Antiviral functions of bone morphogenetic proteins and the activins

Kinda Al-Hourani



Merton College
&
MRC Weatherall Institute of Molecular Medicine

Medical Sciences Division

Supervised by Prof Hal Drakesmith, PhD

Thesis submitted for the degree of Doctor of Philosophy

University of Oxford

Michaelmas Term 2015

Antiviral functions of bone morphogenetic proteins and the activins

Kinda Al-Hourani, Merton College, D.Phil., Michaelmas Term 2015

Abstract

Previous work in the Drakesmith lab has revealed a novel anti-HCV function of bone morphogenetic protein 6 (BMP6), a TGFβ-superfamily cytokine unrelated to type I IFN. Recombinant BMP6 is antiviral against both replication-competent HCV and a full-length genomic replicon model. Data presented in this thesis demonstrate that an anti-HCV effect extends to multiple BMPs and segregates with ability to ligate the type I BMP receptor. Canonically, the type I BMP receptor signals intracellularly via phosphorylation of SMAD1/5/8 transcription factors.

Prior work in the lab shows that BMP6 exerts both type I IFN-dependent and type I IFN-independent antiviral effects. In terms of delineating mechanistic basis for the latter, we have formulated a model whereby BMP6 induces cell cycle arrest in phases characterized by reduced cytosolic nucleotide availability, and which are therefore less permissive to viral replication.

A recent report indicates that another TGFβ-type cytokine, activin B, is able to signal through a non-classical type I BMP receptor dependent mechanism. Activin A and B have multiple established roles in innate immunity and inflammatory responses. However, no direct link between activin A and B and the early response to viral infection has been described. Given their "immune precedent" within the literature, and their high level of structural and phylogenetic homology to the BMPs, both activin A and B represented promising candidates to explore for an antiviral effect.

Our data indicate that activin A mRNA, encoded by the *INHBA* gene, is induced upon activation of RIG-I, MDA5 and TLR7/8 viral nucleic acid sensors *in vitro*, across multiple cell lines and also in PBMCs. *In vitro* infection of A549 lung adenocarcinoma-derived cells and Huh7 hepatoma-derived cells with the murine paramyxovirus Sendai Virus also elicits robust *INHBA* induction. *In vitro* dengue virus infection also elicits *INHBA* upregulation by Huh7.5 hepatoma cells. *In vivo*, infection of mice with influenza A PR8 also elicits induction of activin A message within the lung.

Treatment of Huh7 cells with activin A increases transcription of multiple type I IFN transduction elements; moreover, co-incubation of Huh7 cells with IFNα and either activin A or B augments transcriptional induction of key anti-HCV enzymes. This boosting of type I IFN extends to a functional enhancement: activin A elicits a synergistic, dose-dependent enhancement of both type I and type III IFN's antiviral effect against a full-length HCV genomic replicon. In a full-length genomic replicon model of HCV, both activin A and B alone exert a potent, dose-dependent antiviral effect that is contingent upon signalling via type I BMP receptor. A component of the activins' antiviral effect does not require intact type I IFN signalling. A small-molecule inhibitor of signalling downstream of type I IFN receptor blocks the anti-HCV effect of IFNα but does not impair the antiviral effects of activin A. Both BMP6 and activin A exert dose-dependent antiviral effects against Hepatitis B Virus infection *in vitro*.

Of note, SMAD1/5/8-binding sites have been identified in the promoter sequences of multiple antiviral Interferon Stimulated Genes (ISG), providing a possible route for the enhancement of ISG induction by the SMAD1/5/8 axis. Furthermore, strong topological homology exists between of the transactivation domains of the SMADs and Interferon Response Factors (IRF), which postulated to have diverged from a common ancestor in early metazoans. Preliminary bioinformatic analyses reveal striking parallels between the genome-wide binding profiles of activated SMAD1 and IRF1, including proximal to genes encoding antiviral effectors.

The observations presented in this study may represent the first characterization of a non-IFN intracellular antiviral response in human cells, with implications for the development of targeted therapies against diverse viral diseases. Moreover, these data reveal a novel facet of activin biology, in addition to in part elucidating the nature of the genomic interactions between BMP-SMAD and IFN-IRF signalling.

Declaration

The work presented in this thesis was carried out at the MRC Weatherall Institute of Molecular Medicine, University of Oxford, under the supervision of Prof Hal Drakesmith. I have carried out and developed the majority of the work described in this thesis. Those parts accomplished by others have been clearly indicated. No part of this thesis has been submitted for examination for a degree at this or any other university.

Kinda Al-Hourani

10th October 2015

Acknowledgements

Firstly, I would like to thank my supervisor, Prof Hal Drakesmith, for all of the opportunities, academic challenges and support he has given during the course of my DPhil. I am indebted to him for such a formative and tremendously fun four years. I am also incredibly grateful to Dr Lucy Eddowes, in part for being my Oracle during the early phases of the project, but principally for being so generous with her time, ideas and indefatigable gumption.

I am grateful to Dr Andrew Armitage for his invaluable advice and generosity with his time, expertise and proclivity for wordplay; and also to Dr Sant-Rayn Pasricha, for sharing his infectious passions for both translational research and the Australian alternative music scene. Thank you to Dr Sarah Gooding for offering vital morale boosts, scientific insights and copious LDN-193189; terimah kasih to Pei Jin Lim for sharing her unique scientific ingenuity, tremendous help and never failing to appreciate the value of a kentang besar. I am grateful to Kate Wray for her sharing her excellent proofreading talents. I would like to thank Dr John Ryan for his insights into liver disease, and the many other members and allies of the Drakesmith lab, including Rachel Kandt, Dr Emma Bowles and Shivani Khandwala, who made it such a fantastic environment to study in. Especially, I would like to thank the inimitable Dr Natasha Spottiswoode for her impossibly generous assistance and inestimable friendship throughout the DPhil.

I would like to thank Prof Paul Klenerman and Dr Narayan Ramamurthy for the ongoing collaboration that facilitated extension of our observations to HBV infection and for many rewarding scientific discussions. I am especially grateful to Prof Jan Rehwinkel and Dr Rachel Rigby, in addition to other members of the Rehwinkel lab (notably Dr Jonathan Maelfait and Dr Alice Mayer), for providing indispensible practical expertise, reagents and stimulating scientific conversations. Thank you very much to Prof Alain Townsend and his lab (Dr Tim Powell, Lisa Smith and Pramila Rijal) for their encouragement and insights into influenza infection.

I am very grateful to Prof Nicole Zitzmann and Dr Joanna Miller for the experiments on dengue infection, and also to Prof Frances Platt both for kindly helping to initiate this collaboration and for pastoral guidance. Thank you to Dr Tom Milne, Ross Thorne and the WIMM CBRG for key insights into bioinformatics and igniting my interest in computational biology. I am grateful to Dr Lonnie Swift and Prof Peter McHugh for practical help and theoretical insights into cell cycle biology. Thank you to Prof Angela Russell and her lab at the Department of Chemistry for collaborating on the BMP agonist design project. Thank you to the volunteers who kindly donated blood samples to this project, in addition to those who phlebotomized them.

In addition, I would like to thank profusely my friends and housemates for their support in infinitely varied ways during the past four years. I am lucky that there are too many to list here, but especial gratitude to Melissa, Jeanne, Ai, Lucy, the Merton College Squash Ladder and Plod Club; thank you also to Rosie and Heidi for first galvanizing me to apply for a DPhil.

I am grateful to the Nuffield Department of Medicine Prize Studentship/RDM Scholarship and the Medical Research Council for funding my studies.

Finally, I would like to thank my parents and Ghassan for their unwavering love, support and enthusiasm for all of my scientific endeavours and adventures.

This thesis is dedicated to Mama and Baba, with gratitude beyond words: I can never thank you enough for giving me the opportunities that ultimately made this work possible.

Abbreviations

5'ppp	5' triphosphate moiety
A	Adenine
ac	Acetylation
ALK	Activin receptor-like kinase
ANOVA	Analysis of variance
ATM	Ataxia telangiectasia mutated protein
ATR	Ataxia telangiectasia and Rad3-related protein
ATP	Adenine triphosphate
BMP	Bone morphogenetic protein
bp	Base pair
BrdU	5'-bromo-2'-deoxyuridine
BRE	BMP responsive element
BSA	Bovine serum albumin
C	Cytosine
C. albicans	*Candida albicans*
CARD	Caspase activation and recruitment domain
CD	Cluster of differentiation
CDK	Cyclin dependent kinase
cDNA	Complementary DNA
cGAS	Cyclic GMP-AMP synthase
cHCV	Chronic HCV
ChIP	Chromatin immunoprecipitation
ChIP-seq	Chromatin immunoprecipitation-sequencing
CNS	Central nervous system
Co-SMAD	Common mediator SMAD
CpG	C-phosphate-G- linkage
Ct	Cycle threshold
CTD	C-terminal domain
CTG	Cell Titer Glo ®
CTL	Cytotoxic T lymphocyte
DENV	Dengue virus
DI	Defective interfering (particle)
DMEM	Dulbecco's Modified Eagle's Medium
DMSO	Dimethyl sulphoxide
DNA	Deoxyribonucleic acid
dNTP	Deoxyribonucleoside triphosphate
d.p.i.	Days post infection
DSB	Double strand break
dsRNA	Double stranded RNA
E. coli	*Escherichia coli*
EBI-ENA	European Bioinformatics Institute-European Nucleotide Archive
EDTA	Ethylenediaminetetraacetic acid
EGF	Epidermal growth factor
ELISA	Enzyme-linked immunosorbent assay
ENCODE	Encyclopedia of DNA elements
eQTL	Expression quantitative trait locus
ER	Endoplasmic reticulum
ERK	Extracellular signal-regulated kinase
EtOH	Ethanol
FACS	Fluorescence activated cell sorting
FCS	Foetal calf serum
FLUAV	Influenza A virus

G	Guanine
GAPDH	Glyceraldehyde -3-phosphate dehydrogenase
GAS	Gamma-activated sequence
G-CSF	Granulocyte-colony stimulating factor
GDF	Growth and differentiation factor
GFP	Green fluorescent protein
GO	Gene ontology
GSEA	Gene set enrichment analysis
GWA(S)	Genome-wide association (study)
h.p.i.	Hours post infection
HA	Haemagglutinin
HAU	Haemagglutination unit
HBsAg	HBV surface antigen
HBV	Hepatitis B virus
HCC	Hepatocellular carcinoma
HCV	Hepatitis C virus
hg19	Human genome assembly 19
HIV-1	Human immunodeficiency virus-1
Hprt	Hypoxanthine-guanosine phosphoribosyltransferase
HSV	Herpes simplex virus
IAD	RF-association domain
IC_{50}	50% inhibitory concentration
IFN	Interferon
IFNAR	IFN alpha receptor
IFNLR	FN lambda receptor
IL	Interleukin
Ig	Immunoglobulin
i.n.	Intranasal
INHBA	Inhibin beta A subunit
INHBB	Inhibin beta B subunit
i.p.	Intraperitoneal
IRES	Internal ribosomal entry site
IRF	Interferon response factor
ISG	IFN-stimulated gene
I-SMAD	Inhibitory SMAD
ISRE	IFN-stimulated response element
IVT-RNA	*In vitro* transcribed RNA
JAK	Janus kinase
K	Lysine
kb	Kilobase
KO	Knockout
L. monocytogenes	*Listeria monocytogenes*
LD_{50}	50% lethal dose
LPS	Lipopolysaccharide
LTR	Long terminal repeat
MAPK	Mitogen-activated protein kinase
MAVS	Mitochondrial antiviral signalling protein
MDA5	Melanoma differentiation associated factor 5
mDC	Myeloid dendritic cell
Me	Methylation
MH1/2	Mad homology 1/2 domain
miRNA	MicroRNA
MOI	Multiplicity of infection
mRNA	Messenger RNA
MX1	Myxovirus Resistance 1

NA	Neuraminidase
NCBI	National Center for Biotechnology Information
NFκB	Nuclear factor kappa B
NGS	Next-generation sequencing
NHEJ	Non-homologous end joining
NR	Non-response
nt	Nucleotide
OAS	Oligoadenylate synthetase
ODN	Oligodeoxynucleotide
PAMP	Pathogen-associated molecular pattern
PBMC	Peripheral blood mononuclear cell
PBS	Phosphate buffered saline
PCR	Polymerase chain reaction
pDC	Plasmacytoid dendritic cell
PEG	Polyethylene glycol
pgRNA	Pregenomic RNA
PI	Propidium iodide
PKR	Protein kinase R
poly dA:dT/pdAT	poly(deoxyadenylic-deoxythymidylic) acid
poly(I:C)	polyinosinic:polycytidylic acid
PRR	Pattern recognition receptor
pfu	Plaque forming unit
polyU/UC	polyuridine/uridine-cytosine
RBV	Ribavirin
RIG-I	Retinoic acid inducible gene-1
RLR	RIG-I like receptor
RLuc	Renilla luciferase
RNA	Ribonucleic acid
RNA Pol	RNA polymerase
rpm	revolutions per minute
RPMI-1640	Roswell Park Memorial Institute 1640
rRNA	Ribosomal RNA
R-SMAD	Receptor-activated SMAD
RT-qPCR	Real-time quantitative PCR
SEM	Standard error of the mean
SeV	Sendai virus
SMAD	Sons of mothers against decapentaplegic homologue
snoRNA	Small nucleolar RNA
SNP	Single nucleotide polymorphism
ssRNA	Single stranded RNA
SSH/ftp	Secure shell/file transfer protocol
STAT	Signal transducer and activator of transcription
SVR	Sustained virological response
T	Thymidine
TGFβ	Transforming growth factor beta
Th	Helper T lymphocyte
TLR	Toll-like receptor
TNFα	Tumour necrosis factor alpha
tRNA	Transfer RNA
TSS	Transcription start site
U	Uracil
UTR	Untranslated region
v/v	Volume per volume
w/w	Weight per weight
WT	Wild type

Table of Contents

Abstract ..... **ii**

Declaration ..... **iii**

Acknowledgements ..... **iv**

Abbreviations ..... **v**

Chapter 1 ..... **13**

Introduction to bone morphogenetic proteins, the activins and the immune response to Hepatitis C Virus infection **13**

1.1 Biology of the TGFβ cytokine superfamily **14**

1.1.1 Discovery and phylogeny of the TGFβ superfamily: 14

1.1.2 BMPs: identification, structure and function 15

1.1.3 BMP signal transduction 16

1.1.4 Activins 21

1.1.5 Roles of the TGFβ superfamily cytokines in immune and inflammatory processes 22

1.1.6 Virus-BMP/SMAD interactions 24

1.2 Intracellular innate immunity: the type I IFN response **25**

1.2.1 Classes of IFN response and ligands: a summary 26

1.2.2 Pattern Recognition Receptors and IFN 26

1.2.3 Type I IFN signal transduction (figure 1.7) 27

1.2.4 Interferon Stimulated Genes and effector mechanisms 28

1.3 Hepatitis C Virus **30**

1.3.1 HCV clinical presentation and epidemiology 30

1.3.2 HCV virology and replication cycle 32

1.3.3 In vitro and in vivo HCV infection models 35

1.3.4 HCV therapies: from recombinant IFN to DAAs 36

1.3.5 Immune response to HCV infection 40

1.3.5.1 Adaptive immunity 40

1.3.5.2 Non-IFN innate immunity 42

1.3.6 Type I/III IFN response to HCV infection 44

1.3.6.1 Recognition of HCV by PRRs 44

1.3.6.2 HCV evasion of pattern recognition 45

1.3.6.3 Type I/III IFN and ISG expression during HCV infection 46

1.3.6.4 Inhibition of type I /III IFN by HCV (figure 1.11) 49

1.4 The BMP-SMAD link **50**

1.4.1 Introducing hepcidin, and its dysregulation by HCV 50

1.4.2 Previous antiviral observations from the Drakesmith lab 51

1.5 Thesis Summary **51**

1.6 Thesis Overview **52**

Chapter 2 ..... **53**

General materials and methods **53**

2.1 Cell Culture **54**

2.1.1 Hepatoma-derived cell lines 54

2.1.2 Hepatoma-derived HCV replicon cell lines 54

2.1.3 Monocytic cell lines 54

2.1.4 Lung adenocarcinoma-derived cell lines 54

2.1.5 Fibroblast-derived cell lines 55

2.1.6 PBMC Isolation 55

2.2 Quantitative real-time polymerase chain reaction (RT-qPCR) 55
2.2.1 TaqMan™ probe technology 55
2.2.2 SYBR® Green I technology 57
2.2.3 Passive reference signal 58
2.2.4 RNA isolation 58
2.2.5 RNA quantification and storage 58
2.2.6 cDNA synthesis 58
2.2.7 RT-qPCR reaction 58
2.2.8 Quantification of gene expression 61
2.3 HCV replicon model and luciferase assays 62
2.3.1 The OR6 replicon model 62
2.3.2 Measurement of Renilla luciferase activity 63
2.3.2 Cell Titer Glo viability assay 63
2.4 Data analysis and software 63

Chapter 3 65

Extension of an anti-HCV effect to multiple BMP/TGFβ ligands and exploration of its mechanistic basis 65
3.1 Context and experimental precedents 66
3.1.1 Suppression of hepcidin by HCV reveals antiviral function of BMP6 66
3.1.2 Cell cycle regulation: a summary 70
3.1.3 Cell cycle regulation by BMP/SMAD signalling 71
3.1.4 BMP-SMAD axis and the DNA damage response 73
3.1.5 Some viruses can cause arrest in S-phase 75
3.1.6 Summary and aims 76
3.2 Materials and methods 76
3.2.1 Pharmacological induction of cell cycle arrest 76
3.2.2 BrdU/PI analysis of cell cycle phase distribution 77
3.2.3 Effects of cell cycle inhibition on HCV replication 78
3.2.4 Analysis of CHEK2 and CDKN1A expression in Huh7 cells 78
3.2.5 Screening of BMP/TGFβ superfamily ligands for an anti-HCV effect: 78
3.2.5.1 BMP4 78
3.2.5.2 Activin A and activin B 78
3.2.5.3 BMP15, GDF1, GDF15 79
3.2.6 Investigating the ALK2/3 and IFNAR2 dependency of an anti-HCV effect 79
3.2.6.1 LDN-193189 79
3.2.6.2 Ruxolitinib 79
3.2.6.2 SB-431542 80
3.3 Results: Cell cycle modulation and HCV replication 80
3.3.1 Effect of recombinant BMP6 on cell cycle progression in Huh7 cells 80
3.3.2 Pharmacological induction of cell cycle arrest and HCV replication 88
3.4 Results: Extension of an anti-HCV effect to other BMP/TGFβ-type cytokines 90
3.4.1 Anti-HCV effects of recombinant BMP4, activin A and activin B 91
3.4.2 Testing the ALK2/3, IFNAR2/JAK1 and ALK4/5/7 dependency of the activins' anti-HCV effect 93
3.4.3 Testing peripheral BMP family members for an antiviral effect: GDF15, GDF1 and BMP15 96
3.4.4 The anti-HCV effect of ribavirin is not dependent upon type I BMP receptor activity 99
3.5 Summary and discussion 99

Chapter 4 106

Activin A induction by innate immune and infectious stimuli 106
4.1 Introduction: pattern recognition receptors and innate immune signalling 107
4.1.1 RIG-I-like receptors: biology and function 108
4.1.1.2 RIG-I 108
4.1.1.3 MDA5 109
4.1.1.4 LGP2 110
4.1.1.5 RLR-MAVS interactions 110
4.1.2 Toll-like receptors: biology and function 111
4.1.3 cGAS-STING axis and the innate response to cytosolic DNA 112
4.1.4 PRR signal transduction: induction of pro-inflammatory cytokines and IFN 114
4.1.4.1 Type I IFN induction 114
4.1.4.2 Type III IFN induction 116
4.1.5 PRR activation by specific pathogens and synthetic PAMPs 117
4.1.5.1 Sendai virus: virology and detection 117
4.1.5.2 Dengue virus: virology and detection 117
4.1.5.3 Influenza A virus: virology and detection 118
4.1.5.4 Synthetic agonists of intracellular nucleic acid sensors 119
4.1.6 Summary and aims: 120
4.2 Materials and methods 121
4.2.1 In vitro experiments 121
4.2.1.1 Synthetic nucleic acids and base analogues 121
4.2.1.2 Nucleic acid transfection protocols: cell lines 121
4.2.1.3 Nucleic acid transfection and incubation protocols: human PBMC 122
4.2.1.4 In vitro SeV infection 122
4.2.1.5 In vitro DENV infection 123
4.2.1.6 In vitro HCV infection 123
4.2.1.7 RT-qPCR and ELISA 123
4.2.2 In vivo experiments 124
4.2.2.1 FLUAV infection 124
4.3 Results 125
4.3.1 Activin A mRNA is induced by synthetic agonists of viral PRRs in vitro 125
4.3.2 Induction of activin A and B mRNA by viral infection in vitro 132
4.3.3 Activin A mRNA expression is modulated during in vivo infections 138
4.4 Summary and discussion 142

Chapter 5 147

Modulation of IFN effector 147

functions by activins 147
5.1 Introduction 148
5.1.1 ISG effector mechanisms: a summary 148
5.1.2 Synergistic interactions of BMP and IFNα signalling 151
5.2 Materials and methods 153
5.2.1 HCV replicon antiviral assays 153
5.2.2 Bliss independence test for synergy 153
5.2.3 RT-qPCR quantification of ISG induction in transformed cells 153
5.2.4 RT-qPCR quantification of ISG induction in PBMCs 154
5.2.5 RT-qPCR quantification of IFN signalling components 154
5.2.6 Inspection of ISG promoter regions for BRE motifs 154
5.3 Results 155
5.3.1 Activin A synergistically enhances the anti-HCV effects of IFNα and IL28B . 155

5.3.2 Activin A, activin B and BMP6 modulate ISG induction by IFNα in cell-type specific manner 158
5.3.3 Activin A upregulates transcription of key IFN signalling components 163
5.4 Summary and discussion 164

Chapter 6 168

Bioinformatic comparison of SMAD and IRF 168

genomic interactions 168
6.1 Introduction 169
6.1.1 SMAD structure-function relationship 169
6.1.2 IRF structure-function relationship 170
6.1.3 SMAD and IRF proteins demonstrate strong structural homology 171
6.1.4 Exploring a role for SMAD-IRF interactions in the regulation of antiviral immunity 172
6.1.5 Summary 175
6.2 Materials and methods 175
6.2.1 ChIP-seq databases interrogated 175
6.2.2 Bioinformatic analyses 177
6.2.3 RT-qPCR validation 179
6.3 Results 179
6.3.1 GSE analysis demonstrates significant enrichment for IFN-associated gene sets in the BMP4-SMAD1 dataset 179
6.3.2 Multiple antiviral effector genes are associated with overlapping SMAD1 and IRF1 binding, co-incident with active chromatin marks 183
6.3.3 Genome-wide, SMAD1 binding is enriched proximal to IRF1 188
6.3.4 Statistical appraisal of SMAD1-IRF1 overlap genome-wide 193
6.3.5 Comparison of BMP-induced gene sets between the BMP6/Huh7 microarray and BMP4/K562 ChIP-seq derived datasets 195
6.4 Summary and discussion 197

Chapter 7 200

Investigating the effects of activin and BMP signalling against Hepatitis B Virus, Dengue Virus and Influenza A infection 200
7.1 Introduction 201
7.1.1 Hepatitis B Virus (HBV): virology, pathology and immunology 201
7.1.2 DENV: experimental models and immunology 204
7.1.3 Influenza A (FLUAV): experimental models and immunity 205
7.1.4 Aims and summary 208
7.2 Materials and methods 209
7.2.1 HBV infection 209
7.2.2 DENV infection 210
7.2.3 Influenza A infection/LDN-193189 co-administration 211
7.3 Results 211
7.3.1 Activin A and BMP6 are antiviral against HBV in vitro 211
7.3.2 Investigating an antiviral role for activin A during DENV infection 213
7.3.3 Investigating the effects of LDN-193189 during murine influenza A infection 218
7.4 Summary and discussion 221
7.4.1 HBV infection 221
7.4.2 DENV infection 222
7.4.3 FLUAV infection 222
7.4.4 Screening novel and existing BMP/activin agonists for antiviral effects 226

Chapter 8 ..... **230**

Final summary and discussion **230**

8.1 Summary **231**

8.2 Discussion 233

8.2.1 Is there a role for ECSIT in the interaction of BMP and IFN signalling? 233

8.2.2 Implications for therapeutic modulation of activin signalling 234

8.2.3 Implications for the study of intrauterine viral infection 236

8.2.4 Implications for our understanding of the evolution of intracellular innate immunity 237

8.3 Further investigations **239**

8.4 Future perspectives **241**

Appendix I **242**

Appendix II **250**

Appendix III **252**

Appendix IV **266**

Appendix V **270**

References **287**

Chapter 1

Introduction to bone morphogenetic proteins, the activins and the immune response to Hepatitis C Virus infection

1.1 Biology of the TGFβ cytokine superfamily

Transforming growth factor beta (TGFβ) cytokines perform critical functions in the organogenesis, tissue homeostasis and adaptive immune response of higher vertebrates. Dysregulation of TGFβ signalling is implicated in multiple disease mechanisms, including fibrosis and carcinogenesis.

1.1.1 Discovery and phylogeny of the TGFβ superfamily:

The mechanistic basis for the escape of malignant cells from physiologic growth constraints posed an enigmatic challenge for cell biologists during the late 1970s. Identification of the molecules driving their deregulated growth patterns was accelerated by the observation that virally-transformed cells induce transformation of non-malignant neighbours via a secreted protein, initially termed the "sarcoma growth factor" (SGF) (1). Gel filtration analyses revealed two species composed SGF, neither bioactive in isolation (2): an EGF-like protein afforded the epithet transforming growth factor α (TGFα) and a second structurally dissimilar, but more potently pro-proliferative, TGFβ.

Following the cloning of TGFβ1 in 1985 (3), a series of structurally similar, secreted, disulphide-linked dimeric polypeptides were identified in rapid succession. Whilst the prototypical TGFβ proteins are only expressed in vertebrates, they constitute only a subset within a highly diversified TGFβ superfamily, a group of proteins with a common dimeric structure, overlapping receptor specificities and shared regulatory mechanisms (reviewed by 4,5). Figure 1.1 depicts the phylogenetic relations of the TGFβ superfamily ligands.

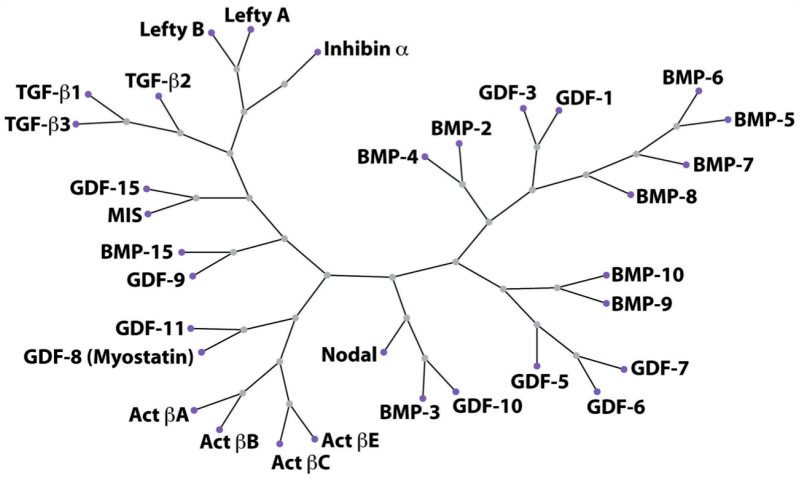


Figure 1.1: Phylogenetic tree of the TGF β superfamily

Mature ligands aligned in accordance with their C-terminal sequence similarity.

Extracted from Hinck, AP Structural studies of the TGF βs their receptors: Insights into the evolution of the TGF β superfamily *FEBS Lett.* 2012 586: 14 1860-1870

Members of the superfamily include modulators of reproductive physiology (activins, inhibins and anti-Müllerian hormone); neurotrophic factors including BDNF and NGFβ; patterning molecules such as Nodal and Lefty, regulators of body plan symmetry (6,7); and the pleiotropic bone morphogenetic proteins (BMP) and related growth and differentiation factors (GDF). Of note, multiple members, including nodal, lefty A, BMP4 and activin A have established roles in liver differentiation from the definitive endoderm germ layer (8,9). Putatively the phylogenetically oldest members of the family, BMP/GDFs have orthologues in both *C. elegans* and *D. melanogaster* (10–12). They are hypothesized to have diverged first to yield activins/inhibins, orthologues of which are expressed by *Drosophila* (13); and subsequently to yield TGFβ1-3, ligands unique to vertebrates.

1.1.2 BMPs: identification, structure and function

Mediating well-established roles in mesenchymal osteogenesis (14), neuronal differentiation (15) and more recently iron metabolism (16), the BMPs are a pleiotropic set of 14 structurally homologous cytokines. Despite their name, the osteoinductive potency of the BMP ligands is highly variable, being highest for BMP2, 6 and 9 (17).

Orthologues of the BMP/GDF ligands and their signalling apparatus are present in diverse animal phyla. Comparative molecular anatomy reveals that BMPs modulate cell fate decisions during the embryogenesis of most bilaterian organisms, including, arthropods, annelids, planarians and all deuterostomata, with increasing complexity of the organism positively correlated with ligand diversity (18,19).

In 1965 Marshall Urist published an elegant series of experiments demonstrating that transplantation of decalcified bone matrix into muscle tissue induced ectopic trabecular bone formation. This osteogenic effect could be ablated by trypsin digestion of the demineralized matrix, conferring the name “bone morphogenetic proteins” to these diffusible inducers of bone formation (20,21). Three decades later, cDNAs encoding BMP2 and 3 were cloned from highly-purified bovine bone extracts by Wozney and colleagues at Genetics Institute (22), followed by isolation of BMP2/7 heterodimers in similar preparations (23). Subsequently, the remaining family members were identified by molecular cloning and mapped to their respective chromosomal loci (24,25).

Despite significant amino acid homology between all BMP/GDFs, they can be categorized into multiple subgroups based on structural homology as illustrated by figure 1.2 (5). The

distinction between BMP and GDF is largely semantic, with nomenclature being guided by the context in which the ligands, or their closest homologues, were first characterized: during osteogenesis for the BMPs, or during more broad developmental and patterning programs for the GDFs.

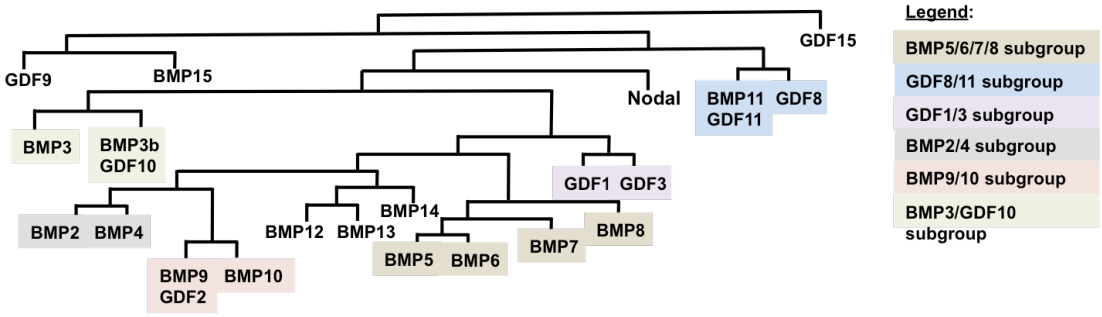


Figure 1.2: Classification of the BMP family by structural similarity

On the basis of their amino acid homology, the BMP/GDF ligands may be divided into a number of subgroups sharing highly conserved sequences, illustrated on the phylogenetic tree. Alternative ligand names are included beneath the primary abbreviation.

The subgroups comprise: BMP2/4; BMP5/6/7/8; GDF-8/-11; BMP9/BMP10; GDF1/3; and BMP3/GDF10.

1.1.3 BMP signal transduction

Akin to other TGFβ cytokines, mature BMPs form either homo- or heterodimeric complexes linked by an intramolecular disulphide bond, approximately 13kDa in molecular weight (reviewed by Rider and Mulloy 2010). A "cysteine-knot" domain, a ring formed by four highly conserved cysteine residues located at the carboxy-terminus, characterizes their structure (27,28).

Whilst multiple cytokine classes share the cysteine knot motif, the presence of a stop codon immediately adjacent to the final cysteine residue is a distinctive consensus feature of the TGFβ superfamily. Figure 1.3 illustrates the crystal structure of BMP9, a prototypic example. BMPs are translated as pre-pro-proteins, and require processing by furin convertases at a conserved RXXR cleavage site before being released from the Golgi network as mature dimers (29,30).

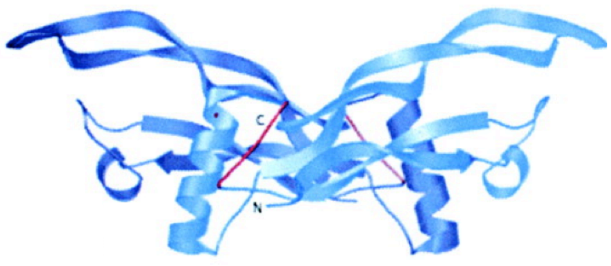


Figure 1.3: Crystal structure of recombinant human BMP9

Ribbon depiction of homodimeric BMP9 at 2.32 Å resolution, representing the prototypic BMP "cysteine knot" structure. The red portion represents the regions including the determinants of receptor specificity.

Extracted from Brown et al. Crystal Structure of BMP-9 and Functional Interactions with Pro-region and Receptors *J Biol Chem* 2005 280: 26 25111-25118

Crystal structures of the BMP ligand/receptor ternary complex reveal that BMP dimers recruit two pairs of receptor symmetrically, producing a heterotetrameric assembly of type I and type II receptors. Despite a diverse repertoire of type I and type II receptors, receptor-ligand binding position and orientation are largely conserved, with the ligand specificity of each receptor principally governed by key amino acid residues at the binding interface (4,5).

ALK1 (ACVRL1), ALK2 (ACVR1), ALK3 (BMPR1A) and ALK6 (BMPR1B) are well-characterized type I BMP receptors, first cloned from human cDNA libraries based upon their homology to the Daf1 receptor encoded by *C. elegans* (31–33). The type 2 BMP receptor species are BMPR2, ActRII (ACVR2A) and ActRIIB (ACVR2B), the latter two being shared with the activins (4).

Associations with co-receptors may be necessary for signal transduction in ligand and tissue-specific contexts, for example hemojuvelin (HJV) for hepatic BMP signalling (16); the type I membrane glycoprotein endoglin as an auxiliary to BMP9/10-mediated angiogenic signalling (34); and the dependence of nodal bioactivity upon Cripto expression (35). The critical regulatory functions performed by these co-receptors are exemplified by the severe pathologies resulting from their dysfunction. Non-functional HJV results in the paediatric iron-overload disorder juvenile haemochromatosis (36); whereas the arteriovenous patterning disorder hereditary haemorrhagic telangiectasia type 1 (37) and accelerated malignant transformation are associated with endoglin and Cripto dysfunction respectively (38).

Upon ligand binding, the constitutively active intracellular kinase domain of the type II receptor phosphorylates the glycine-serine domain of its cognate type I receptor. The type I receptor's activated serine-threonine kinase domain is then able to phosphorylate cytoplasmic substrates and elicit downstream signal transduction. Aberrant constitutive activity of the type I receptor can lead to hyperactive BMP signalling, as seen in the devastating disorder fibrodysplasia ossificans progressive (FOP), characterized by ectopic chondrogenesis within soft tissues (39). In transgenic mice harbouring a constitutively active type I BMP receptor, pharmacological inhibition is sufficient to reduce ectopic endochondral ossification (40). In contrast, truncated type I receptors act as dominant negative inhibitors of the BMP pathway in both *Xenopus* and mice; clinically, they are associated with impaired limb development (41–43).

The classical substrates of the type I BMP receptor are Sons of Mothers Against Decapentaplegia (SMAD) proteins, so-named after their orthologues in *Drosophila* (MAD) and *C. elegans* (sma). Phosphorylation of the receptor-regulated SMADs (R-SMADs)

SMAD1, SMAD 5 and SMAD8 by the type I BMP receptor initiates their association with SMAD4 and subsequent nuclear translocation (44). The SMAD complex binds to GC-rich BMP-responsive elements (BRE) in the promoter region of target genes, initiating their transcription (45). Early-immediate SMAD-responsive genes include the *ID* family of basic helix-loop-helix transcription factors and the inhibitory SMADs (I-SMADs) *SMAD6* and *SMAD7* (46–48). The canonical SMAD-dependent signalling pathway is summarized in figure 1.4.

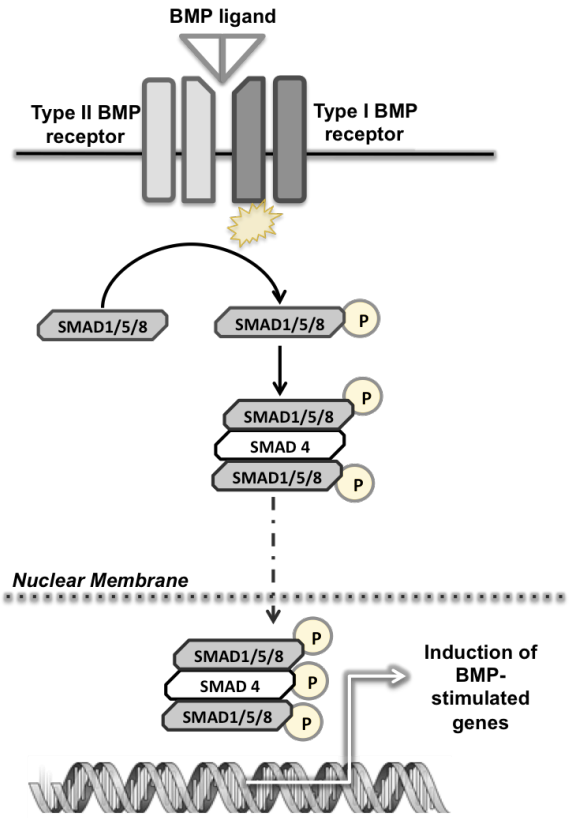


Figure 1.4: The canonical BMP-SMAD signalling cascade

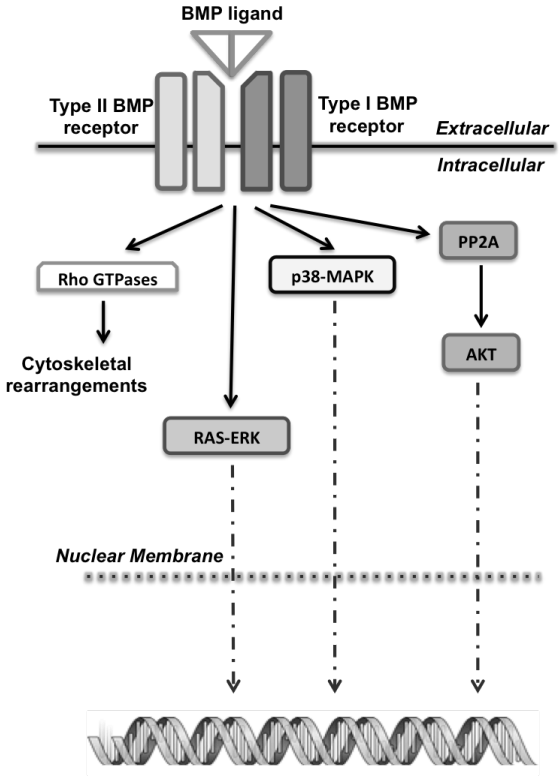
BMP ligands bind to the BMP receptor complex at the cell surface, resulting in activation of the type I receptor's integral serine-threonine kinase and subsequent phosphorylation of the SMAD1/5/8.

Two SMAD1/5/8 molecules associate with a single SMAD4, forming a transcriptionally active complex that translocates to the nucleus and activates BMP-stimulated gene expression.

Non-SMAD signalling mechanisms activated downstream of the BMP receptor include the TAK1/MEKK1 MAPK pathway; RAS-ERK signalling; Rho GTPases involved in cytoskeletal remodelling; and PP2A (49) [figure 1.5]. Of note, functional genomic studies implicate multiple mediators of BMP signalling in the propagation of the HCV replication cycle, including the Rho GTPase RAC1 and the I-SMAD SMAD6 (50).

Figure 1.5: Non-canonical mechanisms of BMP signal transduction

Multiple non-SMAD signal transduction mechanisms are activated downstream, of the BMP receptor complex, including the p38-MAPK pathway, PI3K-AKT and multiple Rho GTPases implicated in remodeling of the actin cytoskeleton.



BMP signalling is regulated by both extracellular and intracellular mechanisms. In the extracellular compartment secreted BMP antagonists, for example noggin, chordin, gremlin and DAN proteins, sequester mature BMPs albeit with variation in their affinities for particular ligands. At the membrane, the BMP-inducible pseudoreceptor BAMBI acts as a dominant negative inhibitor of BMP signalling, lacking an intracellular catalytic domain [figure 1.6].

Intracellularly, SMAD6 and SMAD7 abrogate BMP signalling via multiple mechanisms, including direct disruption of the SMAD4-SMAD1/5/8 association; competitive inhibition of the type I BMP receptor kinase domain; and blocking the SMAD-DNA interaction interface. The I-SMADs also target both R-SMADs and BMP receptor complexes for proteasomal degradation via recruitment of the HECT-type E3 ubiquitin ligases SMURF1 and 2 (51,52) [figure 1.6].

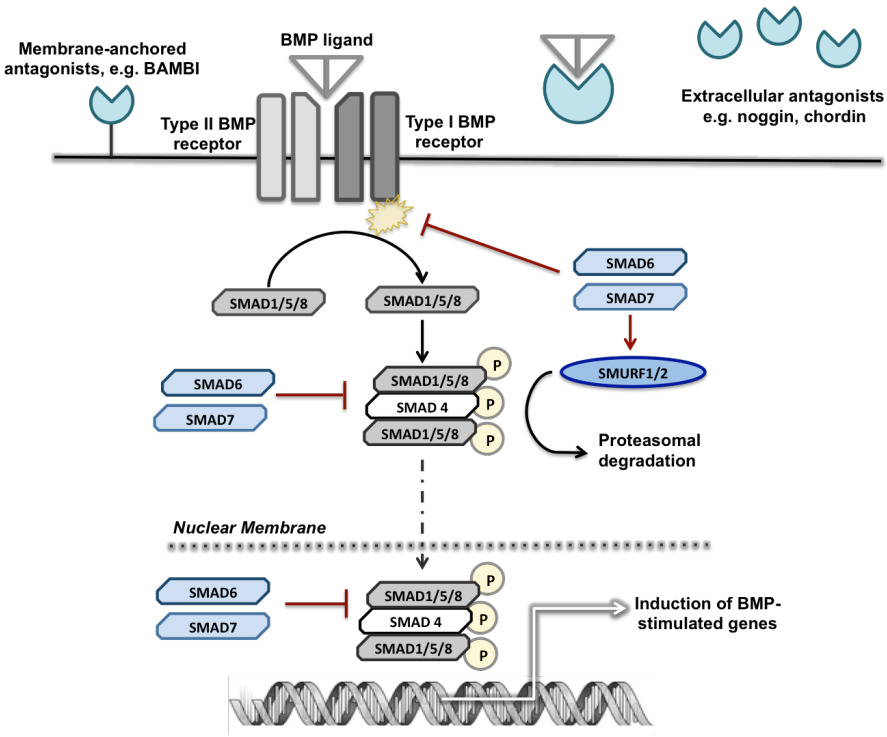


Figure 1.6: Negative regulation of BMP-SMAD signalling

Extracellularly, BMP ligands are sequestered by soluble ligand traps such as noggin and chordin, or membrane-tethered pseudo-receptors such as BAMBI. Intracellularly, the I-SMADs SMAD6 and SMAD7 are induced as a negative feedback response to elevated BMP signalling.

SMAD6/7 act via multiple mechanisms, including: inhibition of SMAD1/5/8 nuclear translocation; direct inhibition of the type I BMP receptor integral kinase domain; recruitment of the SMURF1/2 HECT-type E3 ubiquitin ligases; and direct disruption of the SMAD-DNA binding interface.

Whilst SMAD7 strongly inhibits both BMP and activin/TGFβ signalling, antagonism by SMAD6 is more specific to the BMP axis (51). Availability of SMAD4 to bind R-SMADs is also modulated by proteasomal degradation, the level of which is determined by the balance of activity between the monoubiquitin ligase ectodermin and its antagonist, the deubiquitinase FAM/Usp9x (53,54). Extracellular potentiation of BMP/SMAD signalling can occur either by association with surface-expressed co-receptors, for example the GPI-anchored members of the repulsive guidance molecule (RGM) family (that includes HJV), or via liberation of ligands sequestered by extracellular matrix glycoproteins or soluble antagonists by the matrix metalloproteinase OP-1, or its orthologues Tolloid and Xolloid (55–57). Matriptase-2, encoded by *TMPRSS6*, is proposed to cleave membrane-anchored HJV, thereby attenuating the activity of BMP6 in hepatocytes (58).

Within the nucleus, transcriptionally active SMAD complexes may associate with the cofactors p300 and C/EBPα, augmenting their transcriptional capacity, or interact with master

regulators of cell fate, for example the erythroid lineage regulator GATA1, during lineage commitment (59–61).

In terms of pharmacological manipulation, numerous antagonists of BMP pathway are available, mostly notably small-molecule inhibitors of the type I BMP receptor kinase domain, including dorsomorphin and its more specific derivative LDN-193189 (62,63).

1.1.4 Activins

First identified as regulators of ovarian folliculogenesis, the activins are disulphide-linked dimers formed by association of multiple inhibin β subunits (64–66). The best characterized species are activin A (homodimer of inhibin βA) subunits, activin B (homodimer of inhibin βB) and activin AB (an inhibin βA inhibin βB heterodimer).

Activins were initially described as modulators of follicle stimulating hormone release by the anterior pituitary, but have since been implicated in diverse biological processes. Activin A positively regulates wound healing; keratinocyte proliferation and epidermal morphogenesis; cardiac remodelling during myocardial ischaemia and tissue fibrosis. With regard to expression patterns, activin A is constitutively produced at high concentrations by ovarian granulosa cells, the Sertoli cells of the testis and the anterior pituitary (67). It may be upregulated secondary to inflammatory stimuli (namely TNF, IL1 and LPS) in cells of myeloid origin, including monocytes, myeloid dendritic cells (mDC) and macrophages (68,69), but is also inducible in diverse cell types including hepatocytes, hepatic stellate cells and respiratory epithelia (70).

Activin signalling is mediated by binding to a heterotetrameric cell-surface receptor assembly composed of type I (ACVR1A, ACVR1B and ACVR1C) and type II (ACVR2A and ACVR2B) chains. Canonically, their integral receptor serine/threonine kinase domain phosphorylates SMAD2/3 transcriptions factors, which associate with SMAD4 and translocate to the nucleus to modulate gene expression (67). SMAD2/3 complexes bind a well-conserved “CAGA-box” (AG(C/A)CAGACA) motif in the promoter region of activin target genes, which include the serine protease inhibitor *SERPINE1* and the inhibitor of tissue plasminogen activation *PAI* (71). Increasing evidence exists for non-canonical activin signalling via SMAD1/5/8, akin to BMPs (72).

Negative regulation of activin signalling is mediated intracellularly by SMAD6 and SMAD7, akin to modulation of the BMP axis (73). Extracellularly, the soluble multimeric protein follistatin (FST) binds with high affinity to all activin species, abrogating interaction with cell surface receptors by concealing their receptor binding motifs (67). Binding to certain BMP/GDF family members, including BMP2/5/7/8 and GDF8/9, has also been reported, albeit with an approximately ten-fold reduced affinity (70). FST exists in three isoforms (FST-288, FST-315 and FST-300), the former two derived from post-transcriptional alternative splicing of the primary *FST* mRNA transcript and the latter by post-translational truncation of the primary amino acid chain (74). *FST* is itself induced as a part of a negative feedback response to high levels of activin signalling (75,76). Subtle variations in the cell-type specificity, ligand binding affinities and regulatory function of each isoform are postulated, with evidence from radio-labelled thymidine incorporation assays that FST preferentially inhibits the anti-proliferative effects of exogenous activin, but does not impair autocrine signalling by endogenous activin (77). FST might also regulate activin bioavailability at the level of protein turnover: FST-288 is proposed to induce internalization and lysosomal degradation of activin A (78).

1.1.5 Roles of the TGFβ superfamily cytokines in immune and inflammatory processes

Previous studies regarding the antiviral behaviour of TGFβ have been equivocal: pro-viral and antiviral effects of TGFβ1 upon human immunodeficiency virus-1 (HIV-1) and hepatitis C virus (HCV) replication *in vitro* have been reported (79,80). Akin to the activins, TGFβ signals via SMAD2/3 transcription factors in association with SMAD4 upon ligation of a heterotetrameric TGFβ receptor complex (81). Paradoxically, polymorphisms conferring both elevated TGFβ production and the absence of TGFβ-producing T cells have been vaunted as positive prognostic markers in HIV-HCV co-infected patients (82,83). Such observations further the enigmatic possibility of a systemic role for TGFβ superfamily signalling in the response to acute viral infection. Local, intrahepatic activation of latent TGFβ by HCV infection, mediated by the viral core protein, has been reported in both murine infection models and *in vitro* hepatoma cell-based culture systems (84).

Autocrine BMP signalling is reportedly required for NK cell proliferation; production of IFNγ and chemokines in response to IL2/IL12 stimulation; and paracrine interactions of NK cells with myeloid dendritic cells (85–87). *In vitro*, NK cell activation by a stimulatory cocktail of IL2/IL12/poly(I:C) increases expression of mRNA encoding *BMP2*, *BMPR1A* and

SMAD1, whilst repressing transcription of the BMP-inhibitors *SMAD7* and *BAMBI*. *In* vitro incubation of NK cells with a small-molecule inhibitor of BMP signalling impairs their ability to kill K562 MHC class I-deficient target cells (68,88). Autocrine BMP signalling in mDC promotes expression of the inhibitory ligands PD-L1 and PD-L2, diminishing their capacity to activate antiviral effector T lymphocytes and NK cells (87).

Activin A and B have multiple established roles in innate immunity. Activin A is induced in peripheral blood mononuclear cells (PBMCs) exposed to pro-inflammatory stimuli and associated cytokines, including TNFα, GM-CSF and IFNγ (69,89), neutrophil granules are also a rich source of pre-formed activin A protein (90). In contrast, glucocorticoid exposure suppresses activin A expression (91).

Activin A exerts anti-proliferative effects against T-cells, both thymic and peripheral (92,93). Whilst recombinant activin A reduced proliferation of B9 murine hybridoma cells *in vitro* (94), pharmacological inhibition of activin signalling is associated with reduced immunoglobulin secretion, including IgA and IgE isotypes *in vitro* and *in vivo* respectively (95,96). Activin A also promotes differentiation of immunomodulatory Foxp3+ regulatory T cells from uncommitted precursors *in vitro* (97).

A consensus as to whether activin A signalling predominantly mediates pro- or anti-inflammatory effects has yet to be established, and may represent a cell-type and context-dependent phenomenon. Sierra-Filardi and colleagues report that pharmacological inhibition of activin signalling impairs induction of a pro-inflammatory M1 phenotype after GM-CSF incubation of human monocyte-derived macrophages (98). In rat bone marrow-derived macrophages activin A induces cyclooxygenase 2 expression, with concomitantly increased synthesis of pro-inflammatory arachidonic acid derivatives, including prostaglandin E2 and thromboxane A2 (99).

In vivo, the induction kinetics of activin A and FST in response to systemic inflammatory stimuli were initially characterized in sheep, with induction of activin A and FST occurring 1h and 4h after intravenous injection of LPS, preceding induction of TNFα and IL6 and independently of both prostaglandin release and the febrile response (100). Similarly, both activin A protein in the serum and activin B message in the liver increase rapidly during LPS-induced endotoxaemic shock in mice; administration of recombinant follistatin is sufficient to reduce subsequent mortality (101).

Clinically, activin A expression is positively associated with disease course in acute bacterial septicaemia, but administration of recombinant follistatin does not prevent mortality during virulent *E. coli* K1 infection in mice (102,103). Roles for local elevated activin A are also posited in the pathophysiology of chronic inflammatory bowel disease and rheumatoid arthritis (104,105). In the context of viral infection, a recent clinical study demonstrated that serum levels of both activin A and its soluble binding partner follistatin were significantly elevated in H1N1 influenza-infected patients admitted to intensive care (106). However, no direct link between activin A and B and the early response to viral infection has been described as yet. As discussed later, this topic becomes of some importance in the context of data generated during the course of this research.

1.1.6 Virus-BMP/SMAD interactions

Targeted disruption of the BMP/activin/SMAD axis is a motif of numerous viral infections, and is reminiscent of their antagonism of the type I IFN innate intracellular antiviral response.

HIV-1 Tat protein, a soluble transactivator expressed early in the viral life cycle, is reported to repress transcription of *BMPR2*, encoding an isoform of the type II BMP receptor, in the U937 monocytic cell line. Both HIV-1 infection and exogenous Tat protein dose-dependently repress *BMPR2* mRNA level in U937 cells, with the repressive interaction occurring within the first 208bp of the *BMPR2* promoter (107).

Kaposi's sarcoma herpesvirus (KSHV) targets the BMPR2 protein for lysosomal degradation, via the E3 ubiquitin ligase activity of the membrane-associated viral KS protein (108). Interestingly, KSHV infection in pulmonary endothelial cells is associated with the smooth muscle proliferation and vascular remodelling seen in primary pulmonary arterial hypertension (PAH) (109). Familial forms of PAH are conferred by germline loss of function mutations in *BMPR2* (110).

The KSHV viral microRNA miR-K12-11 suppresses translation of *SMAD5*, thereby impairing BMP signal transduction, whereas Epstein-Barr Virus (EBV) induces expression of the host oncogenic miR-155, the seed sequence of which is both complimentary to, and functionally antagonizes, the *SMAD5* 3'-UTR (111).

Interestingly, the *SMAD5* locus is also a recurrent target site for HBV integration, according to a study isolating and mapping viral integration in HBV-associated HCC tissue by massively parallel sequencing (112). The functional significance of this, however, is unclear.

BMP signalling is activated in the brains of mouse pups infected with reovirus, a neurotropic dsRNA virus that causes encephalitis secondary to caspase 3-dependent apoptosis of infected neurons. Whole brain lysates at six days post-infection showed both elevated BMPR1 protein by immunoblot and increased SMAD1 phosphorylation. Daily supplementation of reovirus-infected mouse cortical cultures with recombinant murine BMP6 reduced caspase-3 activation at 5 days post-infection and preserved neuronal morphology, but did not exert a direct effect on viral replication (113).

Analysis of miRNAs regulated by enterovirus 71 (EV71), the causative agent of hand, foot and mouth disease, *in vitro* suggests targeting of multiple TGFβ/BMP signalling molecules (114). Similarly, microarray analysis of Chikungunya Virus (CHIKV) infected HEK293T cells reveals differential regulation of the TGFβ pathway by CHIKV, including *SMAD6*, observations which were validated by qPCR in primary dermal fibroblasts (115). *SMAD6* induction is also reported in the cortical neurons of mice infected with West Nile Virus (WNV), a *Flavivirus* related to HCV. The same authors reported that siRNA-knockdown of *SMAD6* significantly reduced WNV replication in an *in vitro* system at 48h post-infection (116).

With the exception of the effects of reovirus, the findings above in general describe viral infections impairing BMP signalling by various mechanisms, suggesting that intact BMP signalling may have some antiviral properties, akin to type I IFN signalling – again this topic will be returned to later in the thesis.

1.2 Intracellular innate immunity: the type I IFN response

Interferon (IFN) was first identified by Isaacs and Lindenmann as a soluble factor produced by chick chorio-allantoic membranes exposed to heat-inactivated influenza virus which, when applied to fresh tissue, prevented the replication of live virus (117,118). The biological activities of IFNs have since been extensively characterized, and include antiviral response; immunomodulation, including regulation of MHC expression; and regulation of cell proliferation and differentiation.

1.2.1 Classes of IFN response and ligands: a summary

IFNs comprise three main classes, namely type I, II and III IFN. IFNγ is the sole type II IFN, and despite a sharing a critical role in the systemic immune response to viral infection, is a structurally distinct cytokine with a distinct receptor complex, induction kinetics and chromosomal location. Unlike the BMP/GDF and activin proteins, the expression of type I IFN is restricted to chordates (119). In contrast, 19 mammalian type I IFNs have been discovered, of which 17 are expressed in humans: 13 subtypes of IFNα, IFNβ, IFNε, IFNκ and IFNω. Encoded on chromosome 9q in humans and chromosome 4 in mice, the family diversified as a consequence of repeated gene duplication events. For all members, a single exon encodes a 165-166 residue protein forming a common secondary structure of 5 α-helices clustered by a pair of intramolecular disulphide bonds (119).

Type III IFNs are described in more detail in chapter 5. In brief, three type III IFNs have been characterized, namely IFNλ1-3, encoded by *IL29*, *IL28A* and *IL28B* respectively, in addition to an *IL28B* splice variant encoding IFNλ4. Type III IFNs signal via a multimeric complex composed of an IL10R chain and the IL28Rα receptor subunit, eliciting similar intracellular signalling cascades to type I IFNs (120,121). The type III IFN receptor shows a more tissue-restricted expression pattern than the near-ubiquitous type I IFN receptor, being highly expressed on both B-lymphocytes and endothelial cells, but low on endothelial cells, monocytes, T-lymphocytes and neurons (122).

1.2.2 Pattern Recognition Receptors and IFN

Innate immune detection of microbial infection is contingent upon recognition of pathogen-specific molecular patterns (PAMP). PAMPs include a diverse array of conserved non-self molecules, including foreign nucleic acid structures, for example double-stranded RNA (dsRNA) and non-host surface molecules such as bacterial lipopolysaccharides, lipoteichoic acid and capsular peptidoglycans.

PAMPs are detected by five main categories of pattern recognition receptor (PRR), namely the Toll-like receptors (TLRs); RIG-I-like receptors (RLRs); Nod-like Receptors; C-type lectins (CLRs), including the dectins; and the cGAS-STING cytosolic DNA-sensing axis (123–126). PRR activation and signal transduction mechanisms are described extensively in chapter 4.

Activation of PRRs triggers signalling via a number of adaptor proteins and downstream cascades, including via MYD88/TRIF (TLRs), MAVS/TRAF (RLRs) and STING (cGAS). All mechanisms, however, culminate in phosphorylation of the NFκB transcription factor subunits p50/p65 or the Interferon Response Factor 3 (IRF3), resulting in induction of pro-inflammatory cytokine and Interferon Stimulated Gene (ISG) expression respectively (summarized by (127)).

Phosphorylated IRF3 homodimers translocate to the nucleus and bind to Interferon-stimulated response elements (ISRE) in the promoter of the *IFNβ* gene (128). Secreted IFNβ acts in an autocrine and paracrine manner to promote induction of an "antiviral state" within both the infected cell and its neighbours. IFNβ represents the "first-wave" IFN molecule induced; it in turn activates expression of IFNα and other "second-wave" IFNs, thereby amplifying the response (119,129).

1.2.3 Type I IFN signal transduction (figure 1.7)

Type I IFN signalling occurs via ligation of the surface-expressed IFN receptor complex, comprised of two multimeric receptor chains, IFNAR1 and IFNAR2 (130–132). Type I IFNs have an approximately 1000-fold lower dissociation constant for their interaction with IFNAR2 compared to their interaction with IFNAR1; as such, it is hypothesized that IFNs first bind with high affinity to IFNAR2, with subsequent recruitment of IFNAR1 allowing formation of the ternary receptor complex (133).

IFNAR1 and IFNAR2 constitutively interact with the intracellular kinases TYK2 and JAK1 respectively (134,135). In the majority of cell types, activation of the ternary complex initiates tyrosine phosphorylation of the signal transducer and activator of transcription (STAT) proteins STAT1, STAT2, STAT3 and STAT5, although tissue-specific activation of STAT4 and STAT6 has also been reported (119,136). Phosphorylated STAT (pSTAT) proteins may homo- or heterodimerize; after translocating to the nucleus, these pSTAT dimers, of which the most common species are STAT1 and STAT2 composites, bind to gamma-activated sequences (GAS) in the promoter region of target genes and induce transcription (137). GAS sequences are so-termed by virtue of their initial characterization in the transcriptional regulation of immunoglobulin Fc domain receptors by IFNγ (138).

pSTAT1/2 heterodimers may also associate with the non-phosphorylated transcription factor IRF9 to form the ISGF3 complex. ISGF3 interacts with an Interferon Stimulated Response

Element (ISRE) upstream of its target genes, eliciting induction of a specific repertoire of early phase antiviral Interferon Stimulated Genes (ISG) (139). The promoter region of ISGs may contain exclusively GAS, exclusively ISRE or both sequences, resulting in variation in the profile of IFNs that can induce given ISGs. For example, the multifunctional effector IFITM proteins are inducible by both type I IFNs and IFNγ, whereas the nucleotidyltransferase 2'5'-OAS is selectively induced by IFNα and IFNβ only (140).

Alternative modes of type IFN signal transduction include: the p38-MAPK pathway, activated by JAK1/TYK2 phosphorylation of the guanine nucleotide exchange factors and required for induction of specific ISGs in response to STAT1; IFNα/β-induced anti-apoptotic PI3K-AKT signalling; and modulation of translation via mTOR activation (141).

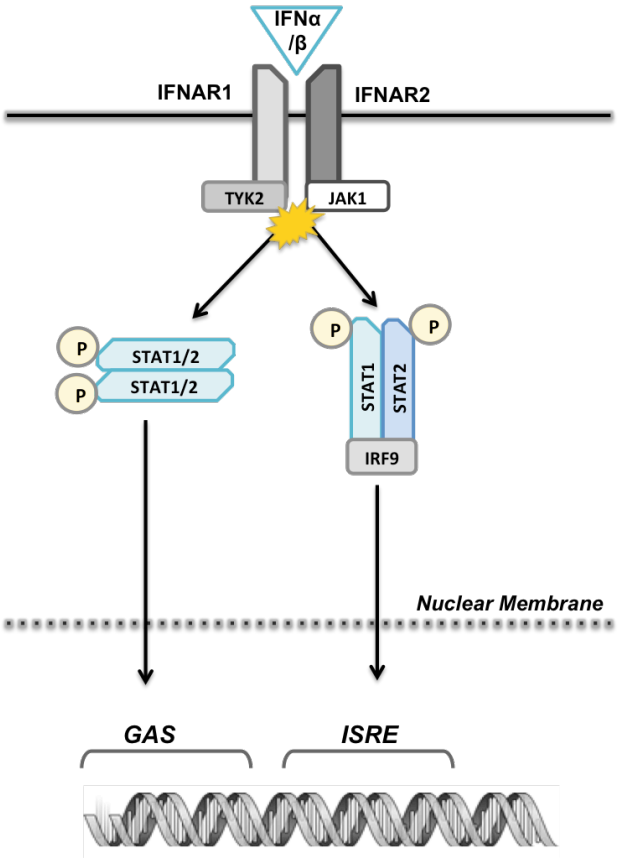


Figure 1.7: Basic scheme of type I IFN signalling

Ligation of the type I IFN receptor complex elicits activation of the constitutively-associated tyrosine kinases JAK1 and TYK2, resulting in phosphorylation of STAT1/2 transcription factors. STAT1/2 may homo- or hetero-dimerize prior to nuclear translocation and binding to gamma-activated sequences (GAS) in the promoters of their target genes.

Phosphorylated STAT1 and 2 also form the ISGF3 tertiary complex with IRF9, which modulates gene expression via binding to Interferon stimulated response elements (ISRE) at target loci.

1.2.4 Interferon Stimulated Genes and effector mechanisms

The effectors of the type I IFN response are the ISGs, which mediate antiviral effects through a diverse set of mechanisms. Up to 2,000 putative ISGs have been identified, through a combination of either discovery-based screens of genes induced by experimental viral

infection, or more hypothesis-driven overexpression studies, in which candidate genes are tested for an antiviral effect against a panel of *in vitro* viral infections (142–144).

Antiviral effector ISGs show a spectrum of potencies, with the most highly active mediators, for example, MX1, OAS and PKR, being discovered during the early days of IFN research (145–147). More recently identified highly potent ISGs include TRIM5, ZC3HAV1, the IFITM proteins and APOBEC3G (148–151). Especially in the case of weaker ISGs (those with less highly active antiviral effects), simultaneous expression of different effectors synergistically enhances their potency (142).

ISG antiviral mechanisms fall into a number of paradigms (142). A first mode of action is to enhance capacity for IFN induction and downstream signalling. Many components of the viral sensing apparatus, for example RIG-I, are IFN-inducible. Type I IFNs also induce key transcription factors, including IRF1 and the master regulator of IFN signalling IRF7, resulting in amplification of the response through a positive feedback loop. IRF7 is absolutely required for the antiviral activity of type I IFN downstream of viral sensing, and is capable of inducing ISG transcription in the absence of IFNα and IFNβ expression (152). Secondly, enzymatic ISGs such as MX1 directly degrade viral nucleic acids, whereas the zinc finger antiviral protein, encoded by *ZC3HAV1*, specifically targets viral RNAs for decay (153,154). ISGs disrupt every stage of the viral life cycle: from inhibition of virus particle –to-cell membrane fusion by soluble hydroxycholesterols produced by the ISG CH25H; to inhibition of intracellular trafficking, in the case of the IFITM proteins; and blockade of budding from the cell surface, as per viperin and tetherin. Moreover, ISGs may modulate host processes to reduce cellular permissiveness to viral replication, as exemplified by the ubiquitin-like adduct ISG15 ("ISGylation"), the RNA editing enzyme ADAR1 and the RNAi component MOV10 (155–158).

Aberrant IFN signalling can result in significant damage to the host. An extreme example is the life-limiting neurodevelopmental disorder Aicardi-Goutières syndrome (AGS), characterized by inappropriate and excessively high type I IFN production. Aetiologically, AGS is genetic heterogeneous, resulting from mutations in any of seven genes associated with intracellular nucleic acid regulation, including the 3'-repair exonuclease *TREX1*, the dNTP triphosphohydrolase *SAMHD1* and the cytosolic dsRNA sensor MDA5 (159,160). For this reason, multiple negative feedback mechanisms curtail the IFN response. The suppressor of cytokine signalling (SOCS) proteins bind to and inhibit signalling via the IFNAR1 receptor chain, whereas protein inhibitor of activated STATs (PIAS) antagonizes DNA-binding of

STATs (161,162). The pleiotropic inhibitor USP18 in part acts by reversal of IFN-induced ISGylation (163,164).

Clinically, type I IFN has been prescribed as an antiviral therapeutic, most prominently against chronic HBV and HCV infection (described further in section 1.3.4). Studies also demonstrate efficacy of intranasal IFNα and topical IFNβ against respiratory rhinovirus and genital herpes infections respectively, but clinical use for these indications is not approved (165,166).

Recombinant IFNα has been deployed as an anti-proliferative agent against a number of solid and haematological malignancies, including renal cell carcinoma and hairy cell leukaemia (167). Notably recombinant IFNβ is a mainstay of therapy for multiple sclerosis, a degenerative neurological disease with an autoimmune component that might be relieved by exogenous IFN (168).

1.3 Hepatitis C Virus

Despite recent radical advances in therapeutic options, hepatitis C virus (HCV) infection remains a significant global health burden. 180 million people worldwide are chronically infected with HCV, a condition that represents the leading indication for liver transplantation in the United States and Europe (169,170). The complex interactions between the type I IFN response and HCV infection are well-characterized, but increasing evidence, both described within this introductory chapter and in the body of this thesis, exists for a link to BMP and activin signalling in the host response to HCV.

1.3.1 HCV clinical presentation and epidemiology

2.8% of the world's population are estimated to be seropositive for anti-HCV antibodies, with the highest prevalence in Central and East Asia (171). All six HCV genotypes (GT1-6) are distributed globally, although GT1, 2, 4 and 5 are hypothesized to have evolved in Africa, whereas GT3 and 6 are endemic to East Asia. In the UK, GT1 and GT3a are co-dominant (172).

Whilst the co-ordinated activities of CD4+/CD8+ T cells, in conjunction with humoral immunity, lead to spontaneous eradication in 15% of infected individuals, HCV persists in 80-85% of cases. Spontaneous clearance rates are higher in women and children, but significantly lower in HIV co-infection (173,174).

Acute HCV infection is associated with a mild, self-limiting febrile illness, with elevated serum aminotransferases in a subset of patients (175). Chronic infection may be clinically silent or manifest with mild non-specific symptoms such as fatigue and myalgia. Severe chronic infection leads to hepatic fibrosis, portal hypertension, liver cirrhosis, and ultimately, in 1-5% of patients per year, culminating in difficult-to-treat hepatocellular carcinoma (HCC) (169,176). Chronic HCV (cHCV) is responsible for an estimated 350,000 deaths annually, accounting for the aetiology of up to 50% of HCC cases in areas of high prevalence (177).

As a blood-borne virus, the principal modes of HCV transmission include high-risk sexual contact; infected blood transfusions; and exchange of contaminated intravenous needles (178). Vertical transmission from infected mothers to their newborns is a significant source of paediatric infections, occurring in 2% to 8% of births to monoinfected, viraemic mothers (179). Iatrogenic transmission is responsible for widespread dissemination of the virus in countries including Italy and Egypt, where use of unsterilized needles during an anti-schistosomiasis control initiative extensively propagated the virus (180,181). Perinatal administration of contaminated anti-Rhesus D immunoglobulin to new mothers resulted in an extensive single-source GT1 outbreak in Ireland; numerous smaller single-source nosocomial outbreaks have been documented in the United States (182,183).

Age at infection, male sex and hepatic steatosis are significant risk factors for progression to advanced fibrosis (184,185). Mode of HCV acquisition is also vaunted as affecting fibrotic progression, with recipients of contaminated blood transfusions possibly more likely to progress to decompensated liver failure than with other infection routes. HBV and/or HIV co-infection, obesity, insulin resistance and diabetes mellitus are positively associated with accelerated fibrosis; diabetes itself is an independent prognostic factor for development of HCC in cHCV patients (186–188). Cohort studies suggest that intrahepatic iron loading is associated with accelerated development of fibrosis in cHCV. The role of heterozygous mutations in the HFE gene (which, in homozygotes, result in the congenital iron overload disorder hereditary haemochromatosis) in the exacerbation of cHCV pathology is controversial, being vaunted as a co-morbid factor in multiple cohort studies, despite meta-analyses suggesting that it is not associated with hepatic iron content.

HBV/HCV co-infection is common, with an estimated prevalence of 5-20% total HCV cases, and widely reported to exacerbate progression to cirrhosis (189). Occult co-infection is

common, with an unexpectedly high proportion of HBV-DNA positive HCV patients lacking serologic evidence of HBV infection, nor expression of HbSAg (190).
Progression to HCC is not ubiquitous, occurring in approximately 20% of patients with HCV-induced liver cirrhosis. GT1 and GT3 infection are most frequently associated with carcinogenesis. In terms of host factors associated with HCC development, multiple SNPs associated with progression to HCC in HCV-infected persons have been identified, most prominently in *MICA* (encoding the MHC class I polypeptide related sequence A), although the mechanistic basis for their association is unclear.

The primary cell type targeted by HCV is the hepatocyte, but evidence of extrahepatic replication has been detected in monocytic cells, peripheral circulating dendritic cells, granulocytes and B-cells *in vivo*. Associated extrahepatic pathologies include dermatological manifestations including porphyria cutanea tarda; and haematological complications including essential mixed cryoglobulinaemia and monoclonal gammopathies (191). Meta-analyses suggests that the prevalence of non-Hodgkin's lymphoma, mainly diffuse large B cell lymphoma, is 10-fold higher in cHCV patients compared to the population average, implying a possible causative role for HCV in neoplastic transformation (192). *In vitro*, HCV negative strand RNA can be detected in PMA-stimulated monocytic cell lines (including Monomac and U937), but not lymphoblastoid lines (193). Cognitive impairment, especially deficits in sustained attention and executive function, is also associated with cHCV. Analysis of brain metabolite composition by proton MS reveals focally elevated choline/creatine ratio in the basal ganglia and white matter of HCV patients compared to healthy controls, a pattern similar to that observed in HIV encephalopathy (194).

1.3.2 HCV virology and replication cycle

HCV is a member of the *Flaviviridae* family, genus *Hepacivirus*, initially identified as the aetiologic agent of "non-A non-B hepatitis" in 1989 (195). It is a small (55-65nM) enveloped positive-sense, single-stranded RNA virus (+ssRNA). Natural HCV infection is restricted to humans, although canine, equine and bat homologues have been described (196). Within the host HCV exists as a quasispecies, with diverse viral sequences generated by the error-prone viral RNA polymerase. Natural intergenotypic recombination (GT1/GT2) has been detected in intravenous drug users in St Petersburg, who risk multiple exposures around the point of primary HCV infection; intragenotypic recombination (GT1a/1b) has been observed in a Peruvian cohort (197,198).

The 9379-nucleotide HCV genome encodes a polyprotein of 3,011 amino acids, comprised of non-structural and structural domains encoding ten viral proteins. The 5'NTR encodes an internal ribosomal entry site, permitting cap-independent translation of the single open-reading frame. Upon entry to the cytosol, the structural region of the viral polyprotein is cleaved by host enzymes, including signal peptidase and signal peptide peptidase, liberating the Core, E1, E2 and p7 proteins. The viral NS2 protease cleaves the NS2-NS3 junction, with subsequent cleavage of the non-structural domain by the NS3/4A serine protease, releasing NS4B, NS5A and NS5B.

Virions are internalized by low pH-dependent clathrin-mediated endocytosis following interaction with a cocktail of entry factors, namely: SR-B1, a high-density lipoprotein receptor that binds host ApoC1/E moieties incorporated into the virion; CD81, a tetraspannin expressed by both hepatocytes and B-lymphocytes; and the intercellular tight junction components claudin-1 and occludin (199–202) [figure 1.9]. The Niemman-Pick C1-like receptor (NPC1LR), part of the host cholesterol sequestration apparatus, is also required for viral entry. Blockade of NPC1LR with the small-molecule inhibitor ezetimibe is a well-tolerated intervention for hypercholesterolaemia, raising the possibility of its use as an adjunct to current HCV therapies (203).

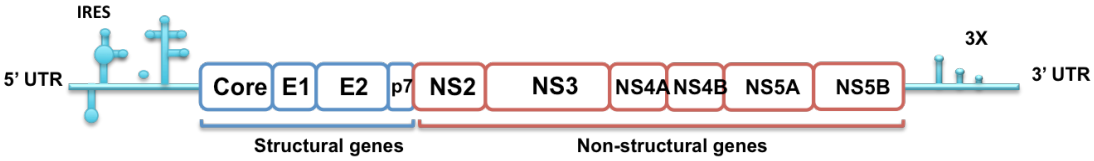


Figure 1.8: Schematic representation of the HCV genome

HCV contains a positive-sense ssRNA genome with highly structured 5' and 3' UTRs. Translation occurs in a cap-independent manner via recruitment of the ribosome to the 5' IRES, yielding an approx. 3,000-amino acid viral polyprotein.

Cleavage of the HCV polyprotein by both host and viral enzymes yields 10 products: 4 structural proteins, denoted in blue, and 6 non-structural, denoted in red. Three conserved stem-loop motifs in the 3' UTR facilitate the intragenomic interactions with the opposite pole of the molecule necessary during viral replication.

The viral RNA-dependent RNA-polymerase, NS5B, mediates HCV genomic replication, with progeny +ssRNA transcribed via a negative-sense RNA intermediate (204). HCV genomic replication and virion assembly occur at the intracellular "membranous web", a system of cholesterol-rich lipid rafts derived from viral modification of the host endoplasmic reticulum (ER) (205). Replication is proposed to occur in large "replication factories", at which hundreds of non-structural proteins aggregate about a single negative-sense RNA template (206) [figure 1.10].

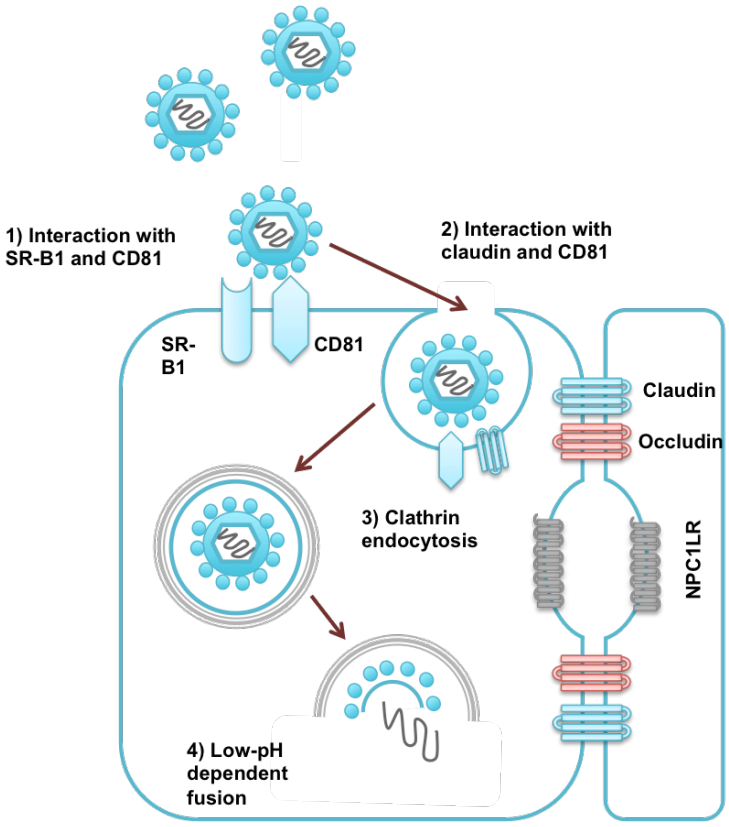


Figure 1.9: HCV intracellular entry mechanisms

After initial binding to the cell-surface scavenger receptor SR-B1 and the tetraspannin CD81, HCV virions further interact with the intercellular gap-junction proteins claudin and occludin, in addition to the lipid transported NPC1LR, before internalization by clathrin-mediated endocytosis. Intracellularly, low-pH mediated fusion results in disintegration of the viral envelope and capsid, liberating its genomic material into the cytosol.

Adapted from Lindenbach BD and Rice CM, The ins and outs of hepatitis C virus entry and assembly. *Nature Medicine* 2013 11: 10 686-700

HCV RNA is translated in a cap-independent process by recruitment of the ribosome to the highly conserved internal ribosomal entry site (IRES) located within the 5'-UTR of the viral transcript. The HCV IRES, composed of a 340-nt stretch forming a tertiary structure under physiological salt conditions, induces conformational changes in the 40S ribosome that compensate for absent translation initiation factors. Subsequent binding of eIF2 and 3 facilitate recruitment of the large ribosomal subunit, driven by GTP hydrolysis, forming the complete 80S translation initiation complex (207,208).

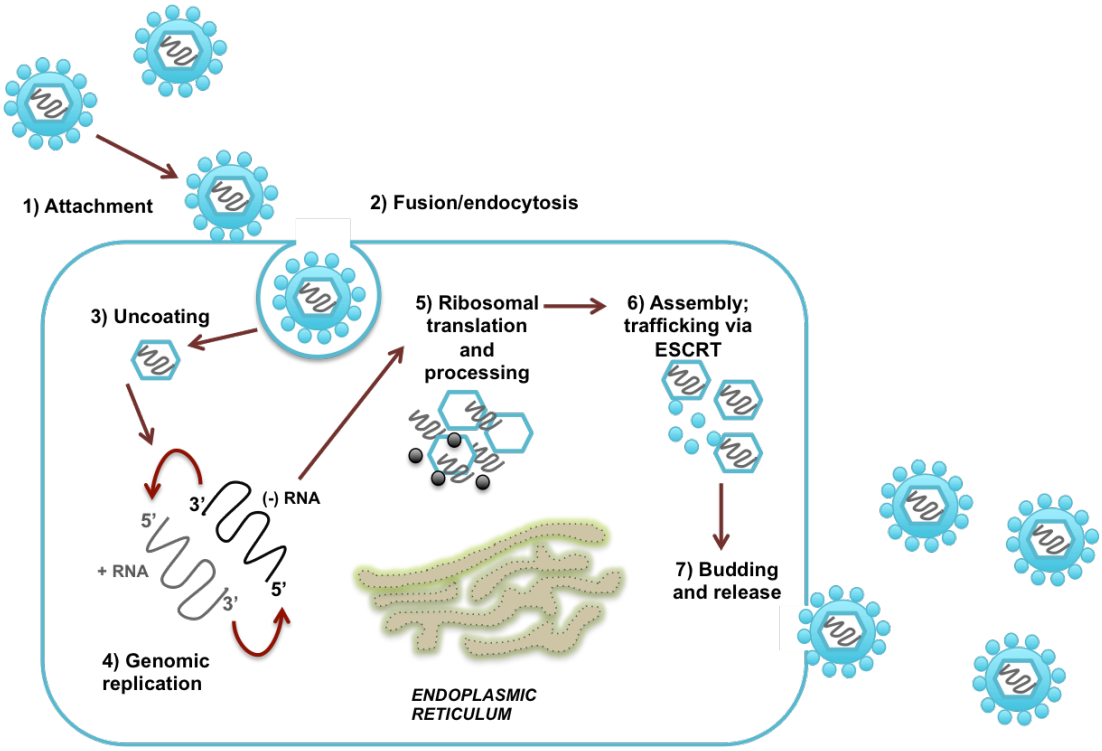


Figure 1.10: HCV replication cycle

Following internalization and uncoating, HCV genomic replication occurs proximal to the endoplasmic reticulum, mediated by the viral RNA-dependent RNA-polymerase, encoded by *NS5B*. At the membranous web, a region of modified endoplasmic reticulum, ribosomes are recruited to the positive sense HCV transcript via the IRES, resulting in translation and cleavage of the polypeptide to release ten HCV structural and non-structural proteins. HCV assembly occurs at the membranous web, followed by trafficking to the surface via the ESCRT pathway, in parallel with glycosylation of the envelope glycoproteins. Viral egress occurs by membrane fission.

During virion assembly, HCV core protein is recruited from cytosolic lipid droplets to the modified ER, where the viral envelope proteins E1/E2 are retained as non-covalent heterodimers. Upon assembly of the icosahedral viral capsid, nascent virions are trafficked via a pH-buffered (mediated by the p7 viroporin) secretory pathway to the cell-surface, acquiring complex glycosylation of the envelope proteins and incorporation of low-density lipoproteins to form mature low-density lipoviral particles. HCV egress occurs by membrane fission facilitated by the ESCRT (endosomal sorting complexes required for transport) pathway, a common mechanism of viral release into the extracellular compartment (209).

1.3.3 In vitro and in vivo HCV infection models

Mechanistic studies of HCV infection were hampered by the specific tropism of HCV for human hosts and the lack of a replication-competent *in vitro* infection system, until the establishment of the JFH1 model in 2005 (210). Earlier subgenomic replicon models, including the initial Con1-strain GT1b model established in Huh7 hepatoma-derived cells,

facilitated radical advances in basic HCV research (211). Despite being ultimately established for full-length genomic constructs, the utility of a replicon model is constrained by the absence of viral entry and egress. Examination of viral entry kinetics became possible with the generation of pseudotyped HCV particles (HCVpp) expressing native E1 and E2 envelope glycoproteins assembled onto retroviral core proteins (212,213).

In the JFH1 model, production of infectious viral particles is sustained following transfection of Huh7 cells with a full-length GT2a genome cloned from a patient with fulminant hepatitis (210). Subsequent iterations of this model included the use of Huh7.5.1 cells, which are more permissive to HCV replication due to defective expression of the cytosolic viral RNA sensor RIG-I; and the use of chimeric HCV clones with faster replication kinetics (214,215).

Both primary human hepatocytes and primary hepatocytes from the tree shrew *Tupaia belangeri* have been successfully infected with both serum-derived HCV particles and pseudotyped retroviral virions (216,217). *T. belangeri*, however, are not characterized as a natural reservoir of HCV.

Whilst artificial infection of chimpanzees is technically possible, use of non-human primates to study HCV *in vivo* is prohibitively expensive and ethically controversial. *In vivo* HCV infections have been established in immunosuppressed *Tupaia belangeri*, whereas tamarin monkeys (*Saguinas ursula*) and marmosets (*Callithrix jacchus*) are susceptible to the related hepacivirus GBV-B (218).

Two experimental murine infection models currently exist. The human liver-uPA-SCID model consists of immunodeficient mice with transgene-induced liver necrosis. Transplantation with primary human hepatocytes after birth permits reconstitution with functional human liver tissue permissive to subsequent HCV infection (219). In a separate chimeric model, immunocompetent mice stably expressing human claudin-1 and occludin, the minimally required HCV entry factors, are able to sustain entry and replication of HCV, with the infection subject to restriction by both innate and adaptive immune responses (220).

1.3.4 HCV therapies: from recombinant IFN to DAAs

Early clinical interventions for HCV included corticosteroid therapy and intravenous administration of the synthetic acyclic nucleoside acyclovir; a phase I trial of the latter elicited no amelioration of biochemical or histological indices in chronically infected patients (221,222).

Motivated by the broad-spectrum *in vitro* antiviral activity of IFNα, including against HAV, HBV and the hepatitis deltavirus, the first trials of recombinant IFNα for "non-A non-B hepatitis" were initiated before Choo and colleagues' identification of HCV as its aetiologic agent. The initial trial consisted of twice-daily subcutaneous administration of recombinant IFNα 2b (5MU or 1MU) to ten patients, six of whom demonstrated a sustained reduction in serum aminotransferase (AT) level, an index of liver damage, in addition to reduced portal inflammation and total eradication of parenchymal hepatocytic necrosis. Subsequent re-analysis of these patients following the biochemical characterization of HCV revealed a correlation of reduced serum AT with reduced HCV-RNA, with one of the study participants representing the first case of HCV clearance following antiviral therapy (223,224).

FDA-approval of recombinant IFNα-2b for HCV followed in 1991, following two multicentre randomized controlled trials (RCT) comparing the efficacy of subcutaneous IFNα-2b administered three times weekly for six months versus placebo. Both studies recorded precipitous declines in serum AT in parallel with improved liver histology, including regression of periportal inflammation and diminished hepatocytic necrosis(225,226).

IFNα monotherapy remained thwarted by a low incidence of SVR, prompting efforts to augment it by co-administration of a directly antiviral agent. Based upon its broad-spectrum antiviral activity *in vitro*, the orally-bioavailable guanosine analogue ribavirin (RBV) entered two trials as an anti-HCV monotherapy, administered at either a single dose twice-daily for 12 weeks or in escalating doses over 24 weeks. Whilst in both studies RBV elicited a potent reduction in serum AT, this effect was reversed only 6 weeks after cessation of treatment (227,228). Subsequent phase II trials examining the response of IFNα 2b and RBV co-treatment, however, demonstrated much greater promise, with an Italian cohort obtaining a 40% SVR rate following 24 weeks co-administration, and a Swedish trial achieving total viral clearance in 90% of patients who had relapsed following previous IFNα 2b monotherapy (229). The therapeutic mechanism of ribavirin, however, remains a point of controversy, with hypotheses ranging from inhibition of eukaryotic initiation factors; induction of viral mutagenesis; disruption of host cell purine metabolism; and direct inhibition of the viral RNA-dependent RNA-polymerase (230).

A European multicentre phase III RCT vindicated the choice of IFNα 2b and RBV combined therapy versus IFNα monotherapy, with 43% of patients attaining SVR in the combined arm versus 19% in IFNα only group. Replication of this observation in a US Phase III RCT established IFNα/RBV co-treatment as the standard-of-care for HCV infection, albeit with

marked variation in the efficacy of the regimen against different viral genotypes, with genotype 1 infection requiring longer treatment windows than genotype 2/3 (231,232).

Multiple studies have shown that the viral load kinetics following initial administration of IFNα are biphasic: an initial exponential reduction in serum HCV-RNA, with rebounds corresponding to reduction in bioactive IFNα, followed by a sustained, slower decline (233). The advent of pegylated-IFN circumvented this jagged variation in HCV-RNA content; conjugation of a polyethylene glycol (peg) oligomer to IFNα and IFNβ increased their serum elimination half-lives to 75h and 30h respectively, thereby allowing sustained bioactivity following initial administration. Numerous phase III trials of intravenous peg-IFNα/oral RBV therapy demonstrated SVR could be established in 20-30 % genotype 1/4 infections and approximately 80% genotype 2/3 cases (approximately 50% success across all genotypes) following 48 and 24-week courses respectively, thereby establishing this regimen as the first-line anti-HCV treatment (234).

Sadly, this regimen is blighted with limitations. Adverse effects of peg-IFNα include cytopaenias, flu-like symptoms and fatigue, all of which reduce patient compliance (235). Furthermore, significant differences in response exist across the major HCV genotypes and between ethnic groups (236). On the conventional peg IFNα /RBV regimen, only 40-50% patients with genotype 1 HCV achieved a sustained virological response (SVR), defined as undetectable viral RNA in the plasma 24 weeks after cessation of treatment (169).

The pre-eminence of peg-IFNα/RBV persisted for a decade, until the emergence of a new breed of anti-HCV pharmaceuticals: the orally-bioavailable directly acting antivirals (DAA).

An initial proof-of-concept study showed a precipitous decline in HCV-RNA in 8 patients administered the first-in-class NS3/4A protease inhibitor BILN 2061, a macrocyclic organic compound (237). Whilst development of BILN 2061 was terminated due to cardiotoxicity in later preclinical studies, subsequent iterations of macrocyclic NS3/4A inhibitors, such as boceprevir and telaprevir gained traction for genotype I infection. The NS3/4A protease is a challenging therapeutic target for the design of small-molecule inhibitors due to the large and shallow active site, with no discrete cleft for the intercalation of a drug (238). Boceprevir, teleprevir and related drugs are metabolised *in vivo* to α-keto peptidomimetics capable of forming a reversible covalent bond with NS3/4A's catalytic serine residue, ablating its proteolytic activity (239). Side effects of NS3/4A inhibitors include, akin to IFNα/RBV regimens, fatigue and nausea, although anaemia is specifically associated with boceprevir (240).

Given the error-prone nature of the HCV RNA-dependent RNA polymerase and the high virion production rate (estimated at $1.3x10^{12}$ day^{-1}), the viral mutation rate is high, with an estimated incidence of 1 mutation per 10^5 nucleotides per replication cycle (241). Initial protease inhibitor (PI) monotherapy was associated with the rapid emergence of resistance, with two mutations (R155K and A156S) conferring resistance to all first-generation PIs (242). Sexual transmission of PI-resistant variants has been documented (243). Second-wave PIs with a non-covalent mechanism of action, such as simeprevir and danoprevir, are clinically better tolerated and demonstrate activity against all HCV strains except genotype 3; however, they remain blighted by a low barrier to resistance. Current attention focuses on a second-generation of allosteric NS3/4A inhibitors with pan-genotypic activity and a higher barrier to resistance. The prototypic example of this class, grazoprevir, is presently in phase III clinical trials in conjunction with the NS5A inhibitor MK-8742 (244).

Two inhibitor classes target the catalytic subunit of the HCV RNA-dependent RNA-polymerase (RdRp), encoded by the viral NS5B; non-nucleoside inhibitors (NNI) and nucleos(t)ide analogues (NA). The former, which are principally active against genotype 1 infections, interact with poorly conserved surface regions of NS5B, eliciting allosteric inhibition of RNA synthesis. NAs, in contrast, mimic the natural substrates of the RdRp and upon incorporation into the nascent RNA molecule elicit premature chain termination. By virtue of not interacting directly with NS5B catalytic residues, the NAs have both a high barrier to resistance and show pan-genotypic activity (238). *In vitro*, long-term serial passage of Huh7 cells harbouring a GT1a subgenomic replicon with mericitabine, a first-generation NA, elicited emergence of single base substitution conferring reduced drug sensitivity, S282T. S282T mutants demonstrate a reduction in fitness to 15% of wildtype *in vitro* (245). Transient emergence of S282T resistant variants has been documented by deep sequencing of viral isolates from relapsed patients receiving monotherapy with sofosbuvir, an NA entering widespread clinical practice. In all cases examined the resistant variant reverted to wildtype, and patients were successfully cured following addition of RBV to their treatment regimen (246,247).

Inhibition of the viral NS5A by palindromic small molecule inhibitors, such as daclatasivr and ledipasvir, abrogates function of the HCV replicase by disrupting cofactor recruitment. Cation channel blockers, including rimantidine derivatives, have been tested against the HCV viroporin p7, but results of these studies have been equivocal (244).

Whilst IFN-free regimes consisting of have shown remarkable efficacy in clinical trials, with up to 97% of non-cirrhotic GT1 patients attaining SVR with a 12-week course of sofosbuvir, RBV and NS5A inhibitor, they remain prohibitively expensive for many healthcare systems (248,249). A 12-week course of sofosbuvir alone is estimated to cost £35,000, but is presently approved by NICE for the treatment of cirrhotic GT1 patients in conjunction with peg-IFNα/RBV (250). It is not likely that the costly new drugs will be available to impact the vast majority of HCV-infected individuals who live in resource-limited settings in the near future. A clear rationale remains for exploring the host immune response to HCV and possible strategies for its therapeutic enhancement.

Despite the advent of DAA regimes, HCV vaccine research continues apace, with a focus upon preventing the establishment of persistent infection, rather than the induction of sterilizing immunity to counter initial infection (251). The genotypic diversity of HCV poses a significant challenge to the development of an effective vaccine. Two vaccine regimes, both with the aim of preventing HCV chronicity, have entered phase I/II clinical trials: the Chiron vaccine, composed of E1/E2 subunit glycoproteins delivered with a squalene lipid adjuvant (252); and the Okairos vaccine, consisting of the HCV NS3-NS5b encoded by viral vectors (253).

1.3.5 Immune response to HCV infection

1.3.5.1 Adaptive immunity

Adaptive immune responses to HCV can be challenging to study due to the tolerogenic environment of the liver, which prevents induction of aberrant immune responses to the many potentially antigenic stimuli passing through each second, including gut-derived nutrients carried in the portal venous blood and neo-antigens produced by detoxification (254).

CD8+ cytotoxic T-lymphocytes (CTL) and CD4+ T-helper (Th) cells predominantly mediate cellular adaptive antiviral responses, along with modulation by FOXP3+ T-regulatory cells (Treg). CTLs mediate direct lysis of infected cells based on recognition of viral peptide epitopes presented by MHC class I; whereas CD4+ helper cells enhance the cytotoxic capacity of CTLs and promote immunoglobulin class-switching by B-lymphocytes, amongst other functions (255–258).

Examination of the intrahepatic T-cell response during acute HCV in chimpanzees reveals that resolution of infection is correlated with a broad CTL response, with induction of

responses against multiple viral target regions; restriction by all six MHC class I allotypes; and long-term persistence of an HCV-specific CTL memory population. In this model, weaker CTL responses, both in terms of epitope breadth and persistence, was associated with chronic viraemia (259). These observations have been replicated in humans, with spontaneous HCV clearance associated with broad CD4+/CD8+ T-cell responses and the persistence of memory CTLs, which are proposed to confer long-term immunity to reinfection after the resolution of clinical hepatitis.

Whilst the CTL response is critical for resolution of acute infection, chronic HCV infection results in exhaustion of intrahepatic T-cells, with loss of function and decreased proliferation. Interestingly, both early administration of IFNα and attainment of SVR are associated with preservation of circulating HCV-specific CD127+ CD8+ memory T-cells (260).

Detection of HCV-specific CD4+ T-cells *ex vivo* is difficult due to the low frequency of tetramer-reactive cells, both circulating and intrahepatocytic (261). Specific CD4+ responses are typically strong during acute infection; waning of this initial response is a hallmark of progression to chronic infection. Intact CD4+ lymphocytes are necessary for memory CTL-mediated protection against secondary HCV infection. Immunodepletion of CD4+ cells before reinfection of immune chimpanzees is reported to result in persistent viraemia and progression to chronicity in spite of unimpaired CD8+ memory T cells (262).

A balance between activation of Th_{17} and FOXP3+ T_{reg} cells is also implicated in cellular immune control of HCV (263). Proliferation of both subsets has been observed in both acute infections, with preferential expansion of Treg cells during persistent infection (264).

In terms of the humoral response to HCV, virus-specific antibodies are detectable in the serum 6-8 weeks post-infection, with rapid induction of cross-reactive neutralizing antibodies correlated with spontaneous clearance (265). Neutralizing antibodies bind directly to the virus and block dependent interactions such as uncoating and entry factor binding. HCV-specific responses are predominantly directed against the E1/E2 envelope glycoproteins, and abrogate their interaction with CD81. Non-neutralizing antibody effector mechanisms include recruitment of complement factors, which are actively antagonized by HCV, and opsonisation of viral particles for Fc-dependent phagocytosis (261,266).

The antibody response has a role in selecting for viral diversity. HCV sequences from patients with concomitant hypogammaglobulinaemia show fewer nucleic acid substitutions in the

hypervariable region (HVR) at the 5' end of E2 (267). The HVR undergoes a much higher rate of nonsynonymous mutation than other regions of the viral genome, leading to the hypothesis that it acts a decoy to direct the focus of the humoral response away from critical conserved epitopes. (268).

Immunization of chimpanzees with E1/E2 glycoproteins conferred some protection to an autologous HCV challenge, an early demonstration of the protective effects of anti-HCV antibodies (269). Human trials of therapeutic neutralizing antibodies have shown variable efficacy, although a recent trial of humanized anti-E2 monoclonal antibody administered after liver transplant to HCV-positive recipients showed a significant delay in the kinetics of viral rebound (270).

As to a role for antibodies in the control of chronic infection, evidence is limited. B-cell depletion with Rituximab resulted in increased serum HCV-RNA during treatment of HCV-positive CD20+ B-cell lymphoma patients, albeit in a small study (271). A Scandinavian cohort of primary hypogammaglobulinaemia patients who contracted HCV from contaminated immunoglobulin preps showed extremely rapid progression to fatal cirrhosis (272).

1.3.5.2 Non-IFN innate immunity

The complement system, an innate immune response comprising a network of soluble factors and cell-surface receptors, enhances antibody responses to viral infection and modulates effector T-cell function. The role of complement in the restriction of HCV is poorly explored. HCV NS5A is reported to repress transcription of the C4 component *in vitro*; this interaction is complemented by the clinical observation that low serum C4 levels are predictive of non-response to IFNα /ribavirin therapy (273,274).

Composing 2-5% of total peripheral blood mononuclear cells (PBMC), Natural Killer (NK) cells are a key component of the antiviral response to HCV, forming a bridge between the innate and adaptive arms of the immune system. NK cell activity is modulated by the integration of activating and inhibitory cues, and constitutively dominated by inhibitory signals from Killer Immunoglobulin Receptors (KIR) recognizing self-MHC class I molecules (275).

A comprehensive genotyping study of over 1,000 patients by Khakoo and colleagues revealed that expression of the inhibitory KIR subtype KIR2DL3 and its class I MHC ligand HLA-C directly influences the resolution of acute HCV infection. A linear relation links KIR2DL3 gene dosing and the odds ratio for spontaneous clearance, with KIR2DL3 homozygotes more likely to spontaneously clear the virus than 2DL3/2DL2 heterozygotes or 2DL2 homozygous individuals. (276). This favourable KIR2DL3-HLAC1 combination is highly prevalent in cohorts of aviraemic intravenous drug users (IDU) multiply exposed to HCV (277).

NK cells from HCV-exposed but uninfected IDUs express significantly higher levels of the activating receptor NKp30; *in vitro* $NKp30^{high}$ NK cells are able to reduce HCV-RNA levels in JFH1-infected Huh7.5 cells in the absence of exogenous stimulation (278).

Dendritic cells (DCs) are professional antigen presenting cells that upon activation (by exposure to pathogen associated molecular patterns (PAMPs), inflammatory cytokines and innate lymphocyte interactions) migrate from sites of local infection to the draining lymph nodes and interact with T and B-lymphocytes to sculpt the epitope specificity of the adaptive response. Dendritic cells can be classified as either myeloid DCs (mDC), with a principal role in antigen presentation, or plasmacytoid DCs (pDC), a morphologically distinct subset associated with prodigious levels of IFNα secretion when exposed to PAMPs, including HCV RNA (279).

The effect of HCV infection on mDC function is poorly defined. *In vitro*, mDCs obtained from HCV-infected patients are reported to elicit reduced alloreactive CTL responses, and transduction of mouse mDCs with a recombinant adenovirus expressing a chimeric HCV Core/NS3 construct impairs CD4+/CD8+ T-cell activation *in vivo* (280). However, a study of chronically infected chimpanzees showed no functional or phenotypic impairment of CD14+ monocyte-derived DCs (281).

pDCs detect HCV RNA either via TLR7 following its endosomal internalization, or via an exosome delivery mechanism dependent upon expression of Annexin A1 and ESCRT machinery (282,283). In the Pelletier et al. prospective study, pDCs expressing the inhibitory ligands PD-L1 and PD-L2 are relatively enriched in frequency in individuals who develop chronic infection, compared to those who spontaneously clear HCV and uninfected controls (284).

1.3.6 Type I/III IFN response to HCV infection

HCV is exquisitely adapted to establish chronic infection by disabling the type I IFN response of infected hepatocytes. It achieves this by a two-step mechanism. Firstly, it disables the PAMP recognition apparatus required for IFNβ induction. Secondly, it attenuates the response of infected cells to type I IFN.

1.3.6.1 Recognition of HCV by PRRs

HCV RNA is detected by RIG-I within hours of infection: nuclear pIRF3-activated by RIG-I and MAVS- is detectable up to 36 hours post-infection in Huh7 cells, before significant viral protein production. As viral protein load increases, however, nuclear pIRF3 diminishes, due to targeted disruption of the RIG-I/MAVS interaction by HCV NS3/4A (285).

The HCV RIG-I PAMP is composed of an exposed 5' triphosphate moiety and a polyU/UC-rich sequence in the viral 3'UTR. The HCV 3'UTR is highly structured, consisting of an initial variable region with secondary structure, a 100bp unstructured polyuridine/ribocytidine-rich tract and a terminal "X" region with three conserved stem-loops (286). During viral replication, intragenomic interactions bring opposite ends of the viral genome into close proximity, and stabilize the PAMP motif (287).

The 5' triphosphate is necessary but not sufficient for recognition of HCV by RIG-I. The 3' polyuridine motif is absolutely required, both *in vitro* and *in vivo* (288).

The endosomal dsRNA sensor TLR3 has a less clear role in the sensing of HCV infection. Expressed by both Kupffer cells and hepatocytes, activated TLR3 engages with its adaptor protein TRIF, culminating in phosphorylation of IRF3 and NFκB (289). Reconstitution of TLR3 in the otherwise TLR3-deficient Huh7 hepatoma-derived cell line elicits transcriptional induction of the antiviral chemokines RANTES and MIP1-1β at 48h post-infection. These delayed induction kinetics, and the observation that UV-inactivated virions do not modulate chemokine transcription, suggest a response to detection of a HCV replication intermediate, rather than viral entry (290). Additionally, in another model, TLR3 reconstitution of Huh7 cells restricts replication of a J6/JFH1 chimeric replicon Whilst the synthetic TLR3 ligand poly(I:C) is able to induce robust *ISG56* and *ISG15* expression with 18h, the kinetics of ISG induction by JFH1 HCV are much slower and weaker, with ISG induction only evident at 4 days post-infection in TLR3-reconstituted Huh7.5 cells (291).

The HCV TLR3 PAMP is proposed to be dsRNA intermediates that accumulate in the later phases of HCV replication. RNA duplexes are readily detectable in cells sustaining HCV replication, forming foci proximal to intracellular lipid droplets (292). It is hypothesized that HCV dsRNAs are exposed to TLR3 after uptake by autophagic vesicles, of after scavenger receptor-mediated endocytosis of dead cell debris (293).

HCV also interacts with the atypical PRR, the dsRNA-activated protein kinase R (PKR). The beta-hairpin RNA structure at the 5' IRES acts as the HCV PAMP for PKR. Recognition of HCV dsRNA by PKR activates its kinase function, resulting in inhibitory phosphorylation of EIF2α and subsequent repression of host mRNA translation. Whilst cap-independent HCV translation is not impaired, reduced translation of viral cofactors and metabolic slowing of the cell elicited by translational repression hampers viral replication rates (294–296).

1.3.6.2 HCV evasion of pattern recognition

The NS3/4A protease cleaves the RIG-I adaptor protein MAVS away from intracellular membranes by proteolysis at C508, preventing its oligomerization and downstream signalling (297–299); a strategy that is also deployed in immune evasion by the related pegivirus GBV-B and the hepatotropic picornavirus Hepatitis A Virus (HAV) (300,301).

Notoriously difficult-to-treat GT1 and GT4 HCV infections are associated with especially high hepatic ISG expression prior to therapy, compared to GT2/3 infections (302). A proposed mechanistic basis for this difference is differential rates of NS3/4A-mediated MAVS cleavage between strains. According to a study of liver biopsies obtained from 129 cHCV patients, MAVS-cleavage is associated with higher serum viral load, and significantly more MAVS cleavage is observed in GT2/3 infections. Moreover, the incidence of MAVS cleavage in cHCV biopsies is negatively correlated with ISG mRNA levels and nuclear localization of pSTAT1 in hepatocytes, both indices of induction of an endogenous IFN response. In this sample, independent of viral genotype, greater MAVS cleavage was observed in biopsies from patients mounting an early virological response (EVR) to therapy, versus NR (303).

It has been suggested that NS3/4A may also proteolytically inactivate the TLR3 adaptor TRIF: whilst the intracellular abundance of TRIF is reduced by HCV infection, intracellular detection of cleaved TRIF fragments have been challenging (304). Interactions of the HCV

core protein with the DEAD-box helicase DDX3 have been reported (305). DDX3 is proposed to enhance IFNβ-promoter activity downstream of TBK1/IKKε; disruption of this interaction has been reported in the context of vaccinia virus (VACV) infection (306).

The HCV E2 envelope glycoprotein is proposed to compete with EIF2a for PKR binding, by virtue of a shared pattern of phosphoresidues, although this observation is poorly reproducible (307). NS5A also antagonizes PKR, by direct binding to its dimerization domain and preventing the oligomerization required for signal transduction and IRF1 phosphorylation (308). Site-directed mutagenesis of NS5A's PKR binding site removed its ability to block IRF1 phosphorylation downstream of dsRNA binding (309).

In macrophages, the NS5A "interferon sensitivity determining region" (ISDR) can bind to the death domain of the TLR adaptor MYD88 and deregulate recruitment of IRAK1; genetic ablation of the NS5A ISDR restores MYD88-linked signalling in macrophages transfected with a HCV expression construct (310).

Early induction of the di-ubiquitin-like molecule *ISG15* by HCV via a MAVS/IRF3-dependent mechanism also regulates RIG-I signalling capacity, with ISGylation of RIG-I targeting it for destruction (294).

1.3.6.3 Type I/III IFN and ISG expression during HCV infection

In 2009 a genome-wide association study (GWAS) by Ge and colleagues demonstrated a striking association of a polymorphism proximal to the *IL28B* gene, encoding IFNλ3, with establishment of SVR following combined peg-IFN/RBV. In 1,671 patients registered with the IDEAL study, a phase III trial of pegylated-IFNα or IFNβ with RBV in treatment-naïve genotype I patients, variant rs12979860 at chr19q13.13, located 3kb upstream of the *IL28B* first exon, showed a positive association with SVR, achieving genome-wide significance at $p=1.37x10^{-28}$ averaged across all population groups. Carriage of the favourable CC genotype is associated with a two-fold greater incidence of SVR across all ancestral populations including in the study. Moreover, CC population frequency is concordant with SVR rates across diverse ethnic groups, being most prevalent in East Asians and of low frequency in populations with African ancestry. The authors estimate that up to 50% of the variation in response to therapy seen between European-American and African-American participants in the IDEAL study can be attributed to the differential frequency of the CC allele between these groups (311).

Intriguingly, CC genotype is significantly associated with higher baseline viral load despite better responses to peg-IFN/RBV therapy. The authors postulate that this may be attributable to the modulation of peg-IFN activity by intrahepatic ISG expression levels prior to therapy.

Ge and colleagues also identified a significant reduction in CC frequency in a cohort of cHCV patients relative to ethnicity-matched controls, proposing that the favourable allele may contribute to spontaneous viral clearance. This was confirmed by a second study, in which 1008 individuals comprising both persistently infected patients and spontaneous clearers from six HCV infection cohorts were genotyped at rs12979680. Spontaneous HCV clearance was associated with a significantly higher incidence of the CC genotype across all ethnic groups (312). Genotyping of over 2,000 individuals from 51 distinct global populations revealed CC to represent the minor allele in African populations; the major allele in Asian groups; and of intermediate frequency in Europeans. The profound discrepancy in natural HCV clearance between African and non-African populations- 9.3% and 36.4% respectively- might be attributable at least in part to this divergence in CC genotype prevalence.

Upon stimulation of primary human hepatocytes, transient induction of a novel *IL28B* frameshift variant, denoted IFNλ4, has been identified. Akin to the other type III IFNs, IFNλ4 is able to induce STAT1/2 phosphorylation *in vitro*. *IFNL4* is encoded within a region containing a dinucleotide substitution that is in high linkage disequilibrium with the rs12979680; in African populations, the presence of this polymorphism is a more accurate predictor of SVR following conventional anti-HCV therapy than rs12979680 (313).

Despite the strong genetic association of the rs12979680 *IL28B* SNP with HCV progression, the strongest predictor of therapeutic response to IFNα/RBV is the pre-existing level of IFN signalling and ISG expression in infected hepatocytes. In a study of hundreds of paired pre- and post-treatment liver biopsies from HCV patients, Sarasin-Filipowicz and colleagues demonstrated that achievement of SVR is associated with low-level ISG expression at baseline, but a strong induction after peg IFNα. Non-response (NR), however, is associated with high ISG expression before therapy and a failure of peg IFNα to induce ISG expression above pre-treatment levels. In non-responsive patients, the IFN axis is pre-activated and refractory to further stimulation; in support of this, IFNα-treatment elicits lower pSTAT1 induction in NR versus SVR patient biopsies (302). Moreover, mRNA expression analysis of liver and peripheral blood samples from patients treated with an IFN-free regimen (namely

ribavirin and sofosbuvir), revealed that attainment of SVR after DAA therapy is contingent upon robust induction of *IFNA2* and effector ISGs upon end of treatment (314).

A study of liver biopsies from 109 cHCV patients, analysed for ISG expression and genotyped at the *IL28B* locus, confirmed that hepatic ISG expression is increased in NR, irrespective of *IL28B* genotype; both variables act as independent predictors of the response to peg-IFNα therapy (315). The unfavourable TT allele is associated with reduced *IL28B* mRNA expression in both liver tissue and peripheral blood mononuclear cells (PBMC) from whole blood; pathway analysis of DNA microarray data from these cell types suggests the unfavourable allele is associated with depressed innate immune and NK cell functionality (316).

Whilst the ISG profiles induced by IFNλ and type I IFN are broadly similar, marked differences in their ISG induction and antiviral kinetics have been observed *in vitro*; in a HCV replicon model, exogenous IFNα is associated with rapid attainment of maximal expression, whereas IFNλ elicited slower and sustained ISG induction. Interestingly, the trend was reversed for the kinetics of STAT1/2 phosphorylation (317).

The IFN species that drive long-term elevations of intrahepatic ISG expression in cHCV have yet to be definitely characterized. Whilst mRNA encoding IFNα and IFNβ is not detectable in HCV-positive biopsies, the profile of ISGs induced during chronic infection is commensurate with a type I/III response, as opposed to IFNγ (140,318). Within the infected liver, IFNα is relatively suppressed by high expression of USP18, a negative regulator with lower potency against IFNβ and no activity against the IFNλ receptor complex (319,320). Transcripts encoding all three IFNλ species are detectable in HCV-positive liver tissue (315), lending credence to the hypothesis that IFNλ, as opposed to type I IFN, mediates the endogenous IFN response during chronic infection (321).

In contrast to hepatocytes, higher pre-treatment ISG expression in Kupffer cells, the resident liver macrophage population, is strong predictor of successful response to therapy. IFNβ production by Kupffer cells is driven by internalization of HCV-RNA fragments released from local infected hepatocytes (322,323). It has been hypothesized that myeloid cell-derived IFNβ is the principal stimulus for ISG induction in infected hepatocyte. Given the cytotoxic profiles of many ISGs after prolonged expression, it is favourable for the cells to develop tolerance to their effects, thereby rendering them refractory to exogenous IFN therapy (324).

A single species of ISG is unlikely to predominate the IFN effector response to HCV; instead, a co-ordinated response of diverse effectors is proposed to spearhead viral clearance. Via an RNAi screen of candidate IFNα and IFNγ-induced ISGs in a Huh7-Lunet reporter cell line, Metz and colleagues were able to identify a number of novel anti-HCV effectors, including *NOS2*, *PLSCR1, TRIM14* and *IFIT3*. Moreover, through a series of combinatorial RNA knockdown experiments, the authors were able to demonstrate that co-expression can synergistically enhance the anti-HCV effect of ISGs, suggesting that an network of effectors is required for successful viral clearance (325).

1.3.6.4 Inhibition of type I /III IFN by HCV (figure 1.11)

There is extensive evidence for a blunting of STAT1/STAT2 mediated signal transduction by HCV, likely via direct induction of protein phosphatase 2A (PP2A) (326). Expression of the HCV core and non-structural proteins inhibits both tyrosine phosphorylation of STAT1 and STAT2 *in vitro* and their DNA binding activity, measured by EMSA using ISRE sequences as an oligonucleotide probe (327). *In vivo*, the same phenomenon is apparent, with liver-specific expression of HCV proteins in transgenic mice resulting in defective STAT-mediated signal transduction and increased susceptibility to a hepatotropic strain of lymphocytic choriomeningitis virus (LCMV) (328) .

HCV core is also able to bind directly to the C-terminus SH2 domain of STAT1(329), preventing assembly of both STAT1-STAT2 heterodimers and the ISGF3 complex and subsequent ISG induction (330).

The HCV core protein also induces expression of *SOCS3*, a negative regulator of the JAK-STAT axis. The SOCS3 N-terminus resembles a JAK substrate, allowing competitive inhibition of the enzyme, with attendant attenuation of IFN signal transduction (331). SOCS3 also binds tightly to the IFNAR receptor, forming a tight SOCS3-JAK-IFNAR ternary complex. This complex is targeted for degradation by ubiquitin ligases recruited via the SOCS3 SH2 adaptor domain (332).

Evidence exists that the antiviral activity of 2'-5'-oligoadenylate synthetase (2'-5'-OAS) is directly blocked by NS5A (333). 2'-5'-OAS proteins are a small family of IFN-induced, template-independent nucleotidyltransferases. With A-form viral dsRNA acting as a co-factor, 2'-5'-OAS synthesizes 2'-5-linked diadenylates, which subsequently recruit RNaseL dimers to digest cytosolic viral RNAs (329).

NS5A is also proposed to transactivate the *IL8* promoter and drive expression of IL8, a CXC chemokine associated with suppression of IFNα signalling (334).

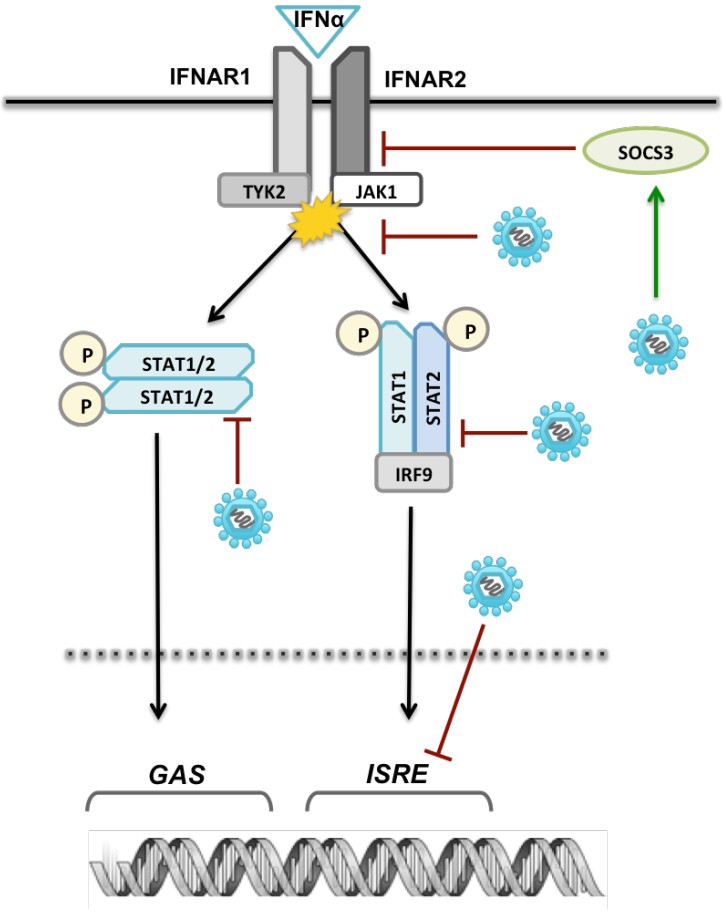


Figure 1.11: Disruption of type I IFN signalling by HCV

Induction of PP2A by HCV inhibits STAT1/2 phosphorylation, whereas HCV core protein binds directly to the C-terminus of STAT1, thereby preventing assembly of transcriptionally active dimers and the ISGF3 complex. HCV core also induces expression of the multifunctional IFNAR inhibitor SOCS3, whereas NS5A induces the CXC chemokine IL8, capable of suppressing IFNα upregulation by infectious stimuli.

1.4 The BMP-SMAD link

1.4.1 Introducing hepcidin, and its dysregulation by HCV

The Drakesmith lab's interest in the role of BMP signaling during HCV infection was sparked by the observation that serum and hepatic levels of the key iron regulatory hormone hepcidin are suppressed during HCV infection (335,336). Hepcidin, encoded by *HAMP* and highly expressed by the liver, reduces dietary iron uptake and promotes sequestration of iron within macrophages by inhibition of the only characterized mammalian iron exporter, ferroportin (337). Accumulation of iron acts as a stimulus to *HAMP* transcription via induction of BMP6-

SMAD signaling as part of a negative feedback loop to prevent deleterious iron overload (56,338,339). However, hepcidin levels are also induced by IL6, IL22 and type I IFN, via the presence of a STAT3-responsive element in the *HAMP* promoter (340,341). Therefore in general, infections and inflammatory conditions lead to increased levels of hepcidin – this may be protective by withholding iron from pathogens that require it in order to grow (342). Increased hepcidin has also been observed in the acute phase of HIV-1 infection that is associated with systemic inflammation (343). The suppression of hepcidin during HCV infection is therefore an enigmatic finding, hinting at a potential dysregulation of BMP signaling by HCV. The Drakesmith lab has investigated the interactions between HCV, hepcidin, BMP signaling and response to interferon. These as-yet unpublished data are described below.

In pre-treatment liver biopsies the ratio of *HAMP* message to BMP6 transcript is lower in non-responders to the first-line anti-HCV therapy of pegylated IFN and ribavirin, compared to uninfected individuals and patients who mount an SVR, suggesting that HCV impairs hepatic BMP6 signaling. Furthermore, HCV blunts the transcriptional response of hepatoma-derived cells to recombinant BMP6 *in vitro* (Eddowes et al. unpublished). This disruption of BMP6 signalling by HCV is reminiscent of its derangement of type I IFN response. It implies that viral impairment of BMP signalling could be an evolutionarily favourable behaviour, if the pathway were to mediate an antiviral effect.

1.4.2 Previous antiviral observations from the Drakesmith lab

Exogenous application of recombinant human BMP6 and 9 to cultured hepatoma-derived cells elicits dose-dependent reductions of HCV RNA *in vitro*, against both a full-length genomic replicon and the replication competent JFH1 virus. (Eddowes et al. unpublished; see appendix I). Lending further credence to this hypothesis, synergistic antiviral effects of BMP7 and IFN-α against HCV *in vitro* have also been reported (344). This research is described in further detail in subsequent chapters.

1.5 Thesis Summary

BMP and activin proteins are implicated in a diverse range of anti-microbial responses and effector pathways. Whilst a functional role of activins in the response to viral infection has yet to be published, their induction in response to acute and chronic inflammatory stimuli, both sterile and infectious, is well described.

Akin to the efficient disablement of type I IFN signalling by virus-encoded proteins, multiple viruses have evolved mechanisms for derangement of BMP/activin/SMAD signalling, targeting each step of the cascade. Blunting of the BMP/SMAD axis by HCV may be a key pathologic process during infection, and our lab has observed an antiviral function of BMP6 and BMP9 during HCV infection *in vitro.*

This thesis seeks to characterize comprehensively the antiviral activity of BMP/activin/SMAD signalling. It focuses upon defining which ligands within the TGFβ family mediate such effects; delineation of the mechanistic basis for their antiviral properties, particular with reference to the type I IFN response; and investigating whether these proteins impair replication of structurally and evolutionarily distinct viruses, including Hepatitis B Virus (HBV), dengue virus (DENV) and influenza A (FLUAV).

1.6 Thesis Overview

Chapter 3 describes the extension of an anti-HCV effect to multiple BMPs and also to activin cytokines. Subsequently, the mechanism for the IFN-independent antiviral effect of BMP6 was investigated, with an especial focus on regulation of cell cycle progression.

Chapter 4 reviews viral sensing and mechanisms of type I IFN induction in greater detail, before examining the induction of activin mRNA by both cytosolic delivery of nucleic acids and true viral infection, both *in vitro* and *in vivo*.

Chapter 5 describes the antiviral effector mechanisms of type I IFN in more detail, before describing our investigations into the interaction between IFN and BMP/activin signalling during antiviral defence. Extending on these *in vitro* observations, chapter 6 presents a bioinformatic comparison of the interactions of SMAD and IRF-linked signalling genome-wide, with a particular focus on the regulation of antiviral loci. The computational analyses were performed using on published datasets and data available from the ENCODE project.

Chapter 7 presents data pertaining to the antiviral effect of BMPs and activins against other viruses, including *in vitro* HBV and DENV infection, obtained in conjunction with the Klenerman and Zitzmann laboratories at the University of Oxford respectively. Our efforts to study a role for BMP signalling in the pathogenesis of murine influenza A infection, in collaboration with the Rehwinkel lab at the University of Oxford, are also detailed.

Chapter 2

General materials and methods

All reagents procured from Sigma-Aldrich (USA), unless specified.

2.1 Cell Culture

All cells were cultured at 37 °C, 5% CO_2 and 20% O_2, unless specified otherwise.

2.1.1 Hepatoma-derived cell lines

Huh7 (ATCC, USA) and Huh7.5.1 (kindly from Prof Raymond Chung [MGH, MA, USA]) cells were maintained in Dulbecco's Modified Eagle's Medium (DMEM), supplemented with 10% foetal calf serum (FCS) (PAA, Pasching, AT or Lonza, Basel, CH), 2 mM glutamine, 100 U/mL penicillin, 0.1 mg/mL streptomycin.

2.1.2 Hepatoma-derived HCV replicon cell lines

OR6 and Cured-OR6 cells (kindly from Prof Raymond Chung [MGH, MA, USA] with permission of Prof Kato and Dr Ikeda [Okayama University, JP]) were cultured in DMEM, supplemented with 10% FCS (PAA, Pasching, AT or Lonza, Basel, CH), 100U/mL penicillin, and 0.1mg/mL streptomycin and 2mM L-glutamine. OR6 cells are stably transfected with a full-length HCV genomic replicon in tandem with a Renilla luciferase reporter and neomycin resistance cassette. Cured-OR6 cells have been serially passaged with high dose recombinant IFNα-2a, eliminating the replicon construct. G418 100 μg/mL was used as a negative selection agent in the OR6 cell cultures.

2.1.3 Monocytic cell lines

THP-1 (ATCC, USA) and U937 (ATCC, USA) were maintained in Roswell Park Memorial Institute-1640 (RPMI-1640) supplemented with 10% FCS (PAA, Pasching, AT or Lonza, Basel, CH) 2 mM glutamine, 100 U/mL penicillin, 0.1 mg/mL streptomycin.

2.1.4 Lung adenocarcinoma-derived cell lines

A549 cells (ATCC, USA) or A549.gfp (a kind gift from Prof Richard Randall, University of St Andrews, Scotland, UK) were maintained in in DMEM, supplemented with 10% FCS (PAA, Pasching, AT or Lonza, Basel, CH), 100U/mL penicillin, and 0.1mg/mL streptomycin and 2mM L-glutamine.

2.1.5 Fibroblast-derived cell lines

HEK293 (ATCC, USA) and 293T cells (ATCC, USA) were maintained in DMEM, supplemented with 10% FCS (PAA, Pasching, AT or Lonza, Basel, CH), 100U/mL penicillin, and 0.1mg/mL streptomycin and 2mM L-glutamine.

2.1.6 PBMC Isolation

Whole blood was procured from healthy volunteer donors in accordance with the MRC WIMM ethical policy and local practices, as described previously(340,345). Blood samples were heparin-treated before immediate layering onto a Ficoll-Pacque Plus^{TM} (GE Healthcare Life Sciences, USA) density centrifugation gradient in a 1:1 volume ratio. Samples were centrifuged in accordance with the manufacturer's protocol and the buffy coat layer aspirated with a pipette. Buffy coat cells were washed three times in 2.5 mM EDTA-PBS at 4°C before dilution and maintenance in RPMI-1640 supplemented with 10% FCS (PAA, Pasching, AT or Lonza, Basel, CH) 2 mM glutamine, 100 U/mL penicillin, 0.1 mg/mL streptomycin.

2.2 Quantitative real-time polymerase chain reaction (RT-qPCR)

RT-qPCR provides a rapid, sensitive and cost-effective method for the quantification of specific RNA molecules, including differentially regulated mRNA transcripts and RNA virus genomes. RT-qPCR technology combines the sensitivity of the polymerase chain reaction (PCR) to detect small quantities of specific nucleic acids with real-time detection of target amplification using fluorescently labelled probes(346).

Two RT-qPCR methodologies were used in this project: TaqMan^{TM} and SYBR Green I technology. Both of these strategies utilize the 5'-exonuclease activity of the *Thermophilus aquaticus* (Taq) polymerase to generate a fluorescent reporter signal proportional to the amount of target cDNA present in a sample.

2.2.1 TaqMan^{TM} probe technology

TaqMan^{TM} probes consist of a 5' reporter fluorophore (6-carboxyfluoroscein, *FAM*) and a 3' quencher moiety (BHQ) linked by an oligonucleotide chain. Both reporter fluorophore and the quencher lie within 100 Å of each other. The probe chain encodes a sequence complimentary to a short region of the cDNA within the PCR primer target sequence. In its intact state, excitement of the fluorophore by an external light source results in light emission.

The quencher molecule absorbs this light by Förster resonance energy transfer (FRET), suppressing the signal generated by the fluorophore. During the PCR reaction, both the probe and the primers bind to the cDNA, recruiting the Taq polymerase upstream of the probe. As DNA polymerization occurs, the Taq 5'-exonuclease activity cleaves the probe oligonucleotide chain, releasing the quencher moiety, which can longer suppress the signal emitted by the reporter fluorophore [summarized in figure 2.1].

Both the TaqMan™ probe and the primers are located within an approximately 100bp sequence, yielding a PCR amplicon of ~100bp. The only PCR products amplified are those resulting from simultaneous probe and primer binding. The primer melting temperature (T_m) gives an indication of DNA-DNA duplex stability: higher T_m is associated with increased risk of secondary annealing. Whilst the optimum T_m for primers used in this assay is 58-60 °C TaqMan™, the probe T_m should be ~10 °C higher, such that it hybridizes to the target DNA first.

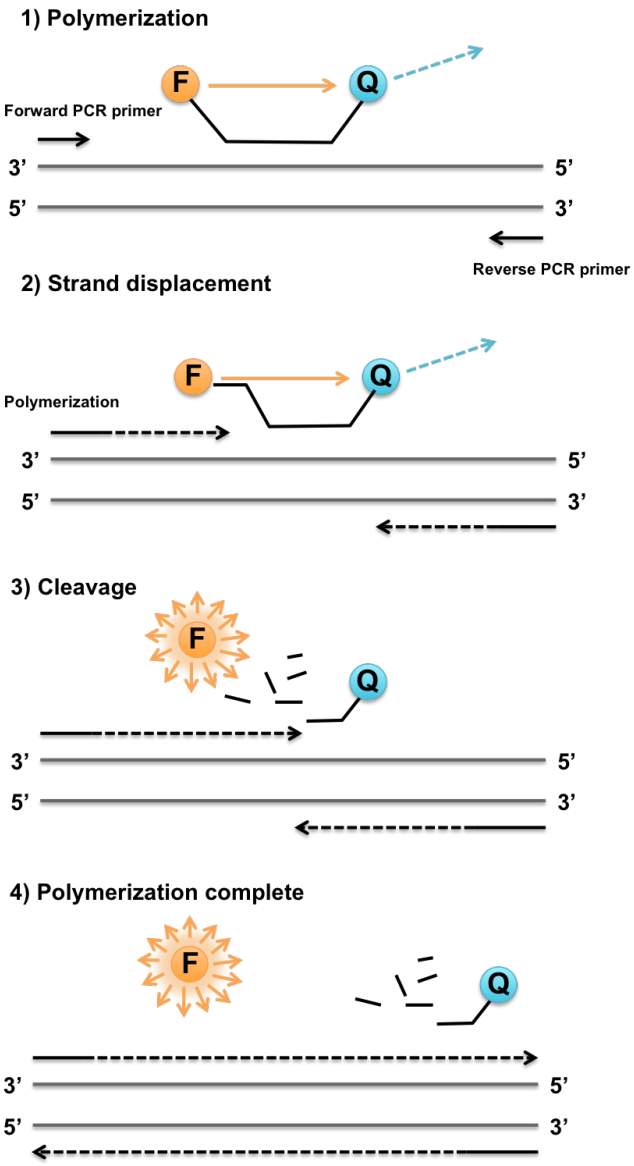


Figure 2.1 Schematic diagram of the TaqMan™ primer-probe system

Upon initial binding of the probe and primer sequences to their complimentary sequences in target nucleotide the TaqMan™ probe is intact and signal from the reporter fluorophore (F) is suppressed by the adjacent quencher (Q).

During polymerization, the 5'-exonuclease activity of the *Taq* polymerase digests the probe's oligonucleotide chain (black), liberating the quencher molecule and removing its suppression of the report fluorophore. The probe is only cleaved if it is hybridized to the target sequence, therefore increasing fluorescence corresponds to an increasing availability of target cDNA as the PCR reaction proceeds.

Adapted from the TaqMan™ Gene Expression Assays Protocol (2010) from Applied Biosystems/Life Technologies.

2.2.2 SYBR® Green I technology

SYBR® Green I n I is DNA-binding dye which intercalates into the minor groove of dsDNA molecules, emitting green light of λ 520 nm after absorption of blue light at λ 497 nm. Akin to the TaqManTM protocol, samples cDNAs are incubated with both the dye and a pair of DNA primers that produce a PCR product of ~100bp. DNA-bound SYBR® Green I emits a stronger fluorescent signal than the unbound dye, therefore as the PCR amplification progresses, the intensity of emitted light increases accordingly [summarized in figure 2.2].

SYBR® Green I can bind to all dsDNA species, irrespective of their sequence, therefore a specificity assessment, most commonly a melt curve/dissociation analysis, should be performed for each primer pair used. During the melt curve analysis, after completion of the final PCR cycle the products of the PCR reaction are gradually melted. When the T_m for a particular DNA duplex is reached, the complex dissociates to form ssDNA, liberating the SYBR® Green dye and reducing its fluorescent intensity. A given target sequence has a specific T_m. Detection of variable T_ms during the melt curve analysis implies the presence of both target and off-target PCR products, suggesting that the PCR amplification reaction is of low-specificity.

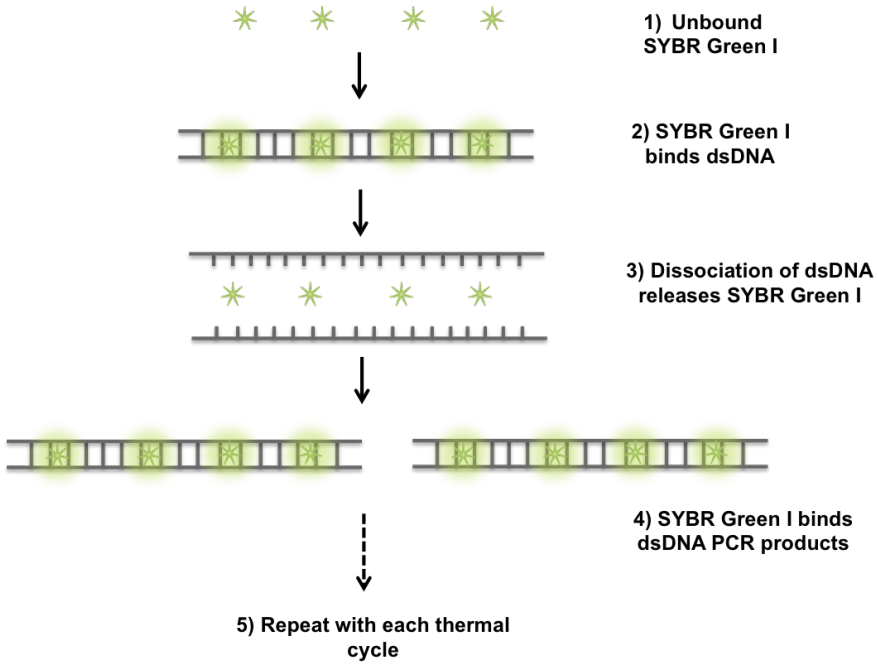


Figure 2.2 Schematic diagram of the SYBR® Green I dye assay

Unbound SYBR Green I dye emits a negligible level of fluorescence. Upon binding to the minor groove of dsDNA, its fluorescent signal greatly increases. Dissociation of the DNA strands liberates the dye molecules, which return to low level fluorescence. After polymerization and DNA duplex formation, SYBR Green I molecules bind to newly formed PCR products and emit a high intensity fluorescent signal, before the process repeats afresh at the start of a new thermal cycle.

2.2.3 Passive reference signal

To correct for variations in signal intensity that are not PCR-based, the signal from a passive reference dye, is used to normalize the signals detected from each reaction. In both TaqMan™ and SYBR® Green I assays, ROX™ fluorescence intensity is measured as a passive reference signal.

2.2.4 RNA isolation

Unless otherwise specified, cell lysates were homogenized with a QIAshredder column (Qiagen, Crawley, UK) and RNA extracted with the RNEasy Mini Kit (Qiagen, Crawley, UK). This extraction method centres around the lysis of cell membrane, linearization of intracellular RNA and inactivation of RNAses by highly concentrated guanidium salts, followed by filtration via a silica membrane, with ultimate elution of purified RNA with water.

2.2.5 RNA quantification and storage

RNA concentration was determined with a NanoDrop 2000 Spectrophotometer (Thermo Fisher Scientific, MA, USA) at 260 nm. RNA samples were stored at -20 °C for short durations (1-3 months) and -80 °C for the longer term.

2.2.6 cDNA synthesis

cDNA was reverse-transcribed from template RNA using the High Capacity RNA-to-cDNA kit (Applied Biosystems, MA, USA) in accordance with the manufacturer's instructions. The following thermocycler program was used: 37 °C for 60 min, followed by 95 °C for 5 min.

2.2.7 RT-qPCR reaction

All RT-qPCR reactions were performed using an Applied Biosystems 7500 Fast Real-Time PCR System (Applied Biosystems, MA, USA), in accordance with the thermal cycling program described in table 2.1.

For TaqMan™ quantification, gene expression was assessed with inventoried TaqMan™ Gene Expression Assays (Applied Biosystems, MA, USA) diluted as per the manufacturer's instructions in TaqMan™ Gene Expression Master Mix (Applied Biosystems, MA, USA).

For SYBR® Green I quantification, gene expression was assessed with specific oligonucleotide primer pairs (Sigma-Aldrich, USA) diluted in Fast SYBR® Green I Master Mix (Applied Biosystems, MA, USA), as per the manufacturer's protocol. Sequences are provided in chapter 7.

Step	Temperature	Time
1	50 °C	20 seconds
2	95 °C	10 minutes
3	95 °C	15 seconds
4	60 °C	1 minute
5	Repeat step 3-4, 40 times	

Table 2.1: Standard thermal cycling program used on the AB 7500 Fast Real-Time PCR System

cDNA samples ere diluted in Ambion non-DEPC treated nuclease-free water (Life Technologies, MA, USA) to a final concentration of 1-3 ng/μL.

Samples were run at a total reaction volume of 20 μL in a duplicate wells of a MicroAmp® Fast Optical 96-well reaction plate covered with MicroAmp® Optical Adhesive Film (both Applied Biosystems, MA, USA). After manual loading, plates were sealed with the adhesive film and briefly centrifuged to eliminate bubbles. No template controls were run in parallel with the experimental samples, consisting of a no RNA control, in which nuclease-free water is substituted for RNA during reverse transcription, and a no RT control in which water was substituted for the reverse transcriptase enzyme.

Gene name (*symbol*)	TaqMan™ inventoried assay ID
Gylceraldehyde-3-phosphate dehydrogenase (*GAPDH*)	Hs99999905_m1
Bone morphogenetic protein 6 (*BMP6*)	Hs01099594_m1
Hepcidin antimicrobial peptide (*HAMP*)	Hs00221783_m1
Inhibitor of DNA binding 1, dominant negative helix-loop-helix protein (*ID1*)	Hs00357821_g1
Inhibin beta A (*INHBA*)	Hs01081598_m1
Inhibin beta B (*INHBB*)	Hs00173582_m1
Tumour necrosis factor alpha (TNF superfamily, member 2) (*TNFA*)	Hs00174128_m1
SMAD family member 6 (*SMAD6*)	Hs00178579_m1
SMAD family member 7 (*SMAD7*)	Hs00998193_m1

Haemochromatosis type 2 (juvenile) (*HFE2*)	Hs00377108_m1
Myxovirus resistance 1, mouse, homolog of (*MX1*)	Hs00895598_m1
Interferon-alpha-inducible-protein 6 (*IFI6*)	Hs00242571_m1
Follistatin (*FST*)	Hs00246256_m1
Interferon alpha, beta and omega, receptor 2 (*IFNAR2*)	Hs01022061_m1
Signal transducer and activator of transcription 2 (*STAT2*)	Hs01013123_m1
Janus kinase 1 (*JAK1*)	Hs01026983_m1
Ubiquitin-like modifier ISG15 (*ISG15*)	Hs01921425_s1
Interferon-induced transmembrane protein 1 (*IFITM1*)	Hs00705137_s1
Interferon-induced protein with tetratricopeptide repeats 3 (*IFIT3*)	Hs01922752_s1
Phospholipid scramblase 1 (*PLSCR1*)	Hs01062171_m1
Ubiquitin-specific protease 18 (*USP18*)	Hs00276441_m1
Interferon regulatory factor 7 (*IRF7*)	Hs01014809_g1
Single-stranded DNA-binding protein (SSBP3)	Hs00401909_m1
Radical S-adenosyl methionine domain-containing protein 2 (RSAD2)	Hs00369813_m1
Zinc Finger CCCH Domain-containing antiviral protein 1*(ZC3HAV1)	Hs00252300_m1

Table 2.2 Human TaqMan™ Gene Expression Assays used in this thesis
The suffix _m1 denotes assays with primers that span exon-exon junctions and therefore do not detect genomic DNA. The suffix _g1 denotes assays designed with primers the lie within a single exon that may amplify genomic DNA. The suffix _s1 denotes assays against genes composed of a single exon that will by definition detect genomic DNA.

Gene name (*symbol*)	TaqMan™ inventoried assay ID
Hypoxanthine-guanosine phosphoribosyltransferase (*Hprt*)	Mm01545399_m1
Tripartite motif-containing protein 14 (*Trim14*)	Mm01352552_m1
Ubiquitin-specific protease 18 (*Usp18*)	Mm01188805_m1
Interferon-induced protein 44 (*Ifi44*)	Mm00505670_m1
Interferon, alpha-4 (*Ifna4*)	Mm00833969_s1
Interferon, beta-1 (*Ifnb1*)	Mm00439546_s1
Inhibin beta A (*Inhba*)	Mm00434339_m1
Inhibin beta B (*Inhbb*)	Mm03023992_m1
Bone morphogenetic protein 6 (*Bmp6*)	Mm01332882_m1
Ubiquitin-like modifier ISG15 (*Isg15*)	Mm01705338_s1
Hepcidin antimicrobial peptide 1 (*Hamp1*)	Mm04231240_s1
SMAD family member 6 (*Smad6*)	Mm00484738_m1
SMAD family member 7 (*Smad7*)	Mm00484742_m1
SEV, Sendai virus genome	Mr04269880_mr

Table 2.3 Non-human TaqMan™ Gene Expression Assays used in this thesis
The prefix "Mm" denotes assays against *Mus musculus*; the prefix and suffix "Mr" is an abbreviation of "Markers and Reporters".

2.2.8 Quantification of gene expression

Gene expression is quantified relative to an endogenous control gene with a constant expression level. In this study, unless otherwise specified, human RNA expression is quantified relative to *GAPDH*, encoding glyceraldehyde -3-phosphate dehydrogenase, and murine RNA expression relative to *Hprt*, encoding hypoxanthine-guanosine phosphoribosyltransferase. Analysis was conducted with either the ΔCt or ΔΔCt methods, denoted in the figure legends as "2^dCt" and "fold change normalized to *GAPDH*/*Hprt*" respectively.

Ct, or "cycle threshold" describes the number of PCR cycles after which the fluorescent signal from a probe reaches a defined threshold. As fluorescence intensity is proportional to the amount of PCR product amplified during a reaction, lower Ct values correspond to a greater quantity of target starting material. A constant threshold was defined across all experiments, unless otherwise specified. For TaqMan™ probes it is assumed that the efficiency of the probe is 1 (i.e. template numbers double after each thermal cycle, resulting in exponential amplification of the target DNA); for the primer pairs used in SYBR® Green I assays this is empirically confirmed in the lab.

To calculate relative gene expression, target gene Ct was subtracted from the endogenous control Ct to give the ΔCt values. To account for exponential amplification during the PCR procedure, ΔCt was transformed by $2^{-\Delta Ct}$, yielding the expression of the target mRNA relative to the endogenous control gene in that sample. To determine the fold change in target gene expression in an experimental sample compared to the untreated/control, the target gene $2^{-\Delta Ct}$ in the experimental condition was divided by respective $2^{-\Delta Ct}$ in the untreated/control sample.

2.3 HCV replicon model and luciferase assays

2.3.1 The OR6 replicon model

The OR6 replicon system consists of the Huh7 hepatoma-derived cell line stably-transfected with a full-length HCV genome sequence, genotype 1b, strain O(347). The construct encodes an EMCV-derived IRES and preserves the 5'UTR and core sequence motifs required for translation of the HCV open-reading frame. Renilla luciferase, derived from the sea pansy *Renilla reniformis*, is expressed in conjunction with a neomycin phosphotransferase [figure 2.3]. Cells are maintained under negative selection with G418.

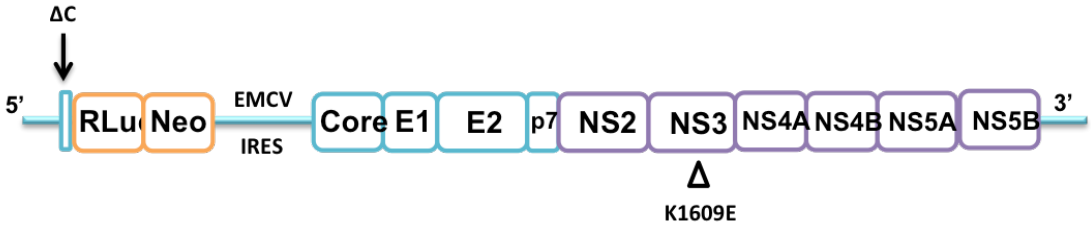


Figure 2.3 Map of the OR6 HCV replicon construct, after Ikeda et al. (2005)

Neomycin phosphotransferase (Neo), conferring resistance to the selection agent G418, is expressed as a fusion protein with the *Renilla* luciferase (RLuc). An adaptive K1609E mutation in the NS3 helicase coding region confers higher rates of replication relative to the wild-type sequence. ΔC denotes the 5'end of the HCV core protein-coding region after which the RLuc-Neo sequence is inserted.

Renilla luciferase catalyses oxidation of a coelenterazine substrate to release light that can be detected with a photomultiplier tube. Luminescence intensity upon exposure to substrate acts as a surrogate for intracellular HCV RNA content.

A sub-line of "Cured-OR6" cells that do not harbour the replicon construct were produced by the authors by serial passage of OR6 cells with 500U/mL recombinant human IFNα, alternated with 300 μg/mL G418) for two weeks. Elimination of the replicon from the Cured-OR6 cells was confirmed by PCR.

OR6 and Cured-OR6 cells were grown to at least 75% confluence before detachment with trypsin-EDTA (Sigma-Aldrich, USA and Lonza, Basel, CH) and pelleting by centrifugation at 1400 rpm for 5 minutes. Cells were counted manually using a Trypan Blue stain. Cells were diluted in DMEM with 10% FCS, 2 mM glutamine, 100 U/mL penicillin and 0.1 mg/mL streptomycin to $3.5x10^4$ per mL and plated at 100uL per well of a 96-well flat-bottomed plate (i.e. $3.5x10^3$ cells per well), unless otherwise specified. A minimum of 18 hours was allowed to ensure adherence before the addition of experimental reagents.

2.3.2 Measurement of Renilla luciferase activity

End-point measurement of luciferase activity was performed with the Renilla-Glo Luciferase Assay System (Promega, WI, USA) as per the manufacturer's instructions.

OR6 and cured-OR6 cells were assayed for *Renilla* luciferase activity via the Renilla-Glo Luciferase Assay System (Promega, Madison, WI, USA). 10uL of cellular lysate were transferred to opaque 96-well plates (PerkinElmer, MA, USA). Luminescence was measured with a Fusion II Luminometer (PerkinElmer, MAS, USA) or a GloMax 96 Microplate Luminometer (Promega, WI, USA).
Relative luciferase activity is calculated by normalizing the absolute luminescence value detected for each condition to the value yielded from untreated OR6 cells. Prior to this, the background luminescence detected from untreated Cured-OR6 cells assayed in parallel is subtracted.

2.3.2 Cell Titer Glo viability assay

Cells were assayed for intracellular ATP content, which may act as index of cell number, with the Cell Titer Glo Assay System (Promega, WI, USA). Lysates were extracted as per the kit's protocol and transferred to an opaque plate before measurement of luminescence intensity as described previously.

2.4 Data analysis and software

Data transformation and analysis was performed with Microsoft Excel (Microsoft Inc., CA, USA). Statistical analysis and data presentation were performed with GraphPad Prism (GraphPad Software Inc., CA, USA). Flow cytometry data was analysed with FlowJo v9 and v10 (TreeStar Inc., OR, USA). The X emulators MobaXterm (Mobatek, Marseille, France)

and X11 (Xquartz, OpenSource) were used to access the command-line; data transfer was performed with the SSH/ftp client Fugu (University of Michigan, MI, USA).

Chapter 3

Extension of an anti-HCV effect to multiple BMP/TGFβ ligands and exploration of its mechanistic basis

3.1 Context and experimental precedents

3.1.1 Suppression of hepcidin by HCV reveals antiviral function of BMP6

Unpublished data from the Drakesmith lab show that the BMP-SMAD signalling axis is suppressed by HCV infection both *in vitro* and *in vivo*, and reveal a novel antiviral function of BMP6 [appendix I]. This chapter investigates the mechanistic basis for a type I IFN-independent component of this antiviral effect, in addition to exploring whether an anti-HCV effect extends to other BMP and TGFβ superfamily cytokines.

The principal research interest of the Drakesmith lab is the modulation of host iron status in response to infection, in particular via the regulatory hormone hepcidin (section 1.4.1). As part of the acute phase response hepcidin is induced by inflammatory and infectious stimuli through the IL-6/STAT3 axis, resulting in a transient hypoferraemia(340). In response to systemic iron balance, however, BMP-SMAD signalling is the principal homeostatic regulator of *HAMP* expression(338,339,348). Analysis of the *HAMP* promoter reveals two BMP-responsive elements, one proximal (-260bp) and a second more distal (-1.6kb) to the transcription start site, both of which are indispensible for maximal hepcidin induction(341). Both *in vitro* and *in vivo*, multiple BMP family members induce HAMP, via ALK2 and ALK3 type I BMP receptors in conjunction with the co-receptor hemojuvelin (HJV)(56). Furthermore, pharmacological inhibition of SMAD1/5/8 signalling ablates *HAMP* induction by both BMP and IL6 stimulation(62).

Clinically, unlike most chronic inflammatory conditions, cHCV infection is associated with suppressed hepcidin expression, both serum peptide and liver *HAMP* mRNA(335,336). Data from the Drakesmith lab, in collaboration with Prof Paul Klenerman's group (University of Oxford), show, using the replication competent JFH1 infection system, that this transcriptional repression of *HAMP* by HCV is recapitulated *in vitro*. HCV infection significantly blunts *HAMP* induction in response to a titration of recombinant BMP6. Concomitant reductions in HJV mRNA and induction of the negative regulators SMAD6 and SMAD7 suggest that HCV infection represses the BMP pathway by modulating the expression of its key signalling components. Similarly, pre-treatment liver biopsies from cHCV patients demonstrate significantly reduced hepcidin mRNA expression, paralleled by raised expression of *SMAD6* and *SMAD7*.

Stratifying these pre-treatment liver biopsies by subsequent response to peg-IFN/RBV therapy reveals that the degree of not only *HAMP* suppression, but also repression of *HJV* and

the BMP-responsive gene *ID1*, is significantly higher in eventual non-responders (NR) compared to either patients mounting a sustained virological response (SVR) or uninfected controls. Extending these observations, the ratio of both *HAMP* and *ID1* mRNA to *BMP6* transcript is similarly lower in NR samples versus SVR or control biopsies, implying greater derangement of BMP signal transduction in non-responsive patients. In terms of a mechanistic basis for this BMP-SMAD antagonism, further unpublished observations from the lab demonstrate that induction of TNFα by HCV elicits transcriptional repression of *HJV* and upregulation of *SMAD6* and *SMAD7*, with increasing suppression at higher multiplicities of infection (MOI). Co-incubation with an anti-TNFα antibody rescues the blunted induction of *HAMP* by BMP6 in the JFH1 infection system.

While these experiments comprise a small patient sample, a possible contribution of BMP signalling to HCV treatment response on the population level has also been identified. As described in chapter 1.3.6.3, a seminal GWAS from Ge and colleagues first identified the prognostic significance of SNPs in the *IL28B* region for patient outcomes following conventional peg-IFN/RBV therapy(311). Re-analysis of this dataset revealed that 14 of the top 100 most significant SNPs pertain to the BMP signalling pathway, including variants in *EVI1*, *FOXG1*, *GRIP1* and *SKIL*, modulators of intracellular BMP signal transduction; *ACVR1*, encoding a type I BMP receptor isoform; and *BMP6* itself. Using the Metacore suite of pathway analysis tools, an interaction network was constructed from the genes annotated to the top 100 SNPs. Gene set enrichment analysis (GSEA) of this hypothetical network revealed a strong association of BMP signalling pathways with response to therapy, with a non-significant probability of false discovery.

In the context of generalized anti-microbial responses, a comprehensive study of signal transduction pathways associated with adaptive events during human evolution hints at positive selection for BMP signalling. Conventional approaches for identifying genes implicated in human evolutionary adaptation frequently focus on single loci associated with extreme phenotypes. However, adaptive events might also require small coordinated changes at multiple loci resulting in much larger combined or epistatic effects. Mindful of this, Daub and colleagues sought evidence for polygenic adaptations within the genome by conducting GSEA on SNPs genotyped from 53 worldwide populations. Given that the response to infection is the major evolutionary selection pressure experienced by *Homo sapiens*, the authors assumed that gene sets under positive selection were likely to be associated with immune functions. The enriched pathways included BMP signalling, speculated by the authors to be implicated in pathogen restriction by virtue of its regulation of hepcidin and

subsequent modulation of iron availability(349). Based upon our data, the antiviral effects of BMP pathway also represent a plausible, evolutionarily favourable, immune function.

Targeted disruption of antiviral signalling is a motif of viral infections; efficient disruption of the type I IFN response by HCV enables it to establish long-term infections (section 1.3.6.4). The disruption of BMP signalling by HCV is reminiscent of its disabling of the IFN response. If BMP signalling is antiviral, its impairment by HCV could represent an evolutionarily favourable viral behaviour.

Indeed, in further unpublished work from the lab, a profound anti-HCV effect of two BMP family members, BMP6 and BMP9, has been identified, both against a full-length HCV replicon and replication-competent infection *in vitro*. In the JFH1 model, titrating doses of recombinant human BMP6 exert a dose-dependent reduction in viral replication. Against the OR6 HCV genomic replicon, incubation with both BMP6 and BMP9 elicits significant, dose-dependent antiviral effects. Co-incubation with either dorsomorphin or LDN-193189, small-molecule inhibitors of the ALK2/ALK3 type I BMP receptors(40,63), abrogates the antiviral effect of BMP6. Our data suggest that a component of BMP6's antiviral effect may also be independent of type I IFN signalling. While co-incubation with an anti-IFNAR2 antibody or ruxolitinib, a pharmacological inhibitor of JAK1/2(350), ablates the antiviral effect of recombinant human IFNα-2a in the OR6 model, the anti-HCV effect of BMP6 is unaffected.

Within the literature, recombinant BMP2, identified by a screen of putative ISGs, is reported to inhibit replication of the murine gammaherpesvirus MHV-68(351). Moreover, Sakamato and colleagues report a synergistic enhancement of IFNα's antiviral effect against a HCV replicon by BMP7, but do not provide a mechanistic basis for this observation(344). Precisely how other BMP/TGFβ ligands could also mediate an antiviral effect is ripe for investigation, a topic explored within this chapter.

To identify a mechanistic basis for the type I IFN-independent component of BMP6's antiviral effect, the whole transcriptome of Huh7.5 cells incubated with BMP6 18nM for 24h was profiled by microarray [see also appendix 1]. Compared to untreated cells, 2207 transcripts were differentially regulated, including well-established BMP-responsive genes including *HAMP*, *ID1* and *ID3*.

As summarized by figure 3.1, pathway analysis with the Metacore GeneGo suite revealed not only statistically significant alteration of the BMP signalling pathway ($p<10^{-4}$) but also statistically significant enrichment of the type I IFN signalling pathway ($p<10^{-4}$). Intriguingly,

multiple gene sets associated with cell cycle regulation were differentially regulated by 24h BMP6 treatment; including the top hit "ATM/ATR regulation of G1/S checkpoint". Since ATM, a serine/threonine kinase recruited to double-strand breaks, is required for HCV replication(352), the possibility that modulation of cell cycle kinetics could at least in part mediate the antiviral effect of BMP6 piqued our interest, and is explored in this chapter. ATM/ATR-associated genes suppressed by BMP6-treatment include the DNA-repair complex components *FANCD2* and *BRCA1*, in addition to the checkpoint regulator *CHK2* and *CDK1* (p34), the catalytic subunit of the protein complex promoting cellular entry into mitosis. Expression of the cyclin dependent kinase inhibitor *CDKN1A* (p21) and the regulator *GADD45A*, a nuclear protein regulating genomic stability and DNA repair, was relatively increased upon BMP6 treatment. The hypothetical network of genetic interactions generated by the Metacore analysis with respect to the "ATM/ATR regulation of G2/M checkpoint" is included in appendix II as an exemplar.

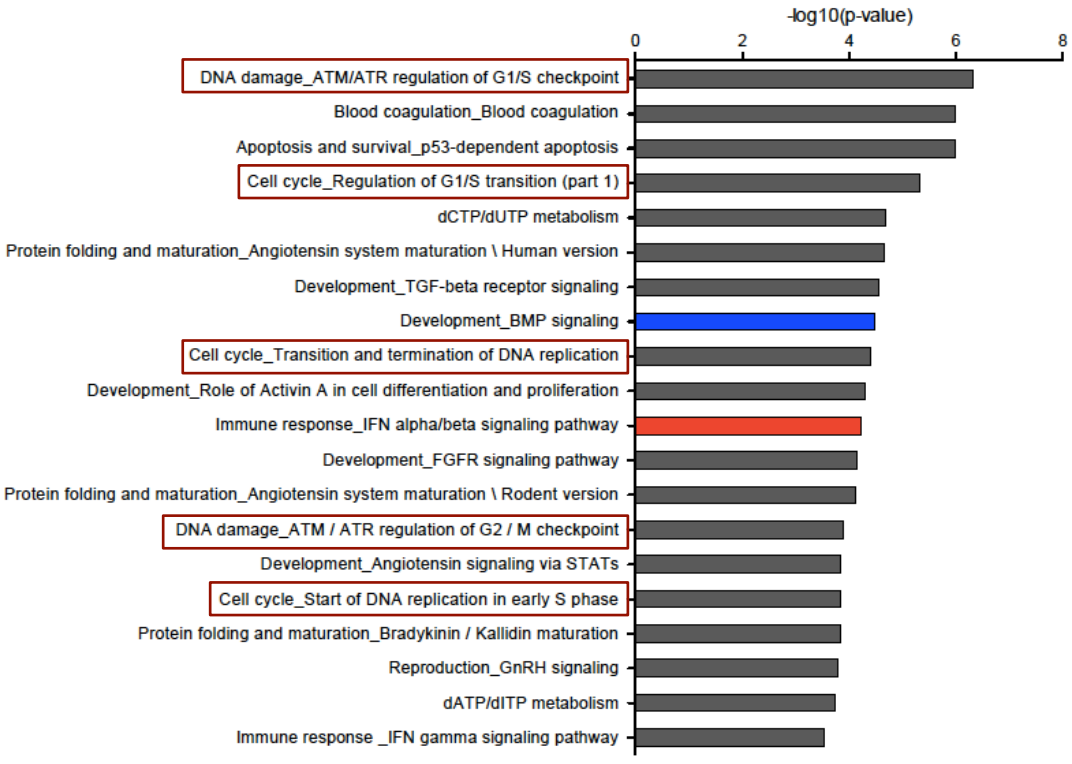


Figure 3.1: Top pathways differentially regulated by BMP6 treatment of Huh7 cells

Huh7 cells were stimulated with 18 nM BMP6 for 24 h followed by extraction of total cellular mRNA. Whole transcriptome analysis performed with the Illumina Human HT12v4.0 Expression BeadChip platform, returning 2275 differentially regulated transcripts. Pathway analysis was performed with MetaCore GeneGo software from Thomson Reuteurs.

Signalling pathways associated with cell-cycle progression and the DNA damage response are highlighted with red boxes.

3.1.2 Cell cycle regulation: a summary

The cell cycle refers to the sequence of intracellular activities that precede mitotic division and cytokinesis. As summarized by figure 3.2, the cell cycle is divided into four main phases: gap 1 (G1), characterized by high rates of protein synthesis, organelle biogenesis and cell growth; synthesis (S), in which DNA replication occurs; gap 2 (G2), a period of further rapid growth and biosynthesis; and mitosis (M), the point of nuclear division. Cells may exit the cell cycle and enter a quiescent phase (G0) either reversibly or irreversibly depending upon their differentiation status(353,354).

Cell cycle progression is governed by a series of checkpoint controls- kinase networks that integrate diverse proliferative and metabolic signals. Checkpoints are regulated by the co-ordinated activities of cyclin-dependent kinases (CDK) and their substrates cyclins. Intracellular levels of both catalytic CDK and regulatory cyclin subunits fluctuate, resulting in oscillating concentrations of the active CDK-cyclin heterodimers that drive transition through cell cycle phases(354,355).

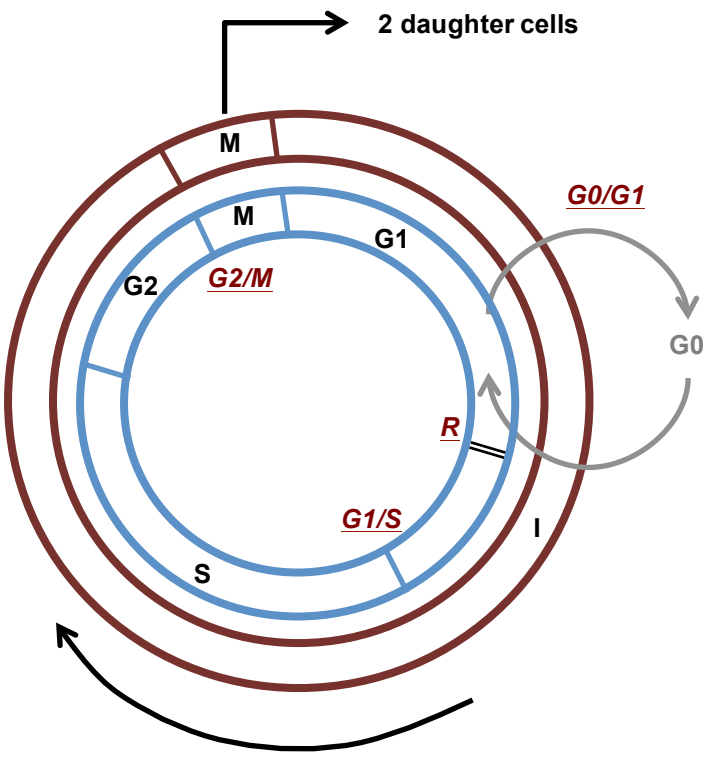


Figure 3.2: Schematic depiction of the mammalian cell cycle

The mammalian cell cycle may be broadly divided into mitosis (M) and interphase (I). Within interphase, the initial G1 phase is associated with cell growth and organelle synthesis.

Mitogenic signals are required to drive progression through G1 until the R-point (denoted by double line) is achieved, at which point extracellular proliferative signals are no longer required. DNA replication occurs during S phase, whereas G2 entails a final burst of biosynthesis before degradation of the nuclear envelope and initiation of mitosis.

After mitosis, two daughter cells are produced. Cells may be actively cycling or enter a state of quiescence (G0), which may be permanent or temporary.

Transcriptional regulation of cyclin and CDK proteins is predominantly mediated by E2F and DP transcription factors. In quiescent cells, the pocket protein p130 binds the majority of E2F-DP heterodimers, preventing their interaction with transcriptional machinery. In G1, however, complexes between the tumour suppressor retinoblastoma protein (Rb) and E2F-DP predominate. During early G1, mitogenic stimuli promote expression of cyclin D, which associates with CDK4/CDK6 and catalyse partial phosphorylation of Rb, weakening its repression of E2F-DP and eliciting downstream transcriptional induction of cyclin E expression. Upon association with cyclin E, CDK2 catalyses total phosphorylation of Rb and release of bound E2F-DP, culminating in transcriptional activation of genes driving the G1/S transition and initiation of DNA replication(353,354,356).

CDK2 and CDK4/6 are negatively regulated by Cip/Kip and INK4 proteins respectively, the prototypic examples of which are $p21^{WAF1}$ and $p16^{INK4A}$. Upon induction by p53 in response to DNA damage, p21 abrogates the cyclin-CDK interaction by simultaneous blockade of motifs in both proteins. In contrast, p16 specifically inhibits the CDK serine-threonine kinase domain(357–359).

During S-phase, cyclin A-CDK2 complexes dominate. Rb remains inactive until the direct action of phosphatases, or attenuation of CDK activity, restore the protein to its hypophosphorylated state and establish quiescence(354,360).

3.1.3 Cell cycle regulation by BMP/SMAD signalling

The pathway analysis of the microarray of Huh7 cells treated with BMP6 indicated regulation of cell cycle was altered. The following two sections will describe what is already known about how other BMPs can alter the cell cycle, and how.

Studies of tooth development provided the first evidence that BMPs are able to regulate p21 expression. In molar precursors explanted from E13 to E14 mouse embryos, beads impregnated with recombinant BMP2 and BMP4 induce focal *p21* expression in the dental epithelium, assayed by *in situ* hybridization(361).

Induction of p21 by recombinant BMP2 has also been shown in the MCF-7 human breast cancer cell line, with associated dampening of its proliferative response to the mitogenic stimulus. Mechanistically, BMP2 is proposed to impair progression to S phase secondary to p21 upregulation and subsequent hypophosphorylation of RB, resulting in G1 arrest(362,363). This mechanism is also proposed to underlie the anti-proliferative effects of

recombinant BMP2 on MDA MB 231 breast cancer cells stimulated with epidermal growth factor; BMP2 on U226 myeloma cells; and BMP7 against a panel of anaplastic thyroid carcinoma lines(364–366). In MDA MB 231 cells, BMP6 is reported to induce expression of miR-192, a microRNA associated with repression of Rb expression. Genetic silencing of this miR-192 ablates the cytostatic effect of BMP6 in this cell line(367).

In vivo, intravenous administration of recombinant BMP2 reduces tumour volume in nude mice xenografted with either MCF-7 and MDA MB 231, an observation attributed to BMP2's cytostatic properties(363). Similarly, expression of a constitutively active type I BMP receptor (ALK6) by PC-3 human prostate cancer cells impairs their tumour-forming capacity after xenograft into nude mice(368).

Contradictory evidence exists for a pro-proliferative effect of SMAD1/5 signalling in primary vascular cells. Zhou and colleagues report that shear stress resulting from turbulent blood flow around atherosclerotic lesions elicits SMAD1/5-phosphylation in rat aortic endothelial cells *in vivo*, in parallel with cyclin A induction and downregulation of p21 and the related CDKI p27(369). However, intra-arterial infusion of noggin, a pan-BMP binding protein, did not block SMAD1/5 phosphorylation nor downstream cell cycle effects, suggesting that SMAD1/5 phosphorylation is likely to be independent of secreted BMP ligands(369).

Evidence exists for an interaction between the pleiotropic non-receptor tyrosine kinase c-ABL, strongly associated with cell proliferation, and the ALK3 type I BMP receptor, resulting in differential activation of $p16^{INK4A}$(370). C-ABL is proposed to regulate the balance of ALK3 signalling output via canonical SMAD1/5/8 and non-canonical ERK1/2 pathways. In the context of osteoblast proliferation, genetic deficiency of C-ABL enhances signalling via ERK1/2, resulting in $p16^{INK4A}$ induction and failed expansion of murine osteoblast progenitors *ex vivo*. C-ABL deficiency is associated with reduced SMAD1 phosphorylation in the residual osteoblast progenitors and downregulation of the BMP target-gene *ID1*, which is itself an activator of $p16^{INK4A}$ transcription(370).

Altogether, the above information show that multiple points of interaction occur between BMP/SMAD signalling and cell cycle regulatory mechanisms, as summarized by figure 3.3.

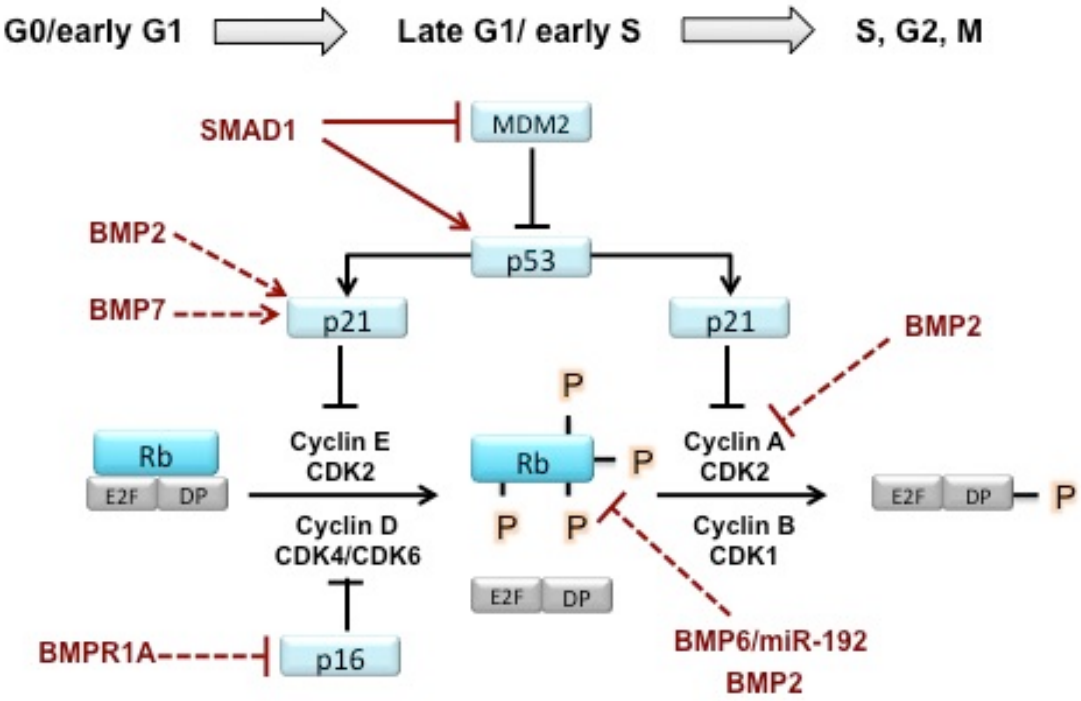


Figure 3.3: Regulation of cell cycle progression by BMP/SMAD signalling

During G0/early G1, hypophosphorylated Rb sequesters E2F-DP transcription factor complexes. As G1 progresses, mitogenic stimuli upregulate expression of cyclin D and E, resulting in catalytic activation of CDK2/4/6 and phosphoprylation of Rb. E2F transcription factors complexes are released from Rb and promote expression of genes driving the cell cycle into S phase. This pathway is negatively regulated by CDKI proteins, including p16 and p21, which is induced in response to p53 activation following DNA damage.

BMP/SMAD signalling is proposed to regulate multiple aspects of this system, including modulation of p21 and p16 levels; activation of p53; and repression of cyclin A expression.

3.1.4 BMP-SMAD axis and the DNA damage response

DNA damage, resulting from intrinsic sources such as reactive oxygen species or external stressors such as ionizing radiation or chemotherapeutic drugs, activates cell cycle checkpoint controls, leading to cell cycle arrest and recruitment of DNA repair machinery. Chk1/ATR and Chk2/ATM, found to be altered by BMP6 in Huh7.5 cells as described in section 3.1.1, [figure 3.1], represent the two best-characterized effector modules recruited to site of DNA damage, being principally induced in response to single-stranded and double-stranded DNA breaks (SSB/DSB) respectively(371). Here, the biological basis of these two repair modules, and their links to BMP signalling, are described.

In terms of the Chk2/ATM response, the trimeric MRN complex, composed of Mre11, Rad50 and Nbs1 subunits, is proposed to detect aberrant chromatin architecture induced by DSBs(372). The Nbs1 C-terminus contains a conserved motif triggering dissociation of inactive ATM trimers and recruitment of active ATM to the site of damage(373). ATM,

truncations of which result in the neurodegenerative syndrome ataxia telangiectasia, is a multifunctional PI-3 kinase(374). It is required for both recruitment of homologous repair and non-homologous end joining apparatus to DNA lesions and activation of downstream effector kinases, including Chk2(375). Threonine phosphorylation of Chk2 induces its oligomerization, enhancing its ability to inactivate the Cdc25 phosphatase family. Cdc25 phosphatases promote cell cycle progression via removal of inhibitory phosphate moieties from the ATP-binding loops of CDK1 and 2, facilitating association with cyclins and passage through the G1/S and G2/M transitions. In a parallel pathway, the PI3K-type kinase ATR is recruited to SSBs, resulting in Chk1 activation, ultimately also convergent upon Cdc25A inactivation(371).

Work by Chau and colleagues suggests that ATM direct activates SMAD1, but not SMAD5 or 8, in response to genotoxic stress(376). In mouse embryonic fibroblasts (MEF) exposed to doxycycline, hydroxyurea or ionising radiation, Smad1 undergoes Atm-dependent phosphorylation in the nucleus, with activation kinetics distinct to those elicited by recombinant Bmp2. Smad1 phosphorylation in this context is sustained, in part due to disruption of its interaction with the protein phosphatase Ppm1(376).

In summary, BMP/SMAD signalling is known to interact with the DNA damage response, especially in the context of genotoxic stress, consistent with the reciprocal modulation of ATM/ATR component expression evident in our microarray study of BMP-treated Huh7.5 cells.

Of note, interactions between HCV and multiple components of the cell cycle regulatory proteins and DNA damage modules have been reported and are posited to contribute to malignant progression. In terms of the cell cycle, Rb protein levels are strongly negatively regulated by HCV in cell culture models, with the binding of the viral polymerase NS5B posited to promote polyubiqitination and proteasomal degradation (377–379).

With regard to induction of genotoxic stress, transgenic expression of HCV core protein in the mouse liver results in increased intracellular ROS, putatively due to disruption of mitochondrial function and depletion of intracellular reserves of reduced glutathione (380,381). In the context of *in vitro* overexpression studies, physical interactions between components of the ATM machinery and HCV NS3/4A have been reported, with concomitant impairment of the cell's ability to respond to ionizing radiation(382). Ariumi and colleagues report that interactions with ATM and CHK2 are proposed to promote viral replication,

suggesting that disruption of the DNA damage response axis represents an evolutionarily favourable viral behaviour (352).

Evidence also exists for modulation of SMAD3-linked TGFβ signalling by the viral core protein, diminishing the anti-proliferative properties of intrahepatic TGFβ yet enhancing its capacity to promote the epithelial-to-mesenchymal transition posited as a precursor to malignant transformation (383,384).

3.1.5 Some viruses can cause arrest in S-phase

We hypothesize that by inducing cell cycle arrest at the G1/S or G2/M checkpoints, possibly through modulation of the DNA damage response, BMP6 could prevent cells from entering S-phase.

Limited evidence exists that the HCV NS2 protein promotes arrest of transformed cells, including Huh7, in S phase, in part by downregulation of cyclin A expression(385). In the PH5CH8 transformed human hepatocyte cell line, expression of HCV NS5B is associated with S-phase arrest, slower rates of DNA synthesis and subsequent delayed progression to G2/M. In this model, despite the absence of replicating viral genomes, the disruption of cell cycle progression is reportedly attributable to IFNβ production downstream of TLR3 activation(386). NS5B is also well described to repress expression of Rb, via direct binding of the viral polymerase to Rb and subsequently targeting it for degradation. In contrast to delaying the cell-cycle, this interaction is posited to promote the activity of E2F-stimualted genes and activate cell proliferation (378). Similar observations have been described for the NS2 encoded by the porcine pathogen classical swine fever virus and the N protein of porcine epidemic diarrhoea virus, both of which promote S-phase arrest and repression of cyclin A(387,388). A distinct mechanism is proposed for S-phase arrest in rubella virus-infected cells *in vitro*, namely disruption of G2/M progression by inhibitory binding of the viral P90 protein to the host CK enzyme that drives cytokinesis(389).

S-phase arrest, associated with reduced CDK2 expression, is a hallmark of transmissible gastroenteritis virus (TGEV) infection. TGEV infection of synchronized cells *in vitro* revealed significantly higher levels of viral genome were detectable by RT-qPCR in cells arrested at either the G1/S or G2/M boundaries (induced by double-thymidine block or nocodazole, respectively) compared to serum-starved cells arrested in G0/G1(390). Clinically, dysregulated expression of cell cycle modulators is also a hallmark of progression from mild

cirrhosis to advanced pathology in an Egyptian cHCV cohort, with particular downregulation of the G2/M checkpoint regulators KNTC1 and MAD2L1(391).

Putting this information together, we hypothesize that the antiviral effect of BMP6 on HCV could be mediated via the induction of cell cycle arrest at the G1/2 or G2/M checkpoints, possibly via modulation of the DNA damage response. Through this mechanism, BMP6 could prevent cells from entering S-phase. S phase is arguably more permissive to replication of viral genomes, both RNA and DNA, than the gap phases due to its high rate of nucleotide biosynthesis and therefore comparative abundance of material for incorporation into nascent viral genomes.

3.1.6 Summary and aims

The data presented within the first half of this chapter extends upon both the results of our transcriptomic analysis and the extensive published interplay between BMP-SMAD signalling and the cell cycle, exploring whether modulation of cell cycle progression could account for at least part of BMP6's IFN-independent antiviral effect. The second half of this chapter explores whether an antiviral effect extends to other BMP/TGFβ-type cytokines by screening diverse ligands for an antiviral effect against the OR6 HCV replicon model.

The key questions were:

1) Does BMP6 induce cell-cycle arrest in Huh7 cells *in vitro*?
2) Is induction of cell-cycle arrest sufficient to reduce HCV replication *in vitro*?
3) Do other BMP or TGFβ-type exert anti-HCV effects, and if so, these also contingent upon intact type I BMP receptor function?

3.2 Materials and methods

3.2.1 Pharmacological induction of cell cycle arrest

As a positive control for the induction of cell cycle arrest, Huh7 or OR6 cells were incubated with the cytostatic agent UCN-01 (Sigma-Aldrich, USA). First identified as protein kinase C inhibitor secreted by *Streptomyces*, UCN-01 elicits cell cycle arrest at the G1/S checkpoint in multiple cell lines via both inhibition of Rb phosphorylation and transcriptional induction of the cyclin-CDK inhibitor p21 and related Cip/Kip proteins(392–394).

3.2.2 BrdU/PI analysis of cell cycle phase distribution

Incorporation of the brominated nucleoside analogue 5'-bromo-2'-deoxyuridine (BrdU) during a pulsed exposure provides an index of DNA replication rates, whereas propidium iodide (PI) intercalates into DNA duplexes, allowing quantification of total cellular DNA. Flow cytometric analysis of immunostained BrdU and PI fluorescence yields a "horseshoe" distribution. Cells in G0/G1 are associated with both minimal BrdU incorporation and 1N quantity of DNA; as S-phase proceeds increasing quantities of BrdU are incorporated and PI signal also increases; cells in G2/M are characterized by 2N DNA content and low BrdU signal.

Huh7 cells were seeded at $7x10^4$ cells/well in a 6-well plate. 24 h after seeding, cells were washed with PBS and replenished with DMEM10 (untreated cells), 100 nM UCN-01 or 18nM recombinant human BMP6 (R&D Systems, MN, USA or courtesy of S. Vukicevic, University of Zagreb, as specified) in duplicate wells per condition. After 48 h incubation, cells were "pulsed" for 30 minutes by addition of the synthetic thymidine analogue BrdU to a final molarity of 10 μM. Cells were detached with 10mM EDTA in PBS, duplicate wells pooled and the cells pelleted by centrifugation at 1400 rpm for 5 min.

After fixation with 70% EtOH at 4 °C for 30min and centrifugation at 1500 rpm for 10 min, cells were subjected to acid denaturation by dropwise addition of 2N HCl+0.5% Triton X-100 followed by a 30 min incubation at room temperature. Cells were spun down in a minifuge at 2400 rpm for 10 min. Acidic pH was neutralized by addition of 0.1 M $Na_2B_4O_7$ and the cells spun down again at 2400 rpm for 10 min, after which the supernatant was aspirated and the cells resuspended in 1mL 0.5% Tween20/1% BSA in PBS. Samples were then divided into two 500 μL aliquots, designated "test" and "control".

Test samples were incubated with rat anti-BrdU monoclonal antibody (cat. number ab6326; Abcam, Cambridge, UK) at 40 μg/mL for 30 min at room temperature whereas control samples were exposed to the antibody diluent (0.5% Tween20/1% BSA) only. After centrifugation at 2400 rpm for 10 min, both test and control cells were incubated with 5 μg/mL goat anti-rat AlexaFluor-488 conjugated polyclonal antibody (cat. Number ab150157) for 30 min, in the dark. Immediately before data acquisition, all cells were spun down at 2400 rpm for 10 minutes and resuspended in 100 μM PI in PBS for 15 min at room temperature.

Data were acquired with a Dako CyAn ADP flow cytometer and analysed with FlowJo v10 (TreeStar Inc. OR, USA).

3.2.3 Effects of cell cycle inhibition on HCV replication

OR6 cells (described in section 2.3.1) were plated at $3.5x10^3$ cells/well in flat-bottomed 96-well plates. After 24h incubation, cells were incubated in triplicate wells with DMEM10 (untreated) or any one of recombinant human IFNα 100U/mL (PBL Assay Science, NJ, USA) or 100 nM, 400 nM or 800 nM UCN-01 for 72 h. At 72 h, cells were assayed for Renilla luciferase activity as a surrogate for intracellular HCV content or with the Cell Titer Glo (Promega) as an index of cell number and viability (methods described in sections 2.3.2 and 2.3.3 respectively).

3.2.4 Analysis of CHEK2 and CDKN1A expression in Huh7 cells

Huh7 cells were plated at $1x10^5$ cells per well in a 12-well plate and incubated for 24 h before a PBS wash and replenishment with DMEM10 (untreated) or recombinant human BMP6 (R&D). After 24 h incubation cellular RNA was harvested for RT-qPCR analysis of *HAMP*, encoding hepcidin, *CHEK2*, encoding CHK2, and *CDKN1A*, encoding p21, expression, as described in section 2.2.

3.2.5 Screening of BMP/TGFβ superfamily ligands for an anti-HCV effect:

3.2.5.1 BMP4

OR6 cells (described in section 2.3.1) were plated at $3.5x10^3$ cells/well in flat-bottomed 96-well plates. After 24h incubation, cells were incubated in triplicate wells with DMEM10 (untreated), recombinant human IFNα 100 U/mL (PBL Assay Science), recombinant human BMP6 (R&D) or a titration of recombinant human BMP4 (R&D) from 0.2 nM to 54 nM, for 72 h. At 72 h, cells were assayed for Renilla luciferase activity, as described in sections 2.3.2.

3.2.5.2 Activin A and activin B

OR6 cells (described in section 2.3.1) were plated at $3.5x10^3$ cells/well in flat-bottomed 96-well plates. After 24h incubation, cells were incubated in triplicate wells with DMEM10 (untreated), recombinant human IFNα 100U/mL (PBL Assay Science), recombinant human BMP6 (R&D) or a titration of recombinant human activin A or activin B (both R&D) from 0.25 nM to 4 nM, for 72 h. At 72 h, cells were assayed for Renilla luciferase activity, as described in sections 2.3.2.

3.2.5.3 BMP15, GDF1, GDF15

OR6 cells (described in section 2.3.1) were plated at $3.5x10^3$ cells/well in flat-bottomed 96-well plates. Recombinant human GDF1, GDF15 and BMP15 were obtained from R&D Systems. At the experimental end-point, cells were assayed for Renilla luciferase activity or with the Cell Titer Glo (Promega) (methods described in sections 2.3.2 and 2.3.3 respectively).

3.2.6 Investigating the ALK2/3 and IFNAR2 dependency of an anti-HCV effect

3.2.6.1 LDN-193189

The ALK2 and ALK3 isoforms of the type I BMP receptor were inhibited by LDN-193189 (Axon Medchem, Groningen, NL) an optimized dorsomorphin derivative and specific inhibitor of their intrinsic intracellular kinase domains(40,63). To assess the effects of LDN-193189 in the OR6 model, OR6 cells were plated at $3.5x10^3$ cells/well in flat-bottomed 96-well plates, in triplicate wells per condition. LDN-193189, at the doses specified within the respective figure legends, was added 30 min prior to incubation with recombinant proteins. Cells were incubated for 72 h and assayed at end-point for Renilla luciferase activity as described in sections 2.3.2.

3.2.6.2 Ruxolitinib

Ruxolitinib (INCB018424) is a small-molecule inhibitor of the JAK1 intracellular kinase required for signal transduction by the IFNAR2 type I IFN receptor chain(350).

OR6 cells were plated at $3.5x10^3$ cells/well in flat-bottomed 96-well plates, triplicate wells per experimental condition. Cells were incubated with 5 μM ruxolitinib (Tocris Bioscience, Bristol, UK) or DMEM10 (untreated) in 50 μL for 30 min, followed by the addition of a unit volume recombinant human IFNα to end-point concentration 100 U/mL (PBL Assay Science) or recombinant human activin A or activin B (both R&D) as 2X solutions giving end-concentrations of 2 nM or 6 nM activin in the presence or absence of 2.5 μM ruxolitinib. Cells were incubated for 72 h and assayed at end-point for Renilla luciferase activity and Cell Titer Glo signal as described in sections 2.3.2 and 2.3.3.

3.2.6.2 SB-431542

SB-431542 is a selective inhibitor of the SMAD2/3-linked ALK4/5/7 isoforms of the type I TGFβ receptor(395).

OR6 cells were plated at $3.5x10^3$ cells/well in flat-bottomed 96-well plates, triplicate wells per experimental condition. Cells were incubated with titrating doses of SB-431542 (Sigma-Aldrich, USA) or DMEM10 (untreated) in 50 μL for 30 min, followed by the addition of a unit volume recombinant human activin A (R&D), giving end-concentrations of 6 nM or 18 nM activin A in the presence or absence of zero ('vehicle'), 1 μM, 5 μM or 10 μM SB-431542. Cells were incubated for 72 h and assayed at end-point for Renilla luciferase activity and Cell Titer Glo signal as described in sections 2.3.2 and 2.3.3.

3.3 Results: Cell cycle modulation and HCV replication

3.3.1 Effect of recombinant BMP6 on cell cycle progression in Huh7 cells

As detailed in section 3.1.3, the cytostatic effects of BMP2, 4 and 7 have been validated against both primary cells and multiple transformed cell line. A cytostatic effect of BMP6 in Huh7 cells, the parent line of the OR6 HCV replicon system, has not yet been formally described. We hypothesized that induction of cell-cycle arrest by BMP6 could reduce the percentage of cells in S-phase, possibly consistent with reduced capacity of the host cell to sustain high-level viral replication.

To address whether BMP6 modulates cell cycle progression in Huh7 cells, we chose to quantify the phase distribution of BMP6-treated cells compared to untreated by BrdU incorporation and PI staining.

As summarized in figure 3.4 and demonstrated by figures 3.5 A-C incubation with either BMP6 or UCN-01 elicits a statistically significant reduction in the percentage of cells in S-phase, associated with a non-significant increase in the percentage of cells in both G0/G1 and G2/M, implying cell cycle arrest at the G1/S and G2/M checkpoints respectively.

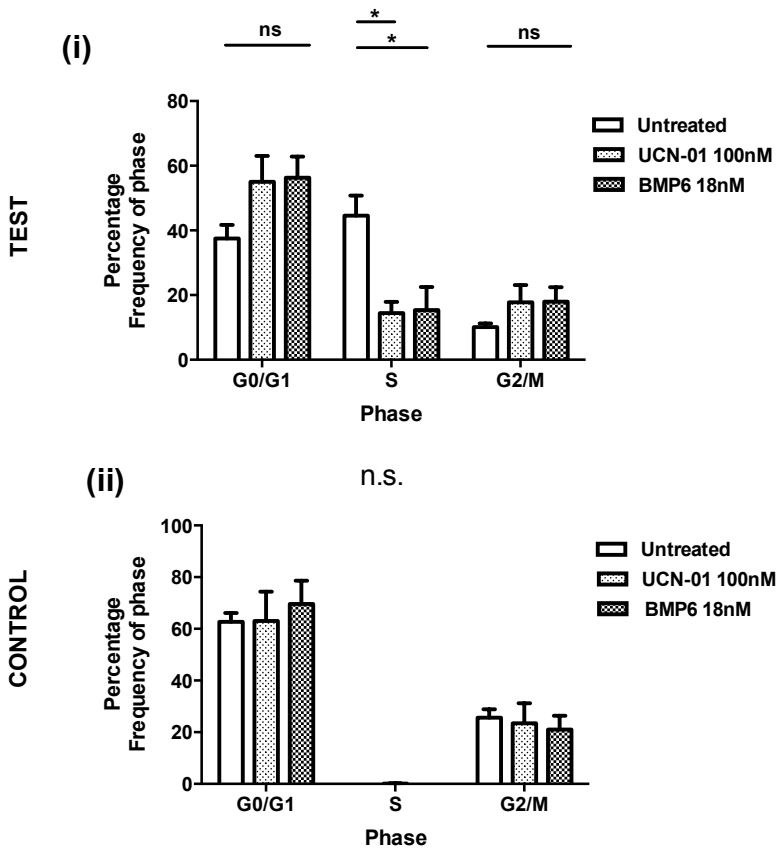


Figure 3.4 BMP6 promotes a shift in cell-cycle kinetics akin to the cytostatic agent UCN-01

Summary of BrdU/PI flow cytometric cell cycle analyses. Huh7 cells were untreated or incubated with the cytostatic agent UCN-01 or recombinant human BMP6 for 48h, followed by 30 minutes pulsed incorporation of BrdU. Cells were harvested and immunostained for incorporated BrdU (test condition only) and exposed to the DNA-intercalating dye propidium iodide (both test and control conditions). Percentages of cells in each phase of the cell cycle were then quantified by two-colour flow-cytometry.

Incubation with BMP6 promotes a shift in phase frequencies akin to that observed with the cytostatic drug UCN-01, characterized by a statistically-significant reduction in the percentage of cells in S-phase, and trend towards accumulation at the G0/G1 and G2/M checkpoints.

Individual flow cytometry plots are shown in figures 3.5 A-C; n=3 independent experiments with each condition in singlicate, except for BMP6 18nM in duplicate in one experiment.

Analysis by ordinary one-way ANOVA within each phase grouping and Bonferroni's multiple comparisons test with respect to untreated cells.

Figure 3.5 A: BrdU/PI cell cycle analysis replicate 1

Control condition flow cytometry plots

Axes: **L-R**: y = SS, x= FS; y = PI linear, x = pulse width; y = BrdU-AF488 log, x = PI area

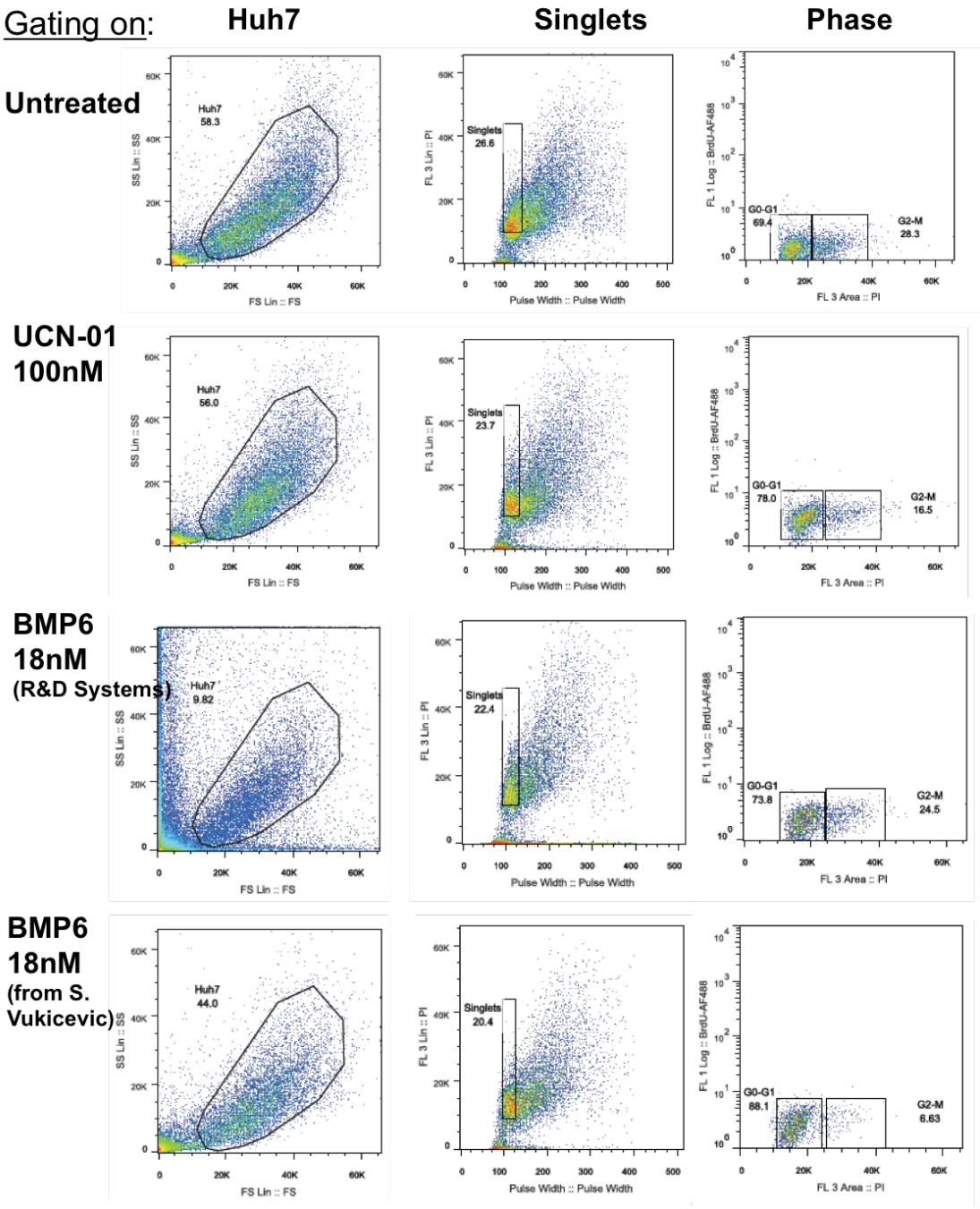


Figure 3.5 A: BrdU/PI cell cycle analysis replicate 1

Test condition flow cytometry plots

Axes: **L-R**: y = SS, x= FS; y = PI linear, x = pulse width; y = BrdU-AF488 log, x = PI area

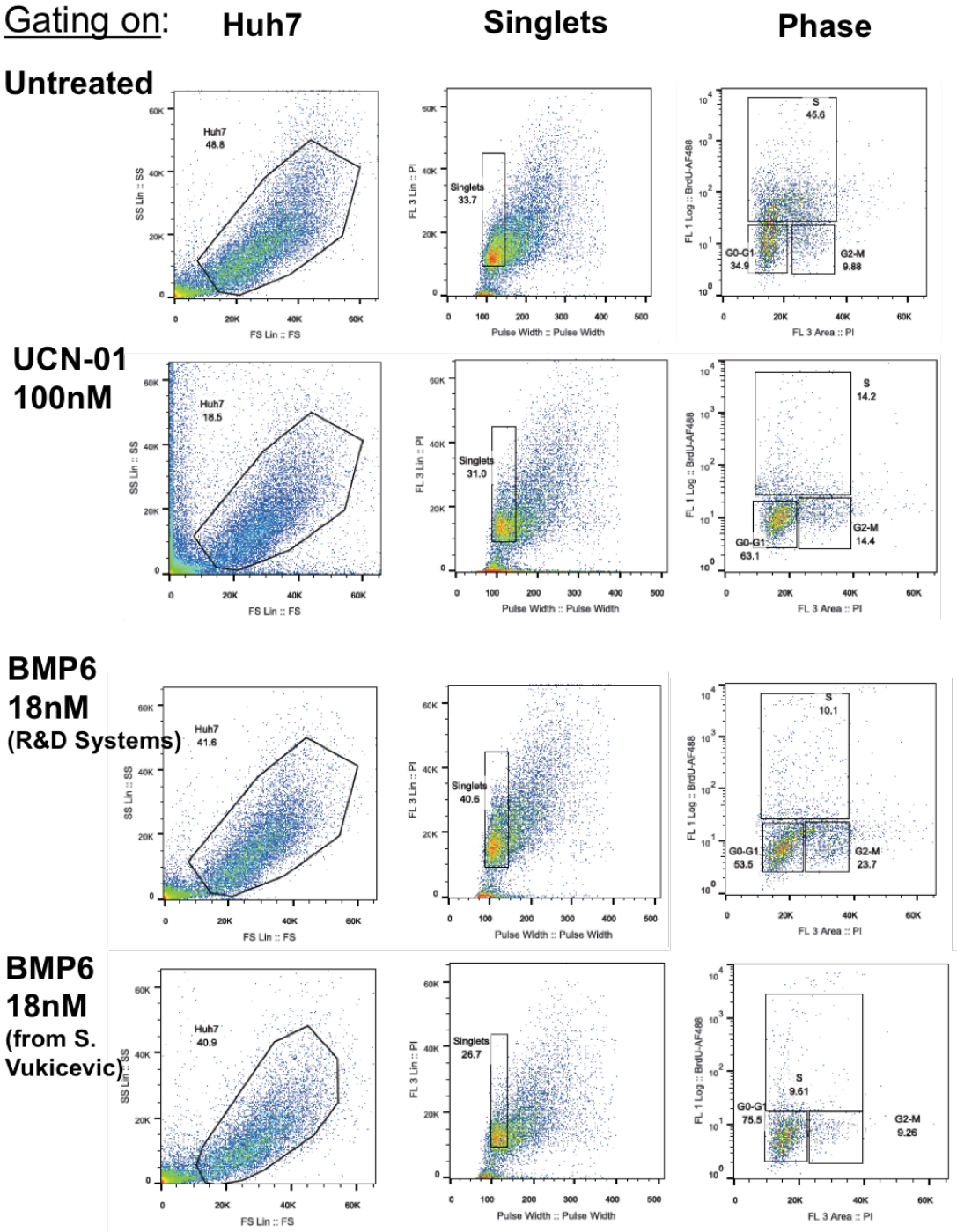


Figure 3.5 B: BrdU/PI cell cycle analysis replicate 2

Control condition flow cytometry plots

Axes: **L-R**: y = SS, x= FS; y = PI linear, x = pulse width; y = BrdU-AF488 log, x = PI area

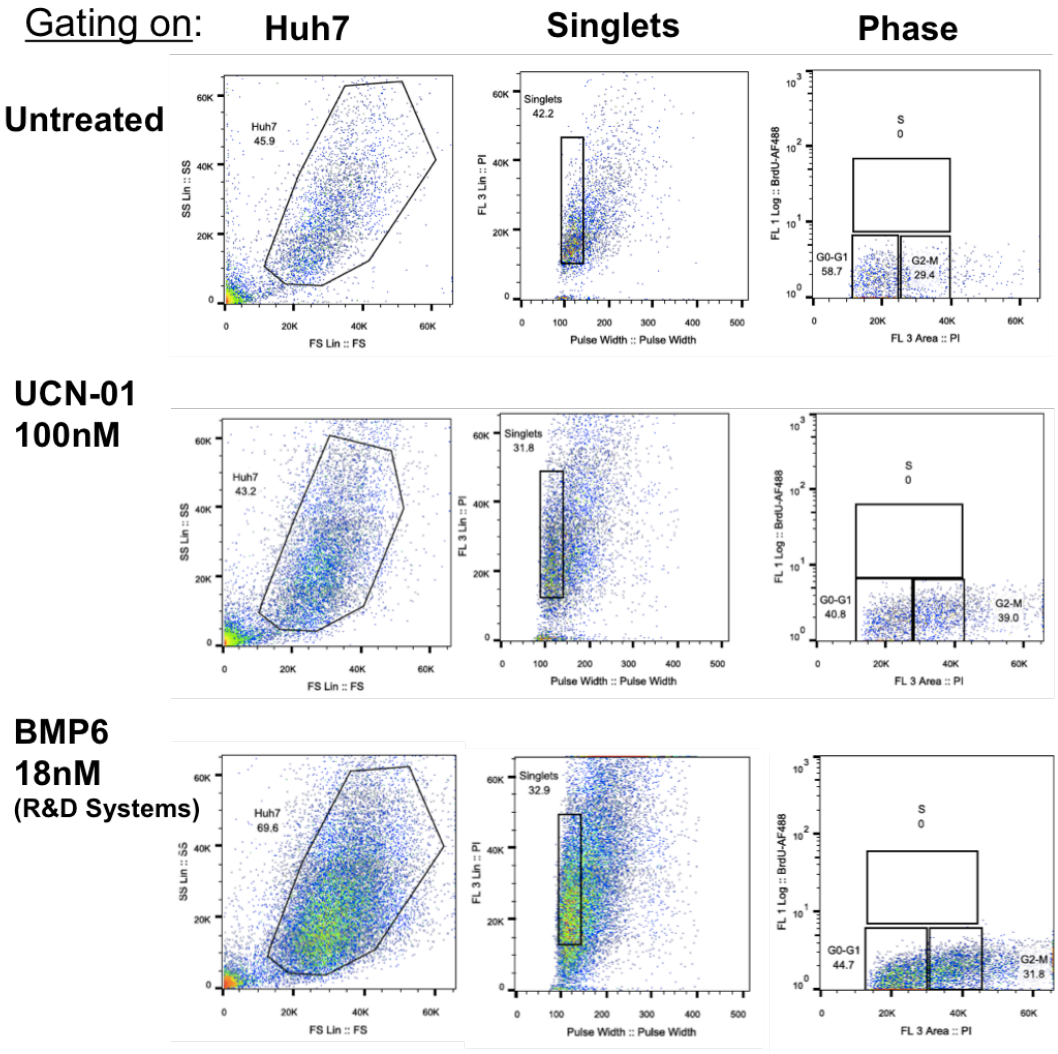


Figure 3.5 B: BrdU/PI cell cycle analysis replicate 2

Test condition flow cytometry plots

Axes: **L-R**: y = SS, x= FS; y = PI linear, x = pulse width; y = BrdU-AF488 log, x = PI area

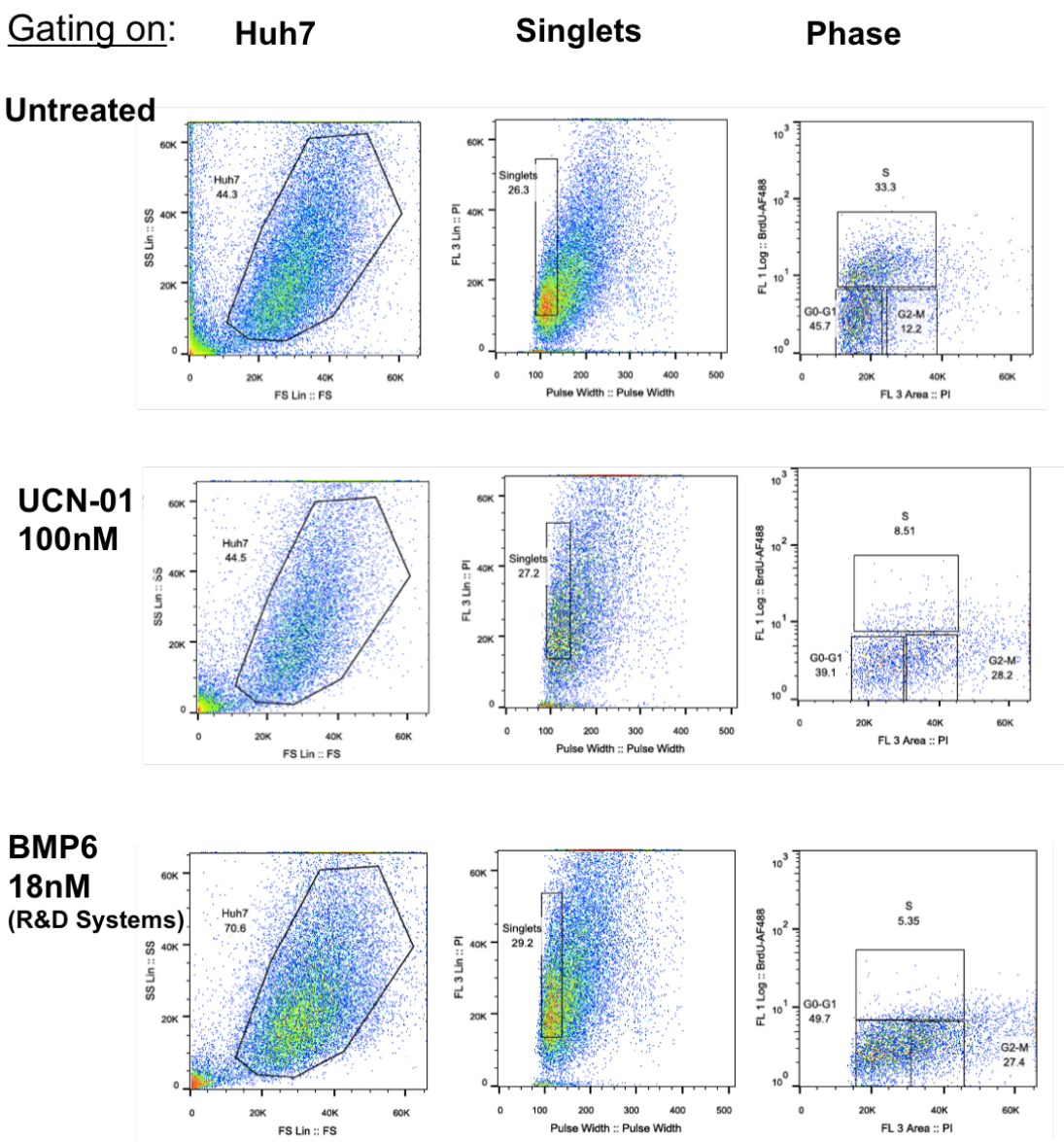


Figure 3.5 C: BrdU/PI cell cycle analysis replicate 3

Control condition flow cytometry plots

Axes: **L-R**: y = SS, x= FS; y = PI linear, x = pulse width; y = BrdU-AF488 log, x = PI area

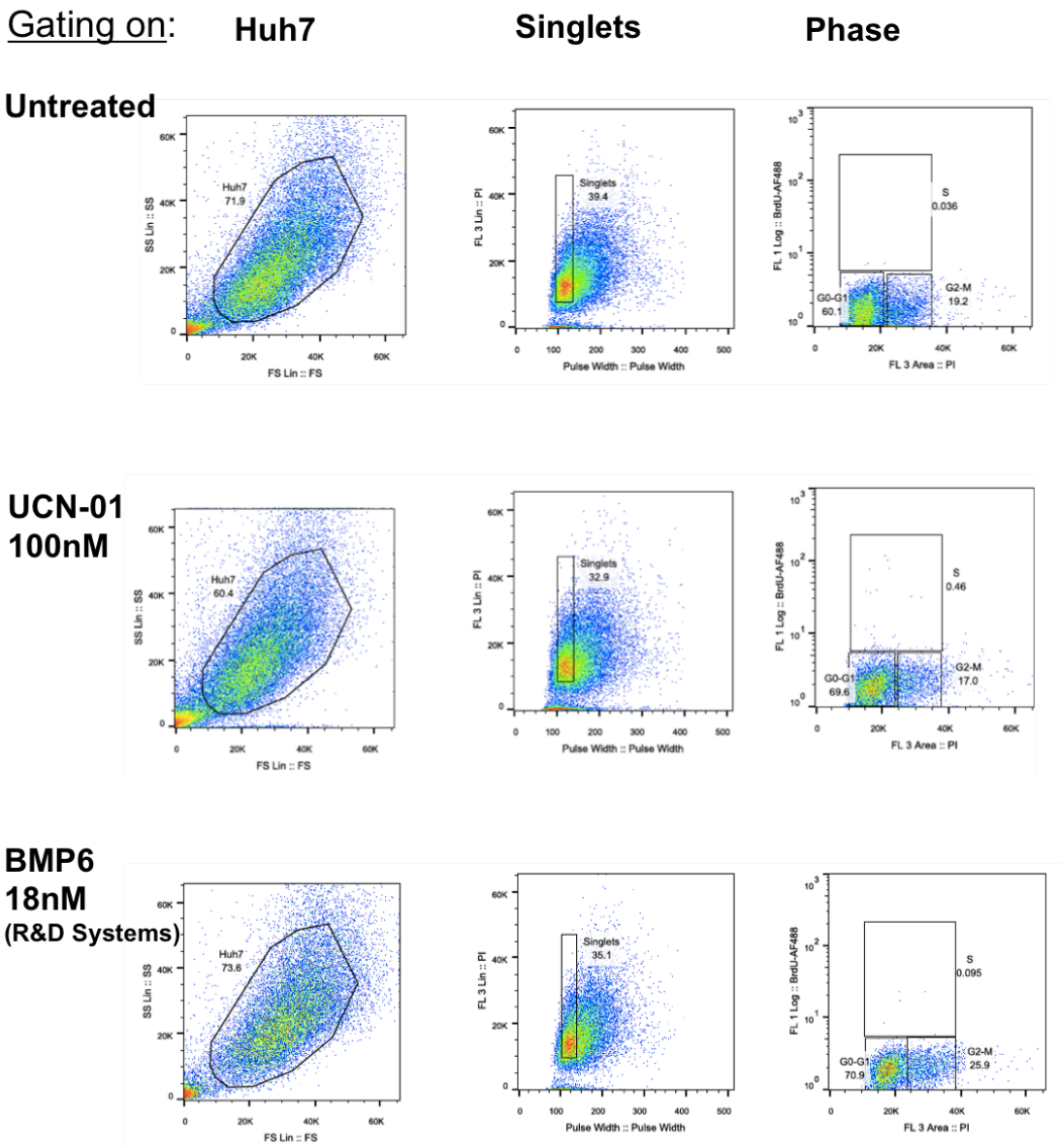
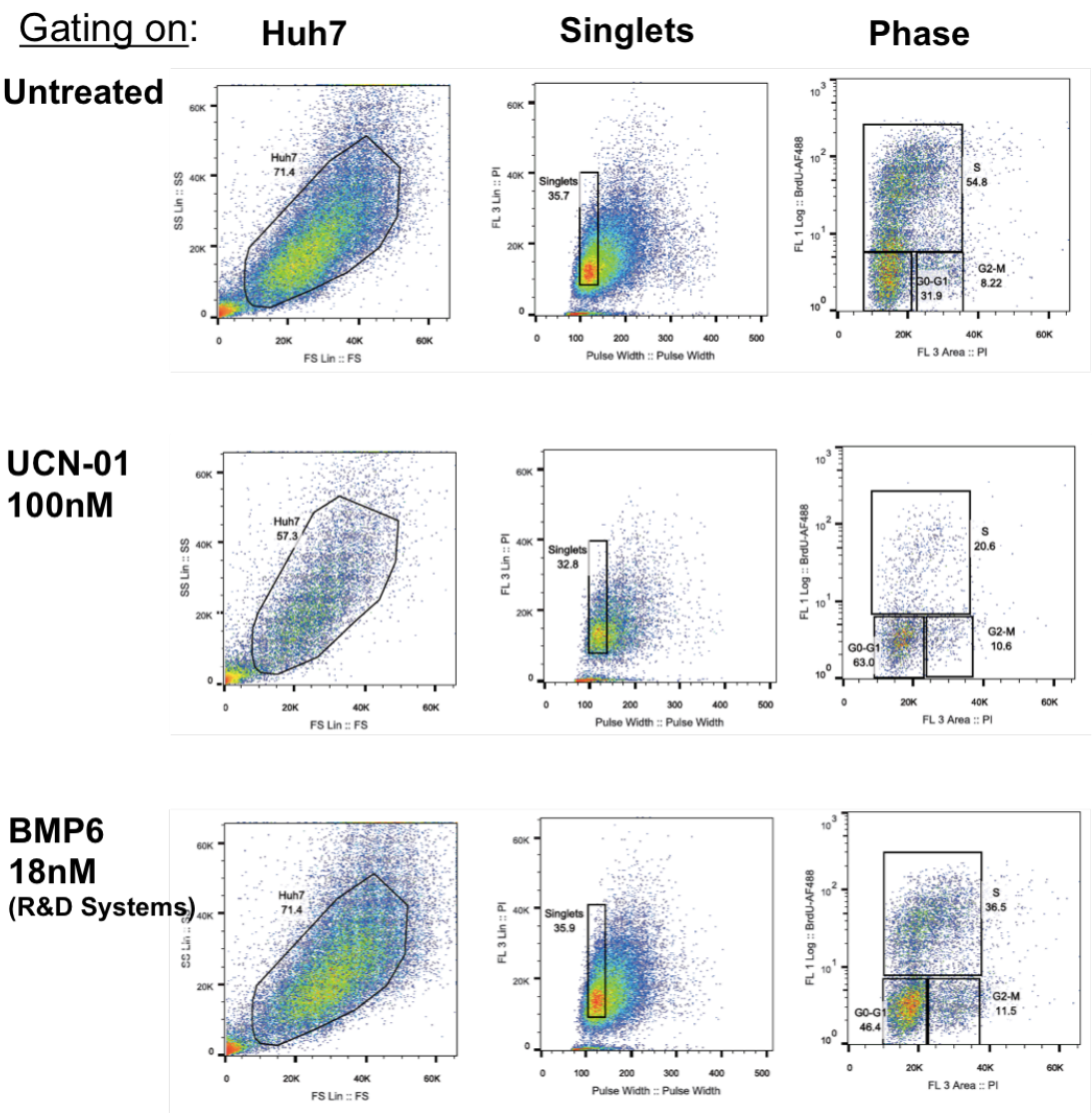


Figure 3.5 C: BrdU/PI cell cycle analysis replicate 3

Test condition flow cytometry plots

Axes: **L-R**: y = SS, x= FS; y = PI linear, x = pulse width; y = BrdU-AF488 log, x = PI area



3.3.2 Pharmacological induction of cell cycle arrest and HCV replication

Figure 3.5 demonstrates that the cell cycle phase distributions of cells treated with BMP6 resembles that of those incubated with the cytostatic agent UCN-01. To determine whether a reduction in the percentage of cells in S-phase is sufficient to reduce HCV replication, OR6 cells were incubated with a titration of UCN-01 for 72 h and assayed at the end-point both for intracellular HCV RNA and with the Cell Titer Glo (CTG) system, an assay for intracellular ATP content within each well (figure 3.6).

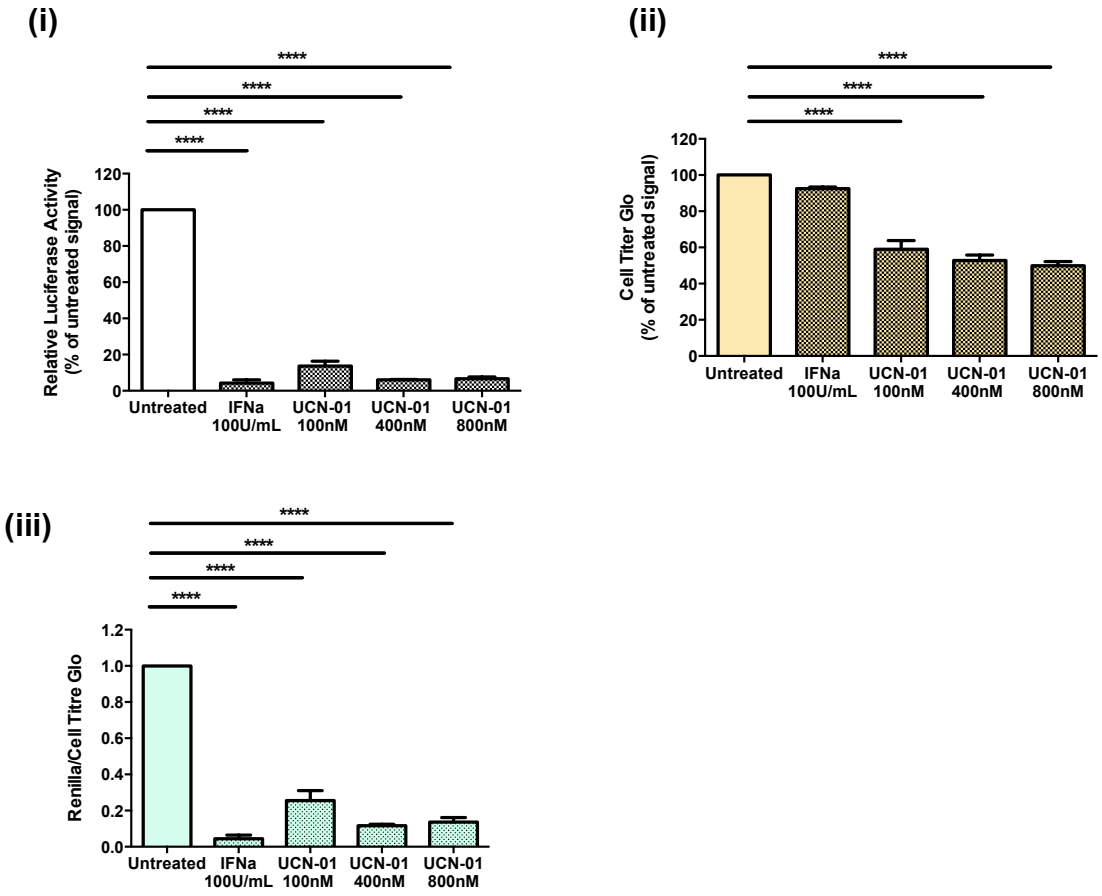


Figure 3.6: Inhibition of cell-cycle progression by UCN-01 is sufficient to reduce HCV replication, independently of an effect on cell number/viability

OR6 cells incubated with recombinant human IFNα-2a or a titration of UCN-01; cells assayed at 72 h post-incubation for Renilla luciferase (i) and Cell Titer Glo (ii), with signal presented relative to the untreated condition. Renilla luciferase is normalized to Cell Titer Glo intensity in (iii).

Incubation with UCN-01 at all doses elicits a significant reduction in intracellular HCV content compared to untreated cells, independently of its attendant statistically-significant diminution of cell number/viability.

n=3 independent experiments conducted in triplicate wells; analysis by ordinary one-way ANOVA and Bonferroni's multiple comparisons test with respect to untreated cells. **** denotes $p<0.001$

Akin to IFNα in this model, incubation with UCN-01 elicits a profound reduction in intracellular HCV content at all doses tested. While IFNα did not alter CTG signal relative to untreated cells, treatment with UCN-01 resulted in a statistically significant, dose-dependent reduction in CTG signal to approximately 50% of the untreated value. However, after normalization of the Renilla luciferase intensity to the respective CTG signal, a strong and statistically significant antiviral effect of UCN-01 remains evident. These data imply that reduction in the S-phase population is a plausible mechanism for the type I IFN-independent component of BMP6's anti-HCV effect.

To control for whether UCN-01 merely inhibited the catalytic activity of the Renilla luciferase reporter enzyme, rather than inhibited replication of the HCV replicon, OR6 cells or Huh7 cells were either incubated with 100 nM UCN-01 for 15 min or left untreated and spiked with stock UCN-01 immediately prior to measurement of luciferase activity [figure 3.7]. As expected, no luciferase activity was detected from Huh7 cells under either condition, as they lack the HCV replicon construct. No difference in luciferase signal was present between untreated OR6 lysates and those spiked with UCN-01, whereas an increased luciferase signal was evident after 15 min incubation with UCN-01. From this preliminary experiment, we were satisfied that the results observed in figure 3.6 are attributable to a direct effect of UCN-01 on replication of the HCV construct.

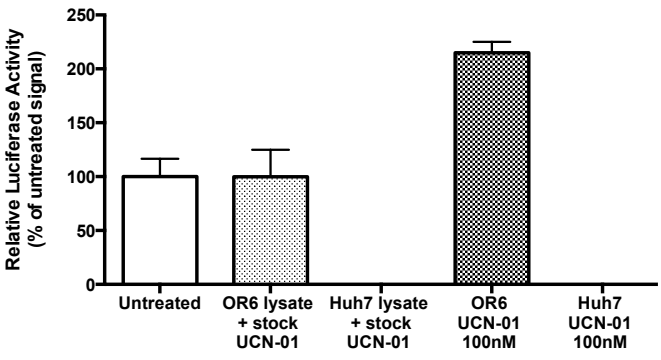


Figure 3.7: UCN-01 does not directly inhibit the Renilla luciferase reporter enzyme expressed by OR6 cells

OR6 and Huh7 cells were either untreated or incubated with UCN-01 100 nM for 15 min. Cells were harvested and lysed for quantification of luciferase activity. Cells which were untreated were left unadulterated ('untreated'; OR6 cells only) or spiked with stock UCN-01 immediately before acquisition of luciferase measurements (OR6 and Huh7 cells).

Neither rapid spiking with UCN-01 nor 15 min incubation with the drug were sufficient to reduce luciferase output compared to untreated OR6 cells. As anticipated, no signal was evident from Huh7 cells under either condition.

n=1 in biological duplicate; mean+SEM presented; statistical analysis precluded due to sample size.

Moving from treatment of OR6 cells with UCN-01 to validation of the observations from our microarray study, incubation of Huh7 cells with BMP6 18 nM for 24 h results in statistically significant upregulation of mRNA encoding p21 (*CDKN1A*) and significant downregulation of CHK2 transcript (*CHEK2*) [figure 3.8].

These transcriptional observations are commensurate with the apparent stalling of entry into S-phase and initiation of mitosis inferred from the G0/G1 and G2/M accumulation seen in figure 3.5. Upregulation of p21 expression by BMP6 could inhibit formation of the cyclin E-CDK2 and cyclin A-CDK2 required to drive progression into S-phase. Moreover, suppression of CHK2 impairs the activation of CDC25 phosphatases, ultimately stalling entry to mitosis. CDC25 phosphatases are responsible for removal of inhibitory an inhibitory phosphate moiety from CDK1, a reaction which induces its nuclear translocation, association with cyclin B and initiation of nuclear division(371,396).

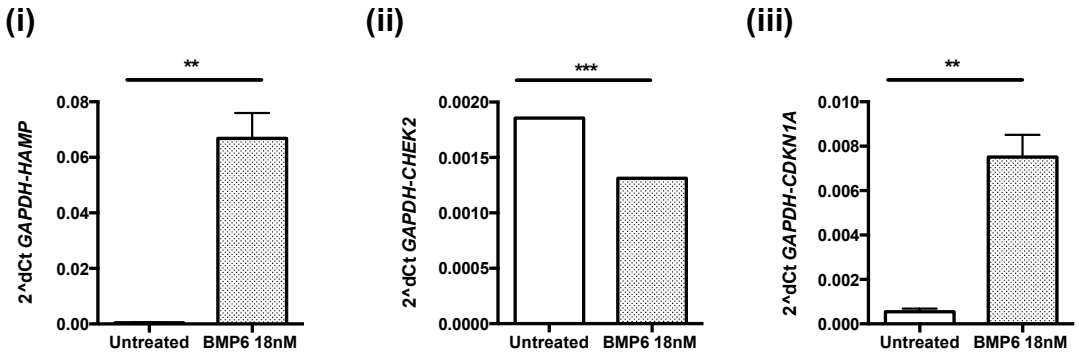


Figure 3.8: BMP6 modulates expression of cell-cycle regulatory genes in Huh7 cells

Huh7 cells were incubated with recombinant human BMP6 18 nM for 24 h, followed by RNA extraction for RT-qPCR analysis of *HAMP*, encoding the established BMP-target gene hepcidin (i); *CHEK2*, encoding CHK2 (ii); and *CDKN1A* (encoding p21) mRNA expression (iii). Data is presented as 2^ΔCt values relative to *GAPDH* (below).

HAMP expression is significantly upregulated by BMP6 (p=0.0063), whereas *CHK2* and *CDKN1A* are significantly suppressed and upregulated respectively (p=0.0009 and p=0.0051).

n=4 independent experiments in duplicate wells; analysis by paired two-tailed t-test.

3.4 Results: Extension of an anti-HCV effect to other BMP/TGFβ-type cytokines

While data from our lab demonstrates anti-HCV effects of BMP6 and BMP9 (see appendix I), and BMP7 is reported to enhance the anti-HCV effect of IFNα(344), direct anti-HCV effects of other BMP/TGFβ cytokines have, to the best of our knowledge, yet to be explored. The TGFβ superfamily consists of many members [see figure 1.3] with different receptor binding patterns and distinct downstream signalling targets. By understanding which family members might possess anti-HCV activity, we hoped to glean further information as to the nature of the antiviral effects observed so far.

3.4.1 Anti-HCV effects of recombinant BMP4, activin A and activin B

The first candidate examined for an antiviral role was BMP4, a member of the BMP2/4 subgroup of the BMP family with non-redundant roles in mesoderm formation during gastrulation, limb patterning and thymus development(397–400). BMP4 signals via a heterotetrameric complex of ALK2 or ALK3 type I BMP receptor chains in conjunction with BMPR2, ACVR2A or ACVR2B type II receptor subunits(5).

Incubation with recombinant BMP4 elicits a statistically significant antiviral effect in the OR6 replicon model at a dose of 54 nM; significant reductions in luciferase signal are not apparent at lower concentrations [figure 3.9].

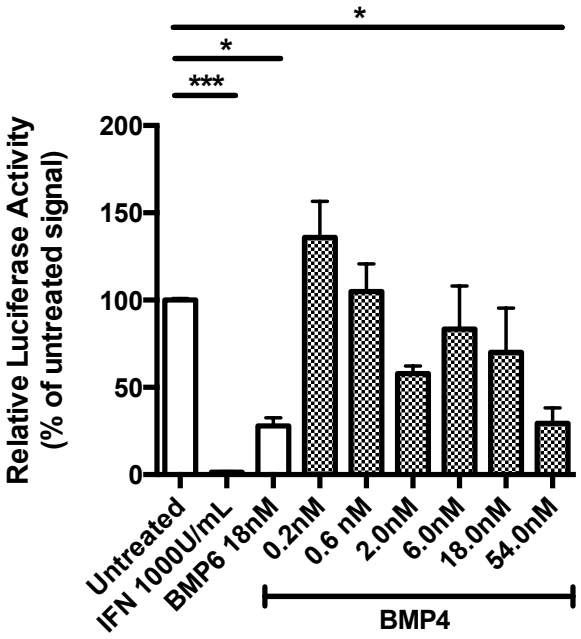


Figure 3.9: 54 nM BMP4 exerts antiviral effects in a HCV genomic replicon model

OR6 cells incubated with recombinant human IFNα-2a 1000 U/mL, recombinant human BMP6 18 nM and a titration of recombinant human BMP4. Renilla luciferase signal assayed at 72 h post-incubation; luciferase signal presented relative to the untreated condition.

n=3 independent experiments in biological triplicate; mean +SEM; analysis by ordinary one-way ANOVA followed by Bonferroni's post-test with respect to the untreated condition

Of note, all of the BMP family members shown to be antiviral, both in work from the Drakesmith lab or the published literature, are able to signal through two particular isoforms of the type I BMP receptor, namely ALK2 and ALK3. Activation of the SMAD1/5/8-linked ALK2 and ALK3 by multiple BMP ligands, including BMP2, 4, 5, 6, 7 and 9, is well validated(5). TGFβ1-3 signal via distinct receptors to activate SMAD2/3 transduction intermediates; interestingly, TGFβ is documented to promote HCV replication *in vitro*(79). However, a 2012 study by Besson-Fournier and colleagues especially piqued our interest with its description of non-canonical, SMAD1/5/8-dependent signalling by activin B(72). Addition of recombinant activin B to human hepatoma-derived HepG2 cells induces both

transcriptional upregulation of hepcidin and phosphorylation of SMAD1/5/8, the latter being inhibited by co-incubation with LDN-193189(72).

Given a precedent for ALK2/3 activation by activin B, we sought to address whether incubation with activin B, or the closely related ligand activin A, could prevent HCV replication in the OR6 model. Activin A, which shares 65% amino acid sequence homology with activin B, also classically signals via SMAD2/3-linked ALK4/5/7 type I receptors(401).

Incubation with a titration of recombinant human activin A or activin B elicits a strong, dose-dependent antiviral effect at all doses tested, with 2 nM of either activin exerting a stronger anti-HCV effect than 18 nM BMP6 [figure 3.10].

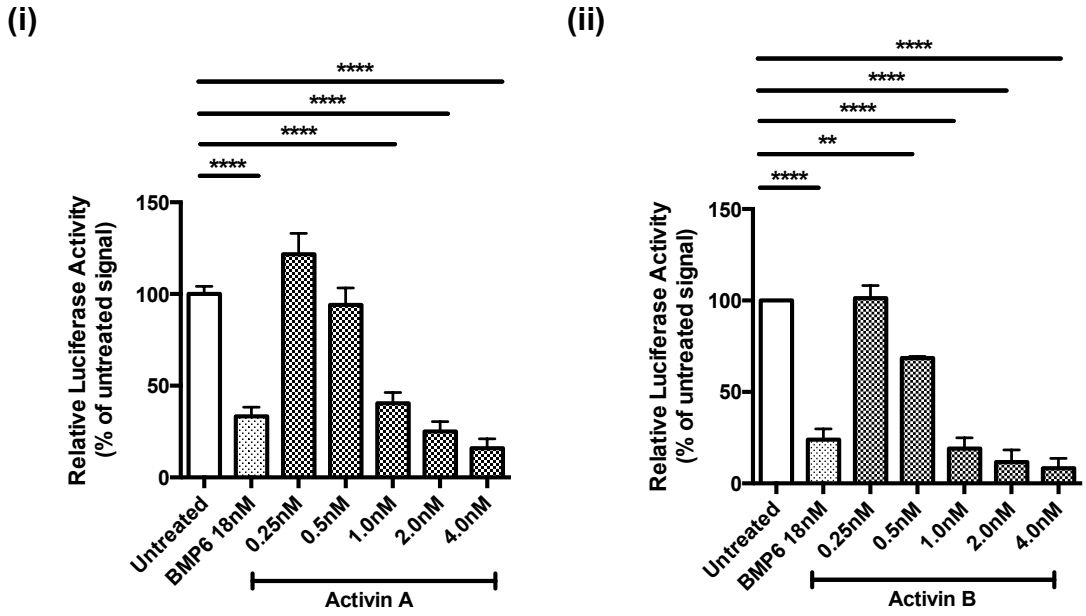


Figure 3.10: Activin A and B exert dose-dependent antiviral effects against a HCV genomic replicon

OR6 cells incubated with recombinant human BMP6 18 nM and a titration of recombinant human activin A (i) or activin B (ii). Renilla luciferase signal assayed at 72h post-incubation; luciferase signal presented relative to the untreated condition.

Both activin A and B elicit significant dose-dependent reductions in intracellular HCV content compared to untreated cells.

n=3 independent experiments conducted in triplicate wells; analysis by ordinary one-way ANOVA and Bonferroni's multiple comparisons test with respect to untreated cells.

CTG assays demonstrate that both activin A and activin B elicit a mild reduction in the ATP content of treated wells, although to a much smaller extent than 18 nM BMP6 in the same experiment [figure 3.11].

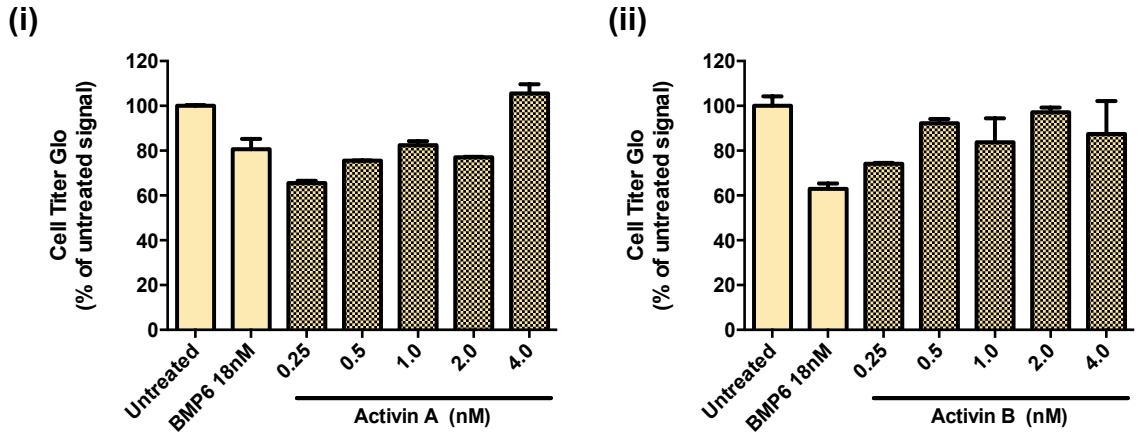


Figure 3.11: Incubation with activin A and B elicits a mild reduction in cell number/viability

OR6 cells incubated with recombinant human BMP6 18 nM and a titration of recombinant human activin A (i) or activin B (ii). Cell Titer Glo signal assayed at 72 h post-incubation; luciferase signal presented relative to the untreated condition. Similarly to BMP6, both activin A and B elicit a mild reduction in Cell Titer Glo signal compared to untreated cells.

n=1 in biological duplicate; mean+SEM presented; statistical analysis precluded due to sample size.

3.4.2 Testing the ALK2/3, IFNAR2/JAK1 and ALK4/5/7 dependency of the activins' anti-HCV effect

To assess whether ALK2/ALK3-dependent signalling is required for the antiviral effect of activin A and B, OR6 cells were co-incubated with titrating doses of both activins in the presence or absence of 100 nM LDN-193189, the small molecule inhibitor of ALK2/3 [figure 3.12]. Co-incubation with LDN-193189 abrogated the antiviral effect of 18 nM BMP6 in this model, but also significantly reduced the antiviral effect of 1.0 nM and 2.0 nM activin A and 1.0 nM activin B. From this, we can conclude that the antiviral effect of activin A and activin B are at least in part dependent upon intact signalling through the ALK2/3 isoforms of the type I BMP receptor or, conversely, that LDN-193189 might exert off-target inhibition of canonical ALK4/5/7-linked activin signalling.

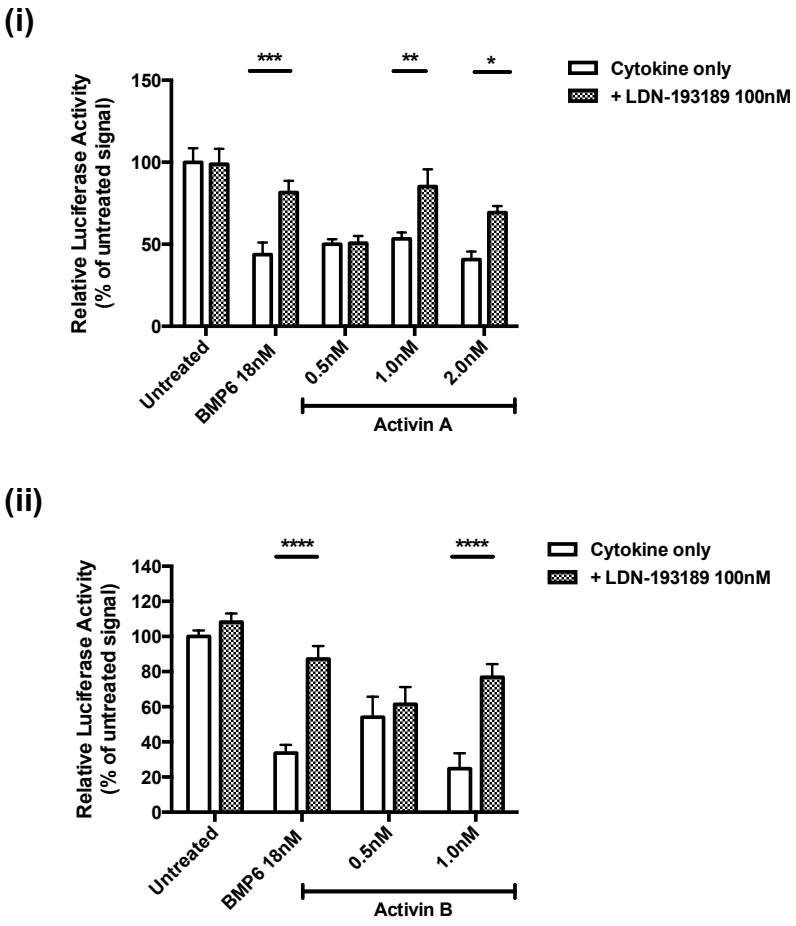


Figure 3.12: The antiviral effects of activin A and B are sensitive to the ALK2/3 type I BMP receptor inhibitor LDN-193189

OR6 cells incubated with recombinant human BMP6 18 nM or a titration of recombinant human activin A (i) or activin B (ii) in the presence or absence of 100 nM LDN-193189; assayed at 72 h post-incubation. Renilla luciferase signal presented relative to the untreated condition. The antiviral effects of both activin A and activin B are at least partially blocked in the presence of LDN-193189.

n=3 independent experiments conducted in triplicate wells; analysis by two-way ANOVA with Bonferroni's multiple comparisons test conducted between respective +/- LDN-193189 conditions.

Previous data from the Drakesmith lab suggests that the antiviral effect of BMP6 is in part independent of signalling through the type I IFN receptor. To investigate whether this IFN-independence extends to activin-mediated antiviral effects, OR6 cells were co-incubated with activin A in the presence of the pharmacological inhibitor of JAK1, ruxolitinib. In this model, ruxolitinib wholly blocks the antiviral effect of 100 U/mL IFNα, but does not impair the anti-HCV effect of either 2 nM or 6 nM activin A. In this model activin A elicits a dose-dependent reduction in CTG signal, but retains a significant antiviral effect at both doses after normalization for this decrement [figure 3.13]. From this data, we can infer that the antiviral effect of activin A is at least in part independent of type I IFN signalling.

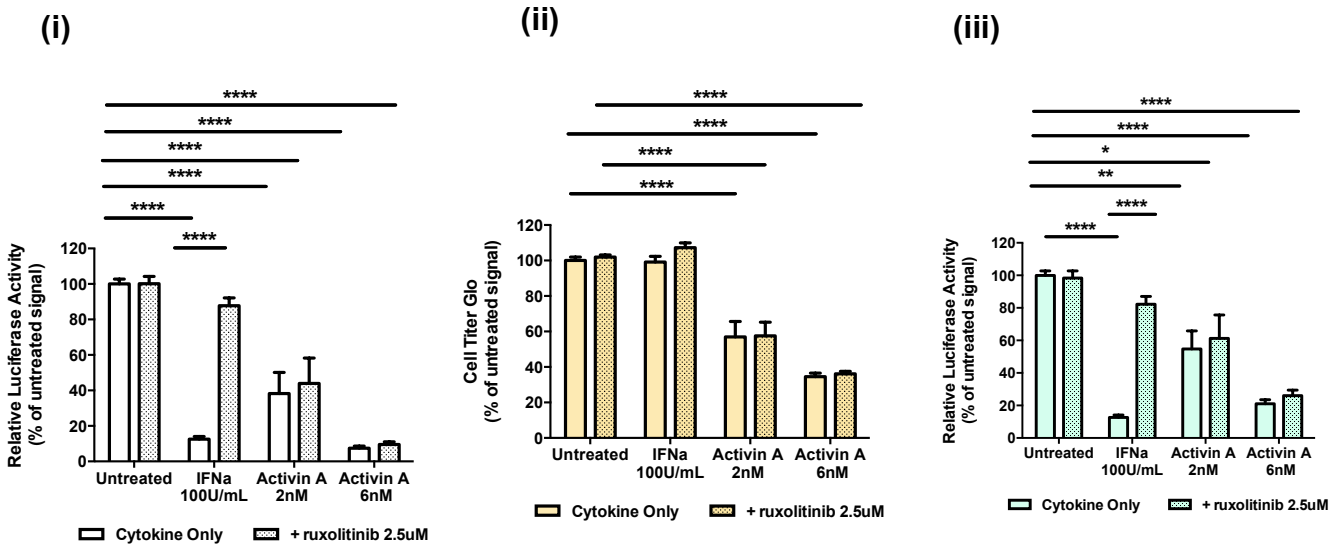


Figure 3.13: Intact type I IFN receptor function is not necessary for the anti-HCV effect of activin A

OR6 cells incubated with recombinant human IFNα-2a or recombinant human activin A in the presence or absence of 2.5 μM ruxolitinib; assayed at 72 h post-incubation for Renilla luciferase activity (i) and Cell Titer Glo (ii), with signal presented relative to the untreated condition. Renilla luciferase is normalized to Cell Titer Glo intensity in (iii).

While the antiviral effect of IFNα is abrogated in the presence of ruxolitinib, the antiviral effect of both 2 nM and 6 nM activin A is unimpaired.

n=3 independent experiments conducted in triplicate wells; analysis by two-way ANOVA with Bonferroni's multiple comparisons test conducted between all groups.

The contribution of IFN-independent components of activin and BMP6 signalling lead to speculation as to whether signalling via the ALK2/ALK3 type I BMP receptors contributes to the anti-HCV effect of recombinant IFNα. To examine this further, OR6 cells were incubated with titrating doses of IFNα in the presence or absence of LDN-193189. While LDN-193189 blocked the antiviral effect of BMP6, no effect of LDN-193189 on IFNα's anti-HCV effect was observed [figure 3.14].

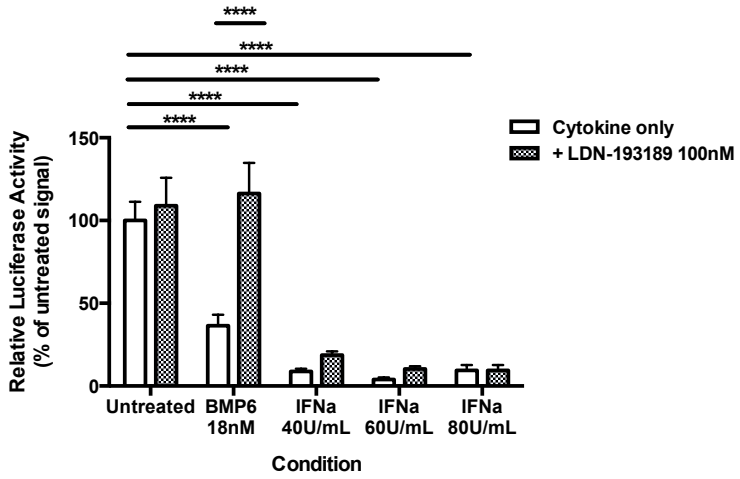


Figure 3.14: The antiviral effect of BMP6, but not that of IFNα-2a, is abrogated by the ALK2/3 type I BMP receptor inhibitor LDN-193189

OR6 cells incubated with recombinant human BMP6 18nM or a titration of recombinant human IFNα-2a in the presence or absence of 100 nM LDN-193189. Renilla luciferase signal assayed at 72 h post-incubation; luciferase signal is presented relative to the untreated condition.

n=4 independent experiments conducted in triplicate wells; analysis by ordinary one-way ANOVA with Bonferroni's multiple comparisons test between all conditions.

Of note, in the majority of the experiments conducted, 100 nM LDN-193189 alone elicited a small increase in luciferase activity, indicative of higher HCV replication. Figure 3.15 summarizes these observations. It is plausible that BMP ligands present in the culture medium or constitutively expressed by the cells restrict replication of the HCV construct and that addition of LDN-193189 ablates this basal suppression of the replicon.

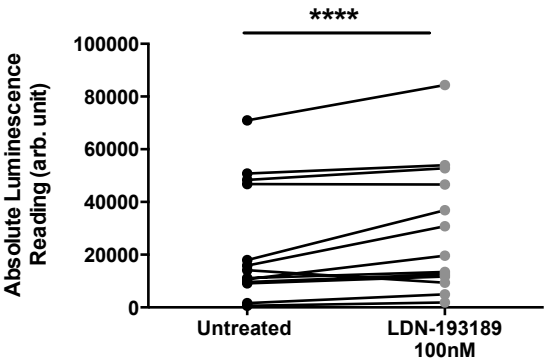


Figure 3.15: Incubation with LDN-193189 elevates intracellular HCV content in the OR6 replicon model

OR6 cells incubated with 100 nM LDN-193189 followed by assay of Renilla luciferase activity at 72 h post-incubation; luciferase signal is presented as absolute values (arbitrary units).

n=13 independent experiments conducted in triplicate wells; analysis by two-tailed t-test

3.4.3 Testing peripheral BMP family members for an antiviral effect: GDF15, GDF1 and BMP15

Having established that the antiviral effects of BMP6 and both activin A and B, but not those of IFNα, are contingent upon intact ALK2/ALK3 receptor function in this model, we were keen to determine whether more peripheral BMP family ligands that do not activate ALK2/ALK3 also exert anti-HCV effects. Three candidate ligands were selected: GDF15, GDF1 and BMP15.

GDF15, a molecule with low sequence similarity to other TGFβ ligands, is highly expressed by liver and kidney and inhibits both inflammatory macrophage activity and integrin-dependent neutrophil migration(5,402,403). Biochemical data on GDF15 is sparse and its receptor is presently unidentified. GDF1 was first cloned from a cDNA library prepared from E8.5 mouse embryos; during embryogenesis it is proposed to have a pivotal role in the patterning of left-right asymmetry, with genetic deficiency resulting in *situs inversus*(403–405). GDF1 signals via the SMAD2/3-linked ALK4 and the co-receptor Cripto in conjunction with the ACVR2A type II BMP receptor(5,406). BMP15, an essential regulator of ovarian follicle development and female fertility is, in contrast, is transduced exclusively by ALK6 (SMAD1/5/8-linked) in conjunction with the BMPR2 type II receptor(5,407).

As demonstrated by both figure 3.16 and figure 3.17, incubation with GDF15, GDF1 or BMP15 did not result in an anti-HCV effect in the OR6 model, nor did any of the ligands

elicit a reduction in CTG signal. While both ALK2 and ALK3 are expressed in both primary liver tissue and the Huh7 cell line(408,409), ALK6 expression has not been reported in the latter, therefore it is possible that BMP15 could not stimulate downstream signalling in this model.

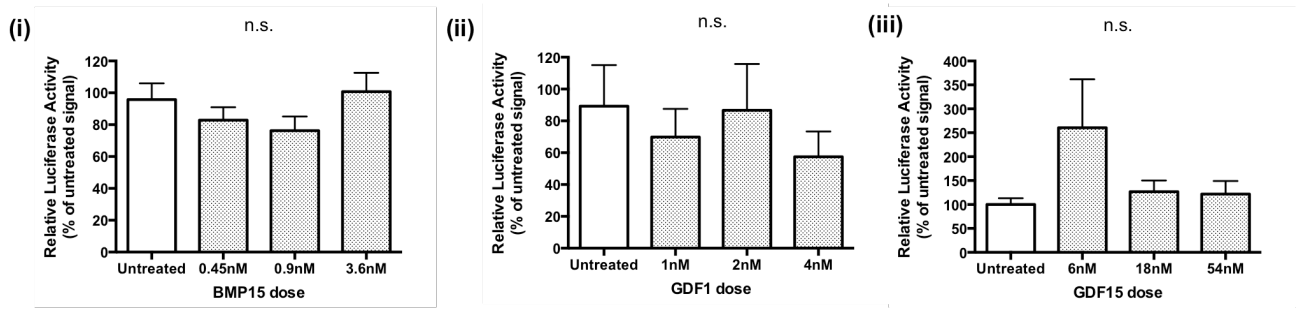


Figure 3.16: Titrated low doses of the peripheral BMP family members BMP15 and GDF1, or high-dose GDF15, are not antiviral against a HCV genomic replicon.

OR6 cells incubated with titrating doses of recombinant human BMP15 (i), GDF1 (ii) or GDF 15 (iii). Renilla luciferase signal assayed at 72 h post-incubation; luciferase signal presented relative to the untreated condition. No significant reductions in intracellular HCV were observed with any ligand.

n=3 independent experiments conducted in triplicate wells; analysis by ordinary one-way ANOVA with Bonferroni's multiple comparisons test with respect to untreated cells.

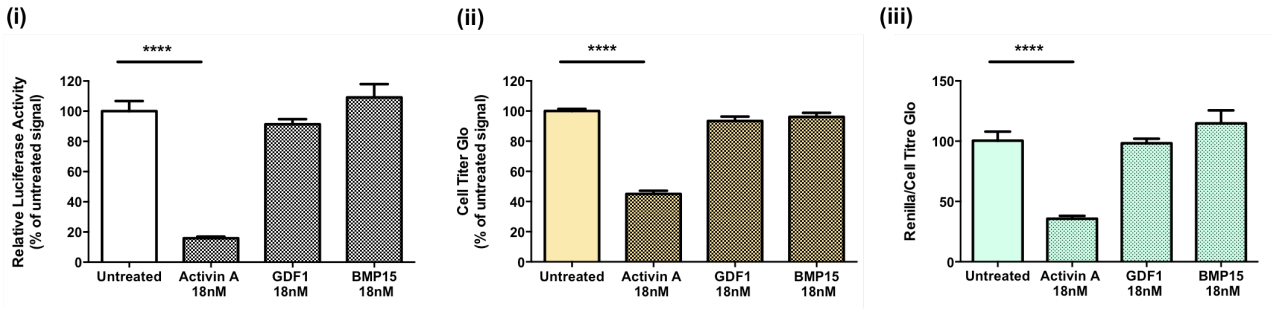


Figure 3.17: GDF1 and BMP15 18 nM do not exert anti-HCV effects in a HCV genomic replicon model, in contrast to activin A 18 nM.

OR6 cells incubated with recombinant human activin A, GDF1 and BMP15 18 nM; cells were assayed at 72 h post-incubation for Renilla luciferase (i) and Cell Titer Glo (ii), with signal presented relative to the untreated condition. Renilla luciferase is normalized to Cell Titer Glo intensity in (iii). Neither GDF1 nor BMP15 affect intracellular HCV or cell viability, whereas activin A elicits a significant decrease in intracellular HCV content, including after normalization for its reduction in cell number/viability.

n=3 independent experiments conducted in triplicate wells; analysis by ordinary one-way ANOVA and Bonferroni's multiple comparisons test with respect to untreated cells.

Of note, a moderate but statistically non-significant increase in luciferase activity was observed in the presence of 6 nM GDF15 [figure 3.16.ii]. While its receptor remains uncharacterized, GDF15 is reported to activate SMAD2/3 intracellularly. Both SMAD1/5/8, activated downstream of ALK2/ALK3 type I BMP receptors, and SMAD2/3, phosphorylated by the ALK4/5/7 type I TGFβ receptors, must complex with SMAD4 to form active

transcriptional complexes(44). As such, SMAD4 availability may be a limiting factor for the activation level of both signalling pathways. Competition between SMAD1/5/8 and SMAD2/3 signalling for SMAD4 has been reported previously. Sartori and colleagues describe enhanced recruitment of pSMAD2/3, measured by ChIP, to the promoter of target genes in the presence of the BMP inhibitor noggin *in vitro*; conversely, knockout of SMAD2/3-linked GDF5 drives increased activity of a luciferase reporter construct under the control of the *ID1* promoter, a well-characterised SMAD1/5/8-responsive gene(410).

To investigate whether endogenous competition for SMAD4 binding could modulate the antiviral effects of a given BMP ligand, OR6 cells were treated with 6 nM or 18 nM activin A in the presence or absence of a titration of SB-431542, a small-molecule inhibitor of the ALK4/5/7 type I TGFβ receptors(395) [figure 3.18]. Interestingly, SB-431542 alone exerted a dose-dependent antiviral effect. In the presence of SB-431542, however, modest but significant antiviral effects of activin A were reversed. Co-incubation with 6 nM activin A and 1 μM SB-431542 resulted in a luciferase signal approximately 2.5-fold greater than in untreated cells.

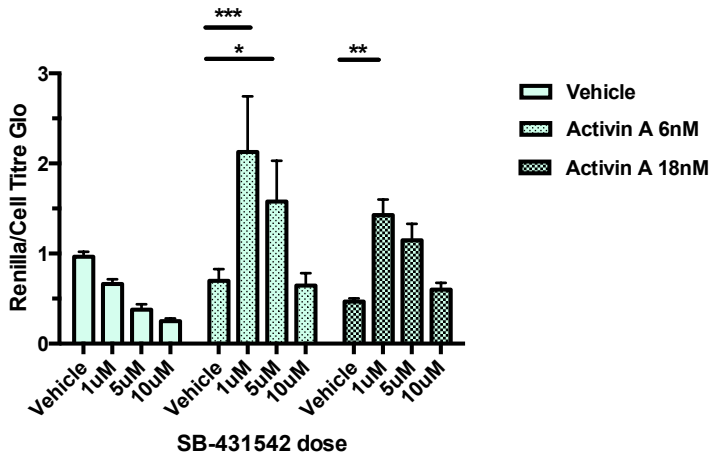


Figure 3.18: The ALK4/5/7 inhibitor SB-431542 elicits an inversely dose-dependent inhibition of activin A's anti-HCV effect

OR6 cells incubated with recombinant human activin A 6 nM or 18 nM, in the presence or absence of SB-431542; cells assayed at 72 h post-incubation for Renilla luciferase and Cell Titer Glo, with signal presented relative to the untreated condition, with Renilla signal normalized to Cell Titer Glo intensity.

A titration of SB-431542 alone shows a strong trend towards a reduction in intracellular HCV, whereas co-incubation with 1 μM SB-431542 abrogates any antiviral effect of activin A 6 nM or 18 nM.

n=3 independent experiments conducted in triplicate wells; analysis by two-way ANOVA and Bonferroni's multiple comparisons test conducted with respect to untreated cells for each group of activin A doses.

3.4.4 The anti-HCV effect of ribavirin is not dependent upon type I BMP receptor activity

In the OR6 model, incubation with a titration of ribavirin for 48 h elicits a dose-dependent reduction in intracellular HCV content [figure 3.1]. While co-incubation with LDN-193189 ablates the antiviral effect of BMP6, it does not impair the activity of IFNα nor ribavirin, implying that intact type I BMP receptor function is not required for either of their antiviral effects [figure 3.19].

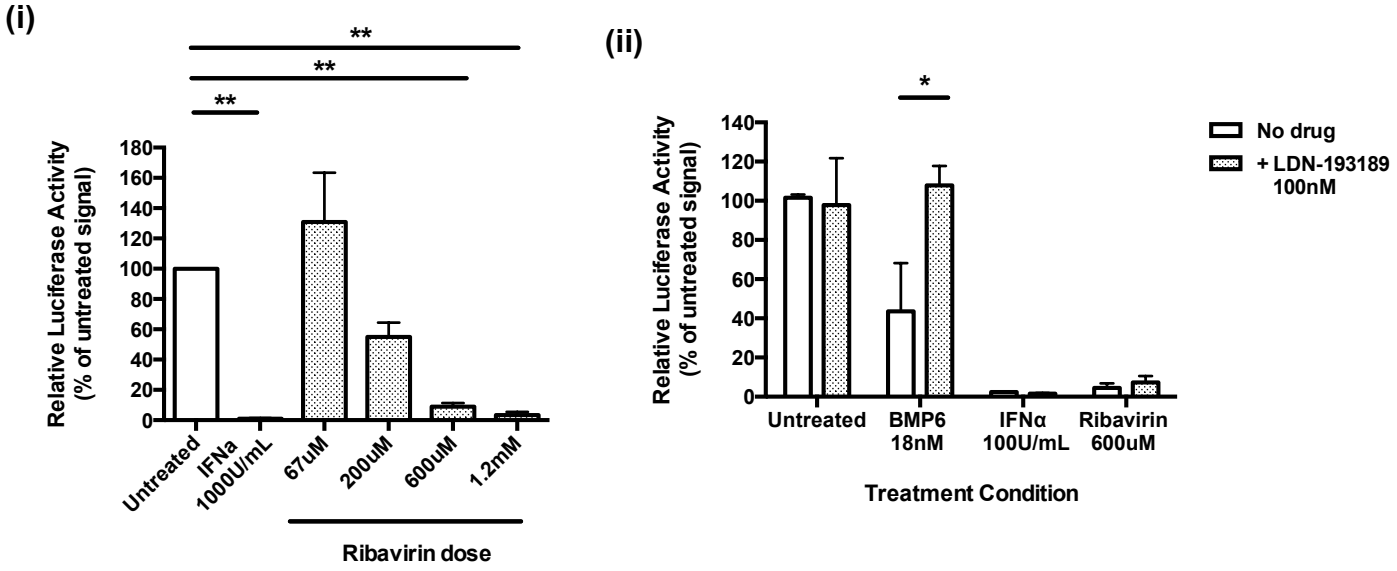


Figure 3.19: The anti-HCV effect of ribavirin does not require intact function of the ALK2/3 type I BMP receptors

In (i) OR6 cells were incubated with IFNα 1000 U/mL or a titration of ribavirin. Renilla luciferase signal assayed at 72 h post-incubation; luciferase signal is presented relative to the untreated condition. Ribavirin elicits a significant dose-dependent reduction in intracellular HCV content, akin to the potent antiviral effect of IFNα. In (ii), OR6 cells were incubated with either BMP6 18nM, IFNα 100 U/mL or 600 uM ribavirin, in the presence or absence of the type I BMP receptor antagonist LDN-193189. At 72h post-incubation, LDN-193189 ablates the antiviral effect of BMP6, but has no effect on that of IFNα nor ribavirin.

n=3 in biological triplicate; mean+SEM. Statistical analysis of (i) by ordinary one-way ANOVA and Bonferroni's multiple comparisons test with respect to untreated cells; analysis of (ii) by two-way ANOVA and Bonferroni's multiple comparisons test conducted between respective +/- LDN-193189 conditions.

3.5 Summary and discussion

The data presented in this chapter provide evidence that the IFN-dependent component of BMP6's antiviral effect in the OR6 model may be due, at least in part, to its modulation of cell cycle progression. Furthermore, the data also suggest that antiviral effect extend to multiple members of the TGFβ superfamily, contingent upon their ability to activate the ALK2 and ALK3 isoforms of the type I BMP receptor.

Interpretation of the observations presented here is clouded by the absence of necessary controls for both the biochemical activity of the drugs we have used to modulate BMP/IFN signalling and the expression levels of the receptors and intracellular signal transduction apparatus through which they are proposed to signal. Subsequent experiments must seek to validate the biochemical activity of LDN-193189 in OR6 cells, preferably via Western blots for intracellular phosphorylated SMAD1/5/8 in the presence of the drug alone and in the presence of an agonist such as BMP6. Additionally, we need to verify the expression of the ALK2/3 type I BMP receptor isoforms in OR6 cells, in addition to the surface levels of ALK6 and ALK4 (through which BMP15 and GDF1 are proposed to signal, respectively). This could be achieved either via immunoblot of lysed cells (for total expression) or via immunohistochemical staining and confocal microscopy for specific surface expression. Similarly, biochemical activity of ruxolitinib must also be validated, in this case via staining for phosphorylated IRF3 in OR6 cells exposed to both exogenous type I IFN and the drug. Additionally, replication of the results obtained with ruxolitinib instead in the presence of an anti-IFNAR2 neutralising antibody would lend further credence to our observations.

RNAi knockdown or ablation of type I BMP receptor genes via CRISPR/Cas9 gene editing would further increase the robustness of the association between ALK2/3 receptor ligation and induction of anti-HCV effects.

In addition to utilising luciferase output as a measure of intracellular HCV content in OR6 cells, it would be more informative to quantitate intracellular HCV RNA by RT-qPCR in concomitantly treated wells. Our present strategy for assessment of HCV content relies upon normalization of the luciferase signal to intracellular ATP content assayed via the Cell Titer Glo proprietary assay system. RT-qPCR measurements (or, alternatively, immunostaining for HCV proteins, such as NS5A) would permit quantification of HCV level on a "per cell" basis, rather than as an aggregate across a whole well, as presented here.

Moreover, this would circumvent the limitations of the Cell Titer Glo assay for the measurement of, and subsequent normalization to, cell number: namely that it cannot sensitively discriminate between changes in cell number versus alterations in the metabolic state of the cells examined, nor can it quantify the levels of apoptosis occurring under exposure to particular experimental conditions. Inclusion of a simple apoptosis assay in parallel, for example the colorimetric MTT assay, would enable us to establish whether any of the ligands tested for an antiviral effect in fact promoted apoptotic death of the OR6 cells.

Incubation of Huh7 cells with BMP6 results in a reduction in the percentage of cells in S-phase and accumulation of cells at the G0/G1 and G2/M checkpoints, mimicking the effects of the cytostatic drug UCN-01. Due to the high rates of ribonucleotide and subsequent deoxyribonucleotide biosynthesis(411), S phase offers an environment arguably more permissive to viral genomic replication, than either G1 or G2. Indeed, disruption of cell-cycle progression by UCN-01 inhibits replication of the OR6 HCV replicon independently of its effects on cell number. Ideally, the effects of BMP6 on cell cycle phase distribution in the OR6 cell line should also be investigated, lest its actions be disrupted by the presence of viral proteins. Given that HCV NS2 is proposed to promote S-phase arrest(385), the phase distribution of untreated OR6 cells might also be different to that of the parent Huh7 cell line at baseline.

Based on our data showing that the antiviral effects of activin A and B can also be abrogated by co-incubation with LDN-193189, we have assumed that the mechanistic basis of their antiviral effect is similar to that of BMP6. To verify this empirically, we need to repeat our cell cycle experiments in the presence of recombinant activin A and B.

Of relevance, the cytostatic effects of IFNα are well described and underlie its clinical use in malignant disease(167,168). These cytostatic effects may also contribute to type I IFN's antiviral activity. Ideally, future experiments should seek to optimize our BrdU/PI assay to assess whether co-incubation with recombinant BMP6 and IFNα enhances their respective effects on the cell cycle.

The data presented in this chapter show that incubation of Huh7 cells with recombinant BMP6 is sufficient both to reduce *CHEK2* expression and to upregulate *CDKN1A* (which encodes the CDKI p21). For more robust conclusions to be drawn, however, these observations must be recapitulated at the level of protein expression, which had not been examined in this study. Both of these observations are consistent with induction of G0/G1 and G2/M arrest, as proposed in section 3.3.1. Further work should validate whether these transcriptional changes are recapitulated at the protein level and, in the case of CHK2, phosphorylation status. Moreover, the results of our previous microarray study (figure 3.1) imply that activation of the ATM kinase upstream of CHK2 is modulated by BMP6 treatment. To validate this, levels of phosphorylated ATM could be quantified by immunoblot of BMP6-treated Huh7 or OR6 cell lysates.

In light of our interest in it's anti-HCV functions, a more appropriate cell line for the study of BMP6's cytostatic effects would be the cured-OR6 cell line described in section 2.1.2. The

OR6 cells are physiologically distinct from the Huh7 line, therefore the IFN-treated cured-OR6 cells represent a better comparator for subsequent studies into the biochemical effects and mechanistic properties of antiviral BMP and activin family ligands.

In addition to its role in the regulation of cell cycle progression, p21 has an emerging function as a regulator of intracellular nucleotide pools, offering a further possible mechanism for modulation of viral replication by BMP signalling.

Suppression of HIV-1 replication in elite controllers - seropositive individuals with undetectable viral replication in CD4+ lymphocytes in the absence of antiretroviral therapy - is associated with elevated p21 expression(412). siRNA knockdown of p21 in CD4+ T cells results in significantly increased synthesis of HIV-1 LTR transcripts, DNA integration and mRNA transcription. Moreover, the effects of p21 silencing were more pronounced in cells from elite controllers versus HIV-1 negative donors, consistent with the enrichment for high p21 expression in the former sample(412).

The mechanistic basis for this effect is controversial. It has been suggested that high p21 expression downregulates expression of the E2F1 transcription factor required for the induction of the ribonucleotide reductase subunit 2 (RNR2), resulting in reduced dNTP synthesis and restriction of viral genomic replication(413). This effect is reportedly independent of p21's interaction with the Rb protein, which sequesters E2F1 in quiescent cells(413). Other reports suggest that the anti-replication effect of p21 is mediated by its interaction with the deoxyribonucleotide triphosphohydrolase SAMHD1, an extensively characterized HIV-1 restriction factor(414). Inhibition of CDK1-cyclin A complexes by p21 reportedly reduces inhibitory phosphorylation of SAMHD1 Thr592, increasing net nucleotide hydrolysis and creating an environment less favourable to viral replication(414).

Given that BMP6 robustly induces p21 expression, the possibility that a component of its antiviral effect is mediated by regulation of intracellular dNTP pools is ripe for investigation. While this effect would obviously not be applicable to HCV replication, being an ssRNA virus, in chapter 7 we describe an antiviral effect of BMP6 and activin A against the DNA virus HBV. Given the published observation that recombinant BMP2 inhibits replication of the DNA virus MHV-68 murine gammaherpesvirus(351), BMP-p21-dNTP interactions could be a fruitful avenue to explore in the context of the DNA virus infection. In this project, quantification of intracellular dNTP concentration in the presence of UCN-01 was attempted, albeit technically unsuccessfully, using a TaqMan-based primer-extension approach described by Wilson and colleagues(415).

The second half of this chapter presents evidence that an anti-HCV effect extends to multiple members of both the BMP and broader TGFβ cytokine families, and segregates with the ability of a ligand to activate the ALK2 and ALK3 isoforms of the type I BMP receptor. A caveat of these observations is that we have not obtained an independent positive control validating the bioactivity of the recombinant proteins utilized. While the suppliers have validated their activity, we have not obtained independent corroboration of their effects.

Testing a larger selection of BMP and TGFβ-type ligands for an anti-HCV effect in the presence or absence of LDN-193189 would provide additional support to our hypothesis that their antiviral effect is ALK2/3 dependent. However, the high cost of recombinant cytokines precluded more extensive screening. As such, our inference relies on the highly selective inhibition of the ALK2/3 receptors by LDN-193189.

The design of isoform-specific inhibitors of the type I BMP and TGFβ receptors is challenging. Both the type I BMP and TGFβ receptors share a high degree of sequence homology, especially in the catalytic kinase domain: ALK3 and ALK5, associated with BMP and TGFβ signalling respectively, share 66% sequence identity(32). Within the type I BMP receptors, the kinase domains of ALK3 and ALK6 are 86% homologous(416).

LDN-193189 is described as a potent and selective ALK2/ALK3 inhibitor. The molecule inhibits a luciferase reporter driven by constitutively active ALK2 and ALK3 with IC_{50} values of 5 nM and 30 nM respectively, approximately 90-fold more potently than its parent molecule dorsomorphin(40,63). However, while dorsomorphin does not modulate SMAD2/3-linked ALK4/ALK5 signalling, high dose LDN-19389 is able to inhibit both of these kinases, albeit with IC_{50} values in the micromolar range (417). Due to the cytotoxic effects of LDN-193189 in OR6 cells at higher doses [data not shown], inhibition of SMAD2/3-linked receptors is unlikely to be biologically relevant in our study, which used LDN-193189 at 100 nM.

Despite its optimized blockade of ALK2 and ALK3, LDN-193189 exerts off-target inhibition of multiple unrelated kinases, including the VEGF receptor and calmodulin kinases (417). In a comprehensive screen of BMP/TGFβ inhibitors against the human kinome, the TNFα receptor-associated kinase RIPK2 and the glucose hexokinase GCK were relatively strongly inhibited by LDN-193189, with IC_{50} concentrations of 0.025 μM and 0.08 μM respectively, values approaching those described for ALK2 and ALK3 in the same study (417). Second generation LDN-193189 derivatives have been developed, including a molecule with 1 log

greater specificity for the ALK2 versus ALK3 receptor isoform *in vitro*, namely LDN-212854(416).

K02288, an ATP-mimetic with ALK2 inhibitory properties similar to LDN-193189 has also been described(418). Intriguingly, this compound bears a striking structural resemblance to the scaffold of a novel antimalarial compound MMV390048(419). In preliminary *in vivo* efficacy studies a single oral dose of MMV390048 is sufficient to eradicate *Plasmodium berghei* infection in mice; presently the drug is undergoing phase I safety and pharmacokinetic profiling in humans (trial I.D. NCT02281344). Malaria infection is associated with transcriptional upregulation of the iron-regulatory hormone hepcidin, resulting in anaemia(420). As hepcidin is a well-characterized SMAD1/5/8-stimulated gene(341,348), it would be intriguing to explore whether MMV390048 manipulates this BMP-associated aspect of malarial pathology, or, alternatively, whether MMV390048 inhibits viral infections *in vitro* via a BMP-linked mechanism, akin to our observations with LDN-193189.

Overexpression of constitutively active ALK2 or ALK3 in OR6 cells offers an alternative strategy to determine whether activation of these receptor isoforms is sufficient for an anti-HCV effect. In transgenic mice, the ALK2 Q207D mutation recapitulates the phenotype of the R206H mutation responsible for sporadic and inherited FOP in humans(421). Both mutations affect the glycine-serine rich extracellular region of ALK2 and impair its association with the extracellular FKBP12 protein, which acts to dampen leaky activation of ALK2 in the absence of ligand. The resultant hyperactivation of mutant ALK2 culminates in the heterotopic ossification and chondrogenesis characteristic of FOP(422–424). Ectopic overexpression of a Q207D or R206H ALK2 constructs in the OR6 model would be of significant future interest.

Intriguingly, FKBP12 is a target of the widely prescribed immunosuppressive drug tacrolimus (FK506). FK506-FKBP12 complexes competitively inhibit the phosphatase calcineurin, preventing dephosphorylation and subsequent activation of the transcription factor NFAT. Inhibition of NFAT ultimately blocks IL-2 production by T-lymphocytes, resulting in profound immunosuppression(425–427). Independently of this activity, FK506 is able to induce osteogenic differentiation in mesenchymal cell lines, via a mechanism sensitive to inhibition by SMAD6(428). Potentiation of BMP signalling by FK506 has also been demonstrated in murine models of pulmonary arterial hypertension (PAH), familial forms of which result from mutations in the BMPR2 type II BMP receptor(429). *In vitro*, FK506 liberated FKBP12 from ALK1, ALK2 and ALK3 receptors and enhanced induction of the

SMAD1/5/8-target gene *ID1*; similar induction of BMP-target genes by FK506, and amelioration of PAH, were observed in mouse models of the disease(429). As such, incubation of OR6 cells with FK506 would offer a third approach to determine whether activation of ALK2/ALK3 signalling is sufficient for an anti-HCV effect.

In conclusion, our data suggest that BMP and activin ligands exert anti-HCV effects *in vitro* via signalling through the ALK2/ALK3 type I BMP receptor. The IFN-independent component of this effect is mediated at least in part by disruption of cell cycle progression.

These antiviral data fit into a broader context of host-pathogen interactions in which BMP/SMAD signalling is not only antagonized by viral infections, but in which polymorphisms in the pathway also correlate with responses to antiviral therapies. These observations are reminiscent of the complex virus-host interplay regulating the type I IFN response. As such, we decided to investigate whether another facet of innate antiviral defence is applicable to BMP/activin signalling: induction in response to pathogen sensing. This is the focus of chapter 4.

Chapter 4

Activin A induction by innate immune and infectious stimuli

4.1 Introduction: pattern recognition receptors and innate immune signalling

First hypothesized by Charles Janeway (430), germline encoded pattern recognition receptors (PRR) survey the extracellular and cytosolic milieu for microbial pathogens, relying upon detection of conserved non-self structural motifs. Sensing of these pathogen-associated molecular patterns (PAMP) by PRRs induces type I/III IFN and pro-inflammatory cytokines, in addition to modulating the adaptive immune response (431,432).

This introduction summarizes the biology of the three principal PRR families implicated in viral sensing, namely the RIG-I-like receptors (RLR), the Toll-like receptors (TLR) [summarized by figure 4.1] and the cGAS-STING axis [figure 4.2]. This will serve as a background to the subsequent experimental studies addressing whether PRR ligation (in the context of viral infection) leads to induction of activins or BMPs.

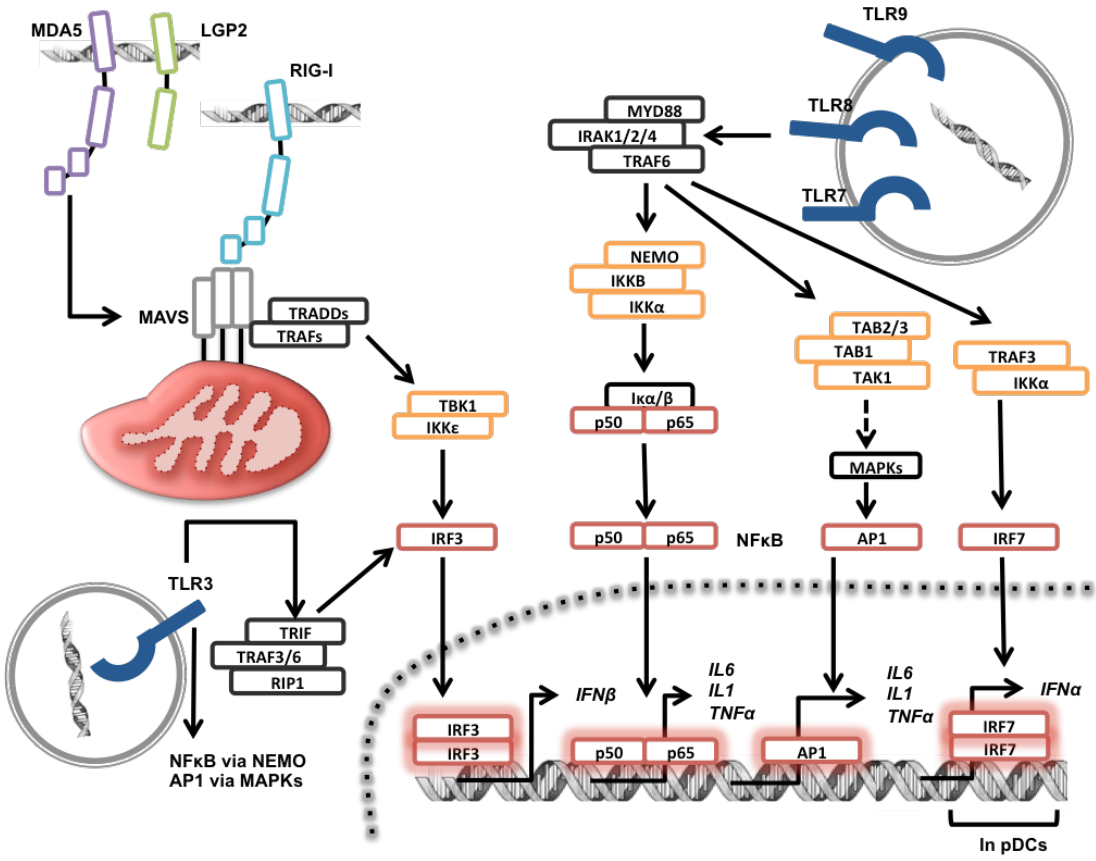


Figure 4.1: Viral nucleic acid sensing by RLR and TLR family members: downstream signal transduction pathways

Ligation of cytosolic RLRs and endosomal TLRs elicits activation of diverse signal transduction pathways in a cell-type and stimulus-dependent manner. Pathways ultimately converge upon transcription factors including IRF3, IRF7, NF κ B and AP1, resulting in expression of pro-inflammatory cytokines and type I IFN.

Adapted from Wu and Chen, Annual Reviews Immunology (2011) and Hornung, V Immunity (2014)

4.1.1 RIG-I-like receptors: biology and function

4.1.1.2 RIG-I

Retinoic acid inducible gene 1 (RIG-I), the prototypic RLR, was identified by screening a cDNA expression library for clones enhancing activation of IRF-reporter construct (433). RIG-I, encoded by *DDX58*, is a multidomain protein composed of a C-terminal domain, an ATP-dependent DExD/H-box helicase and two N-terminal caspase activation and recruitment domains (CARD). While the CARD domains are required for induction of downstream signalling, the helicase domain is indispensible for virus detection, with truncated helicase constructs eliciting dominant negative inhibition of IFNβ induction (433).

RIG-I is preferentially activated by a 5' triphosphate moiety (5'ppp) associated with various non-self RNA structures, including dsRNA and ssRNA encoding polyU/UC tracts. Hornung and colleagues first described the requirement for a direct interaction with 5'ppp in RIG-I activation (434). In eukaryotic cells, newly transcribed RNAs are rapidly capped by 7-methyl-guanosine; hence a 5'ppp is a potent non-self signature. Despite suggestions that modification of the 5'ppp motif attenuates RIG-I signalling (434), subsequent studies have revealed that 5' diphosphate (5'pp) moieties are sufficient to activate RIG-I in response to reovirus genomic dsRNA (435).

In addition to the terminal phosphate groups, composition of the RNA ligand is a key determinant of RIG-I activation. RNA duplexes as short as 23 nucleotides are recognized by RIG-I, with blunt ended molecules eliciting stronger responses than those containing 5' or 3' overhangs (436). Short complimentary regions or panhandle structures are required for RIG-I induction in response to 5'ppp ssRNA viral genomes (437). Interactions with nucleocapsid proteins also modulate the sensitivity of RIG-I to native viral RNA (438). For HCV detection, a polyU/UC tract within the RNA ligand is an absolute requirement for RIG-I activation: deletion of this motif abrogates RIG-I signalling (288).

RIG-I is also activated by 5'ppp RNA duplexes generated during transcription of exogenous poly(dA:dT) templates by RNA Pol III (439,440). Small self-RNAs produced by the host endoribonuclease RNaseL in the presence of 2'5'-OAS can also amplify pre-existing RIG-I activation (441).

Crystal structures suggest that an RNA ligand's terminal α and β phosphate groups intercalate into a basic groove in the RIG-I CTD (442,443), initiating an ATP-dependent conformational

change that relieves repressive intramolecular interactions between the CARD and helicase domains. Activated RIG-I adopts a more condensed conformation, "capping" the 5'ppp terminus of the RNA ligand (444,445).

RIG-I signalling is extensively modulated by ubiquitination and phosphorylation. Associations between the RIG-I CARD domains and unanchored K63-linked chains produced by TRIM25 stabilise the RIG-I/MAVS tetramer (446,447), whereas conjugation of K63 ubiquitin chains to the RIG-I CTD is proposed to release RIG-I from autorepression (448). RIG-I ubiquitination is itself regulated by a number of ubiquitin serine proteases (USP). Deletion of K63-targeting USP21 and USP3 can potentiate IFNβ induction in response to RNA virus infection (449,450). In contrast, deletion of USP4, which specifically degrades K48-linked chains, destabilizes RIG-I expression (451).

In terms of phosphorylation status, removal of inhibitory phosphate moieties from the RIG-I CARD domains by PP1α and PP1γ is required for maximal IFNβ induction in response to diverse RNA virus infections *in vitro* (452).

4.1.1.3 MDA5

Melanoma differentiation associated factor 5, encoded by *IFIH1*, is a paralogue of RIG-I, sharing both its domain architecture and a common downstream signalling pathway. Initially identified as a regulator of growth and apoptosis in transformed cells (453), its role in the sensing of RNA viruses was revealed by Andrejeva and colleagues through their studies of the paramyxovirus V protein, a highly conserved MDA5 antagonist (454). Similarly to RIG-I, MDA5 expression is maintained at low levels is resting cells, but is rapidly induced by both type I IFN and direct IRF3 activation (453,455,456). Unlike RIG-I, MDA5 is not regulated by autorepressive intramolecular interactions (457).

Picornavirus dsRNA replication intermediates were the first characterized MDA5 PAMPs, in addition to the synthetic nucleic acid poly(I:C) (458). Subsequent studies have demonstrated that MDA5 activation in response to dsRNA is length-dependent, with longer nucleic acids eliciting stronger signalling (459).

In contrast to RIG-I, the MDA5 CTD is aligned parallel to the axis of the target dsRNA; while this orientation prevents MDA5 from "capping" its ligand at the 5' end, it allows multiple MDA5 proteins to assemble along dsRNA as a tightly-packed filamentous array (460,461). The MDA5 array is in perpetual flux, rapidly assembling and disassembling in

response to the prevailing ATP availability (462). Similarly to RIG-I, MDA5 activation is also regulated by its phosphorylation status (452).

4.1.1.4 LGP2

The precise function of the third member of the RLR family, laboratory of genetics and physiology 2 (LGP2), remains enigmatic. LGP2, encoded by *DHX58*, contains a CTD and intact helicase but lacks an N-terminal CARD. Crystal structures of LGP2 reveal strong homology between the RIG-I and LGP2 CTD (463).

Initial studies characterized LGP2 as a dominant negative inhibitor of RIG-I and MDA5 *in vitro* (455). *In vivo*, *Lgp2*-/- mice are resistant to lethal challenge with vesicular stomatitis virus (VSV), consistent a role as a negative regulator of RIG-I (464). However, the same authors also demonstrate that IFNβ induction in response to EMCV infection, a virus primarily sensed by MDA5, is blunted in *Lgp2-/-* mice (464). Moreover, immunoprecipitation of LGP2-RNA complexes in EMCV-infected cells enriches for antisense RNA encoding the EMCV L protein, a strong MDA5-stimulus. Together, these observations point towards positive regulation of MDA5 by LGP2 (465).

4.1.1.5 RLR-MAVS interactions

After ligand binding, the liberated CARD domains of both RIG-I and MDA5 are available to interact with the adaptor mitochondrial antiviral signalling protein (MAVS; also known as VISA/IPS-1/CARDIF) (297,466–468). MAVS, the essential host factor required for IFN-induction by RLRs (469,470), is a transmembrane protein localized to the mitochondrial, peroxisome and mitochondria-associated ER membranes (471,472).

In addition to its C-terminal transmembrane domain, MAVS includes three TRAF binding motifs (TBM), required for recruitment of regulatory E3 ubiquitin ligases, a central proline-rich region, and an N-terminal CARD domain (473). CARD-CARD interactions between RLR proteins and MAVS drive its oligomerization. Activated MAVS oligomers, which show prion-like structure properties, recruit multiple adaptor proteins, including multiple TRAF family members, producing a supramolecular ‘MAVS signalosome’ (473,474). This higher-order structure stimulates multiple downstream kinase cascades, including IKK and TBK1 pathways, culminating in phosphorylation and nuclear translocation of IRF3, IRF7 and NFκB (473,474).

Unlike the RLR family, MAVS is not induced by type I IFN (475). Negative regulation can occur by transcription of splice variants with restricted biological functions (476). In terms of translational regulation, the bicistronic *MAVS* mRNA encodes both a full-length 72 kDa protein and 50 kDa truncated variant (miniMAVS), the latter capable of inhibiting IFN induction by full-length MAVS in response to SeV infection (477).

4.1.2 Toll-like receptors: biology and function

Toll-like receptors (TLR), named for their homology to the Drosophila Toll proteins, are the most extensively characterized family of pattern recognition receptors (123). Of the 10 human TLR, 4 are sensitive to non-self nucleic acids, namely TLR3, TLR7, TLR8 and TLR9. In mice, TLR13 detects bacterial 26S ribosomal RNA. These nucleic acid-sensitive TLR are distinguished from other family members by virtue of their robust induction of type I IFN, in addition to the repertoire of pro-inflammatory cytokines common to all TLR signalling pathways (123).

After translation, TLR3 and TLR7-9 are retained at the ER and trafficked to the endosomes via the Golgi body, through a process regulated by the chaperone protein UNC93B1 (478). Post-translational modifications by cathepsins, furin-like convertases and asparagine endopeptidase are required for full-strength TLR signalling, unencumbered by inhibitory portions of their ectodomains (479,480).

Structurally, TLRs consist of a single protein, incorporating an ectodomain conferring ligand specificity, a transmembrane region and a cytosolic Toll/IL-1 receptor (TIR). The TIR interacts with the adaptor proteins MYD88, in the case of TLR7, TLR8 and TLR9, and TRIF, for TLR3, stimulating signalling via IRAK, IKK and TBK1 pathways and ultimate activation of IRF3, IRF7, NFκB and AP1 transcriptional programs (123,481).

In the endosome TLRs are exposed to diverse non-self nucleic acid stimuli. TLR9 senses CpG-rich DNA motifs present in bacterial DNA and the genomes of DNA viruses (482–484).

TLR3, initially identified as a sensor of the synthetic dsRNA poly(I:C) (485), senses viral dsRNA generated either as replication intermediates or from palindromic products of viral transcription (479).

TLR7 and 8, in contrast, sense ssRNA molecules (486,487). Host RNA is unlikely to enter the endolysosomal compartment due to its degradation by cytosolic endoribonucleases. The

acidic endosomal environment, however, promotes disintegration of internalized viral particles, exposing their ssRNA genomes to TLR7/8 (123).

Additionally, viral envelope glycoproteins can be sensed by cell-surface TLRs. Notably, the respiratory syncytial virus (RSV) fusion protein and measles virus haemagglutinin activate the MYD88-linked receptors TLR2 and TLR4 respectively (123).

In terms of expression patterns, TLR3 is IFN-inducible and is expressed by a large number of cells, including various epithelia, multiple glial subtypes and mDC. In the latter, TLR3 can enhance cytotoxic T lymphocyte responses by augmenting cross-presentation of viral antigens (123). Expression of TLR7-9 is highest in the spleen, macrophages and peripheral blood mononuclear cells, with especially high expression of TLR7 by CD14+ monocytes and TLR9 by CD19+ B lymphocytes (488).

4.1.3 cGAS-STING axis and the innate response to cytosolic DNA

Despite a raft of candidates, the sensor responsible for type I IFN induction in response to cytosolic DNA remained elusive until the identification of the cyclic GMP-AMP synthase (cGAS) in 2013 (489).

In contrast, activation of the inflammasome by cytosolic DNA has been extensively characterized. During inflammasome activation, detection of cytosolic DNA by an intracellular PRR promotes its association with the ASC adaptor protein, leading to the recruitment and activation of pro-caspase 1. In turn, caspase-1 cleaves pro-IL-1β and pro-Il-18, culminating in the extracellular release of bioactive pro-inflammatory cytokines (490). PRR domains implicated in the response to viral DNA include AIM2, required for inflammasome activation by vaccinia and mCMV infection (491), and IFI16, a sensor indispensible for inflammasome responses to herpesviruses including KSHV and HSV1 (492).

Five years before the cloning of cGAS, several groups independently identified the ER-associated adaptor protein STING as an essential mediator of the type I IFN response to cytosolic DNA (493–495). *Sting* -/- mice are prone to lethal infection with HSV1 and mount impaired adaptive responses after DNA immunization (496).

Curiously, crystal structures reveal that STING lacks a DNA-binding site. Instead, the STING homodimer is bound at its C-terminus by a 2'-5'-linked cyclic dinucleotide, a secondary messenger commonly found in prokaryotes and archea (124,497,498).

These disparate observations were united upon the discovery of cGAS as the primary sensor of cytosolic DNA. cGAS is ligated by B-form DNA in a sequence-independent manner, mostly through interactions between the DNA ribose-phosphate backbone and an array of positive residues (499). DNA binding induces a conformational switch and activates cGAS' intrinsic nucleotidyltransferase, resulting in synthesis of a novel heterocyclic dinucleotide isoform, 2'3'-cGMP-AMP (cGAMP). cGAMP diffuses to the ER and binds STING, inducing its translocation to the perinuclear Golgi apparatus where it interacts with TBK1 to induce IRF3 phosphorylation (124) [figure 4.2].

cGas -/- mice fail to mount a type I IFN response to DNA virus infections and rapidly succumb to lethal HSV1 infection. The contribution of cGAS signalling to restriction of RNA virus infection remains subject to scrutiny. *In vitro*, the innate immune response to SeV infection is unimpaired in bone marrow-derived mDCs from *cGas -/-* mice (500). However, *in vivo*, cGas deficiency is associated with significantly worse control of positive sense ssRNA Venezuelan equine encephalitis virus (VEEV) compared to wildtype animals (501). In the context of RNA virus infection, it has been proposed that cGAS might sense host DNA released into the cytosol or the extracellular milieu by dead or damaged cells. As a small diffusible molecule, cGAS is also able to spread horizontally from infected cells to uninfected neighbours via gap junctions, facilitating STING activation and induction of an antiviral state in the absence of either cGAS ligands or type I IFN (502). Similarly, incorporation of cytosolic cGAMP into nascent virions facilitates induction of cGAS-independent antiviral responses, an effect independent of both viral nucleic acids and exosomal transfer of cytosolic material (503,504)

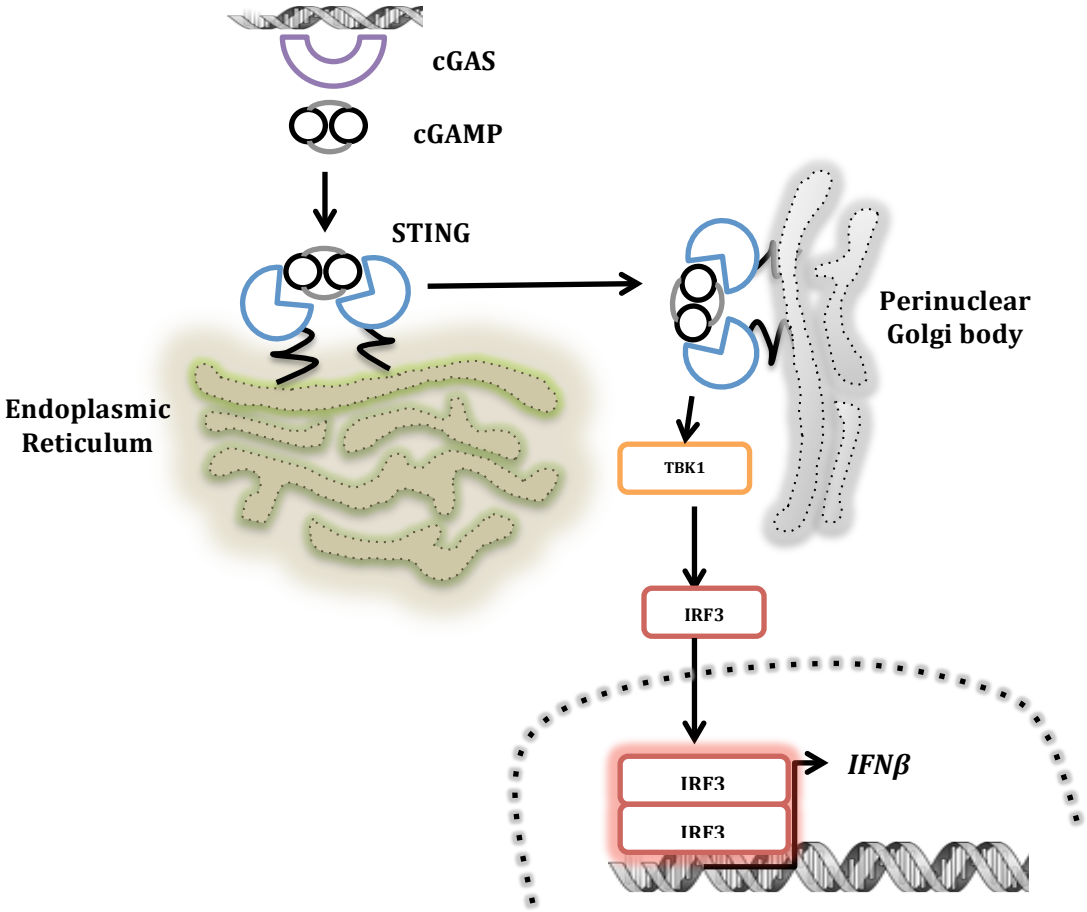


Figure 4.2: Schematic representation of the cGAS-STING pathway

Binding of cytosolic dsDNA to cGAS results in synthesis of cGAMP, which binds the adaptor protein STING and triggers its translocation to the perinuclear Golgi body. AT the Golgi body, STING activates IRF3 phosphorylation, resulting in nuclear translocation of activated IRF3 homodimers and downstream induction of IFN β.

Adapted from Wu, J and Chen, ZJ, Annual Reviews Immunology (2011) and Hornung, V Immunity (2014)

4.1.4 PRR signal transduction: induction of pro-inflammatory cytokines and IFN

Diverse gene products are activated downstream of PRR activation, including type I/III IFN and pro-inflammatory cytokines such as TNFα, IL1 and IL6, as summarized by figures 4.1 and 4.2. The remainder of this chapter focuses on IFN induction.

4.1.4.1 Type I IFN induction

As summarized by figure 4.1 and 4.2, signalling transduction downstream of nucleic acid-responsive PRR converge upon the TBK1 and IKKε serine-threonine kinases responsible for phosphorylation of the IRF3 and IRF7 C-termini (505,506). IRF3 is ubiquitously expressed

and is not induced by viral infection or type I IFN (128). In the resting state, IRF7 expression is absent or negligible in all cells except for pDCs, which are characterized by constitutively high levels of IRF7. In the nucleus, phosphorylated IRF3 homodimers associate with the transcriptional coactivators p300/CBP to induce both IFNβ and IFNα4 (507–509). Subsequent autocrine and paracrine signalling by IFNβ and IFNa4 induces both an antiviral state and expression of a second wave of IFNs (510).

Downstream of the IFNAR-JAK-STAT receptor complex, ISGF3 (section 1.3.6.4) activates *IRF7* transcription. Newly translated IRF7 is phosphorylated by TBK1/IKKε, and these activated IRF7 homodimers promote expression of second-wave IFN (511). IRF7 is vulnerable to proteasomal degradation, preventing excessive amplification of the type I IFN response. A study by Honda and colleague implies that IRF7 is also required for initial IFNβ induction following viral infection, with *IRF7* -/- mice failing to mount a type I IFN response to HSV1 and VSV infection, despite unimpaired IRF3 expression (152). In plasmacytoid dendritic cells, direct activation of IRF7 occurs via TRAF3/IKKα activation downstream of MYD88-linked endosomal TLRs (124).

Other IRFs are posited to regulate type I IFN induction in response to viral infection, in cell-type and pathogen-specific contexts. A restricted set of viruses, including NDV, HSV and VSV, are able to activate IRF5 (512), whereas IRF8 is required to amplify the second wave of IFN induction in NDV-infected pDCs (513). However, IRF1, the first IRF to be identified, is wholly dispensable for induction of type I IFN (514).

The profile of second-wave IFN subtypes is both cell and PAMP-dependent. SeV infection in human PBMCs is reported to induce 9 subtypes of IFNα, predominated by IFNα1 (515). In human pDCs, induction of all 13 IFNα subtypes is detectable, both after viral infection and stimulation with synthetic PRR agonists. Irrespective of the stimulus, both the relative expression magnitude and the induction kinetics of each subtype are rigidly conserved (516). In whole PBMC fractions, however, TLR7 and TLR9 stimulation results in differential induction of IFNα subtypes: TLR7 is associated with a rapid spike in IFNα1, -2, -13 and -14 expression, whereas TLR9 activation elicits slower and sustained induction of subtypes including IFNα1, -2, -4 and -7 (517). Similarly to the observations in pDCs, different ligands activating the same PRR elicit qualitatively similar IFNα subtype profiles.

IFNα subtypes also demonstrate variable ISG-induction potencies, with IFNα1 exhibiting the lowest potency, but IFNα2b, -8 and -10 being amongst the strongest across a broad panel of target genes (518). This differential potential for ISG induction extends to the relative

antiviral potencies of the subtypes *in vitro*. IFNα1 is very weakly antiviral against VSV and Sindbis virus in hepatoma-derived cell lines, whereas IFNα2, -5, -10 and -8 are especially potent against these infections, observations that are recapitulated by *in vitro* models of Semliki Forest virus infection (519,520).

Of note, IFNε is constitutively expressed by the epithelial lining of the female reproductive tract and is not induced downstream of conventional PRR signalling pathways, consistent with the absence of IRF, STAT and NFκB responsive elements proximal to its promoter region. Fung and colleagues characterised IFNε expression as dependent upon prevailing hormonal conditions, peaking at estrus and undergoing a precipitous reduction post-implantation. While their induction kinetics have yet to be characterized, IFNε robustly induces expression of multiple IFN-stimulated antiviral effectors including *OAS*, *IRF7* and *ISG15* in the mouse uterus, with *Ifnε*$^{-/-}$ mice exhibiting deficiencies akin to those seen in *Ifnar1-/-* animals.

Expression of IFNκ, however, is restricted to keratinocytes, being induced by both recombinant IFNβ and IFNγ, in addition to synthetic double-stranded RNA. Its role in response to viral infection is poorly characterized; epigenetic silencing of the IFNκ locus has been reported in the context of human papilloma virus 16 (HPV16).

4.1.4.2 Type III IFN induction

Loss and gain-of-function experiments reveal that induction of IFNλ subtypes during RNA virus infection is also contingent upon IRF3 activation downstream of RIG-I, MAVS and TBK1/IKKε (521). The same study also identified putative IRF and NFκB binding sites upstream of the *IFNλ1* transcriptional start site; ablation of these sequences reduced ISG induction in response to viral infection, indicating a key regulatory function (521). Further characterization demonstrates that while IFNλ1, akin to IFNβ1, is predominantly regulated by IRF3, IFNλ2/3 show delayed induction kinetics and are primarily responsive to IRF7 (522). Maximal induction of IFNλ1 also requires NFκB binding to a cluster of distal promoter elements proposed to derive from Alu and LTR transposable elements (523). Consistent with this, inhibition of NFκB signalling in both mDCs and mice strongly inhibits type III IFN induction in response to a synthetic TLR9 agonist, despite only mild reductions in the type I IFN response (524).

4.1.5 PRR activation by specific pathogens and synthetic PAMPs

In this chapter a range of viral infections and synthetic PRR agonists have been used to investigate whether BMP and activin cytokines are induced downstream of pattern recognition. Their basic biology and signalling characteristics are summarized below.

4.1.5.1 Sendai virus: virology and detection

The murine paramyxovirus SeV is frequently used as an experimental inducer of RIG-I signalling. SeV comprises a lipoprotein envelope enclosing a negative sense, monopartite ssRNA genome. Epizootic and enzootic transmission patterns are observed in rodent colonies; the former typically causes lethal respiratory disease, whereas the latter results in persistent, latent infections, particularly in laboratory animals (525).

In terms of the viral life cycle, after attachment via the asialoglycoprotein receptor, host proteases cleave the viral F protein, mediating fusion of the lipoprotein envelope with the cell membrane and cytosolic injection of the viral genome. Tight encapsulation of the viral genome protects it from cytosolic RNAses and is required for recruitment of the viral RNA-dependent RNA polymerase. Two RNA species are transcribed: mRNA - monocistronic, with the exception of the mRNA encoding the P gene - and positive-sense replication intermediates (525).

Regarding PRR activation by SeV, intact RIG-I, but not MDA5, signalling is necessary for IRF3 phosphorylation and ISG induction *in vitro* (526). In terms of viral PAMPs, it is well-established that SeV defective interfering (DI) particles are potent IFNβ inducers (527). DI particles contain replication-incompetent partial genomes, yet can compete for structural and metabolic substrates in the presence of productive "helper" virions (528). To identify the SeV PAMP, Baum and colleagues immunoprecipitated RIG-I from infected cells and deep sequenced its bound RNA. The pulled-down fraction was significantly enriched for short sequences mapping to a 546nt section of the viral 5'UTR, a region identical to that encoded by "back-copy" DI particles (529). The authors estimate that at 24 h.p.i. *in vitro*, more than 95% of intracellular viral RNA encodes this immunogenic motif.

4.1.5.2 Dengue virus: virology and detection

Dengue virus (DENV) is endemic to 100 countries, resulting in 50 million infections per year. Transmitted by the *Aedes aegypti* mosquito, DENV is an enveloped Flavivirus with a

positive-sense ssRNA genome. While most dengue infections are asymptomatic or characterized by self-limiting febrile phase, severe manifestations include arthralgia, haemorrhage and hypovolaemic shock and, in extreme cases, multi-organ failure. Four antigenically distinct DENV serotypes are currently circulating. Sequential infection by two different viruses is a significant risk factor for severe disease due to antibody-dependent enhancement of viral infectivity (530).

The cellular tropism of DENV during natural infection has proven challenging to define. While it is generally held that the mononuclear phagocytic cells, including monocytes, macrophages and dendritic cells, are the principal cellular targets of DENV *in vivo*, evidence exists for infection of endothelial cells, hepatocytes and neuronal cells *in vitro* (531,532). The essential DENV entry factor is not defined, but interactions with heparan sulphate, CD14 and, in myeloid cells, multiple C-type lectin receptors, have been described.

In terms of innate sensing, DENV activates both RIG-I and MDA5 signalling in murine embryonic fibroblasts. Intact MAVS function is essential for DENV-stimulated IRF3 phosphorylation downstream of either PRR (526). RIG-I and MDA5 knockdown in TLR3-deficient Huh7 cells enhances DENV replication; TLR3 overexpression in these cells curtails both DENV replication and boosts IFNβ induction (533). After co-culture with DENV-infected Huh7.5 cells, primary pDCs release high levels of IFNα in a TLR7-dependent manner (534). Overexpression of TLR8 by HEK293 cells is sufficient for induction of IL-8 in response to DENV infection (535), although neither induction of type I IFN, nor sensing in naturally TLR8-positive cell types, have been described.

4.1.5.3 Influenza A virus: virology and detection

Influenza A virus (FLUAV) is an enveloped negative-sense RNA virus with a segmented genome belonging to the *Orthomyxoviridae* family. Strains are classified by their expression of a given subtype of haemagglutinin (HA) and neuraminidase (NA), surface glycoproteins involved in viral entry and egress respectively (536).

Viral entry involves binding of HA to α-2'3 or α-2'6 linked sialic acid residues present on respiratory epithelial surfaces, followed by endocytosis. Within the endosome, HA undergoes a pH-dependent conformational change, resulting in exposure of a fusion peptide that permits cytosolic injection of the viral ribonucleoproteins (RNP), a process accelerated by pumping of hydrogen ions into the endosome through the M2 viroporin. In the nucleus, the viral RNA-dependent RNA polymerase transcribes two RNA species from the viral genome: cRNA

intermediates from which the genomes of progeny virions are ultimately transcribed in the host cell nucleus, and mRNA templates required for viral protein synthesis. “Cap-snatching”, mediated by the viral PA and PB2 proteins, appends 7-methyl-guanosine capped RNA fragments to the 5’ end of viral mRNA, allowing their nuclear export and translation by the host machinery. Upon assembly and packaging of progeny virions, the sialidase activity of NA liberates the viral particles from the cell surface (536).

In terms of innate sensing, the 5’ppp present on flu genomic ssRNA is a strong RIG-I PAMP (537). Using a FLUAV viral ribonucleoprotein reconstitution system, Rehwinkel and colleagues comprehensively demonstrated that genomic ssRNA bearing 5’ppp is the sole physiological RIG-I stimulus during flu infection (538). In the endosome, flu genomic ssRNA is detected by TLR7, independently of viral replication (486). TLR3-dependent signalling is reported to modulate the pro-inflammatory response to FLUAV. The TLR3 stimulus is likely to be derived from phagocytosis of dead or dying virus-infected cells (539). The role of TLR8 in the sensing of flu infection is presently unknown.

The pleiotropic NS1 protein disrupts host innate immunity through a diverse selection of mechanisms, many of them strain-specific. NS1 can impair RIG-I/MAVS associations, and its RNA-binding domain is hypothesized to out-compete both PKR and OAS for dsRNA produced as a by-product of viral replication. NS1 also exerts a general block on post-transcriptional processing of mRNA produced by RNA Pol II, subsequently disrupting IFNβ synthesis (540).

4.1.5.4 Synthetic agonists of intracellular nucleic acid sensors

Transfection with the synthetic RNA duplex polyinosinic-polycytidylic acid (poly(I:C)) activates MDA5 signalling, whereas endosomal internalization of poly(I:C) is a potent TLR3 stimulus (458,485).

The imidazoquinoline base analogue R837 (imiquimod) is a specific TLR7 agonist, whereas the related compound R848 (resiquimod) functions as a dual stimulus for TLR7 and TLR8 (541).

Short, ssRNA oligodeoxynucleotides (ODN) incorporating unmethylated CpG linkages can stimulate TLR9, although the downstream signalling pathways induced are contingent upon the ligand’s composition. Unlike phosphodiester-linked endogenous DNA, synthetic TLR9 agonists contain a phosphothiorated backbone, conferring resistance to intracellular

nucleases. CpG ODN incorporating a central palindromic region promote high IFNα production, but weakly stimulate NFκB and IL-6. In contrast, linear ODN weakly induce IFNα but are associated with strong NFκB induction, especially in B cells (542,543).

Transfection with *in vitro* transcribed RNA (IVT-RNA) with a 5'ppp moiety elicits RIG-I activation (458). RIG-I can also be stimulated by the synthetic agonist of B-form DNA polydeoxyadenylic-polydeoxythymidylic acid (poly(dA:dT)), by virtue of its transcription into a 5'ppp dsRNA intermediate by RNA Pol III (439,440).

Direct activation of STING can be achieved by exogenous cyclic dinucleotides, including cGAMP, cyclic di-AMP and cyclic di-GMP, in various structural isoforms. cGAS itself can be stimulated by transfection with bacterial and viral dsDNA; experimental ligands are commonly prepared from *L. monocytogenes*, *E. coli* K12 and HSV1 (544).

4.1.6 Summary and aims:

In this chapter, we explore the possibility that BMP and activins might also be induced downstream of viral sensing, both at the mRNA and protein level. Pre-formed activin A is released by neutrophil degranulation in response to pro-inflammatory cytokines, and elevated serum activin A is observed in both HCV and influenza A-infected patients (see section 1.1.5). However, direct induction by viral infection or cytosolic nucleic acids has yet to be experimentally demonstrated.

The key questions addressed by this chapter are:

1) Are BMP6, activin A and activin B induced by viral infection or synthetic mimics thereof, both *in vitro* and *in vivo*?
2) Which PRRs are required for their induction?

4.2 Materials and methods

4.2.1 In vitro experiments

4.2.1.1 Synthetic nucleic acids and base analogues

High molecular weight poly(I:C) [cat I.D. tlrl-pic], poly(dA:dT) [cat. I.D: tlrl-patn], *E. coli* K12 dsDNA [cat. I.D. tlrl-ecdna], ODN 2216 [cat. I.D. tlrl-2216], R837 [cat. I.D. tlrl-imqs], R848 [cat. I.D. tlrl-r848] and ssRNA40/LyoVec™ [cat. I.D. tlrl-lrna40] were purchased from InvivoGen (Toulouse, FR).

IVT-RNA transcribed by the T7 RNA polymerase and corresponding to nucleotides 1-99 of the neomycin phosphotransferase gene (synthesized as described in (538)) was obtained from the Rehwinkel lab (MRC WIMM, University of Oxford).

4.2.1.2 Nucleic acid transfection protocols: cell lines

In all figures, 'medium' denotes cells exposed to equivalent volumes of the reduced serum Opti-MEM (Gibco, Life Technologies, USA) [cat. I.D. 31985-062] used to prepare the stimulatory ligands and transfection reagents. 'Vehicle' denotes cells exposed to transfection reagent only, without its cargo immunostimulus.

THP-1

THP-1 cells were plated at $1x10^5$ cells/well of a 12-well plate and transfected with poly(I:C) or IVT-RNA using Lipofectamine® LTX with PLUS™ [cat. I.D. 15338030] reagent in accordance with the manufacturer's instructions (Life Technologies). Stimulation times and doses are specified by individual figure legends.

293T

293T cells were plated at $5x10^4$ cells/well of a 12-well plate and incubated at 37 °C for 24 h before transfection with poly(dA:dT) and poly(I:C) using Lipofectamine® 2000 (Life Technologies) [cat. I.D. 11668030] in accordance with the manufacturer's instructions. Stimulation times and doses are specified by individual figure legends.

A549.gfp

A549 cells were plated at $5x10^4$ cells/well of a 12-well plate and incubated at 37 °C for 24 h before transfection with poly(dA:dT) and poly(I:C) using Lipofectamine® RNAiMAX (Life

Technologies) [cat. I.D. 13778030] in accordance with the manufacturer's instructions. Stimulation times and doses are specified by individual figure legends.

Huh7

Huh7 cells were plated at $1x10^5$ cells/well of a 12-well plate and incubated at 37 °C for 24 h before transfection with poly(dA:dT) and poly(I:C) using Lipofectamine® LTX with PLUS™ (Life Technologies) [cat. I.D. 13778030] in accordance with the manufacturer's instructions. Stimulation times and doses are specified by individual figure legends.

Primary human dermal fibroblasts

Primary human dermal fibroblasts (F10y isolate; section 2.1.5) were plated at $1x10^5$ cells/well of a 12-well plate and incubated at 37 °C for 24 h before transfection with *E. coli* K12 dsDNA using Lipofectamine® LTX with PLUS™ (Life Technologies) at two doses (100ng and 500ng) for 24 h.

4.2.1.3 Nucleic acid transfection and incubation protocols: human PBMC

Human PBMC were extracted from healthy donors as described in section 2.1.6 and plated at $1x10^6$ cells/well of a 24-well plate. PBMC were transfected with poly(dA:dT) and poly(I:C) using Lipofectamine® LTX with PLUS™ (Life Technologies) in accordance with the manufacturer's instructions. R837, R848, ODN 2216 and ssRNA40 were added to the culture medium in the absence of transfection reagent to the end-point concentrations specified in figure 4.7. Stimulation times and doses are specified by individual figure legends.

4.2.1.4 In vitro SeV infection

Huh7 and Huh7.5

Cantell strain Sendai Virus [cat. I.D. ATCC® VR-907™] was purchased from ATCC. In figure 4.10, Huh7 and Huh7.5 cells were plated at $5x10^4$ cells/well in 12-well plates and incubated at 37 °C for 24 h, the approximate doubling time of the cell lines. Immediately before infection, DMEM10 was aspirated and the monolayers washed twice times with PBS, before addition of SeV at MOI 0.5, MOI 1 and MOI 5 in 500uL serum-free DMEM. Cells were incubated with SeV for 2 h at 37 °C, before removal of the virus, two PBS washes and replenishment with 1 mL DMEM10 (as per section 2.1.1). Infection durations are specified by individual figure legends.

A549.gfp

A549.gfp cells were plated at $1x10^5$ cells/well in 12-well plates and incubated at 37 °C for 24 h, the approximate doubling time of the cell lines, followed by SeV infection as described for Huh7/Huh7.5 cells. Cellular RNA was harvested at 24 h.p.i.

4.2.1.5 In vitro DENV infection

Huh7.5 cells were plated at $3x10^5$ cells/well in 12-well plates and allowed to adhere. Cells were incubated with DENV2 (strain 16681) in serum-free DMEM for 2 h at room temperature with gentle agitation, followed by removal of virus, washing with PBS and incubation at 37 °C for 48 h.

Infection and RNA extraction were performed by Jo Miller (Zitzmann lab, Department of Biochemistry, University of Oxford).

4.2.1.6 In vitro HCV infection

Huh7 or HepG2 cells were plated at 3 $x10^5$ cells/well in 6-well plates and infected with Jc1 strain HCV (GT2a) at MOI 0.05. RNA was harvested at the time intervals indicated and subjected to reverse-transcription and RT-qPCR as described in section 2.2. Jc1 virus was produced following electroporation of Huh7.5 cells with Jc1 RNA, followed by harvesting at 14-20 days post-infection and quantification of viral titre via an immunofluorescence assay(545).

Performed by Narayan Ramamurthy (Klenerman Lab, Peter Medawar Building for Pathogen Research, University of Oxford).

4.2.1.7 RT-qPCR and ELISA

Cellular RNA extraction, cDNA synthesis and RT-qPCR analysis were conducted as described in section 2.2, for the genes specified within each figure.

Culture supernatants harvested for analysis of activin A protein by ELISA were immediately stored at -80 °C. Activin A protein in PBMC culture supernatants was measured with the Human/Mouse/Rat Quantikine ELISA kit [cat. I.D. DAC00B] (R&D Systems), a solid-phase sandwich ELISA. Undiluted samples were assayed in technical duplicate in accordance with the manufacturer's instructions.

4.2.2 In vivo experiments

4.2.2.1 FLUAV infection

For figure 4.14, 6-week old female C57BL/6 mice were anaesthetized and infected intranasally with 3.5 HAU FLUAV PR/8/34 (H1N1), kindly provided by John Skehel (NIMR, Mill Hill, UK). Control mice were administered PBS intranasally. Mice were sacrificed at 3 d.p.i. by asphyxiation.

Whole lungs were immediately lysed in RLT buffer (Qiagen) with 10 μL/mL β-mercaptoethanol and mechanically disrupted with a TissueRuptor (Qiagen), before RNA extraction, cDNA synthesis and RT-qPCR quantification of gene expression as described in section 2.2. Liver explants (~2mm^3) were preserved in RNAlater (Qiagen), before mechanical lysis with a TissueRuptor and RNA extraction, cDNA synthesis and RT-qPCR quantification of gene expression as described in section 2.2.

Infection, RNA extraction and cDNA synthesis were performed by Suzanne Cole and Andrew Armitage (MRC Human Immunology Unit, University of Oxford)

For figure 4.15, 6-week old female wildtype C57BL/6 mice were infected intranasally with increasing titres of wildtype FLUAV PR/8/34 from $4x10^2$ to $5x10^4$ pfu. Control mice were administered DMEM i.n. Mice were sacrificed at 2 d.p.i. by asphyxiation, followed by RNA extraction, cDNA synthesis and RT-qPCR quantification of gene expression as per section 7.2.3

Infection and RNA extraction were performed by Rachel Rigby (MRC Human Immunology Unit, University of Oxford)

For figure 4.17 and 4.18, 6-week old female C57BL/6 mice, both wildtype and MAVS knockout (Cardif KO)(546) were infected intranasally with either $5x10^4$ pfu wildtype (figure 4.18) or NS1-deficient FLUAV PR/8/34 (figure 4.19) bearing two mutations that abrogate its dsRNA binding capacity(547) (kindly gifted by Jan Rehwinkel and Rachel Rigby, produced by the lab of Paul Digard, University of Edinburgh). Mice were sacrificed at 2 d.p.i. by asphyxiation. Control mice were administered DMEM intranasally. Whole lungs were harvested and RNA extracted, followed by cDNA synthesis and RT-qPCR quantification of gene expression as described in section 7.2.3.

Infection and RNA extraction were performed by Rachel Rigby (MRC Human Immunology Unit, University of Oxford)

4.3 Results

4.3.1 Activin A mRNA is induced by synthetic agonists of viral PRRs in vitro

Motivated by our finding that both BMP and activin proteins can exert anti-HCV effects, we initially investigated whether activation of the cytosolic viral RNA sensors RIG-I and MDA5 elicits activin induction *in vitro*.

INHBA mRNA (encoding activin A) is induced, albeit not to statistically significant levels, by transfection of Huh7 hepatoma-derived cells with the indirect RIG-I agonist poly(dA:dT), after both 24 and 48 hours incubation. Transfection with 1 μg/mL poly(dA:dT) elicits 7.5 and 25-fold increases in *INHBA* transcript at 24 and 48 h respectively, paralleled by a very strong induction of the IFN-stimulated GTPase *MX1*, indicating activation of a cellular antiviral state [figure 4.3].
Similarly, in 293T fibroblast-derived cells, *INHBA* mRNA is weakly induced by both 250 ng/mL and 1 μg/mL poly(dA:dT) after 24h incubation, in parallel with a moderate induction of *MX1*. Transfection with poly(I:C), however, induced neither *INHBA* nor *MX1* mRNA [figure 4.3], despite previous reports that biologically active MDA5 is endogenously expressed by 293T cells (452).

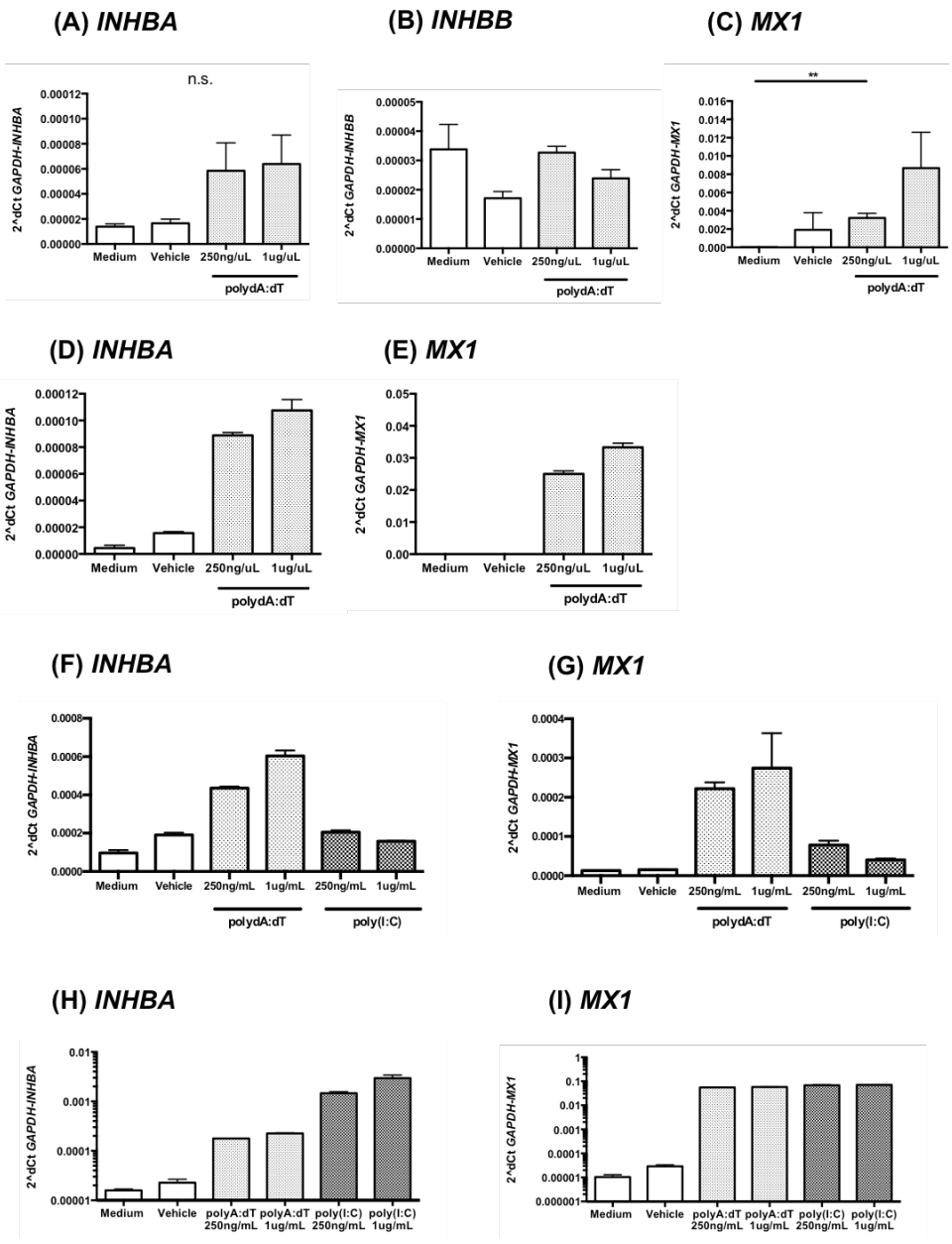
In contrast, in A549 lung adenocarcinoma derived cells, *INHBA* expression is upregulated approximately 150-fold relative to untransfected cells by 1 μg/mL poly(I:C). While *MX1* is upregulated to similar levels by all transfection conditions, poly(dA:dT) transfection at both concentrations elicited only a 10-fold increase in *INHBA* expression compared to uninfected cells [figure 4.3].

Figure 4.3: Transfection of epithelial-like cell lines with poly(dA:dT) and poly(I:C) induces *INHBA* mRNA expression

In (A) to (C) Huh7 cells were transfected with two concentrations of polydA:dT for 24h, followed by RNA extraction and RT-qPCR quantification of transcript for *INHBA* and *MX1*. Data is presented as 2^ΔCt values relative to *GAPDH*. Whilst not reaching statistical significance, there is a marked trend towards induction of *INHBA*, but not *INHBB*, in polydA:dT transfected cells compared to vehicle only. *MX1* is induced significantly by both concentrations of polydA:dT, indicating induction of an antiviral state. In (D) and (E) Huh7 cells were transfected with poly(dA:dT) for 48 h: there is a tendency towards induction of *INHBA* in polydA:dT transfected cells compared to vehicle only. *MX1* is induced to high levels by both concentrations of polydA:dT.

In (F) and (G), 293T cells were transfected with two doses of either polydA:dT or the MDA5 agonist poly (I:C) for 24h, followed by RNA extraction and RT-qPCR quantification of transcript for *INHBA* and *MX1* respectively. *INHBA* is weakly induced by polydA:dT at both doses, in parallel with a modest upregulation of *MX1* expression. Poly(I:C) transfection did not induce *INHBA* expression in the model, nor did it elicit a pronounced induction of *MX1* (H) and (I), A549 cells were transfected with two doses of polydA:dT or poly(I:C) for 24h, followed by RNA extraction and RT-qPCR quantification of transcript for *INHBA* and *MX1* respectively. Whilst *MX1* is strongly induced to equivalent levels by all transfection conditions; *INHBA* mRNA is upregulated approximately 10-fold by polydA:dT transfection, and approximately 150x by poly(I:C) relative to untransfected cells.

For (A) to (C): n=3 in biological duplicate; mean+SEM presented; analysis by ordinary one-way ANOVA and Bonferroni's multiple comparisons test with respect to the vehicle condition. For (D) to (I): n=1 in biological duplicate; mean+SEM presented; statistical analysis precluded due to sample size.



In THP-1 monocytic cells, however, transfection with both 200 ng/mL and 800 ng/mL poly(I:C) results in a trend towards both *INHBA* and *MX1* induction at 48 h.p.i. Transfection of THP-1 cells with titrating doses of the RIG-I ligand IVT-RNA, elicits dose-dependent induction of *INHBA* at both 24 and 48 h incubation, with concomitant upregulation of *MX1* [figure 4.4].

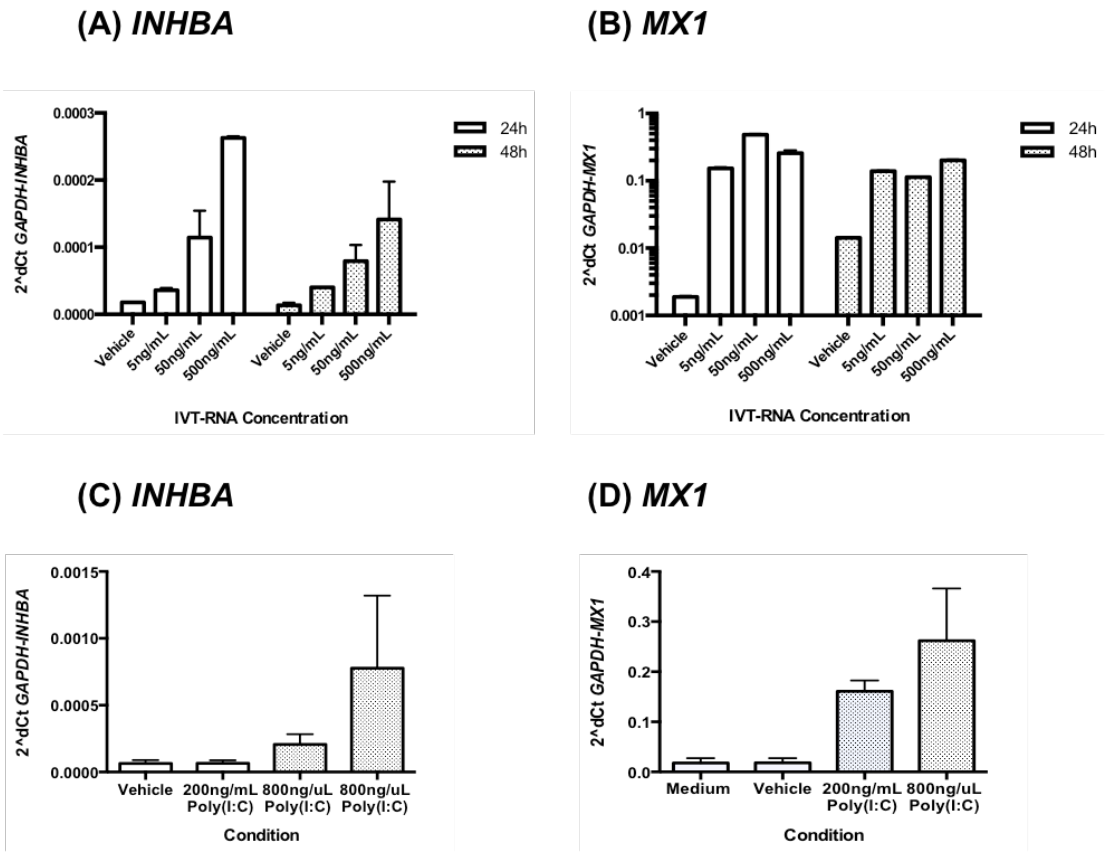


Figure 4.4: Activin A mRNA is induced by the RIG-I agonist IVT-RNA and the MDA5 agonist poly(I:C) in monocytic THP-1 cells

In (A) and (B), THP-1 cells were transfected with titrating doses of IVT-RNA and incubated for 24 or 48h, followed by RNA extraction and RT-qPCR quantification of transcript for *INHBA* (A) and *MX1* (B). Data is presented as 2^ΔCt values relative to *GAPDH*. In (C) and (D), THP-1 cells are transfected with poly(I:C) for 48 h, followed by quantification of *INHBA* (C) and *MX1* (D) expression.

INHBA is dose-dependently induced by IVT-RNA transfection, at both time-points, in parallel with a robust induction of *MX1*, a positive control for induction of an antiviral state following intracellular sensing of IVT-RNA.

n=1 conducted in duplicate wells; mean+SEM; statistical analysis precluded due to sample size.

Having addressed whether agonists of viral RNA sensors transcriptionally induce activins, we turned our attention briefly to activation of cytosolic DNA sensors. Before the identification of cGAS, we attempted to measure *INHBA* induction in Huh7 cells transfected with three exogenous DNA molecules: poly(dA:dT), immunostimulatory DNA (a short non-CpG oligomer derived from the *Listeria monocytogenes* genome) and *E. coli* K12 DNA.

INHBA induction was only evident after poly(dA:dT) transfection, which as previously discussed is likely attributable to detection of an RNA Pol III transcription product by RIG-I [figure 4.5]. As this is a n=1 experiment, only very limited inferences may be drawn. As transformed cell lines are frequently aneuploid and are often selected for on the basis of their permissivity to transfection with DNA plasmids, it is very likely that their cytosolic DNA sensing apparatus is defective. cGAS expression by transformed cell lines is variable, with high expression by THP-1 cells and no expression in HEK293 cells, from which 293T line is derived (489).

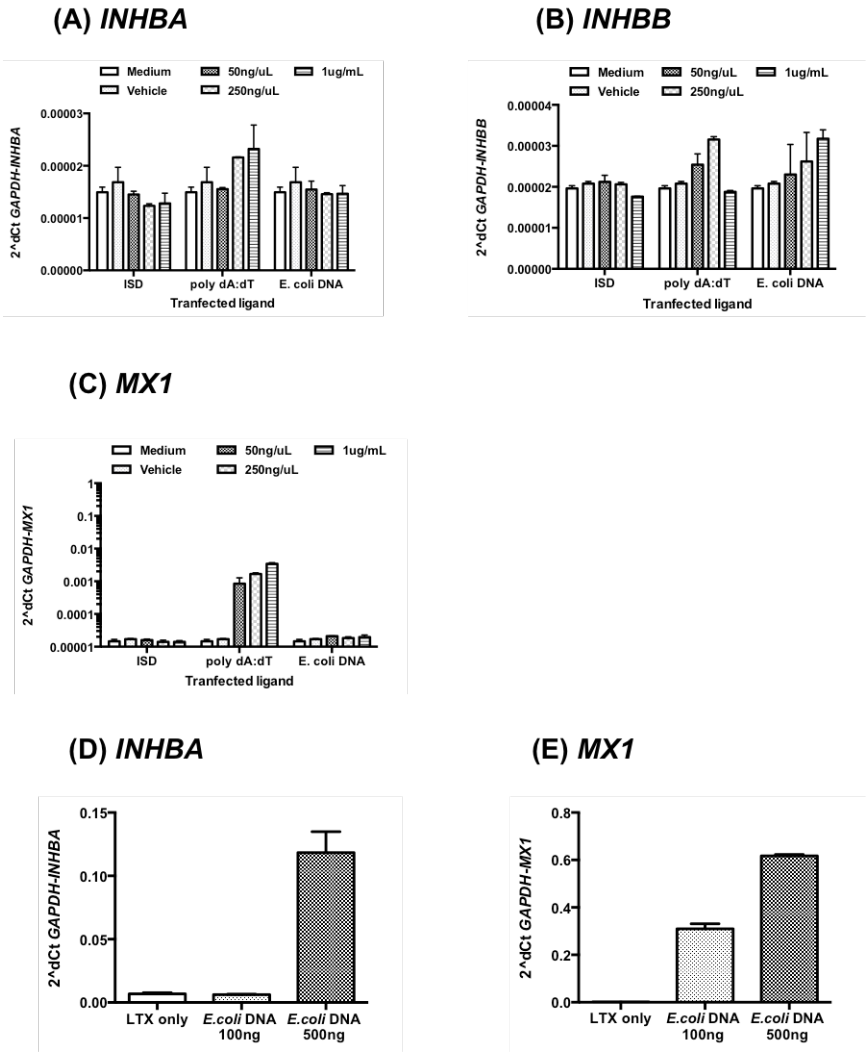


Figure 4.5: Transfection with DNA species induces activin A mRNA in primary human fibroblasts but not in Huh7 cells

In (A) to (C), Huh7 cells were transfected with titrations of three DNA species (immunostimulatory DNA [ISD], poly(dA:dT) and *E. coli* DNA) for 24h, followed by RNA extraction and RT-qPCR quantification for *INHBA* (A), *INHBB* (B) and *MX1* (C). Data is presented as $2^{\Delta Ct}$ values relative to *GAPDH*. Only poly(dA:dT) induced expression of the ISG *MX1*. Neither *INHBA* nor *INHBB* were markedly upregulated by any transfected species, although there is a suggestion of very mild induction above baseline following transfection with higher doses of poly(dA:dT). In (D) and (E), primary human skin fibroblasts were transfected with two doses of *E. coli* DNA, an agonist of intracellular DNA sensing mechanisms, for 24h, followed by quantification of *INHBA* and *MX1* expression. mRNA encoding both *INHBA* and *MX1* are robustly induced by 500ng *E. coli* DNA.

For (A) to (E): n=1 conducted in duplicate wells; mean+SEM; statistical analysis precluded due to sample size.

Given that human skin fibroblasts express all components of the cGAS-STING axis (548), primary dermal fibroblasts were transfected with *E. coli* K12 DNA and both *INHBA* and *MX1* induction measured after 24h incubation. While unfortunately this experiment was only conducted once, sensing of cytosolic DNA appears to induce *INHBA* expression in human fibroblasts, paralleled by dose-dependent induction of *MX1* [figure 4.5].

The data presented in section 3.4.2 suggest that the antiviral effect of activins is at least in part independent of type I IFN. We quantified *INHBA* and *INHBB* expression in Huh7 cells incubated with recombinant IFNα2a, and established that neither are transcriptionally induced by recombinant type I IFN in this cell line [figure 4.6].

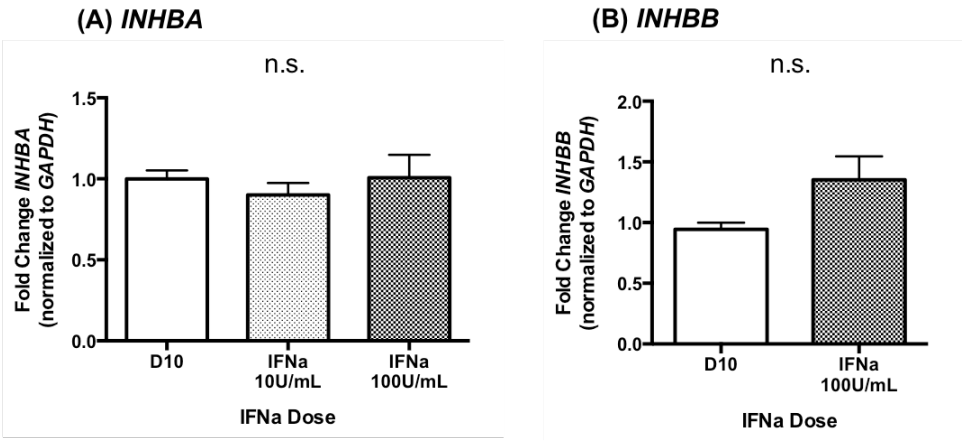


Figure 4.6: Neither *INHBA* nor *INHBB* are transcriptionally induced by recombinant type I IFN in the Huh7 cell line

Huh7 cells were incubated with recombinant IFNα2a for 24h, followed by RNA extraction and RT-qPCR quantification of mRNA encoding *INHBA* (A) and *INHBB* (B). Expression of neither transcript was significantly induced upon treatment with recombinant type I IFN.

n=4 independent experiments; mean + S.E.M.; analysis by two-tailed unpaired t-test.

Moving from transformed cell lines, we examined induction of activin A by PRR stimuli in freshly isolated human PBMC, which express a more extensive repertoire of viral sensors.

Transfection with both IVT-RNA and poly(I:C) at both 250 ng/mL and 1 μg/mL results in a statistically significant upregulation of *INHBA* mRNA, with up to 100-fold induction relative to vehicle only. *INHBA* induction is mirrored by statistically significant induction of the ISGs *MX1* and *IFI6* across all transfection conditions [figure 4.7].

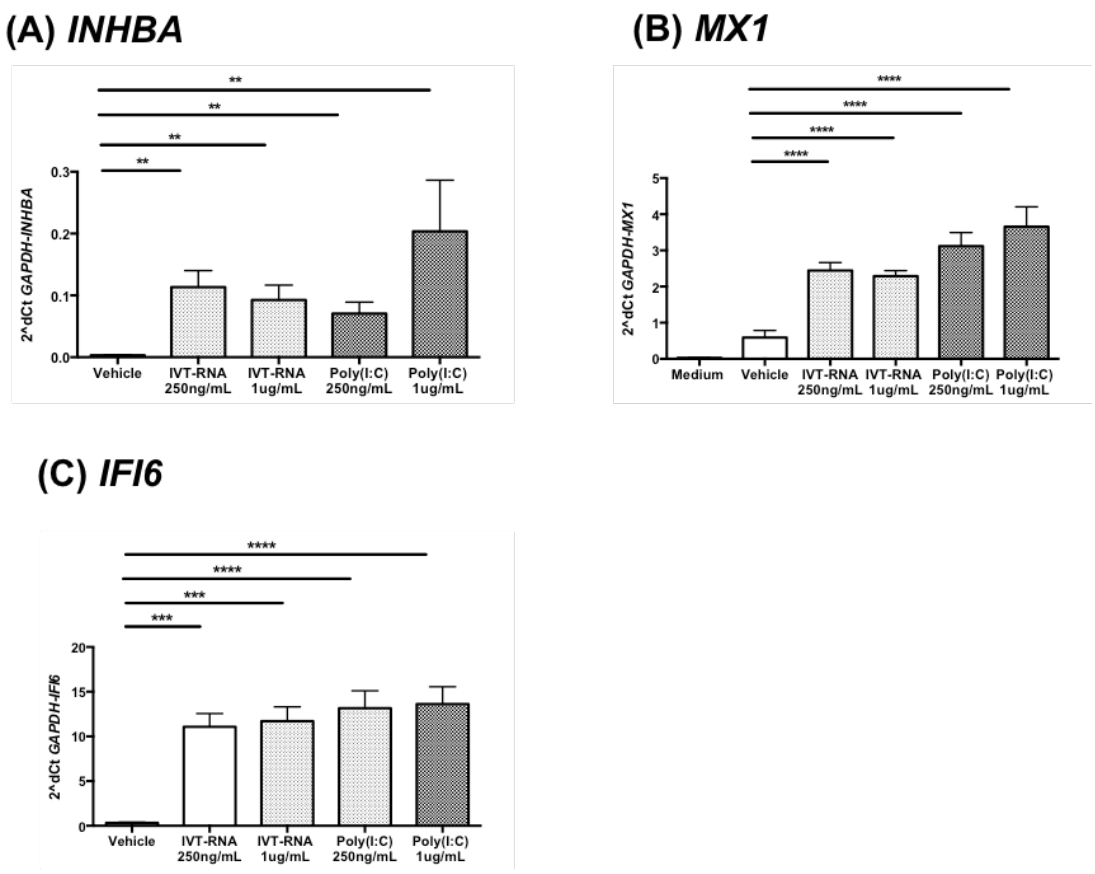


Figure 4.7: IVT-RNA and poly(I:C) induce activin A mRNA in human PBMCs *in vitro*

PBMCs harvested from healthy donors were transfected with IVT-RNA or poly(I:C) at two doses for 24h, followed by RNA extraction and RT-qPCR quantification of transcript for *INHBA* (A), *MX1* (B) and *IFI6*, encoding the ISG IFI6 (C). Data is presented as $2^{\wedge}\Delta Ct$ values relative to *GAPDH*. *INHBA* is significantly induced by both stimuli at both doses, in parallel with significant upregulation of the ISGs *MX1* and *IFI6* across all transfection conditions.

For *INHBA* quantification, n=9 donors; for *MX1*, n=6 donors; for *IFI6*, n=3 donors. Samples transfected in singlicate; mean+SEM presented; analysis by multiple unpaired, two-tailed t-tests.

Incubation with the base analogues R837 and R848 at 1 μg/mL resulted in approximately 15-fold and 50-fold increases in *INHBA* expression respectively, suggesting a role for TLR7 in activin A induction. Conversely, the magnitude of both *MX1* and *IFI6* induction was higher in R837 than R848-treated cells. Consistent with a role for TLR8 in activin A induction, incubation with ssRNA40 at both 1 μg/mL and 5 μg/mL elicited statistically significant *INHBA* upregulation with attendant induction of both *MX1* and *IFI6*. In contrast, despite significant induction of *MX1* and *IFI6* mRNA by the CpG-rich TLR9 agonist ODN 2216, it did not significantly increase *INHBA* expression [figure 4.8].

Neither *INHBB* nor *BMP6* transcript was detectable under any stimulation condition [data not shown].

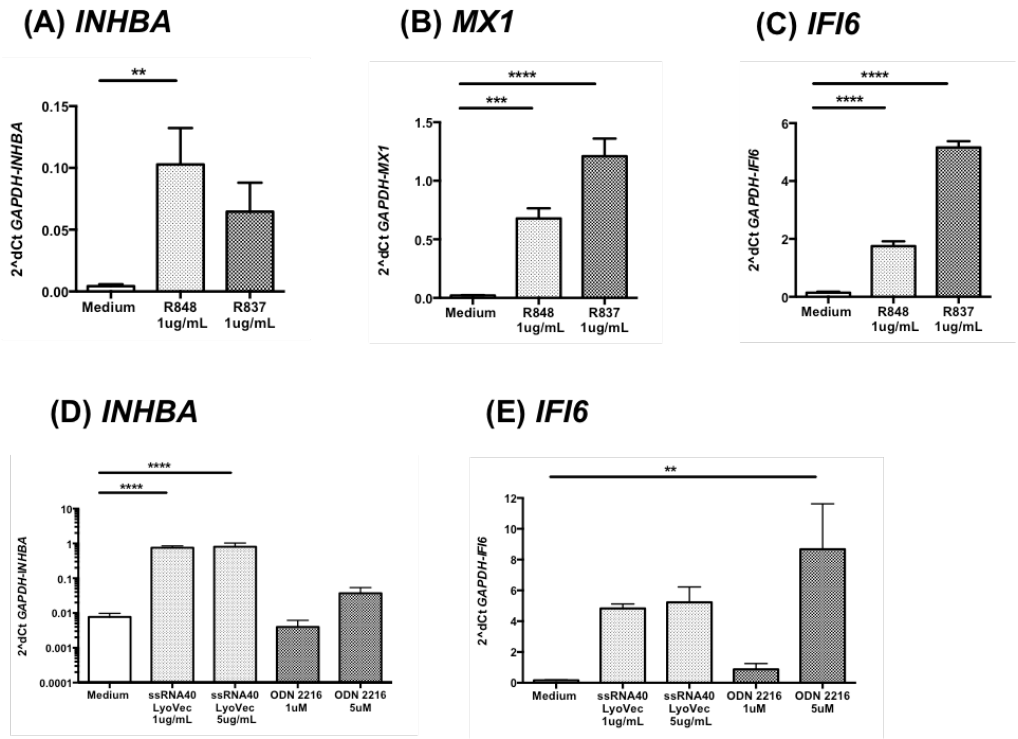


Figure 4.8: TLR7/8 agonists R848, R837 and ssRNA40 induce activin A mRNA in human PBMCs *in vitro*

In (A) to (C), PBMCs harvested from healthy donors were incubated with the TLR7 agonist R837 or the TLR7/8 agonist R848 for 24h, followed by RNA extraction and RT-qPCR quantification of transcript for *INHBA* (A), *MX1* (B) and *IFI6* (C). Data is presented as 2^ Δ Ct values relative to *GAPDH*. In (D) and (E), PBMCs were incubated with the TLR8 agonist ssRNA40 or the TLR9 agonist ODN 2216 for 24h, followed by measurement of *INHBA* (i) and *IFI6* (ii) message.

INHBA is significantly induced by R848, with non-significant upregulation elicited by R837. *MX1* is significantly induced by both ligands, whereas *IFI6* is significantly induced by R848 with non-significant upregulation by R837. *INHBA* message is significantly induced by transfection with both doses of ssRNA40, but not by ODN 2216. In contrast, there is non-significant induction of *IFI6* by ssRNA40, and significant induction by 5uM ODN 2216.

In (A) to (C): for *INHBA* quantification, n=9 donors; for *MX1*, n=6 donors; for *IFI6*, n=3 donors. Samples transfected in singlicate; mean+SEM presented; analysis by ordinary one-way ANOVA and Bonferroni's multiple comparisons test with regard to the medium only condition.

In (D) and (E): n=3 donors for ssRNA40; n=2 donors for ODN 2216. Samples transfected in singlicate; mean+SEM presented; analysis by ordinary one-way ANOVA and Bonferroni's multiple comparisons test with regard to the medium only condition.

To assess whether this transcriptional induction of activin A is mirrored at the level of secreted protein, activin A protein in culture supernatants from the stimulated PBMC was measured by ELISA. PBMCs from three healthy donors were transfected with IVT-RNA or poly(I:C), or stimulated with R837, R848, ssRNA40 or ODN 2216 for 24 h. While marked inter-donor variation is evident, activin A protein was induced by at least one donor with each nucleic acid mimetic. Exposure to the transfection reagent Lipofectamine LTX was sufficient to induce low-level activin A secretion. R848, R837 and ssRNA40 elicited especially high

activin A production, reaching concentrations of the order nanograms per millilitre [figure 4.9]. The detection of activin A protein in culture supernatants from ODN 2216-treated PBMCs is not consistent with observations at the mRNA level.

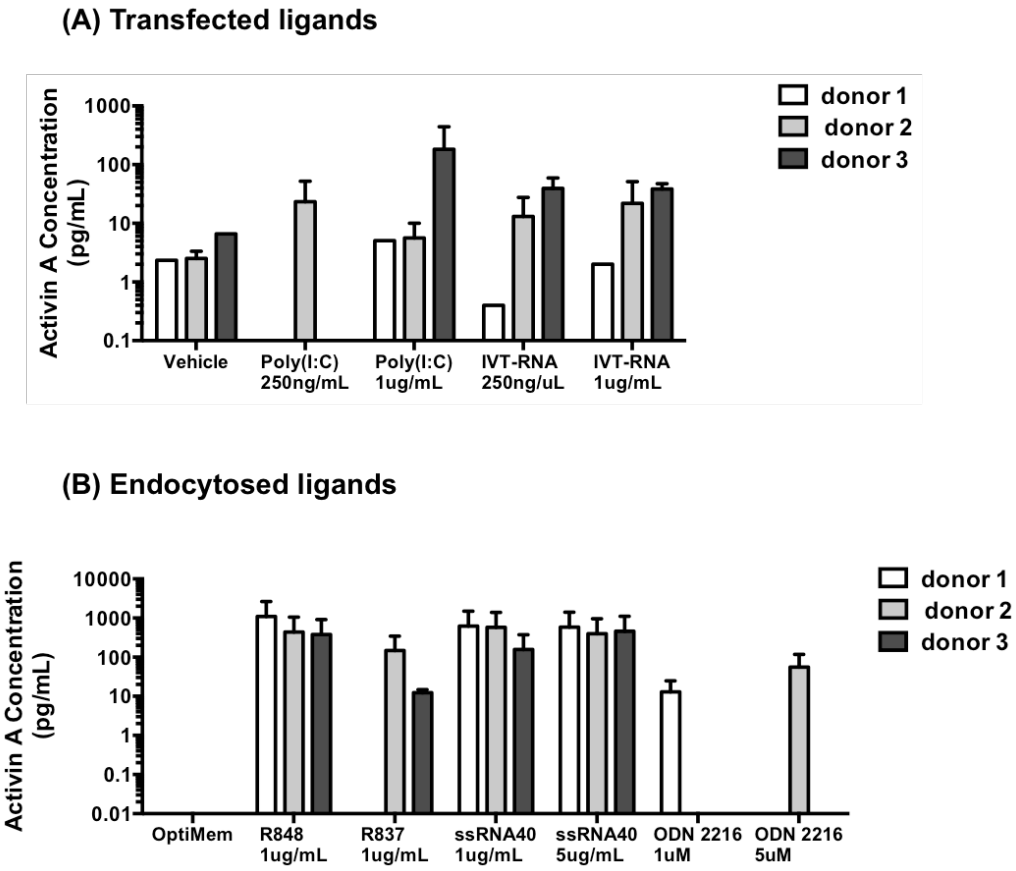


Figure 4.9: Activin A protein is detectable in culture supernatants from human PBMCs stimulated with synthetic nucleic acid mimics of viral infection

PBMCs harvested from three healthy donors were transfected with poly(I:C) or IVT-RNA at two concentrations (A), or exposed to the endosomal TLR agonists R848, R837, ssRNA40 or ODN 2216 (B) for 24h. Conditioned culture supernatants were harvested and activin A protein content measured by ELISA.

Whilst marked inter-donor variability is evident, exposure to all of the nucleic acid mimetics induced activin A release by at least one of the donors, with especially high level production induced by R848, R837 and ssRNA40.

n=3 donors; samples transfected in singlicate; ELISA measurement in duplicate; mean+SEM presented.

4.3.2 Induction of activin A and B mRNA by viral infection in vitro

Having established that *INHBA* mRNA can be induced in cell lines of diverse tissue origin, and in PBMC, by synthetic mimics of viral infection, we explored whether true viral infection *in vitro* induces activin A expression.

In RIG-I/TLR3 replete A549 cells, SeV infection results in a statistically significant, dose-dependent induction of *INHBA* mRNA, paralleled by a strong induction of the antiviral GTPase *MX1* (upregulated approximately 25-fold and 1000-fold at MOI 5.0 respectively) [figure 4.10]. *INHBB* expression was not detectable in this model (data not shown).

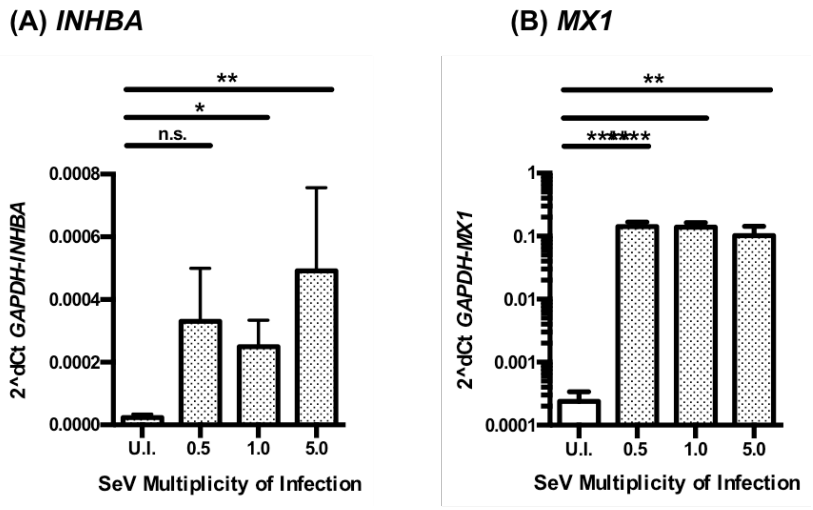


Figure 4.10: Activin A is upregulated 24 h after SeV infection in the A549 lung adenocarcinoma cell line, in parallel with transcriptional induction of MX1

A549.gfp cells were infected with SeV at increasing multiplicities of infection for 24h, followed by RNA extraction and RT-qPCR quantification of *INHBA* (A) and *MX1* (B) expression. Both *INHBA* and *MX1* expression are significantly induced in infected cells compared to uninfected controls (U.I).

n=3 in biological duplicate; mean+SEM; analysis with ordinary one-way ANOVA and Bonferroni's post-test with respect to the uninfected condition.

To further clarify the PRR requirements for *INHBA* induction by SeV, Huh7 and Huh7.5 hepatoma-derived cells were infected with a titration of SeV, and expression of *INHBA, MX1* and genomic SeV quantified by RT-qPCR. The Huh7.5 line was initially derived from Huh7 cells as a clone with exceptionally high permissivity to HCV replication (549), a characteristic attributable to its expression of non-functional RIG-I (550). RIG-I expressed by Huh7.5 encodes an N-terminal point mutation (T55I) that impairs its CARD function, uncoupling downstream signalling from viral sensing (550). Both Huh7 and Huh7.5 cells are deficient in TLR3 expression (551).

In RIG-I wildtype Huh7 cells, SeV infection robustly upregulated *INHBA* expression in a titre-dependent manner, at 48 h.p.i., paralleled by strong induction of the IFN-dependent target gene *MX1*. In Huh7.5 cells, however, neither *INHBA* nor *MX1* message were altered by SeV infection, at either time point. Of note, baseline expression of both *INHBA* and *MX1* is approximately 10-fold higher in uninfected Huh7.5 cells versus Huh7. SeV genomic RNA

levels were comparable in both cell lines, although the signal in the uninfected conditions implies low-level off-target amplification by the Taqman primer/probe set [figure 4.11].

At 24 h.p.i. *INHBB* is not induced by SeV infection in either cell line, if anything showing a trend towards repression with increasing viral titre in Huh7 cells. In contrast to *INHBA*, baseline *INHBB* expression is two-fold lower in Huh7.5 compared to Huh7 cells. Similarly, *FST*, encoding the soluble activin antagonist follistatin, is not induced by SeV infection in either cell line at 24 h.p.i. but shows an approximately three-fold lower expression in uninfected Huh7.5 cells [figure 4.11].

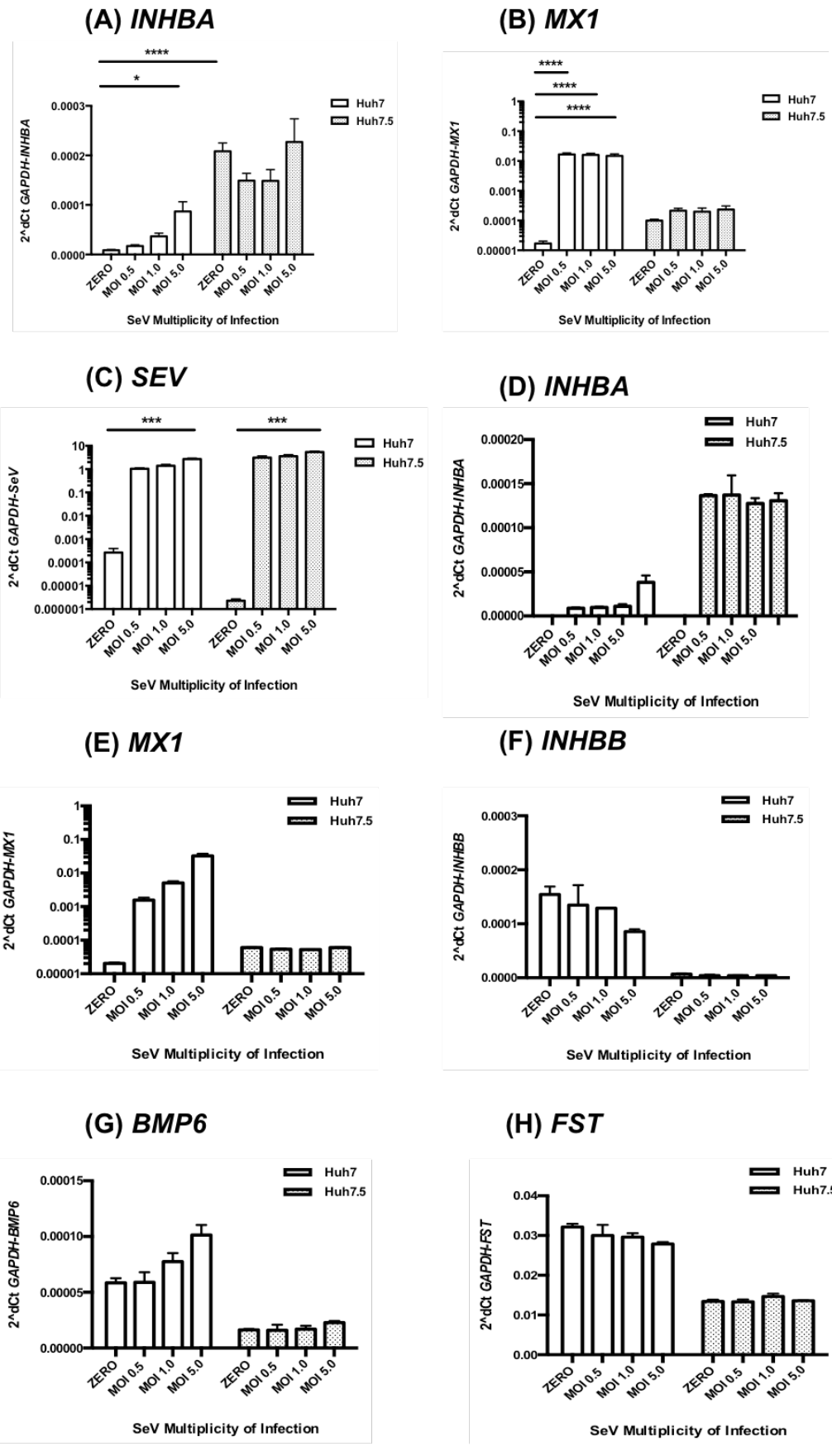
Figure 4.11: Activin A mRNA is upregulated at both 24h and 48h after SeV infection in RIG-I replete Huh7 cells, but not the related RIG-I deficient Huh7.5 cell line (see overleaf)

Huh7 and RIG-I deficient derivative Huh7.5 cells were infected with titrating multiplicities of infection of SeV for 48h, followed by RNA extraction and RT-qPCR quantification of transcript for *INHBA* (A), *MX1* (B) and genomic SeV (C). In the same model at 24h post-infection, expression of *INHBA* (D), *MX1* (E), *INHBB* (F), *BMP6* (G) and *FST* (H) were measured.

At 48 h, in the Huh7 line, *INHBA* mRNA is dose-dependently induced by increasing SeV titre, whereas no induction occurs in RIG-I deficient Huh7.5 cells (A). In parallel, *MX1* is profoundly upregulated upon SeV infection of Huh7 cells, but is not elevated in the Huh7.5 cell line (B). SeV genomic RNA is detected at robust levels upon infection at all titres in both cell lines (C). Both *INHBA* and *MX1* are dose-dependently induced with increasing SeV MOI in Huh7 cells at 24h post-infection (D,E), whereas levels of *INHBB*, *BMP6* and *FST* transcript are unchanged during infection of both cell lines (F-H).

For (A) to (C): n=2 independent experiments, each in biological duplicate; mean + SEM; analysis by two-way ANOVA and Bonferroni's multiple comparisons test with respect to uninfected cells.

For (D) to (H): n=1 in biological duplicate; mean+SEM presented; statistical analysis precluded due to sample size.


(A) INHBA
(B) MX1
(C) SEV
(D) INHBA
(E) MX1
(F) INHBB
(G) BMP6
(H) FST
Huh7
Huh7.5
2^dCt GAPDH-INHBA
2^dCt GAPDH-MX1
2^dCt GAPDH-SeV
2^dCt GAPDH-INHBB
2^dCt GAPDH-BMP6
2^dCt GAPDH-FST
ZERO
MOI 0.5
MOI 1.0
MOI 5.0
SeV Multiplicity of Infection

Being deficient in functional RIG-I and TLR3, MDA5 is likely to be the principal sensor of DENV infection in Huh7.5 cells. At 48 h.p.i. DENV infection results in statistically significant upregulation of mRNA encoding *INHBA* and a strong trend towards induction of *INHBB*, accompanied by a significant upregulation of *MX1*. *BMP6* expression, however, is unchanged in this infection model [figure 4.12].

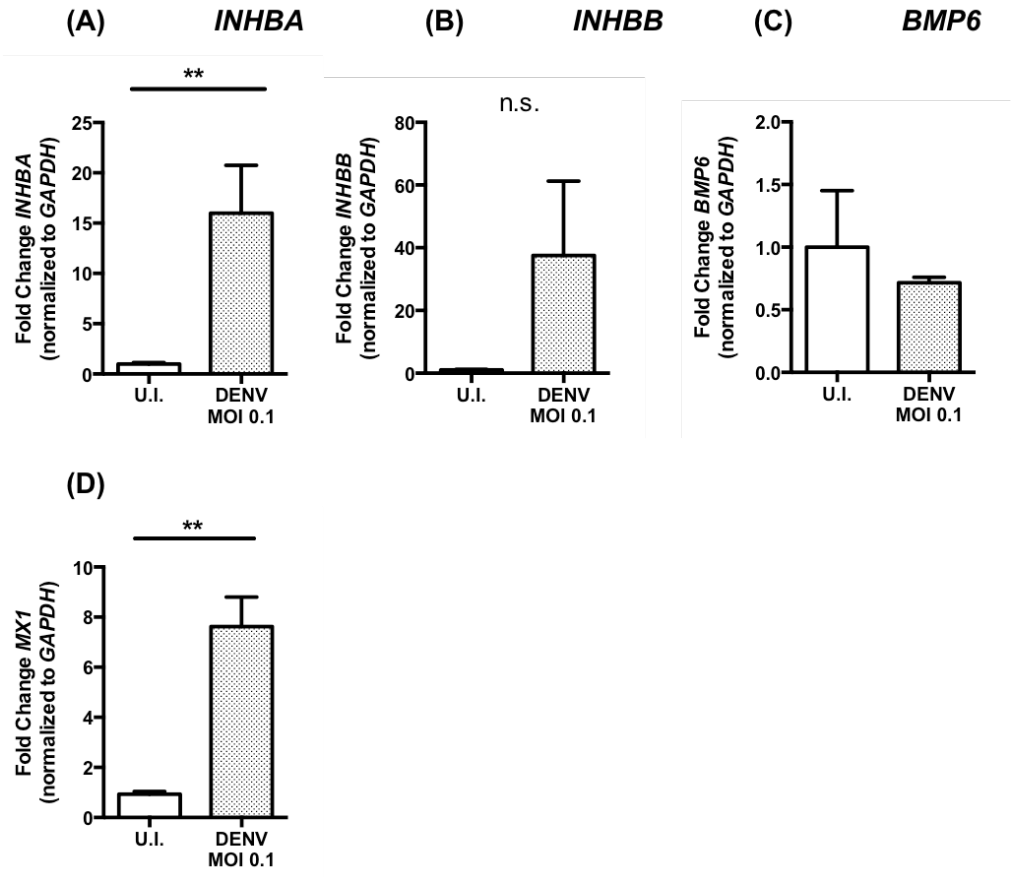


Figure 4.12: Activin A and B mRNA are induced by 48h DENV infection in Huh7.5 cells

Huh7.5 cells were infected with DENV MOI 0.1 and RNA extracted at 48h post-infection, followed by RT-qPCR quantification of transcript encoding *INHBA* (A), *INHBB* (B), *BMP6* (C) and *MX1* (D). Data is presented as fold change compared to uninfected cells.

Both *INHBA* and *MX1* are significantly upregulated in DENV-infected cells relative to uninfected. *INHBB* demonstrated a strong induction by DENV-infection, but this did not attain statistical significance. *BMP6* mRNA level is not modulated by DENV infection.

For *INHBA*, n=4; for *INHBB*, n=3; for *BMP6*, n=2; for *MX1*, n=3; mean+SEM; statistical analysis for all except *BMP6* by unpaired two-tailed t-test.

The hepatoma-derived HepG2 is not usually permissive to HCV infection, unless it is transfected with CD81 expression constructs. However, stimulation of HepG2 cells by Jc1 HCV across a 1 to 6 h time course elicits a mild induction of *INHBA* at 3-6 h post-infection, although this is not accompanied by induction of *MX1*. Neither *INHBB* nor *BMP6* expression were upregulated at any time point [figure 4.13].

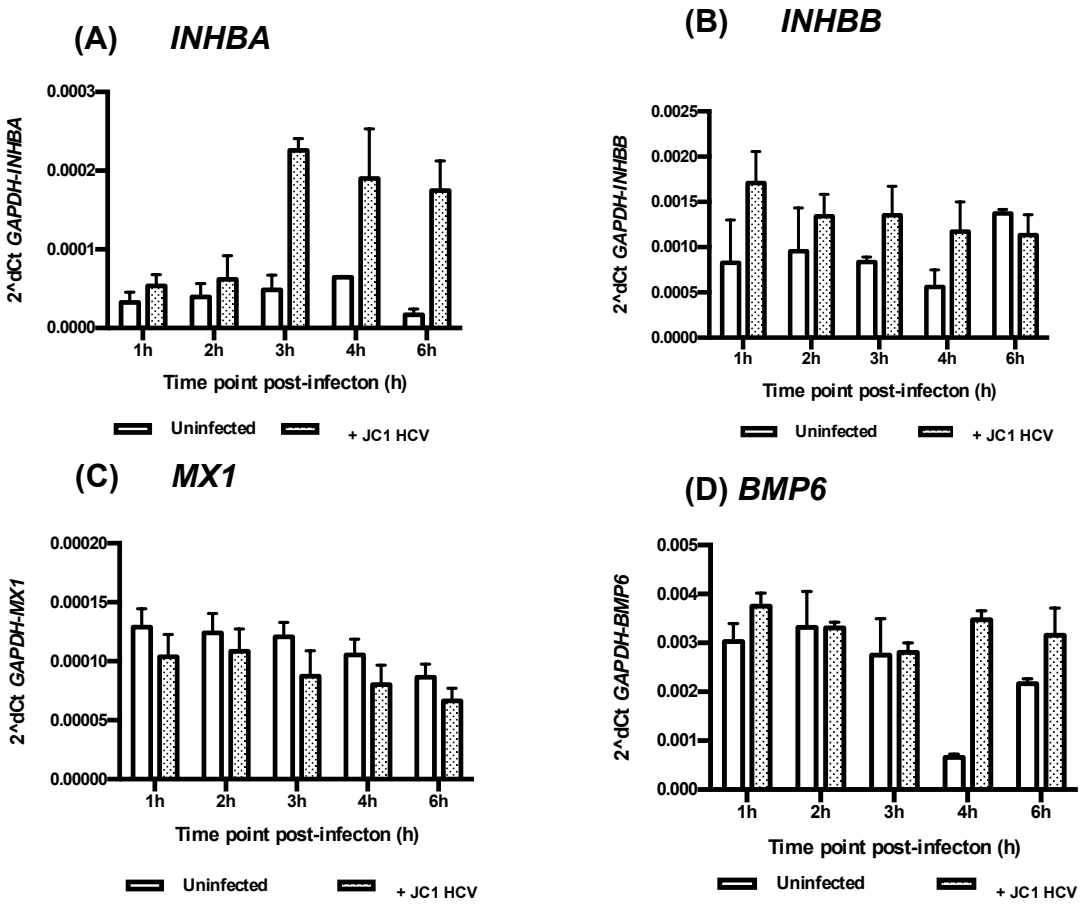


Figure 4.13: Activin A mRNA is induced at 3-6h post-stimulation of HepG2 cells with Jc1 HCV

HepG2 cells were infected with Jc1 strain HCV MOI 0.1. RNA was extracted at hourly intervals from both infected and uninfected control cells across at 6h time course, followed by RT-qPCR quantification of *INHBA* (A), *INHBB* (B), *MX1* (C) and *BMP6* (D) mRNA. Data is presented as 2^ΔCt values relative to *GAPDH*.

INHBA mRNA is elevated in infected relative to uninfected cells at 3h to 6h post-infection, whereas *INHBB* and *BMP6* do not show a consistent change following HCV infection at these time-points. *MX1* transcript is slightly suppressed in infected cells versus uninfected across the time-course.

n=2 independent experiments in biological singlicate; mean+SEM; statistical testing precluded due to small sample size.

In permissive Huh7.5 cells infected with Jc1 HCV, neither *INHBA* nor *MX1* induction was detectable during either 6 h or 72 h time courses, albeit in a single experimental replicate [figure 4.14].

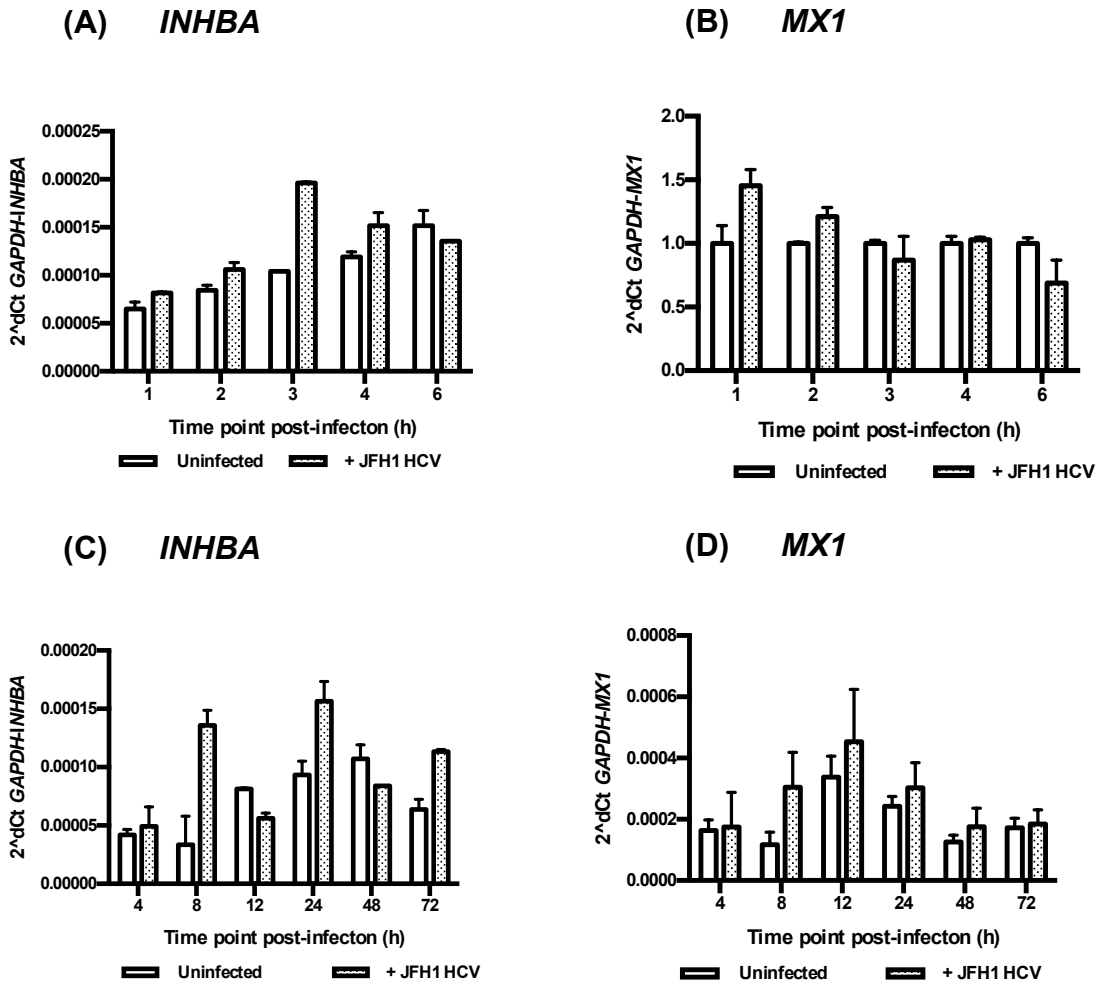


Figure 4.14: Neither Activin A nor MX1 mRNA are induced by Jc1 HCV infection of Huh7.5 cells during both early and late time-points, albeit within a single experimental replicate.

Huh7.5 cells were infected with Jc1 strain HCV MOI 0.1. RNA was extracted at from both infected and uninfected control cells both at hourly intervals across a 6h time course (A,B) and during at 72h period (C,D). *INHBA* (A,C) and *MX1* (B,D) mRNA levels were quantified by RT-qPCR.

In this experiment, neither *INHBA* nor *MX1* message levels demonstrate a consistent pattern infected cells relative to uninfected across ether time course.

n=1 in biological singlicate; mean+SEM; statistical testing precluded due to small sample size.

4.3.3 Activin A mRNA expression is modulated during in vivo infections

Having established that *INHBA*, and in the context of DENV infection *INHBB*, could be induced by viral infection *in vitro*, we chose to examine whether viral infection *in vivo* results in *INHBA* upregulation. Mouse influenza infection presented a readily available model

system. *Inhba* expression is significantly upregulated in the lungs of mice infected intranasally with FLUAV PR/8/34 for three days, compared to uninfected controls. This induction correlates very tightly with that of *Isg15*, encoding a pleiotropic, IFN-stimulated antiviral effector (approximately 10-fold and 40-fold for *Inhba* and *Isg15* respectively). In the liver, however, *Inhba* expression is significantly suppressed by flu infection, despite no alteration in *Isg15* expression [figure 4.15]. Suppression of hepatic *Inhba* expression in the presence of a systemic inflammatory response has been previously reported, albeit in the context of LPS administration (72,552).

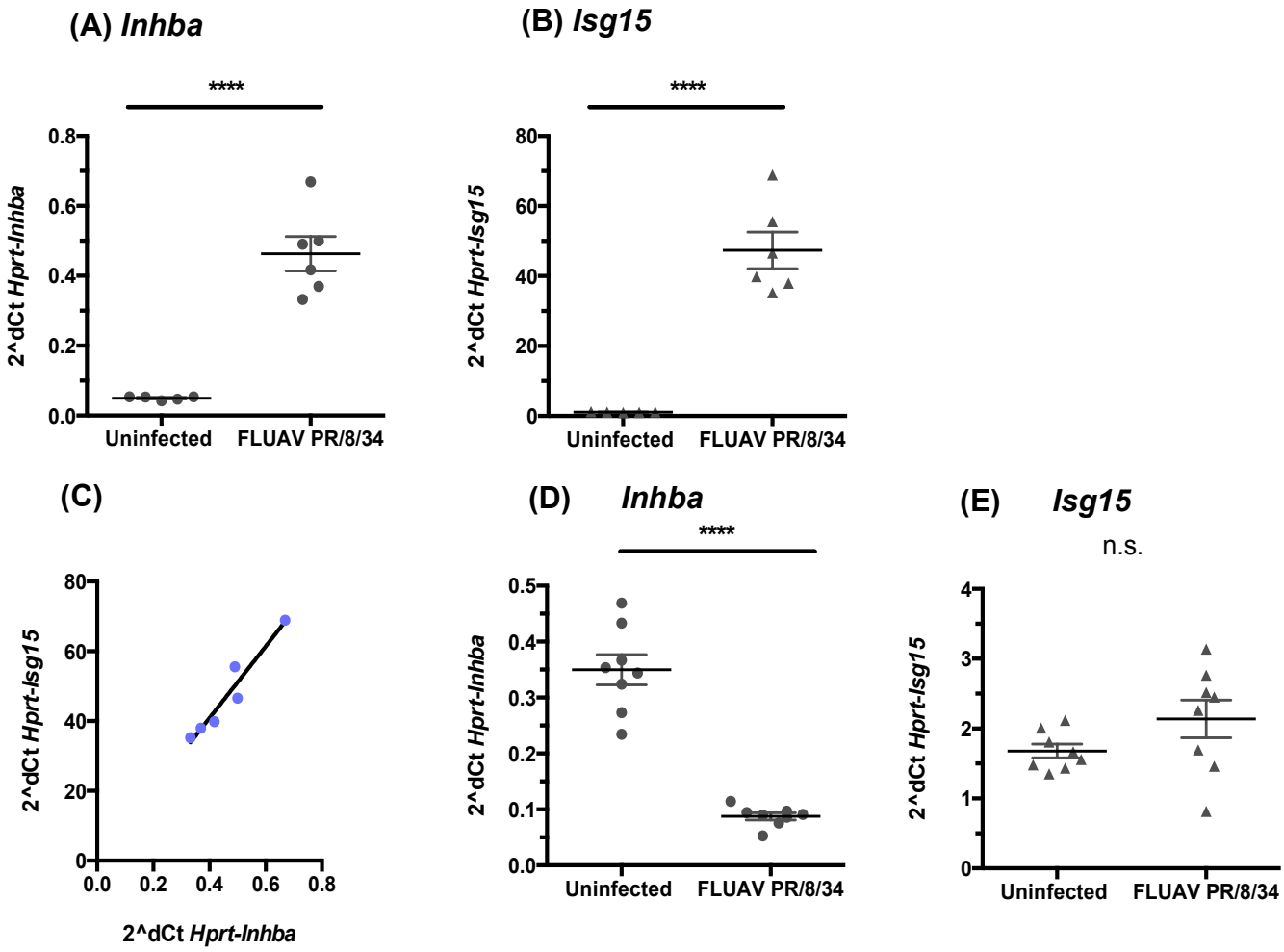


Figure 4.15: Activin A mRNA is upregulated in the lungs of FLUAV PR/8 infected mice at 3 d.p.i. and positively correlates with transcriptional induction of the antiviral effector *Isg15*

Lungs and liver explants were harvested at 3 days post-infection from 6-week old female C57BL/6 mice infected i.n. with 3.5 HAU FLUAV PR/8/34. RNA extracts were analyzed by RT-qPCR for mRNA expression of *Inhba* (A), encoding activin A, and *Isg15* (B), encoding the antiviral effector Isg15. *Isg15* and *Inhba* expression levels are correlated in (C). Data is presented as 2^ΔCt values relative to *Hprt*.

Message encoding both *Inhba* and *Isg15* is significantly upregulated in the lungs of infected mice, and the degree of induction is strongly positively correlated (R^2= 0.9271, p=0.0020). In the liver, *Inhba* message is significantly suppressed in the infected mice, whereas hepatic levels of *Isg15* message do not differ between groups.

For (A) to (C): n=5 uninfected and n=6 infected mice; mean+SEM; analysis by unpaired two-tailed t-test (A,B) and linear regression (C).

For (D) and (E): n=8 mice per group; mean+SEM; analysis by unpaired two-tailed t-test.

In a second infection model, namely intranasal infection with titrating doses of FLUAV, *Inhba* is dose-dependently upregulated at 2 d.p.i., reaching maximal 3-fold increase with the $5x10^4$ pfu inoculum. In contrast, neither *Inhbb* nor *Bmp6* were dose-dependently induced by flu infection; if anything, *Bmp6* transcript was mildly elevated at a low infection titre and then declined to baseline with increasing doses [figure 4.16].

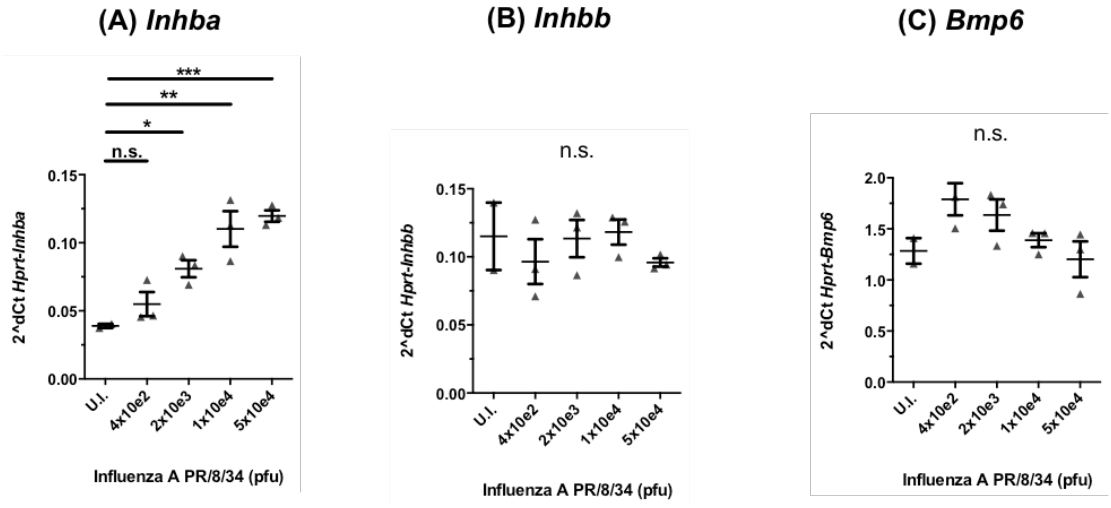


Figure 4.16: Activin A mRNA is dose-dependently induced in the lungs of infected mice by increasing titres of FLUAV, whereas activin B and BMP6 transcript is unchanged

Lungs were harvested at 2 days post-infection from 6-week old female C57BL/6 WT mice infected i.n. with titrating doses of FLUAV PR/8/34. RNA extracts were analyzed by RT-qPCR for mRNA expression of *Inhba* (A), *Inhbb* (B) and *Bmp6* (C). Data is presented as 2^ΔCt values relative to *Hprt*. *Inhba* message is significantly dose-dependently induced by flu infection; there is no difference in *Inhbb* or *Bmp6* induction between groups.

n=3 mice per group; mean+SEM; analysis by ordinary one-way ANOVA and Bonferroni's post-test with respect to uninfected mice.

To further investigate which PRR subsets are responsible for *Inhba* induction during flu infection, we compared *Inhba* expression in lung lysates from both wildtype and Mavs knockout mice. These animals cannot transduce RLR signalling (469). In wildtype mice, *Inhba* expression was significantly increased (approximately four-fold induction) by FLUAV at 2 d.p.i. [figure 4.17].

Inhba expression was also significantly upregulated by FLUAV in Mavs knockout mice.. The ISGs *Isg15* and *Trim14* were significantly induced by infection in both wildtype and Mavs knockout mice. While the magnitude of both *Isg15* and *Trim14* induction was lower in Mavs knockout mice compared to wildtype, this only attained statistical significance for *Isg15* [figure 4.17]. These data suggest a role *Inhba* induction downstream of Mavs-independent pattern recognition, for example via TLR7.

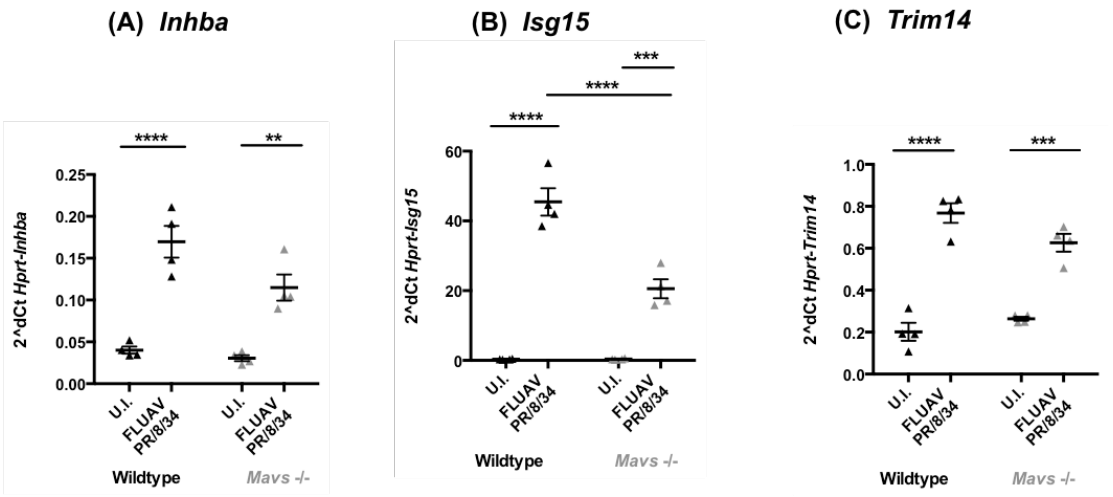


Figure 4.17: Activin A mRNA is significantly upregulated by infection with WT FLUAV PR/8 in the lungs of both WT and MAVS -/- mice at 2 d.p.i.

Lungs were harvested at 2 days post-infection from 6-week old female C57BL/6 mice, either WT or MAVS -/-, infected i.n. with $5x10^4$ pfu FLUAV PR/8/34. RNA extracts were analyzed by RT-qPCR for mRNA expression of *Inhba* (A), *Isg15* (B), and *Trim14* (C). Data is presented as 2^ΔCt values relative to *Hprt* expression.

Message encoding all genes is significantly upregulated in infected mice of both genotypes. Only the level of *Isg15* induction is significantly different between WT and MAVS -/- mice.

n=4 uninfected and n=4 infected mice of each genotype; mean+SEM; analysis by two-way ANOVA and Bonferroni's post-test between all conditions.

The FLUAV NS1 protein antagonizes IFN induction in part by disrupting RIG-I activation, either by suppressing its modification by TRIM25 or sequestering dsRNA ligands (553,554). As our *in vitro* experiments have shown that *INHBA* induction by SeV is RIG-I dependent, and *Inhba* levels are lower in the lungs of flu-infected Mavs knockout mice compared to wildtype, we hypothesized that inhibition of RIG-I by NS1 might also disrupt downstream activin A induction. To address this, we quantified *Inhba* induction in the lungs of both wildtype and Mavs knockout mice at two d.p.i. with NS1-deleted (NS1-del) FLUAV PR/8/34. In this model, while *Inhbb* expression remained unchanged by flu infection in both wildtype and Mavs knockout mice, in both genotypes *Inhba* expression was mildly, but non-significantly, elevated by infection with NS1-del FLUAV. Of note, *Inhba* expression is slightly higher in Mavs knockout versus wildtype mice, despite comparable levels of *Isg15* message [figure 4.18]. As data could only be procured for a single uninfected mouse, scope for interpretation of this experiment is very limited.

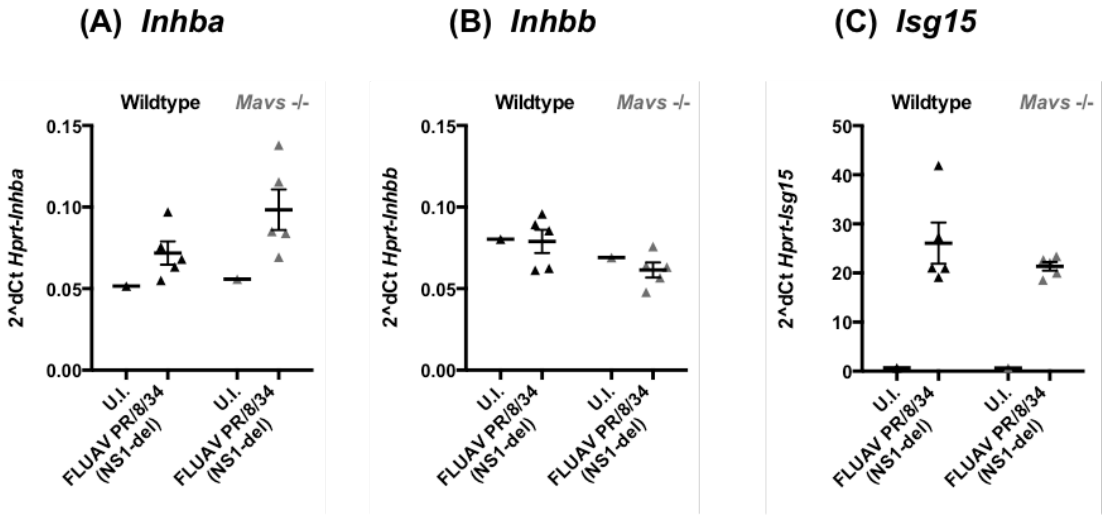


Figure 4.18: Activin A mRNA is mildly elevated in the lungs of both WT and MAVS -/- mice at 48h post-infection with NS1-deleted FLUAV PR/8, whereas activin B message is unchanged.

Lungs were harvested at 2 days post-infection from 6-week old female C57BL/6 mice, either WT or MAVS -/-, infected i.n. with $5x10^4$ pfu NS1-deleted FLUAV PR/8/34. RNA extracts were analyzed by RT-qPCR for mRNA expression of *Inhba* (A), *Inhbb* (B) and *Isg15* (C).

A trend towards mild elevation of *Inhba* is evident upon infection of both genotypes, although there is no difference in *Inhbb* expression between groups. *Isg15* is robustly induced by infection in both genotypes.

Statistical testing precluded due to disparate group sizes: n=1 uninfected mouse per genotype; n=5 infected mice per genotype.

Flu infection appears to induce local expression of *Inhba*, downstream of both Mavs-dependent and independent signalling. We were unable to obtain serum samples from these experiments in which to measure activin A protein.

4.4 Summary and discussion

The data in this chapter provide evidence for induction of activins, at both the transcriptional and protein level, in response to both viral infection and synthetic agonists of viral PRRs.

In vitro, transcriptional upregulation of *INHBA* was detectable in both transformed cells and PBMCs stimulated with synthetic agonists of RIG-I, MDA5, TLR7 and TLR8, albeit with cell-type specific variation. *In vitro*, both SeV and DENV infection elicited strong induction of *INHBA* mRNA; only DENV infection induced *INHBB* in our study. Further experiments should explore whether TLR3 stimulation elicits *INHBA* induction, in both primary cells and TLR3-replete transformed cell lines. In a single experiment we were able to show that detection of cytosolic DNA is sufficient to induce *INHBA* mRNA. In addition to replicating this observation, future work should also examine whether direct STING activation by exogenous cyclic dinucleotides activates *INHBA* transcription.

Activin A protein could not be detected by ELISA in supernatants from transformed cells, either transfected with nucleic acid PRR agonists or infected with SeV. Subsequent experiments should examine expression of activin A protein in cell lysates by Western blot.

To delineate the mechanistic basis for *INHBA* induction following PRR sensing, future work should focus on dissecting the signalling pathways activated in a single cell type, preferably Huh7 or, given their greater similarity to the OR6 HCV replicon model, cured-OR6 cells.

At the protein level, secreted activin A was detectable in culture supernatants from PBMCs stimulated with agonists of RIG-I, MDA5, TLR7, TLR8 and, interestingly, TLR9, albeit with substantial variation between donors. PBMCs are a heterogeneous cell fraction; to identify which cell types are responsible for *INHBA* production in response to PRR activation samples should be sorted into their constituent subsets, either by FACS or magnetic immunodepletion, before stimulation. Monocytes are likely candidates as the principal source of secreted activin A, with existing evidence for activin A expression, both protein and mRNA, by monocytes in response to the PMA, LPS and GM-CSF *in vitro* (69,91,559). Previous studies have described pre-formed granular release of activin A by neutrophils both *in vitro* and *in vivo,* in response to TNFα and LPS respectively. While our PBMC isolation technique sought to exclude granulocytes, the possibility that the cell fractions could have been contaminated by a small neutrophilic fraction remains.

In vivo, wildtype FLUAV significantly upregulated *INHBA* expression in mouse lungs, in parallel with significantly elevated ISG transcription. As these analyses were conducted on whole lung lysates, we cannot infer the specific cell types responsible for this *INHBA* induction. Subsequent experiments should examine activin A localisation in histological sections from infected lungs, either by protein immunohistochemistry or fluorescent *in situ* hybridization against *INHBA* mRNA.

Wu and colleagues report that in the resting state, murine alveolar and bronchial macrophages stain positively for activin A protein; during LPS endotoxaemia, activin A positive neutrophils aggregate in the perialveolar spaces (552). This accumulation of activin A-rich neutrophils in the lung correlates with reduced numbers in the bone marrow, consistent with their migration into the systemic circulation. However, in this study, activin A induction occurred predominantly at the post-transcriptional level, being ablated by cyclohexamide but unaffected by actinomycin D, an inhibitor of transcription initiation (552). In contrast to LPS, in our studies flu infection transcriptionally upregulates *INHBA*, therefore respiratory epithelia and alveolar macrophages are equally plausible candidate sources.

In our studies, there was no significance difference between the magnitude of *INHBA* induction in lungs of flu infected wildtype and MAVS knockout mice, suggesting intact RLR function is not required for *INHBA* upregulation in response to flu infection. To establish whether *INHBA* expression is indeed directly downstream of any viral PRR, the infection could be repeated in either mice deficient in Tbk1, a point of convergence for RLR and TLR3 viral RNA sensing mechanisms, or Mavs/Myd88/Trif triple knockout mice.

The differential induction of *INHBA* and *INHBB* by viral infection and innate immune stimuli is reminiscent of their distinct expression patterns, both spatial and temporal, in other physiological contexts. For example, complementary fluctuations in inhibin βA and βB subunits regulate expression of pituitary gonadotropins during the mammalian reproductive cycle (67). The proximal *INHBA* upstream regulatory region is distinguished from that of *INHBB* by the presence of multiple GATA binding motifs, fewer AP2 consensus sequences and three AP1 binding sites rather than one (401) [figure 4.20].

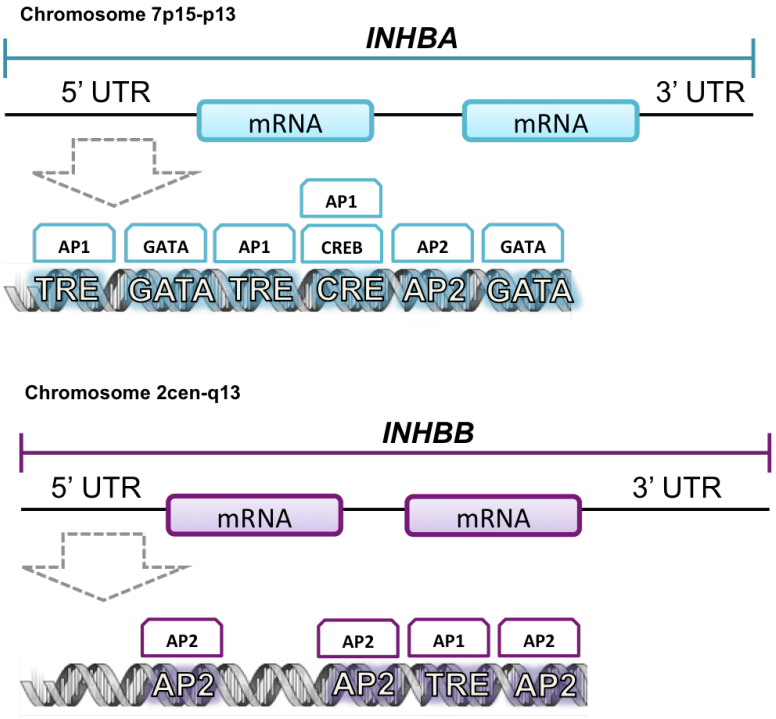


Figure 4.20: Schematic representation of the human *INHBA* and *INHBB* loci, including transcription factor binding sites present in their respective proximal promoter regions

Adapted from Walton et al. The synthesis and secretion of inhibins. *Vitamins and Hormones*, volume 85 (2011)

AP1/2: Activator protein 1/2 transcription factor or consensus sequence
TRE: 12-*O*-Tetradecanoylphorbol-13-acetate
CRE: cAMP responsive element
GATA: GATA-binding factor protein or consensus sequence
CREB: CRE-binding protein

We explored the possibility that *INHBA* could be induced as part of a second wave of cytokine induction, downstream of a primary PRR-induced pro-inflammatory or antiviral cytokine. Recombinant IFNα-2a induces neither *INHBA* nor *INHBB* transcription, an observation consistent with the lack of ISRE or GAS elements in the proximal promoter region of both genes. Comparison of evolutionarily conserved regions of the mouse and human reference genomes, using the NCBI ECR and Mulan sequence comparison tools, does

reveal putative IRF1 and IRF2 binding sites approximately 2 kb upstream of the *INHBA* start site, but the functional ramifications of these are unclear [data not shown] (560). Preliminary efforts were made to identify whether co-incubation with either ruxolitinib or an anti-IFNAR2 neutralizing antibody is sufficient to reduce *INHBA* expression after either SeV infection or IVT-RNA transfection, but these were technically unsuccessful [data not shown].

Activation of the AP1 transcription factor – a heterodimeric assembly of c-FOS, c-JUN and ATF subunits – downstream of TNFα signalling is well characterised (561). Stimulation of the TNF receptor by TNFα elicits activation of a MAPK cascade culminating in phosphorylation of AP1 by JNK (562). Phosphorylation of the NFκB subunits p50 and p65 is also triggered by the TNF receptor, downstream of both the p38α-MAPK and IKK/IκB axes (561). Interaction of TNFα-induced AP1 with TRE and CRE sequences in the *INHBA* promoter is a plausible mechanism for activin A transcriptional induction following viral sensing.

While the interplay between activin A and TNFα has not, to the best of our knowledge, been described during viral infection, numerous studies have explored their interaction in an inflammatory setting. Published *in vitro* data demonstrate that activin A upregulates *TNFA* transcription in rat bone marrow-derived macrophages and human PBMCs (95,99). Recombinant TNFα, by contrast, elicits release of preformed activin A during neutrophil degranulation, but is not associated with transcriptional induction of *INHBA*.

Whole-animal studies examining cytokine kinetics during systemic inflammation suggest that TNFα induction occurs in parallel with, or after, detection of serum activin A peptide. In sheep exposed to LPS, co-administration of a soluble TNFα ligand trap affects neither the kinetics nor the magnitude of serum activin A induction (563). During LPS challenge in mice, intravenous administration of the soluble activin antagonist follistatin reduces peak serum TNFα levels, implying that in this setting induction of TNFα is modulated by activin A (101), rather than the reverse The authors report that infusion with recombinant activin A in the absence of inflammatory stimuli is not sufficient to elevate serum TNFα, suggesting that activin A might enhance pre-existing TNFα release, rather than induce its *de novo* synthesis (101).

We have not yet sought to establish whether the induction of activin A by viral infection or PRR agonists in our experimental models occurs secondary to TNFα signalling. To define the contribution of TNFα signalling to *INHBA* induction, blockade of TNFα signalling during viral infection, for example via administration of the small-molecule RIPK2 inhibitor necrostatin-1 or by incubation with a neutralizing antibody against the TNF receptor

Despite the absence of SMAD-responsive motifs in its proximal promoter *INHBB* is inducible by both canonically SMAD2/3-dependent factors (TGFβ1/2, GDF9, BMP15) and SMAD1/5/8-linked cytokines (BMP2 and BMP6) (401). In cultured ovarian granulosa cells, recombinant activin A is reported to upregulate both *INHBB* and *BMP6* transcripts (564); the possibility that activin A could modulate activin B expression akin to the IFNβ-IFNα interaction is open to investigation. In terms of a mechanistic basis for this interaction, inspection of a SMAD ChIP-seq in BMP4-treated CD34+ erythrocytes reveals a putative SMAD1 binding event approximately 8 kb upstream of the *INHBB* transcription start site (61).

Given that regulation of gene expression also can occur via distal cis-regulatory interactions, we could use chromatin conformational capture-based techniques to characterize more comprehensively the cis-acting elements involved in *INHBA* activation downstream of viral sensing. The transcription factors associated with the identified enhancer elements could then be elucidated with reference to pre-existing ChIP data, and their contribution to *INHBA* induction during infection determined by CRISPR/Cas9 ablation of their respective interaction sites.

Our observations of activin A induction in experimental infection systems correspond with clinical reports of elevated serum activin A in both acute influenza A infection, where it correlates with the degree of respiratory distress, and in chronic HCV (106,565). Interpretation of these patient studies is complicated by the well-established role of activin A and TGFβ signalling in fibrosis (70); it is impossible to dissect whether elevated activin A occurs immediately downstream of viral sensing or as a mediator of fibrotic immune pathology.

In summary, the work presented in this chapter demonstrates that activin is induced by both synthetic analogues of viral nucleic acids and true viral infection, stimuli that are well-characterized inducers of type I and type III IFN. These data tie in with the observations [presented in chapter 3.4] that activins and certain BMPs exert potent anti-HCV effects. In addition, previous data from the lab have also shown that BMP6 and BMP9 could enhance type I IFN activity. Therefore, we were curious to establish whether activins induced during pattern recognition also modulate type I and type III IFN activity. To investigate this, we conducted a series of *in vitro* experiments examining the transcriptional and functional effects of activin and IFN co-incubation, described in chapter 5.

Chapter 5

Modulation of IFN effector functions by activins

5.1 Introduction

Five decades after the initial characterization of the IFN response, up to 2,000 Interferon Stimulated Genes (ISGs) have been identified, initially via genome-wide transcriptome analyses and more recently via functional screening and targeted ablation studies. Induced downstream of type I and type III IFN signalling, ISGs comprise diverse modes of action, including regulation of growth, proliferation and motility, in addition to their direct antiviral effector functions and immumodulatory effects (142). The capacity of type IFN isoforms for ISG induction is hierarchical, with IFNβ reportedly more potent than IFNα, and both type I IFNs stronger than the lambda IFNs (566). ISG induction repertoires vary in accordance with environmental context, including cell type, IFN class and the prevailing cytokine milieu (140,567,568).

This chapter presents data pertaining to the interactions of activin and IFN signalling, both in terms of anti-HCV activity and ISG transcriptional induction. It commences with a brief review of ISG effector mechanisms, before describing previous, largely unpublished, antiviral interactions between IFNα and BMPs.

5.1.1 ISG effector mechanisms: a summary

ISGs can target multiple stages of a viral life cycle, including viral entry or egress, replication and translation. The contributions of individual ISGs to the antiviral immune response is a topic of increasing experimental attention; with the exception of certain mediators conferring broad-spectrum, non-redundant antiviral properties, many ISGs remain poorly characterized, in part due to their functional overlap.

In inbred laboratory mouse strains, associations between extreme susceptibility to influenza infection and variation in the *MX1* locus led to the characterization of MX1 as a strong, broad-spectrum antiviral restriction factor (569). Expressed almost ubiquitously, MX1 encodes a large, multidomain GTPase with a central protein interaction domain that permits binding to viral targets - typically nucleocapsid proteins- resulting in their sequestration and ultimate destruction (570).

MX1 typically inhibits the early stages of viral replication and, in the case of FLUAV, may also disrupt transcription of progeny genomes by direct interaction with the viral RNA-dependent RNA polymerase (571,572).

IFN-induced RNA editing enzymes, including ADAR and APOBEC3G also disrupt synthesis of viral genomic RNA. The former converts adenine to inosine, resulting in unstable IU base pair formation, whereas APOBEC3G's cytidine deaminase activity promotes deleterious hypermutation of HIV-1 replication intermediates (573,574).

Translational inhibition is another common antiviral effector mechanism. IFIT1 disrupts cap-dependent translation by binding to eukaryotic initiation factors required for ribosome activation and is also able to disrupt recruitment of translational machinery to the HCV IRES(575). Ectopic overexpression of IFIT1 is sufficient to inhibit HCV replication *in vitro*. IFIT1 is also implicated in the recognition of viral RNAs that lack 2'-O-methylation at their terminal guanosine, a structural motif common to eukaryotic mRNA (576). Mass spectrometry analysis of intracellular proteins binding a 5'ppp-RNA bait reveal that IFIT1 directly binds 5'ppp-RNA moieties, resulting in recruitment of a trimeric IFIT1/2/3 complex proposed to sequester viral replication intermediates (577).

Antiviral effectors may block viral entry, either by inhibitory association with required viral entry factors or impairment of membrane fusion. For example, IFI6 reportedly impairs co-factor recruitment to the HCV entry receptors CD81 and claudin-1 (578). An analogous function has been described for *IFITM1*, a hepatocellular tight-junction component that mediates CD81-dependent blockade of HCV entry *in vitro* (579). In terms of membrane fusion, the cholesterol hydroxylase CH25H synthesizes soluble lipid derivatives that dose-dependently inhibit membrane fusion by diverse virus classes (580).

IFITM3 knockout mice succumb to severe pneumonia following challenge with low-pathogenicity FLUAV strains; clinically, patients hospitalized with severe influenza during the 2009 pandemic showed increased, significant, enrichment for a variant IFITM3 allele associated with reduced viral restriction *in vitro* (581). IFITM3 is proposed to inhibit membrane fusion of FLUAV in the late endosome, preventing cytosolic injection of viral genomic segments, in addition to its role in modulating intracellular cholesterol homeostasis (582,583).

Numerous effector ISGs target viral egress. The multifunctional antiviral factor viperin, encoded by *RSAD2*, modulates lipid biosynthesis, reducing membrane fluidity and impairing budding of viruses including FLUAV and HIV-1 (584). During DENV, HCV and Chikungunya virus infection, viperin, by virtue of its amphipathic helix domain, is able co-localize with the virion assembly apparatus at the ER membrane, disrupting virion assembly

(585). Direct interactions between viperin and the HCV core and the analogous DENV2 capsid proteins have also been reported (584).

Phospholipid scramblase 1, encoded by *PLSCR1*, is hypothesized to modify phospholipid membrane composition so as to impair the intracellular membrane rearrangements required for establishment of HCV "replication factories" (325).

Multiple ISGs mediate IFN's cytostatic effects, the antiviral effects of which are summarized in section 3.1.4. Additionally, IFIT3 is proposed to prevent proteasomal degradation of the CDKI p27, promoting cell cycle arrest at the G1/S checkpoint (586).

ISGs play a key role in the sensitization of cells to pathogenic stimuli. Multiple PRR signalling components, including RIG-I, MDA5, LGP2 and cGAS are themselves IFN-inducible (433,587,588). While most cells maintain high constitutive expression of STAT1 and IRF9, facilitating rapid amplification of the type I IFN responses following low-level IFNβ secretion, both are also further upregulated by type I IFN and IFNγ respectively (568,589). IRF7, required for second-wave type I IFN induction, is upregulated from very low basal levels by IFNβ in most cell types, facilitating positive-feedback amplification of type I IFN secretion (590,591).

In pDCs, association of viperin with TLR7 and TLR9 facilitates recruitment of IRAK1 and TRAF6 adaptor molecules and subsequent enhancement of IRF7 phosphorylation and IFNα production (592). TRIM14 augments RLR signalling by regulating assembly of the MAVS signalosome and recruiting NFκB; commensurately, TRIM14 knockdown attenuates activation of an ISRE-reporter construct by SeV infection (593).

An array of IFN-inducible negative feedback mechanisms curtail IFN signalling, preventing damaging excess activation, as summarized in section 1.2.4. The viral entry inhibitor IFI6 was initially characterized as a negative regulator of cellular susceptibility to IFN-induced apoptotic signals, hypothetically promoting survival of uninfected cells exposed to pro-apoptotic stimuli (594).

Analogous to the modification of protein function by K48-linked ubiquitin, conjugation of both constitutive and IFN-stimulated target proteins by the IFN-induced polypeptide ISG15 exerts multiple regulatory functions. So-called "ISGylation" stabilizes IRF3 expression and represses the phosphatases that curtail NFκB activation, potentiating induction of IFNβ and pro-inflammatory cytokines (156). ISGylation enhances inhibition of translation by activated

PKR; in contrast, its conjugation to RIG-I reduces IFN induction upon viral infection, suggesting a subtler role for ISG15 in fine-tuning the antiviral response than mere potentiation(595). The OAS-RNaseL axis, a broadly active antiviral mechanism for rapid degradation of cytosolic dsRNA, is also IFN-inducible (571).

ISG15 may also be conjugated directly to viral proteins. ISGylation disrupts viral egress by inhibiting the ubiquitination of Gag and VP40 required for HIV-1 and ebolavirus budding respectively (596,597). Multiple viruses, including SARS coronavirus, Sindbis virus and the emergent pathogen Crimean-Congo fever virus, encode ISG15 de-conjugating mechanisms, illustrating the extent of the selection pressure ISGylation has posed upon viral evolution (598).

Recent data imply that ISG15 negatively regulates the type I IFN response by inhibiting ubiquitination of the negative regulator USP18, thereby promoting its intracellular accumulation and subsequent dampening of the IFNAR complex. In line with this model, patients with homozygous loss of function mutations in *ISG15* show signs of a hyperactive type I IFN axis, exhibiting intracranial calcification and high autoantibody titres reminiscent of Aicardi-Goutières syndrome (599).

A detailed description of adaptive immune modulation by ISGs is beyond the scope of this introduction, but include promotion of Th1 versus Th2 T-lymphocyte polarization; expansion and functional enhancement of Foxp3+ regulatory T-lymphocytes during chronic viral infection; and suppression of Th17 cell differentiation (600).

5.1.2 Synergistic interactions of BMP and IFNα signalling

Previous observations from the Drakesmith laboratory demonstrate that recombinant BMP6 enhances the antiviral function of IFNα-2a against a full-length HCV genomic replicon. Moreover, published data from Sakamoto and colleagues describe synergistic antiviral interaction between BMP7 and IFNα, in both a subgenomic replicon model and against replicating JFH1 HCV (344). In their study, incubation with BMP7 alone did not induce expression of the ISGs *MX1* or *OAS2*, although the authors did not examine other ISGs or the effects of concurrent exposure to BMP7 and IFNα.

Transcriptome analysis in BMP6-treated Huh7 cells (see section 3.1.1) reports induction of multiple components of the type I IFN signal transduction pathway and effectors, including IFNAR2, JAK1, STAT2, IRF9, IFI6 and ISG15, all of which were verified by RT-qPCR.

Increased expression of type I IFN signalling components by BMP6 could increase the capacity available for antiviral signalling, possibly accounting for the boosting of IFNα's anti-HCV effect by BMP6/7 *in vitro*.

Moreover, inspection of the promoter regions of IRF1 and IRF7, both of which can mediate antiviral effects in the absence of added IFN, reveals the presence of multiple BMP-responsive elements (BRE) in the regions 2 kb upstream of each transcription start site. The GGCGCC motif is regarded as a consensus sequence for genomic interactions of BMP-stimulated SMAD1/5/8 transcription factor complexes (601,602) Consistent with this, previous data from the Drakesmith laboratory demonstrates that recombinant BMP6 upregulates *IRF1* and *IRF7* expression *in vitro* [Eddowes et al. unpublished observations; see appendix I].

Integrating these data with the microarray study, it was hypothesized that the IFN-boosting effects of BMP signalling might be in part attributable to increased ISG induction in the presence of both cytokines. Consistent with this, co-incubation of Huh7 cells with recombinant BMP6 and IFNα-2a synergistically enhances induction of a panel of ISGs, including *TRIM14* and *IFI6*, compared to IFNα only [Eddowes et al. unpublished observations; see appendix I].

Given that both activin A and B, akin to BMP6, exert ALK2/3 dependent anti-HCV effects *in vitro*, we were keen to establish whether they also synergised with type I IFN, both in terms of antiviral efficacy and ISG induction. In this chapter, the anti-HCV effects of activin A in the presence of IFNα and IL28B are explored, in addition to the role of activin A and B in ISG induction *in vitro*.

The key questions addressed were:

1) Does activin A enhance the anti-HCV effects of exogenous type I and type III IFN?
2) Do activin A and B modulate ISG induction by type I and III IFN?
3) Does activin A induce expression of type I IFN signalling components?

5.2 Materials and methods

5.2.1 HCV replicon antiviral assays

OR6 cells, maintained as described in section 2.3.1, were plated at $3.5x10^4$ cells/well of flat-bottomed 96-well plates and incubated for 24 h at 37 °C. After aspiration of medium, cells were incubated with 2 nM or 6 nM recombinant human activin A (R&D Systems), in the presence of 10 U/mL or 100 U/mL recombinant human IFNα-2a (PBL Life Sciences) or 10 ng/mL or 100 ng/mL recombinant human IL28B (IFNλ3) (R&D Systems), in triplicate wells per condition. At 72 h post-incubation, cells were assayed for Renilla luciferase signal as a surrogate for intracellular HCV content (as per section 2.3.2) and for cell viability/number with the Promega Cell Titer Glo assay system (as described in section 2.3.3).

5.2.2 Bliss independence test for synergy

To determine whether the observed interactions between activin A and type I/III IFN are additive or synergistic, the data were analyzed with a variant of the Bliss independence test, a common model to determine the anticipated effect magnitude of drugs in combination relative to monotherapy. The model assumes that both drugs act by distinct mechanisms; as such their combined output can be predicted as the product of their individual effects. Yan and colleagues formulated a variant of the Bliss test in which a "synergy assessment factor" is defined by the equation:

$$S = r(a,b) - r(a_o,b) \cdot r(a,b_o)$$

where *S* represents the "synergy assessment factor"; r(a,b) is the actual combined effect; and r(a0,b)*r(a,b0) is the expected combined effect if the drugs are assumed to be synergistic. In this model, synergy is defined as $S<0$, additivity is defined as $S=0$ and antagonism is defined as $S>0$ (603).

5.2.3 RT-qPCR quantification of ISG induction in transformed cells

Cell lines were maintained as described in section 2.1.

Cell lines were plated in either 12-well or 24-well plates and incubated at 37 °C for 24 h, until monolayers reached approximately 70 % confluence. Experiments were conducted in single or duplicate wells as specified in individual figure legends. Cells were incubated with

recombinant human activin A 2 nM, activin B 2nM or BMP6 18 nM (R&D Systems) in the presence or absence of either recombinant human IFNα-2a (PBL Life Sciences) or IL28B (R&D Systems) at the doses specified within the figures. At the experimental end-point, RNA extraction, cDNA synthesis and RT-qPCR quantification of target gene expression were conducted as described in sections 2.2.4-2.2.7.

5.2.4 RT-qPCR quantification of ISG induction in PBMCs

PBMCs were harvested from two healthy donors as described in section 2.1.6. PBMC were plated at $1x10^6$ cells/well of a 24-well plate in RPMI-1640 with 10% FCS (supplemented as per section 2.1.6), with the addition of recombinant human activin A 2nM (R&D Systems) in the presence or absence of recombinant human IFNα-2a (PBL Life Sciences). After 24 h incubation, PBMCs were harvested for RNA extraction, cDNA synthesis and RT-qPCR quantification of target gene expression conducted as described in section 2.2.4-2.2.7.

5.2.5 RT-qPCR quantification of IFN signalling components

In figure 5.9, Huh7 cells were plated at $1x10^5$ cells/well of a 12-well plate, followed by overnight incubation at 37 °C. Cells were then incubated, in either singlicate or duplicate wells, with recombinant human IFNα-2a (PBL Life Sciences) for 24 h, followed by RNA extraction, cDNA synthesis and gene expression analysis by RT-qPCR as detailed in sections 2.2.4-2.2.7.

5.2.6 Inspection of ISG promoter regions for BRE motifs

Genomic regions 2 kb upstream of the transcription start site of a panel of ISGs were extracted from the human reference genome build GRCh37 (UCSC hg19/Feb 2009) using the UCSC genome browser 'Known Genes' table browser (604) and searched for the presence of the GGCGCC BRE consensus sequence.

5.3 Results

5.3.1 Activin A synergistically enhances the anti-HCV effects of IFNα and IL28B

Incubation of OR6 cells with activin A dose-dependently enhances the antiviral effect of both 10 U/mL and 100 U/mL IFNα-2a, normalized for the significant decrement in ATP content within each well upon exposure to activin A [figure 5.1]. The effect of both 2 nM and 6 nM activin A is synergistic, as indicated by the negative Bliss coefficient [table 5.1].

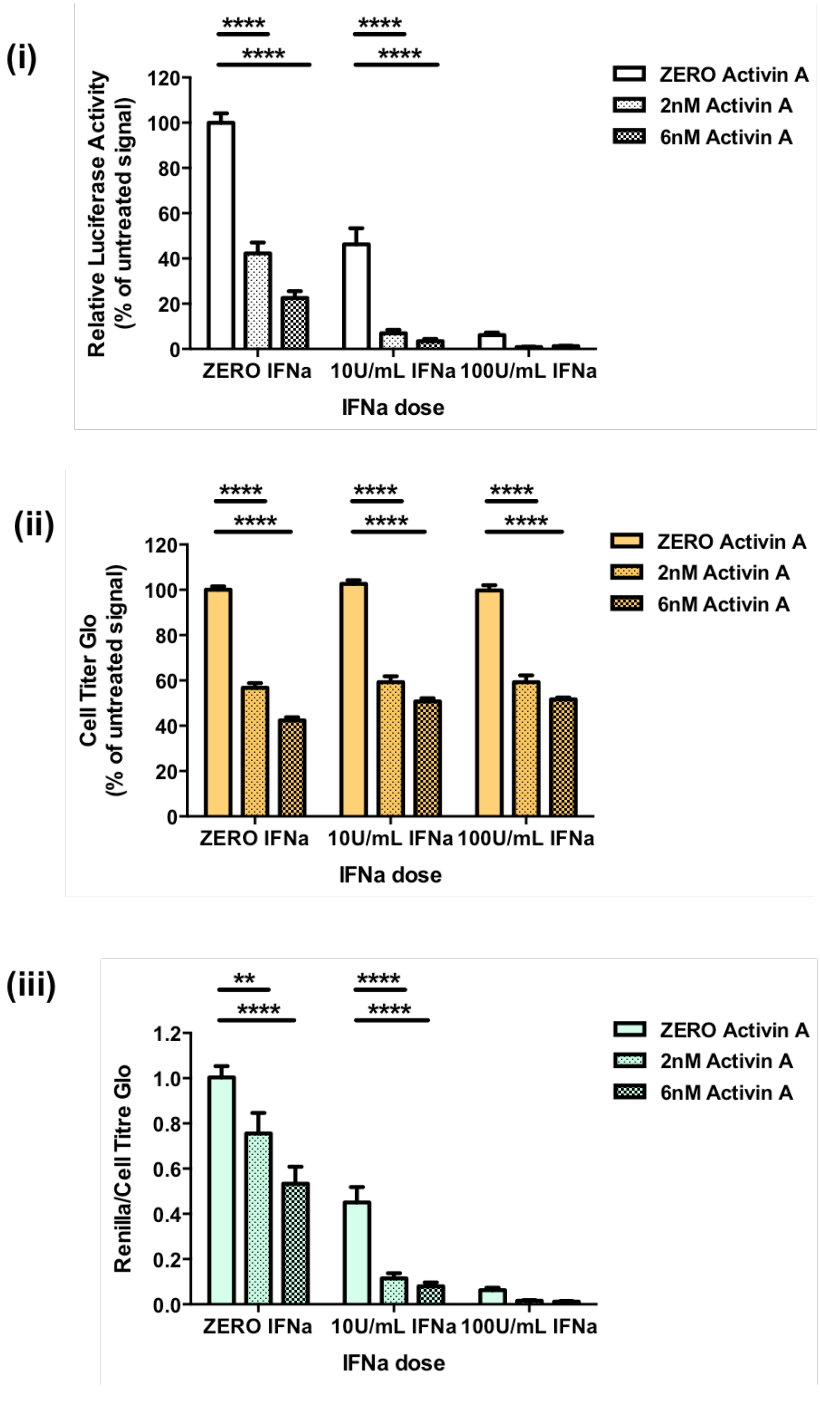


Figure 5.1: Co-incubation with activin A synergistically enhances the antiviral effect of IFNα in the OR6 HCV replicon model

OR6 cells were incubated with a titration of recombinant human IFNα in the presence of titrating doses of recombinant human activin A; cells were assayed at 72 h post-incubation for Renilla luciferase (i) and Cell Titer Glo (ii), with signal presented relative to the untreated condition. Renilla luciferase signal is normalized to Cell Titer Glo intensity, to account for variation in cell number, in (iii).

Normalized for the dose-dependent diminution in cell number/viability caused by activin A, co-incubation with activin A synergistically enhances the antiviral effect of both 10 U/mL and 100 U/mL IFNα.

n=3 independent experiments in biological triplicate; mean+SEM; analysis by 2-way ANOVA and Bonferroni's multiple comparisons test with respect to the ZERO activin A condition within each group.

Activin A Dose	IFNα Dose	Expected Combined Effect (ECE)	Actual Combined Effect (ACE)	S (synergism assessment factor)
ZERO	ZERO	1.003505667	1.003505667	0
ZERO	10 U/mL	0.450429056	0.450429056	0
ZERO	100 U/L	0.062442136	0.062442136	0
2 nM	ZERO	0.755329333	0.755329333	0
2 nM	10 U/mL	0.340222278	0.114883236	-0.225339043
2 nM	100 U/L	0.047164377	0.015327264	-0.031837112
6 nM	ZERO	0.533990433	0.533990433	0
6 nM	10 U/mL	0.240524807	0.079999202	-0.160525604
6 nM	100 U/L	0.033343503	0.011881649	-0.021461854

Table 5.1: Application of the Bliss Independence model to OR6 cells co-incubated with activin A/IFNα

Calculation of the synergism assessment factor for multiple combinations of activin A and IFNα on OR6 cells. Data are derived from the means of three independent experiments, each conducted in biological triplicate.

Similarly, incubation of OR6 cells with activin A dose-dependently boosts the anti-HCV effect of recombinant IL28B, a type III IFN, accounting for reduction in cell number by activin A [figure 5.2]. While the Bliss independence test reports [table 5.2] that enhancement by 2 nM activin A is synergistic, the effect of 6 nM is not, in fact being slightly antagonistic.

Activin A Dose	IL28B Dose	Expected Combined Effect (ECE)	Actual Combined Effect (ACE)	S (synergism assessment factor)
ZERO	ZERO	0.999999967	0.999999967	0
ZERO	10 ng/mL	0.745482467	0.745482467	0
ZERO	100 ng/mL	0.717975887	0.717975887	0
2 nM	ZERO	0.630644433	0.630644433	0
2 nM	10 ng/mL	0.470134368	0.294141743	-0.175992624
2 nM	100 ng/mL	0.452787496	0.287974617	-0.16481288
6 nM	ZERO	0.422242267	0.422242267	0
6 nM	10 ng/mL	0.314774206	0.356520933	0.041746727
6 nM	100 ng/mL	0.303159766	0.365464833	0.062305068

Table 5.2: Application of the Bliss Independence model to OR6 cells co-incubated with activin A/IL28B

Calculation of the synergism assessment factor for multiple combinations of activin A and IFNα on OR6 cells. Data are derived from the means of three independent experiments, each conducted in biological triplicate.

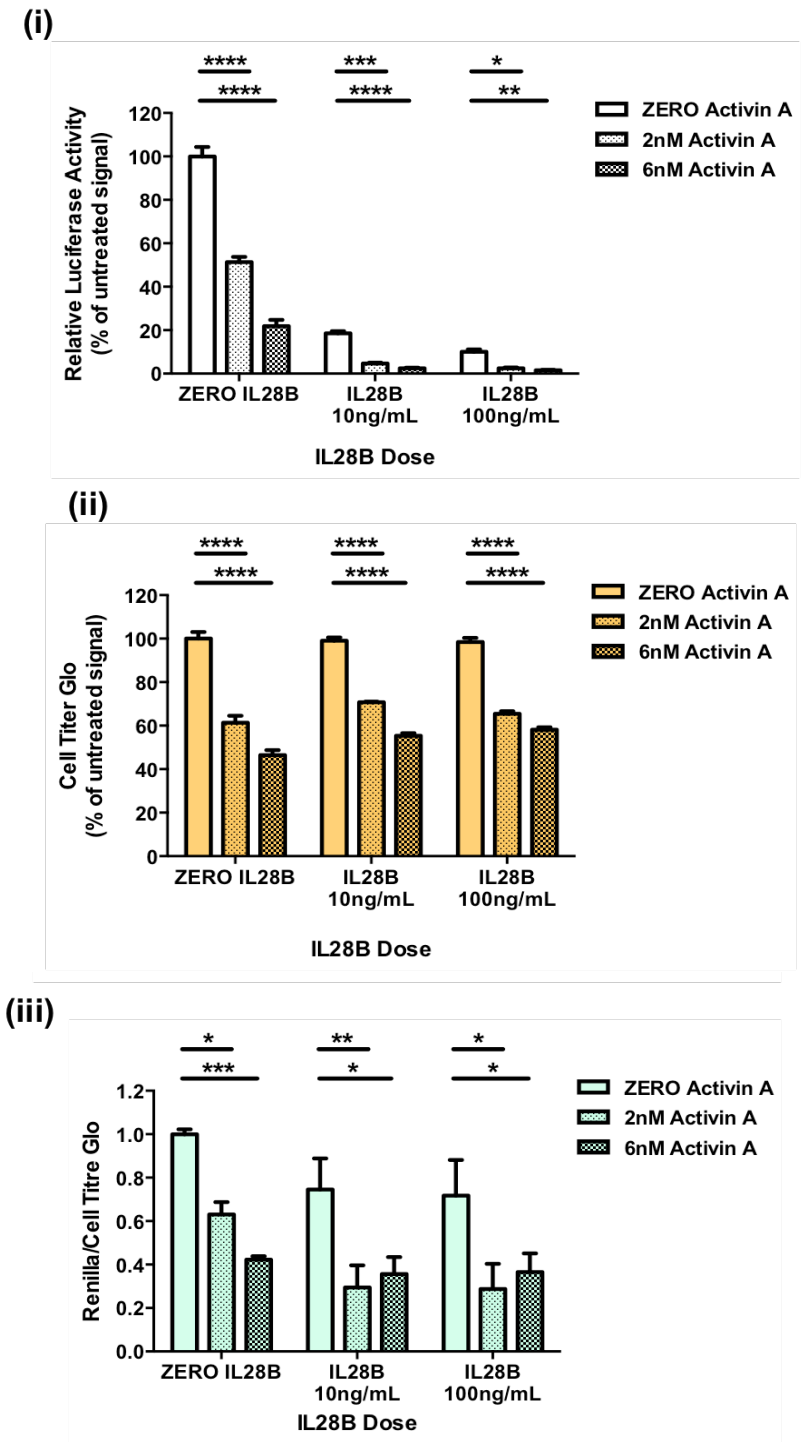


Figure 5.2: Co-incubation with activin A 2nM but not 6nM synergistically enhances the antiviral effect of IL28B in the OR6 HCV replicon model

OR6 cells were incubated with a titration of recombinant human IL28B in the presence of titrating doses of recombinant human activin A; cells were assayed at 72 h post-incubation for Renilla luciferase (i) and Cell Titer Glo (ii), with signal presented relative to the untreated condition. Renilla luciferase signal is normalized to Cell Titer Glo intensity in (iii) to account for variation in cell number.

Normalized for the dose-dependent diminution in cell number/viability caused by activin A, co-incubation with activin A 2 nM synergistically enhances the antiviral effect of both 10 ng/mL and 100 ng/mL IL28B.

n=3 independent experiments in biological triplicate; mean+SEM; analysis by 2-way ANOVA and Bonferroni's multiple comparisons test with respect to the ZERO activin A condition within each group.

5.3.2 Activin A, activin B and BMP6 modulate ISG induction by IFNα in cell-type specific manner

The boosting of IFNα's anti-HCV effect described above is paralleled by enhanced ISG induction by co-incubation with activin A and IFNα, compared to IFNα alone. In Huh7 cells, co-incubation with activin A demonstrates a trend towards induction of mRNA encoding the broad-spectrum antiviral factor *IFITM1* and the extensively characterized restriction factor *MX1*. A trend towards enhanced ISG induction in the presence of activin A extends to a panel of other ISGs, including *IFI6*, *IFIT3*, *PLSCR1* and *USP18* [figure 5.3].

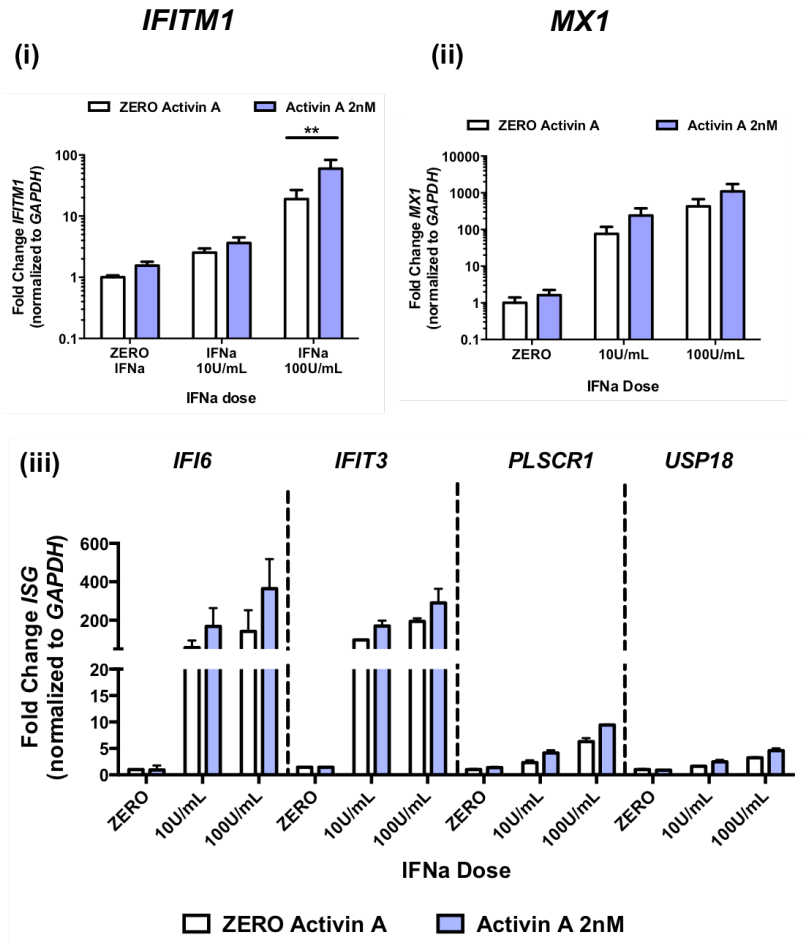


Figure 5.3: In Huh7 cells, co-incubation with activin A enhances transcriptional induction of *IFITM1* by IFNα

Huh7 cells were incubated for 24 h with a titration of recombinant human IFNα in the presence or absence of recombinant human activin A 2 nM, followed by RNA extraction and RT-qPCR quantification of mRNA encoding the ISGs *IFITM1* (i), *MX1* (ii) and *IFI6, IFIT3, PLSCR1* and *USP18* (iii).

Induction of *IFITM1* mRNA is significantly boosted by co-incubation of Huh7 cells with activin A and IFNα, despite no significant induction by activin A treatment alone.

For (i), n=3 in biological duplicate; mean+SEM; analysis by two-way ANOVA with Bonferroni's multiple comparisons test between respective IFNα doses +/- activin A 2 nM. For (ii), n=2 in biological duplicate; mean + SEM. Statistical analysis of (ii) and (iii) precluded due to small sample size.

Similarly, co-incubation with activin B enhances induction by IFNα of *MX1*, *IFITM1*, *IFI6, IFIT3* and *USP18*, but not *PLSCR1*, albeit with varying magnitudes of effect [figure 5.4].

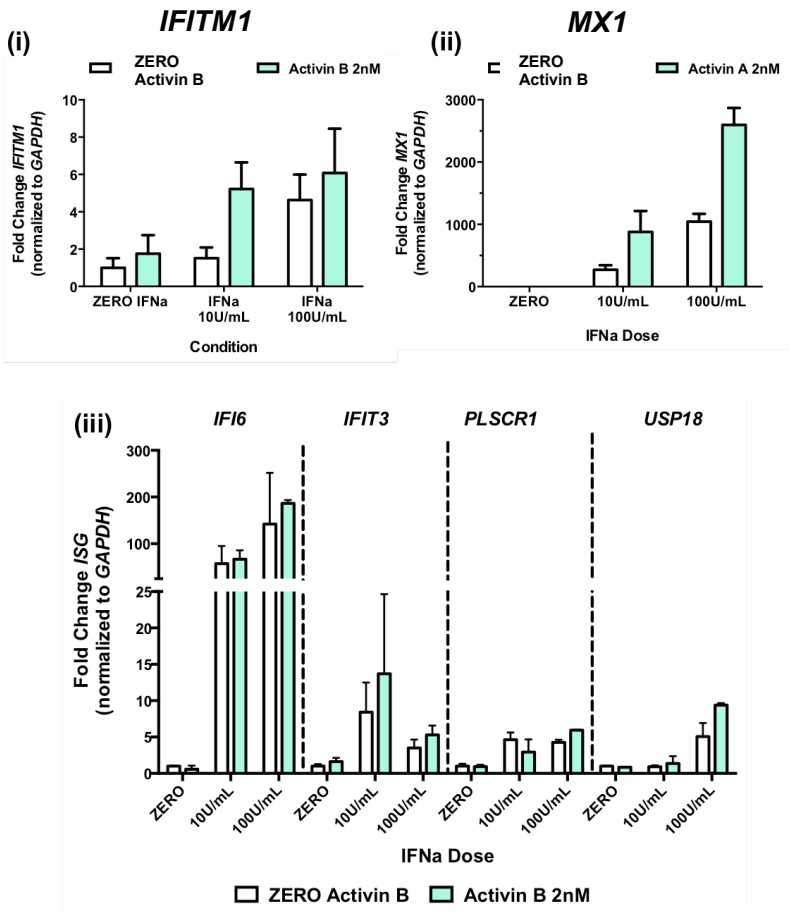


Figure 5.4: In Huh7 cells, co-incubation with activin B enhances transcriptional induction of the antiviral ISGs *IFITM1* and *MX1* by IFNα

Huh7 cells were incubated for 24 h with a titration of recombinant human IFNα in the presence or absence of recombinant human activin B 2 nM, followed by RNA extraction and RT-qPCR quantification of mRNA encoding the ISGs *IFITM1* (i), *MX1* (ii) and IFI6*, IFIT3, PLSCR1* and *USP18* (iii). Data is presented as fold change compared to untreated cells.

There is evidence for enhanced induction of *IFITM1* and *MX1* mRNA by co-incubation of Huh7 cells with activin B and IFNα, despite no induction by incubation by activin B treatment alone.

For (i), n=3 in biological duplicate; mean+SEM; analysis by two-way ANOVA with Bonferroni's multiple comparisons test between respective IFNα doses +/- activin A 2 nM. For (ii), n=2 in biological duplicate; mean + SEM. Statistical analysis of (ii) and (iii) precluded due to small sample size.

In terms of interactions with IL28B, co-incubation with activin A shows a trend towards boosting ISG induction at both 24 h and 48 h incubation (measuring *IFI6* and *ISG15,* and *IFI6* and *MX1* transcript levels respectively). At 24 h, activin B enhanced expression of neither *IFI6* nor *ISG15* mRNA [figure 5.5].

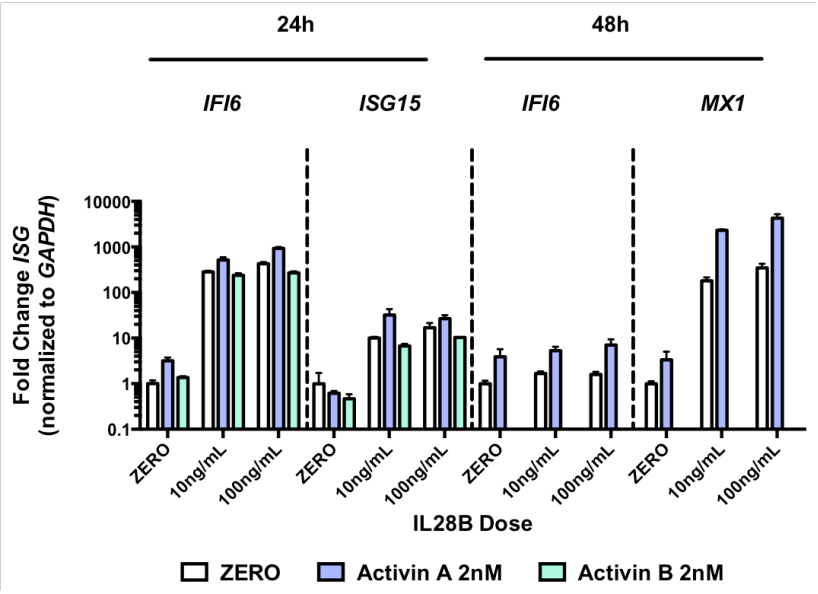


Figure 5.5: In Huh7 cells, co-incubation with activin A, but not B, may enhance transcriptional induction of antiviral ISGs by IL28B

Huh7 cells were incubated for 24 h or 48 h with a titration of recombinant human IL28B in the presence or absence of recombinant human activin A (24 and 48 h) or activin B 2 nM (24 h only), followed by RNA extraction and RT-qPCR quantification of mRNA encoding the ISGs *IFI6, ISG15* and *MX1*. Data is presented as fold change compared to untreated cells.

At 24 h, n=1 in biological duplicate; at 48h, n=2 independent experiments in biological duplicate; mean+SEM; statistical analysis precluded due to small sample size.

To assess whether the transcriptional enhancement of IFNα by activin A is specific to Huh7 cells or a broader phenomenon, the protocol was replicated in three non-hepatoma lines, namely 293T, HeLa and A549.gfp cells. mRNA expression of the ALK2 and AL3 type I BMP receptor isoforms by A549 cells has been reported previously (605). In HEK293 cells, from which the 293T line is derived, SMAD1/5/8 phosphorylation downstream of BMP4 is blocked by the ALK2/3 receptor inhibitor DMH1, suggesting expression of functional ALK2 and/or ALK3 in this cell type (606). In contrast, previous observations report that mRNA expression of ALK2 and ALK3 mRNA in HeLa cells is low (607).

All three ISG transcripts analysed are robustly upregulated by IFNα in all cell lines. Activin A 2 nM in the absence of IFNα, however, has no effect on target mRNA expression. A trend towards slightly enhanced induction of *ISG15* and *IFI6* by IFNα and activin A co-incubation is observed in A549.gfp cells. In 293T cells, induction of all mRNAs is suppressed by co-incubation with activin A compared to IFNα alone, with this effect most pronounced for *MX1* [figure 5.6].

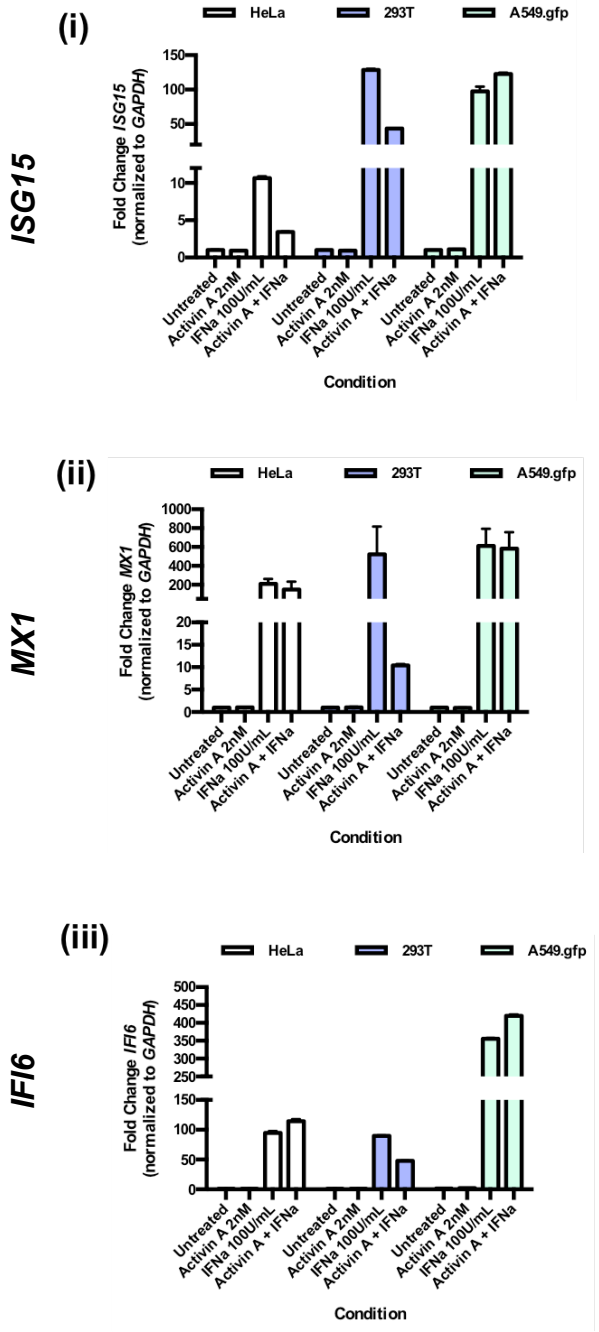


Figure 5.6: Co-incubation with activin A elicits variable effects on ISG induction by IFNα in HeLa, 293T and A549.gfp cells.

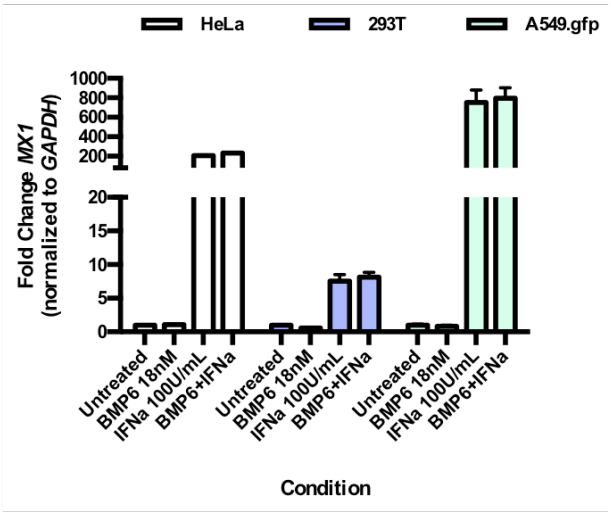
Three cell lines of epithelial origin (HeLa, 293T and A549.gfp) were incubated for 24h with recombinant human activin A 2 nM, recombinant human IFNα 100 U/mL or both, followed by RNA extraction and RT-qPCR quantification of transcript encoding the IFN-stimulated genes *ISG15* (i), *MX1* (ii) and *IFI6* (iii). Data is presented as fold change compared to untreated cells.

Expression of all transcripts is robustly upregulated by IFNα in all cell lines, with no effect of activin A 2nM only. Enhanced induction of *ISG15* and *IFI6* by IFNα/activin A co-incubation is observed in A549.gfp cells. In 293T cells, induction of all mRNAs is suppressed by co-incubation compared to IFNα only, with this effect most pronounced for *MX1*.

For *ISG15* and *IFI6* expression, n=1; for *MX1* expression n=2, in biological singlicate; statistical analysis precluded due to small sample size.

As boosting of ISG induction by BMP6 in Huh7 has also been described in previous work from the Drakesmith lab, we also sought to examine the BMP6/IFNα interaction in HeLa, 293T and A549.gfp cells. Expression of all three transcripts is robustly upregulated by IFNα in all cell lines, with no effect of BMP6 18 nM only. Relative to IFNα only, addition of BMP6 does not enhance *MX1* induction in any cell line. Enhanced induction of *IFI6* by IFNα/BMP6 co-incubation is observed in both HeLa and A549.gfp cells, in contrast to its relative suppression in 293T cells [figure 5.7].

(i)



(ii)

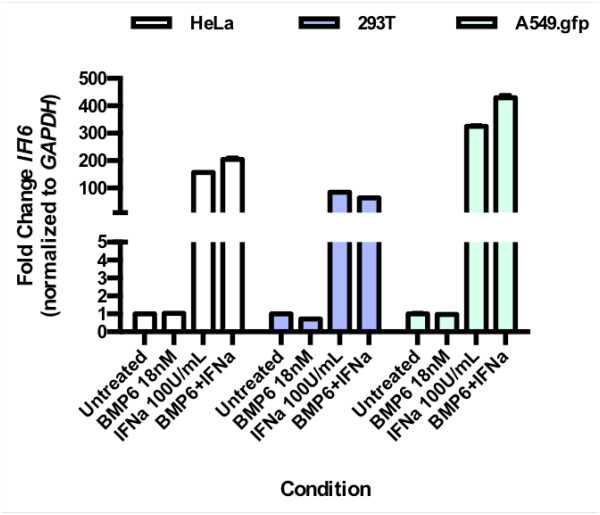


Figure 5.7: Co-incubation with BMP6 elicits variable effects upon ISG induction by IFNα in HeLa, 293T and A549.gfp cells

Three cell lines of epithelial origin (HeLa, 293T and A549.gfp) were incubated for 24 h with recombinant human BMP6 18 nM, recombinant human IFNα 100 U/mL or both, followed by RNA extraction and RT-qPCR quantification of transcript encoding *MX1* (i) and *IFI6* (ii). Data is presented as fold change compared to untreated cells.

Expression of all transcripts is robustly upregulated by IFNα in all cell lines, with no effect of BMP6 18 nM only. *MX1* expression is broadly unchanged relative to IFNα only by BMP6 co-incubation. Enhanced induction of *IFI6* by IFNα/BMP6 co-incubation is observed in both HeLa and A549.gfp cells, in contrast to relative suppression in 293T cells.

n=2 in biological singlicate; mean+SEM; statistical analysis precluded due to small sample size.

Extending our observations to primary cells, co-incubation of PBMCs from two healthy donors with recombinant activin A and IFNα resulted in a modest enhancement of *IFI6* expression relative to IFNα only. However, activin A did not alter the magnitude of *IRF7* or *MX1* upregulation by IFNα, nor did activin A 2 nM alone induce expression of any of the ISGs measured [figure 5.8].

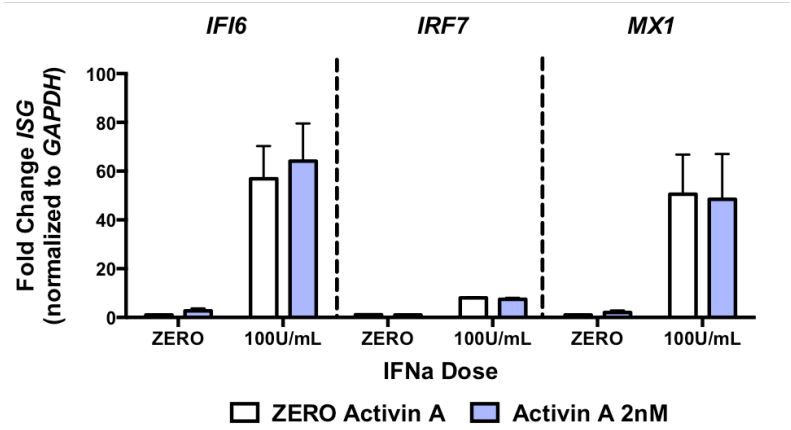


Figure 5.8: In human PBMCs co-incubation with activin A does not markedly enhance the transcriptional induction of antiviral ISGs by IFNα.

PBMCs from two healthy donors were incubated with vehicle or recombinant human IFNα 100 U/mL in the presence or absence of recombinant human activin A 2 nM for 24h, followed by RNA extraction and quantification of *IFI6, IRF7* and *MX1* transcript induction by RT-qPCR. Data is presented as fold change compared to untreated cells.

IFNα treatment, but not activin A, induced expression of all three ISGs at the message level. A small increase in *IFI6* upregulation by co-incubation with activin A is evident, whilst addition of activin A did not boost transcriptional induction of *IRF7* and *MX1* in PBMCs.

n=2 in biological duplicate; mean+SEM; statistical analysis precluded due to small sample size.

5.3.3 Activin A upregulates transcription of key IFN signalling components

Microarray analysis of the transcriptome of BMP6-treated Huh7 cells suggested that BMP6 induces expression of multiple components of the IFN-JAK-STAT signal transduction cascade, an observation that that was validated by RT-qPCR [unpublished data]. Given that activin A enhances expression of antiviral effectors by IFNα, akin to BMP6, we were keen to explore whether it could also induce expression of key signalling components in the absence of exogenous IFN.

As shown in figure 5.9, 24 h incubation of Huh7 cells with recombinant activin A elicits modest but statistically significant upregulation of transcript encoding the type I IFN receptor chain *IFNAR2*, the downstream kinase *JAK1* and the transcription factor *STAT2*, a component of the ISGF3 complex. By contrast, in this model recombinant activin B induces expression of *IFNAR2* mRNA only.

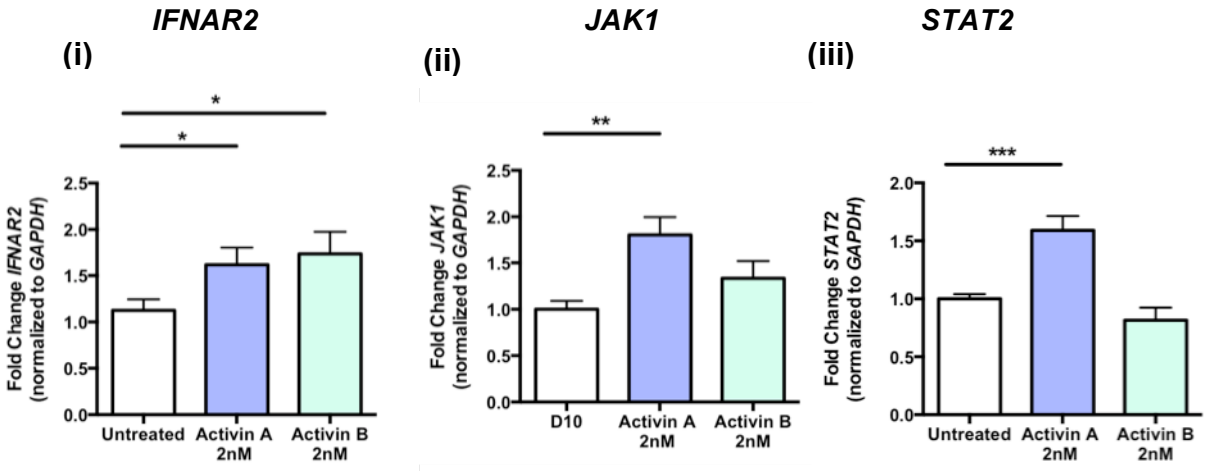


Figure 5.9: Activin A upregulates mRNA expression of key type I IFN signalling components by Huh7 cells

Huh7 cells were incubated with recombinant human activin A or activin B 2 nM for 24 h, followed by RNA extraction and RT-qPCR analysis of *IFNAR2*, encoding a type I IFN receptor subunit (i); *JAK1*, encoding a kinase immediately downstream of the IFNAR complex (ii); and *STAT2* (iii) mRNA expression. Data is presented as fold change compared to untreated cells.

Both activin A and activin B significantly upregulate *IFNAR2* transcript in this model, whereas only activin A induces significant induction of *JAK1* and *STAT2* mRNA.

For activin A, n=6; for activin B, n=4; mean+SEM; analysis by unpaired two-tailed t-test

5.4 Summary and discussion

Chapter 5 presents preliminary evidence for synergistic enhancement by activin A of both IFNα and IL28B's antiviral effects against a HCV genomic replicon construct. Further work should investigate whether this synergy extends both to replication competent HCV infection models and other viruses. A preliminary effort to explore the effects of combined IFNα and activin A against DENV replication *in vitro* is described in section 7.3.2-7.3.3.

The data presented in this chapter demonstrate that, in Huh7 cells at least, transcriptional induction of multiple ISGs, with diverse modes of action and viral specificities, is increased in the presence of either activin A or activin B. The data presented in this chapter, however, are limited, and further experiments are needed for a more robust investigation.

This phenomenon appears to be cell-type specific, with activin A/IFNα co-incubation variably boosting and suppressing ISG expression in non-hepatoma cells lines. Possible explanations for this cell-type specificity include variation in the negative regulation of the IFN pathway between cell lines, or differential epigenetic regulation of ISGs within each cell line, for example in order to modulate their non-immune functions. In the context of dysplastic cell lines, the effect could also be related to nuclear karyotype, with chromosomal

ploidy affecting the number of ISG encoding loci available for activation within each cell line.

Further experiments should seek to characterize the IFN and BMP receptor expression profiles between cell lines, in addition to their susceptibility to toxicity after administration of high dose recombinant cytokines, and then compare these results to the presence or absence of BMP/IFN synergy. To better contextualize these observations with the antiviral studies, the transcriptional effects of BMP/activin and IFN co-incubation should have been explored in the OR6 replicon and cured-OR6 cell lines. As has been previously discussed, these cells represent a distinct lineage to the Huh7 line predominantly utilised in this chapter.

As observations at the mRNA level do not necessarily correlate with protein expression, future experiments should characterize ISG induction at the protein level, either via Western blotting for specific target proteins or comparison of the proteomes following IFNα or IFNα/activin A co-treatment. Co-administration of IFNα and activin A to mice by intraperitoneal injection, followed by quantification of hepatic ISG expression, either by RT-qPCR or immunohistochemistry, would allow assessment of the contribution of activin signalling to ISG induction *in vivo*. A caveat of this approach is that multiple ISGs and IFN-associated signalling components, notably including ISG15, USP18 and STING (156,608), have been observed to have different antiviral effector potencies and biochemical properties to their human orthologues, thereby limiting the utility of murine models when extrapolating to human models of immunity.

Moreover, the data presented here suggest that recombinant activin A is able to increase transcription of the key type I IFN signal transduction components IFNAR2, JAK1 and STAT2 in Huh7 cells. If these changes are recapitulated at the protein level (a question for subsequent investigation), they could confer an increased capacity for IFN signal transduction and subsequent ISG induction.

The presence of BRE motifs in the region immediately upstream of multiple ISGs, including *IFNAR2* and *STAT2*, suggests that activin-induced SMAD1/5/8 might bind to these regions and activate ISG expression. However, numerous ISGs that were transcriptionally boosted by activin A, activin B and BMP6 did not contain BRE motifs in the region 2 kb upstream of their TSS.

Given the previous identification of BRE sequences in the region 2 kb upstream of the IRF1 and IRF7 transcription start site (TSS), the regions upstream of the TSS in a panel of ISGs (predominantly based upon the set of ISGs described by Metz and colleagues to restrict HCV

replication *in vitro* (325), with the inclusion of the three signalling components examined in figure 5.9) were interrogated for the presence of the GGCGCC sequence. Of the genes examined, a single BRE was identified upstream of *IFI6, IFITM1, IFITM3* and *USP18*, whereas two were identified upstream of *TRIM14*. The region 2 kb upstream of *IFNAR2* and *STAT2* also contains BRE motifs. These sequences are depicted in figure 5.10 in addition to those corresponding to the BRE motifs upstream of *HAMP* and *ID1*, extensively characterized BMP-responsive genes.

BRE sequences could not be detected in the 2 kb portion upstream of the *ISG15*, *IFIT3*, *MX1, PLSCR1* and *RSAD2* transcription start sites, nor that of *JAK1*.

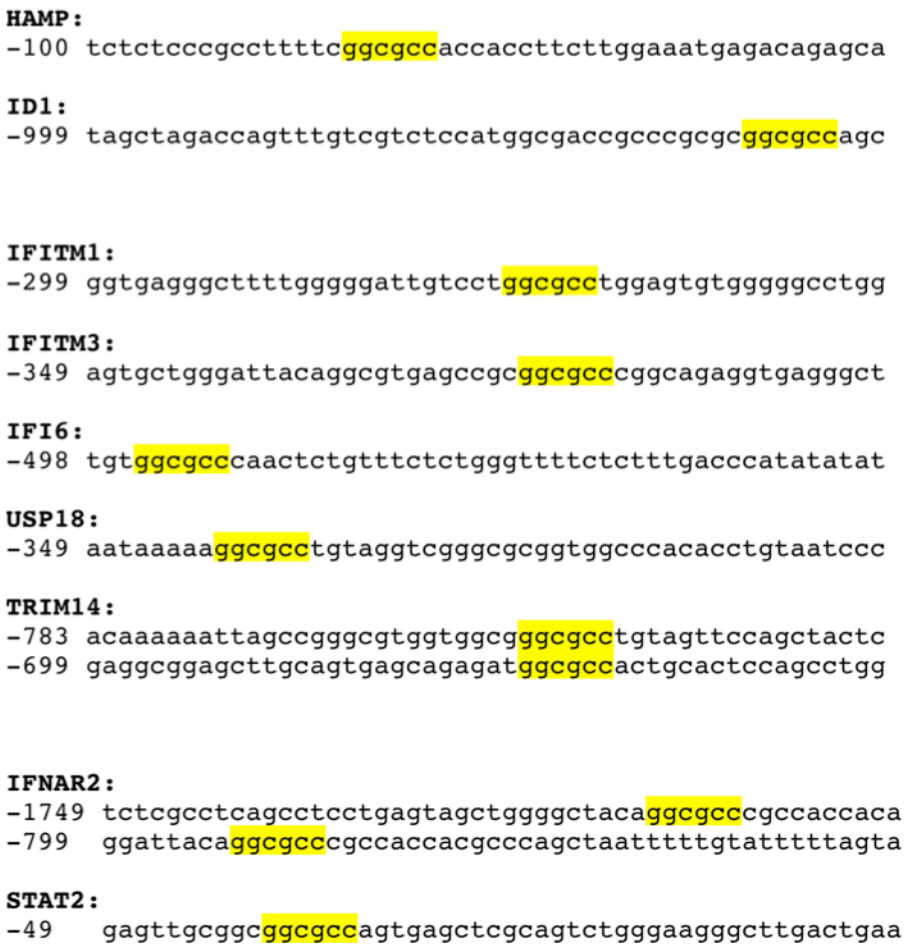


Figure 5.10: BRE motifs are present in the promoter sequence of multiple ISGs

Interrogation of the promoter sequences (defined at the region 2kb upstream of the transcription start site) of selected ISGs reveals the presence of BRE motifs. BRE sequences (ggcgcc) are annotated in the sequence excerpts above. The number denotes the position of the first base in the sequence excerpt relative to the transcription start site.

BRE elements identified in the promoters of the BMP-stimulated genes *HAMP* and *ID1* are included for reference.

Merely screening sequences for pre-defined transcription factor consensus sequences, however, is a crude method for the analysis of gene regulatory mechanisms: gene expression may be regulated by very distal interactions, or binding of transcription factors to non-canonical sequences. Gene expression is also modulated by a myriad of epigenetic cues, including base methylation and the post-translational modification of histone proteins. More informative approaches include genome-wide analysis of transcription factor binding, such as ChIP-seq, and analysis of cis-regulatory interactions with chromatin conformational capture assays.

Of interest, crystal structures of the SMAD transcription factors and IRFs demonstrate remarkable topological and electrostatic homology in their C-terminal dimerization domains (609,610). Based on these observations, they are proposed to have diverged from a common precursor during the early evolution of metazoans (609–611). A possible mechanistic basis for the synergistic enhancement of IFN signalling by the BMP-activin-SMAD axis could be via SMAD-IRF dimerization, thereby increasing the number of transcriptional activators available to induce ISG expression. To begin addressing this possibility, we analysed a number of publicly available ChIP-seq datasets, evaluating both the incidence of SMAD binding at antiviral loci and the similarity of SMAD and IRF binding profiles genome-wide. The results of this exercise are described in chapter 6.

Chapter 6

Bioinformatic comparison of SMAD and IRF genomic interactions

6.1 Introduction

The data presented by this thesis thus far suggest that activin and BMP signalling mediate robust anti-HCV effects, via both type I IFN-dependent and independent mechanisms. In order to dissect the mechanistic basis for their antiviral effect further, we embarked upon a bioinformatic comparison of SMAD and IRF transcription factor binding genome-wide, motivated by structural and biochemical data reporting both structural homology and functional interplay between these transcription factor families.

This introduction briefly summarizes the structure-function relationships of both SMAD and IRF proteins, before reviewing the experimental precedents upon which our exploration of SMAD-IRF genomic interactions is predicated.

6.1.1 SMAD structure-function relationship

Upon activation, the principal substrates of the type I BMP receptor are the SMAD signal transduction proteins, detailed in section 1.1.3. Briefly, phosphorylation of a conserved SSXS motif at the C-terminus of SMAD1, SMAD5 and SMAD8 (the 'R-SMADs') initiates association with SMAD4, resulting in nuclear translocation of transcriptionally active SMAD complexes. Negative regulation is mediated by inhibitory SMAD6 and SMAD7 (the 'I-SMADs'). For ligands signalling via the type I TGFβ receptor, SMAD2 and SMAD3 are the predominant R-SMADs (612,613).

In terms of domain architecture, the R-SMADs are composed of highly conserved Mad homology 1 and 2 (MH1 and MH2) domains bridged by a variable linker sequence. The C-terminal MH2 both encodes the receptor-activated SSXS motif and is required for oligomerization. The SMAD4 MH2 domain lacks an SSXS motif, preventing interactions with the type I BMP receptor kinase. The I-SMADs lack the MH1 domain altogether and do not encode a carboxy-terminal SSXS motif [figure 6.1] (613).

In the R-SMADs, the MH1 domain includes a β-hairpin loop required for binding to the major groove of GC-rich DNA encoding the consensus sequence GGCGCC (46,601,614). The conserved MH2 domain consists of five α-helices and three loop regions enclosing a central β-sheet; in the R-SMADs, it is subtly modified to incorporate a positively charged pocket that facilitates tight binding to a glycine-serine rich region of the type I BMP receptor, bringing the R-SMAD into close association with the receptor's serine-threonine kinase domain (615).

SMAD nuclear translocation is guided by nuclear localization signals at their amino terminus, whereas the MH2 domain includes two nuclear export motifs – short, hydrophobic stretches that promote shuttling into the cytoplasm (616,617). Functional genomic screens have implicated multiple phosphatases, including PPM1A, in SMAD dephosphorylation, a process that promotes their nuclear export and abrogates their transcriptional activity (618).

The SMAD linker region is more variable than the MH1/2 domains, but nevertheless includes a key proline-tyrosine motif required for negative regulation by the SMURF E3 ubiquitin ligases [section 1.1.3] (613).

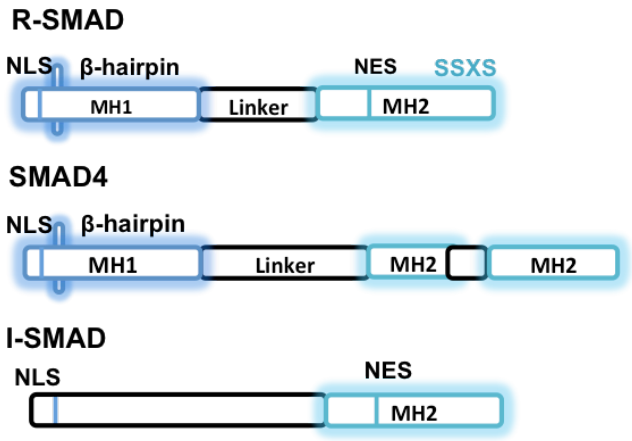


Figure 6.1: Schematic representation of SMAD domain architecture

Adapted from Heldin, C-H; TGF β Signalling from Receptors to SMADs, 2008

NLS: nuclear localisation signal

NES: nuclear export signal;

SSXS: phosphorylation site

6.1.2 IRF structure-function relationship

Following the discovery of IRF1 as a regulator of IFNβ expression in 1988 (619,620), nine IRFs have been identified, each orchestrating distinct facets of the innate and adaptive immune response (621). Diversification of the family is proposed to coincide with the evolution of multicellular organisms (611).

The absolute requirement for IRF3 and IRF7 in complementary aspects of IFNα/β induction has been summarized previously [section 4.1.4.1]. IRF4 expression is restricted to immune cells, where it is required for aspects of both B-cell differentiation and Th2 polarization. IRF4 also negatively regulates induction of pro-inflammatory cytokines by TLR signalling, via an inhibitory association with MYD88. In contrast, IRF5, constitutively expressed by B cells and dendritic cells, enhances induction of inflammatory cytokines following TLR stimulation, with *Irf5-/-* mice being resistant to lethal endotoxic shock. IRF6, primarily expressed in the skin, is poorly characterized, whereas IRF8 is restricted to immune cells and modulates IFNα

production by dendritic cells and macrophage differentiation, amongst other functions. IRF9, as described in section 1.2.3, is a component of the ISGF3 complex, a positive regulator of both ISG expression and the p53 tumour suppressor pathway (589,621,622).

IRF1, inducible by both type I IFN and IFNγ, activates expression of multiple IFN-inducible target genes, including nitric oxide synthase, cyclooxygenase-2 and caspase-1, in addition to enhancing TLR signalling in the presence of IFNγ. During the transactivation of *IFNB*, IRF1 constitutes part of an enhanceosome complex including p300/CBP, NFκB and ATF2/cJun. IRF2, by contrast, acts as repressor of the type I IFN response, via competitive antagonism of IRF1 and IRF9 (589,621,622).

Despite their diverse functions, the domain architecture of the IRFs is highly conserved (621). All nine human IRFs contain an N-terminal DNA binding domain, consisting of a 120-residue helix-turn-helix structure necessary for binding the ISRE consensus sequence, 5'-RNGAAANNGAAACT-3'(623–625).

At their C-termini, IRFs 3-9 contain a conserved IRF-association domain (IAD) required for their homo- and heterodimerization (621,626). Autoinhibitory loops flank the IAD, concealing the hydrophobic interaction surface. Phosphorylation of the IRF C-terminus relieves this repression and permits not only IRF dimerization, but also interaction with unrelated transcription factors, including STAT1/2 and PU.1, the master regulator of macrophage differentiation (609,610). IRF1 and IRF2 do not contain an IAD domain. Instead, they encode C-terminal IAD2 transactivation domains that do not resemble any other tertiary protein folds (611,625). IRF1 and IRF2 retain homology to the remaining human IRFs by virtue of their N-terminal DNA-binding domain.

6.1.3 SMAD and IRF proteins demonstrate strong structural homology

Crystal structures reveal striking topological and electrostatic homology between the SMAD MH2 domain and the IRF-encoded IAD, despite their low sequence similarity (609,610). Comparisons of computer-simulated IRF and SMAD structures had previously hinted at such parallels (626). Both the MH2 and IAD contain a central β-sheet surrounded by five tightly bundled α-helices, in addition to a similar array of hydrophobic residues in their interaction domain [figure 6.2]. Based upon these profound structural similarities, IRFs and SMADs are proposed to have diverged from a common precursor, namely the prokaryotic forkhead association protein (FHA), during the evolution of early multicellular organisms (609,610).

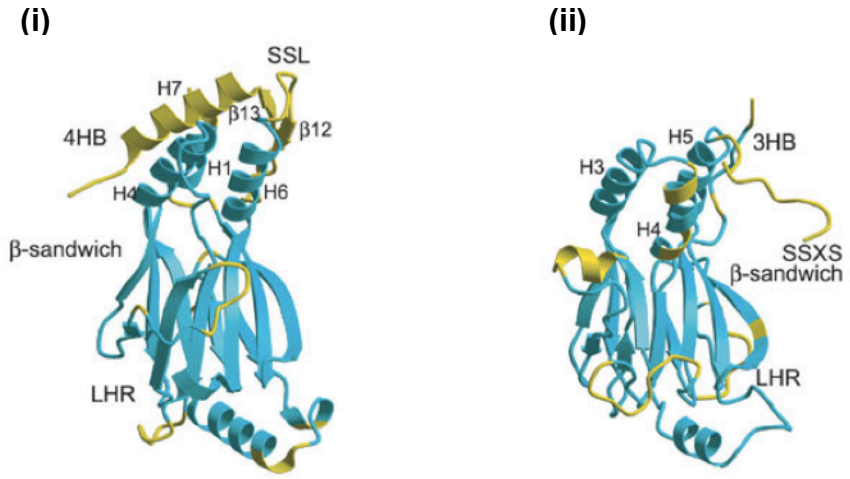


Figure 6.2: Crystal structures of IRF3 and SMAD2 demonstrate marked topological homology at the C-terminus

X-ray crystal structures of an IRF3 fragment (denoted "IRF3 175C" by Takahasi et al.) (i) and SMAD2 (ii) reveal a superimposable β-sandwich structure composed of two antiparallel β-sheets capped by α-helical bundles.

Structures obtained from Takahasi et al. *Nature Structural Biology* **10** 913-921 (2003)

A more recent study has revealed that not only can SMAD and IRF proteins dimerize, as would be predicted from their homologous binding interfaces, but that SMAD-IRF dimers are capable of functionally regulating gene expression. In addition to demonstrating SMAD3-IRF3 association via co-immunoprecipitation, Xu and colleagues report that IRF3 activation, downstream of RLR signalling, is able to inhibit TGFβ-dependent physiological processes, including epithelial-to-mesenchymal transition in transformed keratinocytes and regulatory T cell differentiation *in vitro* (627). Moreover, this SMAD3-IRF3 crosstalk is recapitulated *in vivo*, with significantly reduced expression of multiple TGFβ target genes in the lungs of FLUAV-infected wildtype mice, but not *Irf3-/-* animals (627).

6.1.4 Exploring a role for SMAD-IRF interactions in the regulation of antiviral immunity

Chapter five presented evidence for synergistic enhancement of both type I and type III IFN's anti-HCV effects by activin signalling; additional unpublished data from the lab demonstrates a similar potentiation of IFN by BMP6 [appendix I]. Integrating these observations with both structural and evolutionary homology between SMAD and IRF proteins and the apparent functional capacity of SMAD3-IRF3 heterodimers, we hypothesized that similar genomic interactions, and possibly SMAD-IRF heterodimerization, could provide the mechanistic basis for the enhancement of IFN signalling by both activin and BMP proteins.

To address this possibility, we embarked on a bioinformatic analysis of the most appropriate publicly available ChIP-seq datasets, with two key questions:

1) At the genome level, do SMAD proteins bind DNA near genes with known antiviral activity?
2) Is there similarity in the genomic binding profiles of SMAD and IRF transcription factors?

A ChIP-seq dataset describes the incidence of specific protein-DNA interactions genome-wide. Proteins targeted may include transcription factors and histone proteins, especially with specific post-translational modifications. In brief, the dataset is generated by formaldehyde cross-linking of proteins to their cognate DNA, followed by sequential DNA fragmentation, either by enzymatic shearing or sonication; incubation with an antibody specific to the protein of interest; and immunoprecipitation for bound protein-DNA fragments. The enriched fraction is then de-crosslinked and digested with proteinase K, before library preparation and high-throughput sequencing [summarized in figure 6.3].

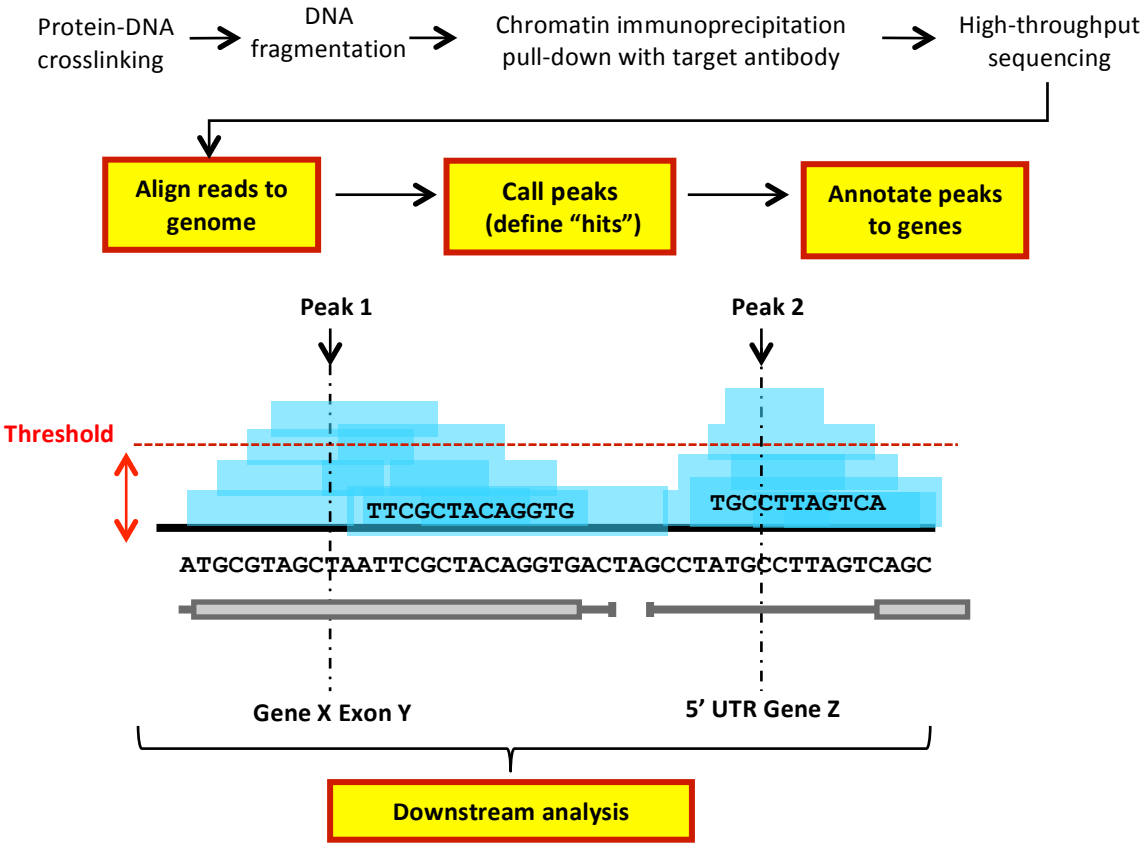


Figure 6.3: Schematic summary of the ChIP-seq experimental process

Obtained reads are subsequently aligned to the reference genome. Regions of transcription factor binding ('peaks') can be inferred from the aggregation of reads at specific genomic positions in the experimental dataset generated with the target antibody compared to an input control dataset. The latter is generated under identical conditions but with a non-specific or irrelevant control antibody. ChIP-seq datasets can be visualized in genome browsers, for example the UCSC browser, and subjected to multiple downstream analyses, including gene set enrichment (GSE). GSE analysis identifies statistically significant differences between datasets in *a priori* defined gene sets, for example corresponding to specific signalling pathways, disease states or regulatory motifs.

For the analyses described below, we investigated published ChIP-seq datasets derived from K562 erythroleukaemic cells. The three principal datasets studied describe SMAD1 binding in cells treated with BMP4 for 2 h (the 'BMP4-SMAD1' dataset) and IRF1 binding in cells treated with IFNα for either 30 min or 6 h ('IFNa30-IRF1' and 'IFNa6h-IRF1' respectively).

Trompouki and colleagues generated the BMP-SMAD1 dataset during their investigation into the role of BMP/SMAD signalling in cell fate decisions during haematopoiesis (61). In this paper, the authors report that SMAD1 co-binds the genome with GATA1, the master regulator of erythroid differentiation, and GATA1 directs SMAD1 away from non-erythroid target genes, implying that SMAD1 and GATA1 are tightly coupled during the determination of haematopoietic cell identity. While this thesis has thus far concentrated upon activin A, activin B and BMP6, we have also reported a dose-dependent antiviral effect of BMP4 against the OR6 HCV replicon [section 3.4.1]. Moreover, BMP4 signalling is SMAD1/5/8-dependent, being transduced by the ALK2 and ALK3 receptor type I BMP receptor isoforms (5), rendering it an appropriate SMAD1 stimulus in the context of our previous work.

IFNa30-IRF1 and IFNa6h-IRF1 datasets were obtained from the ENCODE repository, having been generated by the Snyder laboratory at Yale (628). The ENCODE project is an international research endeavour charged with comprehensively cataloguing functional elements within the human genome via extensive characterization of transcription factor binding sites, epigenetic modifications and chromatin architecture (629). IRF1 would be suboptimal for specific studies of SMAD-IRF heterodimerization, given its lack of an IAD. However, due its conserved N-terminal DNA-binding domain, with high affinity for the ISRE, IRF1 remains an appropriate candidate for our comparison of SMAD and IRF binding patterns genome-wide.

6.1.5 Summary

The bioinformatic analyses presented in this chapter provide evidence for strong similarity in the genome-wide binding profiles of SMAD1 and IRF1, including in the vicinity of genes encoding antiviral effector genes. Gene set enrichment (GSE) analysis reveals enrichment for type I IFN-associated effector functions in the BMP4-SMAD1 dataset, and directly overlapping SMAD1 and IRF1 binding is evident proximal to multiple ISGs. Furthermore, we extend our observations to other haematopoietic cell lines and extend our characterization of the SMAD1/IRF1 binding profiles via comparisons with multiple other ChIP-seq databases. Finally, we formally examine the statistical significance of overlap between SMAD1 and IRF1 with a hypergeometric test.

6.2 Materials and methods

6.2.1 ChIP-seq databases interrogated

Table 6.1 overleaf describes the ChIP-seq databases interrogated, including their stimulation conditions and the accession I.D. for both the ENCODE and NCBI GEO repositories (if applicable).

Table 6.1:

ChIP-seq datasets interrogated in this project

Dataset	Source	NCBI GEO Accession I.D.	ENCODE Accession I.D.	Cell Line	Condition	Antibody
BMP4-SMAD1	Trompouki et al. *Cell* 2011	GSM722416		K562	Human BMP4 @ 25 ng/µL for 2 h	SMAD1
IFNa6h-IRF1	ENCODE; Snyder Lab, Yale		wgEncodeEH001865	K562	Human IFNα; 6 h	IRF1
IFNa30-IRF1	ENCODE; Snyder Lab, Yale	GSM935504	wgEncodeEH002798	K562	Human IFNα; 30 min	IRF1
Input control	ENCODE; Snyder Lab, Yale	GSM935363	wgEncodeEH000615	K562	Unstimulated	IgG
None-ARID3A	ENCODE; Snyder Lab, Yale	GSM935336	wgEncodeEH002861	K562	Unstimulated	ARID3A
None-ELK1	ENCODE; Snyder Lab, Yale		wgEncodeEH003356	K562	Unstimulated	ELK1
None-INI1	ENCODE; Snyder Lab, Yale	GSM935634	wgEncodeEH000725	K562	Unstimulated	INI1
None-RAD21	ENCODE; Snyder Lab, Yale	GSM935319	wgEncodeEH000649	K562	Unstimulated	RAD21
None-XRCC4	ENCODE; Snyder Lab, Yale	GSM935425	wgEncodeEH000650	K562	Unstimulated	XRCC4
Dorso-SMAD1	Trompouki et al. *Cell* 2011	GSM722417		K562	Dorsomorphin @ 20 µM for 2 h	SMAD1
IFNa6h-STAT1	ENCODE; Snyder Lab, Yale		wgEncodeEH000664	K562	Human IFNα; 6 h	STAT1
IFNa6h-STAT2	ENCODE; Snyder Lab, Yale		wgEncodeEH000666	K562	Human IFNα; 6 h	STAT2
BMP4-GATA1	Trompouki et al. *Cell* 2011	GSM722413		K562	Human BMP4 @ 25 ng/µL for 2 h	GATA1
None-RNA Pol II	ENCODE; Snyder Lab, Yale		wgEncodeEH000616	K562	Unstimulated	Pol2
None-RNA Pol III	ENCODE; Snyder Lab, Yale	GSM935481	wgEncodeEH000694	K562	Unstimulated	Pol3
CD34+ BMP4-SMAD1	Trompouki et al. *Cell* 2011	GSM722399		CD34+ progenitors	Human BMP4 @ 25 ng/µL for 2 h	SMAD1
U937 BMP4-SMAD1	Trompouki et al. *Cell* 2011	GSM722425		U937	Human BMP4 @ 25 ng/µL for 2 h	SMAD1
CD34+ Input Control	Wong Lab; UNSW	GSM1097886		CD34+ erythrocytic progenitors	Unstimulated	N/a
U937 Whole Cell Extract	Trompouki et al. *Cell* 2011	GSM722431		U937	Unstimulated	N/a

6.2.2 Bioinformatic analyses

Figure 6.4 summarizes the bioinformatic pipeline.

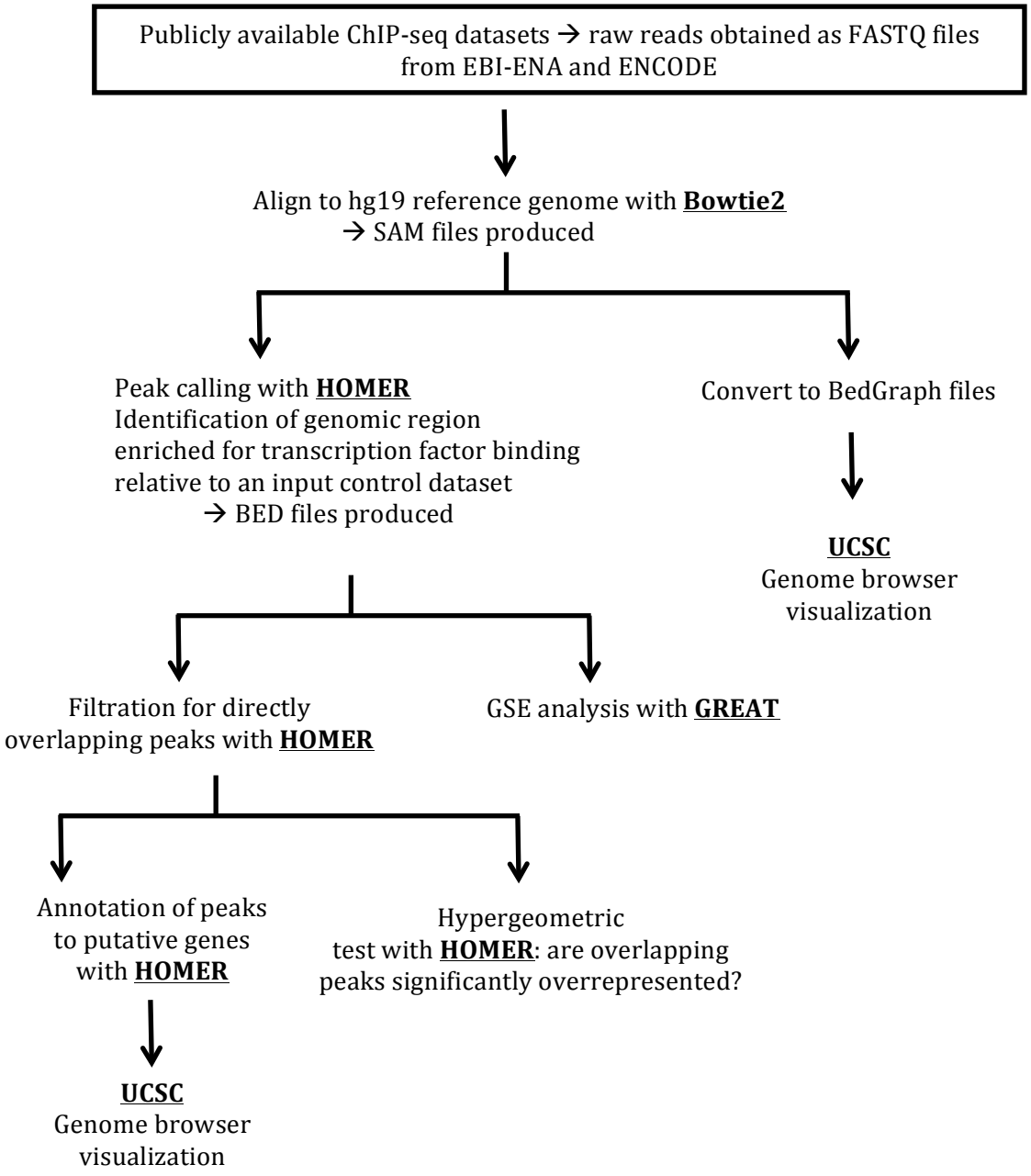


Figure 6.4: Summary of the bioinformatic analysis pipeline

Previously described ChIP-seq datasets were obtained as FASTQ files from the NCBI GEO repository (Series 29196 and Series 31477) (61,628). Adaptor sequences were removed using TrimGalore (Babraham Institute, University of Cambridge). Reads were aligned to the human genome build GRCh37 (UCSC hg19/Feb 2009) with Bowtie2 (v2.2.6) (630). Transcription factor binding profiles were converted to BedGraph files and visualized in the UCSC genome

browser, accompanied by epigenetic modification tracks defined by the ENCODE project (628,631).

For GSE analysis [figure 6.3-6.4] transcription factor binding peaks were identified using the findPeaks program in the HOMER suite of NGS analysis tools, in accordance with the default parameters, and normalized to 10 million total reads per dataset (632). Peaks are identified by both a sequence-depth independent parameter (that is, requiring a four-fold greater density of aligned reads in the target versus the input control dataset) and a sequence-depth dependent parameter, namely the comparison of read densities in the target and input control datasets with the cumulative Poisson distribution, with a threshold p-value of 0.0001 for the designation of a statistically significant peak.

Transcription factor-bound loci were associated with their putative cis-regulated target genes using GREAT (v2.02), an online tool permitting both genome annotation and GSE analysis with reference to multiple ontology databases, including those organized by phenotype, disease and regulatory motifs (633). GREAT calculates the statistical significance of each ontological category within the transcription factor-bound loci with respect to the whole genome. Only ontological categories comprising 10-150 terms inclusive were included in final analyses, to exclude broad, generic pathways and small gene sets liable to be enriched as artefacts of the sampling process.

For comparison of transcription factor binding profiles [figures 6.18-6.21], transcription factor peaks were called with the HOMER findPeaks tool, with each peak defined by 10-fold greater read alignment in the target experiment versus input control and datasets normalized to 10 million total reads. Histograms of transcription factor-binding density were constructed using the annotatePeaks.pl function in HOMER (632).

Peak-sets were compared in a pair-wise fashion to extract directly overlapping peaks, using the mergePeaks function in HOMER, under the default parameters. The statistical significance of the observed overlap was calculated with a hypergeometric test, also in HOMER [described further in section 6.3.4].

6.2.3 RT-qPCR validation

Huh7.5 cells were incubated with recombinant human BMP6, activin A or activin B at 54 nM for 48 h, followed by RNA extraction, cDNA synthesis and RT-qPCR quantification of gene expression as described in section 2.2.

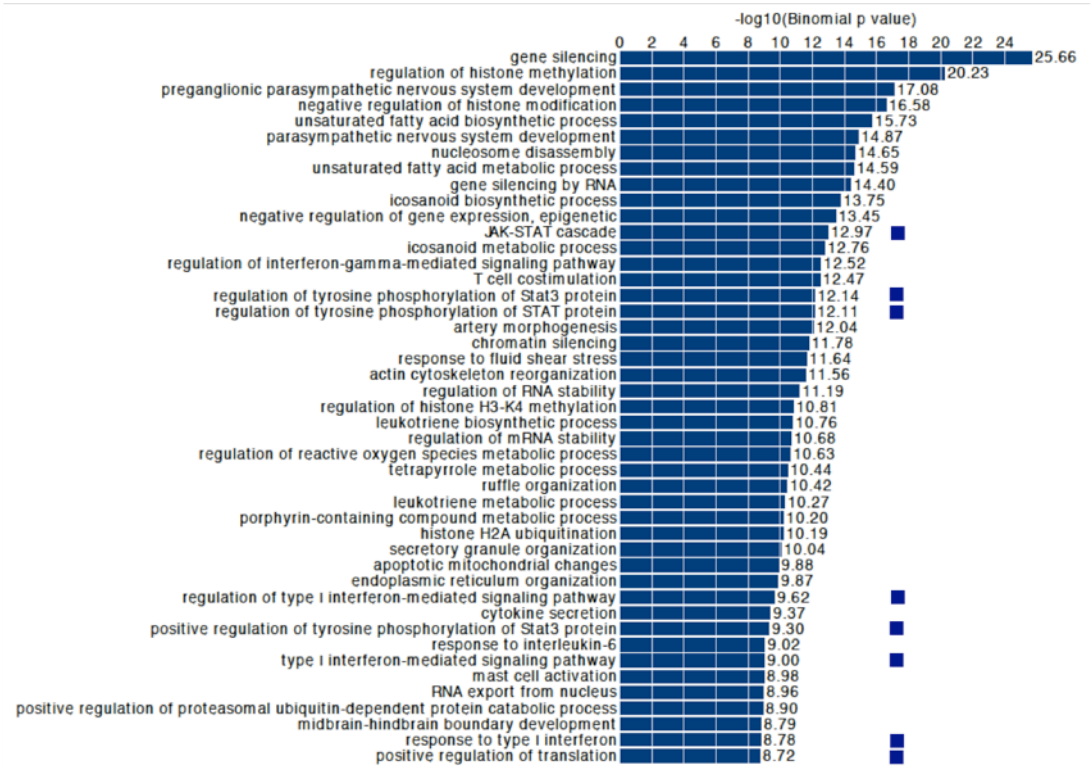
6.3 Results

6.3.1 GSE analysis demonstrates significant enrichment for IFN-associated gene sets in the BMP4-SMAD1 dataset

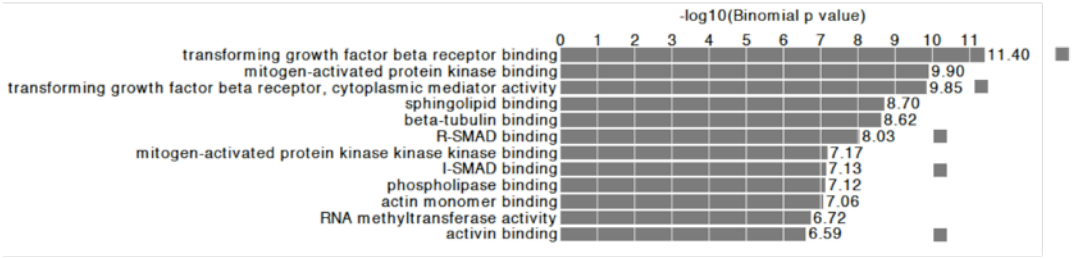
GSE analysis of the BMP4-SMAD1 dataset reveals, as expected, enrichment for SMAD-associated molecular functions, including activation of the TGFβ receptor, R-SMAD activity and I-SMAD binding. The BMP4-SMAD1 dataset also shows significant enrichment for several type I IFN, JAK-STAT and innate antiviral pathways, across multiple ontology databases [figure 6.5].

GSE analysis of the IFNa30-IRF1 and IFNa6h-IRF1 datasets, by contrast, indicate significant enrichment of IFN-associated pathways, as expected, but no reciprocal enrichment for BMP/SMAD-associated gene sets [figure 6.6 and 6.7]. Specific genes driving the associations with the type I IFN response are listed in appendix III.

(i) GO Biological Processes (BMP4-SMAD1)



(ii) GO Molecular Function (BMP4-SMAD1)



(iii) Panther Pathway (BMP4-SMAD1)

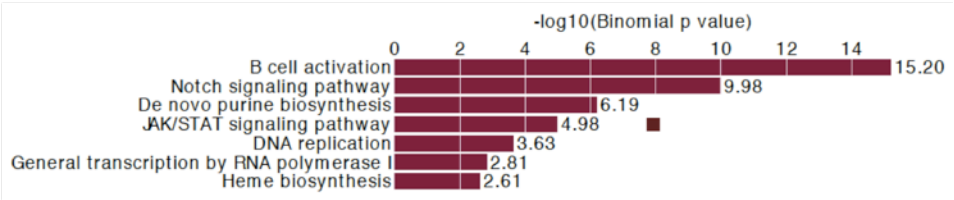


Figure 6.5: GREAT Gene Set Enrichment Analysis (GSEA) for BMP4-SMAD1 peaks

Peaks identified with the Homer peak calling algorithm were subjected to GSEA with the GREAT web-based tool. Pathways defined as significant by region-based binomial analysis with reference to the hg19 GRCh37 genome assembly were reported. GSEA results from interrogation of three databases are illustrated: Gene Ontology (GO) Biological Process (i); GO Molecular Function (ii); and Panther Pathways (iii). Significantly enriched pathways with an annotation count of 10-150 genes inclusive reported.

■ denotes an innate antiviral, IFN, JAK or STAT-signalling associated pathway in (i) and (iii) and a BMP-SMAD associated gene set in (ii)

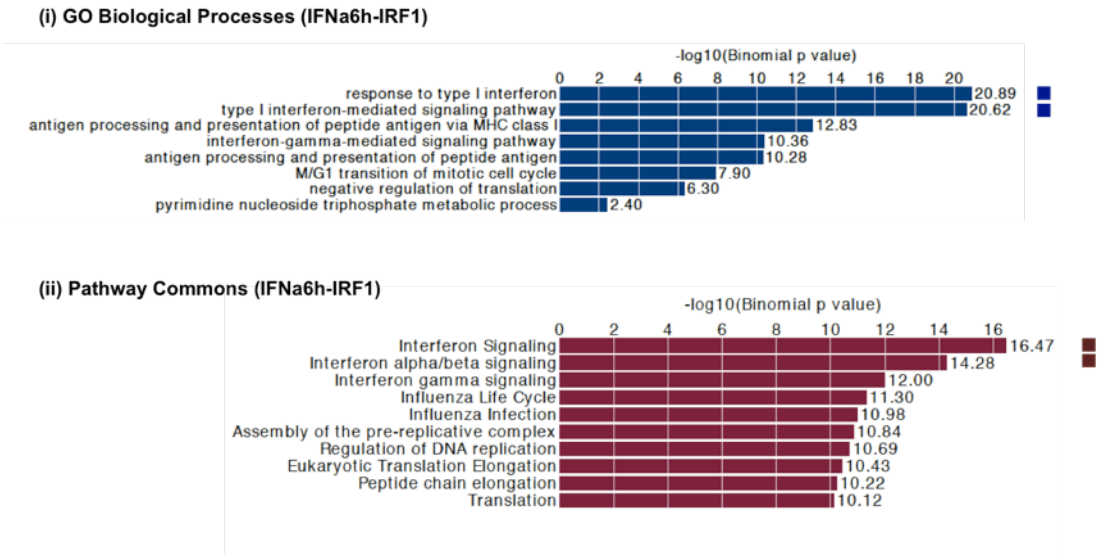


Figure 6.6: GREAT Gene Set Enrichment Analysis (GSEA) for IFNa6h-IRF1 peaks

Peaks identified with the Homer peak calling algorithm were subjected to GSEA with the GREAT web-based tool. Pathways defined as significant by region-based binomial analysis with reference to the hg19 GRCh37 genome assembly were reported. GSEA results from interrogation of two databases are illustrated: Gene Ontology (GO) Biological Process (i) and Pathway Commons (ii). Significantly enriched pathways with an annotation count of 10-150 genes inclusive reported.

■ denotes an innate antiviral, IFN, JAK or STAT-signalling associated pathway

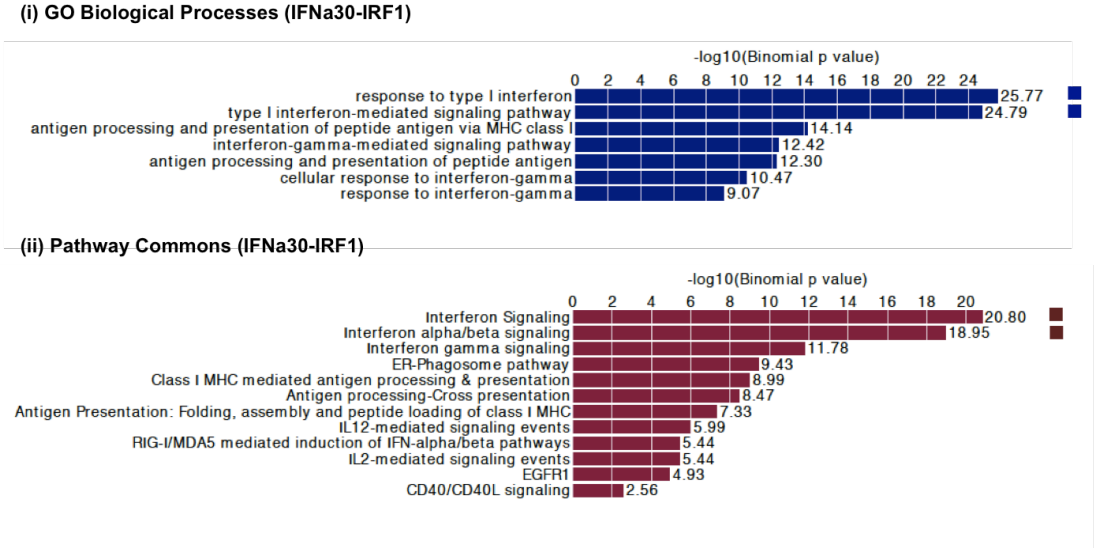


Figure 6.7: GREAT Gene Set Enrichment Analysis (GSEA) for IFNa30-IRF1 peaks

Peaks identified with the Homer peak calling algorithm were subjected to GSEA with the GREAT web-based tool. Pathways designated as significant by region-based binomial analysis with reference to the hg19 GRCh37 genome assembly were reported. GSEA results from interrogation of two databases are illustrated: Gene Ontology (GO) Biological Process (i) and Pathway Commons (ii). Significantly enriched pathways with an annotation count of 10-150 genes inclusive reported.

To examine whether this phenomenon is restricted to K562 cells, the analysis was replicated in an analogous dataset obtained from BMP4-treated U937 cells immunoprecipitated for SMAD1, also generated by Trompouki and colleagues (61). The U937 cell line, derived from a histiocytic lymphoma isolate, exhibits a monocytic phenotype and protein repertoire in culture, in contrast to erythrocyte-like K562 cells (634). In U937 cells treated with BMP4, immunoprecipitation for SMAD1 is associated with enrichment for multiple type I and type II IFN pathways, in addition to significant enrichment for SMAD-associated molecular functions [figure 6.8].

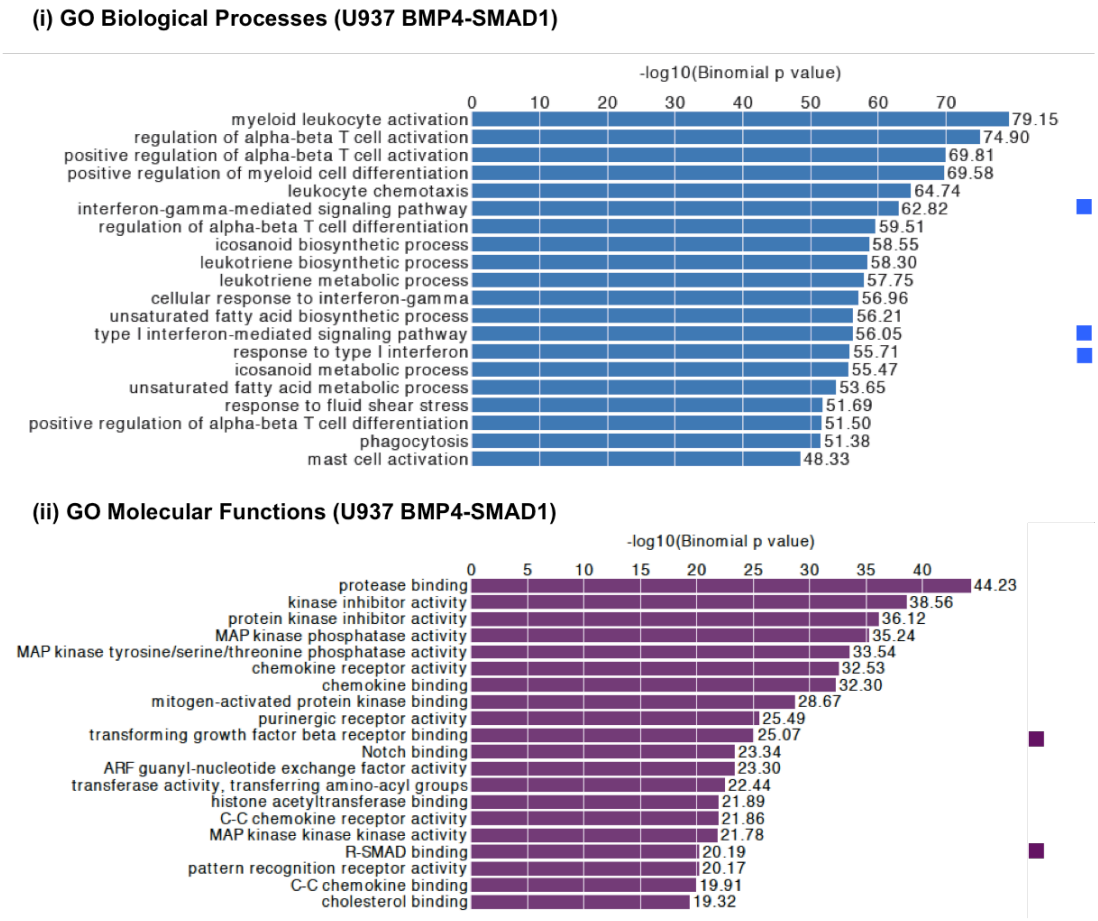


Figure 6.8: GREAT Gene Set Enrichment Analysis (GSEA) for U937 BMP4-SMAD1 peaks

Peaks identified with the Homer peak-calling algorithm were subjected to GSEA with the GREAT web-based tool. Pathways defined as significant by region-based binomial analysis with reference to the hg19 GRCh37 genome assembly were reported. GSEA results from interrogation of two databases are illustrated: Gene Ontology (GO) Biological Process (i) and GO Molecular Functions (ii). Significantly enriched pathways with an annotation count of 10-150 genes inclusive reported.

■ denotes an innate antiviral, IFN, JAK or STAT-signalling associated pathway in (i) and BMP-SMAD associated gene sets in (ii)

Replication of the analysis procedure in a dataset from SMAD1-immunoprecipitated BMP-treated CD34+ erythrocyte progenitors did not yield enrichment for explicitly named "type I IFN response" gene sets. However, upon examination of the genes driving associations between the CD34+ BMP4/SMAD1 dataset and the ontological categories "antigen processing and presentation" and "CD40L signalling pathway" defined by the MgSigDb database [figure 6.9], SMAD1 binding peaks were identified proximal to ten genes encoding type I IFN ligands, in addition to multiple IFN and NFκB-associated signal transduction components (see appendix III).

(i) MgSigDb (CD34+ erythrocytic progenitor BMP4-SMAD1)

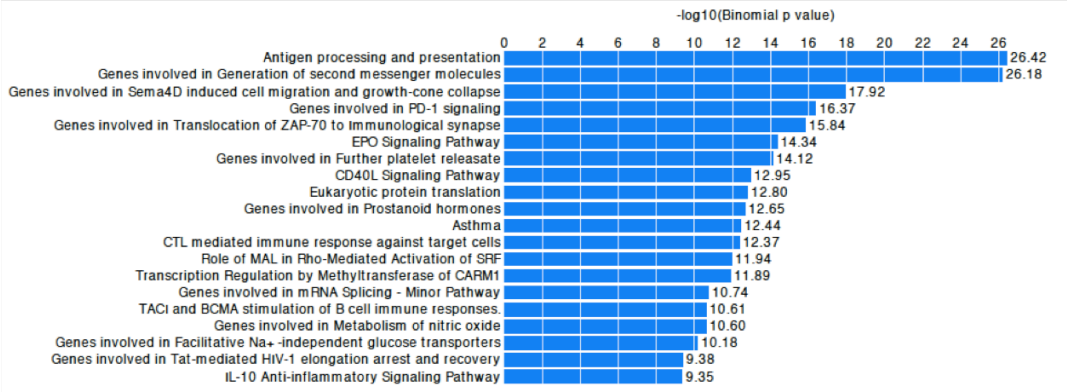


Figure 6.9: GREAT GSEA for CD34+ erythrocytic progenitor BMP4-SMAD1 peaks

Peaks identified with the Homer peak-calling algorithm were subjected to GSEA with the GREAT web-based tool. Pathways defined as significant by region-based binomial analysis with reference to the hg19 GRCh37 genome assembly were reported. GSEA results from the interrogation of the MgSigDb database are reported. Significantly enriched pathways with an annotation count of 10-150 genes inclusive reported.

6.3.2 Multiple antiviral effector genes are associated with overlapping SMAD1 and IRF1 binding, co-incident with active chromatin marks

To identify candidate loci with co-incident IRF1 and SMAD1 binding, we identified peaks showing exact positional overlap in both the BMP4-SMAD1 and IFNa6h-IRF1 datasets and annotated the resulting list to the human reference assembly. Multiple loci associated with antiviral effector genes show direct overlap, at the single nucleotide level, between the centres of IRF1 and SMAD1 peaks. These co-incident peaks are readily apparent upon visualization of the respective ChIP-seq tracks in the UCSC genome browser.

In a number of targets, the height of the SMAD1 binding peak exceeded that of IRF1. These genes include *RSAD2* or viperin; *SSBP3*, encoding a putative HCV restriction factor; *ZC3HAV1*, encoding the zinc-finger antiviral protein; and *MOV10*, a P-body protein that

restricts HCV replication and reduces lentivirus infectivity *in vitro* [figure 6.10-6.13]. Co-incident peaks were also observed at the *IFIT3* locus [see appendix IV]. In Huh7.5 cells, induction of *RSAD2*, *SSBP3* and *ZC3HAV1* by 54 nM BMP6, activin A and activin B was validated by RT-qPCR [figure 6.14].

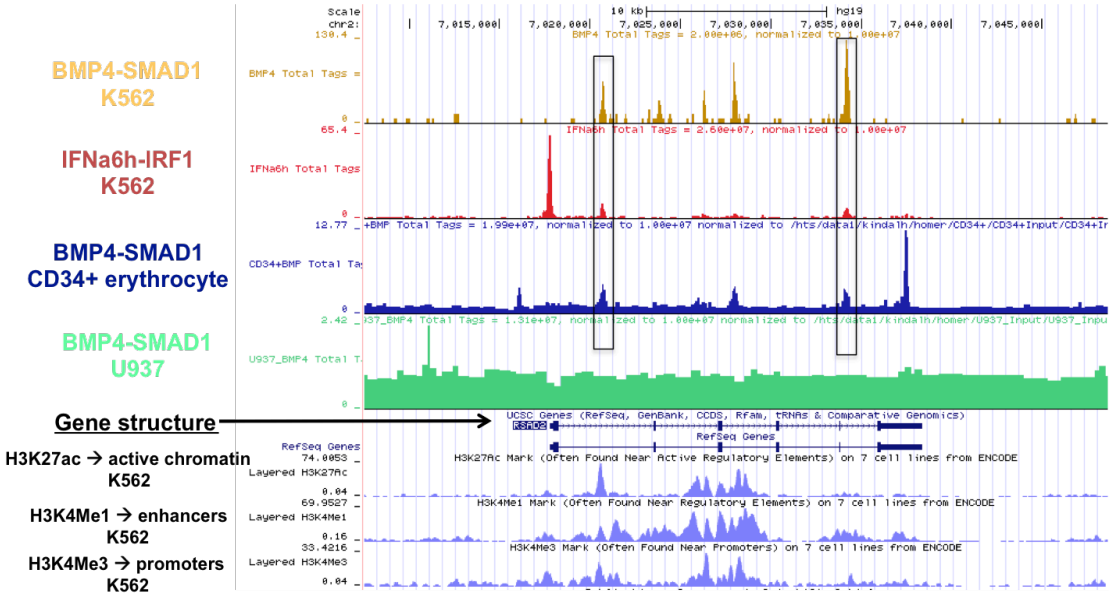


Figure 6.10: UCSC visualization of the *RSAD2* locus, encoding viperin, +/- 10kb.

Instances of peak co-localization denoted by boxes.

Data depicted:

1) ChIP-seq for SMAD1 in BMP4-treated K562 cells [Source: (61)]
2) ChIP-seq for IRF1 in IFN α-treated K562 cells [Source: ENCODE consortium]
3) ChIP-seq for SMAD1 in BMP4-treated CD34+ erythrocyte progenitors [Source: (61)]
4) ChIP-seq for SMAD1 in BMP4-treated U937 cells [Source: (61)]
5) Gene structure, in accordance with RefSeq annotation [Source: RefSeq/UCSC]
6) ChIP-seq for H3K27ac histone mark in K562 cells [Source: ENCODE consortium]
7) ChIP-seq for H3K4Me1 histone mark in K562 cells [Source: ENCODE consortium]
8) ChIP-seq for H3K4Me3 histone mark in K562 cells [Source: ENCODE consortium]

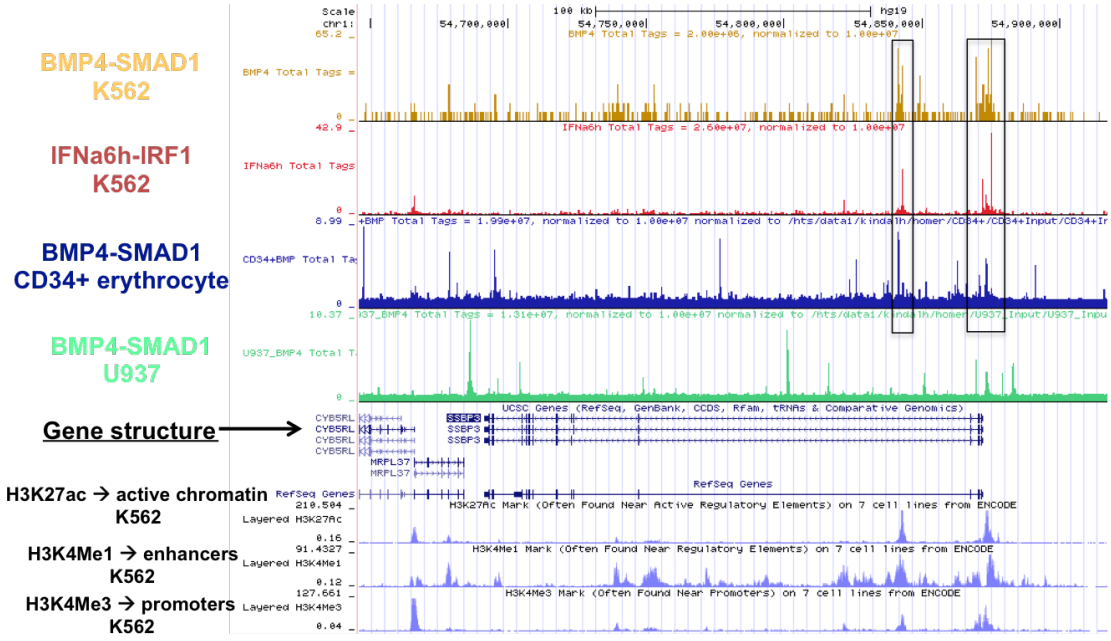


Figure 6.11: UCSC visualization of the *SSBP3* locus, encoding single stranded DNA-binding protein 3, +/- 50kb.

Instances of peak co-localization denoted by boxes. Legend as per figure 6.10

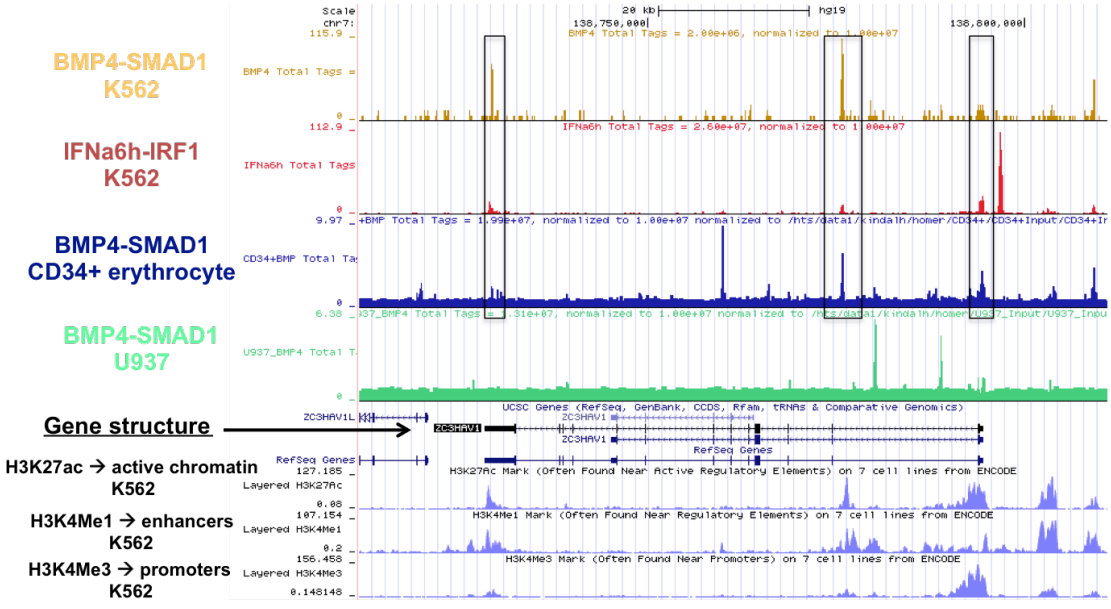


Figure 6.12: UCSC visualization of the *ZC3HAV1* locus, encoding the zinc finger antiviral protein, +/- 20kb.

Instances of peak co-localization denoted by boxes. Legend as per figure 6.10

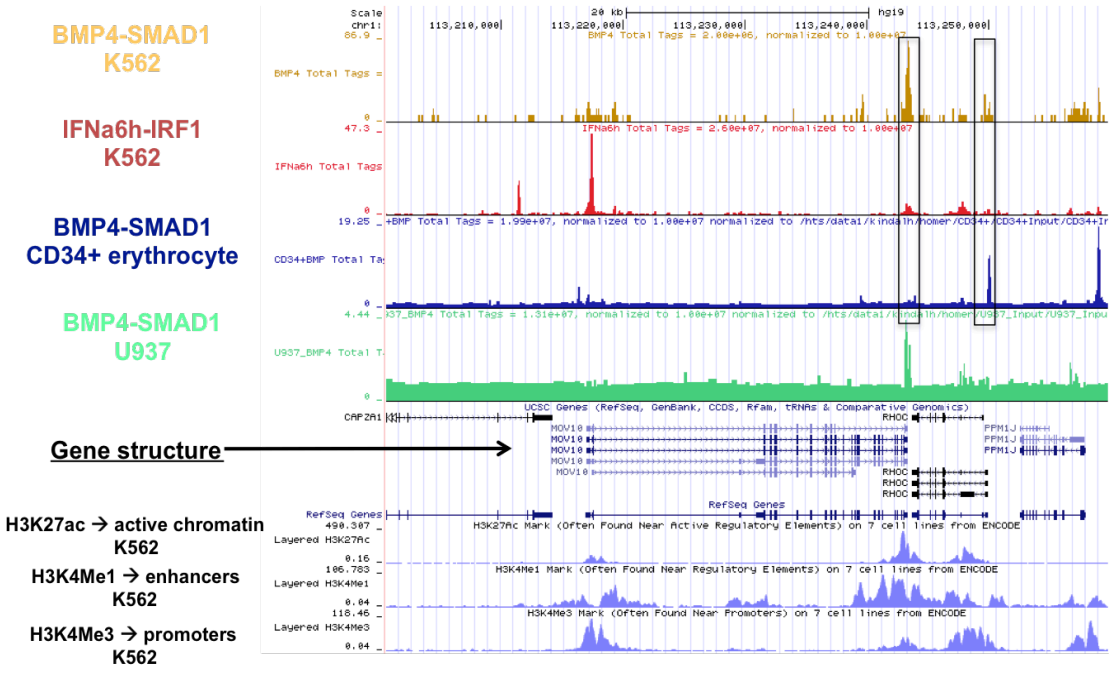


Figure 6.13: UCSC visualization of the *MOV10* locus, encoding Moloney leukaemia virus 10 homologue , +/- 20kb.
Instances of peak co-localization denoted by boxes. Legend as per figure 6.10

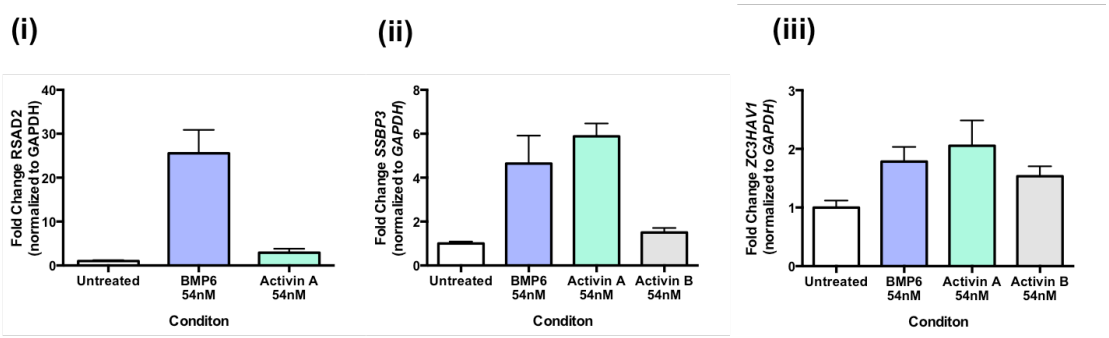


Figure 6.14: BMP6 and activin proteins induce expression of the ISGs *RSAD2*, *SSBP3* and *ZC3HAV1* in Huh7.5 cells

Huh7.5 cells were treated with recombinant human BMP6, activin A or activin B at 54 nM for 72 h, followed by RNA extraction and RT-qPCR quantification of mRNA encoding the antiviral effectors *RSAD2* (i), *SSBP3* (ii) and *ZC3HAV1* (iii). With the exception of *RSAD2*, which was not detected in the presence of activin B, message encoding all genes was induced at 72 h post-incubation, with varying degrees of potency.

n=1 experiment in biological triplicate; mean+SEM

Direct SMAD1/IRF1 overlap is also evident in multiple regions associated with PRR and IFNAR signal transduction components, including *MYD88*, for which SMAD1 binding in the 5'UTR and first exon exceeds that of IRF1; *TBK1*, which also demonstrates stronger SMAD1 versus IRF1 binding; *STAT1* and *STAT2* [see appendix IV for UCSC visualizations]. Of note, directly overlapping SMAD1/IRF1 peaks are also present proximal to the BMP-responsive genes *ID1*, *ID2* and *ID3*, a family of basic helix-loop-helix transcription factors implicated in

cell fate decisions and differentiation (635). However, the magnitude of these IRF1 peaks is much smaller than those corresponding to SMAD1 [figure 6.15 for *ID1*; appendix IV for *ID2* and *ID3*].

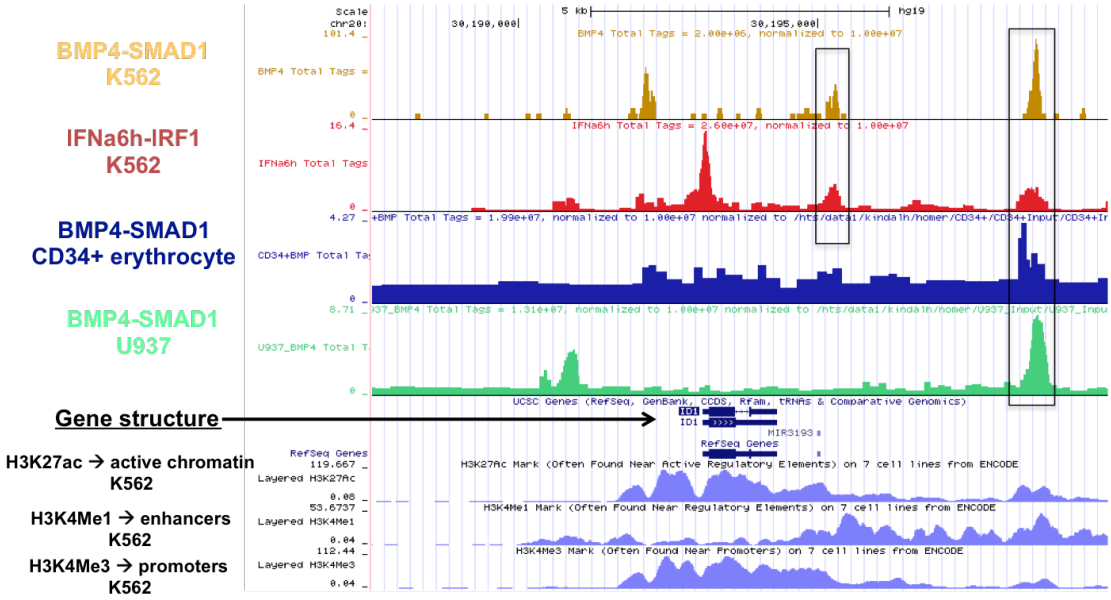


Figure 6.15: UCSC visualization of the *ID1* locus, encoding *inhibitor of DNA binding 1*, +/- 5kb.

Instances of peak co-localization denoted by boxes. Legend as per figure 6.10

Transcription factor binding profiles are frequently cell-type specific, in part due to differential expression of epigenetic marks. To address whether the observed similarity in SMAD1 and IRF1 binding patterns extends to other cell lines, we repeated our analysis on SMAD1 ChIP-seq datasets obtained from transformed monocytic U937 cells and CD34+ erythrocyte progenitors harvested from the peripheral blood of G-CSF mobilized donors (61). Both cell types were stimulated with BMP4, at the same dose and timing as the K562 cells, the datasets being obtained from the same publication.

To determine whether overlapping SMAD1/IRF1 peaks occur in regions of transcriptionally active chromatin, we cross-referenced the binding profiles to ChIP-seq tracks corresponding to three common histone modifications, namely H3K27ac, H3K4Me1 and H3K4Me3. H3K27ac typically maps to transcriptionally active chromatin, whereas H3K4Me1 and H3K4Me3 mark enhancer and promoter regions respectively (629). These tracks were obtained from unstimulated K562 cells, and made publicly available by the ENCODE project. As is evident in the UCSC visualizations [figures 6.10-6.13], multiple antiviral effector genes, including *RSAD2*, *SSBP3*, *ZC3HAV1* and *MOV10* are associated with peaks in the CD34+ progenitor track that directly overlap with both the BMP4-SMAD1 and IRFa6h-IRF1 peak-sets. Moreover, all of the identified overlapping peaks align with regions of active chromatin;

predominantly those enriched for H3K27ac and enhancer-associated H3K4Me1. Fewer instances of positionally conserved peaks were noted in the U937 dataset.

6.3.3 Genome-wide, SMAD1 binding is enriched proximal to IRF1

While the candidate gene approach yielded valuable insights into coincident binding of SMAD1 and IRF1 at specific antiviral effector loci, we were keen to establish whether there is an overlap between SMAD1 and IRF1 binding profiles genome-wide. To tackle this, we devised a second analysis strategy.

A more stringent peak-calling threshold, defined as ten-fold greater read alignment in the target versus input control data set, was applied to the BMP4-SMAD1, IFNa30-IRF1 and IFNa6h-IRF1 datasets. An additional dataset was procured from the Trompouki et al. publication, namely a ChIP-seq for SMAD1 in K562 cells incubated with the type I BMP receptor antagonist dorsomorphin (61). This dataset, referred to as 'dorso-SMAD1' was subjected to identical alignment and analysis protocols.

The analysis procedure is divided into three stages. Firstly, one of the stringently defined peak-sets is selected to act as the 'reference peak-set'. Second, the alignment positions of reads from a second 'comparator' dataset are compared to the centres of the peaks in the reference peak-set. Third, the average densities of the reads in the comparator dataset that align +/- 500 bp about the centre of the reference peaks are binned into 50 bp intervals. Finally, these data are represented as histograms, with 'ChIP fragment depth', an index of read density, plotted against their position relative to the centres of the reference peaks. This approach allows us to interrogate the frequency with which a 'comparator' transcription factor binds in the vicinity of a 'reference' transcription factor across the whole genome.

To validate our methodology, we compared genome-wide binding of RNA Pol II and RNA Pol III in unstimulated K562 cells against the BMP4-SMAD1 and IFNa-IRF1 peak-sets. RNA Pol II is required for transcription of mRNA precursors, miRNA and snoRNA, whereas RNA Pol III synthesizes 5S rRNA, tRNA and various small RNAs including spliceosome components and ribozymes (636). Accordingly, we hypothesized that RNA Pol II binding would be enriched proximal to the peak centres across all of the peak sets, being a necessary constituent of the transcriptional machinery. In contrast, none of the RNA Pol III targets are IFN- or BMP-inducible, to the best of our knowledge. As such, we would anticipate minimal RNA Pol III binding around the centres of the peaks from all of our datasets.

As illustrated in figure 6.16 (i), while RNA Pol II binding in unstimulated K562 cells mirrors that of both SMAD1 in BMP4-treated cells and IRF1 after IFNα stimulation, enrichment for RNA Pol III binding is undetectable in all of the peak-sets [figure 6.16 (ii)].

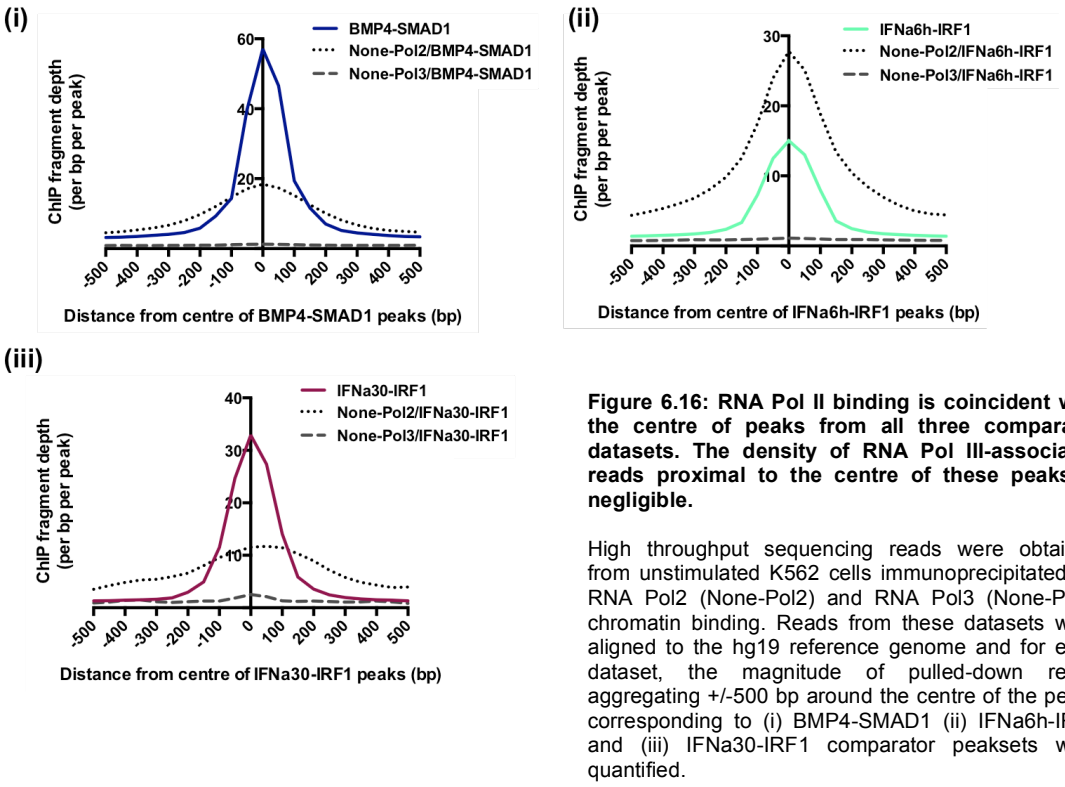


Figure 6.16: RNA Pol II binding is coincident with the centre of peaks from all three comparator datasets. The density of RNA Pol III-associated reads proximal to the centre of these peaks is negligible.

High throughput sequencing reads were obtained from unstimulated K562 cells immunoprecipitated for RNA Pol2 (None-Pol2) and RNA Pol3 (None-Pol3) chromatin binding. Reads from these datasets were aligned to the hg19 reference genome and for each dataset, the magnitude of pulled-down reads aggregating +/-500 bp around the centre of the peaks corresponding to (i) BMP4-SMAD1 (ii) IFNa6h-IRF1 and (iii) IFNa30-IRF1 comparator peaksets were quantified.

In figure 6.17 (i), IRF1 binding in neither the IFNa30-IRF1 nor IFNa6h-IRF1 datasets is enriched proximal to the centre of peaks identified from the BMP4-SMAD1 datasets. As demonstrated by figure 6.17 (ii) and (iii), however, SMAD1 binding is enriched proximal to peaks from both the IFNa6h-IRF1 and IFNa30-IRF1 datasets, albeit more strongly in the former. This enrichment is not observed in cells treated with dorsomorphin, implying that it is contingent upon intact BMP signal transduction. Recapitulating the observations from the GSE analysis, reads from neither the IFNa30-IRF1 nor the IFNa6h-IRF1 datasets are enriched proximal to BMP4-SMAD1 peaks.

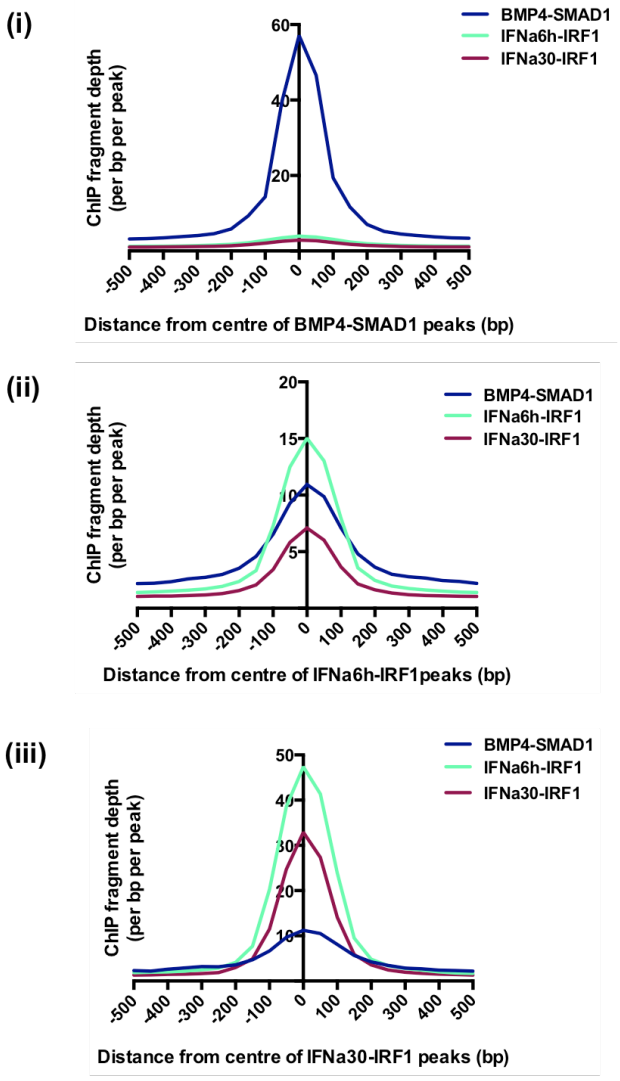


Figure 6.17: SMAD1 binding in BMP-treated K562 cells is enriched proximal to peaks in the IFNa6h-IRF1 and IFNa30-IRF1 datasets
Histograms depict the magnitude of pulled-down reads from each dataset aggregating +/- 500 bp around the centre of the peaks corresponding to (i) BMP4-SMAD1 (ii) IFNa6h-IRF1 and (iii) IFNa30-IRF1 comparator peak-sets.

To gauge whether or not the observed enrichment for SMAD1 proximal to IRF1-bound loci is merely an artefact of the analysis procedure, we extended the analysis to a panel of randomly selected DNA-interacting proteins. Datasets were obtained from ENCODE, and present the genome-wide binding profiles, in unstimulated K562 cells, of ARID3A, ELK1, INI1, RAD21 and XRCC4. The functions and basic biology of these factors are summarized in table 6.2.

DNA-interacting factors	Functions	References
ARID3A	Transactivates heavy-chain immunoglobulin transcription; roles in B-cell development and haematopoiesis	(637,638)
ELK1	Transcription factor activated by MAP kinases and targets the Serum Response Factor sequence upstream of *C-FOS*	(639)
INI1	Component of the SWI/SNF chromatin remodelling complex and maintenance of euploidy.	(640)
RAD21	Cohesin ring subunit; clusters sister chromatids during mitosis	(641)
XCCR4	Component of the NHEJ DNA repair machinery	(642)

Table 6.2: Biological functions of the DNA-binding proteins examined in figure 6.18

As demonstrated in figure 6.18, the binding profiles of none of these randomly selected DNA-binding proteins show strong enrichment proximal to the centre of BMP4-SMAD1 peaks. With reference to the IRF1 peak-sets, ARID3A and RAD21 binding is slightly enriched around the centre of IFNa6h-IRF1 and IFNa30-IRF1 peaks respectively, although neither attained the same maximum fragment depth as SMAD1 binding in BMP4 treated cells. As the reads obtained for each ChIP-seq dataset are normalized to 10 million, we can be assured that enrichment for SMAD1 binding proximal to IRF1 peaks is not an artefact of variation in dataset size.

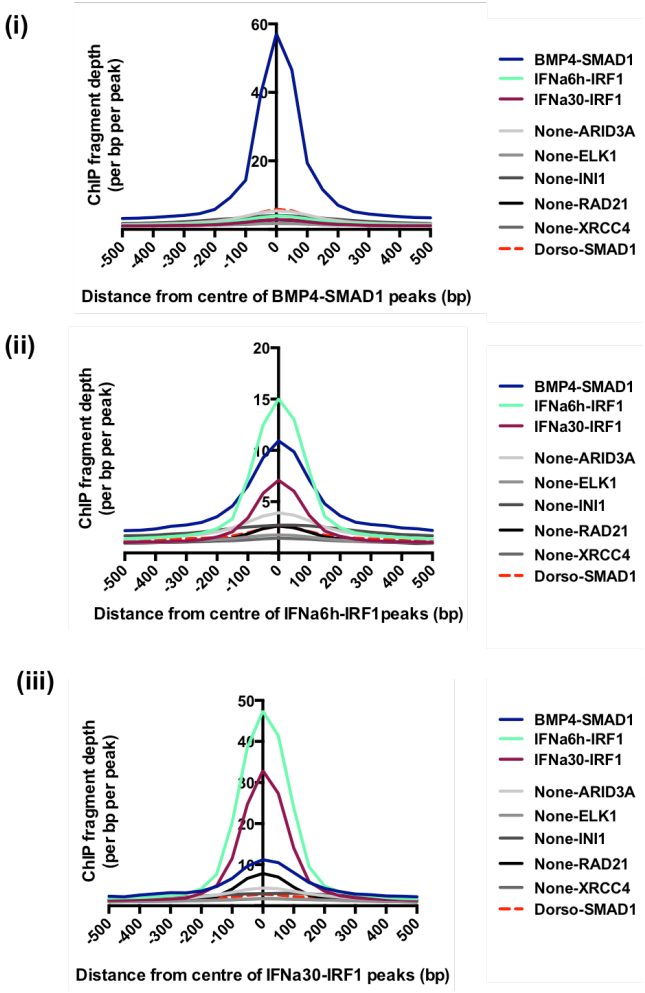


Figure 6.18: SMAD1 binding proximal to the centre of peaks identified from IFNa6h-IRF1 and IFNa30-IRF1 ChIP-seq is enriched compared to a panel of random DNA-interacting factors

High throughput sequencing reads were obtained from unstimulated K562 cells ('None') immunoprecipitated for ARID3A, ELK1, INI1, RAD21, XRCC4 chromatin binding; and SMAD1 binding in K562 cells treated with the BMP signalling inhibitor dorsomorphin ("Dorso-SMAD1").

Reads from these datasets, in addition to the BMP4-SMAD1, IFNa30-IRF1 and IFNa6h-IRF1 datasets described previously, were aligned to the hg19 reference genome and for each dataset, the magnitude of pulled-down reads aggregating +/- 500 bp around the centre of the peaks corresponding to (i) BMP4-SMAD1 (ii) IFNa6h-IRF1 and (iii) IFNa30-IRF1 comparator peaksets were quantified.

To approach the same question from the opposite perspective, we also analysed the incidence of IFNα-induced STAT1 and STAT2 binding proximal to the BMP4-SMAD1, IFNa6h-IRF1 and IFNa30-IRF1 peak-sets. Both STAT1 and STAT2 are phosphorylated downstream of the IFNAR-JAK complex, and transactivate a similar repertoire of ISGs to IRF1 (643). Given this, we would anticipate STAT1 and STAT2 binding to mirror that of IRF1 genome-wide,

reflected in this analysis by enriched transcription factor binding proximal to the IRF1 peak centres.

As illustrated by figure 6.19, both STAT1 and STAT2 binding are enriched in the vicinity of IRF1 peaks from both the IFNa6h-IRF1 and IFNa30-IRF1 datasets, as anticipated. However, neither STAT1 nor STAT2 demonstrate enrichment around the BMP4-SMAD1 peaks, consistent with observations from the IRF1 datasets.

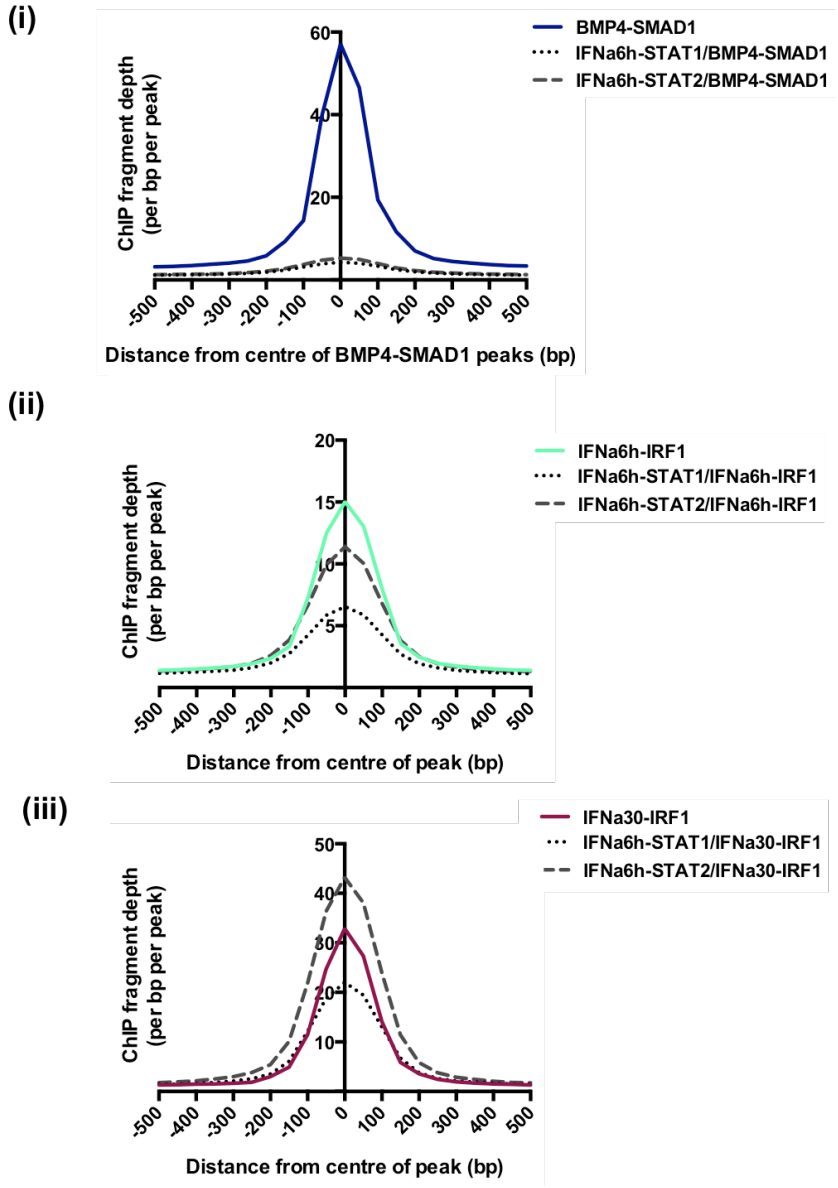


Figure 6.19: STAT1 and STAT2 binding in IFN α -treated K562 cells mirrors that of IRF1, but is not enriched proximal loci bound by SMAD1 in BMP4-treated cells

Histograms depict the magnitude of pulled-down reads aggregating +/- 500 bp around the centre of the peaks corresponding to (i) BMP4-SMAD1 (ii) IFNa6h-IRF1 and (iii) IFNa30-IRF1 comparator peak-sets.

6.3.4 Statistical appraisal of SMAD1-IRF1 overlap genome-wide

To assess the degree of direct overlap between transcription factor binding profiles more formally, the data were analysed by hypergeometric distribution test, a statistical tool available in the HOMER program. In brief, the hypergeometric distribution is a probability distribution (that is, a mathematical description of the odds of every possible outcome in random experiment or dataset) that represents the probability of *k* successes being drawn in *n* attempts, without replacement of the extracted values, from a population of total size *N* containing *K* total successes. In the case of our datasets, *K* represents the total number of directly overlapping peaks, and *N* is the total number of peaks in a given peak-set.

The hypergeometric test itself calculates the statistical significance of drawing *k* successes out of *n* attempts from the aforementioned population, without replacing the extracted values. As such, if *k* or more overlapping peaks are drawn at random from a given peak-set after *n* trials, the statistical significance of this enrichment for peak overlap can be assigned a p-value (632,644).

HOMER reports the enrichment p-value as a natural log. A positive p-value (>=0) represents divergence between two peak-sets whereas increasingly negative values reflect increasing degrees of convergence. While this approach does not allow calculation as to whether the incidence of a transcription factor's binding relative to another is statistically significant, nor permit definition of a biologically significant threshold value, it does provide a quantitative representation of the degree of convergence between transcription factor binding profiles. The percentages of overlapping peaks from all of the analysed datasets with respect to the BMP-SMAD1, IFNa6h-IRF1 and IFNa30-IRF1 peak-sets are also presented as stacked bar charts in figure 6.20.

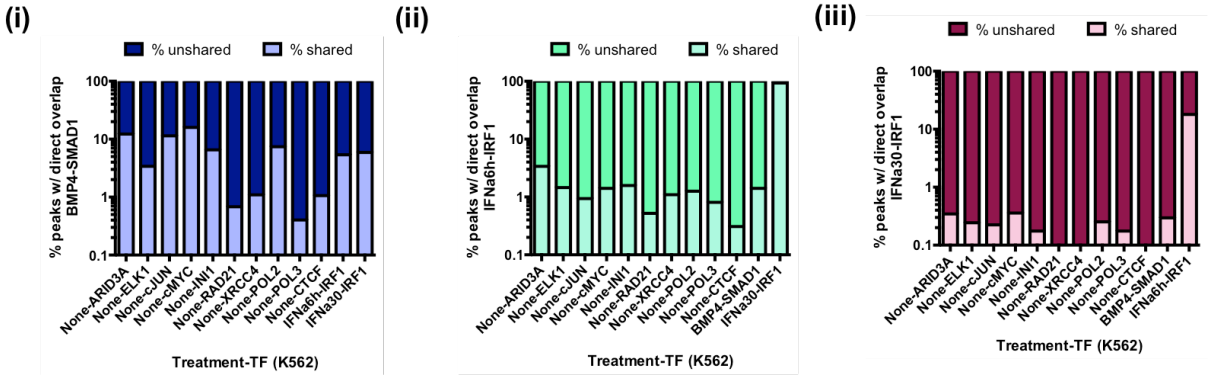


Figure 6.20: Pairwise comparisons of directly overlapping transcription factor binding sites between datasets

Stacked bar charts depict the percentage of overlapping transcription factor binding events as pairwise comparisons with respect to the BMP-SMAD1 (i), IFNa6h-IRF1 (ii) and IFNa30-IRF1 (iii) datasets.

To gauge whether or not this approach can replicate a previously defined association between transcription factor binding profiles, we used the hypergeometric test to assess the significance of overlap between GATA1 and SMAD1 in BMP4-stimulated K562 cells [see table 6.3]. The original publication from Trompouki and colleagues provides extensive evidence that GATA1 and BMP4-stimulated SMAD1 co-occupy DNA sites adjacent to erythroid target genes. Consistent with this, the test yielded an extremely low p-value for the association between GATA1 and SMAD1 in BMP4-stimulated cells. In contrast, the p-value is much higher when the BMP4-GATA1 and dorso-SMAD1 peak-sets are compared, as would be anticipated when BMP4 signal transduction, and subsequent activation of SMAD1, is blocked.

Having validated the test against a well-characterized transcription factor association, we applied it to the other ChIP-seq datasets. The results of this analysis are summarized in table 6.3. From the table, it is clear that RNA Pol III binding shows minimal overlap with any of the BMP4-SMAD1, IFNa6h-IRF1 and IFNa30-IRF1 datasets, as would be expected given the nature of the genes it transcribes: this observation further validates the test's utility.

	BMP4-SMAD1	IFNa6h-IRF1	IFNa30-IRF1	Dorso-SMAD1
BMP4-SMAD1		-263	-60	
IFNa6h-IRF1			-3645	
IFNa30-IRF1				
None-ARID3A	-1522	-462	-37	
None-ELK1	-17	-9	0	
None-INI1	-235	-65	-8	
None-RAD21	-66	-103	-21	
None-XRCC4	-2	-3	0	
Dorso-SMAD1	-2226	-124	-30	
IFNa6h-STAT1	-325	-1889	-1026	-143
IFNa6h-STAT2	-768	-2973	-1415	-231
BMP4-GATA1	-18580	-481	-66	-3210
None-RNA Pol II	-2080	-331	-64	
None-RNA Pol III	0	-3	-15	

Table 6.3: Summary of pairwise hypergeometric testing between ChIP-seq datasets

The results of pairwise hypergeometric testing for overrepresentation of directly overlapping peaks are presented as natural log-transformed p-values: negative values indicate enrichment for overlapping peaks.

The principal question we aim to address with this analysis, however, pertains to the incidence of directly overlapping peaks between the BMP4-SMAD1 and IFNa-IRF1 datasets. By this test, the degree of overlap between the BMP4-SMAD1 and both IFNa-IRF1 peak-sets is greater than that observed for the panel of randomly selected transcription factors, with the exception of ARID3A. In dorsomorphin-treated cells, the significance of enrichment for SMAD1 at IRF1 binding sites is reduced compared to the BMP4-SMAD1 peak-set, suggesting that the similarity in IRF1 and SMAD1 binding is contingent upon active upstream signalling.

As would be expected given their similar repertoire of target genes, IFNα-induced STAT1 and STAT2 binding genome-wide show very significant overlap with IRF1. Both IRF1 and ISGF3 (a heterotrimeric complex of STAT1, STAT2 and IRF9 induced downstream of type I and type III IFN receptor activation) bind the ISRE motif. Induction of activated STAT dimers via the IFNγ receptor drives gene expression via binding to the gamma-activated (GAS) consensus sequence [TTCNNNGAA] (568,645). The presence of ISRE and GAS sequences in the promoter regions of ISGs is not mutually exclusive, with effectors demonstrating variable levels of induction in response to each class of IFN in accordance with the presence of ISRE sequences, GAS elements or both (140,142,325).

By comparison, more modest overlap is evident between the BMP4-SMAD1 peak-set and IFNα-induced STAT1 and STAT2, and the level of co-incidental SMAD1 binding is reduced even further by dorsomorphin treatment.

6.3.5 Comparison of BMP-induced gene sets between the BMP6/Huh7 microarray and BMP4/K562 ChIP-seq derived datasets

The aforementioned analyses suggest a strong association between SMAD1 and IRF1 binding genome-wide in the K562 cell line. Being an erythroleukaemic cell line, however, it is probable that its response to BMP4 (and, indeed to IFNα and other stimuli cytokines) differs from that of liver tissue, both primary human hepatocytes and the transformed Huh7 cells studied extensively in this project. We were unable to replicate the ChIP-seq analysis in Huh7 cells or procure similar data from a related hepatoma-derived cell line. As such, we undertook a specific comparison of the 2,207 genes differentially expressed in our previous microarray of BMP6-treated Huh7 cells [section 3.1.1; figure 3.1] with the loci reported in K562 BMP4-SMAD1 dataset. The genes present in both datasets were the subjected to GREAT GSE analysis.

615 genes (28%) were shared between both the list of 2,206 differentially regulated genes reported by the Huh7/BMP6 microarray and the K562 BMP-SMAD1 ChIP-seq dataset. Many of these genes were associated with multiple SMAD1 binding incidences, as is evident from the comprehensive list of shared genes and their associated SMAD1 peaks presented in appendix V.

Interrogation of the GO Biological Processes database with the resultant list of shared genes yielded enrichment for both TGFβ-associated pathways and JAK-STAT/type I IFN gene sets, akin to the patterns of enrichment evident in the K562 ChIP-seq dataset alone [figure 6.21]. The genes driving the associations with antiviral/IFN-linked pathways are tabulated in appendix VI. From this, we infer that BMP4-treatment of K562 cells and BMP6-treatment of Huh7 cells elicit similar patterns of gene expression. The genes driving associations with two of these gene sets are listed in table 6.4.

(i) GO Biological Processes (K562 BMP-SMAD1 ChIP-seq/Huh7/BMP6 microarray shared genes)

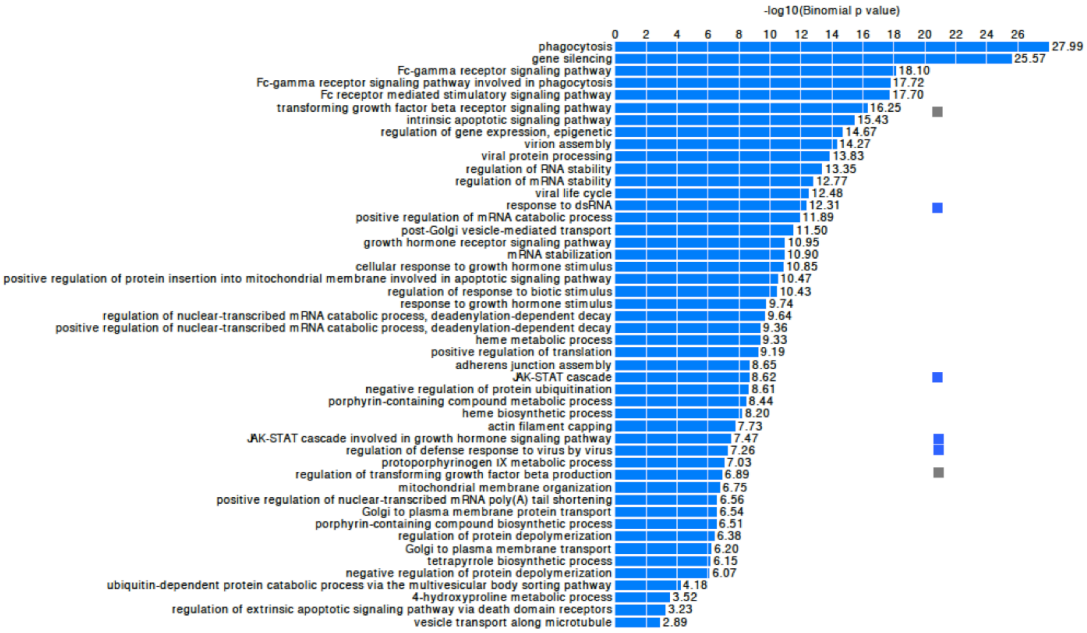


Figure 6.21: GREAT Gene Set Enrichment Analysis (GSEA) for "shared genes"; those both upregulated in the Huh7 +/- BMP6 microarray and associated with peaks in the K562 BMP4-SMAD1 dataset

Peaks identified with the Homer peak-calling algorithm were subjected to GSEA with the GREAT web-based tool. Pathways defined as significant by region-based binomial analysis with reference to the hg19 GRCh37 genome assembly were reported. GSEA results from interrogation of two databases are illustrated: Gene Ontology (GO) Biological Processes. Significantly enriched pathways with an annotation count of 10-150 genes inclusive reported.

■ denotes an innate antiviral, IFN, JAK or STAT-signalling associated pathway; ■ denotes BMP-SMAD associated gene sets

GO Biological Processes: JAK-STAT	GO Biological Processes: Response to dsRNA
ADAM17	CARD9
CISH	DDX1
CTR9	DDX21
EGF	DGCR8
F2R	DICER1
FGFR3	LIN28A
HES1	LIN28B
IFNAR1	MAPK1
IFNAR2	MAVS
IRS1	MB21D1
IRS2	NFKBIA
JAK2	PELI1
LEP	PMAIP1
LYN	PRKRA
MAPK1	SLC3A2
PRL	SMAD1
PTPN1	SMAD2
SOCS1	SMAD3
SOCS3	STAT1
STAT1	TARBP2
STAT2	TICAM1
STAT3	ZC3HAV1
STAT4	ZCCHC11
STAT5A	
STAT5B	

Table 6.4: Summary of genes from the shared list driving associations with antiviral-associated gene sets

Table lists the genes both identified in the K562/BMP4-SMAD1 dataset and differentially regulated in the Huh7/BMP6 microarray that drive associations with GO Biological Processes "JAK-STAT" and "response to dsRNA" gene sets.

6.4 Summary and discussion

Together, these data suggest that the genome-wide binding profile of activated SMAD1 demonstrates very striking parallels to that of IRF1, including proximal to genes encoding antiviral effectors. However, this analysis is subject to a number of constraints and caveats.

An ideal ChIP-seq dataset would be generated from Huh7 hepatoma-derived cells, the line in which all of our antiviral assays have been conducted, or, for a more physiologic representation of the healthy liver, from primary human hepatocytes. Gene expression repertoires, both constitutive and inducible, vary significantly between tissues due to the

activity of tissue-specific promoter elements, variation in chromatin architecture and epigenetic regulation. However, as we could validate the induction of the ISGs *RSAD2*, *SSBP3* and *ZC3HAV1* by activin and BMP6 signalling in Huh7.5 hepatoma-derived cells, it is not improbable that at least some observations from the K562 datasets extrapolate to unrelated cell lines. That the observations from GSE analysis of the K562 BMP4-SMAD1 dataset could in part be replicated in analogous datasets from U937 and CD34+ cells lends some credence to this notion.

Ideally, all of the datasets should be obtained from the same cell clone and under identical laboratory conditions. In this study we have integrated datasets produced by two separate laboratories, with subtly different cross-linking, immunoprecipitation and sequencing protocols. However, given that the quality of the datasets is similar, this is unlikely to detract from the validity of our analyses. All of the datasets analysed have a Phred score (an index of sequencing accuracy) of +33, equivalent to a less than 1 in 1000 probability of an incorrect base call (646). Datasets from both sources show a low clonal read depth (i.e. very few reads mapping to each unique position are replicated), suggesting that none of the experiments were over-sequenced and that the libraries were likely generated from high-quality starting material. For all of the K562 datasets, peaks were called with reference to the same input control dataset from ENCODE, eliminating inter-laboratory variation in this respect.

The initial premise for this study stemmed from the striking structural homology present between the SMAD MH2 domain and IRF-associated IAD domain, both of which mediate protein dimerization (609,610). In terms of its structure, however, IRF1 is an anomaly, lacking a C-terminal IAD domain (621). In an ideal experiment, however, IRF3 or IRF7, under conditions of PRR activation or IFNα stimulation respectively, would be preferable targets.

Thus far, we have not validated our ChIP-seq observations by ChIP-PCR at specific loci: this remains a goal for future experiments. Moreover, co-operative binding of SMAD and IRF proteins could be explored by sequential ChIP-PCR at specific candidate loci, for example *RSAD2* and *SSBP3*.

To elucidate whether simultaneous BMP/activin and IFN signalling induces SMAD-IRF heterodimers, SMAD-IRF protein-protein interactions in fixed, permeabilized cells could be assayed by proximity ligation assay. Alternatively, the presence of SMAD-IRF heterodimers could be probed by conventional immunoprecipitation of both nuclear and cytoplasmic lysates.

Chromatin is a dynamic polymer, forming complex higher-order structures. While the linear DNA sequence is of prime importance for the regulation of gene expression, the spatial organization of the genome also influences gene expression (647). Genes are not necessarily regulated by their nearest transcriptional factor binding event: transactivators might interact tens of kilobases away from a transcription start site, but be brought into contact through changes in DNA secondary structure. Enhancers – regions of DNA that recruit transcriptional activators to a promoter, including chromatin remodelling enzymes, transcription factors and components of the RNA Pol II complex – may be encoded upstream, downstream or even within a gene of interest (648).

To validate whether the SMAD1 binding events identified here do indeed regulate antiviral gene expression, the definitive approach would be to ablate their DNA binding motifs, either by site directed mutagenesis or a CRISPR/Cas9 approach. Clearly, for identical sites bound by IRF1 and SMAD1, this approach would not allow the specific contribution of either transcription factor to be dissected.

The data presented in this chapter provide evidence for significant similarity between SMAD1 and IRF1 genomic interactions, particularly in the region of genes encoding key antiviral effector loci, at least in the context of K562 cells. Having established that parallels between BMP/activin and IFN are not restricted to hepatoma-derived cells, we were keen to establish whether the antiviral effects of BMP/activin signalling extend to other viral infection, including those tropic to non-hepatic tissues, a question addressed by chapter 7.

Chapter 7

Investigating the effects of activin and BMP signalling against Hepatitis B Virus, Dengue Virus and Influenza A infection

7.1 Introduction

Chapter seven explores whether activin and BMP proteins exert antiviral effects against Hepatitis B Virus (HBV) and dengue virus (DENV) *in vitro*. In addition, we describe a preliminary study into the role of ALK2/3-linked signalling during murine influenza A (FLUAV) infection. By way of introduction, the virology, experimental modelling and immune responses to these viruses, if they have not been addressed previously, are reviewed.

7.1.1 Hepatitis B Virus (HBV): virology, pathology and immunology

Worldwide, 240 million people are infected with HBV. The virus is responsible for 1 million deaths annually, resulting from hepatic fibrosis, decompensated liver failure and hepatocellular carcinoma secondary to chronic infection (649). While successful prophylactic vaccines are available, chronic HBV infection is exceptionally difficult to cure, with current regimens, including intravenous peg-IFNα and oral nucleoside analogues, blighted by debilitating side effects and the emergence of resistance respectively (650).

HBV, a member of the Hepadnavirus family, is an enveloped DNA virus encoding a relaxed circular (RC) double-stranded DNA genome (649). Entry to host cells is mediated by NTCP, a hepatic Na^+ bile acid symporter, followed by endosomal internalization (651). Following membrane fusion, HBV nucleocapsids are translocated into the nucleus via importin α/β, whereupon the RC DNA genome is converted, predominately by host factors in concert with the viral HBx protein, to covalently closed circular DNA (cccDNA), the substrate for viral mRNA transcription (649). cccDNA remains in the nucleus as an ectopic minichromosome, and is responsible for viral persistence within hepatocytes after clearance of systemic viraemia (652). Latent cccDNA minichromosomes are replication competent, being reactivated by immunosuppression in patients who had previously resolved infection (653). The HBV life cycle is summarized in figure 7.1.

cccDNA is transcribed into four viral mRNAs, encoding the seven main viral proteins: the viral envelope protein, composed of L, M and S subunit; P, the polymerase; C, the capsid protein; HBx, a multifunctional co-factor; and E, a modified capsid protein secreted by infected cells (649).

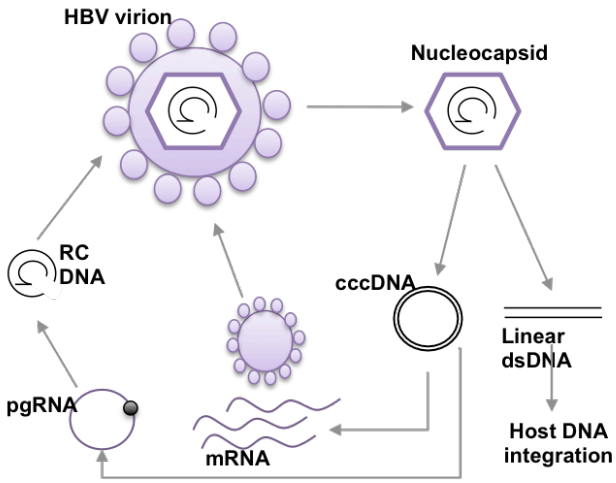


Figure 7.1: The HBV replication cycle

Following internalization, HBV virions shed their external shell, revealing the internal nucleocapsid. Within the host cell nucleus, the relaxed circular DNA (RC DNA) genome is converted to a cccDNA (covalently closed circular DNA) form that acts are a substrate for both viral mRNA synthesis and generation of pregenomic RNA (pgRNA), the precursor of progeny RC DNA genomes. Linear dsDNA molecules are also produced from RC DNA; integration of these linear genomes into the host DNA is not required for HBV replication, but accelerates malignant transformation.

The mRNA encoding the capsid protein also acts as template for reverse transcription of progeny virions, and as such is designated 'pregenomic RNA' (pgRNA). pgRNA undergoes encapsidation within the cytosol and is reverse transcribed to RC DNA within its nucleocapsid shell by the viral polymerase. Intact nucleocapsids are subsequently trafficked to the multivesicular body for assembly of the viral envelope, and mature virions acquire a cholesterol-rich lipid shell before egress (654). Approximately 10% of RC DNA is linearized in the nucleus, and this linear form is capable of integration into the host genome (649,655). Occurring in an estimated 1:10,000 infected hepatocytes, viral integration precedes transformation and development of hepatocellular carcinoma (649). Of relevance to this project, the *SMAD5* locus is recurrent target site for HBV integration (112).

In vivo experimental models are limited to hominid apes and rhesus macaques; animal models of related pathogens include the duck and woodchuck hepatitis viruses. *In vitro*, both primary human hepatocytes and those from the tree shrew *Tupaia belangeri* can sustain HBV replication (656). In terms of transformed cell lines, NTCP transfection renders Huh7 and HepG2 hepatoma-derived cells permissive to infection, whereas the HepaRG line is naturally susceptible to infection and can sustain low-level HBV replication (649,657). In culture, HepaRG cells demonstrate dual hepatocellular and biliary morphology and can successfully propagate HBV when differentiated in the presence of DMSO and corticosteroids (658).

Insights into the contribution of the innate response to HBV control have been hampered by its profound disruption of the type I IFN response. Analysis of the liver transcriptome in acutely infected chimpanzees does not reveal any change in gene expression associated with its entry and expansion (659). *In vitro,* however, strong HBV replication is correlated with robust induction of type I IFN, at least in HepaRG cells transduced with a baculovirus-HBV construct (657). Amongst diverse mechanisms for IFN repression, the HBV polymerase suppresses IRF3 activation downstream of TBK1/IKKε, whereas ectopic overexpression of HbX directly antagonizes MAVS signalling (660,661).

In terms of PRR activation, a recent study reports that RIG-I not only detects the 5'ppp of HBV pgRNA, but also directly represses pgRNA replication by antagonizing its association with the viral polymerase (662). In the same study, type III IFNs were induced by HBV infection in a panel of hepatoma-derived cell lines and primary hepatocytes, but not IFNα or IFNβ. Similarly, in immunodeficient uPA/SCID mice supporting human liver xenografts, HBV infection does not induce type I IFN expression. However, IFNλ subtypes are upregulated, in addition to mRNA encoding *RSAD2*, *CXCL10* and *OAS2* (662). The contribution of the cGAS-STING axis to HBV sensing is not defined, although evidence exists for suppression of STING activation by the viral polymerase (663).

Clinically, HBV infection in immunocompetent adults typically results in an acute, self-limiting hepatitis, with spontaneous clearance observed in 95% of infected individuals, contingent upon polyclonal expansion of HBV-specific CD8+ and CD4+ T-lymphocytes, resulting in destruction of infected hepatocytes and induction of a humoral response respectively (649,650). Diagnosis is made on the basis of serologic parameters, including serum S and E protein levels (HBsAg and HBeAg titres respectively) or serum HBV DNA level. HbSAg seroconversion is indicative of recovery or successful immunization; the simultaneous presence of S antigen and antibody in the plasma is rarely observed, except during fulminant hepatitis (649,664).

First-line HBV therapy includes both peg-IFNα and nucleoside/nucleotide analogues including lamivudine, tenofovir and adefovir (664). Directly antiviral nucleic acid analogues target the viral polymerase, inducing premature chain termination and preventing reverse transcription of genomic RC DNA (665). Total eradication of chronic HBV is difficult to achieve therapeutically, with only 1% of patients sustaining viral clearance after cessation of treatment, in part due to the enduring presence of latent cccDNA minichromosomes (649). Novel strategies to combat HBV infection are much sought after. Recombinant human IFNλ is presently in phase II clinical trials; other experimental approaches including therapeutic

DNA vaccines to stimulate endogenous antiviral responses; TLR7 agonists as innate immune adjuvants; and NTCP inhibition with the anti-cholesterol agent ezetimibe (649,666).

Compared to HCV, HBV demonstrates identical tissue tropism, similar pathology and deploys common mechanisms to disrupt the type I IFN response. Given these similarities, counterbalanced by its radically different viral structure and life cycle, HBV is an excellent candidate to explore for an antiviral effect of activin and BMP signalling.

7.1.2 DENV: experimental models and immunology

The basic virology and clinical manifestations of dengue virus are summarized in [section 4.1.5.2]. In terms of *in vitro* models, DENV replication is sustained in Huh7.5 cells (534), although primary human macrophages, typically differentiated from PBMC, are the mainstay of experimental studies.

In vivo, non-human primates have proven useful for the study of vaccine immunogenicity and induction of correlates of protection, but do not recapitulate human DENV pathology (667). Similarly, infection of wildtype mice results in central nervous system sequelae that do not accurately reflect the human disease trajectory. DENV replication is exquisitely sensitive to type I IFN: the virus is effectively cleared even in IRF3/IRF7 knockout mice, which mount attenuated and delayed type I IFN responses to viral infection. In human cells, DENV efficiently disables the type I IFN response, but a number of these inhibitory mechanisms, including direct inhibitory binding of DENV NS5 to STAT2, are not active during murine experimental infections. Consistent with this, IFNAR deficient mice are capable of sustaining DENV replication and mimic key aspects of human disease, including fever, thrombocytopaenia and elevated vascular permeability (668).

In terms of adaptive responses, humoral immunity plays a key role not only in the in the control of DENV infection, but also its pathogenicity. Maternal transfer of antibodies is proposed to protect infants from severe dengue, with the waning of this protection over the first year of life associated with increasing susceptibility to severe disease (669). Potent neutralizing antibody responses are predominantly directed against epitopes in the viral envelope protein (670). Secondary infection by a heterotypic DENV strain is associated with worse disease, predominately due to antibody dependent cellular cytotoxicity (671). T-cell responses during severe dengue infection are broad, but tend to be associated with higher pro-inflammatory cytokine release as opposed to cytotoxicity (670). Currently, no directly acting

DENV antivirals are available. Clinical management focuses on maintaining fluid balance and provision of symptomatic relief (530).

As a Flavivirus with a similar pattern of type I IFN disruption to HCV, DENV is a clear candidate to examine the antiviral properties of activin and BMP signalling. Of especial interest, DENV is not primarily hepatotropic *in vivo*, and therefore represents an interesting candidate for the extension of an antiviral effect to a non-liver virus. At present, a role for activin, BMP or SMAD signalling in the immune response to DENV has not been described.

7.1.3 Influenza A (FLUAV): experimental models and immunity

As summarized in section 4.1.5.3, FLUAV is a negative-sense ssRNA virus responsible for seasonal and pandemic flu infections. In order to assess whether endogenous BMP/activin signalling exerts an antiviral role *in vivo*, we selected mouse FLUAV infection as model, partly due to its availability, but also due to the well-established role of the innate immune response, including type I IFN, in the restriction of viral replication.

Mice are susceptible to flu infection, although the virus is not propagated by aerosol through laboratory colonies. Ferrets represent popular model for viral transmission; infected animals show similar signs to human patients and high titres of virus can be recovered from the lung. Despite this, mice are the most commonly used experimental model, due to their inexpensive husbandry, amenability to transgenic modification and obvious pathology (672).

Viruses used in murine infection models are typically mouse-adapted by consecutive propagation through multiple mice; this serial passage is associated with characteristic changes in the antigenic composition of the viral haemagglutinin (28). Mouse-adapted strains attach more efficiently to the α-2, 3-linked sialic acid residues that predominate in the mouse respiratory tract (674). The human H1N1 isolate PR/8/34 is one of the most commonly used lab-adapted viruses, and is available in multiple strains exhibiting a range of LD_{50} values in C57BL/6 mice (672).

During the initial stages of intranasal infection, mice develop anorexia, hypothermia and weight loss. Late-stage respiratory pathology includes pulmonary oedema, leukocytic infiltrates and alveolar destruction; unlike human disease, this damage is concentrated in the lower respiratory tract, the main site of viral replication in the mouse. Disease progression and viral pathogenicity is typically tracked by weight loss (672,675).

In response to influenza A infection, CD4+ T helper cells promote differentiation of immature B cells into both FLUAV-specific plasmablasts, responsible for high-level secretion of neutralizing antibody, and a memory B cell population ready for reactivation in response to secondary exposure to cognate antigen. The humoral response facilitates viral clearance via opsonisation of viral particles, fixing complement and promoting phagocytosis of the resulting immune complexes (676).

B-cell activation primarily occurs in regional lymph nodes or mucosal associated tissues. Activation requires antigen presentation by mDC and co-stimulation by CD4+ T cells responsive to antigens presented by MHC class II on the B-cell surface. This interaction promotes immunoglobulin class switching form IgM to IgG or mucosal-associated IgA isotypes (677). Antibodies are primarily directed against the surface proteins haemagglutinin and neuraminidase. Subsequent interactions with CD4+ follicular helper cells trigger somatic hypermutation and affinity maturation, thereby enhancing antibody specificity. Monoclonal expansion of the specific B-cells generates a short-lived plasmablast population, followed by the emergence of a small subset of plasma cells that endure within both the bone marrow and respiratory mucosa, maintaining longer-term antibody expression (676).

While a humoral response is regarded as the best correlate of protection (678), both in the context of vaccine development and recovery from infection, a key role remains for cytotoxic CD8+ T cells in the adaptive response to FLUAV (679).

Given the rapid rates of antigenic drift observed between seasonal flu strains, cross-protective, or heterosubtypic, responses by CD8+ T-cells are proposed to confer at least partial immunity to newly encountered viral variants (679). In 1983, a seminal study by McMichael and colleagues reported that cytotoxic T-cell responses were inversely correlated with viral shedding in a human experimental infection cohort, even in the absence of strain-specific antibodies (680). Epidemiologic data strongly corroborate these observations, suggesting that prior exposure to FLUAV is sufficient to induce heterosubtypic responses to subsequent infection (681). Similarly, in murine infection models, adoptive transfer of virus-specific CD8+ T cells results in protection from severe pathology, whereas immunodepletion of CD8+ cells in the respiratory tract results in significantly higher replication (679). Exuberant immune responses, including high-level systemic pro-inflammatory cytokine and chemokine expression (the ‘cytokine storm’), however, exacerbate tissue damage and contribute to mortality (682).

PRR sensing of FLUAV is summarized in section 4.1.5.3. Regarding the cellular innate immune response, local release of eicosanoids and inflammatory stimuli by infected epithelia recruits NK cells, resulting in destruction of infected cells. Consistent with this, deletion of the NK cell activating receptor NKp46 results in increased FLUAV lethality *in vivo*, emphasizing the critical contribution of NK cells to virus eradication (683). Additionally, phagocytosis by neutrophils, monocytes and macrophages, both infiltrating and tissue-resident, results in clearance of infected cells and opsonized virions (684).

In terms of type I IFN effector mechanisms, multiple ISGs mediate non-redundant roles in the restriction of FLUAV (539). Mx1 [section 5.1.1] is absent from most inbred laboratory mouse strains, although transgenic Mx1 expression is sufficient to protect mice from both intranasal and intracerebral influenza A challenge (685). The IFITM family is highly protective against FLUAV challenge (581). Experimentally, mice deficient in ISGs as diverse as Isg15, PKR, RNaseL and Trim22 show increased susceptibility to flu infection and worse pathology (539).

Evidence exists for distinct contributions of type I and type III IFN to the restriction of influenza A replication. Although both IFNα and IFNλ drive identical IRF3/IRF7-dependent amplification loops in the respiratory epithelium (686), they are posited to induce distinct ISG effector repertoires (687). Airway epithelia are responsive to IFNλ, both *in vitro* and *in vivo* (688). IFNλ is also induced in response to flu infection *in vivo* (43).

In *Mx1*-transgenic mice deficient for IFNAR, recombinant IFNλ3 is sufficient to induce Mx1 expression and enhance protection against FLUAV challenge. While IFNLR deficient mice are only slightly more vulnerable to flu infection than their wildtype counterparts, combined deficiency of IFNAR and IFNLR radically increases their susceptibility, with mice developing severe pneumonia in response to a normally non-pathogenic, NS1-deficient virus (687).

Type I IFN also mediates crosstalk with the adaptive response. IFNα is reported to enhance the cytotoxic capacity of CD8+ T cells by increasing granzyme B expression (690), whereas mice expressing hypomorphic STAT1 demonstrate aberrant polarization towards a Th2 phenotype, resulting in suboptimal IgG response and preference expression of the allergy-associated IgE isotype (689).

The effect of recombinant BMP and activin cytokine on influenza A replication and pathogenesis have not, to the best of our knowledge, been described. Clinically, Linko and colleagues report elevated serum levels of activin A, activin B and the soluble antagonist

follistatin in patients hospitalized by H1N1 infection, although their expression level did not correlate with disease severity or therapeutic outcomes (106).

TGFβ1-3, the prototypic members of the TGFβ cytokine superfamily, have been examined for an antiviral effect during flu infection. *In vitro,* purified flu neuraminidase is able to activate latent forms of TGFβ by modulating its glycosylation patterns (691). *In vivo*, expression of active TGFβ via an adenoviral vector is associated with reduced weight loss and increased survival in mice challenged with H5N1 FLUAV strains. In the same study, TGFβ immunodepletion exacerbates weight loss in response to H1N1 infection and results in higher viral titres in the lung (691). Conversely, while other studies concur that exogenous TGFβ expression can mitigate inflammation; some have failed to replicate an inhibitory effect on viral replication (692).

7.1.4 Aims and summary

This chapter presents preliminary data from efforts to determine whether activin and BMP cytokines exert antiviral effects against HBV and DENV infection *in vitro*.

Data are also presented from a preliminary experiment to determine whether pharmacologic inhibition of the ALK2/3-linked type I BMP receptor affects the course of both FLUAV infection in mice and the kinetics of ISG induction during *in vivo* infection. Based on our *in vitro* evidence suggesting that co-incubation with BMP6 and activin proteins enhances ISG induction by both IFNα and IFNλ, and epidemiologic evidence suggesting that polymorphisms in the BMP signalling pathway can affect outcomes of other viral infections, we hypothesized that inhibition of endogenous BMP-SMAD signalling would exacerbate pathology, enhance viral replication and impair ISG induction.

The key questions addressed were:

1) Do activin A and BMP6 restrict HBV replication *in vitro*?
2) Do activin A, activin B and BMP6 modulate DENV replication *in vitro*, either in isolation or in the presence of exogenous type I IFN?
3) Does treatment of mice with LDN-193189 affect weight loss, viral replication and ISG induction after infection with a lethal dose of FLUAV PR/8/34?

7.2 Materials and methods

7.2.1 HBV infection

HepaRG cells, a HCV-negative hepatoma-derived line exhibiting both hepatocellular and biliary morphologies *in vitro*, were plated in collagen-coated 24-well plates at a density of $5x10^4$cells/well. Cells were allowed to grow in medium for two weeks, before addition of differentiation medium containing 2% (v/v) DMSO and EGF. Cells were cultured for a further two weeks, before infection with a fixed inoculum of HBV [1.5-2.0 x 10^6 genome equivalents per well; corresponding to approximately 10 genome equivalents per cell].

HBV particles were produced and harvested from HepG2 (clone 2.2.15) hepatoblastoma cells as described by Sells et al. (693). Infection continued for 17-20 h at 37 °C, in the presence of 4% (v/v) PEG 8000. Following infection, cells were washed in medium and cultured for seven days in the presence of 2% (v/v) DMSO, 5 µg/mL insulin and 50 mM hydrocortisone. Cells were concurrently incubated with 25 µM lamivudine (Sigma Aldrich), 100 U/mL IFNα (Peprotech) or activin A at 10 µM or 20 µM (R&D Systems).

At day 7 post-infection, culture supernatants were harvested and assayed for the presence of HBsAg with the MONOLISA™ Ultra HBsAg kit [catalogue I.D. 74326] (BioRad, Hercules, CA), in accordance with the manufacturer's instructions.

For the measurement of intracellular RC and cccDNA, DNA was extracted from the HepaRG cells at seven-days post-infection with the PureLink RNA/DNA Viral Mini Kit [Invitrogen], followed by quantification of copy number by RT-qPCR with the following primers:

HBV FORWARD (nucleotide 2259 to 2278):

5'- GGTCTCTTTCGGAGTGTGGA -3'

HBV REV. (nucleotide 2318 to 2299):

5'- ATAGGGGCATTTGGTGGTCT -3'

Infection and analyses were performed by Narayan Ramamurthy, Klenerman Lab, Peter Medawar Building for Pathogen Research, University of Oxford.

7.2.2 DENV infection

Huh7.5.1 cells were seeded in 12-well plates, $3x10^5$ cells per well, followed by 24 h incubation at 37 °C, in the presence of 54 nM recombinant human BMP6, activin A or activin B (all R&D Systems). All conditions were conducted in triplicate.

Cells were washed twice with PBS and infected with DENV2 16681 at MOI 0.1 in fresh serum-free DMEM for 2 h, followed by replenishment with DMEM10 [see section 2.1.1] containing 54 nM BMP6, activin A and activin B.

At 48 h post-infection, % DENV infection was measured by immunofluorescence in a representative well from each condition, and supernatants were harvested for quantification of infectious DENV particles by plaque assay. Plaque assays were conducted in LLC-MK2 cells (a transformed Rhesus monkey kidney line) exposed to experimental supernatants at 10^{-1}, 10^{2}, 10^{-3} and 10^{-4} serial dilutions, with supernatants from DENV-infected macrophages harvested from three healthy donors acting as positive controls. Following addition of an agarose overlay, cells were incubated for 5 days before staining with neutral red and manual counting of plaques.

After extraction of total intracellular RNA, cDNA synthesis as described by section 2.2, target gene expression was quantified by RT-qPCR: host genes by TaqMan Assay [section 2.2.1] and DENV2 NS5 RNA by SYBR Green [section 2.2.2].

Primer sequences used for amplification of positive-sense DENV RNA were obtained from the Zitzmann Lab, University of Oxford:

RT-qPCR of DENV2 16681 NS5 3' Region

ACAAGTCGAACAACCTGGTCCATACATGCTAAACATGAATGGATGACAACGGAAGACATGCT
GACAGTCTGGAACAGGGTGTGGATTCAAGAAAACCCATGGATGGAAGACAAAACTCCAGTGG
AATCATGGGAGGAAATCCCATACTTGGGGAAAAGAGAAGACCAATGGTGCGGC

NS5 3' FOR.: 5'-ACAAGTCGAACAACCTGGTCCAT-3'
NS5 3' REV.: 5'-GCCGCACCATTGGTCTTCTC-3'

DENV infection, immunofluorescence assay, plaque assay and RNA extraction were performed by Jo Miller, Zitzmann Lab, Department of Biochemistry, University of Oxford.

7.2.3 Influenza A infection/LDN-193189 co-administration

8-10 week old female C57BL/6 mice were administered 3.5 mg/kg LDN-193189 (Axon Medchem) or vehicle (serum-free DMEM) by i.p. infection. 30 minutes after injection, mice were infected i.n. with $5x10^4$ pfu influenza A PR/8/34 Mount Sinai strain or mock (PBS). Mice were administered LDN-193189 at 3.5 mg/kg twice daily (08.00 and 17.30), before sacrifice by asphyxiation at 48 h.p.i.

After sacrifice, whole lungs were removed and snap-frozen in liquid N_2. 1 mL Tri Reagent (Sigma-Aldrich) was added to each lung, before lysis with glass beads [cat. I.D. G8772] (Sigma-Aldrich) in a FastPrep Cell Disrupter. RNA was extracted from the lungs with lysates with phenol-chloroform followed by isopropanol precipitation, based on the protocol devised by Chomczynski and Sacchi (694). RNA isolates were further purified, and depleted for genomic DNA, by secondary extraction using the RNeasy Plus kit (Qiagen), in accordance with the manufacturer's instructions. cDNA synthesis and RT-qPCR analysis of gene expression were conducted as described in section 2.2.

For analysis of hepatic gene expression during flu infection, liver explants (~$2mm^3$) were preserved in RNAlater (Qiagen), before mechanical lysis with a TissueRuptor and RNA extraction, cDNA synthesis and RT-qPCR quantification of gene expression as described in section 2.2.

Flu M RNA was quantified by SYBR Green I RT-qPCR, using the primer pairs described by Shin and colleagues(695). Beta-actin was quantified with the following primer sequences, designed by Pei Jin Lim:

F: 5′-AAGGAGCTGCAAAGAAGCTG-3′

R: 5′-GCTGTGGCGTCCTATAAAACC-3′

7.3 Results

7.3.1 Activin A and BMP6 are antiviral against HBV in vitro

HBsAg titre, an index of viral replication, is significantly reduced at seven days post-incubation with 25 μM lamivudine or 1000 U/mL recombinant human IFNα. Lamivudine competes with dCTP for occupation of the HBV polymerase, acting as chain terminator to

inhibit viral replication (696). Similarly, incubation with both 10 nM and 20 nM activin A results in a profound and statistically significant reduction in HBsAg [figure 7.2].

In terms of genomic replication, a trend towards reduction in intracellular RC DNA copy number by both 10 nM and 20 nM activin A is evident, although neither this, nor a reduction in the presence of lamivudine, achieved statistical significance [figure 7.2].

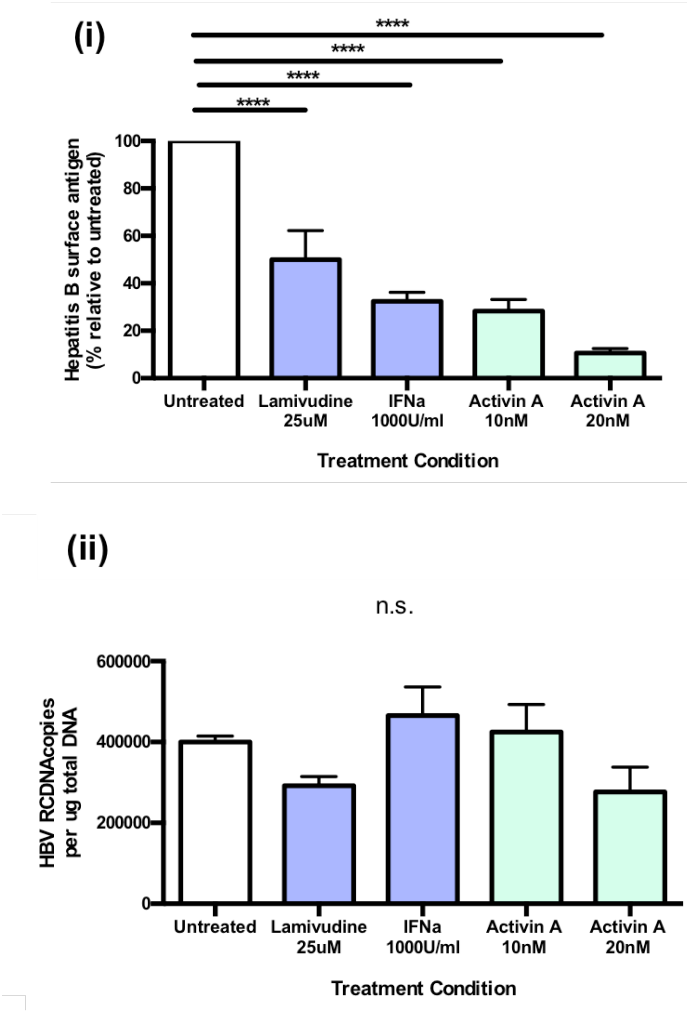


Figure 7.2: Activin A exerts antiviral effects against HBV *in vitro*

HepaRG cells were infected with a fixed inoculum of HBV and incubated for 7 days in the presence of lamivudine 25 μM, IFNα 1000 U/mL or two concentrations of activin A. At the endpoint, supernatants were assayed by ELISA for Hepatitis B surface antigen (HBsAg) (i) and intracellular HBV relaxed circular (RC) DNA.

Activin A 10nM and 20nM both potently decrease HBsAg relative to untreated cells, similarly to the antiviral effects of lamivudine and IFNα. With regard to RC DNA, both lamivudine and activin A 20nM elicit small but statistically non-significant reductions relative to untreated cells.

In (i) for untreated n=5, lamivudine n=4, IFNα n=5, activin A 10 nM n = 5, activin A 20 nM =1 independent experiments; each experiment in biological triplicate; mean + SEM.; analysis by ordinary one-way ANOVA and Bonferroni's post-rest with respect to the untreated condition. In (ii), for all conditions, n =1 experiment in biological triplicate; mean + SEM presented; statistical analysis precluded due to sample size.

Mirroring the effects of activin A, incubation with recombinant BMP6 also elicits a statistically significant, dose-dependent reduction in HBsAg detected in culture supernatants [figure 7.3].

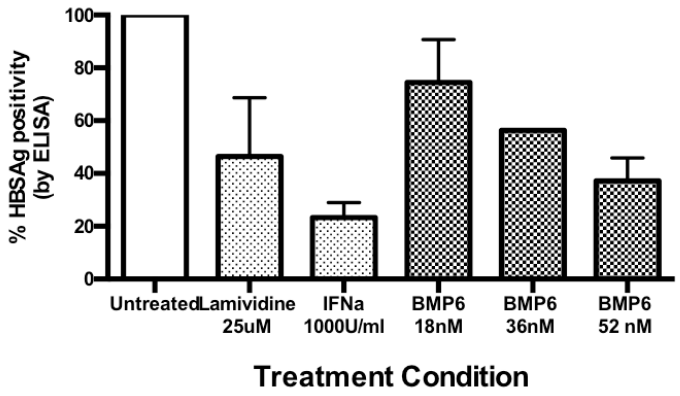


Figure 7.3: BMP6 demonstrates a trend towards reducing HBV replication *in vitro*

HepaRG cells were infected with a fixed inoculum of HBV and incubated for seven days in the presence of lamivudine 25 μM, recombinant human IFNα 1000U/mL or recombinant human BMP6 at 18 nM, 36 nM or 52 nM. At the endpoint, supernatants were assayed by ELISA for Hepatitis B surface antigen (HBsAg).

Both lamivudine and IFNα elicit marked reductions in HBsAg at seven days post-incubation. Incubation with BMP6 also results in a dose-dependent decrement in HBsAg, reaching a maximal reduction to 40% of the untreated value following exposure to 52 nM BMP6.

n=2 independent experiments in biological triplicate; mean + SEM presented; statistical analysis precluded due to small sample size.

7.3.2 Investigating an antiviral role for activin A during DENV infection

Unlike HCV, *in vitro* DENV infection results in upregulation of *HAMP* mRNA. Akin to HCV, however, transcription of inhibitory *SMAD6* and *SMAD7* is significantly induced by DENV infection, in addition to *TNFα* [figure 7.4]. While we were unable to validate whether virus-induced TNFα is responsible for the upregulation of *SMAD6* and *SMAD7*, as has been established for HCV, these findings parallel those previously observed in HCV infection *in vitro* [section 3.1.1].

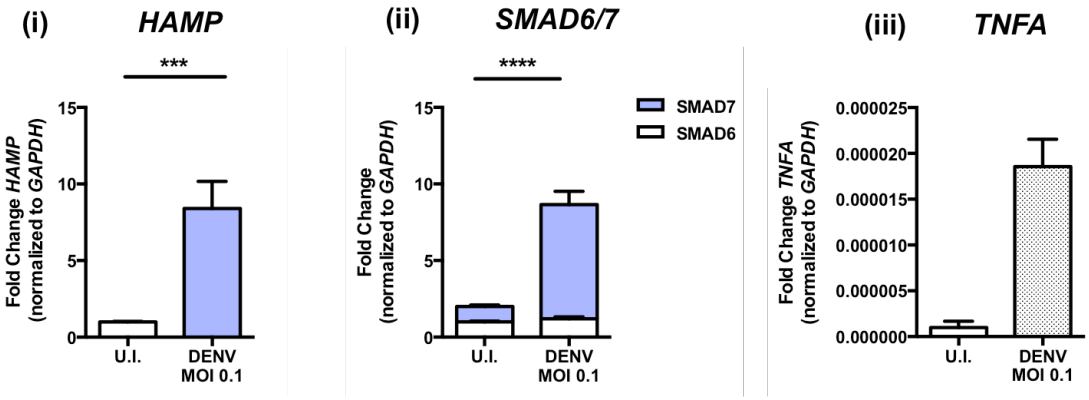


Figure 7.4: DENV infection of Huh7.5 .1 cells elicits upregulation of message encoding hepcidin, SMAD7 and TNFα.

Huh7.5.1 cells were infected with DENV MOI 0.1 and RNA extracted at 48 h post-infection, followed by RT-qPCR quantification of transcript encoding *HAMP* (i), *SMAD6/7* (ii) and *TNFA* (iii). Data is presented as fold change compared to uninfected cells. *HAMP* transcript is significantly increased in DENV-infected versus uninfected cells. Similarly, *SMAD7* is significantly induced upon DENV-infection, whereas *SMAD6* transcript is not changed. A strong trend towards *TNFA* induction upon DENV-infection is also evident.

For *HAMP,* n=4, for *SMAD6/7*, n=3, for *TNFA*, n=2; mean+SEM; analysis by unpaired two-tailed t-test

Based on the results of a plaque assay, activin A, activin B and BMP6 do not exert a significant antiviral effect against DENV *in vitro* [figure 7.5]. Viral titre in supernatants from the untreated condition approximated 2.9 x10^4 pfu/mL. While incubation with all proteins results in an approximately 40% reduction in plaque numbers compared to the untreated control condition, the iminosugar antiviral NB-DNJ reduced numbers to less than the limit of detection (corresponding to a viral titre of < 33 pfu/mL). Given this very modest antiviral effect of the recombinant proteins in isolation, it was decided, based on our observations in HCV infection, to assess whether activin/BMP signalling enhances the antiviral effect of IFNα against DENV.

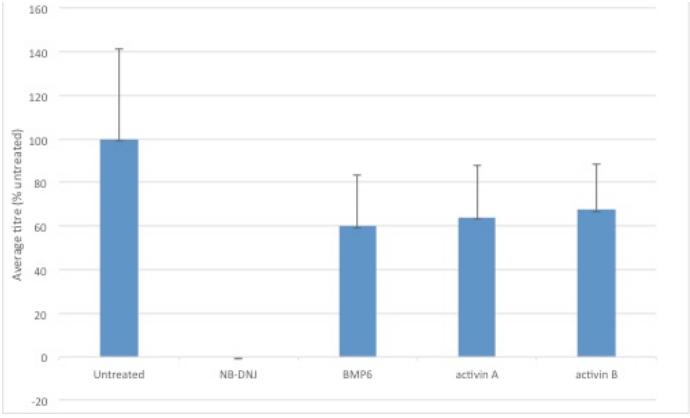


Figure 7.5: Activin A, activin B and BMP6 exert very limited antiviral effects against DENV replication in Huh7.5.1 cells

Huh7.5.1 cells infected with DENV MOI 0.1 for 48 h, preceded and proceeded by incubation with 54 nM recombinant human BMP6, activin A or activin B, or the iminosugar antiviral NB-DNJ at 30 μM. Supernatants from infected cells were analyzed for the presence of infectious virus by plaque assay in MDCK cells. While NB-DNJ resulted in viral titres below the limit of detection, all recombinant proteins exerted a more modest effect, eliciting an approximately 40% reduction in plaque formation.

n=1; all conditions in biological triplicate, each assayed in triplicate wells.

In DENV-infected Huh7.5.1 cells, recombinant IFNα dose-dependently reduces intracellular DENV genomic RNA, quantified by RT-qPCR, and viral replication, measured by plaque assay [figure 7.6]. Consistent with this antiviral effect, treatment with IFNα also dose-dependently upregulated transcription of the ISGs *MX1* and *ISG15*.

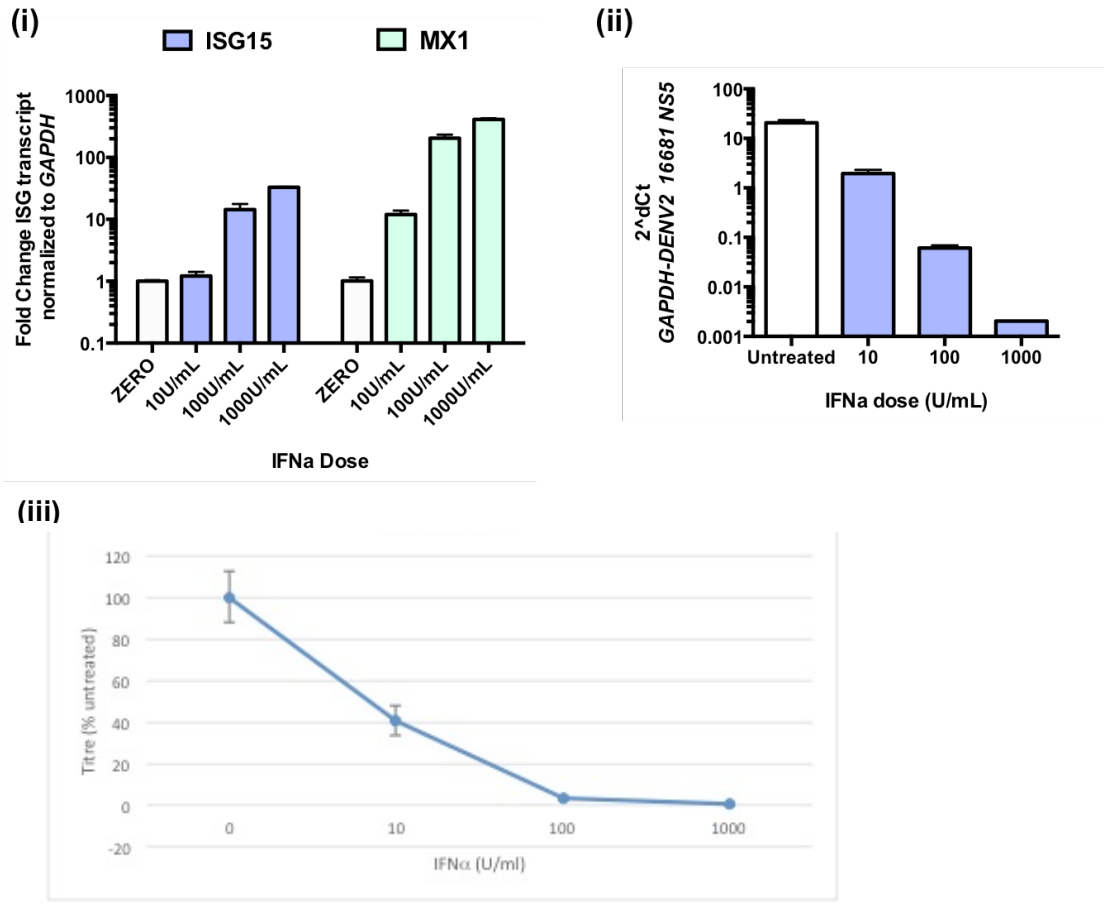


Figure 7.6: Recombinant human IFNα is strongly antiviral against DENV infection of Huh7.5.1 cells

Huh7.5.1 cells were infected with DENV MOI 0.1 for 48h in the presence of titrating doses of recombinant human IFNα, followed by RNA extraction and RT-qPCR quantification of mRNA encoding *ISG15* and *MX1* (i) and positive-sense DENV NS5 RNA (ii). Supernatants from infected cells were examined for the presence of infectious virus by plaque assay (iii).

IFNα dose-dependently induces both *ISG15* and *MX1* in this model, with a concomitant reduction in both DENV NS5 RNA and titres of replication competent virus.

n=1 experiment; biological singlicate; mean+SEM; statistical analysis precluded due to small sample size. (iii) conducted in technical triplicate.

Having established that IFNα is antiviral in the Huh7.5.1 DENV infection model, the possibility of synergistic enhancement by activin A, akin to that observed for HCV infection, was investigated. Due to the protracted optimization of the protocol, only a single replicate of the experiment could be conducted.

As illustrated by figure 7.7, while neither recombinant BMP6 and activin A at 54 nM, nor the iminosugar compound NB-DNJ at 5 μM, were antiviral in isolation, co-incubation with 54 nM activin A enhanced the reduction in DENV genomic RNA by 10 U/mL IFNα.

However, due to the very potent inhibitory effects of IFNα in this experiment, it is not possible to determine by plaque assay whether activin A enhances its inhibition of viral replication. In this experiment, co-incubation with BMP6 or activin A enhanced both MX1 and ISG15 expression by IFNα, of the order 250-fold and 40-fold respectively. By contrast, NB-DNJ did not modulate ISG induction by IFNα [figure 7.7].

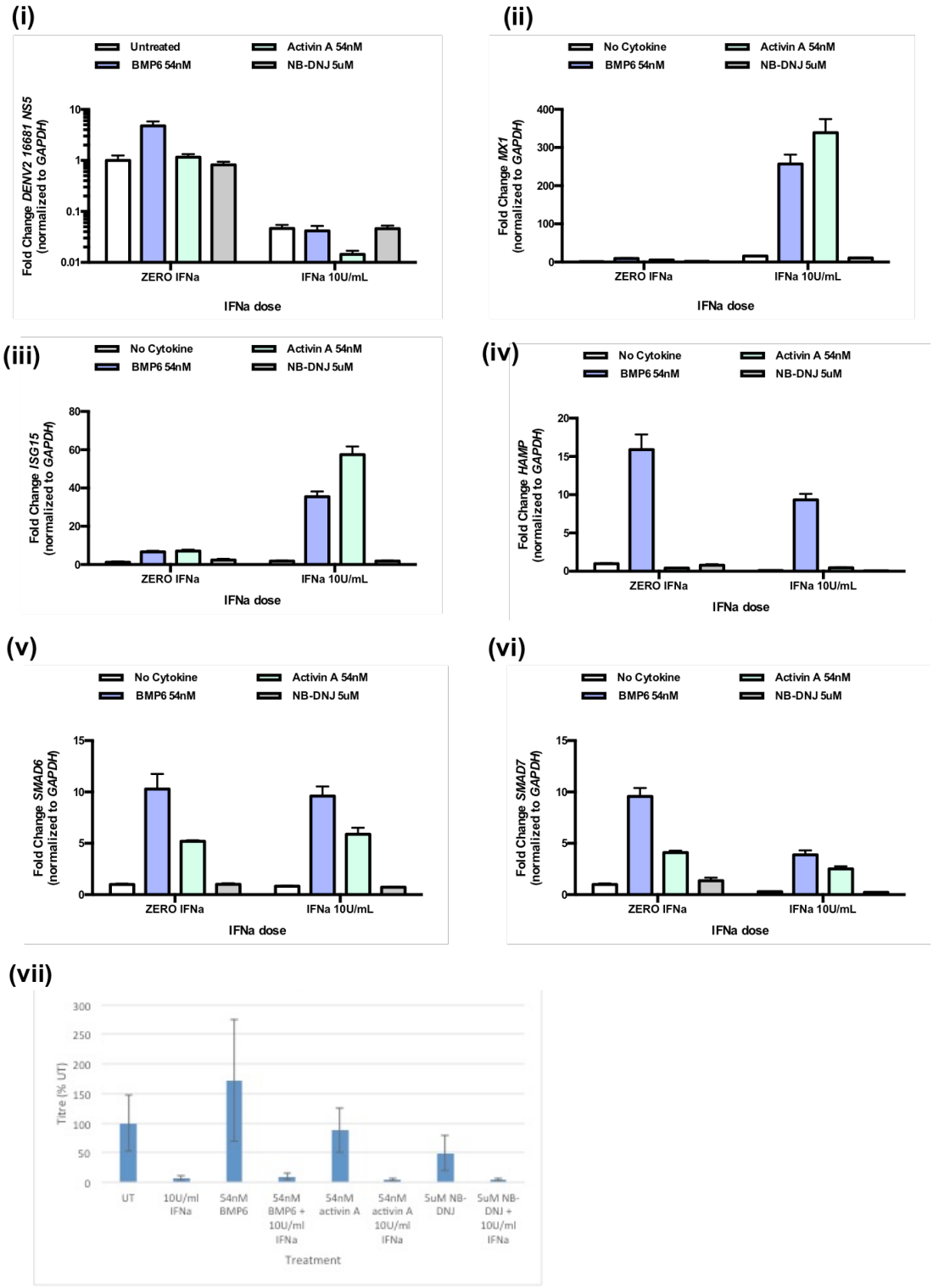


Figure 7.7: Activin A enhances the antiviral effect of IFNα against DENV genome replication in Huh7.5.1 cells at 48 h.p.i.

Huh7.5.1 cells were infected with DENV MOI 0.1 and incubated with BMP6 54 nM, activin A 54 nM or the iminosugar DENV antiviral drug NB-DNJ at 5 μM, in the presence or absence of IFNα 10 U/mL. At 48 h post-infection, RNA was extracted and positive sense DENV NS5 RNA (i), *MX1* (ii), *ISG15* (iii), *HAMP* (iv), *SMAD6* (v) and *SMAD7* (vi) quantified by RT-qPCR. Replicating virus in culture supernatants was measured y plaque assay (vii).

Whilst none of BMP6, activin A nor NB-DNJ elicited an antiviral effect alone, co-incubation with activin A markedly reduced DENV RNA levels in the presence of IFNα. However, this 3-fold reduction in viral RNA was not recapitulated by plaque assay (vii). As observed previously, co-incubation with both BMP6 and activin A enhanced transcriptional induction of the ISGs *MX1* and *ISG15*. As positive controls for bioactivity of BMP6 and activin A, BMP6 alone induced *HAMP*, *SMAD6* and *SMAD7* expression; incubation with activin A alone upregulated both *SMAD6* and *SMAD7*.

n=1 in biological triplicate; mean+SEM; statistical analysis precluded due to small sample size. (vii) conducted in technical triplicate

Interestingly, induction of *HAMP*, *SMAD6* and *SMAD7* mRNA by both BMP6 and activin A is reduced in the presence of IFNα; while this is a single experiment, these observations reflect the trend revealed by chapter 6's bioinformatic analyses, namely that SMAD-linked signalling may potentiate that of IRFs, but not vice versa.

7.3.3 Investigating the effects of LDN-193189 during murine influenza A infection

In part as HCV is tropic only to humans and chimpanzees, murine models of HCV infection are onerous, costly and poorly representative of human pathophysiology. In order to assess whether endogenous BMP/activin signalling exerts an antiviral role *in vivo*, we had recourse to a well-established, more tractable mouse infection model, namely influenza A.

As described in section 7.2.1, mice were administered LDN-193189 i.p. immediately before i.n. infection with a lethal dose of FLUAV PR/8 or mock, with twice-daily LDN-193189 injections, before sacrifice at 48 h post-infection.

As demonstrated by figure 7.8, unlike uninfected animals, flu-infected mice demonstrate significant weight loss during the course of the experiment. However, there is no significant difference between LDN-183189-treated and untreated mice.

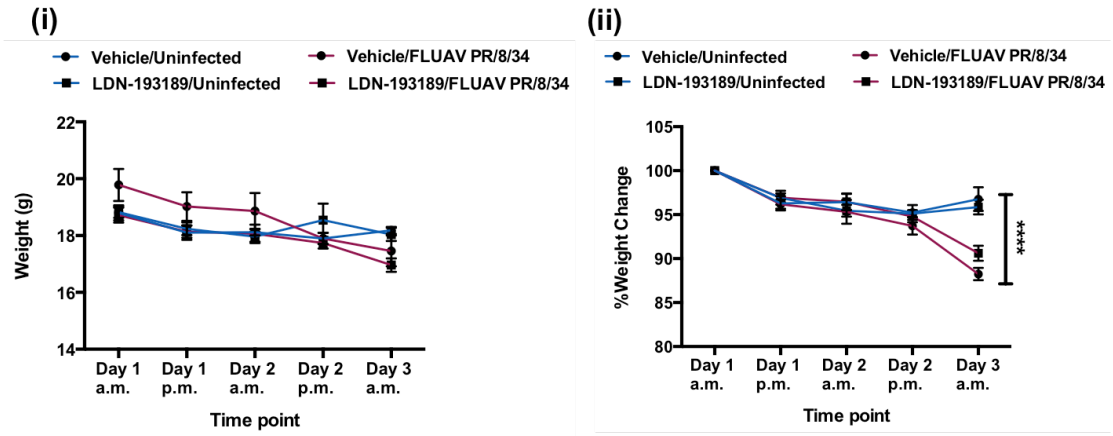


Figure 7.8: Intraperitoneal administration of the type I BMP receptor inhibitor LDN-193189 has no effect on weight loss in a murine model of FLUAV PR/8 infection.

9-10 week old C57BL/6 mice were inoculated i.n. with $5x10^4$ pfu FLUAV PR/8 or medium, in the presence or absence of the type I BMP receptor inhibitor LDN-193189. Mice were weighed twice daily and sacrificed 48 h post-infection. Their weights during the course of infection are displayed as absolute values (i) and as percentage change relative to their starting weight (ii).

By the final time-point, both LDN-193189 and vehicle-treated infected mice has lost a significant percentage of their body mass relative to the uninfected groups. No difference was observed between LDN-193189 and vehicle-treated mice under either infection condition.

n=5 mice per group; mean+SEM; analysis by two-way ANOVA and Bonferroni's multiple comparisons test between all groups

In the liver, expression of *Hamp1*, encoding hepcidin, was significantly increased by infection, consistent with its role as an acute phase regulatory cytokine, and was significantly repressed by treatment with LDN-193189, in line with the major contribution of the BMP-SMAD axis to its homeostatic regulation [figure 7.9]. This observation validates that LDN-193189 exerted biological activity in this model.

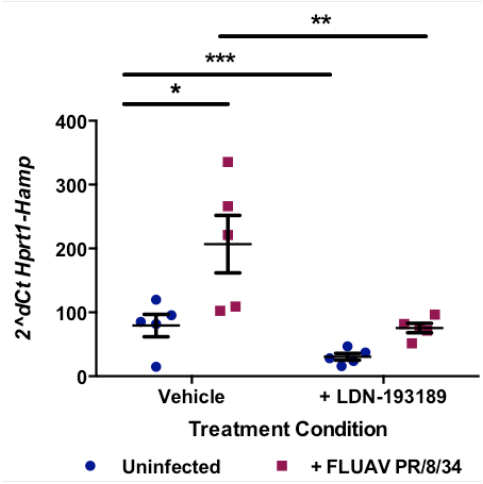


Figure 7.9: LDN-193189 is pharmacologically active in the liver of FLUAV infected mice at 48 h.p.i.

Livers were harvested at 48 h post-infection from 9-10 week old female C57BL/6 mice infected i.n. with $5x10^4$ pfu FLUAV PR/8/34. Mice were administered the type I BMP receptor inhibitor LDN-193189 or vehicle control by i.p. injection twice-daily. RNA extracts were analyzed by RT-qPCR for mRNA encoding hepcidin (*Hamp*). Data is presented as 2^ΔCt values relative to *Hprt*.

Liver *Hamp* mRNA is significantly induced by FLUAV infection, as anticipated as an acute phase marker, and is significantly suppressed by LDN-193189 administration in both infected and uninfected mice.

n=5 mice per group; mean+SEM; analysis by two-way ANOVA and Bonferroni's multiple comparisons test

Extensive efforts to measure replicating virus in lung lysates by TC ID_{50} assay were undertaken, using both haemagglutination assays and NP staining as end-points, but none were technically successful. RT-qPCR quantification of viral genomic RNA is suboptimal assay, as it does not discriminate between genomic RNA from replication-competent and dead virions. Nevertheless, no difference in genomic RNA encoding the M protein was detected in lung lysates from LDN-193189 treated and untreated mice [figure 7.10].

In terms of ISG expression, mRNA encoding *Trim14, Usp18* and *Ifi44* were significantly increased in the lungs of infected mice compared to uninfected animals, although no significant differences in upregulation were observed in the presence of LDN-193189. By contrast, induction of *Ifnα4* by FLUAV was significantly higher in the lungs of LDN-193189 treated mice, compared to vehicle-treated animals. *Ifnb1* expression, while significantly increased by flu-infection, is not differentially upregulated by LDN-193189 [figure 7.10].

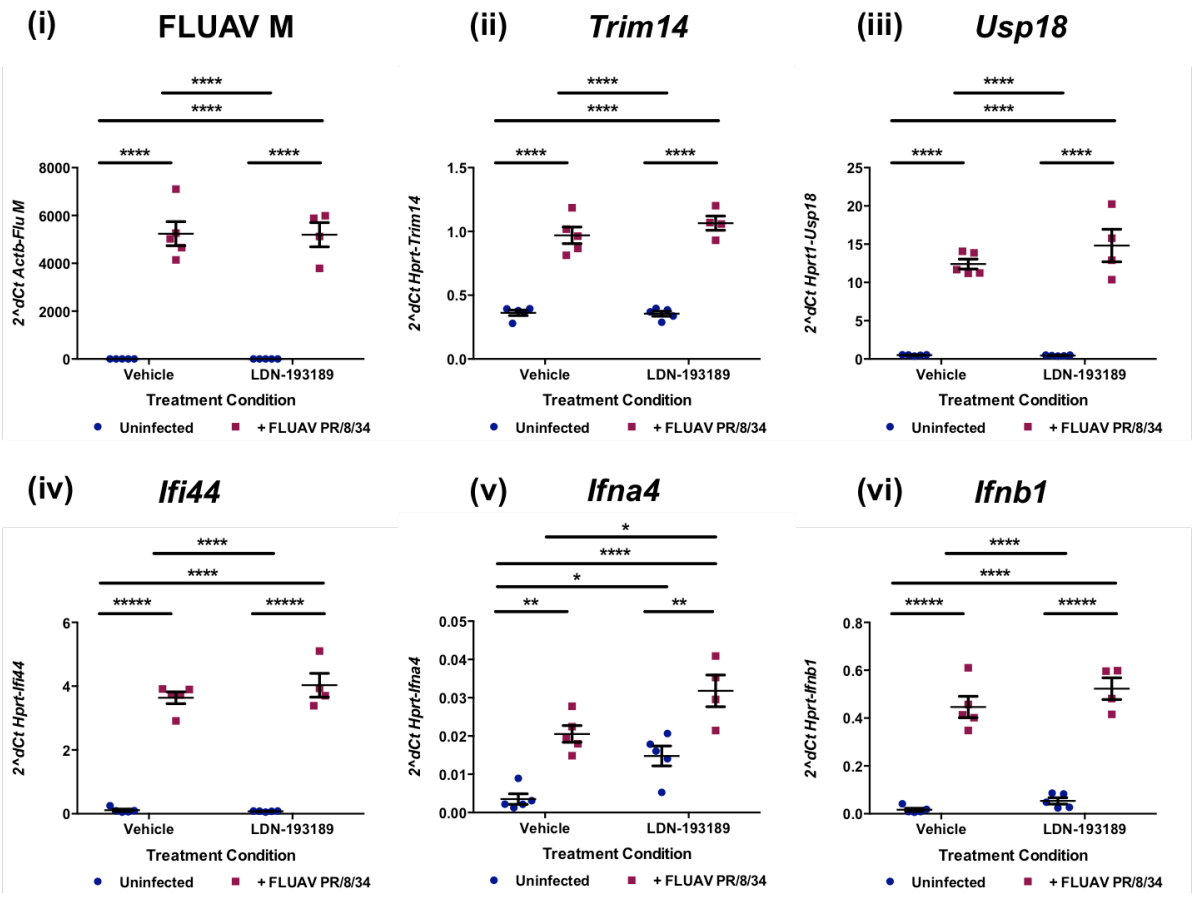


Figure 7.10: Pharmacological blockade of the type I BMP receptor with LDN-193189 has no effect on levels of FLUAV M RNA detected in the lungs of infected mice

Lungs were harvested at 48 h post-infection from 9-10 week old female C57BL/6 mice infected i.n. with $5x10^4$ pfu FLUAV PR/8/34. Mice were administered the type I BMP receptor inhibitor LDN-193189 or vehicle control by i.p. injection twice-daily. RNA extracts were analyzed by RT-qPCR for RNA encoding the Flu M gene (i), *Trim14* (ii), *Usp18* (iii), *Ifi44* (iv), *Ifna4* (v) and *Ifnb1* (vi). Data is presented as 2^ΔCt values relative to *Actb* or *Hprt*.

RNA encoding Flu M is detectable following infection, but there is no difference in level between LDN-193189 and control-treated mice. The ISGs *Trim14, Usp18* and *Ifi44* are significantly upregulated by FLUAV infection, but there are no significant differences between the magnitude of induction in LDN-193189 and vehicle-treated groups. Levels of transcript encoding *Ifna4* and *Ifnb1* are also increased upon infection, with significantly higher *Ifna4* induction in LDN-193189 treated mice.

n=5 mice per group; mean+SEM; analysis by two-way ANOVA and Bonferroni's multiple comparisons test between all groups

7.4 Summary and discussion

This chapter presents the results of multiple experiments to determine whether activin proteins, or ALK2/3-linked signalling, mediate antiviral effects against HBV, DENV and FLUAV infection. In light of our observations, we initiated a screen of small-molecule activin and BMP agonists, in an initial effort to translate our data pertaining to the antiviral effects of activin and BMP proteins against HCV into novel pharmacological strategies.

7.4.1 HBV infection

Activin A elicited a significant reduction in HBsAg and demonstrated a mild trend towards reduction in RC DNA copy number, consistent with an antiviral effect, albeit in a more limited set of experiments.

HBsAg release is tightly correlated with viral replication, both in experimental infections and clinically (657,697). Subsequent experiments should assess whether the anti-HBV effect of activin A requires intact type I BMP receptor expression, via co-incubation with LDN-193189, or whether it's effects are at least in part type I IFN-dependent, by incubation with the JAK1 inhibitor ruxolitinib or an anti-IFNAR neutralizing antibody.

Subsequent experiments should seek not only to extend upon the preliminary observation that activin A reduces intracellular RC DNA content, but also investigate the effects of activin A upon levels of viral cccDNA. Eradication of cccDNA is exceptionally challenging, and its latency in infected hepatocytes is the basis of HBV persistence(649). Total elimination requires direct destruction of the cccDNA destruction or host cell death. As nucleoside analogues, including lamivudine, do not potently repress cccDNA levels and only partially inhibit its *de novo* synthesis, novel agents capable of cccDNA lytic destruction could offer valuable therapeutic tools.

In addition to its potent immunodulatory functions, a recent study by Lucifora and colleagues suggests that IFNα might also induce direct destruction of cccDNA. In infected primary human hepatocytes, administration of recombinant IFNα strongly induces the cytidine deaminases APOBEC3A and APOBEC3G (698). The ensuing deamination of cccDNA, but not the host genome, results in base damage and excision, thereby rendering the viral DNA vulnerable to enzymatic destruction by cellular endonucleases. Subsequent publications have also described a role for TGFβ1-driven cytidine deaminases activity in the repression of intracellular HBV DNA (699).

Given the evidence presented in this thesis for the enhancement of IFNα's anti-HCV effect [chapter 5] by activins, future studies should investigate whether this synergistic boosting of the type I IFN response is applicable during HBV infection, and, moreover, whether it facilitates enhanced cccDNA degradation in association with cytidine deaminase induction.

7.4.2 DENV infection

In isolation, BMP6, activin A and activin B did not exert strong antiviral effects against DENV infection *in vitro*, despite administration at much higher concentrations than is required for an effect against HBV and HCV. Co-incubation of DENV-infected Huh7.5 cells with activin A and IFNα, however, did result in detection of lower viral RNA levels by RT-qPCR compared to IFNα alone. This enhancement was not evident by plaque assay, an index of replicating virus, but this might be attributable to the technique's low resolution and inability to discriminate a small effect of activin A on the background of IFNα's profound antiviral effect.

To circumvent this limitation, IFNα should be titrated to even lower doses in subsequent co-incubation experiments. In future, DENV replication could also be measured by RT-qPCR for negative sense viral RNA, a technique allowing quantification of replicating virus, similarly to plaque assay, but benefiting from the superior sensitivity of RT-qPCR (700). Moreover, while Huh7.5 cells facilitate DENV genomic replication, they do not represent a physiological infection model. Replication of the infection protocol described here in primary monocyte-derived macrophages may offer an experimental context more appropriate to DENV's *in vivo* tissue tropism.

7.4.3 FLUAV infection

Administration of LDN-193189 did not alter the amount of flu genomic RNA detected in the lungs of infected mice. This result, however, needs to be interpreted in the context of two key factors: firstly, the suitability of virus quantification by RT-qPCR, and secondly, whether LDN-193189 was bioactive in the lung after i.p. administration.

While total flu genomic RNA levels were not altered by LDN-193189, the RT-qPCR assay does not discriminate between genomic RNA from replication-competent and incompetent virions. As such, this result does not eliminate the possibility of a specific effect on the levels of live virus. Multiple efforts were made to titre replicating virus in the lungs of infected mice

by $TCID_{50}$ (50% tissue culture infective dose), a standard virological method. In summary, the $TCID_{50}$ assay is an end-point dilution assay that calculates the threshold amount of virus, in this case from lung lysates, required to elicit cytopathic effects in 50% of infected target cells (701). Despite extensive optimization, and the use of two-outputs to measure virus production in MDCK target cells, namely haemagglutination assay and staining for flu nucleoprotein, we were unable to obtain interpretable results. As such, the specific contribution of ALK2/3 inhibition to control of replicating virus cannot be gauged from this experiment.

In terms of bioactivity, both the ALK2 and ALK3 receptors targeted by LDN-193189 are expressed in the lung. However, were concerned that entry of LDN-193189 into the systemic circulation would be subject to a first-pass effect, in which the drug is first delivered to the liver by hepatic portal vein system and subsequently metabolised. To address this possibility, we compared expression of BMP target genes in the liver and lungs of LDN-193189 treated mice.

In the liver, LDN-193189 demonstrated clear activity: mRNA encoding the BMP-stimulated gene *Hamp1* is significantly reduced by LDN-193189, and the I-SMAD *Smad7* shows a strong trend towards repression by the drug. In the lung, by contrast, LDN-193189 did not repress expression of the BMP target gene *Id1*. Similarly, despite being a well-characterised SMAD1/5-dependent gene – its 5' UTR encodes four GC-rich BRE sequences (702) – *Smad6* mRNA levels in the lung were also not altered by LDN-193189 [data not shown]. Together, these observations are consistent with reduced bioavailability in the lung, possibly due to a first-pass effect.

Published data suggest that LDN-193189 plasma concentration rises rapidly immediately after administration, before a precipitous decrease within 1 h post-administration and slower decline thereafter. In a pharmacokinetic study in C57BL/6 mice, Yu and colleagues report that 8 h after i.p. injection at a dose of 3 mg/kg, plasma drug concentration is of the order 80 nM, almost 5 times higher than their reported IC_{50} for phosphorylation of SMAD1/5/8 *in vitro*. It is difficult to reconcile this report with the findings, albeit limited, observed in our study.

Given the suboptimal pharmacokinetics of LDN-193189 *in vivo*, its multiple reported off-target effects [section 3.5] and ethical constraints on the frequency of i.p. injections, future experiments should consider alternative strategies for *in vivo* ablation of ALK2/3-linked signalling.

As BMP6 is not induced by *in vitro* nor *in vivo* viral infections, *Bmp6 -/-* mice are not appropriate candidates. Germline *Inhba* knockout results in perinatal lethality, although *Inhbb* homozygous null mice are both viable and fertile (703,704). Germline *Inhba* deficiency can be partially compensated for by substitution of an *Inhbb* allele in the *Inhba* coding region: craniofacial development is rescued in these chimeric animals, although they are subfertile and show other developmental abnormalities (705).

To circumvent the perinatal lethality and developmental defects associated with germline knockout, inducible activin A knockout models are available. In this project, we explored the possibility of infecting a pan-tissue, post-natal knockout driven by ubiquitin-Cre. However, as an antiviral effect extends to multiple ALK2/3-linked cytokines [section 3.2.5], any effect seen in the absence of a single cytokine is likely to be equivocal, given the range of (*in vitro*, at least) redundant TGFβ/activin antiviral family members.

An ideal transgenic model would ablate the entire signalling axis: few candidate models, however, are available. Germline *Smad4* knockout embryos fail to gastrulate (706), whereas *Smad1* and *Smad5* homozygous null mice die between E9.5 and E11.5 (59,60). Both ALK2 and ALK3 are required for early embryogenesis (709,710). Similarly, germline knockout of *Bmpr2*, the type II BMP receptor isoform required for ALK2/ALK3 signal transduction, arrests embryonic development at the egg cylinder stage, resulting in death at E9.5 (711). While tissue-specific knockout is theoretically feasible, as we have yet to establish which cell types are responsible for *Inhba* upregulation during flu-infection, this approach is presently sub-optimal.

An alternative approach is the use of transgenic mice overexpressing follistatin, the soluble negative regulator of activin signalling. In addition to activins, follistatin has a strong affinity for multiple ALK2/3-linked BMP molecules, including BMP2, BMP4 and BMP7, and can functionally antagonize their effects *in vitro* (712). Follistatin gain-of-function mutants, generated by expression of a follistatin transgene downstream of a ubiquitous MT-1 promoter, are viable, if subfertile, with abundant follistatin transcript detectable in the lung (713). Further work would initially seek to validate whether recombinant follistatin is sufficient to inhibit the antiviral effect of activin and BMP cytokines *in vitro*, before addressing the effect of its overexpression on viral replication *in vivo*.

In the experiment described here, *Inhba* mRNA in the lung was significantly upregulated by flu infection, despite no change in serum activin A peptide. However, it is probable that

changes in serum activin A peptide and tissue mRNA during infection are decoupled from one another.

Previous reports suggest that serum activin A levels rise precipitously approximately 1 h after exposure to an inflammatory stimulus, rapid induction kinetics that suggest regulation at the post-transcriptional level (552,563). Inflammatory stimuli rapidly mobilize activin A-rich neutrophils from the bone marrow into the systemic circulation (552).

It is possible that an initial surge in serum levels, akin to that seen after LPS administration, occurs during the early stages of infection, but wanes as intracellular reserves of pre-formed protein were exhausted. Our study measured serum activin A at only point of sacrifice, missing any induction at early time-points. Equally, local activin A at the site of infection exert restricted autocrine and paracrine antiviral effects, with low or modest changes in circulating concentration.

To better establish the kinetics of activin A protein expression during flu-infection, sera could be sampled at regular intervals - initially hourly, then with decreasing frequency - from point of infection to sacrifice. Activin A protein in the lung could be measured by quantitative immunohistochemistry in fixed lung sections, both shortly after infection and at sacrifice. Western blotting for activin A and phosphorylated Smad1/5/8 in lung lysates would allow correlation of *Inhba* upregulation with both local protein synthesis and ALK2/3 activation.

In terms of ISG induction, LDN-193189 did not significantly alter the magnitude of *Trim14, Usp18* and *Ifi44* expression in the lungs of infected mice, although it did elicit a statistically significant increase in *Ifna4* expression. *Ifna4* is a first-wave IFNα subtype strongly induced by IRF3 activation. In line with the observations from Xu and colleagues that SMAD3-IRF3 heterodimerization can impair TGFβ signalling (627), it is possible that inhibition of SMAD1/5/8 phosphorylation by LDN-193189 could impair hypothetical associations between these SMADs and IRF3, increasing the capacity for IRF3 homodimer formation and subsequent *Ifna4* induction.

This study did not examine whether adaptive immune responses were modulated by LDN-193189. Of interest, published data suggest that TGFβ-independent activation of SMAD4 is necessary for differentiation of effector memory T cells and their migration to peripheral lymph nodes. Using an OT-I TCR transgenic mouse model, in which mouse T cells are responsive to the ovalbumin (OVA) SIINFEKL peptide, Hu and colleagues measured effector memory T cell distributions 30 days after infection with an X31-OVA H1N1 virus (714).

Before infection, mice were irradiated and the bone marrow reconstituted with a mix of either Smad4 knockout/wildtype bone marrow, or type II TGFβ receptor knockout/wildtype donor cells. In the Smad4 knockout chimeric animals, differentiation of effector memory T cells, and their migration to peripheral lymph nodes, was significantly compromised. TGFβ receptor knockout chimeras, however, were unimpaired. Functionally, recovery from X31-OVA challenge is delayed in Smad4 knockout chimeras (714).

The authors suggest that development of the effector memory phenotype requires TGFβ-independent activation of SMAD4. In light of our observations, this could hypothetically be attributable to activin expression downstream of TLR signalling, resulting in ALK2/3-linked SMAD4 stimulation. T cells reportedly express multiple TLRs, including those shown in this project to trigger activin expression, and TLR activation is associated with development of the effector memory phenotype (715). Future *in vivo* infection studies could address whether administration of LDN-193189, with or without intact TLR function, modulates effector memory T-cell differentiation, thereby addressing whether ALK2/3 activation is the bridge between TLR activation and T cell maturation.

Extensive efforts were also undertaken to establish an *in vitro* model of Theiler's murine encephalomyelitis virus (TMEV) infection against which to test recombinant activin A and B for antiviral effects. Unfortunately, we were unable to optimize this model, and therefore did not assay activin A and B for an anti-TMEV effect.

7.4.4 Screening novel and existing BMP/activin agonists for antiviral effects

A major limitation of recombinant type I IFN therapy is the high incidence of severe adverse effects, including gastrointestinal and neuropsychiatric complaints, due to the near-ubiquitous tissue expression of the type I IFN receptor (716). ALK2 and ALK3, the receptors that we hypothesize to transduce the antiviral effects of BMP and activin proteins, show a much more restricted expression pattern (32). As such, drugs enhancing the BMP-activin-SMAD axis could offer a much more specific tool against viruses tropic to ALK2/3 expressing tissues, such as the liver, with potential for a lower incidence of adverse off-target effects.

While numerous pharmacological antagonists of the type I BMP receptor have been described - most prominently, dorsomorphin, LDN-193189 and DMH1 (62,63,606) - development of small-molecule BMP agonists is considerably less advanced. Despite this, pharmacological enhancement of BMP signalling demonstrates therapeutic potential in a diverse range of human diseases, including bone damage, organ fibrosis and cancer (717).

In the USA, recombinant BMP2 and BMP7 are licensed for the treatment of non-union fractures. In an extensive randomized controlled trial, local administration of BMP2 significantly reduced infection rates and accelerated healing of open tibial fractures (718). BMP14 has demonstrated some promise as an osteoinductive treatment in patients with chronic periodontal disease. In a phase 2a pilot study, local administration of BMP14, in tandem with conventional surgery, accelerated resolution of jawbone damage, with two-fold greater deposition of new bone compared to control subjects receiving surgical intervention only (719).

Recombinant protein therapies, however, are restricted by both high manufacturing costs and clinical challenges. While prolonged administration via an implant is appropriate mode of delivery for a focal orthopaedic lesion, this is wholly inappropriate in the context of systemic diseases or whole-organ pathologies, for example viral infection. As such, organic small-molecule agonists of BMP signalling, preferably orally-bioavailable, are highly sought after.

To begin translating the antiviral phenomena described in this thesis into potential therapeutic strategies, multiple pharmacological agonists of activin and BMP signalling, both novel and FDA-approved, were screened for an anti-HCV effect *in vitro.*

The organic compound tilorone was identified as a novel agonist of BMP signalling during a screen of FDA-approved drugs to identify novel lead compounds for the treatment of idiopathic pulmonary fibrosis (IPF) (720). A chronic disorder with poor prognosis and limited therapeutic options, IPF is associated with elevated expression of the soluble BMP antagonist Gremlin, leading to reduced pulmonary BMP activity and elevated pro-fibrotic TGFβ signalling (721). Patients present with progressive interstitial lung fibrosis and severely compromised respiratory function that is unresponsive to conventional anti-inflammatory medications (722). *In* vitro, Leppäranata and colleagues were able to demonstrate transcriptional upregulation of both *BMP7* and the BMP/SMAD target gene *ID3* by tilorone *in vitro*. In a mouse model of pulmonary fibrosis secondary to silica inhalation, tilorone reduced both deleterious collagen deposition and infiltration of inflammatory cells (720).

Tilorone piqued our interest further by virtue its initial characterization as an orally-tolerated inducer of type I IFN (723). However, whilst tilorone is documented to offer prophylaxis against multiple RNA and DNA viruses in mice, the protection it confers is not necessarily correlated with levels of type I IFN induction, most notably during murine MM virus

infection (724,725). The mechanism of type I IFN induction by tilorone is presently unknown.

In contrast to IFNα, tilorone did not exert antiviral effects in the OR6 HCV replicon model; to the contrary, it appeared to elevate luciferase activity relative to the untreated cells [data not shown]. These observations might plausibly be explained by tilorone stabilizing the Renilla luciferase in an active conformation or inhibiting its degradation. However, it was beyond the scope of our research interests to probe this effect further.

No small-molecule agonists of activin signalling are presently approved for clinical administration. Experimental candidates, however, have been identified. A screen of 4,000 compounds for expression Sox17, a marker of definitive endoderm, revealed a role for the molecules IDE1 and IDE2 in the chemical induction of endoderm from mouse embryonic stem cells (ESC) (8). Structured around a HDAC inhibitor scaffold, IDE1 and IDE2 promote endodermal differentiation in multiple mouse and human ESC lines, inducing gene expression signatures indistinguishable from activin A-derived definitive endoderm. This chemically derived endoderm is functional, being able to incorporate into nascent foregut structures after introduction to E8.75 embryos. Of especial relevance, IDE1 and IDE2 are able to induce Smad2 phosphorylation in an ALK4/5/7-dependent manner, suggesting that they function as agonists of activin A signalling (8).

Upon incubation of OR6 cells with a broad titration series of IDE1 and IDE2, however, neither compound elicited a reduction in intracellular HCV level, nor either molecule enhanced induction of *ISG15* nor *IFI6* in Huh7 cells co-incubated with recombinant IFNα [data not shown].

In collaboration with Prof Angela Russell's medicinal chemistry group (Department of Chemistry, University of Oxford), we also embarked upon a screening exercise to identify whether novel small-molecule agonists BMP signalling demonstrate antiviral properties against HCV. In the initial phase of the study, a 25,000 member proprietary library of compounds was screened for activation of a BRE-luciferase construct. The medical chemistry laboratory performed extensive structure-activity analyses, and multiple analogues of each lead compound were synthesized. Hit compounds were validated for induction of BMP-stimulated genes and provided to the Drakesmith laboratory for antiviral testing against the OR6 replicon model.

While the preliminary results of this screen, and compound structures cannot be fully reported in this thesis, the study identified a number of candidates as putative antiviral agents. Subsequent structure-function analyses to define the key regions of these molecules mediating their antiviral effects are required. Given the very preliminary nature of the experiments conducted thus far, we cannot be certain that an observed antiviral effect is attributable to activation of the BMP pathway or, indeed, interactions with a host factor at all. *In silico* modelling of binding complementarity, in parallel with selective knockdown of potential host targets, is required to fully define the factors involved.

Further experiments in this series should explore the capacity of other pharmacological BMP-agonists to elicit antiviral effects *in vitro*. Candidates include the putative Smurf1/2 inhibitors described by Cao and colleagues (726); flavonoid derivatives reported to promote BMP-dependent ventralization of zebrafish embryos (727); and the BMP7 peptidomimetic THR-123, initially developed in the context of renal fibrosis (728).

Chapter 8

Final summary and discussion

The aim of this thesis was to characterize the nature of the antiviral effect mediated by BMP and activin proteins. The initial phase of the study concentrated upon identifying which TGFβ superfamily molecules exert anti-HCV effects and delineating the mechanistic basis for their type I IFN-independent antiviral activity. Further to this, we characterized the induction of activins by viral PRR activation and viral infection, both *in vitro* and *in vivo*, and investigated whether the antiviral effect of BMP and activin proteins extended to HBV, DENV and FLUAV infection.

During the latter half of the project, our attention focussed upon delineating the intersection of the BMP-SMAD axis with the type I IFN response, with recourse to both cellular and bioinformatic techniques.

8.1 Summary

Building upon previous observations from the Drakesmith lab that BMP6 and BMP9 exert anti-HCV effects *in vitro*, multiple BMP/GDF cytokines were screened for an antiviral effect against the OR6 genomic replicon. Coupling our observations with the previously described receptor specificities of the ligands tested, the ability of a BMP family cytokine to exert an anti-HCV effect is positively correlated with its ability to activate the type I BMP receptor. An antiviral effect extends to the fellow TGFβ superfamily members activin A and B, cytokines that are best-characterized to signal via the ALK4/5/7 TGFβ receptor isoforms. Similarly to BMP6, the antiviral effects of activin A and B are sensitive to inhibition by the type I BMP receptor antagonist LDN-193189, mirroring observations obtained by investigators in other contexts that activins may be capable of signal transduction via type I BMP receptor chains (72).

While LDN-193189 demonstrates greatest potency against the ALK2/3 isoforms of the type I BMP receptor, it is capable of interactions with other ALK chains at higher concentrations. As we have yet to investigate whether activin A and B elicit phosphorylation of SMAD1/5/8 in the OR6 model, we must exercise a modicum of caution before wholly ascribing their antiviral properties to activation of the type I BMP receptor.

The antiviral effects of both BMP6 [appendix 1] and the activins are not contingent upon intact type I IFN signal transduction, being unimpaired by the small-molecule JAK1/2 inhibitor ruxolitinib. We report that the IFN-independent antiviral effect of BMP6 may be mediated by its disruption of cell-cycle progression via promoting arrest at the G0/G1 and G2/M checkpoints. Moreover, our data suggest that pharmacological induction of cell cycle

arrest in the OR6 model is sufficient to reduce intracellular HCV content indexed by luciferase output. This effect of BMP6 on cell-cycle progression is also analogous to the known cytostatic functions of type I IFN, which likely contribute to IFN's antiviral activity.

Having established that BMP and activin proteins mediate antiviral effects *in vitro* (constituting an effector limb of a potential antiviral feedback circuit), we characterized their induction by viral nucleic acid sensing mechanisms. Activation of the cytosolic viral RNA sensors RIG-I and MDA5 by synthetic nucleic acid agonists induced *INHBA* mRNA in Huh7, A549 and THP-1 transformed cell lines. In PBMC from healthy donors, imidazoquinoline agonists of TLR7 and TLR8, in addition to synthetic nucleic acid agonists of RIG-I and MDA5, elicit transcriptional upregulation of *INHBA*. Activin A protein was also detected by ELISA in the culture supernatants of these stimulated PBMC, albeit with marked inter-donor variation. Commercial ELISA kits for the detection of activin B protein are presently unavailable.

In true viral infections, *INHBA* induced by SeV infection *in vitro*, in a RIG-I dependent manner. DENV infection of Huh7.5 cells induces both *INHBA* and *INHBB* expression. *In vivo*, *Inhba* is detectable in the lungs of FLUAV-infected mice, correlating with the magnitude of local ISG expression. We have not yet investigated the full kinetics of activin induction downstream of PRR activation. Although neither *INHBA* nor *INHBB* mRNA were induced by treatment of Huh7 cells with recombinant IFNα, we have not defined whether activin expression following pathogen detection forms part of the first wave of cytokine activation or if it is secondarily induced by NFκB, TNFα or other inflammatory signalling cascades.

Building on previous observations of synergy between BMP and IFN antiviral signalling [appendix I], we characterized the interactions of IFN and activin signalling *in vitro*, demonstrating that activin A synergistically enhances the antiviral effects of both IFNα and IL28B (IFNλ3) in the OR6 HCV replicon model. Moreover, in Huh7 cells at least, transcriptional induction of multiple ISGs is enhanced in the presence of activin A or activin B.

These *in vitro* observations were extended *in silico*, via a comparison of SMAD1 and IRF1 binding profiles genome-wide, initially in K562 erythroleukaemic cells but subsequently extending to datasets from U937 transformed monocytes and CD34+ erythrocyte progenitors mobilized from the peripheral blood of healthy volunteers. Our bioinformatic analyses suggest that genome-wide, the repertoire of loci bound by activated SMAD1 demonstrates

marked similarity to that of IRF1, including in the vicinity of loci encoding antiviral effectors. These observations establish that parallels between BMP-SMAD and IFN-IRF signalling are not unique to hepatoma-derived cells.

For reasons of time, we were unable to replicate these bioinformatic analyses in datasets derived from BMP6 or activin A or B-treated hepatoma-derived cells or primary human hepatocytes. However, comparison of the loci bound by SMAD1 in BMP4-treated K562 cells with the genes differentially regulated in a microarray of BMP6-treated Huh7 cells suggested enrichment for type I IFN-associated genes in the fraction of hits shared between both datasets.

The final phase of the study sought to assess whether an antiviral effect of BMP6 and activin A proteins extended to HBV and DENV infection *in vitro*. Both BMP6 and activin A elicited antiviral effects against HBV, indexed by reduction in HBsAg levels in culture supernatants. Activin B was not examined in this infection model. Against DENV, our data suggest that activin A, activin B and BMP6 exert very limited antiviral effects in isolation, but preliminary results favour further investigation of the possibility that activin A may potentiate the anti-DENV effects of recombinant IFNα *in vitro*.

8.2 Discussion

8.2.1 Is there a role for ECSIT in the interaction of BMP and IFN signalling?

Data presented in this thesis suggest that SMAD and IRF binding drive similar antiviral gene expression profiles [chapter 6], and this may underlie the IFN-like activity of BMPs and activins. However, parallel genomic regulation by SMADs and IRFs is not the only plausible mechanism by which BMP and IFN signalling could interact. A body of evidence suggests that the ECSIT protein could form a bridge between TLR signalling and SMAD signal transduction. Identified via a yeast 2-hybrid screen for TRAF6 interaction partners, ECSIT is posited to couple TLR to NFκB and AP-1 activation via recruiting, and stabilizing expression of, the MAP kinase MEKK1 (729). MEKK1 is subsequently able to activate both IKK-NFκB and p38-JNK-AP1 axes, both critical for innate immune and pro-inflammatory gene expression programs. Highly evolutionarily conserved, Drosophila ECSIT mediates an orthologous function, positively regulating expression of the insect antimicrobial effectors defensin and attractin (729).

Strikingly, *Ecsit -/-* mice phenocopy the profound development impairment observed in animals deficient in BMP signalling (730). Akin to homozygous loss of BMPR1A, ECSIT knockout is embryonic lethal, with embryos failing to gastrulate or induce mesoderm differentiation. At E7.5, *Ecsit -/-* mice demonstrate reduced cell proliferation, delaying their attainment of the minimal cell number required for tissue migration and initiation of gastrulation.

While Ecsit knockout closely recapitulates Bmpr1a loss, expression of neither Bmpr1a nor Bmp4, the principal BMP driving differentiation on the early embryo, were modulated by Ecsit loss. Expression of *Tlx2,* however, a BMP-stimulated patterning factor required for mesoderm differentiation, is absent in *Ecsit -/* embryos. Moreover, shRNA knockdown of Ecsit *in vitro* elicits dose-dependent suppression of *Tlx2* induction by BMP4, implying that Ecsit functions as an indispensible BMP co-factor in the context of mesoderm formation. Co-immunoprecipitation experiments further confirm a constitutive association between Ecsit and SMAD4, and a BMP4-inducible interaction with SMAD1 (730). *Ecsit* mRNA is inducible by recombinant BMP2 and BMP7 in transformed murine osteoblast progenitor cells (731).

Hypothetically, BMP-mediated activation of ECSIT could enhance NFκB and IKK signalling, subsequently boosting induction of pro-inflammatory cytokines and, via the contribution of NFκB and AP1 to the IRF3 enhanceosome, type I IFN. In addition to its role downstream of TLR signalling, a role for ECSIT in RLR-MAVS interactions has also been posited: ECSIT encodes an N-terminal mitochondrial targeting sequence, and immunofluorescence studies demonstrate co-localization of ECSIT, TRAF6 and MEKK1 with MAVS at the mitochondrial surface (732,733). Ectopic expression of ECSIT dose-dependently activates an IFNβ promoter-driven luciferase reporter construct, an effect ablated by N-terminal ECSIT truncation (732).

While a raft of circumstantial evidence links ECSIT, SMAD and innate immune signalling, to address whether ECSIT contributes to the interplay between BMP/activin and IFN identified in this project, definitive experiments must examine the effects of ECSIT knockdown or elimination upon their antiviral synergy.

8.2.2 Implications for therapeutic modulation of activin signalling

While this thesis posits that activin and BMP agonists may present a novel therapeutic strategy against viral infection, it is important to note that antagonists are gaining traction in

other domains of clinical practice. Soluble ligand traps for activin A have recently entered phase 2 clinical trials for numerous haematological and malignant disorders, including β-thalassaemia (NCT01571635), Diamond-Blackfan anaemia (NCT01464164) and multiple myeloma (NCT01562405). The most prominent of these agents is Sotatercept (ACE-011), a fusion construct composed of the ActR IIA extracellular portion conjugated to the human IgG1 Fc domain.

Bone lesions are a common pathology in multiple myeloma, a cancer of terminally differentiated B cells (plasma cells) responsible for immunoglobulin synthesis. Within the marrow, malignant plasma cells are posited to promote activin A secretion by the marrow stromal cells, with increased activin A driving SMAD2-dependent inhibition of osteoblast differentiation, resulting in osteolysis and resorprtion of mineralized cortical bone (734). Murine analogues of Sotatercept both reduce bone destruction and enhances cortical deposition in mouse models of multiple myeloma, observations that have been recapitulated by early phase 2 clinical studies (735).

The hereditary haematologic disorder β-thalassaemia is characterized by ineffective erythropoiesis, culminating in microcytic anaemia. ActR IIA ligand traps are proposed to sequester GDF11, a cytokine proposed to drive α-globin membrane precipitation in erythroid progenitors, thereby enhancing the differentiation of mature erythrocytes (736). In the congenital erythrocyte aplasia Diamond-Blackfan anaemia (DBA), pre-clinical observations suggest that sequestration of the TGFβ-type cytokine lefty1 by ActR IIA ameliorates a DBA-like erythroid phenotype in transgenic zebrafish, hence the rationale for clinical translation (737).

With the imminent possibility of these activin inhibitors being used in the clinical management of vulnerable immune-compromised patients, fully characterizing the antiviral role of activin signalling is ever more important, lest inhibition of activin signalling exacerbate immunosuppression.

Conversely, agonism of the BMP-activin-SMAD axis might also have a role in sensitizing cells to recombinant type I IFN in other disease contexts. Pegylated-IFNα is used as cytostatic drug in the haematologic disorders polycythaemia vera and essential thrombocythemia (738), and meta-analyses support co-administration of IFNα with conventional chemotherapy in the treatment of adult T-cell leukaemia and lymphoma (739). As our data demonstrate that both BMP and activin proteins can augment the transcriptional effects of type I IFN as part of their antiviral mechanism, the possibility that this IFN-enhancement could be applied in the

context of anti-tumour therapy remains open to investigation.

8.2.3 Implications for the study of intrauterine viral infection

Congenital viral infections are associated with multiple developmental sequelae, including intrauterine growth restriction, neurodevelopmental delay, visual impairment and sensorineural hearing loss. Vertical transmission of rubella, cytomegalovirus (CMV) and herpes simplex-2 (HSV-2) are the most extensively characterized intrauterine viral infections, although transplacental transmission of HBV, HIV-1 and human papilloma virus (HPV) have been documented.

As summarized in section 1.1.6, multiple viral infections disrupt the BMP-SMAD signalling axis, through an array of mechanisms including repression of type I and type II BMP receptor expression and induction of inhibitory miRNA transcripts. Of note, multiple CNS complications associated with congenital viral infections are associated with the genesis of neural structures and organs regulated by BMP family members.

Intrauterine CMV infection results in varied cerebral pathologies, the majority of which disrupt the normal architecture of cerebral neurons, for example polymicrogyria, referring to an excessively convoluted cerebral surface, and ventricular dilatation (740). Dorsoventral patterning of the telencephalon, the primordial structure giving rise to the cerebrum, is guided by BMP signalling, with tissue-specific disruption of *Alk3* expression resulting in failure of the choroid plexus, a critical tissue derived from the midline of the telencephalon, to differentiate (741).

Congenital rubella infection is associated with a clinical triad of sensorineural deafness, defective eye development and cardiac malformations, most frequently pulmonary artery stenosis and persistence of a patent ductus arteriosus (742). BMP-SMAD signalling is intrinsic to the development of these organs.

BMP ligands modulate multiple aspects of eye development, including the maturation of the lens from the optic placode (regulated by BMP7, germline mutations of which wholly ablate lens formation) and the migration of neurons to the nascent retina. The latter requires expression of the ALK6 isoform of the type I BMP receptor by the retinal precursor cells (743). In the developing heart, BMP2 signalling from the embryonic myocardium is absolutely required for the emergence of the endocardial cushion, a cluster of cells which ultimately differentiate to form the valves and septum that divide the cardiac chambers (743).

Similarly, BMP4 is required for atrioventricular septation in mouse models of cardiogenesis; SMAD6 and SMAD7 deficient mice also demonstrate lethal disruption of the ventricular septum and outflow tracts, and in those animals that survive to adulthood, impaired conduction of the cardiac action potential (743–745).

The mechanistic basis for the morphological abnormalities observed during congenital viral infection is poorly defined. In the context of CNS pathology during congenital CMV infection, multiple hypotheses have been defined. Proposed mechanisms include the virus acting as a teratogen to induce direct chromosomal injury and subsequent impairment of gene expression; viral infection promoting apoptotic death of developing neurons; and preferential replication of the virus within, and subsequent depletion of, neural stem cells (746). The pathophysiology underpinning the extracerebral manifestations of intrauterine viral infections, however, remains unclear.

Integrating the above information with the observations in this thesis, it is plausible that dysregulation of the BMP-SMAD signalling axis during congenital viral infection- either its repression by viruses themselves or its activation as part of an innate antiviral response- could disrupt the complex spatiotemporal regulation of BMP signalling components required for their role in embryogenesis, thereby contributing to developmental abnormalities.

8.2.4 Implications for our understanding of the evolution of intracellular innate immunity

Phylogenetic analyses suggest that type I IFN cytokines have been expressed by chordates for the past 500 million years, initially emerging in teleost fish (747). However, signal transduction cascades orthologous to BMP and activin pathways are rather older, being expressed in diverse phyla, including planarians, annelids, arthropods and all deuterostomes (18,19). Given the topological homology between SMAD and IRF proteins and their proposed divergence from a common ancestor as detailed in section 6.1.3], we hypothesize that BMP/activin-SMAD signalling might represent an evolutionary precursor to the vertebrate type I IFN response. While its antiviral potency is surpassed by IFN, it is possible that the BMP/activin-SMAD axis is an "immunological fossil" in vertebrates, retaining only residual functionality, but perhaps being capable of "resurrection" for therapeutic purposes.

In animals that lack IFN, BMP-type signaling is established as having an innate immune role in addition to its function directing developmental processes. In *Drosophila melanogaster*, three BMP-like ligands are expressed: namely *dpp* (decapentaplegic), *scw* (screw) and *gbb*

(Glass bottom boat). *dpp* is structurally and functionally akin to BMP2/4 (748), whereas *gbb* is orthologous to vertebrate BMP5/6/7/8; *scw* represents a product of *gbb* gene duplication and subsequent divergence to form a novel ligand with a more restricted receptor specificity (12). A single activin is encoded by *Drosophila*. In terms of receptors, *tkv* (thickveins) and *sax* (saxophone) are orthologous to vertebrate ALK3/ALK6 and ALK1/2 respectively; *wit* (wishful thinking) and *put* (punt) resemble the type II BMP and activin receptors respectively. Intracellular signal transduction is conveyed by the interaction of the R-SMAD *mad* (mothers against dpp) with the co-SMAD *medea*, the actions of which are antagonized by the I-SMAD *dad* (daughters against decapentaplegic).

The *dpp-mad* axis is a critical mediator of *Drosophila* morphogenesis, being required for the formation of the fly dorsoventral body plan and the antero-posterior patterning of the nascent wing, whereas *gbb* signalling is required both for patterning of the internal viscera and the maintenance of the fly neuromuscular junction (12,749,750).

Both humoral and cellular immunity are present in flies, manifesting as the systemic secretion of antimicrobial peptides (AMP) and the differentiation of circulating hemocytes into specialized phagocytic lamellocytes (751). Activation of the *toll* pathway (evolutionarily conserved as the TLR family in vertebrates) is central to the *Drosophila* antifungal and antibacterial response (751,752). Pathogen structural motifs trigger extracellular proteolysis of the *toll* ligand *spz* (spätzle), resulting in its ligation of *toll* receptors at the cell surface. Akin to *dpp* and BMP proteins, *spz* is a cysteine-knot cytokine. Toll activation induces intracellular degradation of *cactus*, enabling the transcription factors *dif* and *dorsal* to translocate to the nucleus and stimulate AMP expression. *Drosophila* also encodes an orthologue of the mammalian TNFα pathway, namely *imd*. Both *toll* and *imd* activation converge upon NFκB-like transcription factors, *dif* and *rel* respectively (752).

Evidence exists for an immune role of *dpp* signalling in *Drosophila*, albeit not in an antiviral context. Clark and colleagues report that *dpp* is induced by challenge with the bacteria *Micrococcus luteus*, and that this induction requires expression of the NFκB-like factor *rel*. Ultimately, the authors report that activation of the *dpp-Mad* axis curtails AMP expression, suggesting that the role of *dpp* in this infection model is predominantly anti-inflammatory (753). Intact *dpp* signalling is reportedly also required for the differentiation of phagocytic lammellocytes in a *Drosophila* model of *Salmonella* typhimurium infection (754).

Of interest, the mammalian orthologue of *spz* has recently been identified as the neurotrophin NGFβ, a peripheral member of the TGFβ superfamily. Deleterious mutations in NGFβ or its receptor and its receptors result in both hereditary neuropathies, due to defects in both

neuronal survival and the structure of the spinal cord's anterolateral system, and increased susceptibility to Staphylococcal infections (755). Moreover, both *toll* and *imd* are implicated in fly embryogenesis, with *toll* being first identified as a regulator of dorsoventral patterning before the establishment of its role in immunity (752,756,757). Similarly, in the nematode worm *C. elegans*, expression of antifungal compounds in response to infection is modulated by the morphogen *dbl-1*, a ligand orthologous to *Drosophila dpp* and vertebrate BMPs (758). *Dbl*-1 was initially characterized as a regulator of worm body size and reproductive organ patterning (11). Mutants overexpressing *dbl-1* demonstrate elevated expression of enzymes implicated in the antimicrobial response, including lysozymes, saposin and aspartyl protease (759). Conversely, *dbl-1* deletion increases susceptibility of *C.elegans* to fungal infection (758).

These signalling pathways set a precedent for the existence of mechanisms with dual functionality as mediators of morphogenesis and immunity, the model we propose for BMP/activin signalling in this thesis.

8.3 Further investigations

The data presented in this thesis suggest a number of questions for subsequent investigation.

1) Does SMAD-linked BMP/activin signalling contribute to the control of viral replication in *in vivo* models of infection?

Critical to extending the work presented in this thesis are experiments to test for direct *in vivo* evidence that BMP/activin signalling contributes at least in part to the control of viral infection. Strategies to explore this include comparing FLUAV or MCMV replication in activin A conditional knockout mice versus WT littermates (utilizing the murine models described in section 7.4.3) or assessing whether administration of activin ligand traps, such as Sotatercept, influence the course of murine viral infection. Alternatively, the effect of pharmacological inhibition of the type I BMP receptor with LDN-193189 could be assessed in *Ifnar2* knockout mice, allowing us to discern whether the importance of BMP/activin antiviral activity is heightened in the absence of functional type I IFN signalling.

2) Do eQTL driving individual variation in type I IFN and ISG expression map to BMP-SMAD associated genomic loci?

The mapping of expression quantitative trait loci (eQTL) from RNA-seq datasets aims to

delineate the genetic basis of gene expression, via the identification of polymorphisms in proximal (cis) and distal (trans) regulatory elements that associate with variation in the abundance of a particular transcript (760). Genome-wide identification of eQTL is feasible via integration of SNP genotyping and transcriptomic datasets, with statistical genetics techniques used to dissect the genomic components that drive individual variation in gene expression. Such systematic approaches permit the regulatory inputs controlling expression of thousands of transcripts to be addressed in parallel (760).

As detailed in section 3.1.1, SNPs in multiple BMP-SMAD associated genes were identified in the seminal GWA study from Ge and colleagues that identified polymorphisms in *IL28B* as the major genetic determinant in the response of cHCV patients to IFN-based antiviral therapy (311). Extending upon these observations, we propose to examine whether eQTL regulating type I and type III IFN expression map to genomic loci encoding BMP-SMAD signalling components. Marked variation in trans-eQTL expression is observed between tissues, whereas cis-eQTL demonstrate greater conservation between cell and tissue types. To address this, RNA-seq datasets derived from multiple tissue types of diverse origin could be interrogated.

3) Is expression of the "antiviral genes" associated with a signature of SMAD1 binding in K562, U937 and CD34+ erythroid progenitors increased at the mRNA and protein level following exposure of these cell types to recombinant BMP4?

4) Does BMP signalling induce ISG expression in primary human hepatocytes?

Expression of transcript encoding the multiple ISGs, including those identified in chapter 6 as being bound by both SMAD1 and IRF1 in K562 erythroleukaemic cells, will be quantified in primary human hepatocytes treated with recombinant BMP6. Colleagues in the laboratory will conduct these experiments.

In the longer term, prospective avenues for extension of the study include:

5) Is activin expression induced in response to activation of the cGAS-STING axis and does it exert antiviral effects against DNA viruses?

We have embarked only upon very preliminary assessments of activin induction by cGAS activation *in vitro*. Further work should replicate the observation of *INHBA* induction in response to *E. coli* DNA in human primary fibroblasts, and extend these assays to examine

the effect of exogenous cGAMP upon *INHBA* expression. Subsequent *in vivo* studies could seek to address whether *in vivo* infection with DNA viruses elicits activin A induction at both the mRNA and protein level, both locally, for example in the lungs of murine gammaherpesvirus infection, and in the plasma.

6) Does activation of the BMP-SMAD axis by intrauterine viral infection have implications for dorsoventral patterning of the zebrafish embryo?

The effect of viral infection upon embryogenesis and, specifically, whether aberrant BMP signalling contributes to the structural defects observed after congenital infection, could initially be addressed in a zebrafish model. Zebrafish provide the advantage of easily monitored embryonic development and are susceptible to multiple systemic viral infections (761). Using the type I BMP receptor antagonist dorsomorphin as a positive control for disruption of dorsoventral axis patterning, we could compare the development of the fish body plan in infected and uninfected fish, in an effort to discern whether viral infection affects embryonic morphogenesis and, if so, whether activation of the BMP-SMAD pathway is implicated in this effect.

8.4 Future perspectives

This thesis provides evidence that multiple TGFβ superfamily cytokines exert antiviral effects, both in parallel with, and independently of, type I IFN. We have also uncovered unexpected and striking parallels in the repertoire of genes activated by SMAD and IRF binding genome-wide. Moreover, it provides evidence that activin proteins may mediate a novel innate antiviral response mechanism, being both upregulated in response to viral infection or synthetic analogues thereof, and exerting pronounced antiviral effects against HCV and HBV. To the best of our knowledge, these observations could represent the first characterization of a non-IFN intracellular antiviral feedback mechanism in vertebrates. The findings provide a rationale for the continued investigation of activin and BMP agonists as novel therapeutic agents against viral diseases that present a significant burden upon public health.

Appendix I

Suppression of hepcidin by HCV reveals antiviral properties of BMP/SMAD signaling

Lucy A. Eddowes[1]#, Kinda Al-Hourani[1]#, Narayan Ramamurthy[2]#, Cynthia Sandor[3], Andrew E. Armitage[1], John D. Ryan[4], Dahlene N. Fusco[5], João Arezes[1], Eleni Giannoulatou[6], Sara Boninsegna[2,7], Stephane Chevaliez[5], Benjamin M. J. Owens[8], Chia Chi Sun[9], Paolo Fabris[10], Maria Teresa Giordani[10], Diego Martines[7], Slobodan Vukicevic[11], John Crowe[4], Herbert Y. Lin[9], Jodie L. Babitt[9], Raymond T. Chung[5], Matthew W. Lawless[4], Caleb Webber[3], Paul Klenerman[2, 12], and Hal Drakesmith[1, 12]*

1 MRC Human Immunology Unit, MRC Weatherall Institute of Molecular Medicine, University of Oxford, John Radcliffe Hospital, Oxford, UK
2 Peter Medawar Building for Pathogen Research, University of Oxford, South Parks Road, Oxford, UK
3 MRC Functional Genomics Unit, Department of Physiology, Anatomy & Genetics, Oxford University, UK
4 Centre for Liver Disease, Mater Misericordiae University Hospital, 55 Eccles Street, Dublin 7, Ireland
5 Liver Center, Gastrointestinal Unit, Department of Medicine, Massachusetts General Hospital, Harvard Medical School, Boston, Massachusetts, USA
6 Computational Biology Research Group, Weatherall Institute of Molecular Medicine, University of Oxford, John Radcliffe Hospital, Oxford, UK
7 Department of Surgical Gastroenterological Science, University of Padua, Padova, Italy
8 Translational Gastroenterology Unit, Experimental Medicine Division, Nuffield Department of Medicine, John Radcliffe Hospital, Headington, Oxford, UK
9 Program in Anemia Signaling Research, Nephrology Division, Program in Membrane Biology, and Center for Systems Biology, Massachusetts General Hospital, Harvard Medical School, Boston, Massachusetts, USA
10 Department of Infectious Diseases and Tropical Medicine, San Bortolo Hospital, Vicenza, Italy
11 Center for Translational and Clinical Research, School of Medicine, University of Zagreb, Zagreb, Croatia
12 NIHR Biomedical Research Centre, John Radcliffe Hospital, Oxford UK

*Corresponding author. alexander.drakesmith@imm.ox.ac.uk

# These authors made an equal contribution

Hepatitis C virus (HCV) decreases expression of the iron regulatory hormone hepcidin, although how and why this occurs is not well understood. Bone morphogenetic protein (BMP) signaling in the liver controls hepcidin transcription, and we found that HCV blunted induction of hepcidin by BMP6. In HCV-infected patients, disrupted BMP6 signaling and genetic variation associated with the BMP/SMAD pathway correlated with non-response to type I interferon (IFN) and ribavirin therapy. Correspondingly, BMPs induced an antiviral gene repertoire, enhanced response to IFN and suppressed HCV replication. Thus, we reveal an unappreciated role for the BMP/SMAD pathway in inducing antiviral immunity, acting in parallel to and modulating IFN. HCV inhibits BMP/SMAD signaling influencing the response to IFN, and in so doing suppresses hepcidin.

In the liver, signaling by BMPs (most notably BMP6) via SMAD1/5/8 transcription factors controls synthesis of the iron regulatory hormone hepcidin (encoded by *HAMP)*, and is vital for maintaining iron homeostasis(*1-3*). Most infections and inflammation increase hepcidin expression(*4*), but HCV is associated with low hepcidin and a resultant predisposition to iron accumulation(*5, 6*). Defective BMP/SMAD signaling in clinical and experimental genetic disorders causes iron overload due to hepcidin insufficiency(*7-9*), so we hypothesized that HCV infection caused low hepcidin by inhibiting the BMP pathway. RNA-Seq analysis comparing HCV infected versus uninfected HuH7.5 cells(*10*) indicated that expression of the BMP co-receptor hemojuvelin (*HJV)* was decreased in HCV infected cells, while *SMAD7,* which (like the other I-SMAD *SMAD6*) inhibits BMP signaling(*11, 12*), was increased. Confirming this, HuH7.5 cells expressed decreased *HJV* and elevated total *I-SMAD* as a function of increasing viral burden (Fig. 1a). HCV-infected cells exhibited a blunted induction of *HAMP* in response to BMP6 compared with uninfected cells, consistent with viral inhibition of the BMP6 signal (Fig. 1b). A likely contributor to these effects on BMP/SMAD signaling is TNF-alpha: HCV infection increases *TNFA* expression, and TNF-alpha decreases *HJV,* increases *I-*

SMAD expression and inhibits *HAMP* induction by BMP6 (Fig. S1). To seek clinical correlates of these findings, we quantified *HAMP, SMAD6* and *SMAD7* levels in liver biopsies taken before antiviral treatment was initiated from a cohort of patients chronically infected with HCV genotypes 1 or 3 (Table S1). Compared to mRNA levels in control liver tissue, biopsies from HCV patients had significantly reduced *HAMP*, and significantly increased *SMAD6* without a decrease in *SMAD7* (Fig. 1c), so that as with the *in vitro* HCV-infected cells, total *I-SMAD* was increased (Fig. 1d). To investigate the impact of impaired BMP/SMAD signaling on the outcome of chronic HCV infection, we analysed gene expression in pre-treatment biopsies of those patients whose eventual response to antiviral therapy (pegylated type I Interferon and ribavirin) was known (Table S2). Non-responders (NRs) had reduced levels of *HAMP, HJV* and *ID1,* a canonical BMP target gene, compared to sustained virological responders (SVR) (Fig. 1e). Furthermore *ID1* and *HAMP* levels correlated in all groups and were both lowest in NRs (Fig. 1f). We also quantified liver *BMP6* and calculated *HAMP/BMP6* and *ID1/BMP6* ratios as assessments of BMP6 target gene output per BMP6 input. Both of these ratios were significantly reduced in NRs (Fig. 1g), consistent with an impairment of BMP6 signal transduction causing decreased hepcidin and associating with a failure to respond to antiviral treatment. Motivated by this data, we conducted a hypothesis-driven analysis of a previously conducted genome-wide association (GWA) study of response to pegylated IFN and ribavirin in HCV infected patients(*13*); we examined this dataset to investigate whether common genetic variants in the BMP pathway associate with different outcome after therapy. A list of 100 SNPs most associated with differential HCV clearance(*13*) covered 66 independent GWA intervals (see methods) and contained polymorphisms linked to EVI-1 and SKIL (which regulate BMP/SMAD signaling), ACVR1/ALK2 (a BMP Type I receptor), and BMP6, suggesting a potential enrichment of BMP pathway components. To determine the significance of this (see methods), we calculated the likelihood of a) BMP pathway genes occurring in one million randomly generated sets of 66 GWA intervals, and b) genes from one million randomly generated gene-sets of similar size as the BMP pathway (Table S3) occurring within the defined 66 GWA intervals. In both cases, the probability of four genes (ie the number found in ref 13) arising by chance was very low (p=3.89x10e-4 and p<1x10e-6; Fig. 1h); demonstrating that BMP/SMAD pathway genes were significantly over-represented within intervals associated with differential HCV clearance.

To understand how BMP/SMAD signaling could be linked to antiviral immunity, we exposed HuH7 cells to BMP6, measured changes in the transcriptome by microarray, and subjected the results to pathway analysis, which reported that type I IFN signaling (as well as BMP signaling, as expected) was significantly changed (Fig. S2). The specific genes altered in the IFN signaling pathway are shown in Fig. S3a,b, and we confirmed by qPCR that *IFNAR2, JAK1, STAT2, IRF9, IFI6* and *ISG15* were increased by BMP6 in both HuH7 cells and (apart from *JAK1*) primary human hepatocytes (Fig. 2a, Fig. S4). We also found that BMP6 increased expression of *IRF1* and *IRF7*, important components of IFN's activity against many viruses (*14*) (Fig. S4). These alterations suggested that BMP6 may enhance IFN activity, which we tested in four ways: 1) Phosphorylation of STAT1 and STAT3 transcription factors was increased following IFN exposure in cells pretreated with BMP6 (Fig. 2b, Fig. S5). 2) BMP6 pre-treatment significantly enhanced the expression of seven IFN-stimulated genes: *MX1, IFI6, ISG15, IFIT3, IFITM1, PLSCR1, TRIM14* (Fig. 2c and Fig. S6a-e). 3) BMP6 downregulated *USP18* (Fig. 2a), a critical negative feedback inhibitor of IFN(*15, 16*); this downregulation was inhibited by the BMP type I receptor kinase antagonist LDN-193189(*17*) but not by the JAK inhibitor ruxolitinib(*18*), whereas the reverse was true for upregulation of USP18 by IFN (Fig. 2d, e), demonstrating that BMP6 regulates USP18 independently of IFN signaling. 4) BMP6 increased the antiviral activity of IFNalpha and IFNlambda3 in an HCV replicon cell-culture system (OR6) and against replication competent JFH1 HCV in HuH7.5 cells (Fig. 2f, g, Fig. S6f).

The HCV assays indicated that BMP6 has antiviral effects in the absence of added IFN, and we investigated this further. Adding BMP6 immediately after infecting HuH7.5 cells with JFH1 HCV restricted the accumulation of HCV RNA in culture supernatants (Fig. 3a). BMP6 added to cultures in which HCV had already been replicating for 3 days significantly reduced cellular and supernatant viral RNA measured after a further 7 days (Fig. 3b), and suppressed activity of an HCV replicon over time (Fig. 3c). Suppression of HCV replication by BMP6 was prevented by LDN-193189 and a related inhibitor dorsomorphin(*17*) (Fig. 3d), but not by ruxolitinib or anti-IFNAR2 antibodies (Fig. S7). Conversely, anti-IFNAR2 and ruxolitinib, but not LDN-193189 or dorsomorphin, prevented suppression of HCV replication by IFN (Fig. S7). Therefore BMP6 has direct antiviral effects that require kinase activity of BMP type I receptor but do not require IFN-JAK signaling. Receptor usage by members of the TGF-beta

superfamily varies considerably. A previous report suggested BMP7 may have anti-HCV activity(*19*); we also found that BMP9 and BMP4 (which like BMP6 and BMP7 bind the BMP type I receptors ALK2/3), suppress HCV replication, whereas BMP15, GDF15, and GDF1 (which bind other receptors) had no such activity (Fig. S8a-f); TGF-beta, which binds TGF-beta type I and type II receptors, enhances HCV replication(*20*). A non-BMP TGF-beta superfamily member Activin B, which can bind BMP type I receptors(*21*), suppressed HCV replication in a manner partially blocked by LDN-193189 (Fig. 3e, f). Of relevance, BMP2 (which binds ALK2/3) suppresses replication of murine gammaherpes virus(*22*). Therefore, antiviral activity of TGF-beta superfamily members segregates with BMP type I receptor binding (Fig. S8g).

To explore whether BMPs influence antiviral gene signatures in non-liver cell-types, and to investigate the role of BMP-induced transcription factors in regulating antiviral genes, we interrogated genome-wide ChIPseq datasets of BMP4-treated erythroleukemic K562 cells and monocytic U937 cells (Table S4). In both cell types, the BMP pathway transcription factor SMAD1 bound loci of multiple antiviral genes (Table S5, S6), including IFNAR2, JAK1, STAT2 and multiple IRFs, and pathway analysis of genomic loci bound by SMAD1 indicated alteration of the Type I IFN response in these cells (Fig. S10a,b), similar to the results from our microarray analysis of BMP6-treated HuH7 cells (Fig. S2). For K562 cells, available ChIPseq datasets(Table S4, *23, 24*) allowed genomewide comparison of SMAD1 bound loci to loci bound by multiple other transcription factors. The density of SMAD1 binding in BMP4-treated K562 cells was enriched +/- 500bp around the loci bound by IRF1 in IFNalpha-treated K562 cells; this enrichment of SMAD1 binding was not apparent in dorsomorphin-treated cells; and binding of other transcription factors, with the exception of STAT1 and STAT2 (that like IRF1 regulate antiviral immunity), was also not enriched proximal to IRF1-bound loci (Fig. 4a-c). Furthermore, SMAD1 and IRF1 binding peaks were observed in close proximity in active regulatory chromatin regions in K562 cells and primary CD34+ cells near anti-viral effector genes including RSAD2, SSBP3, ZC3HAV1 (Fig. S11a-c). Consistent with a general activating effect of SMAD1 binding on regulation of these genes across different cell types, BMP6 increased mRNA expression of *RSAD2*, *SSBP3*, *ZC3HAV1* in HuH7 cells (Fig. S12). Therefore, induction of a gene repertoire through SMAD1 binding, similar to that targeted by IRF1 after IFN stimulation, is likely to underpin the antiviral activity of BMP/SMAD signaling. Notably, SMADs and IRFs demonstrate strong electrostatic and topological similarity in their C-terminal domains, may derive from a common ancestor(*25-27*), and can potentially directly interact(*28*).

In summary we have described a mutually antagonistic relationship between HCV and BMP/SMAD signaling (Fig. 4d). HCV disrupts BMP/SMAD signaling, thereby suppressing hepcidin and altering the response to IFN-based antiviral response. Genetic variation in the BMP/SMAD pathway is also associated with differential response to antiviral therapy. Conversely BMP/SMAD signaling enhances antiviral genetic networks and inhibits HCV replication. This reciprocal interaction of HCV and BMP/SMAD is reminiscent of that between HCV (and many other viruses) and IFN. Of relevance, in organisms lacking IFN, BMP/SMAD-type signaling is an established mediator of innate immunity(*29, 30*); our data now reveal a similar function of this pathway in humans that acts in parallel to IFN. Further exploration of BMP/SMAD signalling in the context of viral immunity is warranted.

==========

Acknowledgements

We thank the MRC UK (Grant ID 92044), the Wellcome Trust (WT091663MA), NIHR Biomedical Research Centre, Oxford, the Oxford Martin School, the NIH (NIAID U19AI082630, NIDDK R01DK087727, RO1DK-069533 and RO1DK-071837), the Beit Memorial Trust for Medical Research, CORE and the GI Research Fund of Dublin, Ireland for funding. We are grateful to the patients who took part in this study. The microarray was performed in collaboration with the High-Throughput Genomics Group at the Wellcome Trust Centre for Human Genetics, University of Oxford (funded by Wellcome Trust grant reference 090532/Z/09/Z and MRC Hub grant G0900747 91070) and the analysis performed in collaboration with the Computational Biology Research Group, Weatherall Institute of Molecular Medicine, University of Oxford. We thank Alain Townsend and Jan Rehwinkel for many useful discussions.

Author Contributions

LAE, AEA, NR, JDR, SB, DNF, SC, CCH, BMJO and KAH performed experiments and analysed data, EG, LAE and AEA performed bioinformatic analysis, NR, JDR, SB, PF, MTG, DM, MWL, JC and PK collated clinical samples, AEA,

MWL, PK, JDR, JC, SV, HYL, and JLB advised on the study and the manuscript, LAE, RTC, PK and HD designed and funded the study and wrote the manuscript.

References

1. B. Andriopoulos, Jr. *et al.*, BMP6 is a key endogenous regulator of hepcidin expression and iron metabolism. *Nat Genet* **41**, 482 (Apr, 2009).
2. D. Meynard *et al.*, Lack of the bone morphogenetic protein BMP6 induces massive iron overload. *Nat Genet* **41**, 478 (Apr, 2009).
3. T. Ganz, Systemic iron homeostasis. *Physiol Rev.* **93**, 1721 (10/2013, 2013).
4. H. Drakesmith, A. M. Prentice, Hepcidin and the iron-infection axis. *Science* **338**, 768 (Nov 9, 2012).
5. A. E. Armitage *et al.*, Distinct patterns of hepcidin and iron regulation during HIV-1, HBV, and HCV infections. *Proc Natl Acad Sci U S A* **111**, 12187 (Aug 19, 2014).
6. D. Girelli *et al.*, Reduced serum hepcidin levels in patients with chronic hepatitis C. *J Hepatol* **51**, 845 (Nov, 2009).
7. J. D. Ryan, E. Ryan, A. Fabre, M. W. Lawless, J. Crowe, Defective bone morphogenic protein signaling underlies hepcidin deficiency in HFE hereditary hemochromatosis. *Hepatology* **52**, 1266 (Oct, 2010).
8. R. H. Wang *et al.*, A role of SMAD4 in iron metabolism through the positive regulation of hepcidin expression. *Cell Metab* **2**, 399 (Dec, 2005).
9. J. L. Babitt *et al.*, Bone morphogenetic protein signaling by hemojuvelin regulates hepcidin expression. *Nat Genet* **38**, 531 (May, 2006).
10. S. D. Woodhouse *et al.*, Transcriptome sequencing, microarray, and proteomic analyses reveal cellular and metabolic impact of hepatitis C virus infection in vitro. *Hepatology* **52**, 443 (Aug, 2010).
11. K. Goto, Y. Kamiya, T. Imamura, K. Miyazono, K. Miyazawa, Selective inhibitory effects of Smad6 on bone morphogenetic protein type I receptors. *J Biol Chem* **282**, 20603 (Jul 13, 2007).
12. K. Mleczko-Sanecka *et al.*, SMAD7 controls iron metabolism as a potent inhibitor of hepcidin expression. *Blood* **115**, 2657 (Dec 29, 2010).
13. D. Ge *et al.*, Genetic variation in IL28B predicts hepatitis C treatment-induced viral clearance. *Nature* **461**, 399 (Sep 17, 2009).
14. J. W. Schoggins *et al.*, A diverse range of gene products are effectors of the type I interferon antiviral response. *Nature* **472**, 481 (Apr 28, 2011).
15. O. A. Malakhova *et al.*, UBP43 is a novel regulator of interferon signaling independent of its ISG15 isopeptidase activity. *Embo J* **25**, 2358 (Jun 7, 2006).
16. X. Zhang *et al.*, Human intracellular ISG15 prevents interferon-alpha/beta over-amplification and auto-inflammation. *Nature* **517**, 89 (Jan 1, 2015).
17. G. D. Cuny *et al.*, Structure-activity relationship study of bone morphogenetic protein (BMP) signaling inhibitors. *Bioorg Med Chem Lett* **18**, 4388 (Aug 1, 2008).
18. Q. Lin *et al.*, Enantioselective synthesis of Janus kinase inhibitor INCB018424 via an organocatalytic aza-Michael reaction. *Org Lett* **11**, 1999 (May 7, 2009).
19. N. Sakamoto *et al.*, Bone morphogenetic protein-7 and interferon-alpha synergistically suppress hepatitis C virus replicon. *Biochem Biophys Res Commun* **357**, 467 (Jun 1, 2007).
20. W. Lin *et al.*, HIV increases HCV replication in a TGF-beta1-dependent manner. *Gastroenterology* **134**, 803 (Mar, 2008).
21. C. Besson-Fournier *et al.*, Induction of activin B by inflammatory stimuli up-regulates expression of the iron-regulatory peptide hepcidin through Smad1/5/8 signaling. *Blood* **120**, 431 (Jul 12, 2012).
22. S. Y. Liu, D. J. Sanchez, R. Aliyari, S. Lu, G. Cheng, Systematic identification of type I and type II interferon-induced antiviral factors. *Proceedings of the National Academy of Sciences of the United States of America* **109**, 4239 (Mar 13, 2012).
23. E. Trompouki *et al.*, Lineage regulators direct BMP and Wnt pathways to cell-specific programs during differentiation and regeneration. *Cell* **147**, 577 (Oct 28, 2011).
24. K. R. Rosenbloom *et al.*, ENCODE data in the UCSC Genome Browser: year 5 update. *Nucleic Acids Res* **41**, D56 (Jan, 2013).
25. A. Eroshkin, A. Mushegian, Conserved transactivation domain shared by interferon regulatory factors and Smad morphogens. *J Mol Med (Berl)* **77**, 403 (May, 1999).
26. K. Takahasi *et al.*, X-ray crystal structure of IRF-3 and its functional implications. *Nat Struct Biol* **10**, 922 (Nov, 2003).
27. B. Y. Qin *et al.*, Crystal structure of IRF-3 reveals mechanism of autoinhibition and virus-induced phosphoactivation. *Nat Struct Biol* **10**, 913 (Nov, 2003).
28. P. Xu *et al.*, Innate antiviral host defense attenuates TGF-beta function through IRF3-mediated suppression of Smad signaling. *Mol Cell* **56**, 723 (Dec 18, 2014).
29. J. L. Frandsen, B. Gunn, S. Muratoglu, N. Fossett, S. J. Newfeld, Salmonella pathogenesis reveals that BMP signaling regulates blood cell homeostasis and immune responses in Drosophila. *Proc Natl Acad Sci U S A* **105**, 14952 (Sep 30, 2008).
30. O. Zugasti, J. J. Ewbank, Neuroimmune regulation of antimicrobial peptide expression by a noncanonical TGF-beta signaling pathway in Caenorhabditis elegans epidermis. *Nat Immunol* **10**, 249 (Mar, 2009).

Figure Legends

Figure 1: HCV – BMP pathway interactions decrease hepcidin and associate with therapeutic outcome
A *HJV* mRNA levels, quantified by qRT-PCR relative to *GAPDH* expression, declined in HCV-infected HuH7.5 cells with increasing multiplicities of infection (MOI) (n=3); *SMAD6* and *SMAD7* mRNA levels increased with increasing MOI (n=3).
B Uninfected or HCV-infected (MOI = 0.02) HuH7.5 cells were incubated with a titration of BMP6 overnight; *HAMP* mRNA induction in response to BMP6 was significantly suppressed in HCV-infected cells ($P<0.0001$; Wilcoxon matched pairs test; n=6).

C *HAMP* mRNA levels were significantly decreased in HCV liver biopsies (n=57) compared to control liver biopsies (n=8) (P=0.0027; Mann-Whitney test), *SMAD6* mRNA was significantly increased (P=0.0080; Mann-Whitney test); mean *SMAD7* levels were increased but not significantly (unpaired t-test).
D *SMAD6* and *SMAD7* mRNA levels as in **C** normalised to the mean of control group.
E Patients with known treatment outcome (n=26) were separated by outcome (Sustained Virological Response (SVR) and Non-Responder (NR)) and compared to the control group (n=8). *HAMP* mRNA expression was reduced in both groups compared to controls whereas *HJV* and *ID1* (n=17) were significantly reduced only in the NR group (one-way ANOVA, **P<0.01; *P<0.05).
F BMP target genes *ID1* and *HAMP* mRNA were correlated across these three groups (Pearson correlation: r^2=0.5980; P<0.0001).
G Ratio of expression of *HAMP* or *ID1* to *BMP6*, derived to represent an 'output-per-input' ratio. *HAMP/BMP6* was significantly reduced in NRs and SVRs; *ID1/BMP6* was significantly reduced in NRs (one-way ANOVA).
H BMP pathway gene enrichment is linked to HCV clearance. SNPs linked to four BMP-pathway genes (BMP6, ACVR1/ALK2, EVI1, SKIL) were in the top 66 GWA intervals associated with differential clearance of HCV. The frequency of four genes (black dotted line) from a million randomly generated gene-sets of similar size to the BMP pathway occurring in the 66 GWA intervals (Random gene-set, left), or of four BMP pathway genes occurring in a million randomly generated sets of 66 GWA intervals (Shifting of GWA intervals, right), was determined against randomized backgrounds (grey histograms).

Figure 2: BMP6 enhances IFN activity
A Changes in expression of the type I IFN pathway related genes identified by microarray of HuH7.5 cells treated with BMP6 for 24h were confirmed by qRT-PCR; BMP target gene *ID3* was measured as a positive control (n=6; all unpaired t-test, except *ID3* – Mann Whitney test (see methods)).
B STAT1(Y701) phosphorylation analysed by Phosflow in HuH7.5 cells treated with or without BMP6 (18nM, 18-20h) followed by IFN-alpha (100U/mL, 30 minutes). Flow Cytometry analysis from a representative experiment and normalized MFI from 3 independent experiments are shown.
C *TRIM14* and *IFI6* mRNA expression in HuH7.5 cells co-treated with BMP6 (18nM) and an IFN-alpha titration for 24h (repeated measures ANOVA; n=3).
D, E *USP18* mRNA expression in HuH7.5 cells treated with (**D**) LDN-193189 (LDN, 0.2uM) or (**E**) Ruxolitinib (Rux, 2.5uM) prior to co-incubation with BMP6 (18nM, 20h) or IFN-alpha (1000U/mL, 6h) (repeated measures ANOVA; n=3).
F Luciferase activity in OR6 cells (that harbor an HCV-replicon) treated with or without BMP6 (2nM or 18nM, 24h) followed by addition of an IFN-alpha titration (10-1000U/mL, 24h) (n=3; repeated measures ANOVA).
G Luciferase activity in OR6 cells treated with 0nM, 2nM or 18nM BMP6 overnight followed by the addition of a titration of IFN-lambda (2.5-100ng/mL) for 20h. BMP6 increases the antiviral activity of IFN-lambda3 (n=3; repeated measures ANOVA).

Figure 3: BMP6 and Activin B suppress HCV replication
A Left – HCV RNA in supernatants of HuH7.5 cells incubated with a titration of BMP6 (2-52nM) was reduced in BMP6-treated cultures. Right – Supernatant HCV RNA at 5 days post-infection was significantly lower in cultures treated with BMP6 for the duration of the infection. Administration of 1000U/mL IFN-alpha 1 day prior to RNA extraction also resulted in a significant reduction in supernatant HCV RNA (one-way ANOVA; n=3).
B Levels of supernatant and cellular HCV RNA 10 days post-infection were lower in cells treated with 18nM BMP6 for the last 7 days or 1000U/mL IFN-alpha for 1 day compared to untreated infected cells (both repeated measures one-way ANOVA; n=3).
C Timecourse of luciferase activity in OR6 cells treated with 18nM BMP6 or 1000U/mL IFN-alpha (one-way ANOVA for each time point; n=3).
D Luciferase activity 72h in OR6 cells treated with 2uM dorsomorphin or 0.2uM LDN-193189 for 30 minutes prior to addition of 18nM BMP6 or 1000U/mL IFN-alpha for 72h (paired t-test; n=4).
E Luciferase activity in OR6 cells after 72h treatment with 18nM BMP6 or a dose titration of Activin A (left) or B (right). n=3, analysis by ordinary one-way ANOVA and Bonferroni's multiple comparisons test with respect to untreated cells.
F Luciferase activity 72h post-addition in OR6 cells treated with 0.1uM LDN-193189 for 30 minutes prior to addition of 18nM BMP6 or a dose titration of Activin A (left) or B (right). n=3, analysis by two-way ANOVA with Bonferroni's multiple comparisons test conducted between respective +/- LDN-193189 conditions.

Figure 4: Enrichment of SMAD1-bound loci proximal to IRF1-bound loci
A-C Histograms report the density of reads obtained from ChIP-seq of each transcription factor (TF), under the specified stimulation conditions and normalized to 10 million reads in each case, mapping to +/- 500bp of the genomic loci bound by the comparator transcription factor (IRF1 in K562 cells treated with IFNalpha for 6 hours). **A** The density of SMAD1 binding in BMP4-treated K562 is enriched +/- 500bp around loci bound by IRF1 following 6h IFNa stimulation of K562; in cells treated with dorsomorphin, which inhibits SMAD1 activation, SMAD1 binding is not enriched near IRF1-binding. **B** The density of reads derived from ChIP-seq for non-BMP pathway associated transcription factors (ARID3A, ELK1, INI1, RAD21, XRCC4) is not enriched near IRF1-bound loci in unstimulated cells. **C** The density of reads derived from ChIPseq for the Type I IFN-associated transcription factors STAT1 and STAT2 are enriched near IRF1-bound loci in IFN-alpha treated cells.
D mRNA expression of *RSAD2, SSBP3* and *ZC3HAV1* was upregulated after incubation of HuH7.5 cells with 54nM BMP6 for 72h. These gene loci were amongst those associated with colocalised SMAD1 and IRF1 ChIP peaks in active chromatin regions of BMP4-treated and IFN-treated K562 cells respectively (visualised in Fig S11).
E Model of how BMP/SMAD signaling interacts with antiviral immunity and HCV infection. IFN activity and HCV infection are known to be mutually antagonistic; BMP/SMAD signaling is known to control iron homeostasis through regulating hepcidin. Our data show that BMP/SMAD signaling activates a gene repertoire that both boosts IFN activity and has IFN-independent antiviral activity that suppresses HCV replication; conversely HCV inhibits BMP/SMAD signaling, evading antiviral immunity and suppressing hepcidin.

Figure 1: HCV – BMP pathway interactions decrease hepcidin and associate with therapeutic outcome

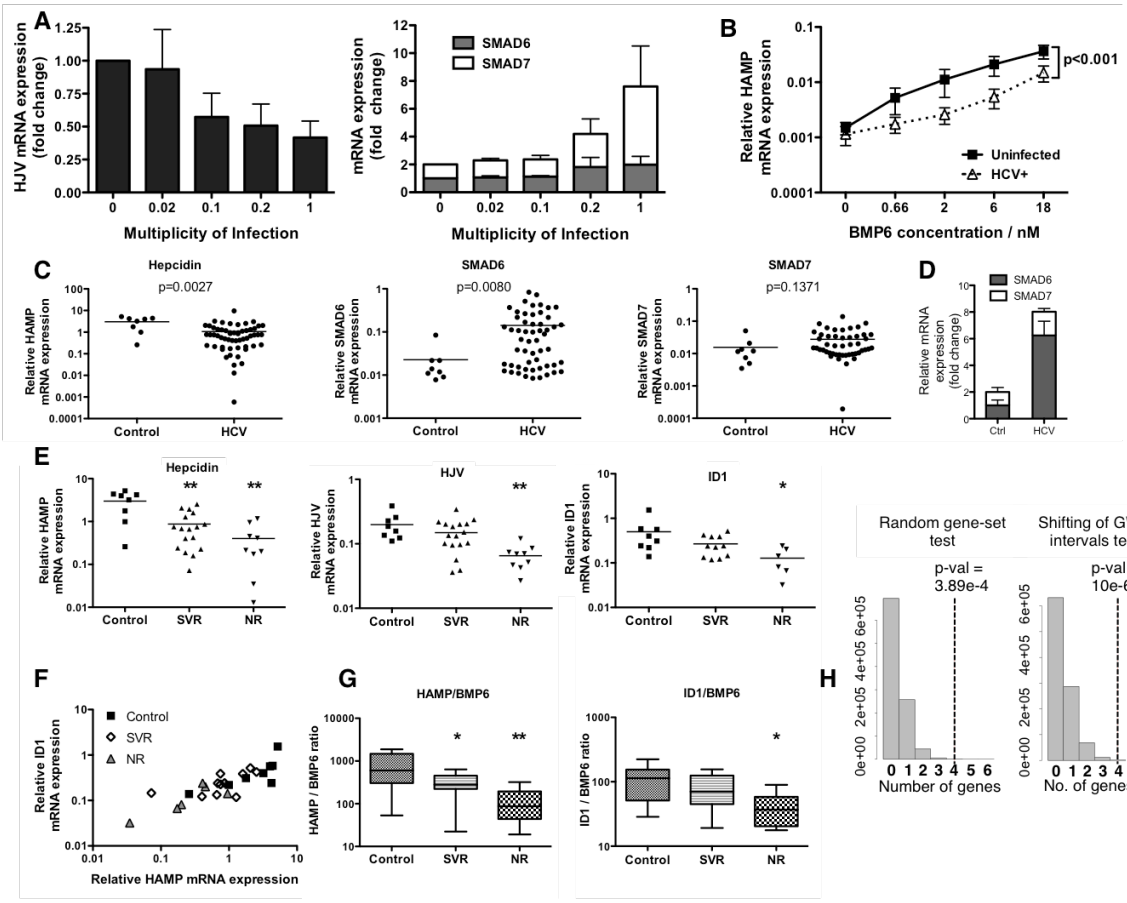


Figure 2: BMP6 enhances IFN activity

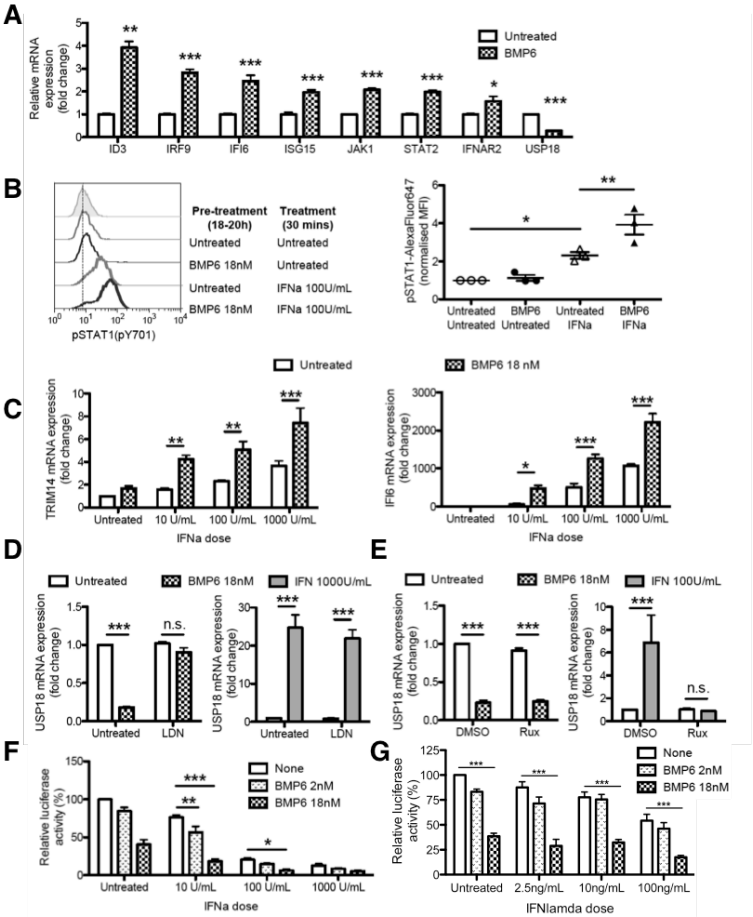


Figure 3: BMP6 and Activins suppress HCV replication

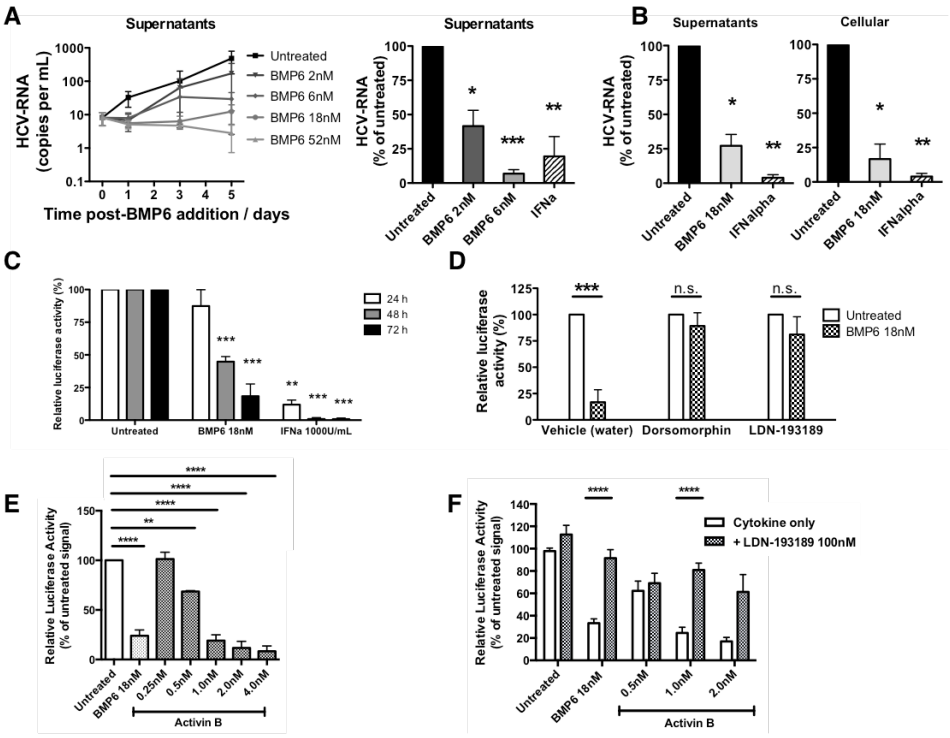
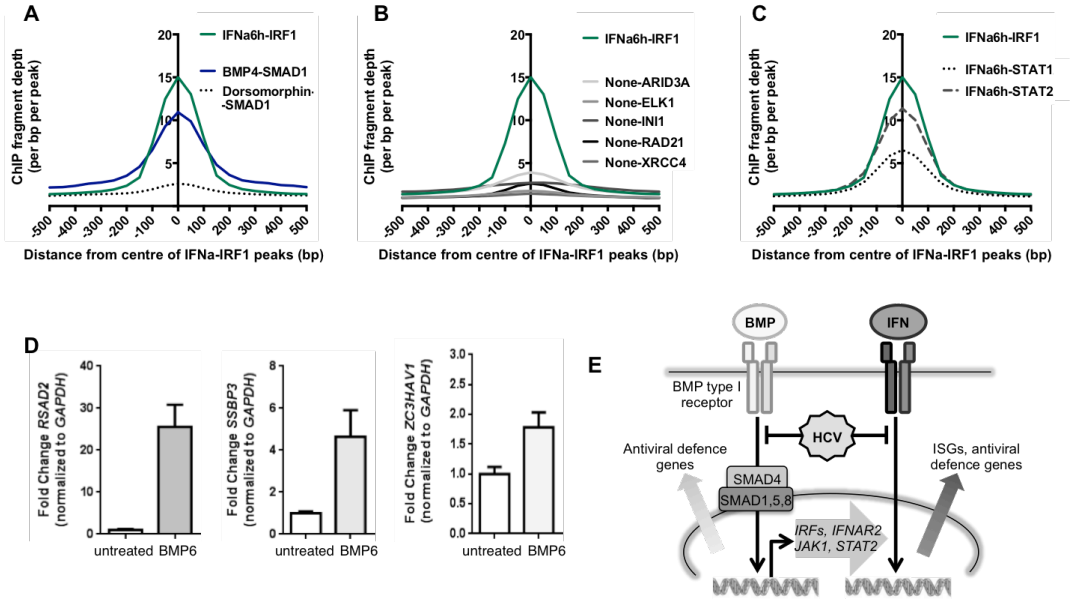


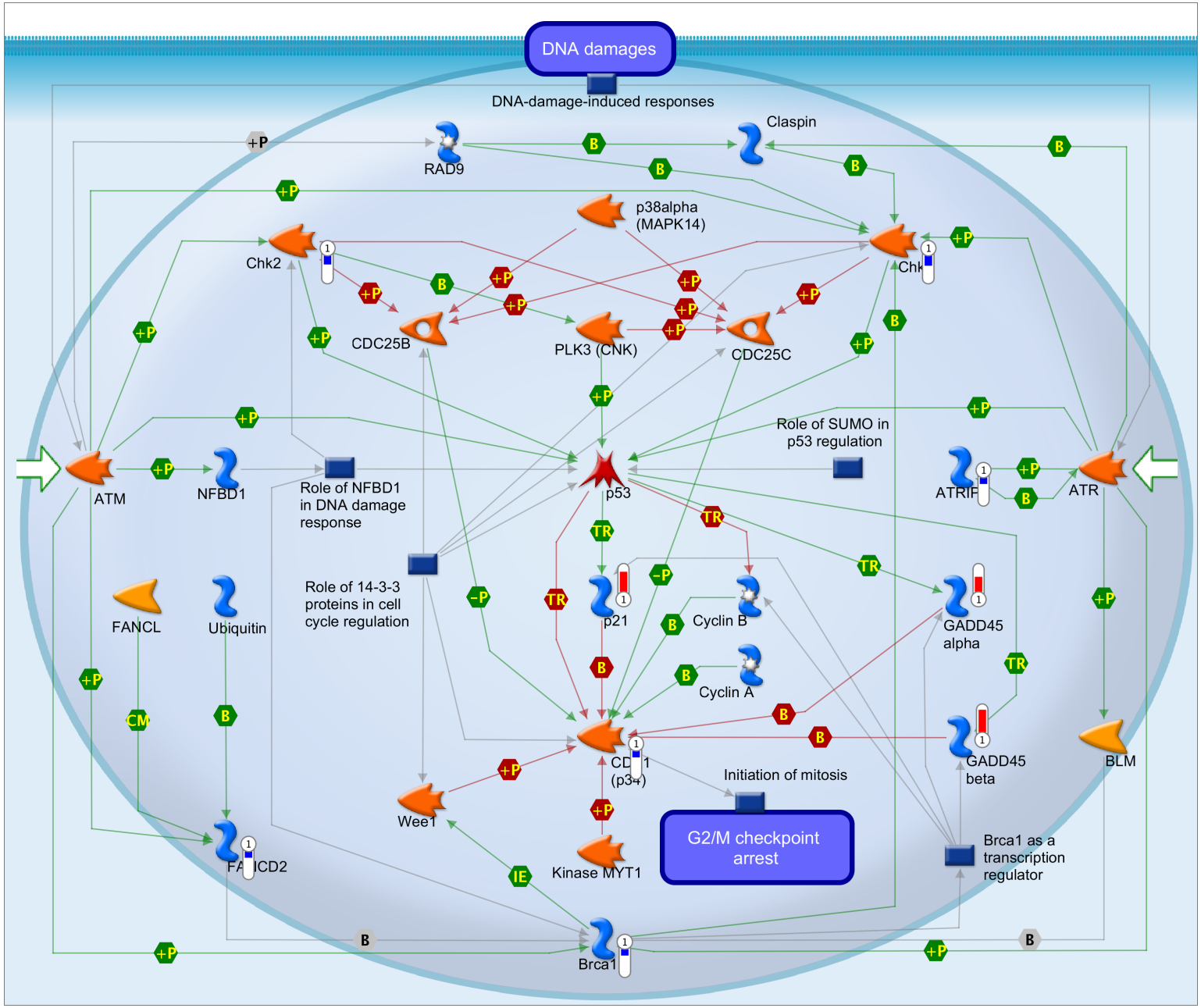
Figure 4: Enrichment of SMAD1-bound loci proximal to IRF1-bound loci



Appendix II

MetaCore™ GeneGo interaction network derived from microarray analysis of BMP6-treated Huh7 cells

Ontological category: G2/M checkpoint arrest


DNA damages
DNA-damage-induced responses
RAD9
Claspin
p38alpha (MAPK14)
Chk2
Chk
CDC25B
PLK3 (CNK)
CDC25C
Role of SUMO in p53 regulation
ATM
NFBD1
Role of NFBD1 in DNA damage response
p53
ATRIP
ATR
Role of 14-3-3 proteins in cell cycle regulation
FANCL
Ubiquitin
p21
Cyclin B
Cyclin A
GADD45 alpha
GADD45 beta
BLM
Wee1
Initiation of mitosis
G2/M checkpoint arrest
Kinase MYT1
Brca1 as a transcription regulator
Brca1

Appendix III

Table of genes driving associations with enriched gene sets identified by GREAT GSE analysis

K562 BMP4-SMAD1 Peakset						
Gene I.D.	JAK-STAT (GO BP)	Regulation of tyrosine phosphorylation of Stat3 (GO BP)	Regulation of type I IFN-mediated signalling pathway (GO BP)	Type I IFN mediated signalling pathway (GO BP)	Response to type I IFN (GO BP)	Genomic regions of peaks (BED format)
ADAR				x	x	chr1-647 (-21086), chr1-2080 (-8907), chr1-2079 (+321), chr1-1464 (+14668)
ARL2BP		x				chr16-528 (+12125), chr16-346 (+21202)
CDKL3		x				chr5-726 (-82), chr5-381 (+82408), chr5-725 (+99320), chr5-723 (+140823), chr5-239 (+179418)
CLCF1	x	x				chr11-487 (+354)
CSF1R		x				chr5-776 (-31136), chr5-532 (-3876), chr5-160 (-2288), chr5-531 (+10266), chr5-530 (+62981), chr5-123 (+86347)
EGF	x					chr4-360 (+253192)
EGR1				x	x	chr5-242 (-55)
F2	x					chr11-11 (+113856)
F2R	x					chr5-97 (-57896), chr5-347 (-53326), chr5-283 (+23120), chr5-649 (+46639), chr5-284 (+90151)
FGFR3	x	x				chr4-86 (-21594), chr4-9 (-7952), chr4-127 (+22)
GBP2				x	x	chr1-1062 (+4245)
HES1	x	x				chr3-402 (-537775), chr3-543 (-536537), chr3-798 (-480164), chr3-99 (-475285), chr3-197 (-447947), chr3-403 (-353799), chr3-148 (-282266), chr3-119 (-225178), chr3-404 (-209816), chr3-75 (-132958), chr3-315 (-84139), chr3-149 (-46313), chr3-100 (-1106), chr3-198 (+3161), chr3-252 (+14339), chr3-546 (+65960), chr3-42 (+119423), chr3-405 (+200732), chr3-406 (+210872)
HES5		x				chr1-932 (-16155), chr1-1214 (-14048)
HLA-A				x	x	chr6-191 (+22541), chr6-270 (+25244)
HLA-C				x	x	chr6-730 (-123929), chr6-1032 (-15655)
HSP90AB1			x			chr6-102 (-21152), chr6-1128 (+399)
IFIT3				x	x	chr10-577 (+30635)
IFITM3				x	x	chr11-568 (-35465)
IFNAR1	x		x	x	x	chr21-140 (-75319), chr21-73 (-58374), chr21-141 (-19899), chr21-9 (+43342), chr21-199 (+55174), chr21-28 (+61679)
IFNAR2	x		x	x	x	chr21-194 (-30994), chr21-72 (-17608), chr21-195 (-88), chr21-140 (+19664), chr21-73 (+36609), chr21-141 (+75084)
IFNGR1						chr6-852 (-72224), chr6-851 (-47)
IFNGR2						chr21-9 (-34646), chr21-199 (-22814), chr21-28 (-16309), chr21-142 (+667)
IL12B		x				chr5-61 (+28026)
IL15		x				chr4-198 (+276408)
IL20		x				chr1-2270 (-37596), chr1-69 (-18104)

K562 BMP4-SMAD1 Peakset						
Gene I.D.	JAK-STAT (GO BP)	Regulation of tyrosine phosphorylation of Stat3 (GO BP)	Regulation of type I IFN-mediated signalling pathway (GO BP)	Type I IFN mediated signalling pathway (GO BP)	Response to type I IFN (GO BP)	Genomic regions of peaks (BED format)
IL23R		x				chr1-496 (+25766)
IL6		x				chr7-274 (-79484), chr7-464 (-59211), chr7-602 (-46546)
IL6R		x				chr1-847 (-51671), chr1-346 (-50534), chr1-2078 (-39015), chr1-513 (-20341), chr1-1463 (+93), chr1-848 (+37097), chr1-347 (+91958)
IL6ST	x	x				chr5-273 (-769171), chr5-67 (-693588), chr5-16 (-681675), chr5-332 (-610383), chr5-450 (-591264), chr5-215 (-507449), chr5-136 (-506964), chr5-272 (-496350), chr5-619 (-414546), chr5-54 (-316036), chr5-33 (-167142), chr5-20 (-128926), chr5-616 (-90428), chr5-447 (-45182), chr5-6 (-42630)
IRF1				x	x	chr5-508 (-216), chr5-717 (+22925), chr5-716 (+53074), chr5-191 (+63993), chr5-29 (+67964)
IRF2				x	x	chr4-124 (+22616)
IRF4				x	x	chr6-246 (+213013), chr6-155 (+266736), chr6-885 (+272295)
JAK1			x	x	x	chr1-336 (-55453), chr1-1948 (+73460), chr1-1947 (+81652), chr1-35 (+102205)
JAK2	x	x				chr9-228 (-186782)
KIT		x				chr4-231 (-207735), chr4-140 (-115273), chr4-173 (-108754), chr4-16 (-86523), chr4-316 (-72145), chr4-232 (-69400)
LEP		x				chr7-741 (-197028), chr7-538 (-36619), chr7-396 (+76208)
LIF	x	x				chr22-68 (+29926), chr22-386 (+62756)
MAVS			x			chr20-323 (-7251), chr20-325 (-3104), chr20-259 (+31988)
NLRC5			x			chr16-109 (+48152)
NR1H2						chr19-780 (+1446)
PPARG						chr3-415 (+54482)
PTPN1			x	x	x	chr20-170 (-312648), chr20-6 (-217614), chr20-32 (-211571), chr20-428 (-191478), chr20-222 (-162049), chr20-39 (-123715), chr20-223 (-122992), chr20-289 (-115560), chr20-224 (-69308), chr20-116 (-54498), chr20-225 (+7615), chr20-290 (+31525), chr20-171 (+48534), chr20-291 (+132192), chr20-431 (+156602), chr20-4 (+181096)
PTPN11			x	x	x	chr12-355 (-4770), chr12-767 (+347)
PTPN2						chr18-97 (+99)
PTPN6			x	x	x	chr12-385 (+14306), chr12-274 (+18670)
SOCS1	x	x	x	x	x	chr16-162 (+407), chr16-105 (+22839), chr16-454 (+54144), chr16-161 (+95372), chr16-46 (+150939), chr16-65 (+283229), chr16-17 (+283764), chr16-160 (+311713), chr16-21 (+369046)

K562 BMP4-SMAD1 Peakset						
Gene I.D.	JAK-STAT (GO BP)	Regulation of tyrosine phosphorylation of Stat3 (GO BP)	Regulation of type I IFN-mediated signalling pathway (GO BP)	Type I IFN mediated signalling pathway (GO BP)	Response to type I IFN (GO BP)	Genomic regions of peaks (BED format)
SOCS3	x		x	x	x	chr17-198 (+48), chr17-163 (+44103), chr17-16 (+87691), chr17-534 (+88138), chr17-80 (+96677), chr17-79 (+101317), chr17-372 (+109018)
SOCS6	x					chr18-290 (+89590), chr18-291 (+140311)
SP100				x	x	chr2-511 (-17177), chr2-91 (+243208)
STAT1	x		x	x	x	chr2-488 (-6284), chr2-847 (-32)
STAT2	x		x	x	x	chr12-654 (+165)
STAT3	x					chr17-443 (-33302), chr17-646 (-26765), chr17-238 (-347), chr17-442 (+19559), chr17-8 (+68341), chr17-7 (+75496)
STAT4	x					chr2-488 (+131062)
STAT5A	x					chr17-7 (+25452), chr17-8 (+32607), chr17-442 (+81389)
STAT5B	x					chr17-441 (+20), chr17-319 (+9031)
SUMO1						chr2-60 (+16563), chr2-861 (+168570), chr2-641 (+168975), chr2-209 (+188547)
TXK						chr4-312 (-113070), chr4-72 (-109372), chr4-71 (-78061), chr4-15 (-69696), chr4-471 (-53710), chr4-48 (+7356)
XAF1				x	x	chr17-396 (-17078)

CD34+ BMP4-SMAD1 Peakset			
Gene I.D.	Antigen Processing and Presentation (MgSigDB)	CD40L Signalling Pathway (MgSigDB)	Genomic regions of peaks (BED format)
B2M	x		chr15-1098 (+65), chr15-671 (+2342), chr15-1260 (+15255)
CALR	x		chr19-1946 (-4728)
CANX	x		chr5-948 (-30355), chr5-2579 (-20617), chr5-1234 (-19675), chr5-2068 (-386)
CD4	x		chr12-18 (-10375)
CD40		x	chr20-969 (+10459), chr20-138 (+14556), chr20-720 (+33776), chr20-287 (+56462), chr20-970 (+97820)
CD40LG		x	chrX-365 (-70435), chrX-45 (-39449), chrX-37 (+46793), chrX-1159 (+60354), chrX-297 (+63180), chrX-1269 (+119134), chrX-650 (+119571)
CD74	x		chr5-407 (-23301)
CD8A	x		chr2-89 (-16803), chr2-968 (+26799), chr2-3433 (+45805)
CD8B	x		chr2-89 (+53407)
CHUK		x	chr10-1308 (-11319)
CIITA	x		chr16-163 (+41730), chr16-531 (+76906), chr16-292 (+87004), chr16-365 (+94472), chr16-989 (+95066), chr16-366 (+104733), chr16-1210 (+140032), chr16-1782 (+217278), chr16-541 (+225202), chr16-918 (+228094), chr16-1783 (+253025), chr16-1477 (+276165), chr16-1613 (+303496), chr16-1211 (+314132), chr16-753 (+347092), chr16-1286 (+347879), chr16-754 (+356102)
CREB1	x		chr2-2591 (-327023), chr2-3064 (-299494), chr2-3860 (-275160), chr2-1367 (-246346), chr2-3065 (-218458), chr2-2592 (-184694), chr2-1980 (-112367), chr2-1838 (-71079), chr2-75 (-56567), chr2-342 (-54825), chr2-3066 (-836), chr2-3861 (-176), chr2-3862 (+4696)
CTSB	x		chr8-1090 (-102528), chr8-168 (-90913), chr8-141 (-75684), chr8-1790 (-68127), chr8-855 (-43824), chr8-40 (-34269), chr8-1556 (-11442), chr8-1234 (+5388), chr8-1233 (+18864), chr8-781 (+22514), chr8-1555 (+34500)
CTSL1	x		chr9-1053 (-225360), chr9-989 (-215903), chr9-1116 (-207271), chr9-2180 (-78107), chr9-155 (-62990), chr9-1117 (-51306), chr9-227 (-47168), chr9-404 (-41291), chr9-1342 (-11103), chr9-601 (+470), chr9-1408 (+5752)
DUSP1		x	chr5-2199 (-36271), chr5-2062 (-31695), chr5-2807 (-18910), chr5-2806 (-18238), chr5-1659 (-6430), chr5-914 (-971), chr5-858 (+425), chr5-199 (+54235), chr5-1401 (+56293), chr5-312 (+57980), chr5-1658 (+63804), chr5-22 (+73518), chr5-2805 (+82371), chr5-1839 (+101672), chr5-504 (+104695), chr5-2804 (+110776), chr5-2564 (+111729)
HLA-A	x		chr6-116 (-107474), chr6-10 (-94249), chr6-2389 (+22547), chr6-2821 (+25433), chr6-1950 (+34211)
HLA-C	x		chr6-724 (-125002), chr6-2827 (-116987), chr6-3097 (-102241), chr6-43 (-94926), chr6-2394 (-111), chr6-1845 (+404), chr6-41 (+74989), chr6-329 (+79410), chr6-2393 (+96026)

CD34+ BMP4-SMAD1 Peakset			
Gene I.D.	Antigen Processing and Presentation (MgSigDB)	CD40L Signalling Pathway (MgSigDB)	Genomic regions of peaks (BED format)
HLA-DMA	x		chr6-600 (-14594), chr6-879 (-288), chr6-1144 (+5134)
HLA-DMB	x		chr6-1144 (-6918), chr6-123 (+7314), chr6-371 (+55187), chr6-341 (+72703)
HLA-DOA	x		chr6-186 (-5344), chr6-82 (+24643)
HLA-DPA1	x		chr6-3109 (-3134), chr6-186 (+58721)
HLA-DPB1	x		chr6-3109 (+885), chr6-158 (+6954), chr6-1108 (+16246), chr6-982 (+42784), chr6-218 (+47984), chr6-930 (+50377), chr6-2838 (+68493), chr6-931 (+72338), chr6-577 (+85701), chr6-444 (+96885), chr6-1849 (+99967)
HLA-DQA2	x		chr6-828 (-49180), chr6-241 (-40688)
HLA-DQB1	x		chr6-241 (-34009), chr6-828 (-25517)
HLA-DRA	x		chr6-135 (-26203), chr6-59 (-24227), chr6-929 (-7653), chr6-1955 (+20869), chr6-2837 (+38150)
HLA-DRB5	x		chr6-2837 (+52237), chr6-1955 (+69518)
HLA-E	x		chr6-3092 (-144175), chr6-2822 (-139441), chr6-1482 (-131661), chr6-2390 (-124596), chr6-2589 (-112789), chr6-118 (-92372), chr6-1388 (-77806), chr6-954 (-35599), chr6-3093 (-8070), chr6-856 (-7179), chr6-2080 (-5528), chr6-3094 (-25), chr6-701 (+7427), chr6-745 (+43219), chr6-169 (+52208), chr6-443 (+55456)
HLA-F	x		chr6-611 (-26615), chr6-1041 (-20639), chr6-612 (-17509), chr6-180 (+14899), chr6-67 (+29903)
HLA-G	x		chr6-116 (+8017), chr6-10 (+21242)
HSP90AA1	x		chr14-1500 (-155782), chr14-125 (-95751), chr14-695 (-74718), chr14-1154 (-69664), chr14-1293 (-67396), chr14-1836 (-51374), chr14-1398 (-17798), chr14-500 (+40818), chr14-300 (+42995), chr14-1397 (+45565), chr14-1041 (+52694), chr14-180 (+76428), chr14-316 (+93148), chr14-1645 (+167133)
HSP90AB1	x		chr6-1781 (-21052), chr6-579 (-12790), chr6-1440 (-12168), chr6-708 (-9006), chr6-1556 (-10), chr6-2873 (+534), chr6-1079 (+6561)
HSPA1A	x		chr6-2397 (+97), chr6-2831 (+2325)
HSPA1B	x		chr6-1954 (+31), chr6-904 (+2366), chr6-2834 (+9156)
HSPA1L	x		chr6-2831 (-2781), chr6-2397 (-553)
HSPA2	x		chr14-467 (-29196), chr14-173 (-5), chr14-270 (+96398), chr14-422 (+131225)
HSPA4	x		chr5-2310 (+70), chr5-30 (+59418), chr5-2311 (+188687), chr5-451 (+196086), chr5-1728 (+208952), chr5-87 (+235722), chr5-1810 (+268356), chr5-2312 (+314658), chr5-1498 (+369629), chr5-369 (+371995), chr5-1138 (+408363), chr5-723 (+501154), chr5-2026 (+559122)
HSPA5	x		chr9-445 (-14801), chr9-2253 (+352)
HSPA6	x		chr1-3941 (-13022), chr1-3706 (-316), chr1-4544 (+305), chr1-4921 (+6097), chr1-1746 (+6937), chr1-2473 (+16037), chr1-3707 (+17931)

CD34+ BMP4-SMAD1 Peakset			
Gene I.D.	Antigen Processing and Presentation (MgSigDB)	CD40L Signalling Pathway (MgSigDB)	Genomic regions of peaks (BED format)
HSPA8	x		chr11-572 (-49397), chr11-1421 (-41234), chr11-2192 (+158), chr11-1185 (+7709), chr11-1880 (+28167), chr11-440 (+38908), chr11-1083 (+41040)
IFI30	x		chr19-1969 (-16471), chr19-238 (-5432)
IFNA1	x		chr9-1389 (-5802), chr9-553 (+15044), chr9-1047 (+25656)
IFNA10	x		chr9-1312 (-6673)
IFNA14	x		chr9-1105 (+4090)
IFNA16	x		chr9-1312 (+3495)
IFNA17	x		chr9-1105 (-7667)
IFNA2	x		chr9-135 (-10926)
IFNA21	x		chr9-2118 (-16620), chr9-1678 (+12546)
IFNA4	x		chr9-1931 (-7706), chr9-2118 (+4319)
IFNA5	x		chr9-451 (-21439), chr9-851 (-13180)
IFNA7	x		chr9-1931 (+6900)
IFNA8	x		chr9-135 (-12824), chr9-1389 (+25505)
IKBKAP		x	chr9-1229 (+347), chr9-1422 (+33234), chr9-1736 (+44574)
IKBKB		x	chr8-1964 (-59), chr8-999 (+497), chr8-324 (+48512)
IKBKG		x	chrX-221 (-14949), chrX-9 (-7258)
KIR3DL3	x		chr19-1191 (-50321), chr19-848 (-48079)
KLRC1	x		chr12-1203 (-154647), chr12-443 (-109118), chr12-1858 (-105634), chr12-700 (-47805)
KLRD1	x		chr12-208 (-71864), chr12-136 (+24035), chr12-699 (+59305), chr12-2384 (+75946)
KLRK1	x		chr12-2384 (+6290), chr12-699 (+22931), chr12-136 (+58201)
LGMN	x		chr14-331 (-35306), chr14-1381 (+19844), chr14-29 (+33801), chr14-693 (+58152), chr14-625 (+61659), chr14-299 (+67443), chr14-741 (+78364), chr14-1821 (+82806), chr14-945 (+92226), chr14-121 (+135433), chr14-487 (+144965), chr14-506 (+159280), chr14-740 (+179822), chr14-624 (+194997), chr14-716 (+197085), chr14-739 (+198624), chr14-1820 (+213322), chr14-1149 (+227991)
LTA	x		chr6-2592 (-11547)
MAP3K1		x	chr5-1612 (-777445), chr5-1363 (-691171), chr5-26 (-613792), chr5-762 (-550486), chr5-268 (-545323), chr5-1 (-544340), chr5-2636 (-526068), chr5-317 (-511375), chr5-1690 (-503999), chr5-1415 (-500329), chr5-1776 (-491318), chr5-1777 (-487128), chr5-955 (-335235), chr5-1249 (-333107), chr5-1873 (-313034), chr5-2638 (-228834), chr5-1778 (-209576), chr5-2427 (-206703), chr5-1462 (-182841), chr5-2639 (-138438), chr5-1364 (-126488), chr5-1416 (-2807), chr5-1691 (+3539), chr5-1974 (+22680), chr5-413 (+23546), chr5-2107 (+41878), chr5-195 (+85957), chr5-1613 (+95005), chr5-2641 (+95729), chr5-1692 (+135668)

CD34+ BMP4-SMAD1 Peakset			
Gene I.D.	Antigen Processing and Presentation (MgSigDB)	CD40L Signalling Pathway (MgSigDB)	Genomic regions of peaks (BED format)
MAP3K14		x	chr17-961 (-78235), chr17-49 (-68645), chr17-1856 (-28687), chr17-2323 (-177), chr17-1349 (+5484), chr17-1749 (+6067), chr17-1748 (+32721), chr17-76 (+39667), chr17-415 (+46004), chr17-2551 (+64229), chr17-1855 (+69915), chr17-484 (+81222), chr17-1348 (+82227)
NFKB1		x	chr4-1676 (-80583), chr4-348 (-69799), chr4-1677 (-56374), chr4-185 (-51380), chr4-1917 (-783), chr4-1005 (+40583), chr4-2213 (+77718), chr4-1678 (+103427), chr4-766 (+108889), chr4-215 (+119499), chr4-166 (+124430), chr4-2419 (+204377), chr4-1183 (+213879), chr4-691 (+242233)
NFKBIA		x	chr14-1327 (-34242), chr14-491 (-17806), chr14-164 (-8664), chr14-147 (-2352), chr14-1428 (+36823), chr14-964 (+62924), chr14-1112 (+71642)
NFYA	x		chr6-1219 (+19657)
NFYB	x		chr12-378 (-63111), chr12-1814 (-39488), chr12-2509 (+53), chr12-93 (+28915)
NFYC	x		chr1-3434 (-43), chr1-1012 (+78392), chr1-201 (+82799)
PDIA3	x		chr15-581 (+23379)
PIK3R2	x		chr19-89 (-40028), chr19-1165 (-480), chr19-1969 (+4092), chr19-238 (+15131)
PSME1	x		chr14-1680 (-2218), chr14-1524 (-460), chr14-1313 (+5059), chr14-923 (+5890)
PSME2	x		chr14-1681 (-514), chr14-923 (+4587), chr14-1313 (+5418)
PSME3	x		chr17-1978 (-297)
RELA		x	chr11-744 (-43487), chr11-2280 (-37672), chr11-2279 (-284), chr11-2278 (+10181)
RFX5	x		chr1-1697 (-23329), chr1-3060 (-20505), chr1-3481 (+220), chr1-2380 (+983), chr1-768 (+6252)
RFXANK	x		chr19-1015 (-6110), chr19-1557 (+7)
RFXAP	x		chr13-347 (-82901), chr13-255 (-3970), chr13-358 (+22398), chr13-649 (+29602), chr13-194 (+39173)
TAP1	x		chr6-211 (-156)
TAP2	x		chr6-55 (-82), chr6-1692 (+12735), chr6-811 (+41604), chr6-576 (+52702)
TNFAIP3		x	chr6-2496 (-277855), chr6-605 (-225776), chr6-871 (-205638), chr6-463 (-161943), chr6-783 (-159383), chr6-537 (-67291), chr6-893 (-21856), chr6-2950 (-15989), chr6-3266 (-10763), chr6-606 (-257), chr6-2712 (+54658), chr6-1584 (+72590), chr6-277 (+77676), chr6-244 (+134511), chr6-1734 (+137146), chr6-1518 (+139658), chr6-3268 (+141510)
TRAF3		x	chr14-501 (-182729), chr14-1093 (-147605), chr14-1502 (-91156), chr14-412 (-82776), chr14-1401 (-60129), chr14-462 (-4081), chr14-137 (-2386), chr14-1838 (+28871), chr14-1295 (+50867)
TRAF6		x	chr11-1337 (-30929), chr11-2120 (+270), chr11-942 (+17416), chr11-816 (+31418), chr11-2806 (+41032)

U937 BMP4-SMAD1 Peakset				
Gene I.D.	Type I IFN-mediated signalling pathway (GO BP)	Response to type I IFN (GO BP)	JAK-STAT Signalling Pathway (Panther Pathway)	Genomic regions of peaks (BED format)
ADAR	x	x		chr1-2962 (-255635), chr1-1314 (-232445), chr1-5863 (-183715), chr1-1879 (-143724), chr1-3393 (-140074), chr1-4957 (-127712), chr1-2708 (-125585), chr1-5862 (-120979), chr1-554 (-112803), chr1-3607 (-111619), chr1-3092 (-106847), chr1-4956 (-17182), chr1-2825 (-15313), chr1-4036 (+33277)
EGR1	x	x		chr5-770 (-6920)
GBP2	x	x		chr1-4884 (-3979), chr1-3992 (-1115), chr1-5308 (-42)
HLA-A	x	x		chr6-2198 (-24431), chr6-336 (+22554), chr6-4512 (+39815)
HLA-C	x	x		chr6-2326 (+42784), chr6-849 (+55692), chr6-848 (+68097), chr6-2465 (+69094)
HLA-F	x	x		chr6-1069 (+11466), chr6-1772 (+39500), chr6-2948 (+40502)
HLA-G	x	x		chr6-2198 (+91060)
IFI35	x	x		chr17-502 (+7726), chr17-288 (+12451)
IFI6	x	x		chr1-698 (+9361), chr1-4186 (+13152)
IFIT1	x	x		chr10-694 (-7434), chr10-1229 (-104), chr10-1173 (+662)
IFIT2	x	x		chr10-3018 (-42885), chr10-404 (-6079), chr10-801 (-5415), chr10-830 (-443), chr10-1550 (+208), chr10-3019 (+24268)
IFIT3	x	x		chr10-3019 (-6265), chr10-1551 (-4537), chr10-693 (-4148), chr10-1718 (-64), chr10-1933 (+529), chr10-1279 (+1019), chr10-1124 (+14105)
IFNA1	x	x		chr9-953 (-28049), chr9-203 (+4001)
IFNA13	x	x		chr9-408 (-13802), chr9-2012 (+10100)
IFNA14	x	x		chr9-1830 (-55392), chr9-2181 (-55103), chr9-2413 (-47602), chr9-611 (-13485), chr9-2180 (-12475)
IFNA2	x	x		chr9-342 (-105), chr9-408 (+3519)
IFNA21	x	x		chr9-590 (+6282), chr9-818 (+13138)
IFNA5	x	x		chr9-1831 (-18046), chr9-1830 (+9942), chr9-2181 (+10231), chr9-2413 (+17732), chr9-611 (+51849), chr9-2180 (+52859)
IFNA6	x	x		chr9-2012 (-7089)
IFNA8	x	x		chr9-953 (+3258)

U937 BMP4-SMAD1 Peakset				
Gene I.D.	Type I IFN-mediated signalling pathway (GO BP)	Response to type I IFN (GO BP)	JAK-STAT Signalling Pathway (Panther Pathway)	Genomic regions of peaks (BED format)
IFNAR1	x	x		chr21-896 (-86537), chr21-651 (-86118), chr21-455 (-82878), chr21-136 (-80679), chr21-343 (-79919), chr21-88 (-77092), chr21-173 (-64686), chr21-17 (-63130), chr21-180 (-59081), chr21-318 (-23775), chr21-373 (-23381), chr21-381 (-20104), chr21-181 (-15861), chr21-690 (-7671), chr21-344 (+37319), chr21-319 (+43371), chr21-802 (+49352), chr21-616 (+49639), chr21-63 (+55134), chr21-155 (+55806), chr21-306 (+58503), chr21-16 (+69524)
IFNAR2	x	x		chr21-217 (-150743), chr21-190 (-140306), chr21-688 (-133282), chr21-191 (-128529), chr21-154 (-120018), chr21-134 (-104800), chr21-275 (-101233), chr21-104 (-31015), chr21-475 (-26007), chr21-56 (-14144), chr21-290 (-13636), chr21-896 (+8446), chr21-651 (+8865), chr21-455 (+12105), chr21-136 (+14304), chr21-343 (+15064), chr21-88 (+17891), chr21-173 (+30297), chr21-17 (+31853), chr21-180 (+35902), chr21-318 (+71208), chr21-373 (+71602), chr21-381 (+74879), chr21-181 (+79122), chr21-690 (+87312)
IFNB1	x	x		chr9-784 (-41364), chr9-881 (-27009), chr9-1573 (-20031), chr9-842 (-19161), chr9-463 (-4245), chr9-988 (+16642), chr9-1684 (+30233)
IP6K2	x	x		chr3-2342 (-127879), chr3-3483 (-94900)
IRF1	x	x		chr5-2856 (-34641), chr5-2610 (-6287), chr5-2609 (-5116), chr5-1960 (+11297), chr5-545 (+22954), chr5-146 (+24117), chr5-461 (+33262), chr5-734 (+34144), chr5-2608 (+53010), chr5-1318 (+62891), chr5-70 (+64056), chr5-689 (+67890), chr5-639 (+69659), chr5-2607 (+75956), chr5-2385 (+100871), chr5-1851 (+102947)
IRF2	x	x		chr4-929 (-60206), chr4-550 (-39937), chr4-286 (-29648), chr4-1512 (-5256), chr4-1785 (-142), chr4-2439 (+13540), chr4-1318 (+20978), chr4-1027 (+22595), chr4-2154 (+56500), chr4-1388 (+78482), chr4-454 (+79576), chr4-810 (+90425), chr4-1952 (+91834), chr4-241 (+119227), chr4-928 (+127211), chr4-2153 (+128953), chr4-1511 (+160081), chr4-1951 (+180832), chr4-608 (+244268)
IRF4	x	x		chr6-753 (-94869), chr6-257 (-92958), chr6-1995 (-78550), chr6-792 (-54863), chr6-909 (-52064), chr6-344 (-50391), chr6-1370 (-19001), chr6-1171 (-7085), chr6-1093 (+31227), chr6-733 (+33605), chr6-1094 (+35070), chr6-1280 (+35405), chr6-3119 (+40552), chr6-2903 (+43050), chr6-2169 (+83260), chr6-1911 (+107431), chr6-2904 (+219305)
IRF5	x	x		chr7-1422 (-13764), chr7-2681 (-12976), chr7-608 (+2745), chr7-409 (+3314), chr7-64 (+10756), chr7-191 (+11197), chr7-1242 (+75618), chr7-549 (+76956)

U937 BMP4-SMAD1 Peakset				
Gene I.D.	Type I IFN-mediated signalling pathway (GO BP)	Response to type I IFN (GO BP)	JAK-STAT Signalling Pathway (Panther Pathway)	Genomic regions of peaks (BED format)
IRF6	x	x		chr1-4097 (-2056), chr1-284 (+36621), chr1-1488 (+37715), chr1-1895 (+38255), chr1-3457 (+44989)
IRF7	x	x		chr11-2015 (-1071)
IRF8	x	x		chr16-2 (-69256), chr16-1902 (-60570), chr16-663 (-47490), chr16-43 (-45301), chr16-789 (-42945), chr16-2127 (-25847), chr16-1903 (-24928), chr16-1333 (-10194), chr16-313 (+6270), chr16-13 (+29458), chr16-486 (+37110), chr16-935 (+37415), chr16-218 (+44738), chr16-233 (+79109), chr16-50 (+83593), chr16-40 (+84591), chr16-301 (+85262), chr16-1906 (+97802), chr16-170 (+111845), chr16-688 (+115456), chr16-1242 (+118794), chr16-147 (+119570), chr16-1337 (+191041), chr16-790 (+270369), chr16-1107 (+314056), chr16-1568 (+408059), chr16-936 (+420984), chr16-664 (+442082), chr16-638 (+454231), chr16-1442 (+456832), chr16-260 (+480400), chr16-1338 (+516377), chr16-566 (+549124), chr16-882 (+549527)
ISG20	x	x		chr15-2334 (-16253), chr15-2862 (-15528), chr15-931 (-59)
JAK1	x	x	x	chr1-370 (-130792), chr1-1606 (-89499), chr1-5736 (-88169), chr1-4868 (+9703), chr1-5287 (+32060), chr1-3362 (+33046), chr1-4239 (+49056), chr1-4867 (+68281), chr1-1995 (+70830), chr1-1866 (+102235), chr1-7092 (+220013)
JAK2			x	chr9-1306 (-134564), chr9-353 (-45968), chr9-749 (-42771)
JAK3			x	chr19-582 (-2616), chr19-2189 (-34), chr19-1585 (+20136)
MAPK14			x	chr6-173 (+1303), chr6-62 (+2014), chr6-32 (+4741)
MX1	x	x		chr21-219 (-29419), chr21-261 (-5780)
MX2	x	x		chr21-370 (+14), chr21-219 (+34609), chr21-261 (+58248)
OAS1	x	x		chr12-3290 (-50853), chr12-795 (-36159), chr12-250 (-19252), chr12-3693 (-13867), chr12-764 (-57), chr12-1227 (+603)
OAS2	x	x		chr12-2145 (-38339), chr12-928 (-64), chr12-1121 (+62301)
OAS3	x	x		chr12-2145 (+1686)
OASL	x	x		chr12-3010 (-71387), chr12-931 (-57537), chr12-1124 (-56690), chr12-735 (-53984), chr12-3317 (-48933), chr12-1231 (-10627), chr12-2736 (+2168), chr12-1176 (+4879)

U937 BMP4-SMAD1 Peakset				
Gene I.D.	Type I IFN-mediated signalling pathway (GO BP)	Response to type I IFN (GO BP)	JAK-STAT Signalling Pathway (Panther Pathway)	Genomic regions of peaks (BED format)
PIAS1			x	chr15-1457 (-214099), chr15-740 (-202695), chr15-1259 (-174576), chr15-609 (-173369), chr15-1709 (-171653), chr15-412 (-99180), chr15-306 (-98753), chr15-848 (-44931), chr15-1207 (+449), chr15-2751 (+129866)
PIAS2			x	chr18-625 (+145043), chr18-1447 (+147340)
PIAS3			x	chr1-457 (-13668), chr1-1011 (-13258)
PSMB8	x	x		chr6-543 (-1622), chr6-2470 (-1186)
PTPN1	x	x		chr20-35 (-288668), chr20-1004 (-249610), chr20-480 (-239621), chr20-110 (-238049), chr20-312 (-235277), chr20-548 (-226294), chr20-245 (-212650), chr20-209 (-207799), chr20-246 (-171500), chr20-654 (-163639), chr20-189 (-162120), chr20-101 (-160896), chr20-257 (-156696), chr20-1254 (-143608), chr20-584 (-138063), chr20-76 (-130955), chr20-1087 (-128016), chr20-1324 (-124192), chr20-2181 (-106582), chr20-247 (-100603), chr20-508 (-97107), chr20-328 (-75497), chr20-786 (-69721), chr20-496 (-69325), chr20-463 (-59340), chr20-105 (-54370), chr20-1191 (-52322), chr20-787 (+6445), chr20-481 (+7600), chr20-58 (+31467), chr20-1192 (+62830), chr20-1632 (+126717), chr20-1193 (+130618), chr20-266 (+142443), chr20-443 (+200475)
PTPN11	x	x		chr12-1782 (+28612), chr12-1226 (+163632), chr12-794 (+181381)
PTPN6	x	x		chr12-3057 (-3014), chr12-2329 (-2608), chr12-1135 (+4704), chr12-536 (+7409), chr12-1915 (+12303), chr12-347 (+12665), chr12-2330 (+15293)
PTPRC			x	chr1-574 (-81852), chr1-1324 (-17345), chr1-1571 (+2), chr1-2407 (+2831), chr1-7440 (+16871), chr1-2617 (+17789), chr1-3281 (+18598), chr1-10 (+42989), chr1-2261 (+124541), chr1-338 (+137822), chr1-1892 (+170486), chr1-1278 (+171105), chr1-3129 (+198650), chr1-5476 (+202621), chr1-222 (+242398), chr1-781 (+278565), chr1-2618 (+290981), chr1-3643 (+295955), chr1-710 (+296697), chr1-5043 (+332032), chr1-2619 (+347614), chr1-1479 (+368616), chr1-3282 (+370634), chr1-2019 (+382116), chr1-7441 (+393638), chr1-614 (+402671), chr1-5044 (+403387), chr1-1433 (+456819), chr1-6653 (+458411), chr1-250 (+484790), chr1-642 (+640243), chr1-3283 (+644060), chr1-3644 (+761115), chr1-5478 (+761537), chr1-6654 (+825842), chr1-6655 (+929321), chr1-6656 (+934207), chr1-2729 (+946575), chr1-125 (+974613)
RNASEL	x	x		chr1-1955 (+48911), chr1-6620 (+68398), chr1-67 (+104425), chr1-512 (+128556), chr1-1775 (+129068)

U937 BMP4-SMAD1 Peakset				
Gene I.D.	Type I IFN-mediated signalling pathway (GO BP)	Response to type I IFN (GO BP)	JAK-STAT Signalling Pathway (Panther Pathway)	Genomic regions of peaks (BED format)
SOCS1	x	x	x	chr16-1602 (-9533), chr16-1122 (-8276), chr16-642 (+19017), chr16-999 (+21978), chr16-455 (+22959), chr16-454 (+36801), chr16-641 (+47142), chr16-593 (+49998), chr16-469 (+54091), chr16-1057 (+74068), chr16-1951 (+110583), chr16-1950 (+117312), chr16-1266 (+119379), chr16-570 (+120608), chr16-1180 (+127211), chr16-1056 (+129345), chr16-1756 (+131751), chr16-468 (+151066), chr16-354 (+161741), chr16-998 (+162078), chr16-362 (+173235), chr16-291 (+176443), chr16-1265 (+189563), chr16-70 (+203644), chr16-668 (+205101), chr16-890 (+207296), chr16-1755 (+221342), chr16-547 (+221972), chr16-1357 (+260483), chr16-1055 (+306607), chr16-438 (+322882), chr16-799 (+370750), chr16-723 (+374370)
SOCS3	x	x		chr17-826 (+16249), chr17-1223 (+22384), chr17-51 (+30513), chr17-525 (+35276), chr17-1950 (+65135), chr17-2529 (+65997), chr17-2119 (+66730), chr17-2756 (+67237), chr17-1827 (+74770), chr17-2118 (+75749)
SP100	x	x		chr2-2369 (-3570), chr2-1251 (+19), chr2-4992 (+2390), chr2-4993 (+23702), chr2-190 (+41431), chr2-6135 (+162016), chr2-3944 (+173551), chr2-475 (+227527), chr2-1817 (+227979), chr2-319 (+244660), chr2-1121 (+252511), chr2-4996 (+253022), chr2-4193 (+262424), chr2-2680 (+284442)
STAT1	x	x	x	chr2-3280 (-100570), chr2-4931 (-37861), chr2-4508 (-24304), chr2-3911 (-6895), chr2-1929 (+17051), chr2-841 (+43193), chr2-2932 (+52159), chr2-3279 (+66201), chr2-3910 (+122614)
STAT2		x		chr12-2875 (+1157)
STAT3			x	chr17-3202 (-29719), chr17-1770 (+772), chr17-1559 (+1066), chr17-549 (+21212), chr17-2210 (+33407), chr17-1664 (+41798), chr17-2898 (+42586), chr17-671 (+45718), chr17-670 (+50773), chr17-2029 (+68330)
STAT4			x	chr2-464 (-71040), chr2-1061 (-42479), chr2-6046 (-16368), chr2-3676 (-6869), chr2-3280 (+36776), chr2-4931 (+99485), chr2-4508 (+113042), chr2-3911 (+130451)
STAT5A			x	chr17-2029 (+32618), chr17-670 (+50175), chr17-671 (+55230), chr17-2898 (+58362), chr17-1664 (+59150), chr17-2210 (+67541), chr17-549 (+79736), chr17-1559 (+99882)
STAT5B			x	chr17-1482 (+25110), chr17-474 (+27642), chr17-2643 (+28469), chr17-878 (+69964)
STAT6			x	chr12-266 (-859), chr12-621 (-444)
TRIM56		x		chr7-1633 (+14780), chr7-341 (+22883)
TYK2	x	x		chr19-577 (+7643)

U937 BMP4-SMAD1 Peakset				
Gene I.D.	Type I IFN-mediated signalling pathway (GO BP)	Response to type I IFN (GO BP)	JAK-STAT Signalling Pathway (Panther Pathway)	Genomic regions of peaks (BED format)
USP18	x	x		chr22-9 (-35843), chr22-503 (-30016)
XAF1	x	x		chr17-341 (-3177), chr17-774 (-2667), chr17-3083 (+40776)

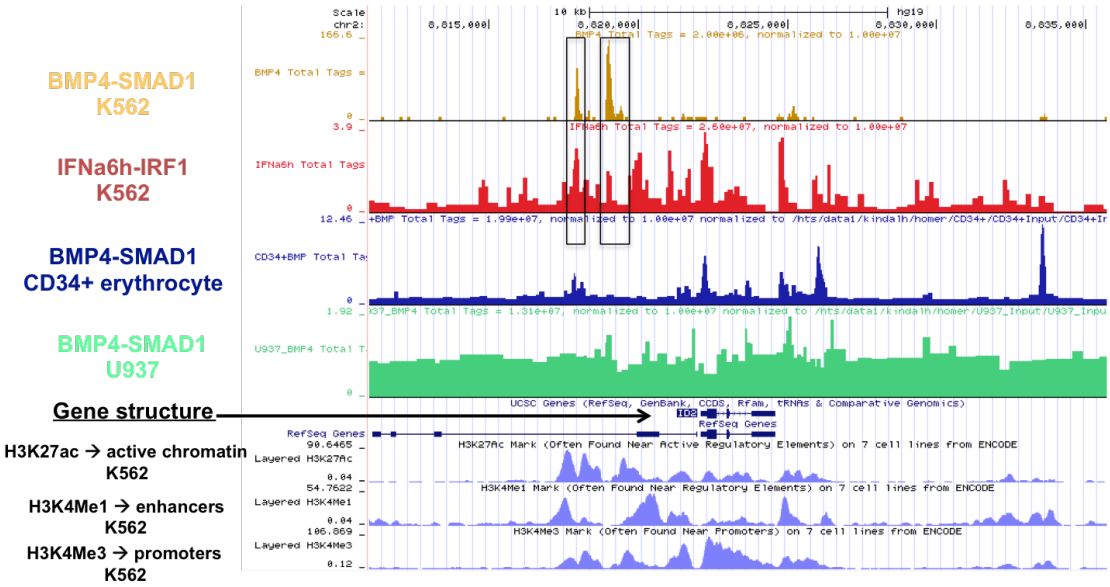
Appendix IV

Appendix IV contains the UCSC track visualizations corresponding to the following loci, in order: *ID2, ID3, IFIT3, MYD88, STAT1, STAT2* and *TBK1*.

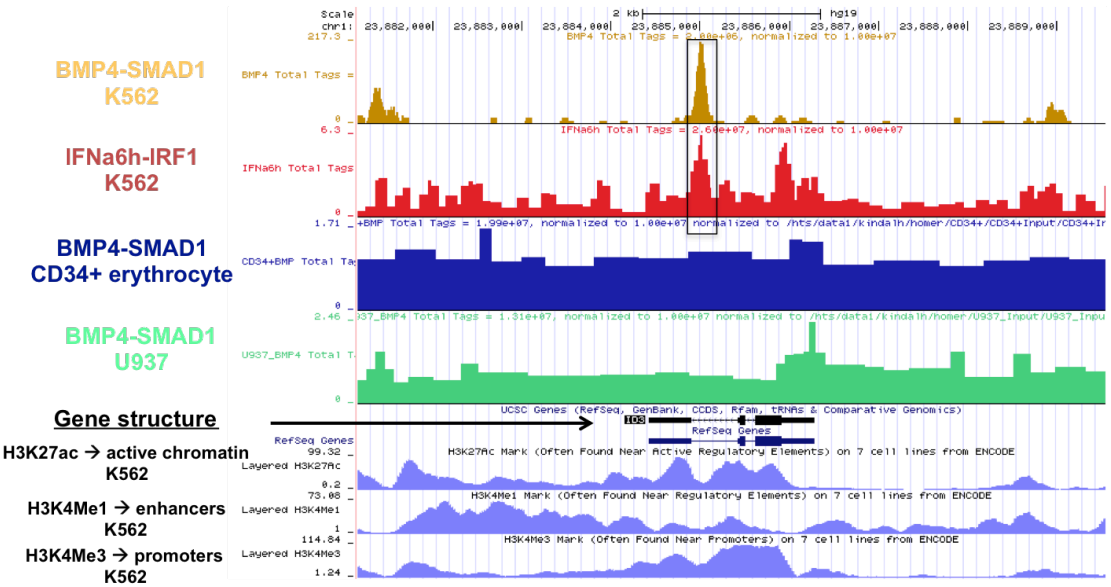
Data depicted:

1) ChIP-seq for SMAD1 in BMP4-treated K562 cells [Source: (61)]
2) ChIP-seq for IRF1 in IFNα-treated K562 cells [Source: ENCODE consortium]
3) ChIP-seq for SMAD1 in BMP4-treated CD34+ erythrocyte progenitors [Source: (61)]
4) ChIP-seq for SMAD1 in BMP4-treated U937 cells [Source: (61)]
5) Gene structure, in accordance with RefSeq annotation [Source: RefSeq/UCSC]
6) ChIP-seq for H3K27ac histone mark in K562 cells [Source: ENCODE consortium]
7) ChIP-seq for H3K4Me1 histone mark in K562 cells [Source: ENCODE consortium]
8) ChIP-seq for H3K4Me3 histone mark in K562 cells [Source: ENCODE consortium]

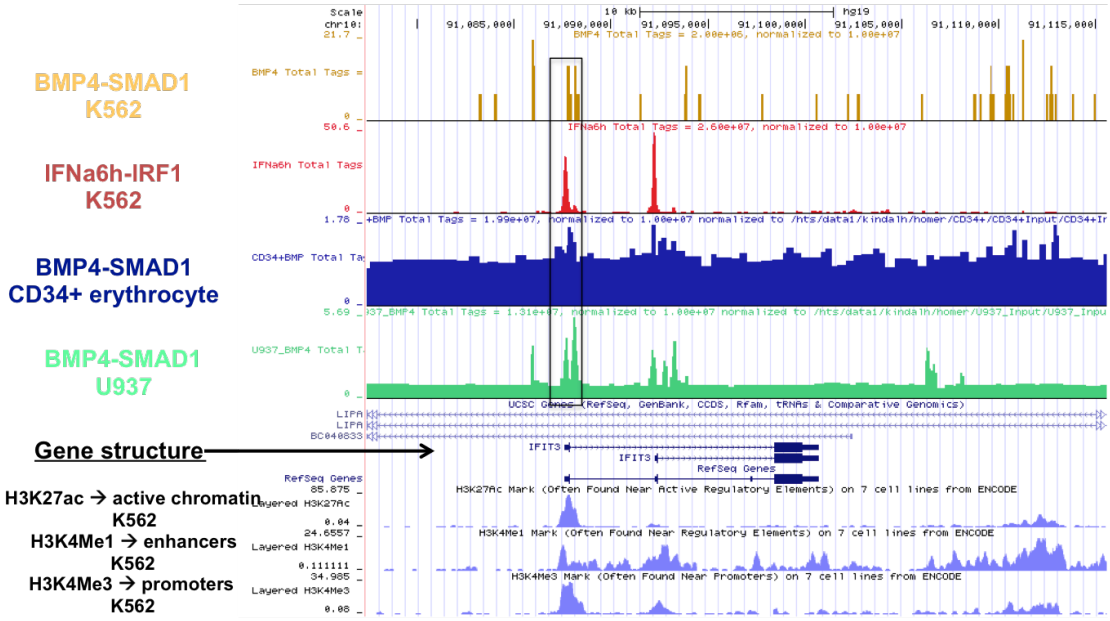
ID2



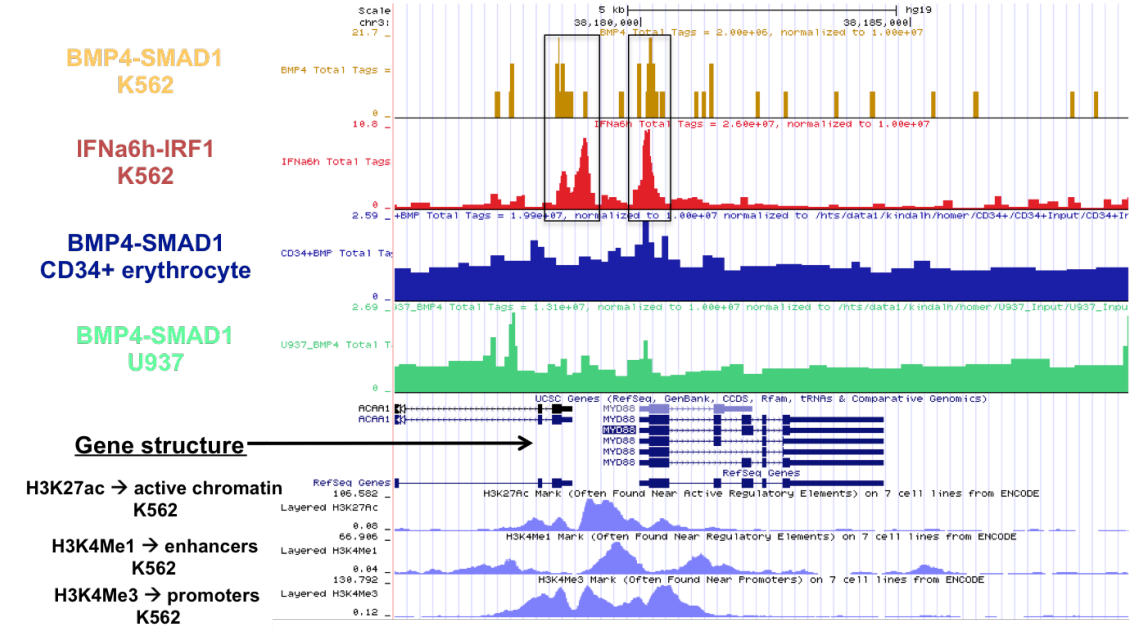
ID3



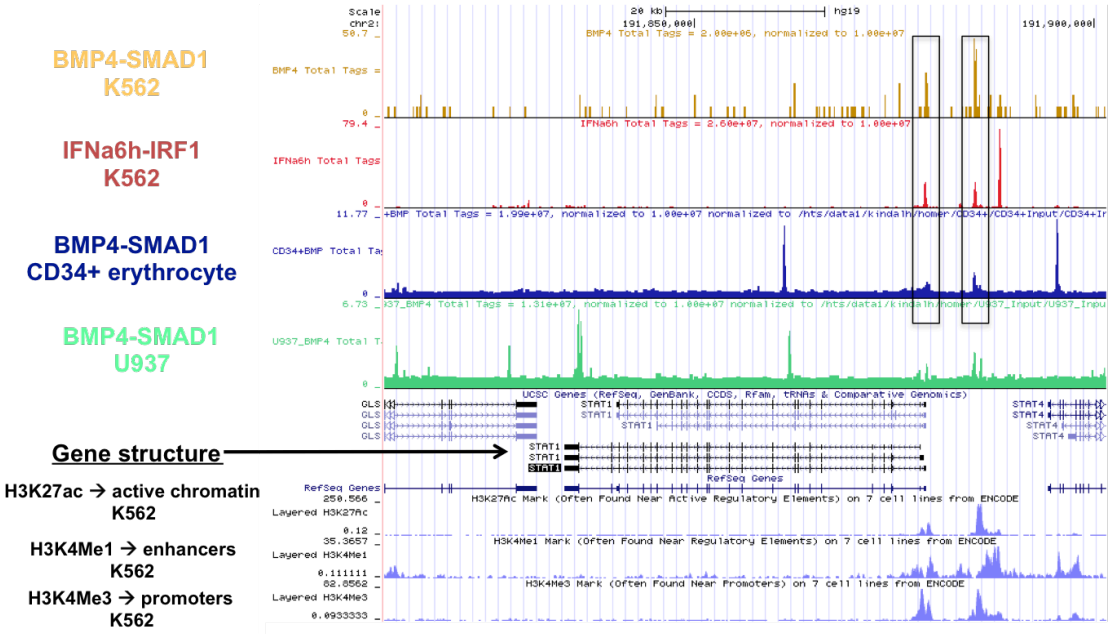
IFIT3



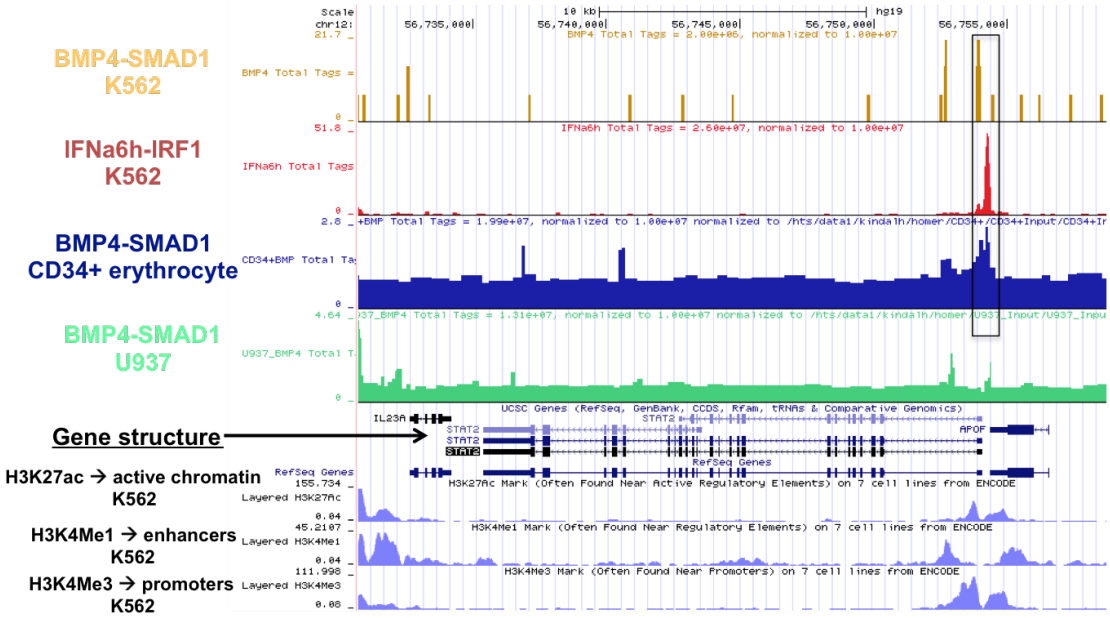
MYD88



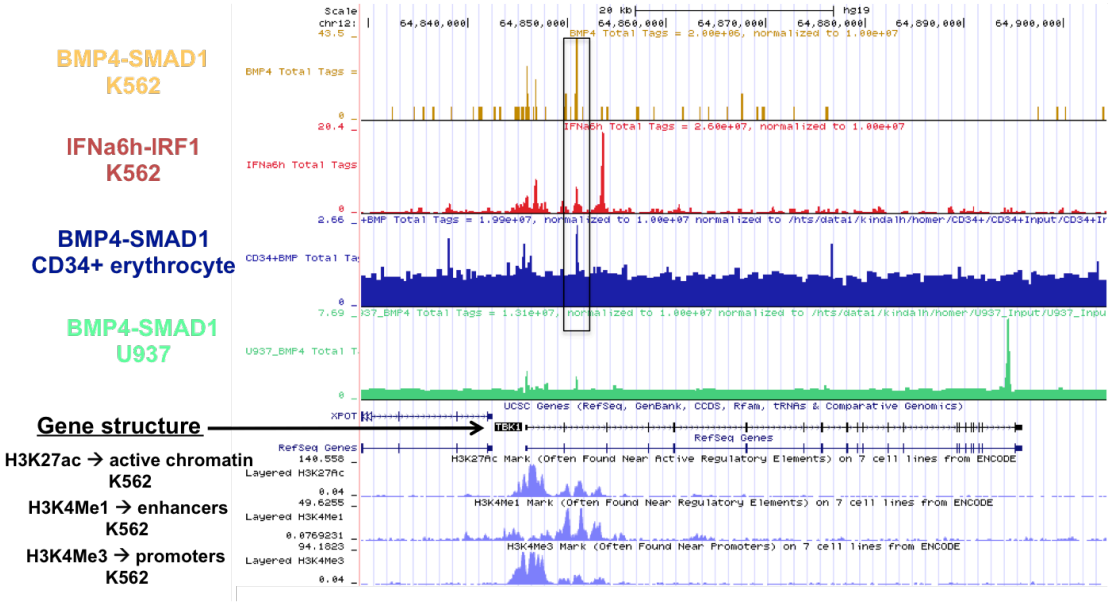
STAT1



STAT2


BMP4-SMAD1
K562
IFNa6h-IRF1
K562
BMP4-SMAD1
CD34+ erythrocyte
BMP4-SMAD1
U937
Gene structure
H3K27ac → active chromatin
K562
H3K4Me1 → enhancers
K562
H3K4Me3 → promoters
K562

TBK1


BMP4-SMAD1
K562
IFNa6h-IRF1
K562
BMP4-SMAD1
CD34+ erythrocyte
BMP4-SMAD1
U937
Gene structure
H3K27ac → active chromatin
K562
H3K4Me1 → enhancers
K562
H3K4Me3 → promoters
K562

Appendix V

List of genes shared between the BMP-SMAD1 ChIP-seq dataset (K562 cells) and microarray of BMP6-treated Huh7 cells.

Key:

Chr: chromosome

S: start base position of SMAD1 peak identified from ChIP-seq

F: finish base position of SMAD1 peak identified from ChIP-seq

Chr	S	F	Gene
chr1	40805447	40805589	**COL9A2**
chr1	43429475	43429617	**SLC2A1**
chr1	43475077	43475219	**SLC2A1**
chr1	43476901	43477043	**SLC2A1**
chr1	44424169	44424311	**DPH2**
chr1	54872438	54872580	**SSBP3**
chr1	68199837	68199979	**GADD45A**
chr1	65886427	65886569	**LEPROT**
chr1	66190878	66191020	**PDE4B**
chr1	85154391	85154533	**SSX2IP**
chr1	85156058	85156200	**SSX2IP**
chr1	87170979	87171121	**SH3GLB1**
chr1	113243334	113243476	**RHOC**
chr1	101445275	101445417	**DPH5**
chr1	117473973	117474115	**PTGFRN**
chr1	181074370	181074512	**IER5**
chr1	206674486	206674628	**RASSF5**
chr1	212408066	212408208	**PPP2R5A**
chr1	226111867	226112009	**PYCR2**
chr1	226119148	226119290	**PYCR2**
chr1	61514660	61514802	**NFIA**
chr1	65878282	65878424	**LEPROT**
chr1	87241228	87241370	**SH3GLB1**
chr1	150518237	150518379	**ADAMTSL4**
chr1	3229795	3229937	**ARHGEF16**
chr1	161136295	161136437	**PPOX**
chr1	16001386	16001528	**PLEKHM2**
chr1	8849484	8849626	**RERE**
chr1	19970633	19970775	**NBL1**
chr1	25092012	25092154	**CLIC4**
chr1	26251108	26251250	**STMN1**
chr1	33840100	33840242	**PHC2**
chr1	40866067	40866209	**SMAP2**
chr1	68199410	68199552	**GADD45A**
chr1	51434157	51434299	**CDKN2C**
chr1	53018293	53018435	**ZCCHC11**
chr1	53018807	53018949	**ZCCHC11**
chr1	54874047	54874189	**SSBP3**
chr1	55030959	55031101	**ACOT11**
chr1	67519657	67519799	**SLC35D1**
chr1	204196576	204196718	**GOLT1A**
chr1	90270301	90270443	**LRRC8D**
chr1	90354207	90354349	**LRRC8D**
chr1	92062161	92062303	**CDC7**

Chr	S	F	Gene
chr2	56075417	56075559	**EFEMP1**
chr2	69997493	69997635	**ANXA4**
chr2	138769771	138769913	**HNMT**
chr2	138776966	138777108	**HNMT**
chr2	153023172	153023314	**STAM2**
chr2	188374625	188374767	**TFPI**
chr2	188417980	188418122	**TFPI**
chr2	191208223	191208365	**INPP1**
chr2	200324171	200324313	**SATB2**
chr2	223695041	223695183	**ACSL3**
chr2	7049982	7050124	**RNF144A**
chr2	219258727	219258869	**CTDSP1**
chr2	219938210	219938352	**IHH**
chr2	8825145	8825287	**ID2**
chr2	10260775	10260917	**RRM2**
chr2	24811153	24811295	**NCOA1**
chr2	24855142	24855284	**NCOA1**
chr2	37617668	37617810	**QPCT**
chr2	37623142	37623284	**QPCT**
chr2	138816043	138816185	**HNMT**
chr2	42300093	42300235	**PKDCC**
chr2	43446824	43446966	**ZFP36L2**
chr2	158786531	158786673	**ACVR1**
chr2	179138528	179138670	**OSBPL6**
chr2	70141514	70141656	**MXD1**
chr2	73471438	73471580	**CCT7**
chr2	43417824	43417966	**ZFP36L2**
chr2	144891541	144891683	**GTDC1**
chr2	144910507	144910649	**GTDC1**
chr2	144988402	144988544	**GTDC1**
chr2	158763603	158763745	**ACVR1**
chr2	159825069	159825211	**TANC1**
chr2	178128177	178128319	**NFE2L2**
chr2	190306170	190306312	**WDR75**
chr2	190330300	190330442	**WDR75**
chr2	190401687	190401829	**SLC40A1**
chr2	190446365	190446507	**SLC40A1**
chr2	191533685	191533827	**NAB1**
chr2	197365474	197365616	**HECW2**
chr2	198317808	198317950	**COQ10B**
chr2	198364588	198364730	**HSPD1**
chr2	24800497	24800639	**NCOA1**
chr2	37720662	37720804	**QPCT**
chr2	56070552	56070694	**EFEMP1**

chr1	94220067	94220209	**BCAR3**	chr20	31340302	31340444	**COMMD7**
chr1	99969102	99969244	**PALMD**	chr20	30294625	30294767	**BCL2L1**
chr1	101491173	101491315	**DPH5**	chr20	36825094	36825236	**TGM2**
chr1	212458770	212458912	**PPP2R5A**	chr20	31319193	31319335	**COMMD7**
chr1	114235740	114235882	**PHTF1**	chr20	35201836	35201978	**TGIF2**
chr1	43428867	43429009	**SLC2A1**	chr20	47804776	47804918	**STAU1**
chr1	173272523	173272665	**TNFSF4**	chr20	36787339	36787481	**TGM2**
chr1	181053657	181053799	**IER5**	chr20	3026579	3026721	**MRPS26**
chr1	181098368	181098510	**IER5**	chr20	32715742	32715884	**EIF2S2**
chr1	202522723	202522865	**PPP1R12B**	chr20	36772184	36772326	**TGM2**
chr1	202546470	202546612	**PPP1R12B**	chr20	30873594	30873736	**KIF3B**
chr1	206329124	206329266	**CTSE**	chr20	25371167	25371309	**ABHD12**
chr1	213218739	213218881	**RPS6KC1**	chr20	30865327	30865469	**KIF3B**
chr1	213219296	213219438	**RPS6KC1**	chr20	17663191	17663333	**RRBP1**
chr1	213298001	213298143	**RPS6KC1**	chr20	25331368	25331510	**ABHD12**
chr1	215821225	215821367	**KCTD3**	chr20	30794996	30795138	**PLAGL2**
chr1	230817489	230817631	**AGT**	chr20	31331113	31331255	**COMMD7**
chr1	9335667	9335809	**SPSB1**	chr20	32723855	32723997	**EIF2S2**
chr1	9353663	9353805	**SPSB1**	chr20	33301291	33301433	**TP53INP2**
chr1	25071839	25071981	**CLIC4**	chr20	57482973	57483115	**GNAS**
chr1	26260966	26261108	**STMN1**	chr20	60641037	60641179	**TAF4**
chr1	203281047	203281189	**BTG2**	chr20	30296339	30296481	**BCL2L1**
chr1	33827175	33827317	**PHC2**	chr20	36755648	36755790	**TGM2**
chr1	877316	877458	**SAMD11**	chr20	36788440	36788582	**TGM2**
chr1	60413120	60413262	**CYP2J2**	chr20	30192058	30192200	**ID1**
chr1	65210502	65210644	**RAVER2**	chr21	44094693	44094835	**PDE9A**
chr1	65350464	65350606	**JAK1**	chr21	44183840	44183982	**PDE9A**
chr1	65358656	65358798	**JAK1**	chr21	46289889	46290031	**PTTG1IP**
chr1	67464732	67464874	**SLC35D1**	chr21	34775798	34775940	**IFNGR2**
chr1	90355805	90355947	**LRRC8D**	chr21	44028782	44028924	**PDE9A**
chr1	95010349	95010491	**F3**	chr21	44572882	44573024	**CRYAA**
chr1	95087185	95087327	**F3**	chr21	16531902	16532044	**NRIP1**
chr1	160990550	160990692	**F11R**	chr21	34602072	34602214	**IFNAR2**
chr1	146849123	146849265	**CHD1L**	chr21	34752317	34752459	**IFNGR2**
chr1	146849583	146849725	**CHD1L**	chr21	44034698	44034840	**PDE9A**
chr1	201122957	201123099	**TMEM9**	chr21	45356991	45357133	**AGPAT3**
chr1	153821867	153822009	**GATAD2B**	chr21	44091199	44091341	**PDE9A**
chr1	11942983	11943125	**NPPB**	chr21	34758822	34758964	**IFNGR2**
chr1	160979602	160979744	**F11R**	chr21	44098002	44098144	**PDE9A**
chr1	167689434	167689576	**MPZL1**	chr21	46494290	46494432	**ADARB1**
chr1	21646700	21646842	**ECE1**	chr21	44085346	44085488	**PDE9A**
chr1	197043341	197043483	**F13B**	chr21	44179393	44179535	**PDE9A**
chr1	33862284	33862426	**PHC2**	chr21	46300866	46301008	**PTTG1IP**
chr1	204207809	204207951	**GOLT1A**	chr21	44184395	44184537	**PDE9A**
chr1	204237353	204237495	**GOLT1A**	chr21	45304130	45304272	**AGPAT3**

chr1	207375700	207375842	**C4BPA**	chr21	45368756	45368898	**AGPAT3**
chr1	54875144	54875286	**SSBP3**	chr21	46274824	46274966	**PTTG1IP**
chr1	213327729	213327871	**RPS6KC1**	chr21	34584552	34584694	**IFNAR2**
chr1	60433152	60433294	**CYP2J2**	chr21	34638769	34638911	**IL10RB**
chr1	221916263	221916405	**DUSP10**	chr21	44119008	44119150	**PDE9A**
chr1	228871031	228871173	**RHOU**	chr21	34740485	34740627	**IFNGR2**
chr1	229761843	229761985	**URB2**	chr22	19879759	19879901	**GNB1L**
chr1	229842956	229843098	**URB2**	chr22	20772567	20772709	**SCARF2**
chr1	68154375	68154517	**GADD45A**	chr22	20783788	20783930	**SCARF2**
chr1	90344641	90344783	**LRRC8D**	chr22	21757173	21757315	**HIC2**
chr1	95113916	95114058	**F3**	chr22	36815500	36815642	**MYH9**
chr1	100237201	100237343	**FRRS1**	chr22	42084748	42084890	**NHP2L1**
chr1	213225071	213225213	**RPS6KC1**	chr22	19879156	19879298	**GNB1L**
chr1	229034473	229034615	**RHOU**	chr22	43579631	43579773	**TTLL12**
chr1	859145	859287	**SAMD11**	chr22	21132125	21132267	**SERPIND1**
chr1	8449181	8449323	**RERE**	chr22	36764692	36764834	**MYH9**
chr1	21647697	21647839	**ECE1**	chr22	31477255	31477397	**SMTN**
chr1	26452849	26452991	**PDIK1L**	chr22	35768058	35768200	**HMOX1**
chr1	55662882	55663024	**USP24**	chr22	36819636	36819778	**MYH9**
chr1	67224014	67224156	**TCTEX1D1**	chr22	21123443	21123585	**SERPIND1**
chr1	206730424	206730566	**RASSF5**	chr22	21997404	21997546	**SDF2L1**
chr1	23888872	23889014	**ID3**	chr22	39679653	39679795	**SNORD83B**
chr1	43833082	43833224	**ELOVL1**	chr22	21131309	21131451	**SERPIND1**
chr1	54953946	54954088	**ACOT11**	chr22	43659899	43660041	**TTLL12**
chr1	100234123	100234265	**FRRS1**	chr3	13049161	13049303	**IQSEC1**
chr1	65329911	65330053	**JAK1**	chr3	145790676	145790818	**PLOD2**
chr1	160959743	160959885	**F11R**	chr3	182502416	182502558	**ATP11B**
chr1	181099056	181099198	**IER5**	chr3	98302645	98302787	**CPOX**
chr1	205676001	205676143	**SLC45A3**	chr3	151961127	151961269	**MBNL1**
chr1	8064945	8065087	**ERRFI1**	chr3	186740236	186740378	**ST6GAL1**
chr1	23893789	23893931	**ID3**	chr3	82179299	82179441	**GBE1**
chr1	181122170	181122312	**IER5**	chr3	182444365	182444507	**ATP11B**
chr1	43833662	43833804	**ELOVL1**	chr3	191047059	191047201	**CCDC50**
chr1	226116237	226116379	**PYCR2**	chr3	43548279	43548421	**ANO10**
chr1	68152461	68152603	**GADD45A**	chr3	158397446	158397588	**LXN**
chr1	94129929	94130071	**BCAR3**	chr3	186650695	186650837	**ST6GAL1**
chr1	94130357	94130499	**BCAR3**	chr3	50283725	50283867	**GNAI2**
chr1	155214540	155214682	**GBA**	chr3	81598652	81598794	**GBE1**
chr1	181120797	181120939	**IER5**	chr3	97630293	97630435	**MINA**
chr1	192955345	192955487	**UCHL5**	chr3	43728504	43728646	**ABHD5**
chr1	875626	875768	**SAMD11**	chr3	57921369	57921511	**FLNB**
chr1	21588407	21588549	**ECE1**	chr3	124595449	124595591	**ITGB5**
chr1	43510591	43510733	**SLC2A1**	chr3	151959031	151959173	**MBNL1**
chr1	53373339	53373481	**ECHDC2**	chr3	170079663	170079805	**SKIL**
chr1	54841378	54841520	**SSBP3**	chr3	182432975	182433117	**ATP11B**

chr1	55645047	55645189	**USP24**	chr3	182505499	182505641	**ATP11B**
chr1	61545654	61545796	**NFIA**	chr3	12994830	12994972	**IQSEC1**
chr1	87254005	87254147	**SH3GLB1**	chr3	186714872	186715014	**ST6GAL1**
chr1	90367933	90368075	**LRRC8D**	chr3	30691164	30691306	**TGFBR2**
chr1	179941123	179941265	**CEP350**	chr3	30708796	30708938	**TGFBR2**
chr1	231201647	231201789	**FAM89A**	chr3	43712739	43712881	**ABHD5**
chr1	3370885	3371027	**ARHGEF16**	chr3	49210860	49211002	**KLHDC8B**
chr1	8686581	8686723	**RERE**	chr3	49503133	49503275	**DAG1**
chr1	21592808	21592950	**ECE1**	chr3	50280422	50280564	**GNAI2**
chr1	47107823	47107965	**ATPAF1**	chr3	43719950	43720092	**ABHD5**
chr1	53079874	53080016	**GPX7**	chr3	58045384	58045526	**FLNB**
chr1	54849143	54849285	**SSBP3**	chr3	58457165	58457307	**KCTD6**
chr1	54946363	54946505	**ACOT11**	chr3	124597868	124598010	**ITGB5**
chr1	55008305	55008447	**ACOT11**	chr3	145831720	145831862	**PLOD2**
chr1	59249656	59249798	**JUN**	chr3	145879078	145879220	**PLOD2**
chr1	61542753	61542895	**NFIA**	chr3	151554951	151555093	**AADAC**
chr1	68112043	68112185	**GADD45A**	chr3	155608665	155608807	**GMPS**
chr1	54930467	54930609	**SSBP3**	chr3	156361674	156361816	**TIPARP**
chr1	68177636	68177778	**GADD45A**	chr3	182433988	182434130	**ATP11B**
chr1	90361855	90361997	**LRRC8D**	chr3	182528459	182528601	**ATP11B**
chr1	160983669	160983811	**F11R**	chr3	186703809	186703951	**ST6GAL1**
chr1	205647831	205647973	**SLC45A3**	chr3	97651357	97651499	**MINA**
chr1	170011026	170011168	**KIFAP3**	chr3	170074813	170074955	**SKIL**
chr1	192946668	192946810	**UCHL5**	chr3	142605859	142606001	**PCOLCE2**
chr1	202777522	202777664	**KDM5B**	chr3	155661961	155662103	**GMPS**
chr1	204232740	204232882	**GOLT1A**	chr3	182484748	182484890	**ATP11B**
chr1	212434899	212435041	**PPP2R5A**	chr3	182513278	182513420	**ATP11B**
chr1	8586111	8586253	**RERE**	chr3	97629945	97630087	**MINA**
chr1	8602373	8602515	**RERE**	chr3	178689584	178689726	**ZMAT3**
chr1	11919466	11919608	**NPPB**	chr4	154059500	154059642	**TRIM2**
chr1	26260015	26260157	**STMN1**	chr4	106918180	106918322	**NPNT**
chr1	53019219	53019361	**ZCCHC11**	chr4	111119789	111119931	**ELOVL6**
chr1	95100648	95100790	**F3**	chr4	1794990	1795132	**FGFR3**
chr1	54869626	54869768	**SSBP3**	chr4	111170089	111170231	**ELOVL6**
chr1	54955110	54955252	**ACOT11**	chr4	25052460	25052602	**LGI2**
chr1	61515699	61515841	**NFIA**	chr4	37661423	37661565	**RELL1**
chr1	23884931	23885073	**ID3**	chr4	106571458	106571600	**INTS12**
chr1	87230870	87231012	**SH3GLB1**	chr4	2869861	2870003	**ADD1**
chr1	87240237	87240379	**SH3GLB1**	chr4	39370981	39371123	**RFC1**
chr1	87254401	87254543	**SH3GLB1**	chr4	80928201	80928343	**ANTXR2**
chr1	87258053	87258195	**SH3GLB1**	chr4	155562173	155562315	**FGG**
chr1	23881288	23881430	**ID3**	chr4	2869612	2869754	**ADD1**
chr1	153895022	153895164	**GATAD2B**	chr4	8200912	8201054	**SH3TC1**
chr1	167664561	167664703	**MPZL1**	chr4	77870899	77871041	**40787**
chr1	170036784	170036926	**KIFAP3**	chr4	78067793	78067935	**CCNG2**

chr1	206728875	206729017	**RASSF5**	chr4	78827131	78827273	**MRPL1**
chr1	206748551	206748693	**RASSF5**	chr4	77222745	77222887	**STBD1**
chr1	206749020	206749162	**RASSF5**	chr4	124365635	124365777	**SPRY1**
chr1	213309805	213309947	**RPS6KC1**	chr4	140374564	140374706	**RAB33B**
chr1	229889577	229889719	**URB2**	chr4	183839088	183839230	**DCTD**
chr1	8137865	8138007	**ERRFI1**	chr4	1037505	1037647	**FGFRL1**
chr1	8487704	8487846	**RERE**	chr4	124270618	124270760	**SPRY1**
chr1	8781879	8782021	**RERE**	chr4	37655291	37655433	**RELL1**
chr1	10777516	10777658	**CASZ1**	chr4	37665283	37665425	**RELL1**
chr1	19383806	19383948	**IFFO2**	chr4	84194116	84194258	**COQ2**
chr1	36621371	36621513	**MAP7D1**	chr4	106884788	106884930	**NPNT**
chr10	15844416	15844558	**FAM188A**	chr4	110497737	110497879	**CCDC109B**
chr10	52339831	52339973	**SGMS1**	chr4	111087161	111087303	**ELOVL6**
chr10	112243536	112243678	**DUSP5**	chr4	135248662	135248804	**PABPC4L**
chr10	17270441	17270583	**VIM**	chr4	154143880	154144022	**TRIM2**
chr10	22096117	22096259	**DNAJC1**	chr4	70411896	70412038	**UGT2B4**
chr10	25040769	25040911	**ARHGAP21**	chr4	74774797	74774939	**CXCL1**
chr10	80938434	80938576	**ZMIZ1**	chr4	77890765	77890907	**40787**
chr10	52337614	52337756	**SGMS1**	chr4	79150561	79150703	**FRAS1**
chr10	73740192	73740334	**CHST3**	chr4	80994309	80994451	**ANTXR2**
chr10	15493334	15493476	**FAM171A1**	chr4	84159669	84159811	**COQ2**
chr10	15355914	15356056	**FAM171A1**	chr4	88312898	88313040	**HSD17B11**
chr10	63590709	63590851	**ARID5B**	chr4	183891234	183891376	**DCTD**
chr10	69644392	69644534	**SIRT1**	chr4	124337247	124337389	**SPRY1**
chr10	98524176	98524318	**PIK3AP1**	chr4	124342460	124342602	**SPRY1**
chr10	99996768	99996910	**LOXL4**	chr4	154074128	154074270	**TRIM2**
chr10	97291878	97292020	**SORBS1**	chr4	155548037	155548179	**FGG**
chr10	80843199	80843341	**ZMIZ1**	chr4	140364872	140365014	**RAB33B**
chr10	102820810	102820952	**KAZALD1**	chr4	1773374	1773516	**FGFR3**
chr10	102831236	102831378	**KAZALD1**	chr4	1787016	1787158	**FGFR3**
chr10	3782635	3782777	**KLF6**	chr5	126307311	126307453	**37681**
chr10	3848160	3848302	**KLF6**	chr5	126312245	126312387	**37681**
chr10	22239633	22239775	**DNAJC1**	chr5	131649896	131650038	**SLC22A4**
chr10	52310193	52310335	**SGMS1**	chr5	172199484	172199626	**DUSP1**
chr10	61473277	61473419	**SLC16A9**	chr5	126257253	126257395	**37681**
chr10	80892624	80892766	**ZMIZ1**	chr5	77883538	77883680	**LHFPL2**
chr10	97227051	97227193	**SORBS1**	chr5	139049556	139049698	**CXXC5**
chr10	97291342	97291484	**SORBS1**	chr5	54872088	54872230	**PPAP2A**
chr10	98588886	98589028	**LCOR**	chr5	95270326	95270468	**ELL2**
chr10	98591548	98591690	**LCOR**	chr5	154317762	154317904	**GEMIN5**
chr10	3827809	3827951	**KLF6**	chr5	66300318	66300460	**MAST4**
chr10	13310936	13311078	**PHYH**	chr5	81047215	81047357	**SSBP2**
chr10	15484160	15484302	**FAM171A1**	chr5	137801055	137801197	**EGR1**
chr10	23336729	23336871	**MSRB2**	chr5	139017450	139017592	**CXXC5**
chr10	52315150	52315292	**SGMS1**	chr5	139026694	139026836	**CXXC5**

chr10	80853551	80853693	**ZMIZ1**	chr5	139990743	139990885	**CD14**
chr10	73669341	73669483	**CHST3**	chr5	60148889	60149031	**ELOVL7**
chr10	97185737	97185879	**SORBS1**	chr5	41925264	41925406	**FBXO4**
chr10	97277402	97277544	**SORBS1**	chr5	66275942	66276084	**MAST4**
chr10	98600754	98600896	**LCOR**	chr5	126312678	126312820	**37681**
chr10	112261072	112261214	**DUSP5**	chr5	76034917	76035059	**F2R**
chr10	3612693	3612835	**KLF6**	chr5	118755898	118756040	**HSD17B4**
chr10	3797256	3797398	**KLF6**	chr5	118774469	118774611	**HSD17B4**
chr10	6281084	6281226	**PFKFB3**	chr5	139016996	139017138	**CXXC5**
chr10	15475969	15476111	**FAM171A1**	chr5	139040636	139040778	**CXXC5**
chr10	15497500	15497642	**FAM171A1**	chr5	139048228	139048370	**CXXC5**
chr10	23384335	23384477	**MSRB2**	chr5	149340040	149340182	**SLC26A2**
chr10	54117810	54117952	**DKK1**	chr5	71616158	71616300	**PTCD2**
chr10	30726093	30726235	**MAP3K8**	chr5	77955587	77955729	**LHFPL2**
chr10	30791276	30791418	**MAP3K8**	chr5	131651351	131651493	**SLC22A4**
chr10	76088236	76088378	**ADK**	chr5	139015383	139015525	**CXXC5**
chr10	89420620	89420762	**PAPSS2**	chr5	139037303	139037445	**CXXC5**
chr10	97157520	97157662	**SORBS1**	chr5	14463795	14463937	**FAM105A**
chr10	99986611	99986753	**LOXL4**	chr5	34008243	34008385	**AMACR**
chr10	99997083	99997225	**LOXL4**	chr5	78067209	78067351	**LHFPL2**
chr10	102831787	102831929	**KAZALD1**	chr5	66192074	66192216	**MAST4**
chr10	100083084	100083226	**LOXL4**	chr5	95352103	95352245	**ELL2**
chr10	3846185	3846327	**KLF6**	chr5	131636326	131636468	**SLC22A4**
chr10	3707749	3707891	**KLF6**	chr5	135585462	135585604	**LOC389332**
chr10	98448667	98448809	**PIK3AP1**	chr5	141675854	141675996	**SPRY4**
chr11	61735149	61735291	**FTH1**	chr5	141703489	141703631	**SPRY4**
chr11	61568216	61568358	**FEN1**	chr5	60116671	60116813	**ELOVL7**
chr11	20016752	20016894	**NAV2**	chr5	42831168	42831310	**SEPP1**
chr11	61734117	61734259	**FTH1**	chr5	52760213	52760355	**FST**
chr11	61739325	61739467	**FTH1**	chr5	54864618	54864760	**PPAP2A**
chr11	86642659	86642801	**FZD4**	chr5	60099676	60099818	**ELOVL7**
chr11	113993542	113993684	**ZBTB16**	chr5	76058436	76058578	**F2R**
chr11	118956301	118956443	**HMBS**	chr5	77822929	77823071	**LHFPL2**
chr11	61054955	61055097	**VWCE**	chr5	95353776	95353918	**ELL2**
chr11	61809584	61809726	**FTH1**	chr5	60274967	60275109	**NDUFAF2**
chr11	61793071	61793213	**FTH1**	chr5	115879301	115879443	**SEMA6A**
chr11	62313153	62313295	**AHNAK**	chr5	149524000	149524142	**PDGFRB**
chr11	67115887	67116029	**POLD4**	chr5	42873052	42873194	**SEPP1**
chr11	73694263	73694405	**UCP2**	chr5	179718994	179719136	**MAPK9**
chr11	125421884	125422026	**EI24**	chr6	19804957	19805099	**ID4**
chr11	20002499	20002641	**NAV2**	chr6	30065785	30065927	**TRIM31**
chr11	57103346	57103488	**SSRP1**	chr6	146870075	146870217	**RAB32**
chr11	65171238	65171380	**FRMD8**	chr6	36067723	36067865	**MAPK13**
chr11	76510416	76510558	**TSKU**	chr6	36493998	36494140	**STK38**
chr11	111781816	111781958	**CRYAB**	chr6	37112334	37112476	**PIM1**

chr11	113969726	113969868	**ZBTB16**	chr6	39961063	39961205	**MOCS1**
chr11	117042587	117042729	**SIDT2**	chr6	71377659	71377801	**SMAP1**
chr11	19977292	19977434	**NAV2**	chr6	106188857	106188999	**PREP**
chr11	19996554	19996696	**NAV2**	chr6	107435601	107435743	**BEND3**
chr11	20046241	20046383	**NAV2**	chr6	16031509	16031651	**MYLIP**
chr11	57200363	57200505	**SLC43A3**	chr6	134516874	134517016	**SGK1**
chr11	64646031	64646173	**EHD1**	chr6	126141297	126141439	**NCOA7**
chr11	57192313	57192455	**SLC43A3**	chr6	144129062	144129204	**LTV1**
chr11	73681160	73681302	**UCP2**	chr6	126160721	126160863	**NCOA7**
chr11	86643119	86643261	**FZD4**	chr6	19996234	19996376	**ID4**
chr11	113953595	113953737	**ZBTB16**	chr6	144127546	144127688	**LTV1**
chr11	125402709	125402851	**EI24**	chr6	25535611	25535753	**SCGN**
chr11	61800961	61801103	**FTH1**	chr6	37151090	37151232	**PIM1**
chr11	76495747	76495889	**TSKU**	chr6	2183602	2183744	**GMDS**
chr11	76526837	76526979	**TSKU**	chr6	14951034	14951176	**JARID2**
chr11	69390874	69391016	**CCND1**	chr6	37145268	37145410	**PIM1**
chr11	114018474	114018616	**ZBTB16**	chr6	15915780	15915922	**MYLIP**
chr11	27393854	27393996	**CCDC34**	chr6	17701073	17701215	**NUP153**
chr11	19429332	19429474	**NAV2**	chr6	25619542	25619684	**SCGN**
chr11	62687402	62687544	**CHRM1**	chr6	37077675	37077817	**PIM1**
chr11	125422962	125423104	**EI24**	chr6	126150683	126150825	**NCOA7**
chr11	118958558	118958700	**HMBS**	chr6	134617262	134617404	**SGK1**
chr11	67211014	67211156	**CORO1B**	chr6	83869999	83870141	**PGM3**
chr11	69453712	69453854	**CCND1**	chr6	3393317	3393459	**SLC22A23**
chr11	70588766	70588908	**SHANK2**	chr6	15097490	15097632	**JARID2**
chr11	876081	876223	**TSPAN4**	chr6	15107298	15107440	**JARID2**
chr12	106752248	106752390	**POLR3B**	chr6	15160153	15160295	**JARID2**
chr12	125292153	125292295	**SCARB1**	chr6	15252540	15252682	**JARID2**
chr12	125371857	125371999	**SCARB1**	chr6	15409629	15409771	**JARID2**
chr12	27674116	27674258	**PPFIBP1**	chr6	17843621	17843763	**NUP153**
chr12	44090099	44090241	**PUS7L**	chr6	30464379	30464521	**HLA-E**
chr12	53319026	53319168	**KRT8**	chr6	36648237	36648379	**CDKN1A**
chr12	56122808	56122950	**CD63**	chr6	117916312	117916454	**GOPC**
chr12	99147864	99148006	**APAF1**	chr6	139696456	139696598	**CITED2**
chr12	110338032	110338174	**TCHP**	chr6	106968803	106968945	**AIM1**
chr12	124451894	124452036	**CCDC92**	chr6	2124733	2124875	**GMDS**
chr12	65114752	65114894	**GNS**	chr6	15434551	15434693	**JARID2**
chr12	76175539	76175681	**PHLDA1**	chr6	39966923	39967065	**MOCS1**
chr12	117489406	117489548	**TESC**	chr6	106874127	106874269	**AIM1**
chr12	6362580	6362722	**CD9**	chr6	134636460	134636602	**SGK1**
chr12	6454808	6454950	**TNFRSF1A**	chr6	146864619	146864761	**RAB32**
chr12	76286770	76286912	**PHLDA1**	chr6	14932774	14932916	**JARID2**
chr12	54319316	54319458	**HOXC13**	chr6	15037118	15037260	**JARID2**
chr12	65176079	65176221	**GNS**	chr6	15081244	15081386	**JARID2**
chr12	71630219	71630361	**TSPAN8**	chr6	15409967	15410109	**JARID2**

chr12	76328349	76328491	**PHLDA1**	chr6	16129029	16129171	**MYLIP**
chr12	117537145	117537287	**TESC**	chr6	25660822	25660964	**SCGN**
chr12	42836889	42837031	**PRICKLE1**	chr6	37159672	37159814	**PIM1**
chr12	125212051	125212193	**SCARB1**	chr6	105403955	105404097	**LIN28B**
chr12	125230623	125230765	**SCARB1**	chr6	111431354	111431496	**SLC16A10**
chr12	132413728	132413870	**PUS1**	chr6	111858238	111858380	**TRAF3IP2**
chr12	7104172	7104314	**LPCAT3**	chr6	15906271	15906413	**MYLIP**
chr12	27702725	27702867	**PPFIBP1**	chr6	25608925	25609067	**SCGN**
chr12	39837125	39837267	**KIF21A**	chr6	3355290	3355432	**SLC22A23**
chr12	42943398	42943540	**PRICKLE1**	chr6	3457513	3457655	**SLC22A23**
chr12	49554188	49554330	**TUBA1A**	chr6	3571548	3571690	**SLC22A23**
chr12	53297778	53297920	**KRT8**	chr6	15081790	15081932	**JARID2**
chr12	125369527	125369669	**SCARB1**	chr6	15400342	15400484	**JARID2**
chr12	57482445	57482587	**NAB2**	chr6	15896520	15896662	**MYLIP**
chr12	76371844	76371986	**PHLDA1**	chr6	30449959	30450101	**HLA-E**
chr12	112851695	112851837	**RPL6**	chr6	43149787	43149929	**CUL9**
chr12	6277032	6277174	**CD9**	chr6	43150138	43150280	**CUL9**
chr12	11877936	11878078	**ETV6**	chr6	46738790	46738932	**MEP1A**
chr12	30910372	30910514	**CAPRIN2**	chr6	83841941	83842083	**PGM3**
chr12	42820694	42820836	**PRICKLE1**	chr6	15062894	15063036	**JARID2**
chr12	42983533	42983675	**PRICKLE1**	chr6	15079637	15079779	**JARID2**
chr12	50170825	50170967	**TMBIM6**	chr6	126111775	126111917	**NCOA7**
chr12	54585312	54585454	**SMUG1**	chr6	1999899	2000041	**GMDS**
chr12	76237941	76238083	**PHLDA1**	chr6	3576112	3576254	**SLC22A23**
chr12	76427194	76427336	**PHLDA1**	chr6	15977243	15977385	**MYLIP**
chr12	89740336	89740478	**DUSP6**	chr6	16007493	16007635	**MYLIP**
chr12	89785214	89785356	**DUSP6**	chr6	17702101	17702243	**NUP153**
chr12	99130741	99130883	**APAF1**	chr6	25670655	25670797	**SCGN**
chr12	99145643	99145785	**APAF1**	chr6	15299985	15300127	**JARID2**
chr12	124457315	124457457	**CCDC92**	chr6	36086497	36086639	**MAPK13**
chr12	125348562	125348704	**SCARB1**	chr6	33584821	33584963	**ITPR3**
chr12	30907735	30907877	**CAPRIN2**	chr6	34164168	34164310	**HMGA1**
chr12	30916058	30916200	**CAPRIN2**	chr6	81840760	81840902	**FAM46A**
chr12	54569262	54569404	**SMUG1**	chr6	106001242	106001384	**PREP**
chr12	76231636	76231778	**PHLDA1**	chr6	107427409	107427551	**BEND3**
chr12	56753801	56753943	**STAT2**	chr6	117882462	117882604	**GOPC**
chr12	57145253	57145395	**PRIM1**	chr6	126245518	126245660	**NCOA7**
chr12	58139076	58139218	**TSPAN31**	chr6	137540543	137540685	**IFNGR1**
chr12	62860505	62860647	**MON2**	chr6	137612720	137612862	**IFNGR1**
chr12	76425233	76425375	**PHLDA1**	chr6	167444092	167444234	**FGFR1OP**
chr12	85964886	85965028	**RASSF9**	chr6	1963898	1964040	**GMDS**
chr12	88828291	88828433	**KITLG**	chr6	3378705	3378847	**SLC22A23**
chr12	6373297	6373439	**PLEKHG6**	chr6	3537903	3538045	**SLC22A23**
chr12	42880329	42880471	**PRICKLE1**	chr6	15369126	15369268	**JARID2**
chr12	133287104	133287246	**PGAM5**	chr6	15411147	15411289	**JARID2**

chr12	89787520	89787662	**DUSP6**	chr6	25524594	25524736	**SCGN**
chr13	24144256	24144398	**TNFRSF19**	chr6	37071191	37071333	**PIM1**
chr13	81166229	81166371	**SPRY2**	chr7	108104122	108104264	**NRCAM**
chr13	110443769	110443911	**IRS2**	chr7	121078532	121078674	**FAM3C**
chr13	24180092	24180234	**TNFRSF19**	chr7	130103752	130103894	**MEST**
chr13	27998736	27998878	**GTF3A**	chr7	155102071	155102213	**INSIG1**
chr13	44942440	44942582	**SERP2**	chr7	103559897	103560039	**RELN**
chr13	44960131	44960273	**SERP2**	chr7	116590178	116590320	**ST7**
chr13	44956908	44957050	**SERP2**	chr7	135602545	135602687	**MTPN**
chr13	41161413	41161555	**FOXO1**	chr7	135614609	135614751	**MTPN**
chr13	44961197	44961339	**SERP2**	chr7	148522600	148522742	**EZH2**
chr13	44933857	44933999	**SERP2**	chr7	5631268	5631410	**FSCN1**
chr13	46674721	46674863	**CPB2**	chr7	50626198	50626340	**DDC**
chr13	76056555	76056697	**TBC1D4**	chr7	149417110	149417252	**KRBA1**
chr13	44943211	44943353	**SERP2**	chr7	103636675	103636817	**RELN**
chr13	41255609	41255751	**FOXO1**	chr7	107476942	107477084	**SLC26A3**
chr13	24230873	24231015	**TNFRSF19**	chr7	86985867	86986009	**CROT**
chr13	46753834	46753976	**LCP1**	chr7	155115693	155115835	**INSIG1**
chr13	44929163	44929305	**SERP2**	chr7	5614048	5614190	**FSCN1**
chr13	75969323	75969465	**TBC1D4**	chr7	43819143	43819285	**BLVRA**
chr14	71353438	71353580	**PCNX**	chr7	92848876	92849018	**HEPACAM2**
chr14	88461814	88461956	**GALC**	chr7	43808233	43808375	**BLVRA**
chr14	24408977	24409119	**DHRS4**	chr7	73027074	73027216	**MLXIPL**
chr14	71351821	71351963	**PCNX**	chr7	103451028	103451170	**RELN**
chr14	25517538	25517680	**STXBP6**	chr7	108059484	108059626	**NRCAM**
chr14	96010996	96011138	**GLRX5**	chr7	116060183	116060325	**CAV2**
chr14	25510703	25510845	**STXBP6**	chr7	148547746	148547888	**EZH2**
chr14	55574603	55574745	**LGALS3**	chr7	155082879	155083021	**INSIG1**
chr14	68089492	68089634	**ARG2**	chr7	5603308	5603450	**FSCN1**
chr14	65346689	65346831	**CHURC1**	chr7	22206692	22206834	**RAPGEF5**
chr14	88459568	88459710	**GALC**	chr7	43790302	43790444	**BLVRA**
chr14	101165543	101165685	**DLK1**	chr7	92219659	92219801	**FAM133B**
chr14	105481665	105481807	**CDCA4**	chr7	100303428	100303570	**POP7**
chr14	97223198	97223340	**VRK1**	chr7	148544920	148545062	**EZH2**
chr14	31291305	31291447	**COCH**	chr7	155089577	155089719	**INSIG1**
chr14	76071846	76071988	**FLVCR2**	chr7	5376622	5376764	**SLC29A4**
chr14	97126526	97126668	**VRK1**	chr7	8171389	8171531	**ICA1**
chr14	101203428	101203570	**DLK1**	chr7	21988122	21988264	**CDCA7L**
chr14	101221999	101222141	**DLK1**	chr7	22386053	22386195	**RAPGEF5**
chr14	25454212	25454354	**STXBP6**	chr7	35077549	35077691	**DPY19L1**
chr14	25390072	25390214	**STXBP6**	chr7	103527617	103527759	**RELN**
chr14	38065245	38065387	**FOXA1**	chr7	149416209	149416351	**KRBA1**
chr15	82031537	82031679	**MEX3B**	chr7	116004211	116004353	**CAV2**
chr15	82237366	82237508	**MEX3B**	chr7	116141647	116141789	**CAV2**
chr15	91384355	91384497	**FURIN**	chr7	121036389	121036531	**FAM3C**

chr15	78857361	78857503	**CHRNA5**	chr7	134519746	134519888	**CALD1**
chr15	80346705	80346847	**ZFAND6**	chr7	135621759	135621901	**MTPN**
chr15	82240722	82240864	**MEX3B**	chr7	146042464	146042606	**CNTNAP2**
chr15	70740315	70740457	**UACA**	chr7	148581769	148581911	**EZH2**
chr15	66947357	66947499	**SMAD6**	chr7	103484330	103484472	**RELN**
chr15	72487572	72487714	**GRAMD2**	chr7	8273114	8273256	**ICA1**
chr15	82234524	82234666	**MEX3B**	chr7	107875573	107875715	**NRCAM**
chr15	91385125	91385267	**FURIN**	chr7	22020679	22020821	**CDCA7L**
chr15	91413110	91413252	**FURIN**	chr7	22327208	22327350	**RAPGEF5**
chr15	58624495	58624637	**LIPC**	chr7	24860938	24861080	**DFNA5**
chr15	40398716	40398858	**BMF**	chr7	5614519	5614661	**FSCN1**
chr15	41788265	41788407	**ITPKA**	chr7	50651091	50651233	**DDC**
chr15	63634224	63634366	**CA12**	chr7	8241512	8241654	**ICA1**
chr15	63655541	63655683	**CA12**	chr7	50860557	50860699	**GRB10**
chr15	82243314	82243456	**MEX3B**	chr7	24835093	24835235	**DFNA5**
chr15	90709092	90709234	**SEMA4B**	chr7	73050785	73050927	**MLXIPL**
chr15	90727382	90727524	**SEMA4B**	chr7	99869781	99869923	**GATS**
chr15	91367441	91367583	**FURIN**	chr7	107876122	107876264	**NRCAM**
chr15	45341052	45341194	**SORD**	chr7	116079172	116079314	**CAV2**
chr15	41624661	41624803	**OIP5**	chr7	5635472	5635614	**FSCN1**
chr15	41860732	41860874	**TYRO3**	chr7	128049779	128049921	**IMPDH1**
chr15	48623553	48623695	**DUT**	chr7	5638527	5638669	**FSCN1**
chr15	70920979	70921121	**UACA**	chr7	5665657	5665799	**FSCN1**
chr15	70925937	70926079	**UACA**	chr7	24859937	24860079	**DFNA5**
chr15	75918066	75918208	**SNUPN**	chr7	26904350	26904492	**SKAP2**
chr15	82333367	82333509	**MEX3B**	chr7	765317	765459	**HEATR2**
chr15	40391044	40391186	**BMF**	chr7	45159265	45159407	**TBRG4**
chr15	90727893	90728035	**SEMA4B**	chr7	22390532	22390674	**RAPGEF5**
chr15	90733182	90733324	**SEMA4B**	chr7	8272681	8272823	**ICA1**
chr15	45341458	45341600	**SORD**	chr7	92262860	92263002	**FAM133B**
chr15	41851005	41851147	**TYRO3**	chr7	103530054	103530196	**RELN**
chr15	41895014	41895156	**TYRO3**	chr8	29083303	29083445	**KIF13B**
chr15	67095643	67095785	**SMAD6**	chr8	37757924	37758066	**RAB11FIP1**
chr15	57675325	57675467	**CGNL1**	chr8	61488581	61488723	**RAB2A**
chr15	63635270	63635412	**CA12**	chr8	26248639	26248781	**BNIP3L**
chr15	64368425	64368567	**FAM96A**	chr8	134552507	134552649	**ST3GAL1**
chr15	64385918	64386060	**FAM96A**	chr8	29107511	29107653	**KIF13B**
chr15	101991584	101991726	**PCSK6**	chr8	37749371	37749513	**RAB11FIP1**
chr15	75917635	75917777	**SNUPN**	chr8	68022109	68022251	**CSPP1**
chr15	77328243	77328385	**TSPAN3**	chr8	56760540	56760682	**LYN**
chr15	72460817	72460959	**GRAMD2**	chr8	29146657	29146799	**KIF13B**
chr15	89531734	89531876	**MFGE8**	chr8	56853814	56853956	**LYN**
chr15	91361461	91361603	**FURIN**	chr8	68167924	68168066	**ARFGEF1**
chr15	99645105	99645247	**SYNM**	chr8	98790748	98790890	**LAPTM4B**
chr15	102018062	102018204	**PCSK6**	chr8	98944270	98944412	**MATN2**

chr15	58722271	58722413	**LIPC**	chr8	103666222	103666364	**KLF10**
chr15	82310688	82310830	**MEX3B**	chr8	66580278	66580420	**MTFR1**
chr15	66972087	66972229	**SMAD6**	chr8	86059797	86059939	**E2F5**
chr15	75899181	75899323	**SNUPN**	chr8	103736120	103736262	**KLF10**
chr15	80352145	80352287	**ZFAND6**	chr8	107182861	107183003	**OXR1**
chr15	67142415	67142557	**SMAD6**	chr8	28243676	28243818	**ZNF395**
chr16	29690907	29691049	**QPRT**	chr8	28260257	28260399	**ZNF395**
chr16	66651786	66651928	**CMTM3**	chr8	29130496	29130638	**KIF13B**
chr16	84947080	84947222	**CRISPLD2**	chr8	30791646	30791788	**TEX15**
chr16	46693060	46693202	**VPS35**	chr8	37739536	37739678	**RAB11FIP1**
chr16	50105109	50105251	**HEATR3**	chr8	56798213	56798355	**LYN**
chr16	58768210	58768352	**GOT2**	chr8	95972214	95972356	**TP53INP1**
chr16	58826240	58826382	**GOT2**	chr8	98790181	98790323	**LAPTM4B**
chr16	88522317	88522459	**ZFPM1**	chr8	98944788	98944930	**MATN2**
chr16	54482170	54482312	**IRX3**	chr8	17388544	17388686	**SLC7A2**
chr16	56459154	56459296	**AMFR**	chr8	29119971	29120113	**KIF13B**
chr16	81465802	81465944	**CMIP**	chr8	56874070	56874212	**LYN**
chr16	58893998	58894140	**GOT2**	chr8	74207214	74207356	**RDH10**
chr16	29700909	29701051	**QPRT**	chr8	91658688	91658830	**TMEM64**
chr16	57300169	57300311	**PLLP**	chr8	56832187	56832329	**LYN**
chr16	57509871	57510013	**DOK4**	chr8	102904095	102904237	**NCALD**
chr16	57640635	57640777	**GPR56**	chr8	134581272	134581414	**ST3GAL1**
chr16	58460158	58460300	**GINS3**	chr8	56852603	56852745	**LYN**
chr16	81515093	81515235	**CMIP**	chr9	123659578	123659720	**PHF19**
chr16	81503505	81503647	**CMIP**	chr9	137248894	137249036	**RXRA**
chr16	89988848	89988990	**TUBB3**	chr9	110778090	110778232	**KLF4**
chr16	231401	231543	**HBQ1**	chr9	90131305	90131447	**DAPK1**
chr16	20837403	20837545	**ERI2**	chr9	114937504	114937646	**SUSD1**
chr16	20843142	20843284	**ERI2**	chr9	131208778	131208920	**ODF2**
chr16	57635751	57635893	**GPR56**	chr9	136024798	136024940	**RALGDS**
chr16	46722225	46722367	**VPS35**	chr9	37592512	37592654	**TOMM5**
chr16	56496378	56496520	**OGFOD1**	chr9	114823686	114823828	**SUSD1**
chr16	57291092	57291234	**ARL2BP**	chr9	38039999	38040141	**SHB**
chr16	58452769	58452911	**GINS3**	chr9	114942738	114942880	**SUSD1**
chr16	90085904	90086046	**DBNDD1**	chr9	129707980	129708122	**RALGPS1**
chr16	81529437	81529579	**CMIP**	chr9	130324231	130324373	**FAM129B**
chr16	84894078	84894220	**CRISPLD2**	chr9	100944532	100944674	**CORO2A**
chr16	75712188	75712330	**TERF2IP**	chr9	139679592	139679734	**TMEM141**
chr17	39949246	39949388	**JUP**	chr9	37336189	37336331	**GRHPR**
chr17	72414925	72415067	**GPRC5C**	chr9	37362531	37362673	**GRHPR**
chr17	75118006	75118148	**SEC14L1**	chr9	37987561	37987703	**SHB**
chr17	75118709	75118851	**SEC14L1**	chr9	38227124	38227266	**SHB**
chr17	49230819	49230961	**NME1-NME2**	chr9	78974317	78974459	**RFK**
chr17	55063176	55063318	**SCPEP1**	chr9	86595563	86595705	**RMI1**
chr17	62084169	62084311	**ICAM2**	chr9	90166797	90166939	**DAPK1**

chr17	73092315	73092457	**SLC16A5**	chr9	108005424	108005566	**SLC44A1**
chr17	76125205	76125347	**TMC6**	chr9	110863793	110863935	**KLF4**
chr17	46949090	46949232	**ATP5G1**	chr9	114855856	114855998	**SUSD1**
chr17	73070752	73070894	**SLC16A5**	chr9	114943462	114943604	**SUSD1**
chr17	73343138	73343280	**SLC25A19**	chr9	110856563	110856705	**KLF4**
chr17	76124876	76125018	**TMC6**	chr9	129949904	129950046	**ANGPTL2**
chr17	79917644	79917786	**NOTUM**	chr9	136009225	136009367	**RALGDS**
chr17	80188856	80188998	**SLC16A3**	chr9	139675121	139675263	**TMEM141**
chr17	80246000	80246142	**CSNK1D**	chr9	19154347	19154489	**PLIN2**
chr17	3570739	3570881	**TAX1BP3**	chr9	90193609	90193751	**DAPK1**
chr17	17109704	17109846	**PLD6**	chr9	123638585	123638727	**PHF19**
chr17	40540789	40540931	**STAT3**	chr9	110871152	110871294	**KLF4**
chr17	55416043	55416185	**MSI2**	chr9	114937027	114937169	**SUSD1**
chr17	55456930	55457072	**MSI2**	chr9	126964730	126964872	**NEK6**
chr17	56495061	56495203	**RNF43**	chr9	129891765	129891907	**ANGPTL2**
chr17	57368034	57368176	**YPEL2**	chr9	135998501	135998643	**RALGDS**
chr17	73068190	73068332	**SLC16A5**	chr9	137168407	137168549	**RXRA**
chr17	79919165	79919307	**NOTUM**	chr9	259768	259910	**DOCK8**
chr17	7386671	7386813	**ZBTB4**	chr9	19161642	19161784	**PLIN2**
chr17	27239489	27239631	**DHRS13**	chr9	37337385	37337527	**GRHPR**
chr17	28690923	28691065	**CPD**	chr9	38108105	38108247	**SHB**
chr17	35849888	35850030	**DUSP14**	chr9	97176044	97176186	**HIATL1**
chr17	39940588	39940730	**JUP**	chr9	100936838	100936980	**CORO2A**
chr17	39941407	39941549	**JUP**	chr9	101094951	101095093	**TBC1D2**
chr17	55417922	55418064	**MSI2**	chr9	110546892	110547034	**KLF4**
chr17	56465279	56465421	**RNF43**	chr9	108006618	108006760	**SLC44A1**
chr17	56514444	56514586	**RNF43**	chr9	110471179	110471321	**KLF4**
chr17	72426845	72426987	**GPRC5C**	chr9	116030529	116030671	**CDC26**
chr17	27234969	27235111	**DHRS13**	chr9	127085067	127085209	**NEK6**
chr17	40520883	40521025	**STAT3**	chr9	129748191	129748333	**RALGPS1**
chr17	40573744	40573886	**PTRF**	chr9	129797102	129797244	**RALGPS1**
chr17	40683560	40683702	**NAGLU**	chr9	130742944	130743086	**FAM102A**
chr17	55453202	55453344	**MSI2**	chr9	110556693	110556835	**KLF4**
chr17	62101588	62101730	**ICAM2**	chr9	114835353	114835495	**SUSD1**
chr17	65653165	65653307	**NOL11**	chr9	137230436	137230578	**RXRA**
chr17	40567207	40567349	**PTRF**	chr9	38390547	38390689	**ALDH1B1**
chr17	48415329	48415471	**XYLT2**	chr9	78977526	78977668	**RFK**
chr17	53528773	53528915	**MMD**	chr9	90133884	90134026	**DAPK1**
chr17	73869064	73869206	**TRIM47**	chr9	110470425	110470567	**KLF4**
chr17	79679128	79679270	**SLC25A10**	chr9	36006679	36006821	**RECK**
chr17	79689497	79689639	**SLC25A10**	chr9	38130836	38130978	**SHB**
chr17	80248145	80248287	**CSNK1D**	chr9	107508293	107508435	**NIPSNAP3A**
chr17	80281541	80281683	**CD7**	chrX	9431169	9431311	**TBL1X**
chr18	47951632	47951774	**SKA1**	chrX	39957084	39957226	**BCOR**
chr18	20780881	20781023	**CABLES1**	chrX	40007829	40007971	**BCOR**

chr18	46355252	46355394	**SMAD7**
chr18	46459510	46459652	**SMAD7**
chr18	9743587	9743729	**RAB31**
chr18	12283739	12283881	**TUBB6**
chr18	12308253	12308395	**TUBB6**
chr18	34048304	34048446	**FHOD3**
chr18	46474876	46475018	**SMAD7**
chr18	46501851	46501993	**SMAD7**
chr18	12302565	12302707	**TUBB6**
chr18	47922445	47922587	**SKA1**
chr18	725163	725305	**ENOSF1**
chr18	9700490	9700632	**RAB31**
chr18	11981088	11981230	**IMPA2**
chr18	47885297	47885439	**SKA1**
chr18	46369154	46369296	**SMAD7**
chr18	48533426	48533568	**SMAD4**
chr18	48737989	48738131	**MEX3C**
chr18	71919097	71919239	**CYB5A**
chr18	11947225	11947367	**IMPA2**
chr18	46423338	46423480	**SMAD7**
chr18	46460439	46460581	**SMAD7**
chr18	71909912	71910054	**CYB5A**
chr18	322660	322802	**THOC1**
chr18	11951586	11951728	**IMPA2**
chr18	46508685	46508827	**SMAD7**
chr18	255334	255476	**THOC1**
chr18	267956	268098	**THOC1**
chr18	11851236	11851378	**CHMP1B**
chr19	8483132	8483274	**37316**
chr19	45245200	45245342	**BCL3**
chr19	13208800	13208942	**LYL1**
chr19	15947473	15947615	**UCA1**
chr19	49376879	49377021	**PPP1R15A**
chr19	39894525	39894667	**ZFP36**
chr19	49375647	49375789	**PPP1R15A**
chr19	3061461	3061603	**AES**
chr19	12904463	12904605	**JUNB**
chr19	21298362	21298504	**ZNF431**
chr19	35466901	35467043	**ZNF792**
chr19	39893192	39893334	**ZFP36**
chr19	45256670	45256812	**BCL3**
chr19	13190349	13190491	**LYL1**
chr19	13180565	13180707	**LYL1**
chr19	21412868	21413010	**ZNF431**
chr19	34745721	34745863	**KIAA0355**
chrX	117748277	117748419	**IL13RA1**
chrX	129216987	129217129	**ELF4**
chrX	9310622	9310764	**TBL1X**
chrX	39710095	39710237	**BCOR**
chrX	39612670	39612812	**BCOR**
chrX	39676266	39676408	**BCOR**
chrX	39949715	39949857	**BCOR**
chrX	39977204	39977346	**BCOR**
chrX	46907566	46907708	**RGN**
chrX	48554794	48554936	**SUV39H1**
chrX	106440656	106440798	**NUP62CL**
chrX	39719814	39719956	**BCOR**
chrX	39813211	39813353	**BCOR**
chrX	39958472	39958614	**BCOR**
chrX	100587856	100587998	**TIMM8A**
chrX	106411572	106411714	**NUP62CL**
chrX	109083841	109083983	**ACSL4**
chrX	129254895	129255037	**ELF4**
chrX	15598089	15598231	**ACE2**
chrX	9484110	9484252	**TBL1X**
chrX	39869828	39869970	**BCOR**
chrX	40032056	40032198	**BCOR**
chrX	22011544	22011686	**PHEX**
chrX	23685440	23685582	**PRDX4**
chrX	23717784	23717926	**PRDX4**
chrX	39874056	39874198	**BCOR**

chr19	35532028	35532170	**HPN**
chr19	2476054	2476196	**GADD45B**
chr19	8420581	8420723	**ANGPTL4**
chr19	11494875	11495017	**EPOR**
chr19	21309916	21310058	**ZNF431**
chr19	33668186	33668328	**LRP3**
chr19	49381958	49382100	**PPP1R15A**
chr19	46405699	46405841	**MYPOP**
chr19	49864751	49864893	**TEAD2**
chr19	16426907	16427049	**KLF2**
chr19	2495015	2495157	**GADD45B**
chr19	14607043	14607185	**GIPC1**
chr19	17357642	17357784	**NR2F6**
chr19	12895504	12895646	**JUNB**
chr19	19171093	19171235	**SLC25A42**
chr19	21323690	21323832	**ZNF431**
chr19	21341486	21341628	**ZNF431**
chr19	40949289	40949431	**SERTAD3**
chr19	35453420	35453562	**ZNF792**
chr19	35760503	35760645	**USF2**
chr19	40931536	40931678	**SERTAD1**
chr19	42432490	42432632	**RABAC1**
chr19	42444264	42444406	**RABAC1**
chr19	15939755	15939897	**UCA1**
chr19	13213617	13213759	**LYL1**
chr19	45996013	45996155	**RTN2**
chr19	15955399	15955541	**UCA1**
chr19	21311705	21311847	**ZNF431**
chr2	47434248	47434390	**CALM2**
chr2	64880410	64880552	**SERTAD2**
chr2	70529178	70529320	**FAM136A**
chr2	43406261	43406403	**ZFP36L2**
chr2	111943286	111943428	**BCL2L11**
chr2	112997501	112997643	**ZC3H8**
chr2	69970772	69970914	**ANXA4**
chr2	149639774	149639916	**KIF5C**
chr2	158755237	158755379	**ACVR1**
chr2	159887398	159887540	**TANC1**
chr2	169115082	169115224	**STK39**
chr2	178146164	178146306	**NFE2L2**
chr2	190381385	190381527	**SLC40A1**
chr2	197425858	197426000	**HECW2**
chr2	198342586	198342728	**HSPD1**
chr2	202824042	202824184	**FZD7**
chr2	202827244	202827386	**FZD7**

chr2	215673779	215673921	**BARD1**
chr2	224810055	224810197	**WDFY1**
chr2	120135359	120135501	**DBI**
chr2	145128583	145128725	**GTDC1**
chr2	179134620	179134762	**OSBPL6**
chr2	219663897	219664039	**CYP27A1**
chr2	21451477	21451619	**APOB**
chr2	64872336	64872478	**SERTAD2**
chr2	169708394	169708536	**SPC25**
chr2	190371479	190371621	**WDR75**
chr2	190446749	190446891	**SLC40A1**
chr2	190477897	190478039	**SLC40A1**
chr2	227637521	227637663	**IRS1**
chr2	30806339	30806481	**LCLAT1**
chr2	192701706	192701848	**SDPR**
chr2	202914704	202914846	**FZD7**
chr2	219262463	219262605	**CTDSP1**
chr2	43395936	43396078	**ZFP36L2**
chr2	70026381	70026523	**GMCL1**
chr2	97485085	97485227	**CNNM3**
chr2	190473628	190473770	**SLC40A1**
chr2	10533305	10533447	**HPCAL1**
chr2	37642335	37642477	**QPCT**
chr2	69971683	69971825	**ANXA4**
chr2	75089576	75089718	**HK2**
chr2	88991136	88991278	**RPIA**
chr2	145090013	145090155	**GTDC1**
chr2	219152593	219152735	**TMBIM1**
chr2	158755894	158756036	**ACVR1**
chr2	188452002	188452144	**TFPI**
chr2	203307658	203307800	**BMPR2**
chr2	9341373	9341515	**ASAP2**
chr2	10483432	10483574	**HPCAL1**
chr2	10510092	10510234	**HPCAL1**
chr2	128165644	128165786	**PROC**
chr2	30736528	30736670	**LCLAT1**
chr2	43405243	43405385	**ZFP36L2**
chr2	47406613	47406755	**CALM2**
chr2	64978566	64978708	**SERTAD2**
chr2	85814845	85814987	**VAMP5**
chr2	138786141	138786283	**HNMT**
chr2	190386507	190386649	**SLC40A1**
chr2	42274748	42274890	**PKDCC**
chr2	47402650	47402792	**CALM2**
chr2	47454767	47454909	**CALM2**

chr2	47464687	47464829	**CALM2**
chr2	64881186	64881328	**SERTAD2**
chr2	70045491	70045633	**GMCL1**
chr2	88982793	88982935	**RPIA**
chr2	102408010	102408152	**MAP4K4**
chr2	144909077	144909219	**GTDC1**
chr2	157198907	157199049	**NR4A2**
chr2	158643445	158643587	**ACVR1**
chr2	178129475	178129617	**NFE2L2**
chr2	188381474	188381616	**TFPI**
chr2	191217651	191217793	**INPP1**
chr2	191513591	191513733	**NAB1**
chr2	200320504	200320646	**SATB2**
chr2	202397513	202397655	**STRADB**
chr2	203283442	203283584	**BMPR2**
chr2	209119108	209119250	**IDH1**
chr2	219287304	219287446	**VIL1**
chr2	223725437	223725579	**ACSL3**
chr2	10418717	10418859	**HPCAL1**
chr2	20425122	20425264	**SDC1**
chr2	27309392	27309534	**KHK**
chr2	30369416	30369558	**YPEL5**

References

1. de Larco JE, Todaro GJ. Growth factors from murine sarcoma virus-transformed cells. Proc Natl Acad Sci U S A. UNITED STATES; 1978 Aug;75(8):4001–5.
2. Roberts AB, Anzano MA, Lamb LC, Smith JM, Sporn MB. New class of transforming growth factors potentiated by epidermal growth factor: isolation from non-neoplastic tissues. Proc Natl Acad Sci U S A. UNITED STATES; 1981 Sep;78(9):5339–43.
3. Derynck R, Jarrett JA, Chen EY, Eaton DH, Bell JR, Assoian RK, et al. Human transforming growth factor-beta complementary DNA sequence and expression in normal and transformed cells. Nature. ENGLAND; 1985 Aug;316(6030):701–5.
4. Hinck AP. Structural studies of the TGF-betas and their receptors - insights into evolution of the TGF-beta superfamily. FEBS Lett. 2012;586(14):1860–70. doi: 10.1016/j.febslet.2012.05.028. Epub .
5. Mueller TD, Nickel J. Promiscuity and specificity in BMP receptor activation. FEBS Lett [Internet]. 2012 Jul 4;586(14):1846–59. Available from: http://www.sciencedirect.com/science/article/pii/S0014579312001664
6. Brennan J, Norris DP, Robertson EJ. Nodal activity in the node governs left-right asymmetry. Genes Dev. United States; 2002 Sep;16(18):2339–44.
7. Meno C, Saijoh Y, Fujii H, Ikeda M, Yokoyama T, Yokoyama M, et al. Left-right asymmetric expression of the TGF beta-family member lefty in mouse embryos. Nature. ENGLAND; 1996 May;381(6578):151–5.
8. Borowiak M, Maehr R, Chen S, Chen AE, Tang W, Fox JL, et al. Small molecules efficiently direct endodermal differentiation of mouse and human embryonic stem cells. Cell Stem Cell. United States; 2009 Apr;4(4):348–58.
9. Rossi JM, Dunn NR, Hogan BLM, Zaret KS. Distinct mesodermal signals, including BMPs from the septum transversum mesenchyme, are required in combination for hepatogenesis from the endoderm. Genes Dev [Internet]. 2001 Aug 1;15 (15):1998–2009. Available from: http://genesdev.cshlp.org/content/15/15/1998.abstract
10. Estevez M, Attisano L, Wrana JL, Albert PS, Massague J, Riddle DL. The daf-4 gene encodes a bone morphogenetic protein receptor controlling C. elegans dauer larva development. Nature. ENGLAND; 1993 Oct;365(6447):644–9.
11. Suzuki Y, Yandell MD, Roy PJ, Krishna S, Savage-Dunn C, Ross RM, et al. A BMP homolog acts as a dose-dependent regulator of body size and male tail patterning in Caenorhabditis elegans. Development. ENGLAND; 1999 Jan;126(2):241–50.
12. Hamaratoglu F, Affolter M, Pyrowolakis G. Dpp/BMP signaling in flies: from molecules to biology. Semin Cell Dev Biol. England; 2014 Aug;32:128–36.
13. Haerry TE, O'Connor MB. Isolation of Drosophila activin and follistatin cDNAs using novel MACH amplification protocols. Gene. Netherlands; 2002 May;291(1-2):85–93.
14. Wang EA, Rosen V, D'Alessandro JS, Bauduy M, Cordes P, Harada T, et al. Recombinant human bone morphogenetic protein induces bone formation. Proc Natl Acad Sci U S A. UNITED STATES; 1990 Mar;87(6):2220–4.
15. Hegarty S V, O'Keeffe GW, Sullivan AM. BMP-Smad 1/5/8 signalling in the development of the nervous system. Prog Neurobiol. England; 2013 Oct;109:28–41.
16. Core AB, Canali S, Babitt JL. Hemojuvelin and bone morphogenetic protein (BMP) signaling in iron homeostasis. Front Pharmacol. Switzerland; 2014;5:104.
17. Cheng H, Jiang W, Phillips FM, Haydon RC, Peng Y, Zhou L, et al. Osteogenic activity of the fourteen types of human bone morphogenetic proteins (BMPs). J Bone Joint Surg Am. United States; 2003 Aug;85-A(8):1544–52.
18. Mieko Mizutani C, Bier E. EvoD/Vo: the origins of BMP signalling in the neuroectoderm. Nat Rev Genet [Internet]. Nature Publishing Group; 2008 Sep;9(9):663–77. Available from: http://dx.doi.org/10.1038/nrg2417
19. Bier E, De Robertis EM. BMP gradients: A paradigm for morphogen-mediated developmental patterning. Sci [Internet]. 2015 Jun 26;348 (6242). Available from: http://www.sciencemag.org/content/348/6242/aaa5838.abstract
20. Urist MR. Bone: Formation by Autoinduction. Sci [Internet]. 1965 Nov 12;150 (3698):893–9. Available from: http://www.sciencemag.org/content/150/3698/893.abstract
21. Urist MR, Strates BS. Bone Morphogenetic Protein. J Dent Res [Internet]. 1971 Nov 1;50 (6):1392–406. Available from: http://jdr.sagepub.com/content/50/6/1392.short
22. Wozney JM, Rosen V, Celeste AJ, Mitsock LM, Whitters MJ, Kriz RW, et al. Novel regulators of bone formation: molecular clones and activities. Science. UNITED STATES; 1988 Dec;242(4885):1528–34.
23. Celeste AJ, Iannazzi JA, Taylor RC, Hewick RM, Rosen V, Wang EA, et al. Identification of transforming growth factor beta family members present in bone-inductive protein purified from bovine bone. Proc Natl Acad Sci U S A. UNITED STATES; 1990 Dec;87(24):9843–7.
24. Hahn G V, Cohen RB, Wozney JM, Levitz CL, Shore EM, Zasloff MA, et al. A bone morphogenetic protein subfamily: chromosomal localization of human genes for BMP5, BMP6, and BMP7. Genomics. UNITED STATES; 1992 Nov;14(3):759–62.
25. Tabas JA, Zasloff M, Wasmuth JJ, Emanuel BS, Altherr MR, McPherson JD, et al. Bone morphogenetic protein: chromosomal localization of human genes for BMP1, BMP2A, and BMP3. Genomics. UNITED STATES; 1991 Feb;9(2):283–9.
26. Rider CC, Mulloy B. Bone morphogenetic protein and growth differentiation factor cytokine families and their protein antagonists. Biochem J. 2010;429(1):1–12. doi: 10.1042/BJ20100305.
27. Brown MA, Zhao Q, Baker KA, Naik C, Chen C, Pukac L, et al. Crystal Structure of BMP-9 and Functional Interactions with Pro-region and Receptors. J Biol Chem [Internet]. 2005 Jul 1;280 (26):25111–8. Available from: http://www.jbc.org/content/280/26/25111.abstract
28. Allendorph GP, Isaacs MJ, Kawakami Y, Izpisua Belmonte JC, Choe S. BMP-3 and BMP-6 Structures Illuminate the Nature of Binding Specificity with Receptors†,‡. Biochemistry [Internet]. American Chemical Society; 2007 Oct 1;46(43):12238–47. Available from: http://dx.doi.org/10.1021/bi700907k
29. Cui Y, Jean F, Thomas G, Christian JL. BMP-4 is proteolytically activated by furin and/or PC6 during vertebrate embryonic development. EMBO J. ENGLAND; 1998 Aug;17(16):4735–43.
30. Cui Y, Hackenmiller R, Berg L, Jean F, Nakayama T, Thomas G, et al. The activity and signaling range of mature BMP-4 is regulated by sequential cleavage at two sites within the prodomain of the precursor. Genes Dev. United States; 2001 Nov;15(21):2797–802.

31. ten Dijke P, Yamashita H, Sampath TK, Reddi AH, Estevez M, Riddle DL, et al. Identification of type I receptors for osteogenic protein-1 and bone morphogenetic protein-4. J Biol Chem. UNITED STATES; 1994 Jun;269(25):16985–8.

32. ten Dijke P, Ichijo H, Franzen P, Schulz P, Saras J, Toyoshima H, et al. Activin receptor-like kinases: a novel subclass of cell-surface receptors with predicted serine/threonine kinase activity. Oncogene. 1993;8(10):2879–87.

33. Ide H, Katoh M, Sasaki H, Yoshida T, Aoki K, Nawa Y, et al. Cloning of human bone morphogenetic protein type IB receptor (BMPR-IB) and its expression in prostate cancer in comparison with other BMPRs. Oncogene. ENGLAND; 1997 Mar;14(11):1377–82.

34. David L, Mallet C, Mazerbourg S, Feige J-J, Bailly S. Identification of BMP9 and BMP10 as functional activators of the orphan activin receptor-like kinase 1 (ALK1) in endothelial cells. Blood. United States; 2007 Mar;109(5):1953–61.

35. Yeo C, Whitman M. Nodal signals to Smads through Cripto-dependent and Cripto-independent mechanisms. Mol Cell. United States; 2001 May;7(5):949–57.

36. Lee PL, Beutler E, Rao S V, Barton JC. Genetic abnormalities and juvenile hemochromatosis: mutations of the HJV gene encoding hemojuvelin. Blood. United States; 2004 Jun;103(12):4669–71.

37. Li DY, Sorensen LK, Brooke BS, Urness LD, Davis EC, Taylor DG, et al. Defective angiogenesis in mice lacking endoglin. Science. UNITED STATES; 1999 May;284(5419):1534–7.

38. Strizzi L, Bianco C, Normanno N, Salomon D. Cripto-1: a multifunctional modulator during embryogenesis and oncogenesis. Oncogene. England; 2005 Aug;24(37):5731–41.

39. Fukuda T, Kohda M, Kanomata K, Nojima J, Nakamura A, Kamizono J, et al. Constitutively activated ALK2 and increased SMAD1/5 cooperatively induce bone morphogenetic protein signaling in fibrodysplasia ossificans progressiva. J Biol Chem. United States; 2009 Mar;284(11):7149–56.

40. Yu PB, Deng DY, Lai CS, Hong CC, Cuny GD, Bouxsein ML, et al. BMP type I receptor inhibition reduces heterotopic [corrected] ossification. Nat Med. United States; 2008 Dec;14(12):1363–9.

41. Xu RH, Kim J, Taira M, Zhan S, Sredni D, Kung HF. A dominant negative bone morphogenetic protein 4 receptor causes neuralization in Xenopus ectoderm. Biochem Biophys Res Commun. UNITED STATES; 1995 Jul;212(1):212–9.

42. Yang C, Yang L, Wan M, Cao X. Generation of a mouse model with expression of bone morphogenetic protein type II receptor lacking the cytoplasmic domain in osteoblasts. Ann N Y Acad Sci. United States; 2010 Mar;1192:286–91.

43. Racacho L, Byrnes AM, MacDonald H, Dranse HJ, Nikkel SM, Allanson J, et al. Two novel disease-causing variants in BMPR1B are associated with brachydactyly type A1. Eur J Hum Genet. 2015 Mar;

44. Miyazono K, Kamiya Y, Morikawa M. Bone morphogenetic protein receptors and signal transduction. J Biochem. England; 2010 Jan;147(1):35–51.

45. Morikawa M, Koinuma D, Miyazono K, Heldin C-H. Genome-wide mechanisms of Smad binding. Oncogene. England; 2013 Mar;32(13):1609–15.

46. Katagiri T, Imada M, Yanai T, Suda T, Takahashi N, Kamijo R. Identification of a BMP-responsive element in Id1, the gene for inhibition of myogenesis. Genes Cells. England; 2002 Sep;7(9):949–60.

47. Takase M, Imamura T, Sampath TK, Takeda K, Ichijo H, Miyazono K, et al. Induction of Smad6 mRNA by bone morphogenetic proteins. Biochem Biophys Res Commun. UNITED STATES; 1998 Mar;244(1):26–9.

48. Pogoda H-M, Meyer D. Zebrafish Smad7 is regulated by Smad3 and BMP signals. Dev Dyn. United States; 2002 Jul;224(3):334–49.

49. Derynck R, Zhang YE. Smad-dependent and Smad-independent pathways in TGF-beta family signalling. Nature. England; 2003 Oct;425(6958):577–84.

50. Li Q, Zhang YY, Chiu S, Hu Z, Lan KH, Cha H, et al. Integrative functional genomics of hepatitis C virus infection identifies host dependencies in complete viral replication cycle. PLoS Pathog. 2014/05/24 ed. 2014;10(5):e1004163.

51. Takenobu K, Tatsua S, Miyazono K. The Bone Morphogenetic Proteins. In: Derynck R, Miyazono K, editors. The TGF-β Family. Cold Sprin. Cold Spring Harbour: Cold Spring Harbour Laboratory Press; 2008. p. 121–49.

52. Zakin L, De Robertis EM. Extracellular regulation of BMP signaling. Curr Biol. England; 2010 Feb;20(3):R89–92.

53. Dupont S, Zacchigna L, Cordenonsi M, Soligo S, Adorno M, Rugge M, et al. Germ-layer specification and control of cell growth by Ectodermin, a Smad4 ubiquitin ligase. Cell. United States; 2005 Apr;121(1):87–99.

54. Dupont S, Mamidi A, Cordenonsi M, Montagner M, Zacchigna L, Adorno M, et al. FAM/USP9x, a deubiquitinating enzyme essential for TGFbeta signaling, controls Smad4 monoubiquitination. Cell. United States; 2009 Jan;136(1):123–35.

55. Babitt JL, Zhang Y, Samad TA, Xia Y, Tang J, Campagna JA, et al. Repulsive guidance molecule (RGMa), a DRAGON homologue, is a bone morphogenetic protein co-receptor. J Biol Chem. United States; 2005 Aug;280(33):29820–7.

56. Babitt JL, Huang FW, Wrighting DM, Xia Y, Sidis Y, Samad TA, et al. Bone morphogenetic protein signaling by hemojuvelin regulates hepcidin expression. Nat Genet. United States; 2006 May;38(5):531–9.

57. Vadon-Le Goff S, Hulmes DJS, Moali C. BMP-1/tolloid-like proteinases synchronize matrix assembly with growth factor activation to promote morphogenesis and tissue remodeling. Matrix biology : journal of the International Society for Matrix Biology. 2015. p. 14–23.

58. Silvestri L, Pagani A, Nai A, De Domenico I, Kaplan J, Camaschella C. THE SERINE PROTEASE MATRIPTASE-2 (TMPRSS6) INHIBITS HEPCIDIN ACTIVATION BY CLEAVING MEMBRANE HEMOJUVELIN. Cell Metab [Internet]. 2008 Dec 30;8(6):502–11. Available from: http://www.ncbi.nlm.nih.gov/pmc/articles/PMC2648389/

59. Pearson KL, Hunter T, Janknecht R. Activation of Smad1-mediated transcription by p300/CBP. Biochim Biophys Acta. NETHERLANDS; 1999 Dec;1489(2-3):354–64.

60. Shikama N, Lutz W, Kretzschmar R, Sauter N, Roth J-F, Marino S, et al. Essential function of p300 acetyltransferase activity in heart, lung and small intestine formation. EMBO J. England; 2003 Oct;22(19):5175–85.

61. Trompouki E, Bowman T V, Lawton LN, Fan ZP, Wu DC, DiBiase A, et al. Lineage regulators direct BMP and Wnt pathways to cell-specific programs during differentiation and regeneration. Cell. 2011/11/01 ed. 2011;147(3):577–89.

62. Yu PB, Hong CC, Sachidanandan C, Babitt JL, Deng DY, Hoyng SA, et al. Dorsomorphin inhibits BMP signals required for embryogenesis and iron metabolism. Nat Chem Biol. United States; 2008 Jan;4(1):33–41.

63. Cuny GD, Yu PB, Laha JK, Xing X, Liu JF, Lai CS, et al. Structure-activity relationship study of bone morphogenetic protein (BMP) signaling inhibitors. Bioorg Med Chem Lett. 2008;18(15):4388–92. doi: 10.1016/j.bmcl.2008.06.052. Epub 200.

64. Ling N, Ying SY, Ueno N, Esch F, Denoroy L, Guillemin R. Isolation and partial characterization of a Mr 32,000 protein with inhibin activity from porcine follicular fluid. Proc Natl Acad Sci U S A. UNITED STATES; 1985 Nov;82(21):7217–21.

65. Ling N, Ying SY, Ueno N, Shimasaki S, Esch F, Hotta M, et al. Pituitary FSH is released by a heterodimer of the beta-subunits from the two forms of inhibin. Nature. 1986;321(6072):779–82.

66. Vale W, Rivier J, Vaughan J, McClintock R, Corrigan A, Woo W, et al. Purification and characterization of an FSH releasing protein from porcine ovarian follicular fluid. Nature. ENGLAND; 1986 Jun;321(6072):776–9.

67. Wiater E, Vale WW. Activins and Inhibins. In: Derynck R, Miyazono K, editors. The TGF-β Family. Cold Sprin. Cold Spring Harbour: Cold Spring Harbour Laboratory Press; 2008. p. 79–120.

68. Robson NC, Phillips DJ, McAlpine T, Shin A, Svobodova S, Toy T, et al. Activin-A: a novel dendritic cell-derived cytokine that potently attenuates CD40 ligand-specific cytokine and chemokine production. Blood. 2008;111(5):2733–43. Epub 2007 Dec 21.

69. Shao L, Frigon Jr. NL, Sehy DW, Yu AL, Lofgren J, Schwall R, et al. Regulation of production of activin A in human marrow stromal cells and monocytes. Exp Hematol. 1992;20(10):1235–42.

70. de Kretser DM, O'Hehir RE, Hardy CL, Hedger MP. The roles of activin A and its binding protein, follistatin, in inflammation and tissue repair. Mol Cell Endocrinol [Internet]. 2012 Aug 15;359(1–2):101–6. Available from: http://www.sciencedirect.com/science/article/pii/S0303720711006058

71. Dennler S, Itoh S, Vivien D, ten Dijke P, Huet S, Gauthier JM. Direct binding of Smad3 and Smad4 to critical TGF beta-inducible elements in the promoter of human plasminogen activator inhibitor-type 1 gene. EMBO J. ENGLAND; 1998 Jun;17(11):3091–100.

72. Besson-Fournier C, Latour C, Kautz L, Bertrand J, Ganz T, Roth MP, et al. Induction of activin B by inflammatory stimuli up-regulates expression of the iron-regulatory peptide hepcidin through Smad1/5/8 signaling. Blood. 2012;120(2):431–9. doi: 10.1182/blood – 2012–02 – 411470. Epub 201.

73. Miyazono K. Regulation of TGF-β Family Signalling by Inhibitory SMADs. In: Derynck R, Miyazono K, editors. The TGF-β Family. Cold Spring Harbour Laboratory Press; 2008. p. 363–87.

74. Saito S, Sidis Y, Mukherjee A, Xia Y, Schneyer A. Differential biosynthesis and intracellular transport of follistatin isoforms and follistatin-like-3. Endocrinology. United States; 2005 Dec;146(12):5052–62.

75. Blount AL, Vaughan JM, Vale WW, Bilezikjian LM. A Smad-binding Element in Intron 1 Participates in Activin-dependent Regulation of the Follistatin Gene. J Biol Chem [Internet]. 2008 Mar 14;283 (11):7016–26. Available from: http://www.jbc.org/content/283/11/7016.abstract

76. Blount AL, Schmidt K, Justice NJ, Vale WW, Fischer WH, Bilezikjian LM, et al. FoxL2 and Smad3 Coordinately Regulate Follistatin Gene Transcription. J Biol Chem [Internet]. 2008 Mar 14;284 (12):7631–45. Available from: http://www.jbc.org/content/283/11/7016.abstract

77. Delbaere A, Sidis Y, Schneyer AL. Differential response to exogenous and endogenous activin in a human ovarian teratocarcinoma-derived cell line (PA-1): regulation by cell surface follistatin. Endocrinology. UNITED STATES; 1999 Jun;140(6):2463–70.

78. Sugino H, Sugino K, Hashimoto O, Shoji H, Nakamura T. Follistatin and its role as an activin-binding protein. J Med Invest. JAPAN; 1997 Aug;44(1-2):1–14.

79. Lin W, Weinberg EM, Tai AW, Peng LF, Brockman MA, Kim K-A, et al. HIV increases HCV replication in a TGF-beta1-dependent manner. Gastroenterology. United States; 2008 Mar;134(3):803–11.

80. Murata T, Ohshima T, Yamaji M, Hosaka M, Miyanari Y, Hijikata M, et al. Suppression of hepatitis C virus replicon by TGF-beta. Virology. United States; 2005 Jan;331(2):407–17.

81. Feng X-H, Derynck R. Specificity and versatility in tgf-beta signaling through Smads. Annu Rev Cell Dev Biol. United States; 2005;21:659–93.

82. Nattermann J, Vogel M, Nischalke HD, Danta M, Ahlenstiel G, Michalk M, et al. The transforming growth factor-beta high-producer genotype is associated with response to hepatitis C virus-specific therapy in HIV-positive patients with acute hepatitis C. AIDS. England; 2008 Jul;22(11):1287–92.

83. Harfouch S, Guiguet M, Valantin M-A, Samri A, Ouazene Z, Slama L, et al. Lack of TGF-beta production by hepatitis C virus-specific T cells during HCV acute phase is associated with HCV clearance in HIV coinfection. J Hepatol. England; 2012 Jun;56(6):1259–68.

84. Benzoubir N, Lejamtel C, Battaglia S, Testoni B, Benassi B, Gondeau C, et al. HCV core-mediated activation of latent TGF-beta via thrombospondin drives the crosstalk between hepatocytes and stromal environment. J Hepatol. Netherlands; 2013 Dec;59(6):1160–8.

85. Hidalgo LMVGVJH-LCVMNNJRZAGSRVAVA. Expression of BMPRIA on human thymic NK cell precursors: role of BMP signaling in intrathymic NK cell development. Blood [Internet]. 2011;119(8):1861–71. Available from: http://www.bloodjournal.org/content/119/8/1861.abstract

86. Robson NC, Hidalgo L, McAlpine T, Wei H, Martinez VG, Entrena A, et al. Optimal effector functions in human natural killer cells rely upon autocrine bone morphogenetic protein signaling. Cancer Res. United States; 2014 Sep;74(18):5019–31.

87. Martínez VG, Hidalgo L, Valencia J, Hernández-López C, Entrena A, del Amo BG, et al. Autocrine activation of canonical BMP signaling regulates PD-L1 and PD-L2 expression in human dendritic cells. Eur J Immunol [Internet]. 2014;44(4):1031–8. Available from: http://dx.doi.org/10.1002/eji.201343693

88. Robson NC, Wei H, McAlpine T, Kirkpatrick N, Cebon J, Maraskovsky E. Activin-A attenuates several human natural killer cell functions. Blood. 2009;113(14):3218–25. doi: 10.1182/blood – 2008–07 – 166926. Epub 2.

89. Shao L-E, Frigon Normand L. J, Yu A, Palyash J, Yu J. CONTRASTING EFFECTS OF INFLAMMATROY CYTOKINES AND GLUCOCORTICOIDS ON THE PRODUCTION OF ACTIVIN A IN HUMAN MARROW STROMAL CELLS AND THEIR IMPLICATIONS. Cytokine [Internet]. 1998 Mar;10(3):227–35. Available from: http://www.sciencedirect.com/science/article/pii/S1043466697902829

90. Chen Y, Wu H, Winnall WR, Loveland KL, Makanji Y, Phillips DJ, et al. Tumour necrosis factor-alpha stimulates human neutrophils to release preformed activin A. Immunol Cell Biol. 2011;89(8):889–96. doi: 10.1038/icb.2011.12. Epub 2011 Mar 29.

91. Yu J, Shao LE, Frigon NLJ, Lofgren J, Schwall R. Induced expression of the new cytokine, activin A, in human monocytes: inhibition by glucocorticoids and retinoic acid. Immunology. ENGLAND; 1996 Jul;88(3):368–74.

92. Hedger MP, Drummond AE, Robertson DM, Risbridger GP, de Kretse DM. Inhibin and activin regulate [3H]thymidine uptake by rat thymocytes and 3T3 cells in vitro. Mol Cell Endocrinol [Internet]. 1989;61(1):133–8. Available from: http://www.scopus.com/inward/record.url?eid=2-s2.0-0024558747&partnerID=40&md5=61b90ae28baaf1472d546a10a03138a4

93. Hedger MP, Clarke L. Isolation of rat blood lymphocytes using a two-step Percoll density gradient. Effect of activin (erythroid differentiation factor) on peripheral T lymphocyte proliferation in vitro. J Immunol Methods [Internet]. 1993;163(1):133–6. Available from: http://www.scopus.com/inward/record.url?eid=2-s2.0-0027205498&partnerID=40&md5=c6c4c47a3db09b83ad6e8a809004af4d

94. Brosh N, Sternberg D, Honigwachs-Sha'anani J, Lee B-C, Shav-Tal Y, Tzehoval E, et al. The plasmacytoma growth inhibitor restrictin-P is an antagonist of interleukin 6 and interleukin 11: Identification as a stroma-derived activin A. J Biol Chem [Internet]. 1995;270(49):29594–600. Available from: http://www.scopus.com/inward/record.url?eid=2-s2.0-0028818438&partnerID=40&md5=8f2d1b03a3c2549a1bdb4367cc690b71

95. Yamashita N, Nakajima T, Takahashi H, Kaneoka H, Mizushima Y, Sakane T. Effects of activin A on IgE synthesis and cytokine production by human peripheral mononuclear cells. Clin Exp Immunol [Internet]. 1993;94(1):214–9. Available from: http://www.scopus.com/inward/record.url?eid=2-s2.0-0027378407&partnerID=40&md5=6e1cbf1e59abad98851cf87465a0306e

96. Ogawa K, Funaba M, Tsujimoto M. A dual role of activin A in regulating immunoglobulin production of B cells. J Leukoc Biol [Internet]. 2008 Jun 1;83 (6):1451–8. Available from: http://www.jleukbio.org/content/83/6/1451.abstract

97. Huber S, Stahl FR, Schrader J, Luth S, Presser K, Carambia A, et al. Activin a promotes the TGF-beta-induced conversion of CD4+CD25- T cells into Foxp3+ induced regulatory T cells. J Immunol. 2009;182(8):4633–40. doi: 10.4049/jimmunol.0803143.

98. Sierra-Filardi E, Puig-Kröger A, Blanco FJ, Nieto C, Bragado R, Palomero MI, et al. Activin A skews macrophage polarization by promoting a proinflammatory phenotype and inhibiting the acquisition of anti-inflammatory macrophage markers. Blood [Internet]. 2011 Mar 9;117(19):5092–101. Available from: http://www.bloodjournal.org/content/117/19/5092.abstract

99. Nüsing RM, Barsig J. Induction of prostanoid, nitric oxide, and cytokine formation in rat bone marrow derived macrophages by activin A. Br J Pharmacol [Internet]. 1999;127(4):919–26. Available from: http://www.scopus.com/inward/record.url?eid=2-s2.0-0032984838&partnerID=40&md5=057492d8825d22d3f703a73a0c6512b4

100. Jones KL, Brauman JN, Groome NP, De Kretser DM, Phillips DJ. Activin A release into the circulation is an early event in systemic inflammation and precedes the release of follistatin. Endocrinology [Internet]. 2000;141(5):1905–8. Available from: http://www.scopus.com/inward/record.url?eid=2-s2.0-0034457246&partnerID=40&md5=dce9a9d3db469b599e0d8818616407d0

101. Jones KL, Mansell A, Patella S, Scott BJ, Hedger MP, de Kretser DM, et al. Activin A is a critical component of the inflammatory response, and its binding protein, follistatin, reduces mortality in endotoxemia. Proc Natl Acad Sci U S A. 2007;104(41):16239–44. Epub 2007 Oct 2.

102. Michel U, Ebert S, Phillips D, Nau R. Serum concentrations of activin and follistatin are elevated and run in parallel in patients with septicemia. Eur J Endocrinol [Internet]. 2003;148(5):559–64. Available from: http://www.scopus.com/inward/record.url?eid=2-s2.0-0038237434&partnerID=40&md5=3648bf316d3986622622c117c39b15be

103. Dieelberg C, Ribes S, Michel U, Redlich S, Bruck W, Nau R, et al. Follistatin does not influence the course of Escherichia coli K1 sepsis in a mouse model. Shock. United States; 2012 Dec;38(6):615–9.

104. Dignass AU, Jung S, Harder-d'Heureuse J, Wiedenmann B. Functional relevance of activin A in the intestinal epithelium. Scand J Gastroenterol. Norway; 2002 Aug;37(8):936–43.

105. Hermansson M, Sawaji Y, Bolton M, Alexander S, Wallace A, Begum S, et al. Proteomic analysis of articular cartilage shows increased type II collagen synthesis in osteoarthritis and expression of inhibin betaA (activin A), a regulatory molecule for chondrocytes. J Biol Chem. United States; 2004 Oct;279(42):43514–21.

106. Linko R, Hedger MP, Pettila V, Ruokonen E, Ala-Kokko T, Ludlow H, et al. Serum activin A and B, and follistatin in critically ill patients with influenza A(H1N1) infection. BMC Infect Dis. 2014;14(doi):10.1186/1471–2334 – 14–253.

107. Caldwell RL, Gadipatti R, Lane KB, Shepherd VL. HIV-1 TAT represses transcription of the bone morphogenic protein receptor-2 in U937 monocytic cells. J Leukoc Biol. 2005/11/12 ed. 2006;79(1):192–201.

108. Durrington HJ, Upton PD, Hoer S, Boname J, Dunmore BJ, Yang J, et al. Identification of a Lysosomal Pathway Regulating Degradation of the Bone Morphogenetic Protein Receptor Type II. J Biol Chem [Internet]. 2010;285(48):37641–9. Available from: http://www.jbc.org/content/285/48/37641.abstract

109. Henke-Gendo C, Schulz T, Hoeper M. HHV-8 in Pulmonary Hypertension. N Engl J Med [Internet]. Massachusetts Medical Society; 2004 Jan 8;350(2):194–5. Available from: http://dx.doi.org/10.1056/NEJM200401083500221

110. Machado RD, Aldred MA, James V, Harrison RE, Patel B, Schwalbe EC, et al. Mutations of the TGF-beta type II receptor BMPR2 in pulmonary arterial hypertension. Hum Mutat. United States; 2006 Feb;27(2):121–32.

111. Liu Y, Sun R, Lin X, Liang D, Deng Q, Lan K. Kaposi's sarcoma-associated herpesvirus-encoded microRNA miR-K12-11 attenuates transforming growth factor beta signaling through suppression of SMAD5. J Virol. 2012;86(3):1372–81. doi: 10.1128/JVI.06245–11. Epub 2011 Oct .

112. Ding D, Lou X, Hua D, Yu W, Li L, Wang J, et al. Recurrent targeted genes of hepatitis B virus in the liver cancer genomes identified by a next-generation sequencing-based approach. PLoS Genet. 2012;8(12):e1003065. doi: 10.1371/journal.pgen.1003065. Epub .

113. Beckham JD, Tuttle K, Tyler KL. Reovirus activates transforming growth factor beta and bone morphogenetic protein signaling pathways in the central nervous system that contribute to neuronal survival following infection. J Virol. 2009/03/13 ed. 2009;83(10):5035–45.

114. Bian L, Wang Y, Liu Q, Xia J, Long JE. Prediction of signaling pathways involved in enterovirus 71 infection by algorithm analysis based on miRNA profiles and their target genes. Arch Virol. 2014/10/08 ed. 2014;

115. Saxena T, Tandon B, Sharma S, Chameettachal S, Ray P, Ray AR, et al. Combined miRNA and mRNA signature identifies key molecular players and pathways involved in chikungunya virus infection in human cells. PLoS One. 2013/11/28 ed. 2013;8(11):e79886.

116. Sultana H, Neelakanta G, Foellmer HG, Montgomery RR, Anderson JF, Koski RA, et al. Semaphorin 7A contributes to West Nile virus pathogenesis through TGF-beta1/Smad6 signaling. J Immunol. 2012/08/17 ed. 2012;189(6):3150–8.

117. ISAACS A, LINDENMANN J. Virus interference. I. The interferon. Proc R Soc London Ser B, Biol Sci. Not Available; 1957 Sep;147(927):258–67.

118. ISAACS A, LINDENMANN J, VALENTINE RC. Virus interference. II. Some properties of interferon. Proc R Soc London Ser B, Biol Sci. Not Available; 1957 Sep;147(927):268–73.

119. Pestka S, Krause CD, Walter MR. Interferons, interferon-like cytokines, and their receptors. Immunol Rev. 2004;202:8–32.

120. Kotenko S V, Gallagher G, Baurin V V, Lewis-Antes A, Shen M, Shah NK, et al. IFN-lambdas mediate antiviral protection through a distinct class II cytokine receptor complex. Nat Immunol. United States; 2003 Jan;4(1):69–77.

121. Sheppard P, Kindsvogel W, Xu W, Henderson K, Schlutsmeyer S, Whitmore TE, et al. IL-28, IL-29 and their class II cytokine receptor

IL-28R. Nat Immunol [Internet]. 2003 Jan;4(1):63–8. Available from: http://dx.doi.org/10.1038/ni873

122. Kelly C, Klenerman P, Barnes E. Interferon lambdas: the next cytokine storm. Gut. England; 2011 Sep;60(9):1284–93.

123. Kawai T, Akira S. Toll-like receptors and their crosstalk with other innate receptors in infection and immunity. Immunity. United States; 2011 May;34(5):637–50.

124. Wu J, Chen ZJ. Innate immune sensing and signaling of cytosolic nucleic acids. Annu Rev Immunol. United States; 2014;32:461–88.

125. Dambuza IM, Brown GD. C-type lectins in immunity: recent developments. Curr Opin Immunol. England; 2015 Feb;32:21–7.

126. Caruso R, Warner N, Inohara N, Nunez G. NOD1 and NOD2: signaling, host defense, and inflammatory disease. Immunity. United States; 2014 Dec;41(6):898–908.

127. Hornung V. SnapShot: Nucleic Acid Immune Sensors, Part 2. Immunity [Internet]. Elsevier; 2015 Jul 5;41(6):1066–1066.e1. Available from: http://dx.doi.org/10.1016/j.immuni.2014.10.006

128. Au WC, Moore PA, Lowther W, Juang YT, Pitha PM. Identification of a member of the interferon regulatory factor family that binds to the interferon-stimulated response element and activates expression of interferon-induced genes. Proc Natl Acad Sci U S A. UNITED STATES; 1995 Dec;92(25):11657–61.

129. Hertzog PJ, Williams BRG. Fine tuning type I interferon responses. Cytokine Growth Factor Rev [Internet]. 2013 Jun;24(3):217–25. Available from: http://www.sciencedirect.com/science/article/pii/S1359610113000300

130. De Weerd NA, Samarajiwa SA, Hertzog PJ. Type I interferon receptors: Biochemistry and biological functions. J Biol Chem [Internet]. 2007;282(28):20053–7. Available from: http://www.scopus.com/inward/record.url?eid=2-s2.0-34547116656&partnerID=40&md5=a91c9355d271bc76902b88a3b9be67bd

131. Novick D, Cohen B, Rubinstein M. The human interferon α β receptor: Characterization and molecular cloning. Cell [Internet]. 1994;77(3):391–400. Available from: http://www.scopus.com/inward/record.url?eid=2-s2.0-0028299340&partnerID=40&md5=9ae77201f9650aec0caa66f02df47191

132. Lutfalla G, Holland SJ, Cinato E, Monneron D, Reboul J, Rogers NC, et al. Mutant U5A cells are complemented by an interferon-αβ receptor subunit generated by alternative processing of a new member of a cytokine receptor gene cluster. EMBO J [Internet]. 1995;14(20):5100–8. Available from: http://www.scopus.com/inward/record.url?eid=2-s2.0-0028820423&partnerID=40&md5=d82973a46cb5358680811decd77dca98

133. Piehler J, Thomas C, Christopher Garcia K, Schreiber G. Structural and dynamic determinants of type I interferon receptor assembly and their functional interpretation. Immunol Rev [Internet]. 2012;250(1):317–34. Available from: http://www.scopus.com/inward/record.url?eid=2-s2.0-84867411811&partnerID=40&md5=e9ce69ab7bab074093f86727bd17c6ed

134. Yan H, Krishnan K, Lim JTE, Contillo LG, Krolewski JJ. Molecular characterization of an alpha interferon receptor 1 subunit (IFNaR1) domain required for TYK2 binding and signal transduction. Mol Cell Biol [Internet]. 1996;16(5):2074–82. Available from: http://www.scopus.com/inward/record.url?eid=2-s2.0-0029863420&partnerID=40&md5=c8804ad54da3b57f2047d15a51e93767

135. Domanski P, Fish E, Nadeau OW, Witte M, Platanias LC, Yan H, et al. A region of the β subunit of the interferon α receptor different from Box 1 interacts with Jak1 and is sufficient to activate the Jak-Stat pathway and induce an antiviral state. J Biol Chem [Internet]. 1997;272(42):26388–93. Available from: http://www.scopus.com/inward/record.url?eid=2-s2.0-0030671276&partnerID=40&md5=1a60ce4e983648ac23ca4ee2a82aa77f

136. Nguyen KB, Watford WT, Salomon R, Hofmann SR, Pien GC, Morinobu A, et al. Critical role for STAT4 activation by type 1 interferons in the interferon-gamma response to viral infection. Science. United States; 2002 Sep;297(5589):2063–6.

137. Darnell JEJ, Kerr IM, Stark GR. Jak-STAT pathways and transcriptional activation in response to IFNs and other extracellular signaling proteins. Science. UNITED STATES; 1994 Jun;264(5164):1415–21.

138. Paquette RL, Minosa MR, Verma MC, Nimer SD, Koeffler HP. An interferon-gamma activation sequence mediates the transcriptional regulation of the IgG Fc receptor type IC gene by interferon-gamma. Mol Immunol. ENGLAND; 1995 Aug;32(12):841–51.

139. Kessler DS, Veals SA, Fu XY, Levy DE. Interferon-alpha regulates nuclear translocation and DNA-binding affinity of ISGF3, a multimeric transcriptional activator. Genes Dev. UNITED STATES; 1990 Oct;4(10):1753–65.

140. Der SD, Zhou A, Williams BRG, Silverman RH. Identification of genes differentially regulated by interferon α, β, or γ using oligonucleotide arrays. Proc Natl Acad Sci [Internet]. 1998 Dec 22;95 (26):15623–8. Available from: http://www.pnas.org/content/95/26/15623.abstract

141. Platanias LC. Mechanisms of type-I- and type-II-interferon-mediated signalling. Nat Rev Immunol [Internet]. 2005 May;5(5):375–86. Available from: http://dx.doi.org/10.1038/nri1604

142. Schoggins JW, Rice CM. Interferon-stimulated genes and their antiviral effector functions. Curr Opin Virol [Internet]. 2011 Dec;1(6):519–25. Available from: http://www.ncbi.nlm.nih.gov/pmc/articles/PMC3274382/

143. Schoggins JW, Wilson SJ, Panis M, Murphy MY, Jones CT, Bieniasz P, et al. A diverse range of gene products are effectors of the type I interferon antiviral response. Nature. 2011;472(7344):481–5. doi: 10.1038/nature09907. Epub 2011 Apr 10.

144. Schoggins JW. Interferon-stimulated genes: roles in viral pathogenesis. Curr Opin Virol [Internet]. 2014 Jun 5;0:40–6. Available from: http://www.ncbi.nlm.nih.gov/pmc/articles/PMC4077717/

145. Knight E, Korant BD. Fibroblast interferon induces synthesis of four proteins in human fibroblast cells. Proc Natl Acad Sci U S A [Internet]. 1979 Apr;76(4):1824–7. Available from: http://www.ncbi.nlm.nih.gov/pmc/articles/PMC383484/

146. Larner AC, Jonak G, Cheng YS, Korant B, Knight E, Darnell JEJ. Transcriptional induction of two genes in human cells by beta interferon. Proc Natl Acad Sci U S A. UNITED STATES; 1984 Nov;81(21):6733–7.

147. Hovanessian AG. On the discovery of interferon-inducible, double-stranded RNA activated enzymes: the 2'-5'oligoadenylate synthetases and the protein kinase PKR. Cytokine Growth Factor Rev. England; 2007;18(5-6):351–61.

148. Yap MW, Nisole S, Lynch C, Stoye JP. Trim5alpha protein restricts both HIV-1 and murine leukemia virus. Proc Natl Acad Sci U S A. United States; 2004 Jul;101(29):10786–91.

149. Zhang Y, Burke CW, Ryman KD, Klimstra WB. Identification and characterization of interferon-induced proteins that inhibit alphavirus replication. J Virol. United States; 2007 Oct;81(20):11246–55.

150. Brass AL, Huang I-C, Benita Y, John SP, Krishnan MN, Feeley EM, et al. The IFITM proteins mediate cellular resistance to influenza A H1N1 virus, West Nile virus, and dengue virus. Cell. United States; 2009 Dec;139(7):1243–54.

151. Sheehy AM, Gaddis NC, Choi JD, Malim MH. Isolation of a human gene that inhibits HIV-1 infection and is suppressed by the viral Vif protein. Nature. England; 2002 Aug;418(6898):646–50.

152. Honda K, Yanai H, Negishi H, Asagiri M, Sato M, Mizutani T, et al. IRF-7 is the master regulator of type-I interferon-dependent immune responses. Nature [Internet]. 2005 Apr 7;434(7034):772–7. Available from: http://dx.doi.org/10.1038/nature03464

153. Muller S, Moller P, Bick MJ, Wurr S, Becker S, Gunther S, et al. Inhibition of filovirus replication by the zinc finger antiviral protein. J Virol. 2006/12/22 ed. 2007;81(5):2391–400.

154. Zhu Y, Chen G, Lv F, Wang X, Ji X, Xu Y, et al. Zinc-finger antiviral protein inhibits HIV-1 infection by selectively targeting multiply spliced viral mRNAs for degradation. Proc Natl Acad Sci U S A. United States; 2011 Sep;108(38):15834–9.

155. Zhao C, Collins MN, Hsiang T-Y, Krug RM. Interferon-induced ISG15 pathway: an ongoing virus-host battle. Trends Microbiol. England; 2013 Apr;21(4):181–6.

156. Morales DJ, Lenschow DJ. The antiviral activities of ISG15. J Mol Biol. England; 2013 Dec;425(24):4995–5008.

157. Abudu A, Wang X, Dang Y, Zhou T, Xiang S-H, Zheng Y-H. Identification of molecular determinants from Moloney leukemia virus 10 homolog (MOV10) protein for virion packaging and anti-HIV-1 activity. J Biol Chem. United States; 2012 Jan;287(2):1220–8.

158. Samuel CE. Adenosine deaminases acting on RNA (ADARs) are both antiviral and proviral. Virology. United States; 2011 Mar;411(2):180–93.

159. Hofer MJ, Campbell IL. Type I interferon in neurological disease-the devil from within. Cytokine Growth Factor Rev. England; 2013 Jun;24(3):257–67.

160. Crow YJ, Manel N. Aicardi-Goutieres syndrome and the type I interferonopathies. Nat Rev Immunol. England; 2015 Jul;15(7):429–40.

161. Piganis RAR, De Weerd NA, Gould JA, Schindler CW, Mansell A, Nicholson SE, et al. Suppressor of Cytokine Signaling (SOCS) 1 inhibits type I interferon (IFN) signaling via the interferon α receptor (IFNAR1)-associated tyrosine kinase tyk2. J Biol Chem [Internet]. 2011;286(39):33811–8. Available from: http://www.scopus.com/inward/record.url?eid=2-s2.0-80053210241&partnerID=40&md5=82336080260b2460a3edce6814fdc870

162. Shuai K, Liu B. Regulation of gene-activation pathways by PIAS proteins in the immune system. Nat Rev Immunol. England; 2005 Aug;5(8):593–605.

163. Malakhova OA, Kim K Il, Luo J-K, Zou W, Kumar KGS, Fuchs SY, et al. UBP43 is a novel regulator of interferon signaling independent of its ISG15 isopeptidase activity. EMBO J. England; 2006 Jun;25(11):2358–67.

164. Malakhov MP, Malakhova OA, Kim K Il, Ritchie KJ, Zhang D-E. UBP43 (USP18) specifically removes ISG15 from conjugated proteins. J Biol Chem. United States; 2002 Mar;277(12):9976–81.

165. Monto AS, Shope TC, Schwartz SA, Albrecht JK. Intranasal interferon-alpha 2b for seasonal prophylaxis of respiratory infection. J Infect Dis. UNITED STATES; 1986 Jul;154(1):128–33.

166. Ophir J, Brenner S, Bali R, Kriss-Leventon S, Smetana Z, Revel M. Effect of topical interferon-beta on recurrence rates in genital herpes: a double-blind, placebo-controlled, randomized study. J Interferon Cytokine Res. UNITED STATES; 1995 Jul;15(7):625–31.

167. Bekisz J, Sato Y, Johnson C, Husain SR, Puri RK, Zoon KC. Immunomodulatory effects of interferons in malignancies. J Interferon Cytokine Res. United States; 2013 Apr;33(4):154–61.

168. Reder AT, Feng X. How type I interferons work in multiple sclerosis and other diseases: some unexpected mechanisms. J Interferon Cytokine Res. United States; 2014 Aug;34(8):589–99.

169. Rosen HR. Clinical practice. Chronic hepatitis C infection. N Engl J Med. 2011;364(25):2429–38. doi: 10.1056/NEJMcp1006613.

170. Davis GL, Albright JE, Cook SF, Rosenberg DM. Projecting future complications of chronic hepatitis C in the United States. Liver Transpl. 2003;9(4):331–8.

171. Mohd Hanafiah K, Groeger J, Flaxman AD, Wiersma ST. Global epidemiology of hepatitis C virus infection: New estimates of age-specific antibody to HCV seroprevalence. Hepatology [Internet]. Wiley Subscription Services, Inc., A Wiley Company; 2013 Apr 1;57(4):1333–42. Available from: http://dx.doi.org/10.1002/hep.26141

172. Messina JP, Humphreys I, Flaxman A, Brown A, Cooke GS, Pybus OG, et al. Global distribution and prevalence of hepatitis C virus genotypes. Hepatology [Internet]. 2015 Jan 1;61(1):77–87. Available from: http://dx.doi.org/10.1002/hep.27259

173. Thomson EC, Fleming VM, Main J, Klenerman P, Weber J, Eliahoo J, et al. Predicting spontaneous clearance of acute hepatitis C virus in a large cohort of HIV-1-infected men. Gut [Internet]. 2011;60(6):837–45. Available from: http://www.scopus.com/inward/record.url?eid=2-s2.0-79955800187&partnerID=40&md5=b454bc5ecda444af3af9d999000e9a19

174. Webster DP, Klenerman P, Dusheiko GM. Hepatitis C. Lancet [Internet]. 21AD Mar 27;385(9973):1124–35. Available from: http://www.sciencedirect.com/science/article/pii/S0140673614624016

175. Hoofnagle JH. Course and outcome of hepatitis C. Hepatology [Internet]. W.B. Saunders; 2002 Nov 1;36(S1):S21–9. Available from: http://dx.doi.org/10.1002/hep.1840360704

176. Kenny-Walsh E. Clinical outcomes after hepatitis C infection from contaminated anti-D immune globulin. Irish Hepatology Research Group. N Engl J Med. UNITED STATES; 1999 Apr;340(16):1228–33.

177. Lin M V, King LY, Chung RT. Hepatitis C virus-associated cancer. Annu Rev Pathol. United States; 2015;10:345–70.

178. Hajarizadeh B, Grebely J, Dore GJ. Epidemiology and natural history of HCV infection. Nat Rev Gastroenterol Hepatol [Internet]. Nature Publishing Group, a division of Macmillan Publishers Limited. All Rights Reserved.; 2013 Sep;10(9):553–62. Available from: http://dx.doi.org/10.1038/nrgastro.2013.107

179. Prasad MR, Honegger JR. Hepatitis C virus in pregnancy. Am J Perinatol [Internet]. 2013;30(2):149–59. Available from: http://www.scopus.com/inward/record.url?eid=2-s2.0-84874111399&partnerID=40&md5=8fdf399b4b29a812c4108c5b375e404f

180. Ciccozzi M, Lo Presti A, Ciccaglione AR, Zehender G, Ciotti M. Phylogeny and phylodinamic of Hepatitis C in Italy. BMC Infect Dis. England; 2012;12 Suppl 2:S5.

181. Frank C, Mohamed MK, Strickland GT, Lavanchy D, Arthur RR, Magder LS, et al. The role of parenteral antischistosomal therapy in the spread of hepatitis C virus in Egypt. Lancet (London, England). ENGLAND; 2000 Mar;355(9207):887–91.

182. Power JP, Lawlor E, Davidson F, Holmes EC, Yap PL, Simmonds P. Molecular epidemiology of an outbreak of infection with hepatitis C virus in recipients of anti-D immunoglobulin. Lancet. ENGLAND; 1995 May;345(8959):1211–3.

183. Armstrong GL, Wasley A, Simard EP, McQuillan GM, Kuhnert WL, Alter MJ. The Prevalence of Hepatitis C Virus Infection in the United States, 1999 through 2002. Ann Intern Med [Internet]. 2006 May 16;144(10):705–14. Available from: http://dx.doi.org/10.7326/0003-4819-144-10-200605160-00004

184. Minola E, Prati D, Suter F, Maggiolo F, Caprioli F, Sonzogni A, et al. Age at infection affects the long-term outcome of transfusion-associated chronic hepatitis C. Blood. United States; 2002 Jun;99(12):4588–91.

185. Leandro G, Mangia A, Hui J, Fabris P, Rubbia-Brandt L, Colloredo G, et al. Relationship between steatosis, inflammation, and fibrosis in chronic hepatitis C: a meta-analysis of individual patient data. Gastroenterology. United States; 2006 May;130(6):1636–42.

186. Gaeta GB, Stornaiuolo G, Precone DF, Lobello S, Chiaramonte M, Stroffolini T, et al. Epidemiological and clinical burden of chronic hepatitis B virus/hepatitis C virus infection. A multicenter Italian study. J Hepatol. England; 2003 Dec;39(6):1036–41.

187. Graham CS, Baden LR, Yu E, Mrus JM, Carnie J, Heeren T, et al. Influence of human immunodeficiency virus infection on the course of hepatitis C virus infection: a meta-analysis. Clin Infect Dis. United States; 2001 Aug;33(4):562–9.

188. Hourigan LF, Macdonald GA, Purdie D, Whitehall VH, Shorthouse C, Clouston A, et al. Fibrosis in chronic hepatitis C correlates significantly with body mass index and steatosis. Hepatology. UNITED STATES; 1999 Apr;29(4):1215–9.

189. Konstantinou D, Deutsch M. The spectrum of HBV/HCV coinfection: epidemiology, clinical characteristics, viralinteractions and management. Ann Gastroenterol Q Publ Hell Soc Gastroenterol [Internet]. Greece: Hellenic Society of Gastroenterology; 2015 Sep 1;28(2):221–8. Available from: http://www.ncbi.nlm.nih.gov/pmc/articles/PMC4367211/

190. Cacciola I, Pollicino T, Squadrito G, Cerenzia G, Orlando ME, Raimondo G. Occult hepatitis B virus infection in patients with chronic hepatitis C liver disease. N Engl J Med. UNITED STATES; 1999 Jul;341(1):22–6.

191. Blackard JT, Kemmer N, Sherman KE. Extrahepatic replication of HCV: Insights into clinical manifestations and biological consequences. Hepatology [Internet]. Wiley Subscription Services, Inc., A Wiley Company; 2006 Jul 1;44(1):15–22. Available from: http://dx.doi.org/10.1002/hep.21283

192. Hartridge-Lambert SK, Stein EM, Markowitz AJ, Portlock CS. Hepatitis C and non-Hodgkin lymphoma: the clinical perspective. Hepatology. United States; 2012 Feb;55(2):634–41.

193. Marino R, Deibis L, De Sanctis J, Bianco N, Toro F. Interaction of immune complexes isolated from hepatitis C virus-infected individuals with human cell lines. Med Microbiol Immunol [Internet]. Springer-Verlag; 2005;194(1-2):73–80. Available from: http://dx.doi.org/10.1007/s00430-003-0216-8

194. Forton DM, Allsop JM, Cox IJ, Hamilton G, Wesnes K, Thomas HC, et al. A review of cognitive impairment and cerebral metabolite abnormalities in patients with hepatitis C infection. AIDS. England; 2005 Oct;19 Suppl 3:S53–63.

195. Choo QL, Kuo G, Weiner AJ, Overby LR, Bradley DW, Houghton M. Isolation of a cDNA clone derived from a blood-borne non-A, non-B viral hepatitis genome. Science. UNITED STATES; 1989 Apr;244(4902):359–62.

196. Scheel TKH, Simmonds P, Kapoor A. Surveying the global virome: identification and characterization of HCV-related animal hepaciviruses. Antiviral Res. Netherlands; 2015 Mar;115:83–93.

197. Kalinina O, Norder H, Mukomolov S, Magnius LO. A Natural Intergenotypic Recombinant of Hepatitis C Virus Identified in St. Petersburg. J Virol [Internet]. 2002 Apr 15;76 (8):4034–43. Available from: http://jvi.asm.org/content/76/8/4034.abstract

198. Moreno MP, Casane D, López L, Cristina J. Evidence of recombination in quasispecies populations of a Hepatitis C Virus patient undergoing anti-viral therapy. Virol J [Internet]. London: BioMed Central; 2006 Oct 24;3:87. Available from: http://www.ncbi.nlm.nih.gov/pmc/articles/PMC1635042/

199. Pileri P, Uematsu Y, Campagnoli S, Galli G, Falugi F, Petracca R, et al. Binding of hepatitis C virus to CD81. Science. UNITED STATES; 1998 Oct;282(5390):938–41.

200. Scarselli E, Ansuini H, Cerino R, Roccasecca RM, Acali S, Filocamo G, et al. The human scavenger receptor class B type I is a novel candidate receptor for the hepatitis C virus. EMBO J. England; 2002 Oct;21(19):5017–25.

201. Evans MJ, von Hahn T, Tscherne DM, Syder AJ, Panis M, Wolk B, et al. Claudin-1 is a hepatitis C virus co-receptor required for a late step in entry. Nature. England; 2007 Apr;446(7137):801–5.

202. Ploss A, Evans MJ, Gaysinskaya VA, Panis M, You H, de Jong YP, et al. Human occludin is a hepatitis C virus entry factor required for infection of mouse cells. Nature. England; 2009 Feb;457(7231):882–6.

203. Sainz BJ, Barretto N, Martin DN, Hiraga N, Imamura M, Hussain S, et al. Identification of the Niemann-Pick C1-like 1 cholesterol absorption receptor as a new hepatitis C virus entry factor. Nat Med. United States; 2012 Feb;18(2):281–5.

204. Behrens SE, Tomei L, De Francesco R. Identification and properties of the RNA-dependent RNA polymerase of hepatitis C virus. EMBO J. ENGLAND; 1996 Jan;15(1):12–22.

205. Gosert R, Egger D, Lohmann V, Bartenschlager R, Blum HE, Bienz K, et al. Identification of the Hepatitis C Virus RNA Replication Complex in Huh-7 Cells Harboring Subgenomic Replicons. J Virol [Internet]. American Society for Microbiology; 2003 May 18;77(9):5487–92. Available from: http://www.ncbi.nlm.nih.gov/pmc/articles/PMC153965/

206. Romero-Brey I, Merz A, Chiramel A, Lee J-Y, Chlanda P, Haselman U, et al. Three-dimensional architecture and biogenesis of membrane structures associated with hepatitis C virus replication. PLoS Pathog. United States; 2012;8(12):e1003056.

207. Spahn CM, Kieft JS, Grassucci RA, Penczek PA, Zhou K, Doudna JA, et al. Hepatitis C virus IRES RNA-induced changes in the conformation of the 40s ribosomal subunit. Science. United States; 2001 Mar;291(5510):1959–62.

208. Fraser CS, Doudna JA. Structural and mechanistic insights into hepatitis C viral translation initiation. Nat Rev Micro [Internet]. 2007 Jan;5(1):29–38. Available from: http://dx.doi.org/10.1038/nrmicro1558

209. Lindenbach BD, Rice CM. The ins and outs of hepatitis C virus entry and assembly. Nat Rev Microbiol [Internet]. 2013;11(10):688–700. Available from: http://www.pubmedcentral.nih.gov/articlerender.fcgi?artid=3897199&tool=pmcentrez&rendertype=abstract

210. Wakita T, Pietschmann T, Kato T, Date T, Miyamoto M, Zhao Z, et al. Production of infectious hepatitis C virus in tissue culture from a cloned viral genome. Nat Med. United States; 2005 Jul;11(7):791–6.

211. Lohmann V, Körner F, Koch J-O, Herian U, Theilmann L, Bartenschlager R. Replication of Subgenomic Hepatitis C Virus RNAs in a Hepatoma Cell Line. Sci [Internet]. 1999 Jul 2;285 (5424):110–3. Available from: http://www.sciencemag.org/content/285/5424/110.abstract

212. Bartosch B, Dubuisson J, Cosset F-L. Infectious Hepatitis C Virus Pseudo-particles Containing Functional E1–E2 Envelope Protein Complexes. J Exp Med [Internet]. 2003 Mar 3;197 (5):633–42. Available from: http://jem.rupress.org/content/197/5/633.abstract

213. Hsu M, Zhang J, Flint M, Logvinoff C, Cheng-Mayer C, Rice CM, et al. Hepatitis C virus glycoproteins mediate pH-dependent cell entry of pseudotyped retroviral particles. Proc Natl Acad Sci [Internet]. 2003 Jun 10;100 (12):7271–6. Available from: http://www.pnas.org/content/100/12/7271.abstract

214. Zhong J, Gastaminza P, Cheng G, Kapadia S, Kato T, Burton DR, et al. Robust hepatitis C virus infection in vitro. Proc Natl Acad Sci

United States Am [Internet]. 2005 Jun 28;102 (26):9294–9. Available from: http://www.pnas.org/content/102/26/9294.abstract

215. Pietschmann T, Kaul A, Koutsoudakis G, Shavinskaya A, Kallis S, Steinmann E, et al. Construction and characterization of infectious intragenotypic and intergenotypic hepatitis C virus chimeras. Proc Natl Acad Sci [Internet]. 2006 May 9;103 (19):7408–13. Available from: http://www.pnas.org/content/103/19/7408.abstract

216. Zhao X, Tang Z-Y, Klumpp B, Wolff-Vorbeck G, Barth H, Levy S, et al. Primary hepatocytes of Tupaia belangeri as a potential model for hepatitis C virus infection. J Clin Invest [Internet]. The American Society for Clinical Investigation; 2002 Jan 15;109(2):221–32. Available from: http://www.jci.org/articles/view/13011

217. Castet V, Fournier C, Soulier A, Brillet R, Coste J, Larrey D, et al. Alpha Interferon Inhibits Hepatitis C Virus Replication in Primary Human Hepatocytes Infected In Vitro. J Virol [Internet]. 2002 Aug 15;76 (16):8189–99. Available from: http://jvi.asm.org/content/76/16/8189.abstract

218. Brass V, Moradpour D, Blum HE. Hepatitis C virus infection: in vivo and in vitro models. J Viral Hepat [Internet]. Blackwell Publishing Ltd; 2007 Nov 1;14:64–7. Available from: http://dx.doi.org/10.1111/j.1365-2893.2007.00918.x

219. Mercer DF, Schiller DE, Elliott JF, Douglas DN, Hao C, Rinfret A, et al. Hepatitis C virus replication in mice with chimeric human livers. Nat Med. 2001;7(8):927–33.

220. Dorner M, Horwitz JA, Donovan BM, Labitt RN, Budell WC, Friling T, et al. Completion of the entire hepatitis C virus life cycle in genetically humanized mice. Nature [Internet]. Nature Publishing Group, a division of Macmillan Publishers Limited. All Rights Reserved.; 2013 Sep 12;501(7466):237–41. Available from: http://dx.doi.org/10.1038/nature12427

221. Fong TL, Valinluck B, Govindarajan S, Charboneau F, Adkins RH, Redeker AG. Short-term prednisone therapy affects aminotransferase activity and hepatitis C virus RNA levels in chronic hepatitis C. Gastroenterology. UNITED STATES; 1994 Jul;107(1):196–9.

222. Pappas SC, Hoofnagle JH, Young N, Straus SE, Jones EA. Treatment of chronic non-A, non-B hepatitis with acyclovir: Pilot study. J Med Virol [Internet]. 1985;15(1):1–9. Available from: http://www.scopus.com/inward/record.url?eid=2-s2.0-0021934088&partnerID=40&md5=1da4dcaa46edc39f8e47f4614bfdce51

223. Shindo M, Di Bisceglie AM, Cheung L, Shih JW-K, Cristiano K, Feinstone SM, et al. Decrease in serum hepatitis C viral RNA during alpha-interferon therapy for chronic hepatitis C. Ann Intern Med [Internet]. 1991;115(9):700–4. Available from: http://www.scopus.com/inward/record.url?eid=2-s2.0-0026002152&partnerID=40&md5=1c842d592307fb4470fcbca412f41631

224. Hoofnagle JH, Mullen KD, Jones DB, Rustgi V, Di Bisceglie A, Peters M, et al. Treatment of Chronic Non-A, Non-B Hepatitis with Recombinant Human Alpha Interferon. N Engl J Med [Internet]. Massachusetts Medical Society; 1986 Dec 18;315(25):1575–8. Available from: http://dx.doi.org/10.1056/NEJM198612183152503

225. Davis GL, Balart LA, Schiff ER, Lindsay K, Bodenheimer Jr. HC, Perrillo RP, et al. Treatment of chronic hepatitis C with recombinant interferon alfa. A multicenter randomized, controlled trial. N Engl J Med [Internet]. 1989;321(22):1501–6. Available from: http://www.scopus.com/inward/record.url?eid=2-s2.0-0024368522&partnerID=40&md5=6344818e031b0c228dafbe51e28143b9

226. Di Bisceglie AM, Martin P, Kassianides C, Lisker-Melman M, Murray L, Waggoner J, et al. Recombinant interferon alfa therapy for chronic hepatitis C. A randomized, double-blind, placebo-controlled trial. N Engl J Med [Internet]. 1989;321(22):1506–10. Available from: http://www.scopus.com/inward/record.url?eid=2-s2.0-0024981607&partnerID=40&md5=a74c92433fb51a89a8d208d5809293ae

227. Reichard O, Andersson J, Schvarcz R, Weiland O. Ribavirin treatment for chronic hepatitis C. Lancet [Internet]. 1991;337(8749):1058–61. Available from: http://www.scopus.com/inward/record.url?eid=2-s2.0-0025847155&partnerID=40&md5=473b07f5b511557687479815bde1d082

228. Di Bisceglie AM, Shindo M, Fong T-L, Fried MW, Swain MG, Bergasa N V, et al. A pilot study of ribavirin therapy for chronic hepatitis C. Hepatology [Internet]. 1992;16(3):649–54. Available from: http://www.scopus.com/inward/record.url?eid=2-s2.0-0026733674&partnerID=40&md5=386cf378f8ac46155cc9f3ce5519352d

229. Schvarcz R, Ando Y, Sonnerborg A, Weiland O. Combination treatment with interferon alfa-2b and ribavirin for chronic hepatitis C in patients who have failed to achieve sustained response to interferon alone: Swedish experience. J Hepatol Suppl [Internet]. 1995;23(2):17–21. Available from: http://www.scopus.com/inward/record.url?eid=2-s2.0-0029589231&partnerID=40&md5=4c9697c058af2a610a0c9b10bb4be50a

230. Paeshuyse J, Dallmeier K, Neyts J. Ribavirin for the treatment of chronic hepatitis C virus infection: a review of the proposed mechanisms of action. Curr Opin Virol. Netherlands; 2011 Dec;1(6):590–8.

231. Poynard T, Marcellin P, Lee SS, Niederau C, Minuk GS, Ideo G, et al. Randomised trial of interferon α2b plus ribavirin for 48 weeks or for 24 weeks versus interferon α2b plus placebo for 48 weeks for treatment of chronic infection with hepatitis C virus. Lancet [Internet]. 1998;352(9138):1426–32. Available from: http://www.scopus.com/inward/record.url?eid=2-s2.0-0032585237&partnerID=40&md5=f6cd179a7b10433c18067c58285feb37

232. McHutchison JG, Gordon SC, Schiff ER, Shiffman ML, Lee WM, Rustgi VK, et al. Interferon alfa-2b alone or in combination with ribavirin as initial treatment for chronic hepatitis C. Hepatitis Interventional Therapy Group. N Engl J Med. UNITED STATES; 1998 Nov;339(21):1485–92.

233. Neumann AU, Lam NP, Dahari H, Gretch DR, Wiley TE, Layden TJ, et al. Hepatitis C viral dynamics in vivo and the antiviral efficacy of interferon-α therapy. Science (80-) [Internet]. 1998;282(5386):103–7. Available from: http://www.scopus.com/inward/record.url?eid=2-s2.0-0032475822&partnerID=40&md5=f61dd2113b74b69f6902ce38c971cc3b

234. Pawlotsky J-M, Feld JJ, Zeuzem S, Hoofnagle JH. From non-A, non-B hepatitis to hepatitis C virus cure. J Hepatol [Internet]. 2015 Apr [cited 2015 Apr 29];62(1S):S87–99. Available from: http://www.sciencedirect.com/science/article/pii/S016882781500080X

235. Fried MW. Side effects of therapy of hepatitis C and their management. Hepatology. 2002;36(5 Suppl 1):S237–44.

236. Conjeevaram HS, Fried MW, Jeffers LJ, Terrault NA, Wiley-Lucas TE, Afdhal N, et al. Peginterferon and ribavirin treatment in African American and Caucasian American patients with hepatitis C genotype 1. Gastroenterology. 2006;131(2):470–7.

237. Lamarre D, Anderson PC, Bailey M, Beaulieu P, Bolger G, Bonneau P, et al. An NS3 protease inhibitor with antiviral effects in humans infected with hepatitis C virus. Nature [Internet]. Macmillian Magazines Ltd.; 2003 Nov 13;426(6963):186–9. Available from: http://dx.doi.org/10.1038/nature02099

238. De Francesco R, Migliaccio G. Challenges and successes in developing new therapies for hepatitis C. Nature. England; 2005 Aug;436(7053):953–60.

239. Lin C, Lin K, Luong Y-P, Rao BG, Wei Y-Y, Brennan DL, et al. In vitro resistance studies of hepatitis C virus serine protease inhibitors, VX-950 and BILN 2061: structural analysis indicates different resistance mechanisms. J Biol Chem. United States; 2004 Apr;279(17):17508–14.

240. Jazwinski AB, Muir AJ. Direct-Acting Antiviral Medications for Chronic Hepatitis C Virus Infection. Gastroenterol Hepatol (N Y) [Internet]. Millennium Medical Publishing; 2011 Mar;7(3):154–62. Available from: http://www.ncbi.nlm.nih.gov/pmc/articles/PMC3079144/

241. Ogata N, Alter HJ, Miller RH, Purcell RH. Nucleotide sequence and mutation rate of the H strain of hepatitis C virus. Proc Natl Acad Sci U S A. UNITED STATES; 1991 Apr;88(8):3392–6.

242. Sarrazin C, Kieffer TL, Bartels D, Hanzelka B, Müh U, Welker M, et al. Dynamic Hepatitis C Virus Genotypic and Phenotypic Changes in Patients Treated With the Protease Inhibitor Telaprevir. Gastroenterology [Internet]. 2007 May;132(5):1767–77. Available from: http://www.sciencedirect.com/science/article/pii/S0016508507003940

243. Franco S, Tural C, Nevot M, Molto J, Rockstroh JK, Clotet B, et al. Detection of a Sexually Transmitted HCV Protease Inhibitor-Resistance Variant in a HIV-infected Homosexual Man. Gastroenterology. 2014;21(14):651–8.

244. Aghemo A, De Francesco R. New horizons in hepatitis C antiviral therapy with direct-acting antivirals. Hepatology. United States; 2013 Jul;58(1):428–38.

245. Pawlotsky J-M, Najera I, Jacobson I. Resistance to mericitabine, a nucleoside analogue inhibitor of HCV RNA-dependent RNA polymerase. Antivir Ther. England; 2012;17(3):411–23.

246. Migliaccio G, Tomassini JE, Carroll SS, Tomei L, Altamura S, Bhat B, et al. Characterization of resistance to non-obligate chain-terminating ribonucleoside analogs that inhibit hepatitis C virus replication in vitro. J Biol Chem. United States; 2003 Dec;278(49):49164–70.

247. Donaldson EF, Harrington PR, O'Rear JJ, Naeger LK. Clinical evidence and bioinformatics characterization of potential hepatitis C virus resistance pathways for sofosbuvir. Hepatology. United States; 2015 Jan;61(1):56–65.

248. Lawitz E, Poordad FF, Pang PS, Hyland RH, Ding X, Mo H, et al. Sofosbuvir and ledipasvir fixed-dose combination with and without ribavirin in treatment-naive and previously treated patients with genotype 1 hepatitis C virus infection (LONESTAR): an open-label, randomised, phase 2 trial. Lancet. 2014;383(9916):515–23. doi: 10.1016/S0140–6736(13)62121–2. Epub 2.

249. Afdhal N, Reddy KR, Nelson DR, Lawitz E, Gordon SC, Schiff E, et al. Ledipasvir and sofosbuvir for previously treated HCV genotype 1 infection. N Engl J Med. United States; 2014 Apr;370(16):1483–93.

250. NICE. Sofosbuvir for treating chronic hepatitis C. 2015. 1-109 p.

251. Walker CM, Grakoui A. Hepatitis C virus: why do we need a vaccine to prevent a curable persistent infection? Curr Opin Immunol [Internet]. 2015 Aug;35:137–43. Available from: http://www.sciencedirect.com/science/article/pii/S0952791515000916

252. Frey SE, Houghton M, Coates S, Abrignani S, Chien D, Rosa D, et al. Safety and Immunogenicity of HCV E1E2 Vaccine Adjuvanted with MF59 Administered to Healthy Adults. Vaccine [Internet]. 2010 Aug 31;28(38):6367–73. Available from: http://www.ncbi.nlm.nih.gov/pmc/articles/PMC2923449/

253. Folgori A, Capone S, Ruggeri L, Meola A, Sporeno E, Ercole BB, et al. A T-cell HCV vaccine eliciting effective immunity against heterologous virus challenge in chimpanzees. Nat Med [Internet]. Nature Publishing Group; 2006 Feb;12(2):190–7. Available from: http://dx.doi.org/10.1038/nm1353

254. Jenne CN, Kubes P. Immune surveillance by the liver. Nat Immunol [Internet]. Nature Publishing Group, a division of Macmillan Publishers Limited. All Rights Reserved.; 2013 Oct;14(10):996–1006. Available from: http://dx.doi.org/10.1038/ni.2691

255. Wong P, Pamer EG. CD8 T CELL RESPONSES TO INFECTIOUS PATHOGENS. Annu Rev Immunol [Internet]. Annual Reviews; 2003 Apr 1;21(1):29–70. Available from: http://dx.doi.org/10.1146/annurev.immunol.21.120601.141114

256. Zhu J, Yamane H, Paul WE. Differentiation of Effector CD4 T Cell Populations*. Annu Rev Immunol [Internet]. Annual Reviews; 2010 Mar 1;28(1):445–89. Available from: http://dx.doi.org/10.1146/annurev-immunol-030409-101212

257. Mills KHG. Regulatory T cells: friend or foe in immunity to infection? Nat Rev Immunol [Internet]. 2004 Nov;4(11):841–55. Available from: http://dx.doi.org/10.1038/nri1485

258. Batista FD, Harwood NE. The who, how and where of antigen presentation to B cells. Nat Rev Immunol. England; 2009 Jan;9(1):15–27.

259. Cooper S, Erickson AL, Adams EJ, Kansopon J, Weiner AJ, Chien DY, et al. Analysis of a successful immune response against hepatitis C virus. Immunity. UNITED STATES; 1999 Apr;10(4):439–49.

260. Badr G, Bedard N, Abdel-Hakeem MS, Trautmann L, Willems B, Villeneuve J-P, et al. Early interferon therapy for hepatitis C virus infection rescues polyfunctional, long-lived CD8+ memory T cells. J Virol. United States; 2008 Oct;82(20):10017–31.

261. Bowen DG, Walker CM. Adaptive immune responses in acute and chronic hepatitis C virus infection. Nature [Internet]. 2005 Aug 18;436(7053):946–52. Available from: http://dx.doi.org/10.1038/nature04079

262. Grakoui A, Shoukry NH, Woollard DJ, Han J-H, Hanson HL, Ghrayeb J, et al. HCV persistence and immune evasion in the absence of memory T cell help. Science. United States; 2003 Oct;302(5645):659–62.

263. Hao C, Zhou Y, He Y, Fan C, Sun L, Wei X, et al. Imbalance of regulatory T cells and T helper type 17 cells in patients with chronic hepatitis C. Immunology. England; 2014 Dec;143(4):531–8.

264. Rushbrook SM, Ward SM, Unitt E, Vowler SL, Lucas M, Klenerman P, et al. Regulatory T Cells Suppress In Vitro Proliferation of Virus-Specific CD8+ T Cells during Persistent Hepatitis C Virus Infection. J Virol [Internet]. 2005 Jun 15;79 (12):7852–9. Available from: http://jvi.asm.org/content/79/12/7852.abstract

265. Pestka JM, Zeisel MB, Bläser E, Schürmann P, Bartosch B, Cosset F-L, et al. Rapid induction of virus-neutralizing antibodies and viral clearance in a single-source outbreak of hepatitis C. Proc Natl Acad Sci [Internet]. 2007 Apr 3;104 (14):6025–30. Available from: http://www.pnas.org/content/104/14/6025.abstract

266. Abdel-Hakeem MS, Shoukry NH. Protective Immunity Against Hepatitis C: Many Shades of Gray. Front Immunol [Internet]. Frontiers Media S.A.; 2014 Jun 16;5:274. Available from: http://www.ncbi.nlm.nih.gov/pmc/articles/PMC4058636/

267. Booth JC, Kumar U, Webster D, Monjardino J, Thomas HC. Comparison of the rate of sequence variation in the hypervariable region of E2/NS1 region of hepatitis C virus in normal and hypogammaglobulinemic patients. Hepatology. UNITED STATES; 1998 Jan;27(1):223–7.

268. Liu L, Fisher BE, Dowd KA, Astemborski J, Cox AL, Ray SC. Acceleration of hepatitis C virus envelope evolution in humans is consistent with progressive humoral immune selection during the transition from acute to chronic infection. J Virol. United States; 2010 May;84(10):5067–77.

269. Choo QL, Kuo G, Ralston R, Weiner A, Chien D, Van Nest G, et al. Vaccination of chimpanzees against infection by the hepatitis C

virus. Proc Natl Acad Sci U S A. UNITED STATES; 1994 Feb;91(4):1294–8.

270. Chung RT, Gordon FD, Curry MP, Schiano TD, Emre S, Corey K, et al. Human monoclonal antibody MBL-HCV1 delays HCV viral rebound following liver transplantation: a randomized controlled study. Am J Transplant. United States; 2013 Apr;13(4):1047–54.

271. Hsieh C-Y, Huang H-H, Lin C-Y, Chung LW, Liao Y-M, Bai L-Y, et al. Rituximab-induced hepatitis C virus reactivation after spontaneous remission in diffuse large B-cell lymphoma. J Clin Oncol. United States; 2008 May;26(15):2584–6.

272. Bjoro K, Froland SS, Yun Z, Samdal HH, Haaland T. Hepatitis C infection in patients with primary hypogammaglobulinemia after treatment with contaminated immune globulin. N Engl J Med. UNITED STATES; 1994 Dec;331(24):1607–11.

273. Banerjee A, Mazumdar B, Meyer K, Di Bisceglie AM, Ray RB, Ray R. Transcriptional Repression of C4 Complement by Hepatitis C Virus Proteins. J Virol [Internet]. 1752 N St., N.W., Washington, DC: American Society for Microbiology; 2011 May 23;85(9):4157–66. Available from: http://www.ncbi.nlm.nih.gov/pmc/articles/PMC3126272/

274. Dumestre-Perard C, Ponard D, Drouet C, Leroy V, Zarski J-P, Dutertre N, et al. Complement C4 monitoring in the follow-up of chronic hepatitis C treatment. Clin Exp Immunol [Internet]. Blackwell Science Ltd.; 2002 Jan 1;127(1):131–6. Available from: http://dx.doi.org/10.1046/j.1365-2249.2002.01729.x

275. Jost S, Altfeld M. Control of Human Viral Infections by Natural Killer Cells. Annu Rev Immunol [Internet]. Annual Reviews; 2013 Mar 21;31(1):163–94. Available from: http://dx.doi.org/10.1146/annurev-immunol-032712-100001

276. Khakoo SI, Thio CL, Martin MP, Brooks CR, Gao X, Astemborski J, et al. HLA and NK Cell Inhibitory Receptor Genes in Resolving Hepatitis C Virus Infection. Sci [Internet]. 2004 Aug 6;305 (5685):872–4. Available from: http://www.sciencemag.org/content/305/5685/872.abstract

277. Knapp S, Warshow U, Hegazy D, Brackenbury L, Guha IN, Fowell A, et al. Consistent beneficial effects of killer cell immunoglobulin-like receptor 2DL3 and group 1 human leukocyte antigen-C following exposure to hepatitis C virus. Hepatology. United States; 2010 Apr;51(4):1168–75.

278. Golden-Mason L, Cox AL, Randall JA, Cheng L, Rosen HR. Increased natural killer cell cytotoxicity and NKp30 expression protects against hepatitis C virus infection in high-risk individuals and inhibits replication in vitro. Hepatology. United States; 2010 Nov;52(5):1581–9.

279. Reizis B, Bunin A, Ghosh HS, Lewis KL, Sisirak V. Plasmacytoid Dendritic Cells: Recent Progress and Open Questions. Annu Rev Immunol [Internet]. Annual Reviews; 2011 Mar 22;29(1):163–83. Available from: http://dx.doi.org/10.1146/annurev-immunol-031210-101345

280. Sarobe P, Lasarte JJ, Zabaleta A, Arribillaga L, Arina A, Melero I, et al. Hepatitis C Virus Structural Proteins Impair Dendritic Cell Maturation and Inhibit In Vivo Induction of Cellular Immune Responses. J Virol [Internet]. 2003 Oct 15;77 (20):10862–71. Available from: http://jvi.asm.org/content/77/20/10862.abstract

281. Larsson M, Babcock E, Grakoui A, Shoukry N, Lauer G, Rice C, et al. Lack of phenotypic and functional impairment in dendritic cells from chimpanzees chronically infected with hepatitis C virus. J Virol. United States; 2004 Jun;78(12):6151–61.

282. Takahashi K, Asabe S, Wieland S, Garaigorta U, Gastaminza P, Isogawa M, et al. Plasmacytoid dendritic cells sense hepatitis C virus-infected cells, produce interferon, and inhibit infection. Proc Natl Acad Sci U S A. United States; 2010 Apr;107(16):7431–6.

283. Dreux M, Garaigorta U, Boyd B, Decembre E, Chung J, Whitten-Bauer C, et al. Short-range exosomal transfer of viral RNA from infected cells to plasmacytoid dendritic cells triggers innate immunity. Cell Host Microbe. United States; 2012 Oct;12(4):558–70.

284. Pelletier S, Bedard N, Said E, Ancuta P, Bruneau J, Shoukry NH. Sustained hyperresponsiveness of dendritic cells is associated with spontaneous resolution of acute hepatitis C. J Virol. United States; 2013 Jun;87(12):6769–81.

285. Loo Y-M, Owen DM, Li K, Erickson AK, Johnson CL, Fish PM, et al. Viral and therapeutic control of IFN-β promoter stimulator 1 during hepatitis C virus infection. Proc Natl Acad Sci U S A [Internet]. National Academy of Sciences; 2006 Apr 11;103(15):6001–6. Available from: http://www.ncbi.nlm.nih.gov/pmc/articles/PMC1458687/

286. Kolykhalov AA, Feinstone SM, Rice CM. Identification of a highly conserved sequence element at the 3' terminus of hepatitis C virus genome RNA. J Virol. UNITED STATES; 1996 Jun;70(6):3363–71.

287. You S, Rice CM. 3' RNA elements in hepatitis C virus replication: kissing partners and long poly(U). J Virol. United States; 2008 Jan;82(1):184–95.

288. Saito T, Owen DM, Jiang F, Marcotrigiano J, Gale MJ. Innate immunity induced by composition-dependent RIG-I recognition of hepatitis C virus RNA. Nature. England; 2008 Jul;454(7203):523–7.

289. Wu J, Meng Z, Jiang M, Zhang E, Trippler M, Broering R, et al. Toll-like receptor-induced innate immune responses in non-parenchymal liver cells are cell type-specific. Immunology. England; 2010 Mar;129(3):363–74.

290. Li K, Li NL, Wei D, Pfeffer SR, Fan M, Pfeffer LM. Activation of chemokine and inflammatory cytokine response in HCV-infected hepatocytes depends on TLR3 sensing of HCV dsRNA intermediates. Hepatology [Internet]. 2012 Mar 30;55(3):666–75. Available from: http://www.ncbi.nlm.nih.gov/pmc/articles/PMC3272326/

291. Wang N, Liang Y, Devaraj S, Wang J, Lemon SM, Li K. Toll-Like Receptor 3 Mediates Establishment of an Antiviral State against Hepatitis C Virus in Hepatoma Cells . J Virol [Internet]. American Society for Microbiology (ASM); 2009 Oct 22;83(19):9824–34. Available from: http://www.ncbi.nlm.nih.gov/pmc/articles/PMC2747996/

292. Targett-Adams P, Boulant S, McLauchlan J. Visualization of double-stranded RNA in cells supporting hepatitis C virus RNA replication. J Virol. United States; 2008 Mar;82(5):2182–95.

293. Dansako H, Yamane D, Welsch C, McGivern DR, Hu F, Kato N, et al. Class A Scavenger Receptor 1 (MSR1) Restricts Hepatitis C Virus Replication by Mediating Toll-like Receptor 3 Recognition of Viral RNAs Produced in Neighboring Cells. PLoS Pathog [Internet]. Public Library of Science; 2013 May 23;9(5):e1003345. Available from: http://dx.doi.org/10.1371%2Fjournal.ppat.1003345

294. Arnaud N, Dabo S, Akazawa D, Fukasawa M, Shinkai-Ouchi F, Hugon J, et al. Hepatitis C Virus Reveals a Novel Early Control in Acute Immune Response. PLoS Pathog [Internet]. Public Library of Science; 2011 Oct 13;7(10):e1002289. Available from: http://dx.doi.org/10.1371%2Fjournal.ppat.1002289

295. Shimoike T, McKenna SA, Lindhout DA, Puglisi JD. Translational insensitivity to potent activation of PKR by HCV IRES RNA. Antiviral Res [Internet]. 2009 Sep;83(3):228–37. Available from: http://www.sciencedirect.com/science/article/pii/S0166354209003246

296. Garaigorta U, Chisari F V. Hepatitis C Virus Blocks Interferon Effector Function by Inducing Protein Kinase R Phosphorylation. Cell Host Microbe [Internet]. 2009 Dec 17;6(6):513–22. Available from: http://www.sciencedirect.com/science/article/pii/S1931312809003813

297. Meylan E, Curran J, Hofmann K, Moradpour D, Binder M, Bartenschlager R, et al. Cardif is an adaptor protein in the RIG-I antiviral

pathway and is targeted by hepatitis C virus. Nature. England; 2005 Oct;437(7062):1167–72.

298. Baril M, Racine M-E, Penin F, Lamarre D. MAVS Dimer Is a Crucial Signaling Component of Innate Immunity and the Target of Hepatitis C Virus NS3/4A Protease. J Virol [Internet]. 2009 Feb 1;83 (3):1299–311. Available from: http://jvi.asm.org/content/83/3/1299.abstract

299. Li X-D, Sun L, Seth RB, Pineda G, Chen ZJ. Hepatitis C virus protease NS3/4A cleaves mitochondrial antiviral signaling protein off the mitochondria to evade innate immunity. Proc Natl Acad Sci United States Am [Internet]. 2005 Dec 6;102 (49):17717–22. Available from: http://www.pnas.org/content/102/49/17717.abstract

300. Chen Z, Benureau Y, Rijnbrand R, Yi J, Wang T, Warter L, et al. GB Virus B Disrupts RIG-I Signaling by NS3/4A-Mediated Cleavage of the Adaptor Protein MAVS. J Virol [Internet]. 2007 Jan 15;81 (2):964–76. Available from: http://jvi.asm.org/content/81/2/964.abstract

301. Yang Y, Liang Y, Qu L, Chen Z, Yi M, Li K, et al. Disruption of innate immunity due to mitochondrial targeting of a picornaviral protease precursor. Proc Natl Acad Sci [Internet]. 2007 Apr 24;104 (17):7253–8. Available from: http://www.pnas.org/content/104/17/7253.abstract

302. Sarasin-Filipowicz M, Oakeley EJ, Duong FHT, Christen V, Terracciano L, Filipowicz W, et al. Interferon signaling and treatment outcome in chronic hepatitis C. Proc Natl Acad Sci U S A. United States; 2008 May;105(19):7034–9.

303. Bellecave P, Sarasin-Filipowicz M, Donze O, Kennel A, Gouttenoire J, Meylan E, et al. Cleavage of mitochondrial antiviral signaling protein in the liver of patients with chronic hepatitis C correlates with a reduced activation of the endogenous interferon system. Hepatology. United States; 2010 Apr;51(4):1127–36.

304. Li K, Foy E, Ferreon JC, Nakamura M, Ferreon AC, Ikeda M, et al. Immune evasion by hepatitis C virus NS3/4A protease-mediated cleavage of the Toll-like receptor 3 adaptor protein TRIF. Proc Natl Acad Sci U S A. 2005;102(8):2992–7. Epub 2005 Feb 14.

305. Oshiumi H, Ikeda M, Matsumoto M, Watanabe A, Takeuchi O, Akira S, et al. Hepatitis C virus core protein abrogates the DDX3 function that enhances IPS-1-mediated IFN-beta induction. PLoS One. United States; 2010;5(12):e14258.

306. Schröder M, Baran M, Bowie AG. Viral targeting of DEAD box protein 3 reveals its role in TBK1/IKKε-mediated IRF activation. EMBO J [Internet]. Nature Publishing Group; 2008 Aug 6;27(15):2147–57. Available from: http://www.ncbi.nlm.nih.gov/pmc/articles/PMC2516890/

307. Taylor DR, Shi ST, Romano PR, Barber GN, Lai MMC. Inhibition of the Interferon- Inducible Protein Kinase PKR by HCV E2 Protein. Sci [Internet]. 1999 Jul 2;285 (5424):107–10. Available from: http://www.sciencemag.org/content/285/5424/107.abstract

308. Gale Jr. MJ, Korth MJ, Tang NM, Tan S-L, Hopkins DA, Dever TE, et al. Evidence That Hepatitis C Virus Resistance to Interferon Is Mediated through Repression of the PKR Protein Kinase by the Nonstructural 5A Protein. Virology [Internet]. 1997 Apr 14;230(2):217–27. Available from: http://www.sciencedirect.com/science/article/pii/S0042682297984932

309. Pflugheber J, Fredericksen B, Sumpter RJ, Wang C, Ware F, Sodora DL, et al. Regulation of PKR and IRF-1 during hepatitis C virus RNA replication. Proc Natl Acad Sci U S A. United States; 2002 Apr;99(7):4650–5.

310. Abe T, Kaname Y, Hamamoto I, Tsuda Y, Wen X, Taguwa S, et al. Hepatitis C virus nonstructural protein 5A modulates the toll-like receptor-MyD88-dependent signaling pathway in macrophage cell lines. J Virol. United States; 2007 Sep;81(17):8953–66.

311. Ge D, Fellay J, Thompson AJ, Simon JS, Shianna K V, Urban TJ, et al. Genetic variation in IL28B predicts hepatitis C treatment-induced viral clearance. Nature [Internet]. Macmillan Publishers Limited. All rights reserved; 2009 Sep 17;461(7262):399–401. Available from: http://dx.doi.org/10.1038/nature08309

312. Thomas DL, Thio CL, Martin MP, Qi Y, Ge D, O/'hUigin C, et al. Genetic variation in IL28B and spontaneous clearance of hepatitis C virus. Nature [Internet]. Macmillan Publishers Limited. All rights reserved; 2009 Oct 8;461(7265):798–801. Available from: http://dx.doi.org/10.1038/nature08463

313. Prokunina-Olsson L, Muchmore B, Tang W, Pfeiffer RM, Park H, Dickensheets H, et al. A variant upstream of IFNL3 (IL28B) creating a new interferon gene IFNL4 is associated with impaired clearance of hepatitis C virus. Nat Genet [Internet]. Nature Publishing Group, a division of Macmillan Publishers Limited. All Rights Reserved.; 2013 Feb;45(2):164–71. Available from: http://dx.doi.org/10.1038/ng.2521

314. Meissner EG, Wu D, Osinusi A, Bon D, Virtaneva K, Sturdevant D, et al. Endogenous intrahepatic IFNs and association with IFN-free HCV treatment outcome. J Clin Invest [Internet]. The American Society for Clinical Investigation; 124(8):3352–63. Available from: http://dx.doi.org/10.1172/JCI75938

315. Dill MT, Duong FHT, Vogt JE, Bibert S, Bochud P-Y, Terracciano L, et al. Interferon-induced gene expression is a stronger predictor of treatment response than IL28B genotype in patients with hepatitis C. Gastroenterology. United States; 2011 Mar;140(3):1021–31.

316. Naggie S, Osinusi A, Katsounas A, Lempicki R, Herrmann E, Thompson AJ, et al. Dysregulation of innate immunity in hepatitis C virus genotype 1 IL28B-unfavorable genotype patients: impaired viral kinetics and therapeutic response. Hepatology. United States; 2012 Aug;56(2):444–54.

317. Marcello T, Grakoui A, Barba–Spaeth G, Machlin ES, Kotenko S V, Macdonald MR, et al. Interferons α and λ Inhibit Hepatitis C Virus Replication With Distinct Signal Transduction and Gene Regulation Kinetics. Gastroenterology [Internet]. 2006 Dec;131(6):1887–98. Available from: http://www.sciencedirect.com/science/article/pii/S0016508506022207

318. Mihm S, Frese M, Meier V, Wietzke-Braun P, Scharf J-G, Bartenschlager R, et al. Interferon type I gene expression in chronic hepatitis C. Lab Invest [Internet]. 2004 Jun 21;84(9):1148–59. Available from: http://dx.doi.org/10.1038/labinvest.3700135

319. Sarasin-Filipowicz M, Wang X, Yan M, Duong FHT, Poli V, Hilton DJ, et al. Alpha interferon induces long-lasting refractoriness of JAK-STAT signaling in the mouse liver through induction of USP18/UBP43. Mol Cell Biol [Internet]. 2009;29(17):4841–51. Available from: http://www.scopus.com/inward/record.url?eid=2-s2.0-68849096074&partnerID=40&md5=6103fec617e84c35cc279c61dd33d7e2

320. Makowska Z, Duong FHT, Trincucci G, Tough DF, Heim MH. Interferon-beta and interferon-lambda signaling is not affected by interferon-induced refractoriness to interferon-alpha in vivo. Hepatology. United States; 2011 Apr;53(4):1154–63.

321. Heim MH. Innate immunity and HCV. J Hepatol. Netherlands; 2013 Mar;58(3):564–74.

322. Chen L, Borozan I, Sun J, Guindi M, Fischer S, Feld J, et al. Cell-type specific gene expression signature in liver underlies response to interferon therapy in chronic hepatitis C infection. Gastroenterology. United States; 2010 Mar;138(3):1123.

323. McGilvray I, Feld JJ, Chen L, Pattullo V, Guindi M, Fischer S, et al. Hepatic Cell–Type Specific Gene Expression Better Predicts HCV Treatment Outcome Than IL28B Genotype. Gastroenterology [Internet]. 2012 May;142(5):1122–31.e1. Available from: http://www.sciencedirect.com/science/article/pii/S001650851200145X

324. Lau DT –Y., Negash A, Chen J, Crochet N, Sinha M, Zhang Y, et al. Innate Immune Tolerance and the Role of Kupffer Cells in

Differential Responses to Interferon Therapy Among Patients With HCV Genotype 1 Infection. Gastroenterology [Internet]. 2013 Feb;144(2):402–13.e12. Available from: http://www.sciencedirect.com/science/article/pii/S0016508512016022

325. Metz P, Dazert E, Ruggieri A, Mazur J, Kaderali L, Kaul A, et al. Identification of type I and type II interferon-induced effectors controlling hepatitis C virus replication. Hepatology. 2012;56(6):2082–93. doi: 10.1002/hep.25908. Epub 2012 Oct 14.

326. Duong FHT, Filipowicz M, Tripodi M, La Monica N, Heim MH. Hepatitis C virus inhibits interferon signaling through up-regulation of protein phosphatase 2A. Gastroenterology. United States; 2004 Jan;126(1):263–77.

327. Heim MH, Moradpour D, Blum HE. Expression of Hepatitis C Virus Proteins Inhibits Signal Transduction through the Jak-STAT Pathway. J Virol [Internet]. 1999 Oct 1;73 (10):8469–75. Available from: http://jvi.asm.org/content/73/10/8469.abstract

328. Kriegs M, Burckstummer T, Himmelsbach K, Bruns M, Frelin L, Ahlen G, et al. The hepatitis C virus non-structural NS5A protein impairs both the innate and adaptive hepatic immune response in vivo. J Biol Chem. United States; 2009 Oct;284(41):28343–51.

329. Hornung V, Hartmann R, Ablasser A, Hopfner K-P. OAS proteins and cGAS: unifying concepts in sensing and responding to cytosolic nucleic acids. Nat Rev Immunol. England; 2014 Aug;14(8):521–8.

330. Lin W, Kim SS, Yeung E, Kamegaya Y, Blackard JT, Kim KA, et al. Hepatitis C virus core protein blocks interferon signaling by interaction with the STAT1 SH2 domain. J Virol. United States; 2006 Sep;80(18):9226–35.

331. Bode JG, Ludwig S, Ehrhardt C, Albrecht U, Erhardt A, Schaper F, et al. IFN-alpha antagonistic activity of HCV core protein involves induction of suppressor of cytokine signaling-3. FASEB J Off Publ Fed Am Soc Exp Biol. United States; 2003 Mar;17(3):488–90.

332. Carow B, Rottenberg ME. SOCS3, a Major Regulator of Infection and Inflammation. Front Immunol. Switzerland; 2014;5:58.

333. Taguchi T, Nagano-Fujii M, Akutsu M, Kadoya H, Ohgimoto S, Ishido S, et al. Hepatitis C virus NS5A protein interacts with 2',5'-oligoadenylate synthetase and inhibits antiviral activity of IFN in an IFN sensitivity-determining region-independent manner. J Gen Virol. England; 2004 Apr;85(Pt 4):959–69.

334. Polyak SJ, Khabar KS, Paschal DM, Ezelle HJ, Duverlie G, Barber GN, et al. Hepatitis C virus nonstructural 5A protein induces interleukin-8, leading to partial inhibition of the interferon-induced antiviral response. J Virol. United States; 2001 Jul;75(13):6095–106.

335. Girelli D, Pasino M, Goodnough JB, Nemeth E, Guido M, Castagna A, et al. Reduced serum hepcidin levels in patients with chronic hepatitis C. J Hepatol. 2009;51(5):845–52. doi: 10.1016/j.jhep.2009.06.027. Epub 2009.

336. Fujita N, Sugimoto R, Takeo M, Urawa N, Mifuji R, Tanaka H, et al. Hepcidin expression in the liver: relatively low level in patients with chronic hepatitis C. Mol Med. 2007;13(1-2):97–104.

337. Nemeth E, Tuttle MS, Powelson J, Vaughn MB, Donovan A, Ward DM, et al. Hepcidin regulates cellular iron efflux by binding to ferroportin and inducing its internalization. Science. United States; 2004 Dec;306(5704):2090–3.

338. Andriopoulos Jr B, Corradini E, Xia Y, Faasse SA, Chen S, Grgurevic L, et al. BMP6 is a key endogenous regulator of hepcidin expression and iron metabolism. Nat Genet [Internet]. Nature Publishing Group; 2009 Apr;41(4):482–7. Available from: http://dx.doi.org/10.1038/ng.335

339. Meynard D, Kautz L, Darnaud V, Canonne-Hergaux F, Coppin H, Roth M-P. Lack of the bone morphogenetic protein BMP6 induces massive iron overload. Nat Genet [Internet]. Nature Publishing Group; 2009 Apr;41(4):478–81. Available from: http://dx.doi.org/10.1038/ng.320

340. Armitage AE, Eddowes LA, Gileadi U, Cole S, Spottiswoode N, Selvakumar TA, et al. Hepcidin regulation by innate immune and infectious stimuli. Blood. United States; 2011 Oct;118(15):4129–39.

341. Truksa J, Lee P, Beutler E. Two BMP responsive elements, STAT, and bZIP/HNF4/COUP motifs of the hepcidin promoter are critical for BMP, SMAD1, and HJV responsiveness. Blood. United States; 2009 Jan;113(3):688–95.

342. Arezes J, Jung G, Gabayan V, Valore E, Ruchala P, Gulig PA, et al. Hepcidin-induced hypoferremia is a critical host defense mechanism against the siderophilic bacterium Vibrio vulnificus. Cell Host Microbe. United States; 2015 Jan;17(1):47–57.

343. Armitage AE, Stacey AR, Giannoulatou E, Marshall E, Sturges P, Chatha K, et al. Distinct patterns of hepcidin and iron regulation during HIV-1, HBV, and HCV infections. Proc Natl Acad Sci U S A. United States; 2014 Aug;111(33):12187–92.

344. Sakamoto N, Yoshimura M, Kimura T, Toyama K, Sekine-Osajima Y, Watanabe M, et al. Bone morphogenetic protein-7 and interferon-alpha synergistically suppress hepatitis C virus replicon. Biochem Biophys Res Commun. 2007;357(2):467–73. Epub 2007 Apr 5.

345. Armitage AE, Pinches R, Eddowes LA, Newbold CI, Drakesmith H. Plasmodium falciparum infected erythrocytes induce hepcidin (HAMP) mRNA synthesis by peripheral blood mononuclear cells. Br J Haematol [Internet]. Blackwell Publishing Ltd; 2009 Dec 1;147(5):769–71. Available from: http://dx.doi.org/10.1111/j.1365-2141.2009.07880.x

346. Heid CA, Stevens J, Livak KJ, Williams PM. Real time quantitative PCR. Genome Res. UNITED STATES; 1996 Oct;6(10):986–94.

347. Ikeda M, Abe K, Dansako H, Nakamura T, Naka K, Kato N. Efficient replication of a full-length hepatitis C virus genome, strain O, in cell culture, and development of a luciferase reporter system. Biochem Biophys Res Commun. 2005;329(4):1350–9.

348. Wang R-H, Li C, Xu X, Zheng Y, Xiao C, Zerfas P, et al. A role of SMAD4 in iron metabolism through the positive regulation of hepcidin expression. Cell Metab. United States; 2005 Dec;2(6):399–409.

349. Daub JT, Hofer T, Cutivet E, Dupanloup I, Quintana-Murci L, Robinson-Rechavi M, et al. Evidence for Polygenic Adaptation to Pathogens in the Human Genome. Mol Biol Evol [Internet]. 2013 Jul 1;30 (7):1544–58. Available from: http://mbe.oxfordjournals.org/content/30/7/1544.abstract

350. Quintás-Cardama A, Vaddi K, Liu P, Manshouri T, Li J, Scherle PA, et al. Preclinical characterization of the selective JAK1/2 inhibitor INCB018424: therapeutic implications for the treatment of myeloproliferative neoplasms. Blood [Internet]. 2010 Feb 3;115(15):3109–17. Available from: http://www.bloodjournal.org/content/115/15/3109.abstract

351. Liu S-Y, Sanchez DJ, Aliyari R, Lu S, Cheng G. Systematic identification of type I and type II interferon-induced antiviral factors. Proc Natl Acad Sci [Internet]. 2012 Mar 13;109 (11):4239–44. Available from: http://www.pnas.org/content/109/11/4239.abstract

352. Ariumi Y, Kuroki M, Dansako H, Abe K-I, Ikeda M, Wakita T, et al. The DNA Damage Sensors Ataxia-Telangiectasia Mutated Kinase and Checkpoint Kinase 2 Are Required for Hepatitis C Virus RNA Replication . J Virol [Internet]. American Society for Microbiology (ASM); 2008 Oct 30;82(19):9639–46. Available from: http://www.ncbi.nlm.nih.gov/pmc/articles/PMC2546985/

353. Malumbres M, Barbacid M. Milestones in cell division : To cycle or not to cycle: a critical decision in cancer. Nat Rev Cancer [Internet]. 2001 Dec;1(3):222–31. Available from: http://dx.doi.org/10.1038/35106065

354. Duronio RJ, Xiong Y. Signaling Pathways that Control Cell Proliferation. Cold Spring Harb Perspect Biol [Internet]. 2013 Mar 1;5 (3). Available from: http://cshperspectives.cshlp.org/content/5/3/a008904.abstract

355. Hochegger H, Takeda S, Hunt T. Cyclin-dependent kinases and cell-cycle transitions: does one fit all? Nat Rev Mol Cell Biol [Internet]. Nature Publishing Group; 2008 Nov;9(11):910–6. Available from: http://dx.doi.org/10.1038/nrm2510

356. Rhind N, Russell P. Signaling Pathways that Regulate Cell Division. Cold Spring Harb Perspect Biol [Internet]. 2012 Oct 1;4 (10). Available from: http://cshperspectives.cshlp.org/content/4/10/a005942.abstract

357. Xiong Y, Hannon GJ, Zhang H, Casso D, Kobayashi R, Beach D. p21 is a universal inhibitor of cyclin kinases. Nature [Internet]. 1993 Dec 16;366(6456):701–4. Available from: http://dx.doi.org/10.1038/366701a0

358. Wade Harper J, Adami GR, Wei N, Keyomarsi K, Elledge SJ. The p21 Cdk-interacting protein Cip1 is a potent inhibitor of G1 cyclin-dependent kinases. Cell [Internet]. 1993 Nov 19;75(4):805–16. Available from: http://www.sciencedirect.com/science/article/pii/009286749390499G

359. Serrano M, Hannon GJ, Beach D. A new regulatory motif in cell-cycle control causing specific inhibition of cyclin D/CDK4. Nature. ENGLAND; 1993 Dec;366(6456):704–7.

360. Knudsen ES, Knudsen KE. Tailoring to RB: tumour suppressor status and therapeutic response. Nat Rev Cancer [Internet]. Nature Publishing Group; 2008 Sep;8(9):714–24. Available from: http://dx.doi.org/10.1038/nrc2401

361. Jernvall J, Aberg T, Kettunen P, Keranen S, Thesleff I. The life history of an embryonic signaling center: BMP-4 induces p21 and is associated with apoptosis in the mouse tooth enamel knot. Dev [Internet]. 1998 Jan 15;125 (2):161–9. Available from: http://dev.biologists.org/content/125/2/161.abstract

362. Ghosh-Choudhury N, Ghosh-Choudhury G, Celeste A, Ghosh PM, Moyer M, Abboud SL, et al. Bone morphogenetic protein-2 induces cyclin kinase inhibitor p21 and hypophosphorylation of retinoblastoma protein in estradiol-treated MCF-7 human breast cancer cells. Biochim Biophys Acta. NETHERLANDS; 2000 Jul;1497(2):186–96.

363. Chen A, Wang D, Liu X, He S, Yu Z, Wang J. Inhibitory effect of BMP-2 on the proliferation of breast cancer cells. Mol Med Rep. Greece; 2012 Sep;6(3):615–20.

364. Ghosh-Choudhury N, Woodruff K, Qi W, Celeste A, Abboud SL, Ghosh Choudhury G. Bone morphogenetic protein-2 blocks MDA MB 231 human breast cancer cell proliferation by inhibiting cyclin-dependent kinase-mediated retinoblastoma protein phosphorylation. Biochem Biophys Res Commun. UNITED STATES; 2000 Jun;272(3):705–11.

365. Kawamura C, Kizaki M, Yamato K, Uchida H, Fukuchi Y, Hattori Y, et al. Bone morphogenetic protein-2 induces apoptosis in human myeloma cells with modulation of STAT3. Blood [Internet]. 2000 Sep 15;96(6):2005–11. Available from: http://www.bloodjournal.org/content/96/6/2005.abstract

366. Franzen A, Heldin NE. BMP-7-induced cell cycle arrest of anaplastic thyroid carcinoma cells via p21(CIP1) and p27(KIP1). Biochem Biophys Res Commun. United States; 2001 Jul;285(3):773–81.

367. Hu F, Meng X, Tong Q, Liang L, Xiang R, Zhu T, et al. BMP-6 inhibits cell proliferation by targeting microRNA-192 in breast cancer. Biochim Biophys Acta. Netherlands; 2013 Dec;1832(12):2379–90.

368. Miyazaki H, Watabe T, Kitamura T, Miyazono K. BMP signals inhibit proliferation and in vivo tumor growth of androgen-insensitive prostate carcinoma cells. Oncogene. England; 2004 Dec;23(58):9326–35.

369. Zhou J, Lee P-L, Tsai C-S, Lee C-I, Yang T-L, Chuang H-S, et al. Force-specific activation of Smad1/5 regulates vascular endothelial cell cycle progression in response to disturbed flow. Proc Natl Acad Sci [Internet]. 2012 May 15;109 (20):7770–5. Available from: http://www.pnas.org/content/109/20/7770.abstract

370. Kua H-Y, Liu H, Leong WF, Li L, Jia D, Ma G, et al. c-Abl promotes osteoblast expansion by differentially regulating canonical and non-canonical BMP pathways and p16INK4a expression. Nat Cell Biol [Internet]. Nature Publishing Group, a division of Macmillan Publishers Limited. All Rights Reserved.; 2012 Jul;14(7):727–37. Available from: http://dx.doi.org/10.1038/ncb2528

371. Reinhardt HC, Yaffe MB. Kinases that control the cell cycle in response to DNA damage: Chk1, Chk2, and MK2. Curr Opin Cell Biol [Internet]. 2009 Apr;21(2):245–55. Available from: http://www.sciencedirect.com/science/article/pii/S0955067409000246

372. Downs JA, Nussenzweig MC, Nussenzweig A. Chromatin dynamics and the preservation of genetic information. Nature [Internet]. 2007;447(7147):951–8. Available from: http://www.scopus.com/inward/record.url?eid=2-s2.0-34250820438&partnerID=40&md5=bd4e424a330636569728030efb8379d1

373. Falck J, Coates J, Jackson SP. Conserved modes of recruitment of ATM, ATR and DNA-PKcs to sites of DNA damage. Nature [Internet]. 2005;434(7033):605–11. Available from: http://www.scopus.com/inward/record.url?eid=2-s2.0-15844394846&partnerID=40&md5=27e4c134cbdf9dbea98c5bf7922214de

374. Savitsky K, Bar-Shira A, Gilad S, Rotman G, Ziv Y, Vanagaite L, et al. A single ataxia telangiectasia gene with a product similar to PI-3 kinase. Science. UNITED STATES; 1995 Jun;268(5218):1749–53.

375. Marechal A, Zou L. DNA damage sensing by the ATM and ATR kinases. Cold Spring Harb Perspect Biol. United States; 2013 Sep;5(9).

376. Chau JFL, Jia D, Wang Z, Liu Z, Hu Y, Zhang X, et al. A crucial role for bone morphogenetic protein-Smad1 signalling in the DNA damage response. Nat Commun. England; 2012;3:836.

377. Munakata T, Liang Y, Kim S, McGivern DR, Huibregtse J, Nomoto A, et al. Hepatitis C Virus Induces E6AP-Dependent Degradation of the Retinoblastoma Protein. Young JAT, editor. PLoS Pathog [Internet]. San Francisco, USA: Public Library of Science; 2007 Sep 28;3(9):e139. Available from: http://www.ncbi.nlm.nih.gov/pmc/articles/PMC2323300/

378. Munakata T, Nakamura M, Liang Y, Li K, Lemon SM. Down-regulation of the retinoblastoma tumor suppressor by the hepatitis C virus NS5B RNA-dependent RNA polymerase. Proc Natl Acad Sci U S A [Internet]. National Academy of Sciences; 2005 Dec 13;102(50):18159–64. Available from: http://www.ncbi.nlm.nih.gov/pmc/articles/PMC1307512/

379. Mitchell JK, Lemon SM, McGivern DR. How do persistent infections with hepatitis C virus cause liver cancer? Curr Opin Virol [Internet]. 2015 Oct;14:101–8. Available from: http://www.sciencedirect.com/science/article/pii/S1879625715001388

380. McGivern DR, Lemon SM. Virus-specific mechanisms of carcinogenesis in hepatitis C virus associated liver cancer. Oncogene [Internet]. Macmillan Publishers Limited; 2011 Apr 28;30(17):1969–83. Available from: http://dx.doi.org/10.1038/onc.2010.594

381. Korenaga M, Wang T, Li Y, Showalter LA, Chan T, Sun J, et al. Hepatitis C Virus Core Protein Inhibits Mitochondrial Electron Transport and Increases Reactive Oxygen Species (ROS) Production. J Biol Chem [Internet]. 2005 Nov 11;280 (45):37481–8. Available from: http://www.jbc.org/content/280/45/37481.abstract

382. Lai C-K, Jeng K-S, Machida K, Cheng Y-S, Lai MMC. Hepatitis C virus NS3/4A protein interacts with ATM, impairs DNA repair and enhances sensitivity to ionizing radiation. Virology [Internet]. 2008 Jan 20;370(2):295–309. Available from: http://www.sciencedirect.com/science/article/pii/S0042682207005661

383. Battaglia S, Benzoubir N, Nobilet S, Charneau P, Samuel D, Zignego AL, et al. Liver Cancer-Derived Hepatitis C Virus Core Proteins Shift TGF-Beta Responses from Tumor Suppression to Epithelial-Mesenchymal Transition. Rojas M, editor. PLoS One [Internet]. San Francisco, USA: Public Library of Science; 2009 Feb 3;4(2):e4355. Available from: http://www.ncbi.nlm.nih.gov/pmc/articles/PMC2629560/

384. Cheng P-L, Chang M-H, Chao C-H, Lee Y-HW. Hepatitis C viral proteins interact with Smad3 and differentially regulate TGF-[beta]//Smad3-mediated transcriptional activation. Oncogene [Internet]. Nature Publishing Group; 2004 Aug 30;23(47):7821–38. Available from: http://dx.doi.org/10.1038/sj.onc.1208066

385. Yang X-J, Liu J, Ye L, Liao Q-J, Wu J-G, Gao J-R, et al. HCV NS2 protein inhibits cell proliferation and induces cell cycle arrest in the S-phase in mammalian cells through down-regulation of cyclin A expression. Virus Res [Internet]. 2006 Nov;121(2):134–43. Available from: http://www.sciencedirect.com/science/article/pii/S0168170206000657

386. Naka K, Dansako H, Kobayashi N, Ikeda M, Kato N. Hepatitis C virus NS5B delays cell cycle progression by inducing interferon-β via Toll-like receptor 3 signaling pathway without replicating viral genomes. Virology [Internet]. 2006 Mar 15;346(2):348–62. Available from: http://www.sciencedirect.com/science/article/pii/S0042682205006732

387. Tang Q, Zhang Y, Fan L, Tong G, He L, Dai C. Classic swine fever virus NS2 protein leads to the induction of cell cycle arrest at S-phase and endoplasmic reticulum stress. Virol J [Internet]. BioMed Central; 2010 Jan 11;7:4. Available from: http://www.ncbi.nlm.nih.gov/pmc/articles/PMC2819037/

388. Xu X, Zhang H, Zhang Q, Huang Y, Dong J, Liang Y, et al. Porcine epidemic diarrhea virus N protein prolongs S-phase cell cycle, induces endoplasmic reticulum stress, and up-regulates interleukin-8 expression. Vet Microbiol [Internet]. 2013 Jun 28;164(3–4):212–21. Available from: http://www.sciencedirect.com/science/article/pii/S0378113513000862

389. Atreya CD, Kulkarni S, Mohan KVK. Rubella virus P90 associates with the cytokinesis regulatory protein Citron-K kinase and the viral infection and constitutive expression of P90 protein both induce cell cycle arrest following S phase in cell culture. Arch Virol [Internet]. Springer-Verlag; 2004;149(4):779–89. Available from: http://dx.doi.org/10.1007/s00705-003-0267-6

390. Ding L, Huang Y, Dai M, Zhao X, Du Q, Dong F, et al. Transmissible gastroenteritis virus infection induces cell cycle arrest at S and G2/M phases via p53-dependent pathway. Virus Res. Netherlands; 2013 Dec;178(2):241–51.

391. Sarfraz S, Hamid S, Ali S, Jafri W, Siddiqui AA. Modulations of cell cycle checkpoints during HCV associated disease. BMC Infect Dis. England; 2009;9:125.

392. Takahashi I, Kobayashi E, Asano K, Yoshida M, Nakano H. UCN-01, a selective inhibitor of protein kinase C from Streptomyces. J Antibiot (Tokyo). JAPAN; 1987 Dec;40(12):1782–4.

393. Kawakami K, Futami H, Takahara J, Yamaguchi K. UCN-01, 7-hydroxyl-staurosporine, inhibits kinase activity of cyclin-dependent kinases and reduces the phosphorylation of the retinoblastoma susceptibility gene product in A549 human lung cancer cell line. Biochem Biophys Res Commun. UNITED STATES; 1996 Feb;219(3):778–83.

394. Akiyama T, Yoshida T, Tsujita T, Shimizu M, Mizukami T, Okabe M, et al. G1 phase accumulation induced by UCN-01 is associated with dephosphorylation of Rb and CDK2 proteins as well as induction of CDK inhibitor p21/Cip1/WAF1/Sdi1 in p53-mutated human epidermoid carcinoma A431 cells. Cancer Res. UNITED STATES; 1997 Apr;57(8):1495–501.

395. Inman GJ, Nicolás FJ, Callahan JF, Harling JD, Gaster LM, Reith AD, et al. SB-431542 Is a Potent and Specific Inhibitor of Transforming Growth Factor-β Superfamily Type I Activin Receptor-Like Kinase (ALK) Receptors ALK4, ALK5, and ALK7. Mol Pharmacol [Internet]. 2002 Jul 1;62 (1):65–74. Available from: http://molpharm.aspetjournals.org/content/62/1/65.abstract

396. De Wulf P, Montani F, Visintin R. Protein phosphatases take the mitotic stage. Curr Opin Cell Biol. England; 2009 Dec;21(6):806–15.

397. Amita M, Adachi K, Alexenko AP, Sinha S, Schust DJ, Schulz LC, et al. Complete and unidirectional conversion of human embryonic stem cells to trophoblast by BMP4. Proc Natl Acad Sci [Internet]. 2013;110(13):E1212–21. Available from: http://www.pnas.org/content/110/13/E1212.abstract

398. Bandyopadhyay A, Tsuji K, Cox K, Harfe BD, Rosen V, Tabin CJ. Genetic analysis of the roles of BMP2, BMP4, and BMP7 in limb patterning and skeletogenesis. PLoS Genet [Internet]. 2006;2(12). Available from: http://www.scopus.com/inward/record.url?eid=2-s2.0-34748859165&partnerID=40&md5=a4d0eaa45f3705f4e27e933db472d503

399. Gordon J, Patel SR, Mishina Y, Manley NR. Evidence for an early role for BMP4 signaling in thymus and parathyroid morphogenesis. Dev Biol [Internet]. 2010;339(1):141–54. Available from: http://www.scopus.com/inward/record.url?eid=2-s2.0-77649191415&partnerID=40&md5=52a4cea74aea940821c255b08547546c

400. Parent AV, Russ HA, Khan IS, LaFlam TN, Metzger TC, Anderson MS, et al. Generation of Functional Thymic Epithelium from Human Embryonic Stem Cells that Supports Host T Cell Development. Cell Stem Cell [Internet]. 2013;13(2):219–29. Available from: http://www.sciencedirect.com/science/article/pii/S1934590913001409

401. Hedger MP, Winnall WR, Phillips DJ, de Kretser DM. Chapter Thirteen - The Regulation and Functions of Activin and Follistatin in Inflammation and Immunity. In: Hormones GLBT-V&, editor. Activins and Inhibins [Internet]. Academic Press; 2011. p. 255–97. Available from: http://www.sciencedirect.com/science/article/pii/B9780123859617000135

402. Bootcov MR, Bauskin AR, Valenzuela SM, Moore AG, Bansal M, He XY, et al. MIC-1, a novel macrophage inhibitory cytokine, is a divergent member of the TGF-β superfamily. Proc Natl Acad Sci [Internet]. 1997 Oct 14;94 (21):11514–9. Available from: http://www.pnas.org/content/94/21/11514.abstract

403. Xu J, Kimball TR, Lorenz JN, Brown DA, Bauskin AR, Klevitsky R, et al. GDF15/MIC-1 functions as a protective and antihypertrophic factor released from the myocardium in association with SMAD protein activation. Circ Res. United States; 2006 Feb;98(3):342–50.

404. Lee S-J. Identification of a Novel Member (GDF-1) of the Transforming Growth Factor-β Superfamily. Mol Endocrinol [Internet]. The Endocrine Society; 1990 Jul 1;4(7):1034–40. Available from: http://dx.doi.org/10.1210/mend-4-7-1034

405. Rankin CT, Bunton T, Lawler AM, Lee SJ. Regulation of left-right patterning in mice by growth/differentiation factor-1. Nat Genet. UNITED STATES; 2000 Mar;24(3):262–5.

406. Gray PC, Vale W. Cripto/GRP78 modulation of the TGF-beta pathway in development and oncogenesis. FEBS Lett. Netherlands; 2012 Jul;586(14):1836–45.

407. Peng J, Li Q, Wigglesworth K, Rangarajan A, Kattamuri C, Peterson RT, et al. Growth differentiation factor 9:bone morphogenetic protein 15 heterodimers are potent regulators of ovarian functions. Proc Natl Acad Sci U S A. United States; 2013 Feb;110(8):E776–85.

408. Xia Y, Babitt JL, Sidis Y, Chung RT, Lin HY. Hemojuvelin regulates hepcidin expression via a selective subset of BMP ligands and receptors independently of neogenin. Blood. United States; 2008 May;111(10):5195–204.

409. Mayeur C, Lohmeyer LK, Leyton P, Kao SM, Pappas AE, Kolodziej SA, et al. The type I BMP receptor, Alk3, is required for the

induction of hepatic hepcidin gene expression by interleukin-6. Blood. 2014;5:5.

410. Sartori R, Schirwis E, Blaauw B, Bortolanza S, Zhao J, Enzo E, et al. BMP signaling controls muscle mass. Nat Genet [Internet]. Nature Publishing Group, a division of Macmillan Publishers Limited. All Rights Reserved.; 2013 Nov;45(11):1309–18. Available from: http://dx.doi.org/10.1038/ng.2772

411. Lane AN, Fan TW-M. Regulation of mammalian nucleotide metabolism and biosynthesis. Nucleic Acids Res [Internet]. 2015 Jan 27; Available from: http://nar.oxfordjournals.org/content/early/2015/01/24/nar.gkv047.abstract

412. Chen H, Li C, Huang J, Cung T, Seiss K, Beamon J, et al. CD4+ T cells from elite controllers resist HIV-1 infection by selective upregulation of p21. J Clin Invest. United States; 2011 Apr;121(4):1549–60.

413. Allouch A, David A, Amie SM, Lahouassa H, Chartier L, Margottin-Goguet F, et al. p21-mediated RNR2 repression restricts HIV-1 replication in macrophages by inhibiting dNTP biosynthesis pathway. Proc Natl Acad Sci U S A. 2013;110(42):E3997–4006. doi: 10.1073/pnas.1306719110. Epub 201.

414. Pauls E, Ruiz A, Riveira-Muñoz E, Permanyer M, Badia R, Clotet B, et al. p21 regulates the HIV-1 restriction factor SAMHD1. Proc Natl Acad Sci [Internet]. 2014 Apr 8;111 (14):E1322–4. Available from: http://www.pnas.org/content/111/14/E1322.short

415. Wilson PM, Labonte MJ, Russell J, Louie S, Ghobrial AA, Ladner RD. A novel fluorescence-based assay for the rapid detection and quantification of cellular deoxyribonucleoside triphosphates. Nucleic Acids Res. England; 2011 Sep;39(17):e112.

416. Mohedas AH, Xing X, Armstrong KA, Bullock AN, Cuny GD, Yu PB. Development of an ALK2-Biased BMP Type I Receptor Kinase Inhibitor. ACS Chem Biol [Internet]. American Chemical Society; 2013 Jun 21;8(6):1291–302. Available from: http://dx.doi.org/10.1021/cb300655w

417. Vogt J, Traynor R, Sapkota GP. The specificities of small molecule inhibitors of the TGFß and BMP pathways. Cell Signal [Internet]. 2011 Nov;23(11):1831–42. Available from: http://www.sciencedirect.com/science/article/pii/S0898656811001914

418. Sanvitale CE, Kerr G, Chaikuad A, Ramel M-C, Mohedas AH, Reichert S, et al. A new class of small molecule inhibitor of BMP signaling. PLoS One. United States; 2013;8(4):e62721.

419. Younis Y, Douelle F, Feng T-S, Cabrera DG, Manach C Le, Nchinda AT, et al. 3,5-Diaryl-2-aminopyridines as a Novel Class of Orally Active Antimalarials Demonstrating Single Dose Cure in Mice and Clinical Candidate Potential. J Med Chem [Internet]. American Chemical Society; 2012 Apr 12;55(7):3479–87. Available from: http://dx.doi.org/10.1021/jm3001373

420. Spottiswoode N, Duffy P, Drakesmith H. Iron, anemia and hepcidin in malaria [Internet]. Frontiers in Pharmacology . 2014. Available from: http://www.frontiersin.org/Journal/Abstract.aspx?s=323&name=drug_metabolism_and_transport&ART_DOI=10.3389/fphar.2014.00125

421. Fukuda T, Scott G, Komatsu Y, Araya R, Kawano M, Ray MK, et al. Generation of a mouse with conditionally activated signaling through the BMP receptor, ALK2. Genesis. United States; 2006 Apr;44(4):159–67.

422. van Dinther M, Visser N, de Gorter DJJ, Doorn J, Goumans M-J, de Boer J, et al. ALK2 R206H mutation linked to fibrodysplasia ossificans progressiva confers constitutive activity to the BMP type I receptor and sensitizes mesenchymal cells to BMP-induced osteoblast differentiation and bone formation. J Bone Miner Res. United States; 2010 Jun;25(6):1208–15.

423. Song G-A, Kim H-J, Woo K-M, Baek J-H, Kim G-S, Choi J-Y, et al. Molecular Consequences of the ACVR1R206H Mutation of Fibrodysplasia Ossificans Progressiva. J Biol Chem [Internet]. 2010 Jul 16;285 (29):22542–53. Available from: http://www.jbc.org/content/285/29/22542.abstract

424. Shore EM, Xu M, Feldman GJ, Fenstermacher DA, Cho T-J, Choi IH, et al. A recurrent mutation in the BMP type I receptor ACVR1 causes inherited and sporadic fibrodysplasia ossificans progressiva. Nat Genet [Internet]. 2006 May;38(5):525–7. Available from: http://dx.doi.org/10.1038/ng1783

425. Liu J, Farmer Jr. JD, Lane WS, Friedman J, Weissman I, Schreiber SL. Calcineurin is a common target of cyclophilin-cyclosporin A and FKBP-FK506 complexes. Cell [Internet]. 1991 Aug 23;66(4):807–15. Available from: http://www.sciencedirect.com/science/article/pii/009286749190124H

426. Mukai H, Kuno T, Chang CD, Lane B, Luly JR, Tanaka C. FKBP12-FK506 complex inhibits phosphatase activity of two mammalian isoforms of calcineurin irrespective of their substrates or activation mechanisms. J Biochem. JAPAN; 1993 Mar;113(3):292–8.

427. Clipstone NA, Crabtree GR. Identification of calcineurin as a key signalling enzyme in T-lymphocyte activation. Nature. ENGLAND; 1992 Jun;357(6380):695–7.

428. Kugimiya F, Yano F, Ohba S, Igawa K, Nakamura K, Kawaguchi H, et al. Mechanism of osteogenic induction by FK506 via BMP/Smad pathways. Biochem Biophys Res Commun. United States; 2005 Dec;338(2):872–9.

429. Spiekerkoetter E, Tian X, Cai J, Hopper RK, Sudheendra D, Li CG, et al. FK506 activates BMPR2, rescues endothelial dysfunction, and reverses pulmonary hypertension. J Clin Invest [Internet]. The American Society for Clinical Investigation; 2013 Aug 1;123(8):3600–13. Available from: http://www.jci.org/articles/view/65592

430. Janeway CAJ. Approaching the asymptote? Evolution and revolution in immunology. Cold Spring Harb Symp Quant Biol. UNITED STATES; 1989;54 Pt 1:1–13.

431. Akira S, Uematsu S, Takeuchi O. Pathogen Recognition and Innate Immunity. Cell [Internet]. 2006 Feb 24;124(4):783–801. Available from: http://www.sciencedirect.com/science/article/pii/S0092867406001905

432. Brubaker SW, Bonham KS, Zanoni I, Kagan JC. Innate Immune Pattern Recognition: A Cell Biological Perspective. Annu Rev Immunol [Internet]. Annual Reviews; 2015 Mar 21;33(1):257–90. Available from: http://dx.doi.org/10.1146/annurev-immunol-032414-112240

433. Yoneyama M, Kikuchi M, Natsukawa T, Shinobu N, Imaizumi T, Miyagishi M, et al. The RNA helicase RIG-I has an essential function in double-stranded RNA-induced innate antiviral responses. Nat Immunol [Internet]. 2004;5(7):730–7. Available from: http://www.scopus.com/inward/record.url?eid=2-s2.0-3242813113&partnerID=40&md5=780d974f865b002010cfc69272fbc356

434. Hornung V, Ellegast J, Kim S, Brzózka K, Jung A, Kato H, et al. 5'-Triphosphate RNA Is the Ligand for RIG-I. Science (80-) [Internet]. 2006 Nov 10;314(5801):994–7. Available from: http://www.sciencemag.org/content/314/5801/994.abstract

435. Goubau D, Schlee M, Deddouche S, Pruijssers AJ, Zillinger T, Goldeck M, et al. Antiviral immunity via RIG-I-mediated recognition of RNA bearing 5[prime]-diphosphates. Nature [Internet]. Nature Publishing Group, a division of Macmillan Publishers Limited. All Rights Reserved.; 2014 Oct 16;514(7522):372–5. Available from: http://dx.doi.org/10.1038/nature13590

436. Marques JT, Devosse T, Wang D, Zamanian-Daryoush M, Serbinowski P, Hartmann R, et al. A structural basis for discriminating between self and nonself double-stranded RNAs in mammalian cells. Nat Biotechnol [Internet]. 2006;24(5):559–65. Available from:

http://www.scopus.com/inward/record.url?eid=2-s2.0-33646561864&partnerID=40&md5=977930f8ec0ca6d42fafa25a5b3dd4ee

437. Schlee M, Roth A, Hornung V, Hagmann CA, Wimmenauer V, Barchet W, et al. Recognition of 5′ Triphosphate by RIG-I Helicase Requires Short Blunt Double-Stranded RNA as Contained in Panhandle of Negative-Strand Virus. Immunity [Internet]. 2009 Jul 17;31(1):25–34. Available from: http://www.sciencedirect.com/science/article/pii/S1074761309002714

438. Weber M, Gawanbacht A, Habjan M, Rang A, Borner C, Schmidt AM, et al. Incoming RNA virus nucleocapsids containing a 5′-triphosphorylated genome activate RIG-I and antiviral signaling. Cell Host Microbe [Internet]. 2013;13(3):336–46. Available from: http://www.scopus.com/inward/record.url?eid=2-s2.0-84875167118&partnerID=40&md5=43aed6fdb8a1a794b3098711e57f5457

439. Ablasser A, Bauernfeind F, Hartmann G, Latz E, Fitzgerald KA, Hornung V. RIG-I-dependent sensing of poly(dA:dT) through the induction of an RNA polymerase III-transcribed RNA intermediate. Nat Immunol. 2009;10(10):1065–72. doi: 10.1038/ni.1779. Epub 2009 Jul 16.

440. Chiu Y-H, MacMillan JB, Chen ZJ. RNA Polymerase III Detects Cytosolic DNA and Induces Type I Interferons through the RIG-I Pathway. Cell [Internet]. 2009 Aug 7;138(3):576–91. Available from: http://www.sciencedirect.com/science/article/pii/S0092867409007144

441. Malathi K, Dong B, Gale Jr. M, Silverman RH. Small self-RNA generated by RNase L amplifies antiviral innate immunity. Nature [Internet]. 2007;448(7155):816–9. Available from: http://www.scopus.com/inward/record.url?eid=2-s2.0-34547960175&partnerID=40&md5=da7beebe9dc4429cd89a0468b1d24cb8

442. Cui S, Eisenächer K, Kirchhofer A, Brzózka K, Lammens A, Lammens K, et al. The C-Terminal Regulatory Domain Is the RNA 5′-Triphosphate Sensor of RIG-I. Mol Cell [Internet]. 2008;29(2):169–79. Available from: http://www.scopus.com/inward/record.url?eid=2-s2.0-38649089789&partnerID=40&md5=3d00689154aac2a1c574b71fa85d8e49

443. Lu C, Xu H, Ranjith-Kumar CT, Brooks MT, Hou TY, Hu F, et al. The structural basis of 5′ triphosphate double-stranded RNA recognition by RIG-I C-terminal domain. Structure [Internet]. 2010;18(8):1032–43. Available from: http://www.scopus.com/inward/record.url?eid=2-s2.0-77955481642&partnerID=40&md5=5846919a393e93a74beab417dec968f2

444. Civril F, Bennett M, Moldt M, Deimling T, Witte G, Schiesser S, et al. The RIG-I ATPase domain structure reveals insights into ATP-dependent antiviral signalling. EMBO Rep [Internet]. 2011;12(11):1127–34. Available from: http://www.scopus.com/inward/record.url?eid=2-s2.0-80255141860&partnerID=40&md5=88159366d2bd591f89102d5601cf723b

445. Kowalinski E, Lunardi T, McCarthy AA, Louber J, Brunel J, Grigorov B, et al. Structural basis for the activation of innate immune pattern-recognition receptor RIG-I by viral RNA. Cell [Internet]. 2011;147(2):423–35. Available from: http://www.scopus.com/inward/record.url?eid=2-s2.0-80054703126&partnerID=40&md5=6a51a6190a184aaef637145b063a9aa7

446. Zeng W, Sun L, Jiang X, Chen X, Hou F, Adhikari A, et al. Reconstitution of the RIG-I Pathway Reveals a Signaling Role of Unanchored Polyubiquitin Chains in Innate Immunity. Cell [Internet]. 2010 Apr 16;141(2):315–30. Available from: http://www.sciencedirect.com/science/article/pii/S009286741000317X

447. Peisley A, Wu B, Xu H, Chen ZJ, Hur S. Structural basis for ubiquitin-mediated antiviral signal activation by RIG-I. Nature [Internet]. 2014;508(7498):110–4. Available from: http://www.scopus.com/inward/record.url?eid=2-s2.0-84899957213&partnerID=40&md5=451d261306caeee0bb5b895c149080ca

448. Oshiumi H, Miyashita M, Matsumoto M, Seya T. A Distinct Role of Riplet-Mediated K63-Linked Polyubiquitination of the RIG-I Repressor Domain in Human Antiviral Innate Immune Responses. PLoS Pathog [Internet]. Public Library of Science; 2013 Aug 8;9(8):e1003533. Available from: http://dx.doi.org/10.1371%2Fjournal.ppat.1003533

449. Fan Y, Mao R, Yu Y, Liu S, Shi Z, Cheng J, et al. USP21 negatively regulates antiviral response by acting as a RIG-I deubiquitinase. J Exp Med [Internet]. 2014;211(2):313–28. Available from: http://www.scopus.com/inward/record.url?eid=2-s2.0-84893721948&partnerID=40&md5=bb98582fd26f2d49625093fd0d5a88c9

450. Cui J, Song Y, Li Y, Zhu Q, Tan P, Qin Y, et al. USP3 inhibits type i interferon signaling by deubiquitinating RIG-I-like receptors. Cell Res [Internet]. 2014;24(4):400–16. Available from: http://www.scopus.com/inward/record.url?eid=2-s2.0-84898040489&partnerID=40&md5=1ccd7f26a62483c8a0bc6f5bf29f758c

451. Wang L, Zhao W, Zhang M, Wang P, Zhao K, Zhao X, et al. USP4 Positively regulates RIG-I-Mediated antiviral response through deubiquitination and stabilization of RIG-I. J Virol [Internet]. 2013;87(8):4507–15. Available from: http://www.scopus.com/inward/record.url?eid=2-s2.0-84875789033&partnerID=40&md5=86899ddddecd0f12af89eac93dcf4eeb

452. Wies E, Wang MK, Maharaj NP, Chen K, Zhou S, Finberg RW, et al. Dephosphorylation of the RNA Sensors RIG-I and MDA5 by the Phosphatase PP1 Is Essential for Innate Immune Signaling. Immunity [Internet]. 2013;38(3):437–49. Available from: http://www.scopus.com/inward/record.url?eid=2-s2.0-84875542059&partnerID=40&md5=97369dba795ae88da9eb8e4f6d347158

453. Kang D-C, Gopalkrishnan R V, Lin L, Randolph A, Valerie K, Pestka S, et al. Expression analysis and genomic characterization of human melanoma differentiation associated gene-5, mda-5: A novel type I interferon-responsive apoptosis-inducing gene. Oncogene [Internet]. 2004;23(9):1789–800. Available from: http://www.scopus.com/inward/record.url?eid=2-s2.0-1642348822&partnerID=40&md5=d5c0224c6db420c747dbf015728516fb

454. Andrejeva J, Childs KS, Young DF, Carlos TS, Stock N, Goodbourn S, et al. The V proteins of paramyxoviruses bind the IFN-inducible RNA helicase, mda-5, and inhibit its activation of the IFN-β promoter. Proc Natl Acad Sci U S A [Internet]. 2004;101(49):17264–9. Available from: http://www.scopus.com/inward/record.url?eid=2-s2.0-10344259136&partnerID=40&md5=436f835ca6513de15cba657e4ee807b1

455. Yoneyama M, Kikuchi M, Matsumoto K, Imaizumi T, Miyagishi M, Taira K, et al. Shared and unique functions of the DExD/H-box helicases RIG-I, MDA5, and LGP2 in antiviral innate immunity. J Immunol [Internet]. 2005;175(5):2851–8. Available from: http://www.scopus.com/inward/record.url?eid=2-s2.0-23844438864&partnerID=40&md5=d8131a7a402f3e804e6ee4af38249ad4

456. Yount JS, Moran TM, López CB. Cytokine-independent upregulation of MDA5 in viral infection. J Virol [Internet]. 2007;81(13):7316–9. Available from: http://www.scopus.com/inward/record.url?eid=2-s2.0-34250863768&partnerID=40&md5=a6b8b444ef8339dacdf7e7ee849718e6

457. Saito T, Hirai R, Loo Y-M, Owen D, Johnson CL, Sinha SC, et al. Regulation of innate antiviral defenses through a shared repressor domain in RIG-1 and LGP2. Proc Natl Acad Sci U S A [Internet]. 2007;104(2):582–7. Available from: http://www.scopus.com/inward/record.url?eid=2-s2.0-33846307026&partnerID=40&md5=bd7c8435331785710b2ab8048d1b78c4

458. Kato H, Takeuchi O, Sato S, Yoneyama M, Yamamoto M, Matsui K, et al. Differential roles of MDA5 and RIG-I helicases in the recognition of RNA viruses. Nature. 2006;441(7089):101–5. Epub 2006 Apr 9.

459. Kato H, Takeuchi O, Mikamo-Satoh E, Hirai R, Kawai T, Matsushita K, et al. Length-dependent recognition of double-stranded ribonucleic acids by retinoic acid-inducible gene-I and melanoma differentiation-associated gene 5. J Exp Med [Internet]. 2008;205(7):1601–10. Available from: http://www.scopus.com/inward/record.url?eid=2-s2.0-46949097299&partnerID=40&md5=67cf3e2612191d3e12525947afd91761

460. Takahasi K, Kumeta H, Tsuduki N, Narita R, Shigemoto T, Hirai R, et al. Solution structures of cytosolic RNA sensor MDA5 and LGP2 C-terminal domains: Identification of the RNA recognition loop in RIG-I-like receptors. J Biol Chem [Internet]. 2009;284(26):17465–74. Available from: http://www.scopus.com/inward/record.url?eid=2-s2.0-67650510680&partnerID=40&md5=644b65483c120afb6a669c785378cbaf

461. Wu B, Peisley A, Richards C, Yao H, Zeng X, Lin C, et al. Structural basis for dsRNA recognition, filament formation, and antiviral signal activation by MDA5. Cell [Internet]. 2013;152(1-2):276–89. Available from: http://www.scopus.com/inward/record.url?eid=2-s2.0-84872604349&partnerID=40&md5=5d63188f5ef42a4b0589e9f0e340245d

462. del Toro Duany Y, Wu B, Hur S. MDA5 — filament, dynamics and disease. Curr Opin Virol [Internet]. 2015 Jun;12:20–5. Available from: http://www.sciencedirect.com/science/article/pii/S1879625715000139

463. Yoneyama M, Onomoto K, Jogi M, Akaboshi T, Fujita T. Viral RNA detection by RIG-I-like receptors. Curr Opin Immunol [Internet]. 2015 Feb;32:48–53. Available from: http://www.sciencedirect.com/science/article/pii/S0952791514001605

464. Venkataraman T, Valdes M, Elsby R, Kakuta S, Caceres G, Saijo S, et al. Loss of DExD/H Box RNA Helicase LGP2 Manifests Disparate Antiviral Responses. J Immunol [Internet]. 2007 May 15;178 (10):6444–55. Available from: http://www.jimmunol.org/content/178/10/6444.abstract

465. Deddouche S, Goubau D, Rehwinkel J, Chakravarty P, Begum S, Maillard P V, et al. Identification of an LGP2-associated MDA5 agonist in picornavirus-infected cells. Chen ZJ, editor. Elife [Internet]. 2014 Feb 18;3. Available from: http://elifesciences.org/content/3/e01535.abstract

466. Seth RB, Sun L, Ea C-K, Chen ZJ. Identification and Characterization of MAVS, a Mitochondrial Antiviral Signaling Protein that Activates NF-κB and IRF3. Cell [Internet]. 2005 Sep 9;122(5):669–82. Available from: http://www.sciencedirect.com/science/article/pii/S0092867405008160

467. Kawai T, Takahashi K, Sato S, Coban C, Kumar H, Kato H, et al. IPS-1, an adaptor triggering RIG-I- and Mda5-mediated type I interferon induction. Nat Immunol. 2005;6(10):981–8. Epub 2005 Aug 28.

468. Xu L-G, Wang Y-Y, Han K-J, Li L-Y, Zhai Z, Shu H-B. VISA is an adapter protein required for virus-triggered IFN-β signaling. Mol Cell [Internet]. 2005;19(6):727–40. Available from: http://www.scopus.com/inward/record.url?eid=2-s2.0-24944538819&partnerID=40&md5=9f65f65430a3dbe3795567fac34a404e

469. Sun Q, Sun L, Liu H-H, Chen X, Seth RB, Forman J, et al. The Specific and Essential Role of MAVS in Antiviral Innate Immune Responses. Immunity [Internet]. 2006 May;24(5):633–42. Available from: http://www.sciencedirect.com/science/article/pii/S1074761306002202

470. Kumar H, Kawai T, Kato H, Sato S, Takahashi K, Coban C, et al. Essential role of IPS-1 in innate immune responses against RNA viruses. J Exp Med [Internet]. 2006 Jul 10;203 (7):1795–803. Available from: http://jem.rupress.org/content/203/7/1795.abstract

471. Dixit E, Boulant S, Zhang Y, Lee ASY, Odendall C, Shum B, et al. Peroxisomes Are Signaling Platforms for Antiviral Innate Immunity. Cell [Internet]. 2010;141(4):668–81. Available from: http://www.scopus.com/inward/record.url?eid=2-s2.0-77952503750&partnerID=40&md5=29e0a61585d0067cb1ba26ebc6defd2d

472. Horner SM, Liu HM, Park HS, Briley J, Gale Jr. M. Mitochondrial-associated endoplasmic reticulum membranes (MAM) form innate immune synapses and are targeted by hepatitis C virus. Proc Natl Acad Sci U S A [Internet]. 2011;108(35):14590–5. Available from: http://www.scopus.com/inward/record.url?eid=2-s2.0-80052281413&partnerID=40&md5=4cc65d683282ebf9a47b6c04f73f6977

473. West AP, Shadel GS, Ghosh S. Mitochondria in innate immune responses. Nat Rev Immunol [Internet]. Nature Publishing Group, a division of Macmillan Publishers Limited. All Rights Reserved.; 2011 Jun;11(6):389–402. Available from: http://dx.doi.org/10.1038/nri2975

474. Koshiba T. Mitochondrial-mediated antiviral immunity. Biochim Biophys Acta - Mol Cell Res [Internet]. 2013 Jan;1833(1):225–32. Available from: http://www.sciencedirect.com/science/article/pii/S0167488912000651

475. Vazquez C, Horner SM. MAVS Coordination of Antiviral Innate Immunity. J Virol [Internet]. 2015 Jul 15;89 (14):6974–7. Available from: http://jvi.asm.org/content/89/14/6974.abstract

476. Lad SP, Yang G, Scott DA, Chao T-H, Correia J da S, de la Torre JC, et al. Identification of MAVS splicing variants that interfere with RIGI/MAVS pathway signaling. Mol Immunol [Internet]. 2008 Apr;45(8):2277–87. Available from: http://www.sciencedirect.com/science/article/pii/S0161589007008577

477. Brubaker SW, Gauthier AE, Mills EW, Ingolia NT, Kagan JC. A Bicistronic MAVS Transcript Highlights a Class of Truncated Variants in Antiviral Immunity. Cell [Internet]. Elsevier; 2015 Jul 21;156(4):800–11. Available from: http://dx.doi.org/10.1016/j.cell.2014.01.021

478. Kim Y-M, Brinkmann MM, Paquet M-E, Ploegh HL. UNC93B1 delivers nucleotide-sensing toll-like receptors to endolysosomes. Nature [Internet]. 2008;452(7184):234–8. Available from: http://www.scopus.com/inward/record.url?eid=2-s2.0-40749098665&partnerID=40&md5=a6088478b3b319571f8e9c811fd517ed

479. Blasius AL, Beutler B. Intracellular Toll-like Receptors. Immunity [Internet]. 2010;32(3):305–15. Available from: http://www.scopus.com/inward/record.url?eid=2-s2.0-77949940198&partnerID=40&md5=295e9e9034d2ec7965d79c3cd74c0baf

480. Hipp MM, Shepherd D, Gileadi U, Aichinger MC, Kessler BM, Edelmann MJ, et al. Processing of human toll-like receptor 7 by furin-like proprotein convertases is required for its accumulation and activity in endosomes. Immunity. United States; 2013 Oct;39(4):711–21.

481. West AP, Koblansky AA, Ghosh S. Recognition and Signaling by Toll-Like Receptors. Annu Rev Cell Dev Biol [Internet]. Annual Reviews; 2006 Oct 9;22(1):409–37. Available from: http://dx.doi.org/10.1146/annurev.cellbio.21.122303.115827

482. Hemmi H, Takeuchi O, Kawai T, Kaisho T, Sato S, Sanjo H, et al. A Toll-like receptor recognizes bacterial DNA. Nature [Internet]. Macmillian Magazines Ltd.; 2000 Dec 7;408(6813):740–5. Available from: http://dx.doi.org/10.1038/35047123

483. Lund J, Sato A, Akira S, Medzhitov R, Iwasaki A. Toll-like Receptor 9–mediated Recognition of Herpes Simplex Virus-2 by Plasmacytoid Dendritic Cells. J Exp Med [Internet]. 2003 Aug 4;198 (3):513–20. Available from: http://jem.rupress.org/content/198/3/513.abstract

484. Krug A, Luker GD, Barchet W, Leib DA, Akira S, Colonna M. Herpes simplex virus type 1 activates murine natural interferon-producing cells through toll-like receptor 9. Blood [Internet]. 2003 Oct 16;103(4):1433–7. Available from: http://www.bloodjournal.org/content/103/4/1433.abstract

485. Alexopoulou L, Holt AC, Medzhitov R, Flavell RA. Recognition of double-stranded RNA and activation of NF-[kappa]B by Toll-like receptor 3. Nature [Internet]. 2001 Oct 18;413(6857):732–8. Available from: http://dx.doi.org/10.1038/35099560

486. Diebold SS, Kaisho T, Hemmi H, Akira S, Reis E Sousa C. Innate Antiviral Responses by Means of TLR7-Mediated Recognition of

Single-Stranded RNA. Science (80-) [Internet]. 2004;303(5663):1529–31. Available from: http://www.scopus.com/inward/record.url?eid=2-s2.0-1542317550&partnerID=40&md5=85428d4cbb00d1d317b69b768e906c8b

487. Heil F, Hemmi H, Hochrein H, Ampenberger F, Kirschning C, Akira S, et al. Species-Specific Recognition of Single-Stranded RNA via Toll-like Receptor 7 and 8. Sci [Internet]. 2004 Mar 5;303 (5663):1526–9. Available from: http://www.sciencemag.org/content/303/5663/1526.abstract

488. Zarember KA, Godowski PJ. Tissue Expression of Human Toll-Like Receptors and Differential Regulation of Toll-Like Receptor mRNAs in Leukocytes in Response to Microbes, Their Products, and Cytokines. J Immunol [Internet]. 2002 Jan 15;168 (2):554–61. Available from: http://www.jimmunol.org/content/168/2/554.abstract

489. Sun L, Wu J, Du F, Chen X, Chen ZJ. Cyclic GMP-AMP Synthase Is a Cytosolic DNA Sensor That Activates the Type I Interferon Pathway. Sci [Internet]. 2013 Feb 15;339 (6121):786–91. Available from: http://www.sciencemag.org/content/339/6121/786.abstract

490. Lupfer C, Malik A, Kanneganti T-D. Inflammasome control of viral infection. Current opinion in virology. 2015. p. 38–46.

491. Hornung V, Ablasser A, Charrel-Dennis M, Bauernfeind F, Horvath G, Caffrey DR, et al. AIM2 recognizes cytosolic dsDNA and forms a caspase-1-activating inflammasome with ASC. Nature [Internet]. Macmillan Publishers Limited. All rights reserved; 2009 Mar 26;458(7237):514–8. Available from: http://dx.doi.org/10.1038/nature07725

492. Kerur N, Veettil M V, Sharma-Walia N, Bottero V, Sadagopan S, Otageri P, et al. IFI16 acts as a nuclear pathogen sensor to induce the inflammasome in response to Kaposi Sarcoma-associated herpesvirus infection. Cell Host Microbe [Internet]. 2011;9(5):363–75. Available from: http://www.scopus.com/inward/record.url?eid=2-s2.0-79956061094&partnerID=40&md5=35c5c916152f51ca233670a9eee6c86f

493. Ishikawa H, Barber GN. STING is an endoplasmic reticulum adaptor that facilitates innate immune signalling. Nature [Internet]. Macmillan Publishers Limited. All rights reserved; 2008 Oct 2;455(7213):674–8. Available from: http://dx.doi.org/10.1038/nature07317

494. Zhong B, Yang Y, Li S, Wang Y-Y, Li Y, Diao F, et al. The Adaptor Protein MITA Links Virus-Sensing Receptors to IRF3 Transcription Factor Activation. Immunity [Internet]. 2008 Oct 17;29(4):538–50. Available from: http://www.sciencedirect.com/science/article/pii/S1074761308004068

495. Sun W, Li Y, Chen L, Chen H, You F, Zhou X, et al. ERIS, an endoplasmic reticulum IFN stimulator, activates innate immune signaling through dimerization. Proc Natl Acad Sci [Internet]. 2009 May 26;106 (21):8653–8. Available from: http://www.pnas.org/content/106/21/8653.abstract

496. Ishikawa H, Ma Z, Barber GN. STING regulates intracellular DNA-mediated, type I interferon-dependent innate immunity. Nature [Internet]. Macmillan Publishers Limited. All rights reserved; 2009 Oct 8;461(7265):788–92. Available from: http://dx.doi.org/10.1038/nature08476

497. Shang G, Zhu D, Li N, Zhang J, Zhu C, Lu D, et al. Crystal structures of STING protein reveal basis for recognition of cyclic di-GMP. Nat Struct Mol Biol [Internet]. Nature Publishing Group, a division of Macmillan Publishers Limited. All Rights Reserved.; 2012 Jul;19(7):725–7. Available from: http://dx.doi.org/10.1038/nsmb.2332

498. Burdette DL, Monroe KM, Sotelo-Troha K, Iwig JS, Eckert B, Hyodo M, et al. STING is a direct innate immune sensor of cyclic di-GMP. Nature [Internet]. Nature Publishing Group, a division of Macmillan Publishers Limited. All Rights Reserved.; 2011 Oct 27;478(7370):515–8. Available from: http://dx.doi.org/10.1038/nature10429

499. Civril F, Deimling T, de Oliveira Mann CC, Ablasser A, Moldt M, Witte G, et al. Structural mechanism of cytosolic DNA sensing by cGAS. Nature [Internet]. Nature Publishing Group, a division of Macmillan Publishers Limited. All Rights Reserved.; 2013 Jun 20;498(7454):332–7. Available from: http://dx.doi.org/10.1038/nature12305

500. Li X-D, Wu J, Gao D, Wang H, Sun L, Chen ZJ. Pivotal Roles of cGAS-cGAMP Signaling in Antiviral Defense and Immune Adjuvant Effects. Sci [Internet]. 2013 Sep 20;341 (6152):1390–4. Available from: http://www.sciencemag.org/content/341/6152/1390.abstract

501. Schoggins JW, MacDuff DA, Imanaka N, Gainey MD, Shrestha B, Eitson JL, et al. Pan-viral specificity of IFN-induced genes reveals new roles for cGAS in innate immunity. Nature. 2014;505(7485):691–5. doi: 10.1038/nature12862. Epub 2013 Nov 27.

502. Ablasser A, Schmid-Burgk JL, Hemmerling I, Horvath GL, Schmidt T, Latz E, et al. Cell intrinsic immunity spreads to bystander cells via the intercellular transfer of cGAMP. Nature. England; 2013 Nov;503(7477):530–4.

503. Bridgeman A, Maelfait J, Davenne T, Partridge T, Peng Y, Mayer A, et al. Viruses transfer the antiviral second messenger cGAMP between cells. Sci [Internet]. 2015 Sep 11;349 (6253):1228–32. Available from: http://www.sciencemag.org/content/349/6253/1228.abstract

504. Gentili M, Kowal J, Tkach M, Satoh T, Lahaye X, Conrad C, et al. Transmission of innate immune signaling by packaging of cGAMP in viral particles. Sci [Internet]. 2015 Sep 11;349 (6253):1232–6. Available from: http://www.sciencemag.org/content/349/6253/1232.abstract

505. Fitzgerald KA, McWhirter SM, Faia KL, Rowe DC, Latz E, Golenbock DT, et al. IKKE and TBKI are essential components of the IRF3 signalling pathway. Nat Immunol [Internet]. 2003;4(5):491–6. Available from: http://www.scopus.com/inward/record.url?eid=2-s2.0-0038393016&partnerID=40&md5=e591427fef5d4b5ef85bc358fea2f130

506. Sharma S, tenOever BR, Grandvaux N, Zhou G-P, Lin R, Hiscott J. Triggering the Interferon Antiviral Response Through an IKK-Related Pathway. Sci [Internet]. 2003 May 16;300 (5622):1148–51. Available from: http://www.sciencemag.org/content/300/5622/1148.abstract

507. Juang Y-T, Lowther W, Kellum M, Au W-C, Lin R, Hiscott J, et al. Primary activation of interferon A and interferon B gene transcription by interferon regulatory factor 3. Proc Natl Acad Sci [Internet]. 1998 Aug 18;95 (17):9837–42. Available from: http://www.pnas.org/content/95/17/9837.abstract

508. Marié I, Durbin JE, Levy DE. Differential viral induction of distinct interferon-α genes by positive feedback through interferon regulatory factor-7. EMBO J [Internet]. 1998 Nov 16;17(22):6660–9. Available from: http://emboj.embopress.org/content/17/22/6660.abstract

509. Yoneyama M, Suhara W, Fukuhara Y, Fukuda M, Nishida E, Fujita T. Direct triggering of the type I interferon system by virus infection: activation of a transcription factor complex containing IRF-3 and CBP/p300. EMBO J [Internet]. 1998 Feb 16;17(4):1087–95. Available from: http://www.ncbi.nlm.nih.gov/pmc/articles/PMC1170457/

510. McNab F, Mayer-Barber K, Sher A, Wack A, O'Garra A. Type I interferons in infectious disease. Nat Rev Immunol [Internet]. Nature Publishing Group, a division of Macmillan Publishers Limited. All Rights Reserved.; 2015 Feb;15(2):87–103. Available from: http://dx.doi.org/10.1038/nri3787

511. Sato M, Hata N, Asagiri M, Nakaya T, Taniguchi T, Tanaka N. Positive feedback regulation of type I IFN genes by the IFN-inducible transcription factor IRF-7. FEBS Lett [Internet]. 1998 Dec 11;441(1):106–10. Available from:

http://www.sciencedirect.com/science/article/pii/S0014579398015142

512. Barnes BJ, Kellum MJ, Field AE, Pitha PM. Multiple regulatory domains of IRF-5 control activation, cellular localization, and induction of chemokines that mediate recruitment of T lymphocytes. Mol Cell Biol. United States; 2002 Aug;22(16):5721–40.

513. Tailor P, Tamura T, Kong HJ, Kubota T, Kubota M, Borghi P, et al. The Feedback Phase of Type I Interferon Induction in Dendritic Cells Requires Interferon Regulatory Factor 8. Immunity [Internet]. 2007 Aug 24;27(2):228–39. Available from: http://www.sciencedirect.com/science/article/pii/S1074761307003688

514. Reis LF, Ruffner H, Stark G, Aguet M, Weissmann C. Mice devoid of interferon regulatory factor 1 (IRF-1) show normal expression of type I interferon genes. EMBO J [Internet]. 1994 Oct 17;13(20):4798–806. Available from: http://www.ncbi.nlm.nih.gov/pmc/articles/PMC395418/

515. Nyman TA, Tolo H, Parkkinen J, Kalkkinen N. Identification of nine interferon-alpha subtypes produced by Sendai virus-induced human peripheral blood leucocytes. Biochem J. ENGLAND; 1998 Jan;329 (Pt 2:295–302.

516. Szubin R, Chang WLW, Greasby T, Beckett L, Baumgarth N. Rigid Interferon-α Subtype Responses of Human Plasmacytoid Dendritic Cells. J Interf Cytokine Res [Internet]. Mary Ann Liebert, Inc., publishers; 2008 Oct 20;28(12):749–63. Available from: http://dx.doi.org/10.1089/jir.2008.0037

517. Puig M, Tosh KW, Schramm LM, Grajkowska LT, Kirschman KD, Tami C, et al. TLR9 and TLR7 agonists mediate distinct type I IFN responses in humans and nonhuman primates in vitro and in vivo. J Leukoc Biol [Internet]. 2012 Jan 1;91 (1):147–58. Available from: http://www.jleukbio.org/content/91/1/147.abstract

518. Moll HP, Maier T, Zommer A, Lavoie T, Brostjan C. The differential activity of interferon-α subtypes is consistent among distinct target genes and cell types. Cytokine [Internet]. Academic Press; 2011 Jan 30;53(1):52–9. Available from: http://www.ncbi.nlm.nih.gov/pmc/articles/PMC3020287/

519. Yamamoto S, Yano H, Sanou O, Ikegami H, Kurimoto M, Kojiro M. Different antiviral activities of IFN-α subtypes in human liver cell lines: synergism between IFN-α2 and IFN-α8. Hepatol Res [Internet]. 2002 Oct;24(2):99–106. Available from: http://www.sciencedirect.com/science/article/pii/S1386634602000207

520. Yamaoka T, Kojima S, Ichi S, Kashiwazaki Y, Koide T, Sokawa Y. Biologic and binding activities of IFN-alpha subtypes in ACHN human renal cell carcinoma cells and Daudi Burkitt's lymphoma cells. J Interferon Cytokine Res. UNITED STATES; 1999 Dec;19(12):1343–9.

521. Onoguchi K, Yoneyama M, Takemura A, Akira S, Taniguchi T, Namiki H, et al. Viral Infections Activate Types I and III Interferon Genes through a Common Mechanism. J Biol Chem [Internet]. 2007 Mar 9;282 (10):7576–81. Available from: http://www.jbc.org/content/282/10/7576.abstract

522. Österlund PI, Pietilä TE, Veckman V, Kotenko S V, Julkunen I. IFN Regulatory Factor Family Members Differentially Regulate the Expression of Type III IFN (IFN-λ) Genes. J Immunol [Internet]. 2007 Sep 15;179 (6):3434–42. Available from: http://www.jimmunol.org/content/179/6/3434.abstract

523. Thomson SJP, Goh FG, Banks H, Krausgruber T, Kotenko S V, Foxwell BMJ, et al. The role of transposable elements in the regulation of IFN-λ1 gene expression. Proc Natl Acad Sci [Internet]. 2009 Jul 14;106 (28):11564–9. Available from: http://www.pnas.org/content/106/28/11564.abstract

524. Iversen MB, Ank N, Melchjorsen J, Paludan SR. Expression of Type III Interferon (IFN) in the Vaginal Mucosa Is Mediated Primarily by Dendritic Cells and Displays Stronger Dependence on NF-κB than Type I IFNs . J Virol [Internet]. American Society for Microbiology (ASM); 2010 May 24;84(9):4579–86. Available from: http://www.ncbi.nlm.nih.gov/pmc/articles/PMC2863761/

525. Faísca P, Desmecht D. Sendai virus, the mouse parainfluenza type 1: A longstanding pathogen that remains up-to-date. Res Vet Sci [Internet]. 2007 Feb;82(1):115–25. Available from: http://www.sciencedirect.com/science/article/pii/S0034528806000701

526. Loo Y-M, Fornek J, Crochet N, Bajwa G, Perwitasari O, Martinez-Sobrido L, et al. Distinct RIG-I and MDA5 signaling by RNA viruses in innate immunity. J Virol [Internet]. 2008;82(1):335–45. Available from: http://www.scopus.com/inward/record.url?eid=2-s2.0-37349052379&partnerID=40&md5=fcaab0d12d4206a4cd06f9ed4bbf49a0

527. Strahle L, Garcin D, Kolakofsky D. Sendai virus defective-interfering genomes and the activation of interferon-beta. Virology [Internet]. 2006 Jul 20;351(1):101–11. Available from: http://www.sciencedirect.com/science/article/pii/S0042682206001826

528. Lazzarini RA, Keene JD, Schubert M. The origins of defective interfering particles of the negative-strand RNA viruses. Cell [Internet]. 1981 Oct;26(2, Part 2):145–54. Available from: http://www.sciencedirect.com/science/article/pii/0092867481902981

529. Baum A, Sachidanandam R, García-Sastre A. Preference of RIG-I for short viral RNA molecules in infected cells revealed by next-generation sequencing. Proc Natl Acad Sci [Internet]. 2010 Sep 14;107 (37):16303–8. Available from: http://www.pnas.org/content/107/37/16303.abstract

530. Simmons CP, Farrar JJ, van Vinh Chau N, Wills B. Dengue. N Engl J Med [Internet]. Massachusetts Medical Society; 2012 Apr 11;366(15):1423–32. Available from: http://dx.doi.org/10.1056/NEJMra1110265

531. Balsitis SJ, Coloma J, Castro G, Alava A, Flores D, McKerrow JH, et al. Tropism of dengue virus in mice and humans defined by viral nonstructural protein 3-specific immunostaining. Am J Trop Med Hyg. United States; 2009 Mar;80(3):416–24.

532. Rodenhuis-Zybert IA, Wilschut J, Smit JM. Dengue virus life cycle: viral and host factors modulating infectivity. Cell Mol Life Sci. Switzerland; 2010 Aug;67(16):2773–86.

533. Nasirudeen AMA, Wong HH, Thien P, Xu S, Lam K-P, Liu DX. RIG-I, MDA5 and TLR3 Synergistically Play an Important Role in Restriction of Dengue Virus Infection. PLoS Negl Trop Dis [Internet]. Public Library of Science; 2011 Jan 4;5(1):e926. Available from: http://dx.doi.org/10.1371%2Fjournal.pntd.0000926

534. Décembre E, Assil S, Hillaire MLB, Dejnirattisai W, Mongkolsapaya J, Screaton GR, et al. Sensing of Immature Particles Produced by Dengue Virus Infected Cells Induces an Antiviral Response by Plasmacytoid Dendritic Cells. PLoS Pathog [Internet]. Public Library of Science; 2014 Oct 23;10(10):e1004434. Available from: http://dx.doi.org/10.1371%2Fjournal.ppat.1004434

535. Tsai Y-T, Chang S-Y, Lee C-N, Kao C-L. Human TLR3 recognizes dengue virus and modulates viral replication in vitro. Cell Microbiol [Internet]. Blackwell Publishing Ltd; 2009 Apr 1;11(4):604–15. Available from: http://dx.doi.org/10.1111/j.1462-5822.2008.01277.x

536. Bouvier NM, Palese P. THE BIOLOGY OF INFLUENZA VIRUSES. Vaccine [Internet]. 2008 Sep 12;26(Suppl 4):D49–53. Available from: http://www.ncbi.nlm.nih.gov/pmc/articles/PMC3074182/

537. Pichlmair A, Schulz O, Tan CP, Näslund TI, Liljeström P, Weber F, et al. RIG-I-Mediated Antiviral Responses to Single-Stranded RNA Bearing 5'-Phosphates. Sci [Internet]. 2006 Nov 10;314 (5801):997–1001. Available from: http://www.sciencemag.org/content/314/5801/997.abstract

538. Rehwinkel J, Tan CP, Goubau D, Schulz O, Pichlmair A, Bier K, et al. RIG-I Detects Viral Genomic RNA during Negative-Strand RNA Virus Infection. Cell [Internet]. 2010 Feb 5;140(3):397–408. Available from: http://www.sciencedirect.com/science/article/pii/S0092867410000218

539. Iwasaki A, Pillai PS. Innate immunity to influenza virus infection. Nat Rev Immunol [Internet]. Nature Publishing Group, a division of Macmillan Publishers Limited. All Rights Reserved.; 2014 May;14(5):315–28. Available from: http://dx.doi.org/10.1038/nri3665

540. Hale BG, Randall RE, Ortin J, Jackson D. The multifunctional NS1 protein of influenza A viruses. J Gen Virol. 2008;89(Pt 10):2359–76. doi: 10.1099/vir.0.2008/004606–0.

541. Hemmi H, Kaisho T, Takeuchi O, Sato S, Sanjo H, Hoshino K, et al. Small anti-viral compounds activate immune cells via the TLR7 MyD88-dependent signaling pathway. Nat Immunol. United States; 2002 Feb;3(2):196–200.

542. Vollmer J, Weeratna R, Payette P, Jurk M, Schetter C, Laucht M, et al. Characterization of three CpG oligodeoxynucleotide classes with distinct immunostimulatory activities. Eur J Immunol. Germany; 2004 Jan;34(1):251–62.

543. Dorn A, Kippenberger S. Clinical application of CpG-, non-CpG-, and antisense oligodeoxynucleotides as immunomodulators. Curr Opin Mol Ther. England; 2008 Feb;10(1):10–20.

544. Cai X, Chiu Y-H, Chen ZJ. The cGAS-cGAMP-STING Pathway of Cytosolic DNA Sensing and Signaling. Mol Cell [Internet]. 2014 Apr 24;54(2):289–96. Available from: http://www.sciencedirect.com/science/article/pii/S1097276514002731

545. Kato T, Date T, Murayama A, Morikawa K, Akazawa D, Wakita T. Cell culture and infection system for hepatitis C virus. Nat Protoc [Internet]. Nature Publishing Group; 2006 Dec;1(5):2334–9. Available from: http://dx.doi.org/10.1038/nprot.2006.395

546. Michallet M-C, Meylan E, Ermolaeva MA, Vazquez J, Rebsamen M, Curran J, et al. TRADD protein is an essential component of the RIG-like helicase antiviral pathway. Immunity. United States; 2008 May;28(5):651–61.

547. Wang W, Riedel K, Lynch P, Chien CY, Montelione GT, Krug RM. RNA binding by the novel helical domain of the influenza virus NS1 protein requires its dimer structure and a small number of specific basic amino acids. RNA [Internet]. 1999 Feb 1;5 (2):195–205. Available from: http://rnajournal.cshlp.org/content/5/2/195.abstract

548. Orzalli MH, Broekema NM, Diner BA, Hancks DC, Elde NC, Cristea IM, et al. cGAS-mediated stabilization of IFI16 promotes innate signaling during herpes simplex virus infection. Proc Natl Acad Sci [Internet]. 2015 Apr 7;112 (14):E1773–81. Available from: http://www.pnas.org/content/112/14/E1773.abstract

549. Blight KJ, McKeating JA, Rice CM. Highly Permissive Cell Lines for Subgenomic and Genomic Hepatitis C Virus RNA Replication. J Virol [Internet]. 2002 Dec 15;76 (24):13001–14. Available from: http://jvi.asm.org/content/76/24/13001.abstract

550. Sumpter R, Loo Y-M, Foy E, Li K, Yoneyama M, Fujita T, et al. Regulating Intracellular Antiviral Defense and Permissiveness to Hepatitis C Virus RNA Replication through a Cellular RNA Helicase, RIG-I. J Virol [Internet]. 2005 Mar 1;79 (5):2689–99. Available from: http://jvi.asm.org/content/79/5/2689.abstract

551. Li K, Chen Z, Kato N, Gale M, Lemon SM. Distinct Poly(I-C) and Virus-activated Signaling Pathways Leading to Interferon-β Production in Hepatocytes. J Biol Chem [Internet]. 2005 Apr 29;280 (17):16739–47. Available from: http://www.jbc.org/content/280/17/16739.abstract

552. Wu H, Chen Y, Winnall WR, Phillips DJ, Hedger MP. Acute regulation of activin A and its binding protein, follistatin, in serum and tissues following lipopolysaccharide treatment of adult male mice. Am J Physiol - Regul Integr Comp Physiol [Internet]. 2012 Sep 15;303(6):R665–75. Available from: http://ajpregu.physiology.org/content/303/6/R665.abstract

553. Gack MU, Shin YC, Joo C-H, Urano T, Liang C, Sun L, et al. TRIM25 RING-finger E3 ubiquitin ligase is essential for RIG-I-mediated antiviral activity. Nature [Internet]. 2007 Apr 19;446(7138):916–20. Available from: http://dx.doi.org/10.1038/nature05732

554. Mibayashi M, Martinez-Sobrido L, Loo Y-M, Cardenas WB, Gale MJ, Garcia-Sastre A. Inhibition of retinoic acid-inducible gene I-mediated induction of beta interferon by the NS1 protein of influenza A virus. J Virol. United States; 2007 Jan;81(2):514–24.

555. Cheng S-C, Joosten LAB, Kullberg B-J, Netea MG. Interplay between Candida albicans and the Mammalian Innate Host Defense. Infect Immun [Internet]. 2012 Apr 1;80 (4):1304–13. Available from: http://iai.asm.org/content/80/4/1304.abstract

556. Michel U, Gerber J, O'Connor AE, Bunkowski S, Brück W, Nau R, et al. Increased activin levels in cerebrospinal fluid of rabbits with bacterial meningitis are associated with activation of microglia. J Neurochem [Internet]. 2003;86(1):238–45. Available from: http://www.scopus.com/inward/record.url?eid=2-s2.0-0038647411&partnerID=40&md5=7b959b274a4a512fc185a57946ce63e7

557. Michel U, Shintani Y, Nau R. Serum follistatin concentrations are increased in patients with septicaemia. Clin Endocrinol (Oxf) [Internet]. Blackwell Science Ltd, UK; 1998 Apr 1;48(4):413–7. Available from: http://dx.doi.org/10.1046/j.1365-2265.1998.00484.x

558. Ebert S, Phillips DJ, Jenzewski P, Nau R, O'Connor AE, Michel U. Activin A concentrations in human cerebrospinal fluid are age-dependent and elevated in meningitis. J Neurol Sci [Internet]. Elsevier; 2015 Jul 25;250(1):50–7. Available from: http://dx.doi.org/10.1016/j.jns.2006.06.026

559. Erämaa M, Hildén K, Tuuri T, Ritvos O. Regulation of inhibin/activin subunit messenger ribonucleic acids (mRNAs) by activin A and expression of activin receptor mRNAs in cultured human granulosa-luteal cells. Endocrinology [Internet]. The Endocrine Society; 1995 Oct 1;136(10):4382–9. Available from: http://dx.doi.org/10.1210/endo.136.10.7664658

560. Loots GG, Ovcharenko I. Dcode.org anthology of comparative genomic tools. Nucleic Acids Res [Internet]. Oxford University Press; 2005 Jul 1;33(Web Server issue):W56–64. Available from: http://www.ncbi.nlm.nih.gov/pmc/articles/PMC1160116/

561. Newton K, Dixit VM. Signaling in Innate Immunity and Inflammation. Cold Spring Harb Perspect Biol [Internet]. 2012 Mar 1;4 (3). Available from: http://cshperspectives.cshlp.org/content/4/3/a006049.abstract

562. Westwick JK, Weitzel C, Minden A, Karin M, Brenner DA. Tumor necrosis factor alpha stimulates AP-1 activity through prolonged activation of the c-Jun kinase. J Biol Chem [Internet]. 1994 Oct 21;269 (42):26396–401. Available from: http://www.jbc.org/content/269/42/26396.abstract

563. Jones KL, de Kretser DM, Clarke IJ, Scheerlinck JP, Phillips DJ. Characterisation of the rapid release of activin A following acute lipopolysaccharide challenge in the ewe. J Endocrinol [Internet]. 2004 Jul 1;182 (1):69–80. Available from: http://joe.endocrinology-journals.org/content/182/1/69.abstract

564. Shi J, Yoshino O, Osuga Y, Koga K, Hirota Y, Hirata T, et al. Bone morphogenetic protein-6 stimulates gene expression of follicle-stimulating hormone receptor, inhibin/activin β subunits, and anti-Müllerian hormone in human granulosa cells. Fertil Steril [Internet]. 2009 Nov;92(5):1794–8. Available from: http://www.sciencedirect.com/science/article/pii/S0015028209010759

565. Refaat B, Ashshi A, El-Shemi A, AlZanbagi A. Effects of chronic hepatitis C genotype 1 and 4 on serum activins and follistatin in treatment naïve patients and their correlations with interleukin-6, tumour necrosis factor-α, viral load and liver damage. Clin Exp Med [Internet]. Springer Milan; 2014;1–10. Available from: http://dx.doi.org/10.1007/s10238-014-0297-2

566. Bolen CR, Ding S, Robek MD, Kleinstein SH. Dynamic expression profiling of type I and type III interferon-stimulated hepatocytes reveals a stable hierarchy of gene expression. Hepatology [Internet]. 2014 Apr 18;59(4):1262–72. Available from: http://www.ncbi.nlm.nih.gov/pmc/articles/PMC3938553/

567. Hertzog P, Forster S, Samarajiwa S. Systems biology of interferon responses. J Interferon Cytokine Res. United States; 2011 Jan;31(1):5–11.

568. Ivashkiv LB, Donlin LT. Regulation of type I interferon responses. Nat Rev Immunol [Internet]. Nature Publishing Group, a division of Macmillan Publishers Limited. All Rights Reserved.; 2014 Jan;14(1):36–49. Available from: http://dx.doi.org/10.1038/nri3581

569. LINDENMANN J. Resistance of mice to mouse-adapted influenza A virus. Virology. Not Available; 1962 Feb;16:203–4.

570. Haller O, Kochs G. Human MxA protein: an interferon-induced dynamin-like GTPase with broad antiviral activity. J Interferon Cytokine Res. United States; 2011 Jan;31(1):79–87.

571. Sadler AJ, Williams BRG. Interferon-inducible antiviral effectors. Nat Rev Immunol [Internet]. Nature Publishing Group; 2008 Jul;8(7):559–68. Available from: http://dx.doi.org/10.1038/nri2314

572. MacMicking JD. IFN-inducible GTPases and immunity to intracellular pathogens. Trends Immunol [Internet]. 2004 Nov;25(11):601–9. Available from: http://www.sciencedirect.com/science/article/pii/S1471490604002467

573. Samuel CE. ADARs, Viruses and Innate Immunity. Curr Top Microbiol Immunol [Internet]. 2012;353:10.1007/82_2011_148. Available from: http://www.ncbi.nlm.nih.gov/pmc/articles/PMC3867276/

574. Suspène R, Sommer P, Henry M, Ferris S, Guétard D, Pochet S, et al. APOBEC3G is a single-stranded DNA cytidine deaminase and functions independently of HIV reverse transcriptase. Nucleic Acids Res [Internet]. Oxford, UK: Oxford University Press; 2004 Apr 30;32(8):2421–9. Available from: http://www.ncbi.nlm.nih.gov/pmc/articles/PMC419444/

575. Diamond MS, Farzan M. The broad-spectrum antiviral functions of IFIT and IFITM proteins. Nat Rev Immunol [Internet]. Nature Publishing Group, a division of Macmillan Publishers Limited. All Rights Reserved.; 2013 Jan;13(1):46–57. Available from: http://dx.doi.org/10.1038/nri3344

576. Szretter KJ, Daniels BP, Cho H, Gainey MD, Yokoyama WM, Gale M, et al. 2′-O Methylation of the Viral mRNA Cap by West Nile Virus Evades Ifit1-Dependent and -Independent Mechanisms of Host Restriction In Vivo. Gack MU, editor. PLoS Pathog [Internet]. San Francisco, USA: Public Library of Science; 2012 May 10;8(5):e1002698. Available from: http://www.ncbi.nlm.nih.gov/pmc/articles/PMC3349756/

577. Pichlmair A, Lassnig C, Eberle C-A, Gorna MW, Baumann CL, Burkard TR, et al. IFIT1 is an antiviral protein that recognizes 5[prime]-triphosphate RNA. Nat Immunol [Internet]. Nature Publishing Group, a division of Macmillan Publishers Limited. All Rights Reserved.; 2011 Jul;12(7):624–30. Available from: http://dx.doi.org/10.1038/ni.2048

578. Meyer K, Kwon Y-C, Liu S, Hagedorn CH, Ray RB, Ray R. Interferon-α inducible protein 6 impairs EGFR activation by CD81 and inhibits hepatitis C virus infection. Sci Rep [Internet]. Macmillan Publishers Limited. All rights reserved; 2015 Mar 11;5. Available from: http://dx.doi.org/10.1038/srep09012

579. Wilkins C, Woodward J, Lau DT-Y, Barnes A, Joyce M, McFarlane N, et al. IFITM1 is a tight junction protein that inhibits hepatitis C virus entry. Hepatology [Internet]. 2013 Feb 12;57(2):461–9. Available from: http://www.ncbi.nlm.nih.gov/pmc/articles/PMC3566288/

580. Liu S-Y, Aliyari R, Chikere K, Li G, Marsden MD, Smith JK, et al. Interferon-Inducible Cholesterol-25-Hydroxylase Broadly Inhibits Viral Entry by Production of 25-Hydroxycholesterol. Immunity [Internet]. 2013 Jan 24;38(1):92–105. Available from: http://www.sciencedirect.com/science/article/pii/S1074761312005109

581. Everitt AR, Clare S, Pertel T, John SP, Wash RS, Smith SE, et al. IFITM3 restricts the morbidity and mortality associated with influenza. Nature [Internet]. Nature Publishing Group, a division of Macmillan Publishers Limited. All Rights Reserved.; 2012 Apr 26;484(7395):519–23. Available from: http://dx.doi.org/10.1038/nature10921

582. Feeley EM, Sims JS, John SP, Chin CR, Pertel T, Chen L-M, et al. IFITM3 Inhibits Influenza A Virus Infection by Preventing Cytosolic Entry. PLoS Pathog [Internet]. Public Library of Science; 2011 Oct 27;7(10):e1002337. Available from: http://dx.doi.org/10.1371%2Fjournal.ppat.1002337

583. Amini-Bavil-Olyaee S, Choi YJ, Lee JH, Shi M, Huang I-C, Farzan M, et al. The Antiviral Effector IFITM3 Disrupts Intracellular Cholesterol Homeostasis to Block Viral Entry. Cell Host Microbe [Internet]. 2013 Apr 17;13(4):452–64. Available from: http://www.sciencedirect.com/science/article/pii/S1931312813001169

584. Helbig KJ, Beard MR. The role of viperin in the innate antiviral response. J Mol Biol. 2013/10/26 ed. 2014;426(6):1210–9.

585. Seo J-Y, Yaneva R, Cresswell P. Viperin: a multifunctional, interferon-inducible protein that regulates virus replication. Cell Host Microbe [Internet]. 2011 Dec 15;10(6):534–9. Available from: http://www.ncbi.nlm.nih.gov/pmc/articles/PMC3246677/

586. Xiao S, Li D, Zhu H-Q, Song M-G, Pan X-R, Jia P-M, et al. RIG-G as a key mediator of the antiproliferative activity of interferon-related pathways through enhancing p21 and p27 proteins. Proc Natl Acad Sci U S A [Internet]. National Academy of Sciences; 2006 Oct 31;103(44):16448–53. Available from: http://www.ncbi.nlm.nih.gov/pmc/articles/PMC1637602/

587. Kang D-C, Gopalkrishnan R V, Wu Q, Jankowsky E, Pyle AM, Fisher PB. mda-5: An interferon-inducible putative RNA helicase with double-stranded RNA-dependent ATPase activity and melanoma growth-suppressive properties. Proc Natl Acad Sci U S A [Internet]. 2002;99(2):637–42. Available from: http://www.scopus.com/inward/record.url?eid=2-s2.0-0037154176&partnerID=40&md5=7cdd3107aa7cf896cca58944e3489808

588. Ma F, Li B, Liu S, Iyer SS, Yu Y, Wu A, et al. Positive Feedback Regulation of Type I IFN Production by the IFN-Inducible DNA Sensor cGAS. J Immunol [Internet]. 2015 Jan 21; Available from: http://www.jimmunol.org/content/early/2015/01/20/jimmunol.1402066.abstract

589. Taniguchi T, Ogasawara K, Takaoka A, Tanaka N. IRF family of transcription factors as regulators of host defense. Annu Rev Immunol. 2001/03/13 ed. 2001;19:623–55.

590. Honda K, Takaoka A, Taniguchi T. Type I Inteferon Gene Induction by the Interferon Regulatory Factor Family of Transcription Factors. Immunity [Internet]. 2006 Sep;25(3):349–60. Available from: http://www.sciencedirect.com/science/article/pii/S1074761306003943

591. van Boxel-Dezaire AHH, Rani MRS, Stark GR. Complex Modulation of Cell Type-Specific Signaling in Response to Type I Interferons. Immunity [Internet]. 2006 Sep;25(3):361–72. Available from: http://www.sciencedirect.com/science/article/pii/S1074761306003992

592. Saitoh T, Satoh T, Yamamoto N, Uematsu S, Takeuchi O, Kawai T, et al. Antiviral protein viperin promotes toll-like receptor 7- and toll-like receptor 9-mediated type i interferon production in plasmacytoid dendritic cells. Immunity [Internet]. 2011;34(3):352–63. Available from: http://www.scopus.com/inward/record.url?eid=2-s2.0-

79952762131&partnerID=40&md5=60c74833f53b6ccd49616c572626e6a4

593. Zhou Z, Jia X, Xue Q, Dou Z, Ma Y, Zhao Z, et al. TRIM14 is a mitochondrial adaptor that facilitates retinoic acid-inducible gene-I–like receptor-mediated innate immune response. Proc Natl Acad Sci [Internet]. 2014 Jan 14;111 (2):E245–54. Available from: http://www.pnas.org/content/111/2/E245.abstract

594. Cheriyath V, Glaser KB, Waring JF, Baz R, Hussein MA, Borden EC. G1P3, an IFN-induced survival factor, antagonizes TRAIL-induced apoptosis in human myeloma cells. J Clin Invest [Internet]. The American Society for Clinical Investigation; 2007 Oct 1;117(10):3107–17. Available from: http://www.jci.org/articles/view/31122

595. Kim M-J, Hwang S-Y, Imaizumi T, Yoo J-Y. Negative Feedback Regulation of RIG-I-Mediated Antiviral Signaling by Interferon-Induced ISG15 Conjugation. J Virol [Internet]. 2008 Feb 1;82 (3):1474–83. Available from: http://jvi.asm.org/content/82/3/1474.abstract

596. Okumura A, Lu G, Pitha-Rowe I, Pitha PM. Innate antiviral response targets HIV-1 release by the induction of ubiquitin-like protein ISG15. Proc Natl Acad Sci U S A [Internet]. National Academy of Sciences; 2006 Jan 31;103(5):1440–5. Available from: http://www.ncbi.nlm.nih.gov/pmc/articles/PMC1360585/

597. Okumura A, Pitha PM, Harty RN. ISG15 inhibits Ebola VP40 VLP budding in an L-domain-dependent manner by blocking Nedd4 ligase activity. Proc Natl Acad Sci U S A [Internet]. National Academy of Sciences; 2008 Mar 11;105(10):3974–9. Available from: http://www.ncbi.nlm.nih.gov/pmc/articles/PMC2268823/

598. Lenschow DJ. Antiviral Properties of ISG15. Viruses [Internet]. Molecular Diversity Preservation International (MDPI); 2010 Oct 28;2(10):2154–68. Available from: http://www.ncbi.nlm.nih.gov/pmc/articles/PMC3185569/

599. Zhang X, Bogunovic D, Payelle-Brogard B, Francois-Newton V, Speer SD, Yuan C, et al. Human intracellular ISG15 prevents interferon-[agr]/[bgr] over-amplification and auto-inflammation. Nature [Internet]. Nature Publishing Group, a division of Macmillan Publishers Limited. All Rights Reserved.; 2015;517(7532):89–93. Available from: http://dx.doi.org/10.1038/nature13801

600. González-Navajas JM, Lee J, David M, Raz E. Immunomodulatory functions of type I interferons. Nat Rev Immunol [Internet]. Nature Publishing Group, a division of Macmillan Publishers Limited. All Rights Reserved.; 2012 Feb;12(2):125–35. Available from: http://dx.doi.org/10.1038/nri3133

601. Korchynskyi O, ten Dijke P. Identification and Functional Characterization of Distinct Critically Important Bone Morphogenetic Protein-specific Response Elements in the Id1 Promoter. J Biol Chem [Internet]. 2002 Feb 15;277 (7):4883–91. Available from: http://www.jbc.org/content/277/7/4883.abstract

602. López-Rovira T, Chalaux E, Massagué J, Rosa JL, Ventura F. Direct Binding of Smad1 and Smad4 to Two Distinct Motifs Mediates Bone Morphogenetic Protein-specific Transcriptional Activation ofId1 Gene . J Biol Chem [Internet]. 2002 Feb 1;277 (5):3176–85. Available from: http://www.jbc.org/content/277/5/3176.abstract

603. Yan H, Zhang B, Li S, Zhao Q. A formal model for analyzing drug combination effects and its application in TNF-alpha-induced NFkappaB pathway. BMC Syst Biol. England; 2010;4:50.

604. Kent WJ, Hsu F, Karolchik D, Kuhn RM, Clawson H, Trumbower H, et al. Exploring relationships and mining data with the UCSC Gene Sorter. Genome Res [Internet]. 2005 May 1;15 (5):737–41. Available from: http://genome.cshlp.org/content/15/5/737.abstract

605. Langenfeld E, Hong CC, Lanke G, Langenfeld J. Bone Morphogenetic Protein Type I Receptor Antagonists Decrease Growth and Induce Cell Death of Lung Cancer Cell Lines. PLoS One [Internet]. Public Library of Science; 2013 Apr 12;8(4):e61256. Available from: http://dx.doi.org/10.1371%2Fjournal.pone.0061256

606. Hao J, Ho JN, Lewis JA, Karim KA, Daniels RN, Gentry PR, et al. In Vivo Structure−Activity Relationship Study of Dorsomorphin Analogues Identifies Selective VEGF and BMP Inhibitors. ACS Chem Biol [Internet]. American Chemical Society; 2010 Feb 19;5(2):245–53. Available from: http://dx.doi.org/10.1021/cb9002865

607. Murakami M, Kawachi H, Ogawa K, Nishino Y, Funaba M. Receptor expression modulates the specificity of transforming growth factor-β signaling pathways. Genes to Cells [Internet]. Blackwell Publishing Inc; 2009 Apr 1;14(4):469–82. Available from: http://dx.doi.org/10.1111/j.1365-2443.2009.01283.x

608. Conlon J, Burdette DL, Sharma S, Bhat N, Thompson M, Jiang Z, et al. Mouse, but not human STING, binds and signals in response to the vascular disrupting agent DMXAA. J Immunol [Internet]. 2013 May 15;190(10):5216–25. Available from: http://www.ncbi.nlm.nih.gov/pmc/articles/PMC3647383/

609. Qin BY, Liu C, Lam SS, Srinath H, Delston R, Correia JJ, et al. Crystal structure of IRF-3 reveals mechanism of autoinhibition and virus-induced phosphoactivation. Nat Struct Biol. 2003/10/14 ed. 2003;10(11):913–21.

610. Takahasi K, Suzuki NN, Horiuchi M, Mori M, Suhara W, Okabe Y, et al. X-ray crystal structure of IRF-3 and its functional implications. Nat Struct Biol. 2003/10/14 ed. 2003;10(11):922–7.

611. Nehyba J, Hrdlickova R, Bose HR. Dynamic evolution of immune system regulators: the history of the interferon regulatory factor family. Mol Biol Evol. 2009;26(11):2539–50. doi: 10.1093/molbev/msp167. Epub 2009 Jul.

612. Miyazono K, Maeda S, Imamura T. BMP receptor signaling: transcriptional targets, regulation of signals, and signaling cross-talk. Cytokine Growth Factor Rev. England; 2005 Jun;16(3):251–63.

613. Heldin C-H. TGF-β Signaling from Receptors to Smads. In: Miyazono K, Derynck R, editors. The TGF-β Family. 50th ed. Cold Spring Harbour Laboratory Press; 2008.

614. Shi Y, Wang YF, Jayaraman L, Yang H, Massague J, Pavletich NP. Crystal structure of a Smad MH1 domain bound to DNA: insights on DNA binding in TGF-beta signaling. Cell. UNITED STATES; 1998 Sep;94(5):585–94.

615. Wu G, Chen Y-G, Ozdamar B, Gyuricza CA, Chong PA, Wrana JL, et al. Structural Basis of Smad2 Recognition by the Smad Anchor for Receptor Activation. Sci [Internet]. 2000 Jan 7;287 (5450):92–7. Available from: http://www.sciencemag.org/content/287/5450/92.abstract

616. Xiao Z, Liu X, Henis YI, Lodish HF. A distinct nuclear localization signal in the N terminus of Smad 3 determines its ligand-induced nuclear translocation. Proc Natl Acad Sci U S A [Internet]. The National Academy of Sciences; 2000 Jul 5;97(14):7853–8. Available from: http://www.ncbi.nlm.nih.gov/pmc/articles/PMC16634/

617. Xiao Z, Brownawell AM, Macara IG, Lodish HF. A Novel Nuclear Export Signal in Smad1 Is Essential for Its Signaling Activity. J Biol Chem [Internet]. 2003 Sep 5;278 (36):34245–52. Available from: http://www.jbc.org/content/278/36/34245.abstract

618. Lin X, Duan X, Liang Y-Y, Su Y, Wrighton KH, Long J, et al. PPM1A Functions as a Smad Phosphatase to Terminate TGFβ Signaling. Cell [Internet]. 2006 Jun 2;125(5):915–28. Available from: http://www.sciencedirect.com/science/article/pii/S0092867406005174

619. Miyamoto M, Fujita T, Kimura Y, Maruyama M, Harada H, Sudo Y, et al. Regulated expression of a gene encoding a nuclear factor,

IRF-1, that specifically binds to IFN-beta gene regulatory elements. Cell. 1988/09/09 ed. 1988;54(6):903–13.

620. Fujita T, Sakakibara J, Sudo Y, Miyamoto M, Kimura Y, Taniguchi T. Evidence for a nuclear factor(s), IRF-1, mediating induction and silencing properties to human IFN-beta gene regulatory elements. EMBO J [Internet]. 1988 Nov;7(11):3397–405. Available from: http://www.ncbi.nlm.nih.gov/pmc/articles/PMC454838/

621. Tamura T, Yanai H, Savitsky D, Taniguchi T. The IRF Family Transcription Factors in Immunity and Oncogenesis. Annu Rev Immunol [Internet]. Annual Reviews; 2008 Mar 27;26(1):535–84. Available from: http://dx.doi.org/10.1146/annurev.immunol.26.021607.090400

622. Ikushima H, Negishi H, Taniguchi T. The IRF family transcription factors at the interface of innate and adaptive immune responses. Cold Spring Harb Symp Quant Biol. United States; 2013;78:105–16.

623. Escalante CR, Yie J, Thanos D, Aggarwal AK. Structure of IRF-1 with bound DNA reveals determinants of interferon regulation. Nature [Internet]. 1998 Jan 1;391(6662):103–6. Available from: http://dx.doi.org/10.1038/34224

624. Fujii Y, Shimizu T, Kusumoto M, Kyogoku Y, Taniguchi T, Hakoshima T. Crystal structure of an IRF-DNA complex reveals novel DNA recognition and cooperative binding to a tandem repeat of core sequences. EMBO J [Internet]. 1999 Sep 15;18(18):5028–41. Available from: http://emboj.embopress.org/content/18/18/5028.abstract

625. Harada H, Fujita T, Miyamoto M, Kimura Y, Maruyama M, Furia A, et al. Structurally similar but functionally distinct factors, IRF-1 and IRF-2, bind to the same regulatory elements of IFN and IFN-inducible genes. Cell [Internet]. 1989 Aug 25;58(4):729–39. Available from: http://www.sciencedirect.com/science/article/pii/0092867489901074

626. Eroshkin A, Mushegian A. Conserved transactivation domain shared by interferon regulatory factors and Smad morphogens. J Mol Med (Berl). GERMANY; 1999 May;77(5):403–5.

627. Xu P, Bailey-Bucktrout S, Xi Y, Xu D, Du D, Zhang Q, et al. Innate Antiviral Host Defense Attenuates TGF-β Function through IRF3-Mediated Suppression of Smad Signaling. Mol Cell [Internet]. 2014;56(6):723–37. Available from: http://www.sciencedirect.com/science/article/pii/S1097276514009228

628. Rosenbloom KR, Sloan CA, Malladi VS, Dreszer TR, Learned K, Kirkup VM, et al. ENCODE Data in the UCSC Genome Browser: year 5 update. Nucleic Acids Res [Internet]. 2013;41(D1):D56–63. Available from: http://nar.oxfordjournals.org/content/41/D1/D56.abstract

629. Consortium TEP. An Integrated Encyclopedia of DNA Elements in the Human Genome. Nature [Internet]. 2012 Sep 6;489(7414):57–74. Available from: http://www.ncbi.nlm.nih.gov/pmc/articles/PMC3439153/

630. Langmead B, Salzberg SL. Fast gapped-read alignment with Bowtie 2. Nat Meth [Internet]. Nature Publishing Group, a division of Macmillan Publishers Limited. All Rights Reserved.; 2012 Apr;9(4):357–9. Available from: http://dx.doi.org/10.1038/nmeth.1923

631. Kent WJ, Sugnet CW, Furey TS, Roskin KM, Pringle TH, Zahler AM, et al. The Human Genome Browser at UCSC. Genome Res [Internet]. 2002 Jun 1;12 (6):996–1006. Available from: http://genome.cshlp.org/content/12/6/996.abstract

632. Heinz S, Benner C, Spann N, Bertolino E, Lin YC, Laslo P, et al. Simple combinations of lineage-determining transcription factors prime cis-regulatory elements required for macrophage and B cell identities. Mol Cell. United States; 2010 May;38(4):576–89.

633. McLean CY, Bristor D, Hiller M, Clarke SL, Schaar BT, Lowe CB, et al. GREAT improves functional interpretation of cis-regulatory regions. Nat Biotechnol. 2010/05/04 ed. 2010;28(5):495–501.

634. Sundstrom C, Nilsson K. Establishment and characterization of a human histiocytic lymphoma cell line (U-937). Int J Cancer. DENMARK; 1976 May;17(5):565–77.

635. Perk J, Iavarone A, Benezra R. Id family of helix-loop-helix proteins in cancer. Nat Rev Cancer [Internet]. 2005 Aug;5(8):603–14. Available from: http://dx.doi.org/10.1038/nrc1673

636. Vannini A, Cramer P. Conservation between the RNA Polymerase I, II, and III Transcription Initiation Machineries. Mol Cell [Internet]. 2012 Feb 24;45(4):439–46. Available from: http://www.sciencedirect.com/science/article/pii/S1097276512000895

637. Herrscher RF, Kaplan MH, Lelsz DL, Das C, Scheuermann R, Tucker PW. The immunoglobulin heavy-chain matrix-associating regions are bound by Bright: a B cell-specific trans-activator that describes a new DNA-binding protein family. Genes Dev. UNITED STATES; 1995 Dec;9(24):3067–82.

638. Ratliff ML, Templeton TD, Ward JM, Webb CF. The Bright side of hematopoiesis: Regulatory roles of ARID3a/Bright in human and mouse hematopoiesis. [Internet]. Frontiers in Immunology . 2014. Available from: http://www.frontiersin.org/Journal/Abstract.aspx?s=1176&name=b_cell_biology&ART_DOI=10.3389/fimmu.2014.00113

639. Wang Z, Wang D-Z, Hockemeyer D, McAnally J, Nordheim A, Olson EN. Myocardin and ternary complex factors compete for SRF to control smooth muscle gene expression. Nature [Internet]. 2004 Mar 11;428(6979):185–9. Available from: http://dx.doi.org/10.1038/nature02382

640. Vries RGJ, Bezrookove V, Zuijderduijn LMP, Kia SK, Houweling A, Oruetxebarria I, et al. Cancer-associated mutations in chromatin remodeler hSNF5 promote chromosomal instability by compromising the mitotic checkpoint. Genes Dev [Internet]. 2005 Mar 15;19 (6):665–70. Available from: http://genesdev.cshlp.org/content/19/6/665.abstract

641. Haering CH, Farcas A-M, Arumugam P, Metson J, Nasmyth K. The cohesin ring concatenates sister DNA molecules. Nature [Internet]. Macmillan Publishers Limited. All rights reserved; 2008 Jul 17;454(7202):297–301. Available from: http://dx.doi.org/10.1038/nature07098

642. Li Z, Otevrel T, Gao Y, Cheng H-L, Seed B, Stamato TD, et al. The XRCC4 gene encodes a novel protein involved in DNA double-strand break repair and V(D)J recombination. Cell [Internet]. 1995 Dec 29;83(7):1079–89. Available from: http://www.sciencedirect.com/science/article/pii/0092867495901353

643. Schneider WM, Chevillotte MD, Rice CM. Interferon-Stimulated Genes: A Complex Web of Host Defenses. Annu Rev Immunol [Internet]. Annual Reviews; 2014 Mar 21;32(1):513–45. Available from: http://dx.doi.org/10.1146/annurev-immunol-032713-120231

644. Rivals I, Personnaz L, Taing L, Potier M-C. Enrichment or depletion of a GO category within a class of genes: which test? Bioinforma [Internet]. 2007 Feb 15;23 (4):401–7. Available from: http://bioinformatics.oxfordjournals.org/content/23/4/401.abstract

645. Schmid S, Mordstein M, Kochs G, García-Sastre A, tenOever BR. Transcription Factor Redundancy Ensures Induction of the Antiviral State. J Biol Chem [Internet]. 9650 Rockville Pike, Bethesda, MD 20814, U.S.A.: American Society for Biochemistry and Molecular Biology; 2010 Dec 31;285(53):42013–22. Available from: http://www.ncbi.nlm.nih.gov/pmc/articles/PMC3009927/

646. Stein L. Large Scale Sequencing. Current Protocols in Bioinformatics [Internet]. John Wiley & Sons, Inc.; 2002. Available from: http://dx.doi.org/10.1002/0471250953.bi1101s02

647. Bickmore WA. The Spatial Organization of the Human Genome. Annu Rev Genomics Hum Genet [Internet]. Annual Reviews; 2013 Aug 31;14(1):67–84. Available from: http://dx.doi.org/10.1146/annurev-genom-091212-153515

648. Maston GA, Landt SG, Snyder M, Green MR. Characterization of Enhancer Function from Genome-Wide Analyses. Annu Rev Genomics Hum Genet [Internet]. Annual Reviews; 2012 Sep 12;13(1):29–57. Available from: http://dx.doi.org/10.1146/annurev-genom-090711-163723

649. Zeisel MB, Lucifora J, Mason WS, Sureau C, Beck J, Levrero M, et al. Towards an HBV cure: state-of-the-art and unresolved questions—report of the ANRS workshop on HBV cure. Gut [Internet]. 2015 Feb 10; Available from: http://gut.bmj.com/content/early/2015/02/09/gutjnl-2014-308943.abstract

650. Dienstag JL. Hepatitis B Virus Infection. N Engl J Med [Internet]. Massachusetts Medical Society; 2008 Oct 2;359(14):1486–500. Available from: http://dx.doi.org/10.1056/NEJMra0801644

651. Yan H, Zhong G, Xu G, He W, Jing Z, Gao Z, et al. Sodium taurocholate cotransporting polypeptide is a functional receptor for human hepatitis B and D virus. Chen ZJ, editor. Elife [Internet]. eLife Sciences Publications, Ltd; 2012 Nov 13;1:e00049. Available from: http://www.ncbi.nlm.nih.gov/pmc/articles/PMC3485615/

652. Yang H-C, Kao J-H. Persistence of hepatitis B virus covalently closed circular DNA in hepatocytes: molecular mechanisms and clinical significance. Emerg Microbes Infect [Internet]. Nature Publishing Group; 2014 Sep 17;3(9):e64. Available from: http://www.ncbi.nlm.nih.gov/pmc/articles/PMC4185362/

653. Yeo W, Chan TC, Leung NWY, Lam WY, Mo FKF, Chu MT, et al. Hepatitis B Virus Reactivation in Lymphoma Patients With Prior Resolved Hepatitis B Undergoing Anticancer Therapy With or Without Rituximab. J Clin Oncol [Internet]. 2009 Feb 1;27 (4):605–11. Available from: http://jco.ascopubs.org/content/27/4/605.abstract

654. Watanabe T, Sorensen EM, Naito A, Schott M, Kim S, Ahlquist P. Involvement of host cellular multivesicular body functions in hepatitis B virus budding. Proc Natl Acad Sci [Internet]. 2007 Jun 12;104 (24):10205–10. Available from: http://www.pnas.org/content/104/24/10205.abstract

655. Hino O, Ohtake K, Rogler CE. Features of two hepatitis B virus (HBV) DNA integrations suggest mechanisms of HBV integration. J Virol [Internet]. 1989 Jun 1;63 (6):2638–43. Available from: http://jvi.asm.org/content/63/6/2638.abstract

656. Köck J, Baumert TF, Delaney WE, Blum HE, von Weizsäcker F. Inhibitory effect of adefovir and lamivudine on the initiation of hepatitis B virus infection in primary tupaia hepatocytes. Hepatology [Internet]. W.B. Saunders; 2003 Dec 1;38(6):1410–8. Available from: http://dx.doi.org/10.1016/j.hep.2003.09.009

657. Lucifora J, Durantel D, Testoni B, Hantz O, Levrero M, Zoulim F. Control of hepatitis B virus replication by innate response of HepaRG cells. Hepatology [Internet]. Wiley Subscription Services, Inc., A Wiley Company; 2010 Jan 1;51(1):63–72. Available from: http://dx.doi.org/10.1002/hep.23230

658. Gripon P, Rumin S, Urban S, Le Seyec J, Glaise D, Cannie I, et al. Infection of a human hepatoma cell line by hepatitis B virus. Proc Natl Acad Sci U S A [Internet]. National Academy of Sciences; 2002 Nov 26;99(24):15655–60. Available from: http://www.ncbi.nlm.nih.gov/pmc/articles/PMC137772/

659. Wieland S, Thimme R, Purcell RH, Chisari F V. Genomic analysis of the host response to hepatitis B virus infection. Proc Natl Acad Sci United States Am [Internet]. 2004 Apr 27;101 (17):6669–74. Available from: http://www.pnas.org/content/101/17/6669.abstract

660. Wang H, Ryu W-S. Hepatitis B Virus Polymerase Blocks Pattern Recognition Receptor Signaling via Interaction with DDX3: Implications for Immune Evasion. Ou JJ, editor. PLoS Pathog [Internet]. San Francisco, USA: Public Library of Science; 2010 Jul 15;6(7):e1000986. Available from: http://www.ncbi.nlm.nih.gov/pmc/articles/PMC2904777/

661. Wei C, Ni C, Song T, Liu Y, Yang X, Zheng Z, et al. The Hepatitis B Virus X Protein Disrupts Innate Immunity by Downregulating Mitochondrial Antiviral Signaling Protein. J Immunol [Internet]. 2010 Jul 15;185 (2):1158–68. Available from: http://www.jimmunol.org/content/185/2/1158.abstract

662. Sato S, Li K, Kameyama T, Hayashi T, Ishida Y, Murakami S, et al. The RNA Sensor RIG-I Dually Functions as an Innate Sensor and Direct Antiviral Factor for Hepatitis B Virus. Immunity [Internet]. 2015 Jan 20;42(1):123–32. Available from: http://www.sciencedirect.com/science/article/pii/S107476131400483X

663. Liu Y, Li J, Chen J, Li Y, Wang W, Du X, et al. Hepatitis B Virus Polymerase Disrupts K63-Linked Ubiquitination of STING To Block Innate Cytosolic DNA-Sensing Pathways. J Virol [Internet]. 2015 Feb 15;89 (4):2287–300. Available from: http://jvi.asm.org/content/89/4/2287.abstract

664. Liver EA for the S of the. EASL Clinical Practice Guidelines: Management of chronic hepatitis B virus infection. J Hepatol [Internet]. 2012 Jul;57(1):167–85. Available from: http://www.sciencedirect.com/science/article/pii/S0168827812001675

665. Papatheodoridis G V, Dimou E, Papadimitropoulos V. Nucleoside analogues for chronic hepatitis B: antiviral efficacy and viral resistance. Am J Gastroenterol [Internet]. The American College of Gastroenterology; 2002 Jul;97(7):1618–28. Available from: http://dx.doi.org/10.1111/j.1572-0241.2002.05819.x

666. Bertoletti A, Rivino L. Hepatitis B: future curative strategies. Curr Opin Infect Dis [Internet]. Lippincott Williams & Wilkins; 2014 Dec 30;27(6):528–34. Available from: http://www.ncbi.nlm.nih.gov/pmc/articles/PMC4232294/

667. Clark KB, Onlamoon N, Hsiao H-M, Perng GC, Villinger F. Can non-human primates serve as models for investigating dengue disease pathogenesis? Front Microbiol [Internet]. Frontiers Media S.A.; 2013 Oct 11;4:305. Available from: http://www.ncbi.nlm.nih.gov/pmc/articles/PMC3795305/

668. Zellweger RM, Shresta S. Mouse Models to Study Dengue Virus Immunology and Pathogenesis. Front Immunol [Internet]. Frontiers Media S.A.; 2014 Apr 10;5:151. Available from: http://www.ncbi.nlm.nih.gov/pmc/articles/PMC3989707/

669. Chau TNB, Quyen NTH, Thuy TT, Tuan NM, Hoang DM, Dung NTP, et al. Dengue in Vietnamese Infants—Results of Infection-Enhancement Assays Correlate with Age-Related Disease Epidemiology, and Cellular Immune Responses Correlate with Disease Severity. J Infect Dis [Internet]. 2008 Aug 15;198 (4):516–24. Available from: http://jid.oxfordjournals.org/content/198/4/516.abstract

670. Yacoub S, Mongkolsapaya J, Screaton G. The pathogenesis of dengue. Curr Opin Infect Dis. United States; 2013 Jun;26(3):284–9.

671. Green S, Rothman A. Immunopathological mechanisms in dengue and dengue hemorrhagic fever. Curr Opin Infect Dis. United States; 2006 Oct;19(5):429–36.

672. Bouvier NM, Lowen AC. Animal Models for Influenza Virus Pathogenesis and Transmission. Viruses [Internet]. Molecular Diversity Preservation International (MDPI); 2010 Aug 27;2(8):1530–63. Available from: http://www.ncbi.nlm.nih.gov/pmc/articles/PMC3063653/

673. Gitelman AK, Kaverin N V, Kharitonenkov IG, Rudneva IA, Zhdanov VM. ANTIGENIC CHANGES IN MOUSE-ADAPTED INFLUENZA VIRUS STRAINS. Lancet [Internet]. 1983 May 28;321(8335):1229. Available from: http://www.sciencedirect.com/science/article/pii/S0140673683925205

674. Ibricevic A, Pekosz A, Walter MJ, Newby C, Battaile JT, Brown EG, et al. Influenza Virus Receptor Specificity and Cell Tropism in

Mouse and Human Airway Epithelial Cells. J Virol [Internet]. American Society for Microbiology; 2006 Aug 21;80(15):7469–80. Available from: http://www.ncbi.nlm.nih.gov/pmc/articles/PMC1563738/

675. Sidwell RW, Smee DF. In vitro and in vivo assay systems for study of influenza virus inhibitors. Antiviral Res [Internet]. 2000 Oct;48(1):1–16. Available from: http://www.sciencedirect.com/science/article/pii/S016635420000125X

676. Chiu C, Openshaw PJ. Antiviral B cell and T cell immunity in the lungs. Nat Immunol [Internet]. Nature Publishing Group, a division of Macmillan Publishers Limited. All Rights Reserved.; 2015 Jan;16(1):18–26. Available from: http://dx.doi.org/10.1038/ni.3056

677. Renegar KB, Small PA, Boykins LG, Wright PF. Role of IgA versus IgG in the Control of Influenza Viral Infection in the Murine Respiratory Tract. J Immunol [Internet]. 2004 Aug 1;173 (3):1978–86. Available from: http://www.jimmunol.org/content/173/3/1978.abstract

678. Plotkin SA, Plotkin SA. Correlates of Vaccine-Induced Immunity. Clin Infect Dis [Internet]. 2008 Aug 1;47 (3):401–9. Available from: http://cid.oxfordjournals.org/content/47/3/401.abstract

679. Rimmelzwaan GF, Fouchier RAM, Osterhaus ADME. Influenza virus-specific cytotoxic T lymphocytes: a correlate of protection and a basis for vaccine development. Curr Opin Biotechnol [Internet]. 2007 Dec;18(6):529–36. Available from: http://www.sciencedirect.com/science/article/pii/S0958166907001449

680. McMichael AJ, Gotch FM, Noble GR, Beare PAS. Cytotoxic T-Cell Immunity to Influenza. N Engl J Med [Internet]. Massachusetts Medical Society; 1983 Jul 7;309(1):13–7. Available from: http://dx.doi.org/10.1056/NEJM198307073090103

681. Epstein SL. Prior H1N1 influenza infection and susceptibility of Cleveland Family Study participants during the H2N2 pandemic of 1957: An experiment of nature. J Infect Dis [Internet]. 2006;193(1):49–53. Available from: http://www.scopus.com/inward/record.url?eid=2-s2.0-29744438219&partnerID=40&md5=a17bf36f44807bce0e811e5ccd7559bb

682. de Jong MD, Simmons CP, Thanh TT, Hien VM, Smith GJD, Chau TNB, et al. Fatal outcome of human influenza A (H5N1) is associated with high viral load and hypercytokinemia. Nat Med [Internet]. Nature Publishing Group; 2006 Oct;12(10):1203–7. Available from: http://dx.doi.org/10.1038/nm1477

683. Gazit R, Gruda R, Elboim M, Arnon TI, Katz G, Achdout H, et al. Lethal influenza infection in the absence of the natural killer cell receptor gene Ncr1. Nat Immunol. United States; 2006 May;7(5):517–23.

684. Hashimoto Y, Moki T, Takizawa T, Shiratsuchi A, Nakanishi Y. Evidence for phagocytosis of influenza virus-infected, apoptotic cells by neutrophils and macrophages in mice. J Immunol. United States; 2007 Feb;178(4):2448–57.

685. Pavlovic J, Arzet HA, Hefti HP, Frese M, Rost D, Ernst B, et al. Enhanced virus resistance of transgenic mice expressing the human MxA protein. J Virol [Internet]. 1995 Jul;69(7):4506–10. Available from: http://www.ncbi.nlm.nih.gov/pmc/articles/PMC189194/

686. Crotta S, Davidson S, Mahlakoiv T, Desmet CJ, Buckwalter MR, Albert ML, et al. Type I and Type III Interferons Drive Redundant Amplification Loops to Induce a Transcriptional Signature in Influenza-Infected Airway Epithelia. Kawaoka Y, editor. PLoS Pathog [Internet]. San Francisco, USA: Public Library of Science; 2013 Nov 21;9(11):e1003773. Available from: http://www.ncbi.nlm.nih.gov/pmc/articles/PMC3836735/

687. Mordstein M, Kochs G, Dumoutier L, Renauld J-C, Paludan SR, Klucher K, et al. Interferon-λ Contributes to Innate Immunity of Mice against Influenza A Virus but Not against Hepatotropic Viruses. PLoS Pathog [Internet]. Public Library of Science; 2008 Sep 12;4(9):e1000151. Available from: http://dx.doi.org/10.1371%2Fjournal.ppat.1000151

688. Lazear HM, Nice TJ, Diamond MS. Interferon-λ: Immune Functions at Barrier Surfaces and Beyond. Immunity [Internet]. 2015 Jul 21;43(1):15–28. Available from: http://www.sciencedirect.com/science/article/pii/S107476131500268X

689. Durbin JE, Fernandez-Sesma A, Lee C-K, Rao TD, Frey AB, Moran TM, et al. Type I IFN Modulates Innate and Specific Antiviral Immunity. J Immunol [Internet]. 2000 Apr 15;164 (8):4220–8. Available from: http://www.jimmunol.org/content/164/8/4220.abstract

690. Kohlmeier JE, Cookenham T, Roberts AD, Miller SC, Woodland DL. Type I Interferons Regulate Cytolytic Activity of Memory CD8+ T Cells in the Lung Airways during Respiratory Virus Challenge. Immunity [Internet]. 2010 Jul 23;33(1):96–105. Available from: http://www.sciencedirect.com/science/article/pii/S1074761310002426

691. Carlson CM, Turpin EA, Moser LA, O'Brien KB, Cline TD, Jones JC, et al. Transforming Growth Factor-β: Activation by Neuraminidase and Role in Highly Pathogenic H5N1 Influenza Pathogenesis. PLoS Pathog [Internet]. Public Library of Science; 2010 Oct 7;6(10):e1001136. Available from: http://dx.doi.org/10.1371%2Fjournal.ppat.1001136

692. Williams AE, Humphreys IR, Cornere M, Edwards L, Rae A, Hussell T. TGF-β prevents eosinophilic lung disease but impairs pathogen clearance. Microbes Infect [Internet]. 2005 Mar;7(3):365–74. Available from: http://www.sciencedirect.com/science/article/pii/S1286457905000249

693. Sells MA, Chen ML, Acs G. Production of hepatitis B virus particles in Hep G2 cells transfected with cloned hepatitis B virus DNA. Proc Natl Acad Sci [Internet]. 1987 Feb 1;84 (4):1005–9. Available from: http://www.pnas.org/content/84/4/1005.abstract

694. Chomczynski P, Sacchi N. Single-step method of RNA isolation by acid guanidinium thiocyanate-phenol-chloroform extraction. Anal Biochem. UNITED STATES; 1987 Apr;162(1):156–9.

695. Shin H-B, Choi M-S, Ryu B, Lee N-R, Kim H-I, Choi H-E, et al. Antiviral activity of carnosic acid against respiratory syncytial virus. Virol J [Internet]. 2013;10(1):303. Available from: http://www.virologyj.com/content/10/1/303

696. Severini A, Liu XY, Wilson JS, Tyrrell DL. Mechanism of inhibition of duck hepatitis B virus polymerase by (-)-beta-L-2',3'-dideoxy-3'-thiacytidine. Antimicrob Agents Chemother [Internet]. 1995 Jul;39(7):1430–5. Available from: http://www.ncbi.nlm.nih.gov/pmc/articles/PMC162757/

697. Hsu HC, Lai MY, Su IJ, Chen DS, Chang MH, Yang PM, et al. Correlation of hepatocyte HBsAg expression with virus replication and liver pathology. Hepatology. UNITED STATES; 1988;8(4):749–54.

698. Lucifora J, Xia Y, Reisinger F, Zhang K, Stadler D, Cheng X, et al. Specific and Nonhepatotoxic Degradation of Nuclear Hepatitis B Virus cccDNA. Sci [Internet]. 2014 Mar 14;343 (6176):1221–8. Available from: http://www.sciencemag.org/content/343/6176/1221.abstract

699. Liang G, Liu G, Kitamura K, Wang Z, Chowdhury S, Monjurul AM, et al. TGF-β Suppression of HBV RNA through AID-Dependent Recruitment of an RNA Exosome Complex. Siddiqui A, editor. PLoS Pathog [Internet]. San Francisco, CA USA: Public Library of Science; 2015 Apr 2;11(4):e1004780. Available from: http://www.ncbi.nlm.nih.gov/pmc/articles/PMC4383551/

700. Wang W-K, Sung T-L, Tsai Y-C, Kao C-L, Chang S-M, King C-C. Detection of Dengue Virus Replication in Peripheral Blood Mononuclear Cells from Dengue Virus Type 2-Infected Patients by a Reverse Transcription-Real-Time PCR Assay. J Clin Microbiol [Internet]. 2002 Dec 1;40 (12):4472–8. Available from: http://jcm.asm.org/content/40/12/4472.abstract

701. Fields BN, Knipe DM, Howley PM. Fields Virology [Internet]. 5th ed. Philadephia/London: Wolters Kluwer Health / Lippincott

Williams & Wilkins; 2007. Available from: http://solo.bodleian.ox.ac.uk/OXVU1:oxfaleph016912141

702. Ishida W, Hamamoto T, Kusanagi K, Yagi K, Kawabata M, Takehara K, et al. Smad6 is a Smad1/5-induced smad inhibitor. Characterization of bone morphogenetic protein-responsive element in the mouse Smad6 promoter. J Biol Chem. UNITED STATES; 2000 Mar;275(9):6075–9.

703. Matzuk MM, Kumar TR, Vassalli A, Bickenbach JR, Roop DR, Jaenisch R, et al. Functional analysis of activins during mammalian development. Nature. 1995;374(6520):354–6.

704. Schrewe H, Gendron-Maguire M, Harbison ML, Gridley T. Mice homozygous for a null mutation of activin βB are viable and fertile. Mech Dev [Internet]. 1994;47(1):43–51. Available from: http://www.sciencedirect.com/science/article/pii/0925477394900949

705. Brown CW, Houston-Hawkins DE, Woodruff TK, Matzuk MM. Insertion of Inhbb into the Inhba locus rescues the Inhba-null phenotype and reveals new activin functions. Nat Genet. UNITED STATES; 2000 Aug;25(4):453–7.

706. Sirard C, de la Pompa JL, Elia A, Itie A, Mirtsos C, Cheung A, et al. The tumor suppressor gene Smad4/Dpc4 is required for gastrulation and later for anterior development of the mouse embryo. Genes Dev [Internet]. 1998 Jan 1;12 (1):107–19. Available from: http://genesdev.cshlp.org/content/12/1/107.abstract

707. Tremblay KD, Dunn NR, Robertson EJ. Mouse embryos lacking Smad1 signals display defects in extra-embryonic tissues and germ cell formation. Dev [Internet]. 2001 Sep 15;128 (18):3609–21. Available from: http://dev.biologists.org/content/128/18/3609.abstract

708. Chang H, Matzuk MM. Smad5 is required for mouse primordial germ cell development. Mech Dev [Internet]. 2001;104(1-2):61–7. Available from: http://www.scopus.com/inward/record.url?eid=2-s2.0-0034967992&partnerID=40&md5=acdc2ed016f5fba36609823bd97466ca

709. Mishina Y, Crombie R, Bradley A, Behringer RR. Multiple Roles for Activin-Like Kinase-2 Signaling during Mouse Embryogenesis. Dev Biol [Internet]. 1999 Sep 15;213(2):314–26. Available from: http://www.sciencedirect.com/science/article/pii/S0012160699993788

710. Mishina Y, Suzuki A, Ueno N, Behringer RR. Bmpr encodes a type I bone morphogenetic protein receptor that is essential for gastrulation during mouse embryogenesis. Genes Dev [Internet]. 1995 Dec 15;9 (24):3027–37. Available from: http://genesdev.cshlp.org/content/9/24/3027.abstract

711. Beppu H, Kawabata M, Hamamoto T, Chytil A, Minowa O, Noda T, et al. BMP Type II Receptor Is Required for Gastrulation and Early Development of Mouse Embryos. Dev Biol [Internet]. 2000 May 1;221(1):249–58. Available from: http://www.sciencedirect.com/science/article/pii/S0012160600996702

712. Glister C, Kemp CF, Knight PG. Bone morphogenetic protein (BMP) ligands and receptors in bovine ovarian follicle cells: actions of BMP-4, -6 and -7 on granulosa cells and differential modulation of Smad-1 phosphorylation by follistatin. Reprod [Internet]. 2004 Feb 1;127 (2):239–54. Available from: http://www.reproduction-online.org/content/127/2/239.abstract

713. Guo Q, Kumar TR, Woodruff T, Hadsell LA, DeMayo FJ, Matzuk MM. Overexpression of mouse follistatin causes reproductive defects in transgenic mice. Mol Endocrinol. UNITED STATES; 1998 Jan;12(1):96–106.

714. Hu Y, Lee Y-T, Kaech SM, Garvy B, Cauley LS. Smad4 promotes differentiation of effector and circulating memory CD8 T cells, but is dispensable for tissue resident memory CD8 T cells. J Immunol [Internet]. 2015 Mar 1;194(5):2407–14. Available from: http://www.ncbi.nlm.nih.gov/pmc/articles/PMC4337487/

715. Reynolds JM, Dong C. Toll-like receptor regulation of effector T lymphocyte function. Trends Immunol [Internet]. 2013 Oct;34(10):511–9. Available from: http://www.sciencedirect.com/science/article/pii/S1471490613000938

716. Donnelly RP, Dickensheets H, O'Brien TR. Interferon-lambda and therapy for chronic hepatitis C virus infection. Trends Immunol. 2011;32(9):443–50. doi: 10.1016/j.it.2011.07.002. Epub 2011 A.

717. Brazil DP, Church RH, Surae S, Godson C, Martin F. BMP signalling: agony and antagony in the family. Trends Cell Biol [Internet]. 2015 May;25(5):249–64. Available from: http://www.sciencedirect.com/science/article/pii/S0962892414002141

718. Govender S, Csimma C, Genant HK, Valentin-Opran A, Amit Y, Arbel R, et al. Recombinant human bone morphogenetic protein-2 for treatment of open tibial fractures: a prospective, controlled, randomized study of four hundred and fifty patients. J Bone Joint Surg Am. United States; 2002 Dec;84-A(12):2123–34.

719. Windisch P, Stavropoulos A, Molnár B, Szendrői-Kiss D, Szilágyi E, Rosta P, et al. A phase IIa randomized controlled pilot study evaluating the safety and clinical outcomes following the use of rhGDF-5/β-TCP in regenerative periodontal therapy. Clin Oral Investig [Internet]. Springer-Verlag; 2012;16(4):1181–9. Available from: http://dx.doi.org/10.1007/s00784-011-0610-3

720. Lepparanta O, Tikkanen JM, Bespalov MM, Koli K, Myllarniemi M. Bone morphogenetic protein-inducer tilorone identified by high-throughput screening is antifibrotic in vivo. Am J Respir Cell Mol Biol. United States; 2013 Apr;48(4):448–55.

721. Myllärniemi M, Lindholm P, Ryynänen MJ, Kliment CR, Salmenkivi K, Keski-Oja J, et al. Gremlin-mediated Decrease in Bone Morphogenetic Protein Signaling Promotes Pulmonary Fibrosis. Am J Respir Crit Care Med [Internet]. American Thoracic Society; 2008 Feb 1;177(3):321–9. Available from: http://www.ncbi.nlm.nih.gov/pmc/articles/PMC2218851/

722. Raghu G, Collard HR, Egan JJ, Martinez FJ, Behr J, Brown KK, et al. An official ATS/ERS/JRS/ALAT statement: idiopathic pulmonary fibrosis: evidence-based guidelines for diagnosis and management. Am J Respir Crit Care Med. United States; 2011 Mar;183(6):788–824.

723. Mayer GD, Krueger RF. Tilorone hydrochloride: mode of action. Science. UNITED STATES; 1970 Sep;169(3951):1214–5.

724. Krueger RE, Mayer GD. Tilorone hydrochloride: an orally active antiviral agent. Science. UNITED STATES; 1970 Sep;169(3951):1213–4.

725. Giron DJ, Schmidt JP, Pindak FF. Tilorone hydrochloride: lack of correlation between interferon induction and viral protection. Antimicrob Agents Chemother. UNITED STATES; 1972 Jan;1(1):78–9.

726. Cao Y, Wang C, Zhang X, Xing G, Lu K, Gu Y, et al. Selective Small Molecule Compounds Increase BMP-2 Responsiveness by Inhibiting Smurf1-mediated Smad1/5 Degradation. Sci Rep [Internet]. Nature Publishing Group; 2014 May 14;4:4965. Available from: http://www.ncbi.nlm.nih.gov/pmc/articles/PMC4021816/

727. Vrijens K, Lin W, Cui J, Farmer D, Low J, Pronier E, et al. Identification of Small Molecule Activators of BMP Signaling. PLoS One [Internet]. Public Library of Science; 2013 Mar 19;8(3):e59045. Available from: http://dx.doi.org/10.1371%2Fjournal.pone.0059045

728. Sugimoto H, LeBleu VS, Bosukonda D, Keck P, Taduri G, Bechtel W, et al. Activin-like kinase 3 is important for kidney regeneration and reversal of fibrosis. Nat Med [Internet]. Nature Publishing Group, a division of Macmillan Publishers Limited. All Rights Reserved.; 2012 Mar;18(3):396–404. Available from: http://dx.doi.org/10.1038/nm.2629

729. Kopp E, Medzhitov R, Carothers J, Xiao C, Douglas I, Janeway CA, et al. ECSIT is an evolutionarily conserved intermediate in the Toll/IL-1 signal transduction pathway. Genes Dev [Internet]. Cold Spring Harbor Laboratory Press; 1999 Aug 15;13(16):2059–71.

Available from: http://www.ncbi.nlm.nih.gov/pmc/articles/PMC316957/

730. Xiao C, Shim J, Klüppel M, Zhang SS-M, Dong C, Flavell RA, et al. Ecsit is required for Bmp signaling and mesoderm formation during mouse embryogenesis. Genes Dev [Internet]. 2003 Dec 1;17 (23):2933–49. Available from: http://genesdev.cshlp.org/content/17/23/2933.abstract

731. Bustos-Valenzuela JC, Fujita A, Halcsik E, Granjeiro JM, Sogayar MC. Unveiling novel genes upregulated by both rhBMP2 and rhBMP7 during early osteoblastic transdifferentiation of C2C12 cells. BMC Res Notes [Internet]. BioMed Central; 2011 Sep 26;4:370. Available from: http://www.ncbi.nlm.nih.gov/pmc/articles/PMC3196718/

732. Kondo T, Watanabe M, Hatakeyama S. TRIM59 interacts with ECSIT and negatively regulates NF-κB and IRF-3/7-mediated signal pathways. Biochem Biophys Res Commun [Internet]. 2012 Jun 8;422(3):501–7. Available from: http://www.sciencedirect.com/science/article/pii/S0006291X12008923

733. Lei C-Q, Zhang Y, Li M, Jiang L-Q, Zhong B, Kim YH, et al. ECSIT Bridges RIG-I-Like Receptors to VISA in Signaling Events of Innate Antiviral Responses. J Innate Immun [Internet]. 2015;7(2):153–64. Available from: http://www.karger.com/DOI/10.1159/000365971

734. Vallet S, Mukherjee S, Vaghela N, Hideshima T, Fulciniti M, Pozzi S, et al. Activin A promotes multiple myeloma-induced osteolysis and is a promising target for myeloma bone disease. Proc Natl Acad Sci U S A. United States; 2010 Mar;107(11):5124–9.

735. Abdulkadyrov KM, Salogub GN, Khuazheva NK, Sherman ML, Laadem A, Barger R, et al. Sotatercept in patients with osteolytic lesions of multiple myeloma. Br J Haematol [Internet]. 2014;165(6):814–23. Available from: http://dx.doi.org/10.1111/bjh.12835

736. Dussiot M, Maciel TT, Fricot A, Chartier C, Negre O, Veiga J, et al. An activin receptor IIA ligand trap corrects ineffective erythropoiesis in [beta]-thalassemia. Nat Med [Internet]. Nature Publishing Group, a division of Macmillan Publishers Limited. All Rights Reserved.; 2014;20(4):398–407. Available from: http://dx.doi.org/10.1038/nm.3468

737. Ear J, Huang H, Wilson T, Tehrani Z, Lindgren A, Sung V, et al. RAP-011 improves erythropoiesis in zebrafish model of Diamond-Blackfan anemia through antagonizing lefty1. Blood. United States; 2015 Aug;126(7):880–90.

738. Quintas-Cardama A, Abdel-Wahab O, Manshouri T, Kilpivaara O, Cortes J, Roupie AL, et al. Molecular analysis of patients with polycythemia vera or essential thrombocythemia receiving pegylated interferon alpha-2a. Blood. 2013;122(6):893–901. doi: 10.1182/blood – 2012–07 – 442012. Epub 2.

739. Fields PA, Taylor GP. "Antivirals" in the treatment of adult T cell leukaemia- lymphoma (ATLL). Curr Hematol Malig Rep. 2012;7(4):267–75. doi: 10.1007/s11899–012 – 0139–9.

740. Nijman J, Mandemaker FS, Verboon-Maciolek MA, Aitken SC, van Loon AM, de Vries LS, et al. Genotype Distribution, Viral Load and Clinical Characteristics of Infants with Postnatal or Congenital Cytomegalovirus Infection. Gantt S, editor. PLoS One [Internet]. San Francisco, USA: Public Library of Science; 2014 Sep 30;9(9):e108018. Available from: http://www.ncbi.nlm.nih.gov/pmc/articles/PMC4182318/

741. Hebert JM, Mishina Y, McConnell SK. BMP signaling is required locally to pattern the dorsal telencephalic midline. Neuron. United States; 2002 Sep;35(6):1029–41.

742. RL N, Blanc W. PAthogenesis of congenital rubella. JAMA [Internet]. 1965 Dec 20;194(12):1277–83. Available from: http://dx.doi.org/10.1001/jama.1965.03090250011002

743. Wang RN, Green J, Wang Z, Deng Y, Qiao M, Peabody M, et al. Bone Morphogenetic Protein (BMP) signaling in development and human diseases. Genes Dis [Internet]. 2014 Sep;1(1):87–105. Available from: http://www.sciencedirect.com/science/article/pii/S2352304214000105

744. Liu W, Selever J, Wang D, Lu M-F, Mosest KA, Schwartz RJ, et al. Bmp4 signaling is required for outflow-tract septation and branchial-arch artery remodeling. Proc Natl Acad Sci U S A [Internet]. 2004;101(13):4489–94. Available from: http://www.scopus.com/inward/record.url?eid=2-s2.0-1842481058&partnerID=40&md5=f238105abda578d3e82a2ff0af826ce3

745. Chen Q, Chen H, Zheng D, Kuang C, Fang H, Zou B, et al. Smad7 Is Required for the Development and Function of the Heart. J Biol Chem [Internet]. 2009 Jan 2;284 (1):292–300. Available from: http://www.jbc.org/content/284/1/292.abstract

746. Cheeran MC-J, Lokensgard JR, Schleiss MR. Neuropathogenesis of Congenital Cytomegalovirus Infection: Disease Mechanisms and Prospects for Intervention. Clin Microbiol Rev [Internet]. 2009 Jan 1;22 (1):99–126. Available from: http://cmr.asm.org/content/22/1/99.abstract

747. Robertsen B. The interferon system of teleost fish. Fish Shellfish Immunol [Internet]. 2006 Feb;20(2):172–91. Available from: http://www.sciencedirect.com/science/article/pii/S1050464805000690

748. Padgett RW, Wozney JM, Gelbart WM. Human BMP sequences can confer normal dorsal-ventral patterning in the Drosophila embryo. Proc Natl Acad Sci U S A [Internet]. 1993 Apr 1;90(7):2905–9. Available from: http://www.ncbi.nlm.nih.gov/pmc/articles/PMC46205/

749. Sekelsky JJ, Newfeld SJ, Raftery LA, Chartoff EH, Gelbart WM. Genetic Characterization and Cloning of Mothers against Dpp, a Gene Required for Decapentaplegic Function in Drosophila Melanogaster. Genetics [Internet]. 1995 Mar;139(3):1347–58. Available from: http://www.ncbi.nlm.nih.gov/pmc/articles/PMC1206461/

750. Wharton KA, Cook JM, Torres-Schumann S, de Castro K, Borod E, Phillips DA. Genetic analysis of the bone morphogenetic protein-related gene, gbb, identifies multiple requirements during Drosophila development. Genetics. UNITED STATES; 1999 Jun;152(2):629–40.

751. Lemaitre B, Hoffmann J. The Host Defense of Drosophila melanogaster. Annu Rev Immunol [Internet]. Annual Reviews; 2007 Mar 21;25(1):697–743. Available from: http://dx.doi.org/10.1146/annurev.immunol.25.022106.141615

752. Valanne S, Wang J-H, Rämet M. The Drosophila Toll Signaling Pathway. J Immunol [Internet]. 2011 Jan 15;186 (2):649–56. Available from: http://www.jimmunol.org/content/186/2/649.abstract

753. Clark RI, Woodcock KJ, Geissmann F, Trouillet C, Dionne MS. Multiple TGF-beta superfamily signals modulate the adult Drosophila immune response. Curr Biol. 2011;21(19):1672–7. doi: 10.1016/j.cub.2011.08.048. Epub 2011 .

754. Frandsen JL, Gunn B, Muratoglu S, Fossett N, Newfeld SJ. Salmonella pathogenesis reveals that BMP signaling regulates blood cell homeostasis and immune responses in Drosophila. Proc Natl Acad Sci U S A. 2008/09/26 ed. 2008;105(39):14952–7.

755. Hepburn L, Prajsnar TK, Klapholz C, Moreno P, Loynes CA, Ogryzko N V, et al. A Spaetzle-like role for Nerve Growth Factor β in vertebrate immunity to Staphylococcus aureus. Science [Internet]. 2014 Oct 31;346(6209):641–6. Available from: http://www.ncbi.nlm.nih.gov/pmc/articles/PMC4255479/

756. Hashimoto C, Hudson KL, Anderson K V. The Toll gene of Drosophila, required for dorsal-ventral embryonic polarity, appears to encode a transmembrane protein. Cell. UNITED STATES; 1988 Jan;52(2):269–79.

757. Medzhitov R, Preston-Hurlburt P, Janeway CAJ. A human homologue of the Drosophila Toll protein signals activation of adaptive immunity. Nature. ENGLAND; 1997 Jul;388(6640):394–7.

758. Zugasti O, Ewbank JJ. Neuroimmune regulation of antimicrobial peptide expression by a noncanonical TGF-beta signaling pathway in Caenorhabditis elegans epidermis. Nat Immunol. United States; 2009 Mar;10(3):249–56.

759. Roberts AF, Gumienny TL, Gleason RJ, Wang H, Padgett RW. Regulation of genes affecting body size and innate immunity by the DBL-1/BMP-like pathway in Caenorhabditis elegans. BMC Dev Biol [Internet]. BioMed Central; 2010 Jun 7;10:61. Available from: http://www.ncbi.nlm.nih.gov/pmc/articles/PMC2894779/

760. Fairfax BP, Knight JC. Genetics of gene expression in immunity to infection. Curr Opin Immunol [Internet]. 2014 Oct 31;30:63–71. Available from: http://www.ncbi.nlm.nih.gov/pmc/articles/PMC4426291/

761. Sullivan C, Kim CH. Zebrafish as a model for infectious disease and immune function. Fish Shellfish Immunol [Internet]. 2008 Oct;25(4):341–50. Available from: http://www.sciencedirect.com/science/article/pii/S1050464808001319